

WL-TR-96-3028



**UNIFIED PILOT-INDUCED OSCILLATION THEORY
VOLUME I: PIO ANALYSIS WITH LINEAR AND NONLINEAR
EFFECTIVE VEHICLE CHARACTERISTICS, INCLUDING RATE
LIMITING**

**DAVID H. KLYDE
DUANE T. MCRUER
THOMAS T. MYERS**
*Systems Technology, Inc.
13766 S. Hawthorne Blvd.
Hawthorne CA 90250*

**DECEMBER 1995
FINAL REPORT FOR PERIOD OCTOBER 1994 - SEPTEMBER 1995**

APPROVED FOR PUBLIC RELEASE; DISTRIBUTION IS UNLIMITED.

**FLIGHT DYNAMICS DIRECTORATE
WRIGHT LABORATORY
AIR FORCE MATERIEL COMMAND
WRIGHT-PATTERSON AIR FORCE BASE, OHIO 45433-7562**

19960501 173

DISCLAIMER NOTICE



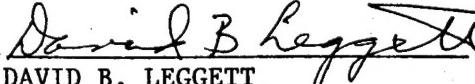
**THIS DOCUMENT IS BEST
QUALITY AVAILABLE. THE
COPY FURNISHED TO DTIC
CONTAINED A SIGNIFICANT
NUMBER OF PAGES WHICH DO
NOT REPRODUCE LEGIBLY.**

NOTICE

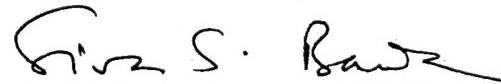
When Government drawings, specifications, or other data are used for any purpose other than in connection with a definitely Government-related procurement, the United States Government incurs no responsibility or any obligation whatsoever. The fact that the government may have formulated or in any way supplied the said drawings, specifications, or other data, is not to be regarded by implication, or otherwise in any manner construed, as licensing the holder, or any other person or corporation; or as conveying any rights or permission to manufacture, use, or sell any patented invention that may in any way be related thereto.

This report is releasable to the National Technical Information Service (NTIS). At NTIS, it will be available to the general public, including foreign nations.

This technical report has been reviewed and is approved for publication.



DAVID B. LEGGETT
Project Engineer
Control Dynamics Branch
Flight Control Division



SIVA S. BANDA, Chief
Control Dynamics Branch
Flight Control Division



DAVID P. LEMASTER
Chief, Flight Control Division
Flight Dynamics Directorate

If your address has changed, if you wish to be removed from our mailing list, or if the addressee is no longer employed by your organization please notify WL/FIGC-2, WPAFB, OH 45433-7531 to help us maintain a current mailing list.

Copies of this report should not be returned unless return is required by security considerations, contractual obligations, or notice on a specific document.

REPORT DOCUMENTATION PAGE

*Form Approved
OMB No. 0704-0188*

Public reporting burden for this collection of information is estimated to average 1 hour per response, including the time for reviewing instructions, searching existing data sources, gathering and maintaining the data needed, and completing and reviewing the collection of information. Send comments regarding this burden estimate or any other aspect of this collection of information, including suggestions for reducing this burden, to Washington Headquarters Services, Directorate for Information Operations and Reports, 1215 Jefferson Davis Highway, Suite 1204, Arlington, VA 22202-4302, and to the Office of Management and Budget, Paperwork Reduction Project (0704-0188), Washington, DC 20503.

1. AGENCY USE ONLY (Leave blank)			2. REPORT DATE December 1995	3. REPORT TYPE AND DATES COVERED Final Report: Oct 94 thru Sep 95	
4. TITLE AND SUBTITLE Unified Pilot-Induced Oscillation Theory, Volume I PIO Analysis with Linear and Nonlinear Effective Vehicle Characteristics Including Rate Limiting			5. FUNDING NUMBERS Contract: F33615-94-C-3613 PE 62201F PR 2403 TA 05 WU 9C		
6. AUTHOR(S) David H. Klyde Duane T. McRuer Thomas T. Myers			8. PERFORMING ORGANIZATION REPORT NUMBER TR No. 1313-1		
7. PERFORMING ORGANIZATION NAME(S) AND ADDRESS(ES) Systems Technology, Inc. 13766 Hawthorne Blvd Hawthorne CA 90250			10. SPONSORING/MONITORING AGENCY REPORT NUMBER WL-TR-96-3028		
9. SPONSORING/MONITORING AGENCY NAME(S) AND ADDRESS(ES) Flight Dynamics Directorate Wright Laboratory Air Force Materiel Command Wright-Patterson AFB OH 45433-7562					
11. SUPPLEMENTARY NOTES					
12a. DISTRIBUTION/AVAILABILITY STATEMENT Approved for public release Distribution unlimited			12b. DISTRIBUTION CODE		
13. ABSTRACT (Maximum 200 words) This work was conducted as part of a USAF initiative to develop a comprehensive theory to predict pilot-induced oscillation (PIO) tendencies due to the combined effect of all influencing elements. A PIO is a very complicated phenomenon stemming from a dynamic interaction between the pilot and the aircraft. When tight control is required from the pilot, an undesired oscillation can result. However, the adaptive nature of the human pilot makes such oscillations difficult to predict. The independent research of STI included: compilation of available PIO time histories and references as an initial step toward a comprehensive PIO database; refinement of the proposed PIO categories defined in NASA CR-4683; development of PIO theories based on these categories; development of methods to handle the higher frequency and nonlinear aspects of PIO analysis with an emphasis on rate limiting; and a review of existing and proposed linear PIO criteria.					
14. SUBJECT TERMS Flying Qualities, Pilot-Induced Oscillation, Rate Limiting, Position Limiting, Pilot Modeling			15. NUMBER OF PAGES 295		
16. PRICE CODE					
17. SECURITY CLASSIFICATION OF REPORT Unclassified	18. SECURITY CLASSIFICATION OF THIS PAGE Unclassified	19. SECURITY CLASSIFICATION OF ABSTRACT Unclassified	20. LIMITATION OF ABSTRACT UL		

FOREWORD

A pilot-induced oscillation (PIO) results from the interaction of the pilot and the dynamics of the vehicle being controlled. It may be caused or affected by several elements of the aircraft design or the mission task. PIO affects the pilot's ability to perform a given task, ranging from an annoying aircraft motion to inability to complete the task to, in the most extreme cases, jeopardizing the safety of the aircraft and crew. Because it occurs sporadically, PIO can be one of the most insidious flying qualities problems.

Criteria currently exist for some of the elements of aircraft design which influence PIO tendencies; however, the criteria in the flying qualities standard (MIL-STD-1797) address the effect of these elements individually rather than cumulatively. These elements include sluggish response modes, low damping, excessive phase lag or time delay, overly sensitive stick gradients, unstable response modes, coupled response modes, etc. Furthermore, there are some elements that are known to influence PIO tendencies which are not addressed in MIL-STD-1797. Some examples of these elements are aerodynamic nonlinearities, control system nonlinearities, actuator rate limits, nonlinear stick gradients, etc.

This report is the first step of an Air Force initiative to develop a comprehensive and unifying theory to explain the nature of the interaction of pilot and vehicle which results in PIO and to develop the capability to predict an aircraft's PIO tendencies due to the combined effect of all influencing elements. This theory must be consistent with several PIOS which have been documented in research, development, and operational aircraft. This effort should also produce design criteria which can be used in the development process to assess the risk of PIO prior to manned simulation.

The four volumes of this report represent a broad-band approach to developing this comprehensive theory. There were five contractors involved: Calspan Corporation; Hoh Aeronautics, Inc.; McDonnell Douglas Aerospace; Systems Technology, Inc.; and Virginia Polytechnic Institute and State University. The objectives of the contractors were to develop their theories and partially validate them against existing data.

Volume I is the work of Systems Technology, Inc. This research included: compilation of available PIO time histories and references as an initial step toward a comprehensive PIO database; refinement of the proposed PIO categories defined in NASA CR-4683; development of PIO theories based on these categories; development of methods to handle the higher frequency and nonlinear aspects of PIO analysis with an emphasis on rate limiting; and a review of existing and proposed linear PIO criteria.

Volume II is the combined work of McDonnell Douglas Aerospace, Advanced Transport Aircraft at Long Beach, CA, McDonnell Douglas Aerospace, Advanced Programs, at St. Louis, MO, and Hoh Aeronautics, Inc. at Lomita, CA. There are primarily two components associated with this study. One element is an examination of PIO events that have occurred in the course of initial flight development on several aircraft produced by

the McDonnell Douglas Corporation. The other element is an exploration of several theories associated with PIOs, particularly those with rate limiting involved.

Volume III was produced by the Virginia Tech Department of Aerospace and Ocean Engineering. This report describes an analysis method capable of predicting PIO tendencies due to several simultaneous factors. A unified approach involving pilot modeling, stability robustness analysis, and multivariable describing function analysis is applied to the problem of identifying aircraft with PIO tendencies. The approach is shown to have ties to existing PIO criteria and is successfully applied to the prediction of PIO tendencies of the M2-F2 lifting body.

Volume IV is the result of Calspan's efforts. This report presents the theory, fundamental principles, and analytical procedures of a quantitative criterion for the prediction of PIO tendencies based on a "time-domain Neal-Smith" approach. The criterion is validated against three very reliable flying qualities data bases. At present the criterion is intentionally limited to the evaluation of pitch control only. No fundamental limitations were discovered which preclude the evolution of this methodology and analytical procedures to PIO analysis of roll control or "outer-loop" longitudinal control, such as control of aircraft flight path.

After further evaluation and deliberation of these reports, the Air Force will pursue the most promising ideas, or combination of ideas, and validate them with further simulation and flight testing.

TABLE OF CONTENTS

LIST OF FIGURES	viii
LIST OF TABLES	xvii
LIST OF SYMBOLS	xix
ACKNOWLEDGMENTS	xviii
I. INTRODUCTION	1
A. OBJECTIVES	1
B. REPORT ORGANIZATION	1
II. BACKGROUND	2
A. HISTORICAL PERSPECTIVE	2
1. Single Axis - Extended Rigid-Body	2
2. Single Axis - Extended Rigid-Body Plus Mechanical Elaborations	2
3. Multiple Axis - Extended Rigid-Body	4
4. Higher Frequency - Non Rigid-Body	4
B. PILOT BEHAVIOR PATTERNS	4
1. Compensatory Behavior	6
2. Pursuit Behavior	8
3. Precognitive Behavior	8
4. Pilot Aberrant Behavior Characteristics	10
C. PROPOSED PIO CATEGORIES	11
III. PIO THEORY	14
A. DEFINITIONS	14
1. Minor Bobbles and Severe PIOS	14
2. Elements of a Severe PIO	15
3. Proposed PIO Categories	17
4. Are PIO Categories Really Needed?	17
5. Distinctions Between Categories II and III	17
B. FACTORS CONTRIBUTING TO CATEGORY I PIOS	18
1. Excessive Lags in the Effective Vehicle	18
2. Mismatched Pilot-Aircraft Interface	19

TABLE OF CONTENTS (continued)

C. FACTORS CONTRIBUTING TO CATEGORY II PIOS	21
1. Series Rate and Position Limiting	21
2. Effector Rate Limiting	22
D. FACTORS CONTRIBUTING TO CATEGORY III PIOS	29
IV. PIO ANALYSIS	30
A. CATEGORY I ANALYSIS	31
B. RATE AND POSITION LIMITING	36
C. DESCRIBING FUNCTIONS FOR SINGLE EFFECTOR RATE LIMITING	36
1. Sinusoidal Input Describing Function Approximation	37
2. Sinusoidal Input/Triangle Output Describing Function Approximation	42
3. Approximate Describing Function Comparison	46
4. Exact Sinusoidal Describing Function	46
5. Nonlinear Bandwidth	49
D. ANALYSIS OF CATEGORY II SITUATIONS	53
1. Analytical Preliminaries and X-15 Case Study Data	54
2. Elementary Series Rate Limiting	58
3. Single Effector Rate Limiting with Finite Actuator Bandwidth	61
4. Category II X-15 Analysis Summary	63
5. Increasing Pilot Gain	66
6. Multiple Rate Limits	67
E. CATEGORY III ANALYSIS	67
1. Analysis Issues	67
2. YF-12 Case Study	70
F. HIGH FREQUENCY PIO ANALYSIS	72
1. Analysis Issues	72
2. Analysis Examples	73
G. ANALYSIS GUIDE	75
1. Delineation of Most Likely Flight Conditions	77
2. Determination of Effective Controlled Element Dynamics	77
3. Pure-Gain-Pilot/Vehicle Closed-Loop System Analysis and Associated Considerations	78
4. Closed-Loop Compensatory Pilot/Vehicle System Analyses	79

TABLE OF CONTENTS (continued)

V. CONSIDERATIONS OF CRITERIA FOR ASSESSMENT OF PIO POTENTIAL	80
A. "CRITERIA" FOR CRITERIA	80
1. Validity	80
2. Selectivity	80
3. Ready Applicability	81
B. PROMINENT CATEGORY I PIO ASSESSMENT CRITERIA	81
1. Bandwidth/Phase Delay (Including Average Phase Rate)	82
2. Smith-Geddes Attitude-Dominant Type III	85
3. Summary Conclusions	89
C. CONSIDERATIONS FOR EXTENSIONS TO TREAT CATEGORY II SITUATIONS	90
1. Conjectures Based on $Y_c = K_c e^{-ts}/s$	90
2. Possibilities Based on X-15 Analyses	93
VI. SUMMARY COMMENTS AND CONCLUSIONS	96
A. PIO CONSTITUENTS	96
1. Aircraft Dynamics Frequency Range	96
2. Pilot Behavioral Dynamics	96
3. Triggers	96
B. PROPOSED PIO CATEGORIES	96
C. STATUS OF ASSESSMENT CAPABILITY	97
1. Category I	97
2. Category II PIOS	98
3. Category III PIOS	98
D. FUNDAMENTAL CONCLUSIONS AND RECOMMENDATIONS	98
VII. REFERENCES	100
APPENDIX A -- A CATALOG OF PIO TIME HISTORIES FOR OPERATIONAL, EXPERIMENTAL, AND RESEARCH AIRCRAFT	A-1
APPENDIX B -- CATEGORY I PIO DATA COMPILATION	B-1

LIST OF FIGURES

1. Simple Compensatory System and Time Responses (Adapted from Ref. 29) -----	7
2. Closed-Loop Pilot-Vehicle System Possibilities (Compensatory and Pursuit) -----	9
3. Pilot Ratings vs. Controlled Element Gain (Ref. 27)-----	20
4. Possible Flight Control System Locations of Rate and Position Limits -----	21
5. Closed-Loop Surface Actuator System -----	22
6. Example Linear Closed-Loop Surface Actuator Response to Command-----	23
7. Example Nonlinear Closed-Loop Surface Actuator Response to a δ_c Step -----	24
8. Closed-Loop Surface Actuator Model Examples-----	26
9. Conditions Associated with PIO -----	32
10. Frequency Responses for Crossover Model -----	34
11. Effective Nonlinear Gain for the Open-Loop Saturation Nonlinearity-----	39
12. Open-Loop Describing Function Representations of the Nonlinear Gain -----	39
13. Saturation Frequency as a Function of the Time Constant Ratio -----	41
14. Rate Limiting Actuator Phase Angle Frequency Response Comparison Between the Near Saturation Describing Function Approximation and the Nonlinear Simulation -----	43
15. Rate Limiting Actuator Phase Angle Frequency Response Comparison Between the Highly Saturated Describing Function Approximation and the Nonlinear Simulation -----	43
16. Rate Limiting Element (RLE) Time Response for a Sinusoidal Input (from Refs. 59 and 67) -----	44
17. Rate Limiting Actuator Phase Angle Frequency Response Comparison Between the Sinusoidal Input/Triangle Output Describing Function Approximation and the Nonlinear Simulation -----	47
18. Approximate Describing Function Time Response Comparison to the Nonlinear Simulation-----	47
19. Exact Sinusoidal Describing Function Comparison with the Nonlinear Simulation -----	48
20. Exact Sinusoidal Describing Function Frequency Response-----	50
21. Frequency Response Difference Between the Exact Sinusoidal Describing Function and the Linear Response -----	51

LIST OF FIGURES (continued)

22. Nonlinear Bandwidth Variation-----	53
23. Synchronous Pilot Closed-Loop System-----	54
24. Sinusoidal Input/Triangle Output Inverse Describing Function-----	55
25. Exact Sinusoidal Inverse Describing Function-----	56
26. Time History of the Landing Flare on X-15 Flight 1-1-5 (from Ref. 5) -----	57
27. X-15 Pitch Attitude (θ/δ) Frequency Response at the Flight 1-1-5 Landing Flare Condition-----	59
28. Normalized Limit Cycle Frequency for Elementary Series Rate Limiting-----	60
29. Limit Cycle Frequency Identification Using the Sinusoidal Input/Triangle Output Inverse Describing Function with the X-15 Example Case-----	62
30. Frequency Response Bode Plot of the X-15 Example Case with First Order Lag Representation of Single Effector Rate Limiting-----	62
31. Normalized Frequency Variation for the X-15 θ/δ_h Transfer Function-----	64
32. Limit Cycle Frequency Identification Using the Exact Sinusoidal Inverse Describing Function with the X-15 Example Case -----	64
33. Frequency Response Bode Plot of the X-15 Example Case with First Order Lag Representation of Single Effector Rate Limiting with Finite Bandwidth -----	65
34. Limit Cycle Frequency Identification Using the Sinusoidal Input/Triangle Output Finite Bandwidth Inverse Describing Function Approximation with the X-15 Example Case-----	65
35. Determining Limit Cycle Stability-----	67
36. Stable Limit Cycle Frequency Variation with Increasing Pilot Gain for the X-15 Example Case -----	68
37. YF-12 Pitch Attitude Frequency Response for an Aerial Refueling Flight Condition -----	71
38. Stick Output Variance Components for Vibratory Forcing (from Ref. 62)-----	73
39. YF-12 System Survey of the Pitch Attitude to Stick Force Transfer Function (from Ref. 7) at the Aerial Refueling Flight Condition -----	74
40. Large Helicopter q/δ_B Response with All SAS Loops Closed -----	76

LIST OF FIGURES (continued)

41. Comparison of Large Helicopter q/δ_B Response with All SAS Loops Closed with and without Desensitizer -----	76
42. Categories B and C Bandwidth/Dropback Requirements for PIO Resistance (from Ref. 2) -----	84
43. Prediction of PIO Susceptibility with Bandwidth/Phase Delay for Example Operational and Test Aircraft -----	84
44. PIO Frequencies of Operational, Test, and Have PIO Data as a Function of Smith-Geddes Criterion Frequency -----	89
45. Ratio of Nonlinear to Linear Bandwidth and Unstable Frequencies as a Function of K' -----	92
46. Bandwidth/Phase Delay Requirements for PIO Resistance Applied to X-15 Example Cases -----	94
47. Comparison of a First Order Lag Representation of the Magnitude Reduction Due to Rate Limiting with the Nonlinear Result for the X-15 Example Cases -----	95
 A-1. C-97 (Ref. A-1)-----	 A-7
A-2. F-101B (Ref. A-2)-----	A-8
A-3. F-101B (Ref. A-2)-----	A-9
A-4. B-52G (Ref. A-3)-----	A-10
A-5. B-52G (Ref. A-3)-----	A-11
A-6. F-104B (Ref. A-4)-----	A-12
A-7. YF-5A (Ref. A-5)-----	A-13
A-8. YF-5A (Ref. A-5)-----	A-14
A-9. X-15 (Ref. A-6)-----	A-15
A-10. T-38A (Ref. A-7)-----	A-16
A-11. M2-F2, Flight 1 (Ref. A-8) -----	A-17
A-12. M2-F2, Flight 10 (Ref. A-8) -----	A-18
A-13. M2-F2, Flight 16 (Ref. A-8) -----	A-19
A-14. YF-16 (Ref. A-9)-----	A-20
A-15. YF-16 (Ref. A-10) -----	A-21

LIST OF FIGURES (continued)

A-16. YF-12 (Ref. A-11) -----	A-22
A-17. YF-12 (Ref. A-11) -----	A-23
A-18. YA-7D Digitac (Ref. A-12)-----	A-24
A-19. Shuttle Orbiter (Ref. A-13)-----	A-25
A-20. F-8 DFBW (Ref. A-14)-----	A-26
A-21. F-15A. (Ref. A-15)-----	A-27
A-22. F-15C (Ref. A-16) -----	A-28
A-23. F-15C (Ref. A-16) -----	A-29
A-24. F-15C (Ref. A-16) -----	A-30
A-25. F/A-18A (Ref. A-17) -----	A-31
A-26. F/A-18, without eddy damper (Ref. A-18)-----	A-32
A-27. F-15E (CAS off) (Ref. A-19)-----	A-33
A-28. F-14A, Dual Hydraulic Failure (Ref. A-20) -----	A-34
A-29. F-14A, Dual Hydraulic Failure (Ref. A-20) -----	A-35
A-30. YF-22A (Ref. A-21) -----	A-36
A-31. B-2 (Ref. A-22)-----	A-37
A-32. B-2 (Ref. A-22)-----	A-38
A-33. X-15 (Ref. 23)-----	A-39
A-34. NT-33A, Configuration 1G (Ref. A-24) -----	A-40
A-35. NT-33A, Configuration 4D (Ref. A-24) -----	A-41
A-36. NT-33A, Configuration 6E (Ref. A-24)-----	A-42
A-37. NT33A, Configuration 14 (Ref. A-25) -----	A-43
A-38. NT-33A, Configuration 1-3 (Ref. A-26) -----	A-44
A-39. NT-33A, Configuration 2-4 (Ref. A-26) -----	A-45
A-40. NT-33A, Configuration 2-4 (Ref. A-26) -----	A-46

LIST OF FIGURES (continued)

A-41. NT-33A, Configuration 2-9 (Ref. A-26) -----	A-47
A-42. NT-33A, Configuration 4-10 (Ref. A-26) -----	A-48
A-43. NT-33A, Configuration 4-10 (Ref. A-26) -----	A-49
A-44. NT-33A, Configuration 5-3 (Ref. A-26) -----	A-50
A-45. NT-33A, Configuration 6-1, YF-17 (Ref. A-26 (Ref. A-26) -----	A-51
A-46. NT-33A, Configuration 6-1, YF-17 (Ref. A-26) -----	A-52
A-47. NT-33A, Configuration P5-1 (Ref. A-27) -----	A-53
A-48. NT-33A, Configuration P10D (Ref. A-27) -----	A-54
A-49. NT-33A, Configuration P11 (Ref. A-27) -----	A-55
A-50. NT-33A, Configuration P12 (Ref. A-27) -----	A-56
A-51. NT-33A, Configuration P12A (Ref. A-27) -----	A-57
A-52. NT-33A, Configuration P12B (Ref. A-27) -----	A-58
A-53. NT-33A, Configuration P13A (Ref. A-27) -----	A-59
A-54. NT-33A, Configuration P14 (Ref. A-27) -----	A-60
A-55. NT-33A, Configuration P15 (Ref. A-27) -----	A-61
A-56. NT-33A, Configuration P16 (Ref. A-27) -----	A-62
A-57. NT-33A, Configuration P16A (Ref. A-27) -----	A-63
A-58. NT-33A, Configuration L8 (Ref. A-27) -----	A-64
A-59. NT-33A, Configuration L8B (Ref. A-27) -----	A-65
A-60. NT-33A, Configuration L10 (Ref. A-27) -----	A-66
A-61. NT-33A, Configuration L11C (Ref. A-27) -----	A-67
A-62. NT-33A, Configuration L11C (Ref. A-27) -----	A-68
A-63. NT-33A, Configuration L14B (Ref. A-27) -----	A-69
A-64. NT-33A, Configuration L16A (Ref. A-27) -----	A-70
A-65. NT-33A, Configuration 5-2 (Ref. A-28) -----	A-71

LIST OF FIGURES (continued)

A-66. TIFS, Configuration X-29A - AR/PA (Ref. A-29)-----	A-72
A-67. TIFS, Configuration 5 + 200ms (Ref. A-30) -----	A-73
A-68. TIFS, Configuration 5 + 200ms (Ref. A-30) -----	A-74
A-69. TIFS, Configuration 11 (Ref. A-30)-----	A-75
A-70. TIFS, Configuration 11 (Ref. A-30)-----	A-76
A-71. TIFS, Configuration 11 (Ref. A-30)-----	A-77
A-72. TIFS, Configuration 11 (Ref. A-30)-----	A-78
A-73. TIFS, Configuration 12 (Ref. A-30)-----	A-79
A-74. TIFS, Configuration 12 (Ref. A-30)-----	A-80
A-75. TIFS, Configuration 13 (Ref. A-30)-----	A-81
A-76. TIFS, Configuration 13 (Ref. A-30)-----	A-82
A-77. TIFS, Configuration 14 (Ref. A-30)-----	A-83
A-78. TIFS, Configuration 14 (Ref. A-30)-----	A-84
A-79. TIFS, Configuration 21 (Ref. A-30)-----	A-85
A-80. TIFS, Configuration 21 (Ref. A-30)-----	A-86
A-81. TIFS, Configuration 21 (Ref. A-30)-----	A-87
A-82. TIFS, Configuration 21 (Ref. A-30)-----	A-88
A-83. TIFS, Configuration 22 (Ref. A-30)-----	A-89
A-84. TIFS, Configuration 22 (Ref. A-30)-----	A-90
A-85. TIFS, Configuration 22 (Ref. A-30)-----	A-91
A-86. TIFS, Configuration 22 (Ref. A-30)-----	A-92
A-87. TIFS, Configuration 22A (Ref. A-30)-----	A-93
A-88. TIFS, Configuration 22A (Ref. A-30)-----	A-94
A-89. TIFS, Configuration 27 (Ref. A-30)-----	A-95
A-90. TIFS, Configuration 27 (Ref. A-30)-----	A-96

LIST OF FIGURES (continued)

A-91. TIFS, Configuration 27 (Ref. A-30) -----	A-97
A-92. TIFS, Configuration 27 (Ref. A-30) -----	A-98
A-93. TIFS, Configuration 27 (Ref. A-30) -----	A-99
A-94. TIFS, Configuration 27 (Ref. A-30) -----	A-100
A-95. TIFS, Configuration 27 (Ref. A-30) -----	A-101
A-96. TIFS, Configuration 27 (Ref. A-30) -----	A-102
A-97. TIFS, Configuration 28 (Ref. A-30) -----	A-103
A-98. TIFS, Configuration 28 (Ref. A-30) -----	A-104
A-99. TIFS, Configuration 28 (Ref. A-30) -----	A-105
A-100. TIFS, Configuration 28 (Ref. A-30) -----	A-106
A-101. TIFS, Configuration 28A (Ref. A-30) -----	A-107
A-102. TIFS, Configuration 28A (Ref. A-30) -----	A-108
A-103. NT-33A, Configuration 2-B (Ref. A-31) -----	A-109
A-104. NT-33A, Configuration 2-5 (Ref. A-31) -----	A-110
A-105. NT-33A, Configuration 2-7 (Ref. A-31) -----	A-111
A-106. NT-33A, Configuration 2-8 (Ref. A-31) -----	A-112
A-107. NT-33A, Configuration 3-1 (Ref. A-31) -----	A-113
A-108. NT-33A, Configuration 3-6 (Ref. A-31) -----	A-114
A-109. NT-33A, Configuration 3-8 (Ref. A-31) -----	A-115
A-110. NT-33A, Configuration 3-12 (Ref. A-31) -----	A-116
A-111. NT-33A, Configuration 3-13 (Ref. A-31) -----	A-117
A-112. NT-33A, Configuration 5-9 (Ref. A-31) -----	A-118
A-113. NT-33A, Configuration 5-10 (Ref. A-31) -----	A-119
A-114. NT-33A, Configuration 5-11 (Ref. A-31) -----	A-120
A-115. NT-33A, Configuration 141F (10) (Ref. A-32) -----	A-121

LIST OF FIGURES (continued)

A-116. NT-33A, Configuration 141F (10) (Ref. A-32)-----	A-122
A-117. NT-33A, Configuration 143P (18) (Ref. A-32)-----	A-123
A-118. C-5A (Ref. A-33)-----	A-126
A-119. F-8 DFBW (Ref. A-34)-----	A-127
A-120. F-8 DFBW (Ref. A-35)-----	A-128
A-121. F-8 DFBW (Ref. A-35)-----	A-129
A-122. Tornado (Ref. A-36)-----	A-130
A-123. Tornado (Ref. A-36)-----	A-131
A-124. Tornado (Ref. A-36)-----	A-132
A-125. Tornado (Ref. A-36)-----	A-133
A-126. NT-33A, Configuration A(F)-5(1) (Ref. A-37)-----	A-134
A-127. NT-33A, Configuration A(F)-5(1) (Ref. A-37)-----	A-135
A-128. NT-33A, Configuration C(F)-5(2.5) (Ref. A-37)-----	A-136
A-129. NT-33A, Configuration C(F)-5(2.5) (Ref. A-37)-----	A-137
A-130. NT-33A, Configuration LA(F)-5(1) (Ref. A-37)-----	A-138
A-131. NT-33A, Configuration LA(F)-5(1) (Ref. A-37)-----	A-139
A-132. NT-33A, Configuration LA(F)-5(1) (Ref. A-37)-----	A-140
A-133. TIFS, Short Aft Tail Configuration (Ref. A-38)-----	A-141
B-1. Have PIO Configuration 2-1 (Baseline) -----	B-7
B-2. Have PIO Configuration 2-5 -----	B-8
B-3. Have PIO Configuration 2-8 -----	B-9
B-4. Have PIO Configuration 3-1 (Baseline) -----	B-10
B-5. Have PIO Configuration 3-12-----	B-11
B-6. Have PIO Configuration 3-13-----	B-12

LIST OF FIGURES (concluded)

B-7. Have PIO Configuration 5-1 (Baseline) -----	B-13
B-8. Have PIO Configuration 5-9 -----	B-14
B-9. Have PIO Configuration 5-10-----	B-15
B-10. X-15 Flight 1-1-5-----	B-16
B-11. T-38 with Bobweight Loop-Closed-----	B-17
B-12. T-38 with Bobweight Loop-Open-----	B-18
B-13. YF-Rigid Body Only-----	B-19
B-14. YF-12 Rigid Body with Flexible Mode -----	B-20
B-15. Shuttle Alt-5 -----	B-21
B-16. Shuttle STS-4 (fit) -----	B-22
B-17. F-8 DFBW CAS Mode + 100msec Added Delay -----	B-23
B-18. F-8 DFBW Direct Mode + 100msec Added Delay -----	B-24
B-19. F-8 DFBW Direct Mode-----	B-25
B-20. F-8 DFBW SAS Mode-----	B-26
B-21. B-2 Off-Nominal Approach (from Ref. 10)-----	B-27
B-22. B-2 Refueling (from Ref. 10)-----	B-28

LIST OF TABLES

1. Operation or Flight Test PIOs (Reduced Set) -----	3
2. Summary of Conditions for Category I PIO-----	33
3. PIO Situations Associated With Rate and Position Limiting -----	36
4. Inverse Describing Function Results-----	66
5. Closed-Loop Characteristics for Synchronous Pilot and Idealized Rate-Command Controlled Elements -----	83
6. Prediction of PIO Susceptibility with Smith Geddes Attitude Dominant Type III for Operational Test Aircraft-----	87
A-1. PIO Events with Documented Time Histories -----	A-3
A-2. Research PIO Events with Documented Time Histories -----	A-4
A-3. Additional Known PIO Cases-----	A-6
A-4. Addendum to PIO Events with Documented Time Histories -----	A-124
A-5. Addendum to Research PIO Events with Documented Time Histories -----	A-125
B-1. Category I PIO Data for Operational and Test Aircraft-----	B-3

ACKNOWLEDGMENTS

The work presented herein was performed during the period from September 1994 to September 1995 under contract F33615-94-C-3613 from the Flight Control Division, Flight Dynamics Directorate, Wright Laboratory, Air Force Materiel Command. The Air Force Project Engineer for the Unified Pilot-Induced Oscillation Theory program was Mr. David B. Leggett. The Air Force Technical Contact for the Systems Technology, Inc. (STI) contract was Mr. Charles F. Suchomel. The initial STI Project Engineer was Mr. Bimal L. Aponso. This duty was later transferred to Mr. David H. Klyde.

The authors wish to acknowledge the contributions of the following individuals. From Hoh Aeronautics, Inc. we gratefully acknowledge the efforts put forth by Mr. David G. Mitchell toward the creation of the PIO time history catalog that is included as an appendix to this report. At STI, we are grateful for the technical assistance provided by Mr. Bimal L. Aponso, Mr. Raymond E. Magdaleno, Ms. Cecy A. Pelz, and Mr. Frederick G. Anderson. We would also like to acknowledge the great efforts of Mr. Charles W. Reaber and Ms. Donna Taylor of the STI publications staff for report graphics, typing, and layout.

LIST OF SYMBOLS

- A** — maximum amplitude of actuator command input sine wave
- b₁** — open-loop actuator system output Fourier fundamental
- E** — magnitude of the input to a rate limiting element for a closed-loop actuator system
- e** — closed-loop actuator model error
- e_L** — rate limit saturation point
- j** — $\sqrt{-1}$
- K'** — ratio of the peak amplitude of a triangle output wave to the peak amplitude of a sinusoidal input wave for a rate limiting element
- K_c** — effective airplane or controlled element gain
- K_p** — pilot gain
- m** — average slope computed for Smith-Geddes criteria (dB/octave)
- s** — Laplace operator
- T** — linear system time constant (sec)
- t_D** — peak to peak time difference between input and output waves for a rate limiting element (sec)
- t_i** — time to peak amplitude for a rate limiting element sinusoidal input (sec)
- T_L** — pilot model lead time constant (sec)
- T_{NL}** — nonlinear system indicial response time constant (sec)
- t_o** — time to peak amplitude for a rate limiting element triangle wave output (sec)
- V_L** — rate limit
- x_i** — rate limiting element sinusoidal input
- \dot{x}_i** — rate limiting element sinusoidal input rate
- x_o** — rate limiting element triangle wave output
- Y_c** — effective airplane describing function

LIST OF SYMBOLS (continued)

- Y_p — pilot describing function
- Y_{pe} — compensatory pilot describing function
- Y_{pi} — pursuit pilot describing function
- δ — effector output surface position
- $\dot{\delta}$ — actuator rate
- δ_c — actuator input position command
- $\dot{\delta}_c$ — actuator input rate command
- $\Delta\phi$ — phase lag between output and input of a rate limiting element
- ζ_{D_f} — flexible mode pole damping ratio
- ζ_{N_f} — flexible mode zero damping ratio
- ζ_{sp} — short period damping ratio
- θ — pitch attitude
- θ_c — pitch attitude command
- θ_e — pitch attitude error
- θ_i — phase angle of actuator command input sine wave
- ϕ_{ω_u} — average phase rate (deg/Hz)
- τ_e — pilot-vehicle system effective time delay (sec)
- τ_h — effective pilot time delay (sec)
- $\tau_{p\theta}$ — pitch attitude phase delay (sec)
- ω — frequency (rad/sec)
- ω_a — linear actuator close-loop bandwidth (or linear actuator gain) (rad/sec)

LIST OF SYMBOLS (concluded)

- ω_a — nonlinear closed-loop actuator bandwidth (or effective nonlinear actuator gain) (rad/sec)
- ω_{BW_0} — pitch attitude airplane bandwidth frequency (rad/sec)
- ω_{BW_f} — flight path airplane bandwidth frequency (rad/sec)
- ω_c — pilot-vehicle crossover model frequency or Smith-Geddes criterion frequency (rad/sec)
- ω_{D_f} — flexible mode pole frequency (rad/sec)
- ω_i — frequency of actuator command input sine wave (rad/sec)
- ω_u — linear system unstable frequency (rad/sec)
- ω_{N_f} — flexible mode zero frequency (rad/sec)
- ω_s — rate limiting element saturation frequency (rad/sec)
- ω_{sp} — short period frequency (rad/sec)

I. INTRODUCTION

A. OBJECTIVES

This report documents the results of a Program Research and Development Announcement (PRDA) contract from the U.S. Air Force, Wright Laboratory. The purpose of this study was to develop a comprehensive unified pilot-induced oscillation (PIO) theory through independent research and direct interaction with the Air Force, other PRDA contractors (i.e., Virginia Polytechnic Institute and McDonnell Douglas Aerospace), and other military and industry groups currently working on PIO problems. As stated by the Air Force a comprehensive PIO theory will predict PIO tendencies due to the combined effect of all influencing elements. The independent research of Systems Technology, Inc. (STI) included the following:

- Compilation of available PIO time histories and references as an initial step toward a comprehensive PIO database;
- Refinement of the proposed PIO categories defined in Ref. 1;
- Development of PIO theories based on these categories;
- Development of methods to handle the higher frequency and nonlinear aspects of PIO analyses with an emphasis on rate limiting; and
- Review of existing and proposed linear PIO criteria.

B. REPORT ORGANIZATION

The potential for PIO is difficult to anticipate with any certainty, and conditions conducive to PIO grow in variety and complexity as aircraft systems improve and become more sophisticated. Existing handling qualities criteria typically emphasize the importance of reducing high-frequency lags. These criteria, however, cannot guarantee the likely presence or absence of PIOs. The primary reason for this is that various additional factors have been identified as contributory factors to PIOs. These include triggering events, pilot behavioral transitions, the impact of nonlinearities such as actuator rate and surface position limiting on closed-loop piloted control, and transitions in effective vehicle dynamics as a function of pilot input amplitude such as those caused by nonlinear gain schedules and stick gearing, and mode switches. To develop a comprehensive unified PIO theory, all of these factors need to be addressed.

The background material of Section II includes a historical perspective of PIO, a review of pilot behavior patterns, and the proposed PIO categories. Much of this material is essentially an overview of Ref. 1. Section III develops a PIO theory in terms of the three proposed PIO categories. The foundation of the STI theory first involves the distinction between minor bobbles and severe PIOs. Then severe PIOs are classified by category, and finally, the factors that contribute to PIO within a given category are identified. In Section IV analysis issues and procedures are presented by category. The major thrust of this section is on the development of analysis methods that encompass the effects of series rate limiting. Section V features a review of existing and proposed linear system predictive PIO criteria. A summary and conclusions are then presented in Section VI.

As a starting point for the creation of a PIO database, available time histories and associated references were collected from available sources. From this effort an extensive, but not yet comprehensive, collection of PIO events was assembled jointly by STI and Hoh Aeronautics, Inc. The time histories and related flight condition information are presented in Appendix A. To complement the Section V criteria review, a compilation of related Category I PIO data is presented in Appendix B.

II. BACKGROUND

A. HISTORICAL PERSPECTIVE

A study of aeronautical history reveals a remarkably diverse set of severe PIOs as exemplified by the listing of "famous" PIOs in Ref. 1. To develop criteria and analysis techniques that can be used to predict and prevent future incidents, a database consisting of time histories, effective vehicle dynamics, pilot comments, etc. from actual PIO events is required. As a first step an Air Force enhanced version of the Ref. 1 listing was used to assemble the catalog of PIO time histories provided in Appendix A. The catalog was assembled from a joint literature search undertaken by STI and Hoh Aeronautics, Inc. that included the extensive STI technical library and material gathered via respective Air Force PRDA and SBIR contracts. The time histories were divided into two distinct groups; (1) operational or flight test PIOs and (2) flight research PIOs. The main difference between the two groups was that the flight research PIOs occurred experimentally with a variable stability aircraft.

Table 1 presents a reduced set of the operational or flight test PIOs. The events selected also fall into two groups. One group represents PIOs for which some representation of the effective vehicle dynamics exists in the published literature (e.g., X-15, T-38, YF-12, Shuttle, F-8 DFBW, CH-53E, and B-2). The remaining events represent PIOs in current military and civilian aircraft (e.g., F/A-18, JAS 39, YF-22, MD-11, etc.). Appropriate references, when available, are given in Table 1, although for many of the PIOs there is little or no data available other than time histories or commentaries. It is useful to describe the Table 1 PIOs in terms of two primary features: the aircraft control axes that are fundamentally involved; and the frequency of the closed-loop oscillation that historically ranges from about 0.2 (1.4 rad/sec) to 4 Hz (25 rad/sec) as presented in the Ref. 2 analysis of the Appendix A data. These distinguishing features are described below. Finally, the Category indicated in the table refers to the proposed PIO categories that are a foundation of this research effort. As such, detailed discussions are provided throughout this report beginning with the category definitions provided at the end of this section.

1. *Single Axis – Extended Rigid-Body*

Most of the PIO research to date has been focused on effective aircraft dynamics that are characteristic of rigid body longitudinal or lateral-directional properties. Higher frequency dynamics representing the control actuators, SAS dynamics effects, digital system time delays, etc. have been incorporated or approximated in an effective time delay. For many PIOs such approximations are both appropriate and adequate. Perhaps best known and surely the most widely viewed lateral PIO in this category was the remarkable unintended "first flight" of the YF-16. A description of the participating events is given in Ref. 6. The longitudinal variety have several dramatic entries including the recent YF-22 and JAS 39 crashes.

2. *Single Axis – Extended Rigid-Body Plus Mechanical Elaborations*

PIOs in this group are similar to those described above, with the addition that the primary mechanical control system plays a major role. The aircraft included are of more traditional design, and typically incorporate such elements as single or dual bobweights, various artificial feel devices, etc. Some older aircraft or modern aircraft with simpler primary controls have tab or servo-tab controls, power boost rather than fully powered surface actuators, etc. System friction and hysteresis effects can be very important, since they tend to create two different sets of effective airplane dynamics (e.g., corresponding to small-amplitude and large-amplitude pilot inputs). In these systems the aircraft dynamics

TABLE 1. OPERATION OR FLIGHT TEST PIOS (REDUCED SET)

Aircraft	Date	PIO Description	Axis/Frequency	Cat.	Ref.
X-15	6/8/59	Gliding flight approach and landing.	Longitudinal - Extended Rigid-Body	II	3
T-38	1/26/60	High speed. Distributed bobweight and primary control system involved.	Longitudinal - Extended Rigid-Body Plus Mechanical Elaborations	III	4
X-15	1961	Research study of ω_4/ω_d effects.	Lateral-Directional - Extended Rigid-Body	I	5
YF-16	1/20/74	"Flight Zero." High speed taxi tests.	Lateral-Directional - Extended Rigid-Body	III	6
YF-12	1975	Aerial refueling with flexible mode interaction.	Higher Frequency Non-Rigid Body	I	7
YF-12	1975	Aerial refueling. Mid-frequency, severe case.	Longitudinal - Extended Rigid-Body	III	7
Shuttle	10/26/77	ALT-5 landing approach glide. Lateral PIO just prior to longitudinal PIO with both attitude and path modes involved.	Multiple Axis - Extended Rigid-Body	II	8
F-8 DFBW	4/18/78	Offset landing. Tail strike trigger on touch and go.	Longitudinal - Extended Rigid-Body	III	1
CH-53E	1978-85	Airplane-pilot coupling with flexible modes. Several major instances in precision hover and with heavy slung loads. Heavy landings, dropped loads, etc.	Higher Frequency Non-Rigid Body	I - II	9 to 11
F/A-18A	1981	Sea trials. Carrier landing.	Lateral-Directional - Extended Rigid-Body	I	12
F-15E	1987	CAS off. Cruise.	Longitudinal - Extended Rigid-Body	I - II	13
V-22	1989-91	1.4 Hz lateral oscillation on the landing gear. 3.4 Hz antisymmetric mode destabilized by pilot aileron control. 4.2 Hz symmetric mode destabilized by pilot collective control.	Higher Frequency Non-Rigid Body	I	14
JAS 39	1990	Power approach.	Longitudinal - Extended Rigid-Body	II - III	none
F-14A	1991	Dual hydraulic failure evaluation. Aerial refueling.	Longitudinal - Extended Rigid-Body	II	15
YF-22	4/25/92	Wave off in afterburner.	Longitudinal - Extended Rigid-Body	III	16
MD-11	4/6/93	China Eastern Airlines Flt. 583. Inadvertent slat deployment.	Longitudinal - Extended Rigid-Body	?	17
JAS 39	1993	Low altitude demonstration.	Longitudinal - Extended Rigid-Body	II - III	none
B-2	1994	Landing and aerial refueling.	Longitudinal - Extended Rigid-Body	?	18
B777	1995	Landing with automatic spoiler deployment at touchdown. 3 Hz bending mode excitation on approach. Control system mistrim during a touch-and-go rollout.	Longitudinal - Extended Rigid-Body and Higher Frequency Non-Rigid Body	I - II and III	19

are still extended rigid body, but the dynamics of the primary control and artificial feel system also contribute. In the simplest situations, the effective airplane dynamics differ primarily as a function of the pilot's output amplitude (e.g., the T-38 PIO of Ref. 4), and the pilot's inability to adapt to large changes from pre- to post-transition effective airplane dynamics is central to the PIO. In some cases the limb-neuromuscular-manipulator system dynamics are major factors, either as a simple effective limb-bobweight combination, or as a much more elaborate dynamic entity.

3. Multiple Axis – Extended Rigid-Body

Of all the essentially rigid body PIOs these are by far the most interesting, dramatic, and least well understood. As noted by Einar Enevoldson, a noted retired NASA Dryden test pilot, “3-D PIOs are extreme, and are present in many aircraft under asymmetric conditions. Besides the oblique wing AD-1, another example was a 3-D PIO in an F-14 at high angle of attack and large sideslip, which resulted in a departure which was very difficult to recover.” Thrust-vectoring aircraft, damaged aircraft, and aircraft with asymmetrically-hung stores, are also subject to unusual asymmetries. Unfortunately, this PIO type is not at all well understood. For aircraft with elevon or ailevator controls, that can create conflicts between axes, the multi-axis PIO phenomenon can be further complicated by position as well as rate limiting.

4. Higher Frequency – Non Rigid-Body

A downside of the trend for more highly integrated aircraft, and especially unstable aircraft that are highly augmented, is the insurgence of the lower frequency flexible modes into the frequency range of stability augmentation and pilot control. For these vehicles the extended rigid body characteristics are not sufficient or, sometimes, even relevant. Cases in which the limb-neuromuscular dynamics are central to pilot-vehicle oscillations are fairly common. The roll ratchet phenomenon is a notable example (e.g., Refs. 20 to 22). Here the characteristic frequency is set primarily by the limb-manipulator combination, tending to range from 2 - 3 Hz. To the extent that this type of PIO is a limb-bobweight phenomenon it is sometimes referred to as Pilot-Augmented Oscillation (PAO). PAO is probably not catastrophic in the safety sense, although it can severely limit the airplane's maneuvering performance. Roll ratchet cases are not included in Table 1, although some of the aircraft listed there have exhibited the characteristic.

Pilot interaction with lower frequency flexible modes can be extremely severe. As reported in Ref. 23 they have been observed on the F-111 at the edges of its flight envelope when loaded with heavy stores, and with the Rutan Voyager. Of the documented cases to date, the flexible mode coupling observed on the YF-12 (Ref. 7) was relatively mild while on the CH-53E the result was quite severe. In fact, the pilot-vehicle interactions encountered with the CH-53E helicopter are extremely important harbingers of things to come as flexible modes become significant elements in aircraft-pilot coupling. They are of particular future concern for large, flexible aircraft such as the High Speed Civil Transport (Ref. 24). In connection with the CH-53E, the severe pilot-aircraft oscillations that occurred were associated with the lower flexible mode frequencies. These were first encountered with the aircraft in precision hover tasks. They were particularly severe when large slung loads were present. The extra dynamics due to the sling load were not an important feature of these oscillations, but the much higher sensitivity to cyclic controls associated with the increased collective needed to support the load was. Several dramatic incidents occurred over a period of years (1978 - 85), including some high-visibility events in which catastrophe was avoided only by dropping the load (in one case a light armored vehicle), that created a great deal of high level attention in the US Navy. The very comprehensive analysis, flight, and ground test program conducted to define and measure all the dynamics and conditions involved (Refs. 9 to 11) make this an unusually well-documented case study. As further noted in Table 1, the CH-53E is not alone among rotorcraft for PIO or PAO. The V-22 tiltrotor aircraft experienced three incidents of this nature in flight test operations (Ref. 14).

B. PILOT BEHAVIOR PATTERNS

A significant attribute of a human pilot is the ability to establish a wide variety of pilot-vehicle system organizations (Refs. 25 to 31). In essence, human adaptive and learning attributes permit the pilot to be simultaneously engaged as the on-going architect and modifier of the pilot-aircraft system itself and as an operating entity within that system. As the pilot “changes” the system organization, his dynamic

behavior is adjusted as appropriate for the overall system. This repertory of behavior is so extensive that, as a learning and adaptive controller operating with an extensive array of endogenous sensing mechanisms, the pilot has capabilities that far exceed those of the most sophisticated unmanned control system.

From the system analysis standpoint this variety is, at first, disconcerting. For many flight control situations, however, the complexities exhibit an orderly character. In controlling any complex system operating at or near its margins, *successful* behavior is very narrowly limited. The very nature of the requirements for "good" system performance and the restrictions imposed by the dynamic characteristics of the aircraft constrain the successful human pilot to operate in accordance with well-established "behavioral laws." When the pilot is well-trained and motivated and the restrictions imposed on pilot-vehicle system performance are severe, the performance of the pilot and the system can be predicted in both qualitative and quantitative terms. In short the pilot-vehicle system is amenable to mathematical analysis like inanimate systems (Ref. 29). Operationally, each of the pilot-organized system structures can be depicted as an effective pilot-vehicle system block diagram that corresponds to a "control law." Thus feedback control system analysis principles can be extended to treat these pilot-vehicle systems. The dynamic behavior of human pilots can be described and quantified by "describing functions" that are akin to the transfer functions used to characterize the airplane dynamics, and an additive pilot-induced noise or "remnant."

The overall result of all this versatility is a variably-configured, task-oriented, pilot-vehicle system that in any of its manifestations is ordinarily admirably suited to accomplish flight control goals with great efficiency and precision. On occasion, however, aberrations in either the pilot's system organization or dynamic behavior appear that induce far from ideal system behavior. PIOS are a notable example.

There are several behavioral modes that can conceivably enter into or influence pilot-induced oscillations. These full attention control architectural patterns are cataloged as follows:

- Compensatory - Pilot response conditioned on errors;
- Pursuit - Response conditioned on errors plus system inputs and outputs;
- Pursuit with Preview - Preview of input added;
- Precognitive - Skilled, essentially open-loop; and
- Precognitive/Compensatory - Dual mode control.

Each pattern can be represented as a specific block diagram showing the essential control pathways that embody that structural form. For example, in "compensatory" behavior the pilot responds primarily to errors in the pilot-vehicle system. The dynamic properties for some of these behavioral patterns will be described later. In principle these modes can exist for a variety of pilot percepts, although visual and acceleration cues are certainly dominant in flight control.

There are also a number of behavior transitions among the above patterns that can sometimes occur (Refs. 26, 27, 31 to 33). The "SOP Progressive Transitions" form a sequence, based on the Successive Organization of Perception (SOP) theory (Refs. 26 to 29). As the system structure established by the pilot changes progressively, overall pilot-vehicle performance improves. Specifically:

- Closed-loop pilot-vehicle system effective bandwidth increases;
- System dynamic response is faster, with less error; and
- Pilot workload is reduced.

The "SOP Regressive Transitions" proceed in the opposite direction.

The consequence on the pilot dynamics of sudden or step-like changes in the effective vehicle dynamics is the "Post-Transition Retention" phase (Ref. 29). During this interval immediately after a sudden change in vehicle characteristics, the pilot dynamics remain those adapted to the vehicle dynamics that were present before the change. This phase is followed by adaptation to the post-transition aircraft dynamics.

The basic behavioral modes pertain to the fundamental human pilot dynamic forms for conditions when the pilot is devoting full attention to control tasks. Additional human pilot dynamic features include divided attention, neuromuscular actuation system phenomena, and acceleration-induced phenomena. The first item, divided attention, is important for many flying tasks, but is seldom pertinent to PIOS because they are invariably full-attention in the developed state. Reduction in divided attention, as in the narrowing of the attentional field with a consequent increased focus on a dominant control variable and increased pilot gain, however, can be a precursor and initiating facet for a PIO. The neuromuscular system dynamics and the acceleration feedthroughs, on the other hand, can be important factors in pilot-aircraft oscillations (Refs. 19, 21, 34 to 39). An example is the high-frequency (2-3 Hz) rolling oscillation that sometimes occurs during rapid rolling maneuvers (i.e., roll ratchet). References 20 and 21 indicate that this can be associated with the neuromuscular actuation system's resonant peak. Acceleration-induced phenomena can appear in several guises. For instance, acceleration feedbacks may be associated with the neuromuscular system limb-manipulator "bobweight" effect or with whole-body acceleration and vibration feedthroughs (Ref. 38); these are both essentially independent of human pilot central processes other than deliberate changes of muscular tension. Accelerations can also act through the human's perceptual processes to set up major feedback pathways that are on a par with visual pathways. In this form, accelerations can conceivably serve in parallel feedback pathways or as one stage in transition processes in which visual and acceleration cues compete for dominance.

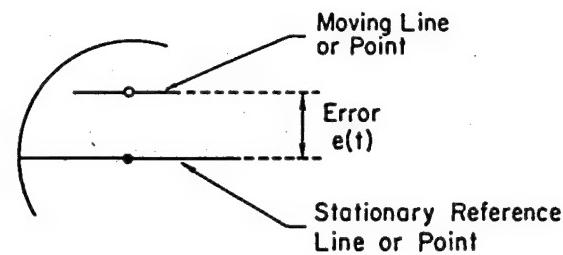
1. Compensatory Behavior

Compensatory behavior will characteristically be present when the commands and disturbances are random-appearing and when the only information acted on by the pilot consists of system errors or aircraft outputs. Under full-attention conditions the pilot exerts continuous closed-loop control on the aircraft so as to minimize system errors in the presence of commands and disturbances.

The time traces of Figure 1 illustrate the nature of compensatory control. The system is a roll-control tracking task in which the rolling velocity becomes proportional to the pilot's command output after a first-order lag given by the roll-subsidence time constant, T_s . Notice that the system output follows the system forcing function command to the closed-loop pilot-vehicle system quite closely. To accomplish this the pilot develops an anticipatory lead ($T_{LS} + 1$) that approximately cancels the roll-subsidence lag $1/(T_s + 1)$ of the airplane. This can be demonstrated using the Figure 1 time traces by comparing the system roll error with the pilot's output lagged by the roll-subsidence lag time constant ($T_s + 1$). When the latter time history is shifted by a time increment τ_h , the two traces are very much alike. This correspondence suggests not only that the pilot has generated a lead to cancel the vehicle lag, but that his higher frequency lags can be approximated at the lower frequencies by the time delay, τ_h . The implication is that, when the pilot's characteristics are represented by a describing function, Y_{pe} , and the aircraft roll angle to aileron dynamics by the transfer function, Y_c , the open-loop describing function for the roll control task of Figure 1 would be,

$$Y_{pe} Y_c \approx K_p e^{-\tau_h j\omega} (T_L j\omega + 1) \frac{K_c}{j\omega(T_j\omega + 1)} \quad (1)$$

which can then be reduced to,



COMPENSATORY DISPLAY

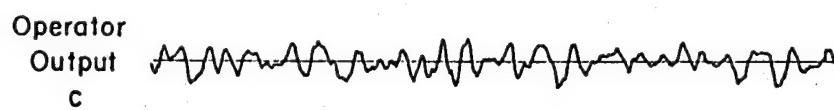
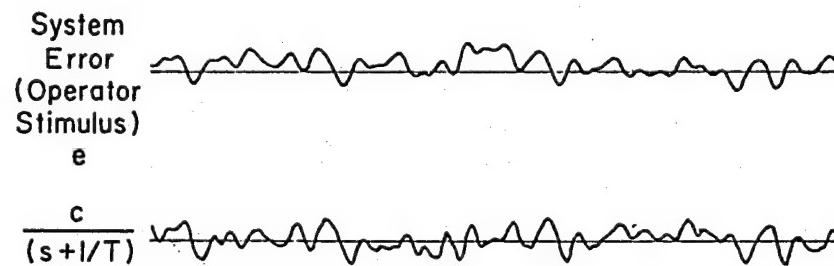
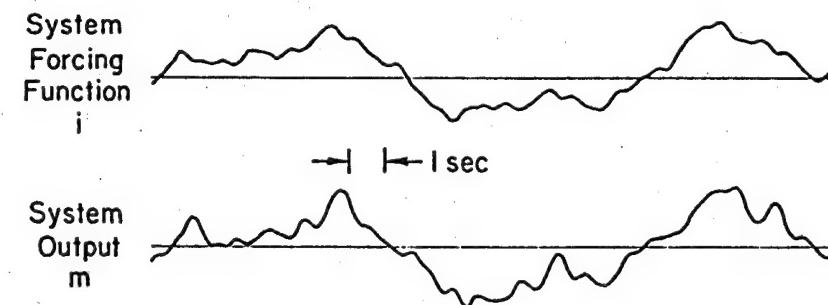
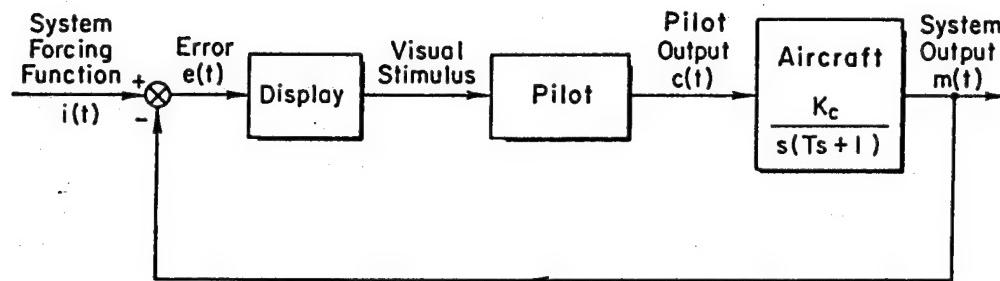


Figure 1. Simple Compensatory System and Time Responses (Adapted from Ref. 29)

$$Y_p Y_c \approx \frac{\omega_c e^{-j\omega t_h}}{j\omega} \text{ for } |\omega| \text{ near } \omega_c \quad (2)$$

where $\omega_c = K_p K_c$. As discussed in Ref. 1, this equation has become ubiquitous in manual control, and is commonly referred to as the "crossover" model or law.

2. Pursuit Behavior

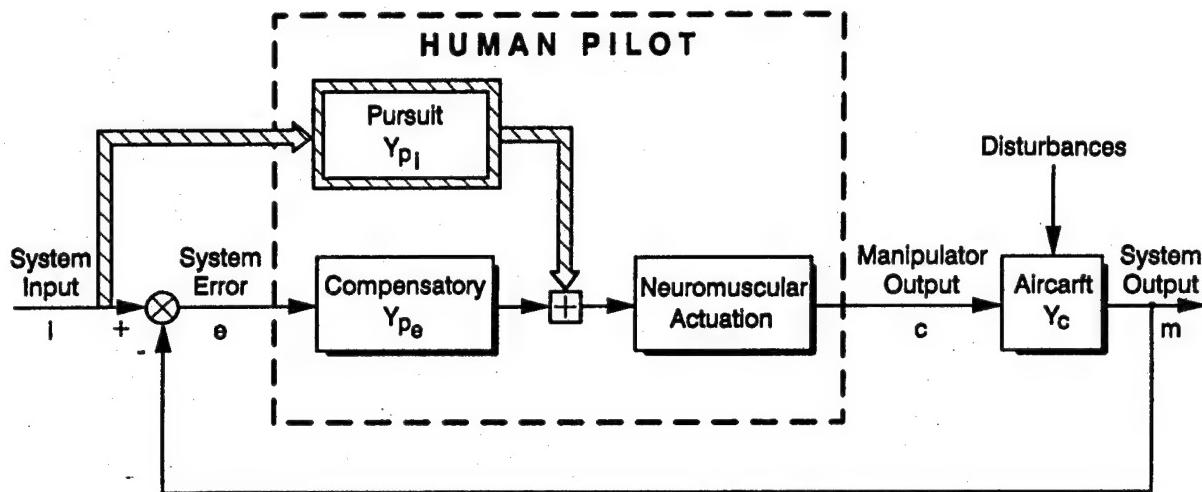
When the command inputs can be distinguished from the system outputs by virtue of a display (e.g., the system input and output are shown or detectable as separate entities relative to a reference) or by preview (e.g., a curved roadway that can be seen far ahead) a *pursuit* block can be added as shown in Figure 2. The introduction of this new signal pathway permits an open-loop control in conjunction with the compensatory closed-loop error correcting action. With the pursuit system organization the error can be reduced by the human's operations in two ways: by making the open-loop describing function large compared with 1; and by generating a pursuit path describing function that tends to be the inverse of the controlled element (Refs. 29 and 32). This can, of course, only be done over a limited range of frequencies. The quality of the overall control in the pursuit case can, in principle, be much superior to that where only compensatory operations are possible.

In many flight phases the pilot has sufficient cues to permit a pursuit system organization. Approach and landing with good runway visual cues and formation flying in clear weather are typical examples. Displays that provide good preview can also serve to support the superior performance available with pursuit organizational structures. When essential cues are lost (e.g., as with reduced effective preview), or are unattended (e.g., when appropriate division of attention and/or situational awareness breaks down), the pilot-vehicle system can change from a pursuit to a compensatory organization. Depending on the precise details, such transitions can introduce PIO triggering inputs as well as greatly reduced closed-loop system performance.

3. Precognitive Behavior

An even higher level of control is possible. When complete familiarity with the controlled element dynamics and the entire perceptual field is achieved, the highly-skilled human pilot can, under certain conditions, generate neuromuscular commands that are deft, discrete, properly timed, scaled and sequenced so as to result in machine outputs that are almost exactly as desired. These neuromuscular commands amount to conditioned responses that may be triggered by the situation and the command and control quantities, but they are not continuously dependent on these quantities (Refs. 25, 26, 29, 31, and 40). This pure open-loop programmed-control-like behavior is called *precognitive*. Most highly-skilled movements that have been so thoroughly locked-in as to be automatic (i.e., without thought) fall under this category. Like the pursuit pathway, it often appears in company with compensatory follow-up or simultaneous operations. This forms a dual-mode form of control in which the pilot's manual output is initially dominated by the precognitive action, which does most of the job, and is then completed when needed by compensatory error-reduction actions.

A special case of precognitive behavior is *Synchronous (Precognitive)* behavior. When sinusoidal inputs appear in pilot-vehicle systems the pilot progresses through several phases adapting to the input. Initially the periodic character is not recognized, and the pilot treats the input as unpredictable and operates off errors only (compensatory behavior). After intermediate adaptation phases (which can include pursuit behavior), the pilot ultimately recognizes that the input is a sinusoid and, up to frequencies of about 3 Hz, can duplicate the sinusoid with no phase lag (Ref. 29). If a transfer characteristic is assigned to this mode the pilot dynamics become $Y_p \approx K_p$. This would represent the pilot's ability to "follow" the sinusoid with no phase lag, although this is not a totally legitimate



TRANSFER CHARACTERISTICS	COMPENSATORY	PURSUIT
Open-Loop Output/Error, $m/e = Y_B$	$Y_{pe} Y_c$	$\frac{(Y_{pI} + Y_{pe}) Y_c}{1 - Y_{pI} Y_c}$
Closed-Loop Output/Input, m/I Error/Input, e/I	$\frac{Y_{pe} Y_c}{1 + Y_{pe} Y_c}$ $\frac{1}{1 + Y_{pe} Y_c}$	$\frac{(Y_{pI} + Y_{pe}) Y_c}{1 + Y_{pe} Y_c}$ $\frac{1 - Y_{pI} Y_c}{1 + Y_{pe} Y_c}$

Figure 2. Closed-Loop Pilot-Vehicle System Possibilities (Compensatory and Pursuit)

"transfer" characteristic. Instead, the pilot is generating the output sinusoid internally; indeed, the pilot's response can continue even if visual inputs are cut off, although there is a drift in frequency as time goes on. In the presence of sustained oscillation, however, the pilot's output does become phase-locked, so the pure gain model is appropriate. Synchronous operations can also occur in which the pilot's outputs are much closer to trapezoidal or even rectangular periodic waves than to sinusoids. In all of these cases the effective pilot describing function will still be a gain.

The stability of both pursuit and compensatory systems is governed by the dynamics of the compensatory elements, Y_p , Y_c .

4. Pilot Aberrant Behavior Characteristics

The above description of pilot behavioral patterns and characteristics suggests that many possible abnormal forms of pilot dynamic behavior can contribute to PIO. These include:

- Inappropriate behavioral organization;
- Inappropriate pilot adaptation within an established behavioral organization;
- Excessive pilot gain that may lead to a conventional compensatory system crossover PIO (2 to 5 Hz), a synchronous pilot PIO (0.5 to 3 Hz), or high frequency ratchet (2 to 3 Hz);
- Transitions in pilot behavior organization such as pursuit to compensatory, precognitive to compensatory, or switching of a key control variable (e.g., pitch attitude to normal acceleration); and
- Post-transition retention.

The first three sources are common in early flight operations with a new aircraft. To the extent that they are associated with pilot inexperience with a particular aircraft situation, they ordinarily disappear as the pilot adopts a more appropriate system organization and/or transfer characteristics. As some of the examples described next will make clear, they remain PIO possibilities for unusual situations in an otherwise very familiar aircraft.

The high-frequency ratchet has already been mentioned. The pilot's neuromuscular system resonance at 2 to 3 Hz may very well couple with higher frequency airplane modes due to flexible structures, mechanical control system dynamics, etc. Desirable stick and rudder inceptor (manipulator) characteristics and associated pilot-command input filtering that minimize such possibilities are underappreciated areas for fruitful research.

Transitions in pilot behavioral organization are probably major sources of pilot-induced upsets that can serve as PIO triggers. Pilot dynamics for pre-transition situations where the pilot is exerting full-attention, high-gain closed-loop control can be estimated using the procedures of Ref. 41. A switch from pursuit to compensatory operation can significantly reduce the available closed-loop system bandwidth, with a concomitant expansion of system error, etc. As an illustrative example, consider driving across a narrow bridge when suddenly presented with an on-coming truck. If the driver abandons a stare mode with a far-ahead fixation point (that permits the separate perception of roadway/bridge and car position and heading relative to the surround needed for pursuit operation) and changes to a closer-in perception of truck/car clearance, the driver will be shifting to compensatory behavior, with a corresponding increase in potential error. Much the same kind of system bandwidth and dynamic performance reduction occurs in carrier approach if the pilot starts to track or "spot" the deck.

The most common pilot behavior shifts involved with PIOs appear to be transitions from full-attention pursuit or compensatory operations in high-gain, high urgency tasks to a synchronous mode of behavior. This leads to significant simplifications for the analytic treatment of fully-developed synchronous PIOs because the pilot's dynamics approximate a pure gain and only the effective controlled element dynamic characteristics enter into the closed-loop situation. The transient nature of the transition itself is, unfortunately, not well understood. Major upsets or triggers, originating from either the pilot (e.g., in dropping a pursuit feedforward, changing attentional focus, etc.) or other system changes are almost invariably involved.

A very important pilot-centered characteristic is post-transition retention. If, for example, the controlled element dynamics change while the pilot is in a full-attention compensatory task, the pilot's characteristics will ultimately be modified as prescribed by the crossover model. But, the modification process has several sequential steps. Initially, with the pre-transition dynamics, Y_{cl} , the pilot's characteristics will be Y_{pl} , and the composite will approximate the crossover model. When the controlled-element transition occurs, the pilot retains the same characteristics adapted to the pre-transition effective vehicle dynamics. Then, at least momentarily, the system describing function is $Y_{pl}Y_{c2}$. If these are inappropriate to the "new" vehicle dynamics, the closed-loop system stability can suffer. The retention phase can last from one or two reaction times to many seconds. The vehicle dynamics transition may be a consequence of an internal shift, such as a change in the vehicle configuration (e.g., power or flap), stability augmenter system, etc. It can also stem from nonlinearities sensitive to pilot input amplitudes, such as rate and position limiting.

One pilot behavioral transition that has been proposed as a source of PIO is an attentional switching from attitude to normal acceleration as the primary control variable (Ref. 42). The hypothesis is that, in the presence of a nearly resonant pilot-vehicle closed-loop attitude system, plus a trigger of some sort, the pilot switches his primary control to normal acceleration. This theory has the undoubted merit that it demands the presence of good acceleration cues if a PIO is to appear. This could help "explain" the generally poor ability to predict PIO from fixed-base simulations. Analyses using the hypothesis have also been fruitful in showing PIO susceptibility.

C. PROPOSED PIO CATEGORIES

The detailed analytical studies (e.g., Refs. 1, 4 to 8, 42 and 43, etc.) of some of the "Famous PIOs," relied on pilot behavioral models and closed-loop analysis procedures to elicit understanding and rationalization of the phenomena and their associations. Then, in some cases, pilot-vehicle behavioral models were used as a basis for designing and assessing changes to the effective vehicle to alleviate the PIO potential. The categories in the classification scheme suggested here follow from the successes of this past experience. Thus, based on utilization of existing pilot behavior models and analysis techniques, the world of potentially severe PIOs is divided into the three categories described below.

- Category I -- Essentially Linear Pilot-Vehicle System Oscillations: The effective controlled element characteristics are essentially linear, and the pilot behavior is also quasi-linear and time-stationary. The oscillations are associated with high open-loop system gain. The pilot dynamic behavior mode may be pursuit, compensatory, or synchronous.

In this category no significant frequency-variant nonlinearities (see, e.g., Ref. 44) are involved in the controlled element dynamics (hence there is just one effective Y_c/K_c) and no behavioral mode shifts occur in the pilot (so Y_p/K_p is fixed). There may be changes in either the pilot or the controlled element gain, so such things as nonlinear stick sensitivity or pilot attention shifts that change K_c and K_p , respectively, may be admissible as features consistent with Category I. The pilot-vehicle oscillations in

this category may be casual, easily repeatable, readily eliminated by loosening control (lowering pilot gain), and generally non-threatening. With a major triggering input, however, the oscillations may be quite severe and catastrophic. More often than not, these situations involve aircraft configurations that are characterized by excessive lags. For a given pilot cue structure, analyses of Category I oscillation possibilities can reveal the oscillatory frequencies consistent with a presumed type of pilot behavior (e.g., compensatory or synchronous), pilot gain levels, nominal high-gain pilot-vehicle system bandwidths, various sensitivities to effective vehicle characteristics, etc.

- Category II -- Quasi-Linear Pilot-Vehicle System Oscillations with Series Rate or Position Limiting: These are severe PIOs, with oscillation amplitudes well into the range where software and/or actuator rate and/or position limiting in series with the pilot are present as primary nonlinearities. Rate limiting, either as a series element or as a rate-limited surface actuator, modifies the Category I situation by adding an amplitude-dependent lag and by setting the limit cycle magnitude. Other simple nonlinearities (e.g., stick command shaping, some aerodynamic characteristics, etc.) may also be present. These are the most common and easiest to analyze true limit-cycle severe PIOs.

Category II PIOs are very similar to those of Category I except for the dominance of key lag-introducing series nonlinearities. They are invariably severe PIOs, whereas Category I covers both small and large amplitude levels.

- Category III--Essentially Nonlinear Pilot-Vehicle System Oscillations with Transitions: These PIOs fundamentally depend on nonlinear transitions in either the effective controlled element dynamics, or in the pilot's behavioral dynamics. The shifts in controlled element dynamics may be associated with the size of the pilot's output, or may be due to internal changes in either control system or aerodynamic/propulsion configurations, mode changes, etc. Pilot transitions may be shifts in dynamic behavioral properties (e.g., from compensatory to synchronous), from modifications in cues (e.g., from attitude to load factor), or from behavioral adjustments to accommodate task modifications.

Category III PIOs can be much more complicated to analyze in that they intrinsically involve transitions in either the pilot or the effective controlled element dynamics. Thus there are a minimum of two sets of effective pilot-vehicle characteristics involved: pre- and post-transition. When these differ greatly, as in the T-38, YF-12, and YF-22 circumstances, very severe PIOs can occur.

Much of the flying qualities and PIO generic data base that can be associated with the reduction of PIO potential (Ref. 2) has dealt with the situations covered by Category I. Consequently, the presence of PIO tendencies in tight tracking tasks can be minimized by simply providing "good" flying qualities as defined by an appropriate selection of the entries available in MIL-STD-1797A (Ref. 45). In this sense, appropriate criteria to avoid Category I PIOs are generally tantamount to those for Level 1 flying qualities, with emphasis on those criteria of most importance in high-gain closed-loop piloting tasks.

A heightened emphasis on PIO has come to the fore as several modern aircraft (e.g., YF-22, C-17, B-2, and JAS 39) with advanced fly-by-wire (FBW) control systems have exhibited PIOs. The juxtaposition of PIO presence with new FBW systems has raised the visibility in much the same way as the shuttle ALT-5 earlier gained high-level attention. Some recommended refinements to MIL-STD-1797A that specifically emphasize the possibility of PIO have recently been put forth (Refs. 46 and 47). These are connected with excessive lag within the context of desirable pilot-vehicle system crossover characteristics. The initial steps taken propose to incorporate into the MIL-STD the "Smith-Geddes" PIO criteria based on Refs. 42, 48, and 49, as well as the "average phase rate," as suggested in Refs. 50

and 51. A version of the latter already appears in the handling qualities specification for the European Fighter Aircraft (Ref. 52). Other criteria, involving aircraft attitude bandwidth, phase-delay and dropback measures have been recommended in Ref. 2. When reduced to attitude control considerations, all of these are attempts to specify effective aircraft frequency domain characteristics over which the pilot can exert precise, high-gain control when needed, with great tolerance for variations in pilot gain (e.g., well-behaved effective aircraft amplitude ratio characteristics, approximating K/s, in which lags are not excessive). It should be noted that those Category I PIOs that are associated with higher-frequency non-rigid-body modes are not currently covered by the proposed criteria. More discussion of Category I criteria is presented in Section V.

Until recently, major PIO issues on new aircraft have usually been confined to factors that can be treated in Categories I and II; however, this may well be changing. The full application of active control technology in flight control systems for modern high performance aircraft invariably results in multiple-redundant, multi-mode, task-tailored, fly-by-wire (or light) systems. Great efforts are taken in design to put limits in the right places, to seamlessly transition from one set of effective aircraft characteristics to another, to foresee all possible contingencies. Unfortunately, with even the most modern and elaborate systems (e.g., YF-22) some upsetting condition within the flight control system itself or pilot behavior transitions within the pilot-vehicle system seem to creep through. In this event, a Category III PIO is a likely consequence when appropriate triggers also arise. Past history indicates that the Category III PIOs are highly unusual but can also be very severe events. The post-transition effective vehicle dynamics are almost always unforeseen, as are the triggering possibilities. This type of PIO is particularly insidious because, in the best modern FBW systems the pre-transition (normal) effective aircraft dynamics are designed to have excellent flying qualities. Most of the system nonlinearities (e.g., limits, fades, mode-switches, etc.) are deliberately introduced to counter anticipated events and problems. In all of these systems the lure of software "solutions" to all sorts of imagined problems has become easy to espouse; but unimagined events can remain submerged only to surface in an untimely way. Indeed, it is usually when the known-problem fixes act in peculiar, unanticipated ways in the presence of large pilot inputs that the "bad" post-transition vehicle dynamics are created. Avoidance of Category III PIOs is one of the great challenges of active control technology applications.

The categories suggested above do not differentiate as to PIO severity (i.e., large-amplitude severe PIOs can occur in all categories). They also have little if anything to say about the subjective and emotional aspects of a severe PIO. The pilot involved cares not at all whether his encounter was a Category I, II, or III! For the analyst, on the other hand, such details are essential to permit the use of available tools and analysis techniques discussed in this report to develop understanding of the event and determine corrective action.

III. PIO THEORY

A. DEFINITIONS

In order to develop a unified theory for pilot-induced oscillations, there must first be some consensus toward an appropriate term and definition. As the name implies, pilot-induced oscillations involve the pilot's active participation in a feedback system. Although the pilot is an active participant in a PIO, the event itself is a "joint enterprise" involving the aircraft as well. As such, the true causes of the PIO may well be, and often are, embedded in the design and operation of the aircraft and its flight control system. In this sense, there may be a set of pre-disposing conditions inadvertently present in the inanimate portions of the system that interact unfavorably with quite normal actions of the pilot to create the PIO. It is important to make such distinctions because, in a climate where accidents and incidents have prescribed causes, the "fault" is often wrongly ascribed to the pilot (after all, the event is a *pilot-induced oscillation*). This usually turns out to be counterproductive because untoward actions of the pilot are seldom the cause of a severe PIO. To alleviate any potential blame placed on the pilot, several new terms have been proposed that tend to de-emphasize the pilot's role as a solitary contributor. These new terms include *Aircraft-Pilot Coupling*, *Pilot-in-the-Loop Oscillations* and *Pilot-Assisted (or Augmented) Oscillations*. Despite good intentions, these new terms seem to only spark additional controversies. Thus because of the weight of history and widespread acceptance in both the pilot and handling qualities communities, it is recommended that the term Pilot-Induced Oscillation or PIO be retained.

The heart of the definition issue revolves around the magnitude and duration of the oscillation. MIL-STD-1797A (Ref. 45) contains the following definition:

Pilot-induced oscillations are sustained or uncontrollable oscillations resulting from efforts of the pilot to control the aircraft.

Although the complexities surrounding PIOS are concealed in the above definition, it does provide a concise statement of the cause (i.e., closed-loop piloted control of an aircraft) and effect (i.e., sustained or uncontrollable oscillations). It should be emphasized again that even though closed-loop piloted control is a necessary cause, there is still no blame placed on the pilot for the resulting oscillations. The following discussion exposes many of the hidden complexities that directly led to the development of the proposed PIO Categories.

1. Minor Bobbles and Severe PIOS

The pilot's dynamic behavior is conditioned by the dynamic behavior of the "effective airplane" with which he interacts. The "effective airplane" dynamics comprise aircraft rigid body and lower frequency flexible modes, manipulator(s) and manipulator restraints, actuation, stability and control augmentation, and "effective display" characteristics. When this combination is consolidated into a single dynamic entity (i.e., controlled element) that is characterized by the describing function $Y_c(j\omega)$, the presence of an oscillation demands that,

$$Y_p(j\omega)Y_c(j\omega) = -1 \quad (3)$$

where $Y_p(j\omega)$ is the describing function of the pilot. While this is a necessary and sufficient condition for an oscillation, it is *not* the *only* condition for the oscillation to be a serious PIO. Instead, the oscillation may be a very temporary, easily corrected, small amplitude "bobble" that is often encountered by pilots when getting used to a new configuration. This is basically a learning experience. It can happen on every airplane, and has undoubtedly been experienced by every pilot at one time or another. Other bobbles often result from lightly damped modes in the effective airplane. These cases, however, rarely

satisfy the Eqn. 3 condition, and so overall system stability is not at issue. A fully-developed, large amplitude oscillation with near or actual catastrophic consequences, on the other hand, is a chilling and terrifying event. This kind of oscillation must be avoided for reasons of safety and operational performance. This effort has, therefore, been concerned primarily with the identification and prevention of large amplitude, potentially catastrophic oscillations, referred to here as severe PIOs. The presence of seemingly moderate oscillations and bobbles must also be carefully examined, however, to reveal any severe PIO potential.

For severe PIOs both pilot and controlled element properties are important in Eqn. 3. In the simplest cases where the pilot-aircraft coupling acts as a predominantly single-loop system, Eqn. 3 creates a useful duality in that either the pilot or the effective vehicle dynamics can be used to quantify matters. It is generally easier to quantify the effective airplane dynamics (Y_c) than the pilot's behavior (Y_p). Further, these dynamics are adjustable by control engineering means and aircraft configuration modifications, and, therefore, it would be convenient to emphasize the well-defined and known effective airplane dynamics in considering criteria and procedures. But there are problems even at this very basic level, that is, what particular Y_c is the important entity in a given PIO? For example, in a longitudinal axis PIO, is Y_c the transfer characteristic relating pilot output to attitude, to normal acceleration at the pilot's location, to some variable on a display, or ...what? Also, what is the pilot's output (input to Y_c); is it force, position, or a composite? Just how much of the limb-neuromuscular-manipulator subsystem is involved?

While PIOs often start with fairly low amplitudes, consistent with small perturbation linear theory, severe ones can become very large. In addition, almost all of the severe PIO time history records available for operational and flight test aircraft (see Appendix A) show surface rate limiting and sometimes stick or surface position limiting as well in the fully developed oscillation. Rate limiting has two major effects: (1) adding to the effective lag in series with the pilot, making the effective aircraft dynamics worse; and (2) limiting of the ultimate amplitude of pilot-vehicle system oscillation that is perhaps a lifesaver. Other particularly insidious nonlinearities are those leading to a sudden change in effective aircraft dynamics in the midst of a high-gain urgent task. Examples of these sudden "transitions" include changes in effective vehicle dynamics due to sudden configuration modifications (e.g., afterburner light-off, engine unstart in hypersonic aircraft, stability augmenter mode changer or failure, asymmetric stores release, etc.). These transitions also include changes driven by pilot output-amplitude shifts from small (e.g., stick motions around trim within a control system hysteresis band) to large (e.g., pilot attempts to counter perceived major upsets). Such cases range from ancient PIOs, where the primary manual control system appeared in several guises (e.g., bobweight-in/bobweight-out in the T-38, see Ref. 4), to many of the most modern PIOs where factors such as actuator rate limiting, surface and SAS position limits, nonlinear stick shaping of pilot commands, and mode transition faders interact to create a confounding variety of input-amplitude-sensitive effective vehicle dynamics. Clearly, attention must be paid both to the linear and nonlinear features of the effective airplane in any adequate PIO theory and data base.

2. *Elements of a Severe PIO*

Several source elements enter into any severe PIO. They can be usefully organized under three headings:

- Effective Aircraft Dynamic Characteristics;
- Pilot Behavior Characteristics; and
- Trigger Mechanisms.

Effective aircraft dynamic characteristics were touched on above; the remaining two characteristics are further introduced below.

Pilot behavior is the source-factor that distinguishes the severe PIO problem from most aircraft flight control-related design problems. The differences reside in those uniquely human properties related to the enormously adaptive characteristics of the human pilot for which there are no parallels in an automatic flight control system. Reference 1 and its shorter recap given in Section II of this report describe the multiplicity of pilot behavior patterns that can conceivably be involved in PIOs. These can, for simplicity, be reduced to two major principles. First, different pilot behavior patterns are associated with different types of PIO (e.g., compensatory behavior and low-frequency neuromuscular dynamics with PIOs in the 0.3 - 0.7 Hz range, synchronous dynamics with PIOs in the 1-3 Hz range and with flexible mode interactions, more complete limb/neuromuscular/manipulator dynamics with PIOs in the 1-3 Hz range, etc.). Second, pilots exhibit peculiar transitions in the organizational structure of the pilot-vehicle system. These transitions can involve both the pilot's compensation (e.g., when a pilot adapted to high-gain compensatory tracking/regulation suddenly shifts to a synchronous pure gain mode) and the effective architecture of his control strategy (i.e., what variables the pilot senses and processes).

"Triggers" are initiating events or upsets that start the PIO sequence. Their great variety renders them difficult to generalize. A few examples for PIOs cited in Table 1 are:

- T-38 – Failed stability augmenter; disconnect sequence created a major upset (see Ref. 4);
- YF-16 – Several undesired inputs coupled with limiting effects (see Ref. 6);
- Shuttle ALT-5 – 30 mph over-speed on very first runway approach; speed brake actuated, nosed down to make desired impact point; pilot plus transient upset basic approach;
- F-8 DFBW – Major unexpected change in effective controlled element dynamics (see Ref. 1);
- YF-22 –Landing gear retraction, pilot input, plus mode transition circuitry interacted to create a major upset; and
- MD-11 – Inadvertent slat extension.

Flying qualities researchers often regard the elimination of the trigger aspect of PIOs as a deceptive goal. The impression is that there are so many and such varied triggers as to make their elimination impossible. This is almost surely true; but efforts intended to minimize trigger/precursors as much as possible are not only well intended but are sure to be beneficial. Indeed, when confronted with a severe PIO the usual classical engineering approach is to consider each PIO a unique case, find out what caused it, and eliminate the "cause." While one might wish that adequate predictive criteria and assessment procedures will indeed result in a new generation of aircraft that are invulnerable to PIO tendencies, this remains a consummation devoutly to be wished. There is no question that future PIOs will be handled in the same old ad hoc fashion. So, one approach to prevention is to search out and then eliminate trigger possibilities.

As emphasized in the previous discussion of pilot behavioral modes, triggering upsets can also arise from shifts in the pilot's organization of behavior. These include changes in the pilot's goals, attention, and neuromuscular tension that reflect into higher pilot gains, controller offsets, or control reversals. A major source of upsets is the surrounding external and internal environment. The latter category includes gusts, wind shears, etc. as well as control system shifts acting on the airplane. It also includes changes that enter the pilot-vehicle system via the pilot, such as drastic evasive maneuvers.

As already noted, great efforts are taken in modern multiple redundant fly-by-wire aircraft to seamlessly transition from one set of aircraft characteristics to another. Unfortunately, with even the most modern and elaborate systems (e.g., the YF-22) some upsetting condition within the flight control system itself, or pilot behavior transitions within the pilot-vehicle system seem to creep through. Possible software "solutions" to all sorts of imagined and projected "problems" may still leave unimagined events submerged only to surface in an untimely way. Upsets can also arise from the surrounding environment (i.e., gusts and wind shears).

3. Proposed PIO Categories

To facilitate a clearer understanding of PIOs through a systematic study of the various influencing factors, the PIOs themselves must be categorized to identify and isolate the key elements. This essentially breaks down a large and complex problem into smaller, more manageable areas. PIOs can range from mild to severe as characterized by the PIOs identified in Table 1. They can also involve varied pilot behavioral models and require differing analysis procedures. This suggests that PIOs can usefully be classified in categories that are based on existing pilot behavior models and analysis techniques. The result is the proposed categories that were discussed in Section I and introduced in Ref. 1. These categories are summarized below.

- Category I – Essentially Linear Pilot-Vehicle System Oscillations;
- Category II – Quasi-Linear Pilot-Vehicle System Oscillations with Series Rate or Position Limiting; and
- Category III – Essentially Nonlinear Pilot-Vehicle System Oscillations with Transitions.

4. Are PIO Categories Really Needed?

As described in Ref. 1 the PIO Categories were proposed as a pilot-behavioral-analysis based classification scheme. In other words, they are useful in developing an *understanding* of specific PIOs. A legitimate question at this stage is to ask whether the complications introduced by distinguishing between various categories are really needed if the focus is solely on the elimination of PIOs. For instance, in those PIOs where Category III circumstances prevailed (and were needed to *understand* the specific phenomenon), did the effective aircraft dynamics meet various Category I specification requirements in the pre-transition state? There are not, as yet, many Category III PIOs for which the data and documentation are sufficient to answer such a question, but there are some pertinent cases. The best well-understood example of a severe Category III PIO is the YF-12 severe PIO. Here consideration of the pilot-amplitude-sensitive transitional properties of the effective vehicle dynamics was essential to understanding, and the describing functions needed to elicit this understanding were very complex. Further, the effective aircraft dynamics, as discussed in Section IV, prior to degradation by virtue of effective vehicle transitions due to large pilot input-amplitudes, were consistent with good values of key flying qualities parameters and Category I PIO-indicators. For instance, the effective-aircraft attitude bandwidth, phase delay, and average phase rate were all well within proposed guidelines, as were metrics associated with a Smith-Geddes Type III attitude PIO (Ref. 49). The YF-22 and some elements of the F-8 DFBW PIOs are also examples of Category III PIOs, but the F-8 DFBW (and perhaps the YF-22) does not have good pre-transition dynamic characteristics.

5. Distinctions Between Categories II and III

In order to avoid any conceptual confusion, the distinction between Category II and Category III PIOs should be explained. In aircraft with a conventional manual primary control system rate limiting

- stems from the surface actuation system. The effect is to put pilot-amplitude-dependent effective lags and amplitude-ratio changes in series with the pilot and aircraft. This converts the effective aircraft dynamics as seen by the pilot into an amplitude-dependent set of dynamic characteristics that still qualify as quasi-stationary. In this sense it is an extended "amplitude-dependent" case of Category I that is special in that fully-developed PIOs can be fairly easily analyzed and understood with simple sinusoidal describing functions. For this reason, and because it is also very commonly encountered, it has been distinguished from Categories I and III. As stability augmentation systems became more complex additional nonlinearities were introduced that no longer were as easily treated with relatively simple describing functions. With fly-by-wire and more extensive application of the principles of active control technology, the potential for a wide variety of effective controlled element amplitude-dependent changes potentially increase enormously. The number of deliberately introduced modes, and mode shifts, may also increase. There is a need, therefore, for a further distinction to cover PIOs that are governed by these more extensive effective transitions in the effective vehicle dynamics. Thus Category III was defined to cover all the more complex cases. Category II is then an intermediate between I and III, being a special "amplitude-dependent" extended case of Category I, as well as being one of the simplest examples of Category III.

B. FACTORS CONTRIBUTING TO CATEGORY I PIOs

1. *Excessive Lags in the Effective Vehicle*

For modern aircraft equipped with stability augmentation that corrects unfavorable aircraft dynamics, the low-frequency effect of higher-frequency lags from assorted sources is by far the most important causal factor in those Category I PIOs that can be "explained" by quasi-linear theory. The assorted sources of excessive lag include actuators, filters, digital system time delays, mechanical control and feel system, structural characteristics, etc. Here "low frequency" refers to the region from pilot-vehicle system crossover (ω_c) to the instability frequency (ω_u) whereas "higher-frequency" refers to those above ω_u .

To better appreciate the qualitative and quantitative aspects of PIOs due to excessive lags they must be considered in the larger context of closed-loop pilot-aircraft interactions in general. These interactions, whether favorable or unfavorable, are part of the flying qualities domain. An aircraft that exhibits a high degree of PIO susceptibility clearly has very poor flying qualities. Starting at the other extreme, the most fundamental attribute of effective airplane dynamics that possess excellent flying qualities is tolerance to adjustments in pilot dynamic characteristics in demanding, high-urgency, closed-loop flying tasks. In the explicit statements of the Cooper-Harper rating scale (Ref. 53) describing Level 1 flying qualities,

"Pilot compensation is not a factor for desired performance" (HQRs of 1 and 2), and
"Minimal pilot compensation required for desired performance" (HQR of 3).

Although there are a variety of detailed pilot-vehicle system factors involved in pilot rating (e.g., Ref. 54), the "Tolerance to Pilot Compensation Variations" is of such central and overriding importance that it can be taken as the governing and guiding principle in considering both favorable and unfavorable (e.g., PIOs) pilot-vehicle interactions or coupling.

For closed-loop full-attention operations the ideal controlled-element dynamics are $Y_c = K_c/s$. This form requires no pilot lead or lag equalization for compensatory operations (the crossover model is "made good" with pilot dynamics that approximate $Y_p = K_p e^{-\tau_h s}$). Further, it supports a range of pilot gains from zero to an octave or so below ω_u with only minor changes in the basic dynamic form of the closed-loop system. The attainable closed-loop system bandwidth and time response performance is, in

fact, limited only by the pilot's effective lag, τ_h . In terms of the pilot-vehicle system output/input properties for low and moderate open-loop gains the dominant closed-loop mode will be approximately:

$$\frac{M(s)}{I(s)} = \frac{1}{(s/\omega_c + 1)}, \quad \omega_c = K_p K_c \quad (4)$$

For this ideal controlled element the pilot has maximum latitude to vary gain, K_p (and thus ω_c), to adjust the closed-loop system response and accuracy as needed to meet varied demands while not materially changing the form of the closed-loop system dynamics. As the pilot attention level, task urgency, or aggressiveness calls for gain modification, the crossover frequency, ω_c , will increase or decrease proportionally, and the dominant closed-loop system time constant, $1/\omega_c$, will wax and wane in corresponding fashion. Thus, there is a very wide range of closed-loop system response properties available that are affected in direct proportion to pilot effort.

Consider as the other extreme a set of effective aircraft dynamics characteristics in the region of pilot-vehicle system crossover that requires a great deal of pilot lead as well as exquisitely precise adjustment of the pilot's equalization and gain to approximate the crossover law and to close the loop in a stable manner. The pilot may be able to exert adequate closed-loop control, but the dynamic quality and even the closed-loop system stability require that the pilot's describing function, Y_p , be precisely tuned to offset the controlled element deficiencies in the crossover region. In the language of the Cooper-Harper Scale, the pilot's compensation in this case can range from "extensive" (HQR of 6) if adequate performance can be attained at all, to "considerable" (HQR of 8) or "intense" (HQR of 9) if retention of control itself is the only issue.

PIO potential fits very nicely into this framework. Clearly the ideal K_c/s vehicle dynamics (with the aircraft gain, K_c , set at an optimum value) is very forgiving and has very low PIO potential, whereas the other example will have a high PIO potential in urgent, high-gain tasks.

2. Mismatched Pilot-Aircraft Interface

It has been well-known for many years that the pilot gain required to accomplish precision high-gain tracking-like tasks is a predominant factor underlying the pilot's assessment of the flying qualities of a particular aircraft configuration (e.g., Ref. 27). If the controlled element gain is varied in such full-attention, high-gain tasks, the crossover frequency of the open-loop pilot-aircraft system is maintained essentially constant by a counteracting self-adjustment of the pilot's gain. The "cost" of such an adjustment is reflected in the pilot rating. Figure 3, from Ref. 27, illustrates the general nature of this relationship for effective vehicle dynamics that approximate an ideal rate control form. Since the approximate transfer characteristic is $Y_c = K_c/s$, other vehicle-dynamics aspects are irrelevant.

Several general observations can be made about the trends of Figure 3. First, there is an optimum controlled element gain for each case. These optima are used as normalizing factors to coalesce the data from the several sources. Second, the optima lie in rather broad regions in which a change of plus or minus 50 percent in controlled element gain, K_c , incurs a penalty of no more than one rating point. This implies that, once the effective vehicle sensitivity is properly adjusted, minor controlled element changes are easily accommodated by the pilot, and are not major factors in pilot rating. Third, outside the broad optimum region, there are major decrements in handling qualities rating associated with either too-sluggish (i.e., K_c too small and pilot gain, K_p , too large) or too-sensitive (i.e., K_c too large and pilot gain, K_p , too small). Either extreme can be connected with a PIO tendency.

The determination of the optimum controlled element gain is clearly a matter of supreme importance to assure a favorable pilot-aircraft interface, effective pilot-vehicle interactions, and an absence of PIO tendencies. With conventional center sticks, pedals, and yokes decades of past practice

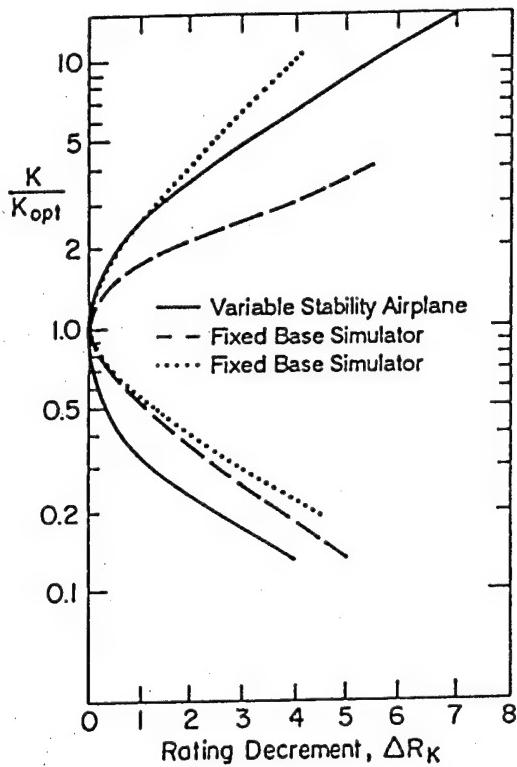


Figure 3. Pilot Ratings vs. Controlled Element Gain (Ref. 27)

provide traditional answers. With the introduction of full-authority stability augmentation and fly-by-wire systems the stick "inceptor" has permitted the introduction of many other options. These range from side versus center cockpit locations, force-alone versus various degrees of motion, etc. Also, the inceptors have become "subsystems" by incorporating sensors and frequency and nonlinear amplitude shaping circuits. Further, the harmonization of within- and between-axis characteristics of cockpit inceptors that share functions, such as the conventional stick as a lateral and longitudinal controller, has new dimensions. Consequently, the proper setting of controlled element gain has become a nontrivial development aspect on every new aircraft that introduces a new inceptor at the pilot-control-system interface. In the absence of an extensive background of data for these there is no basis other than experiment to determine the optimum gains. The pathway to ultimate success has often had many byways, with minor wiggles, bobbles, and ratchets, as well as occasional severe PIOs.

The detailed issues that must be examined for a new inceptor are many and varied. Major questions with a side stick, for instance, include control sensitivity and PIO susceptibility in precision maneuvering, roll (or pitch) ratchet or jerkiness in otherwise steady maneuvers, sensitivity to pilot gripping techniques and arm/hand support characteristics, effective time delay and amplitude and frequency shaping of stick filters, biodynamic interactions, minimum and total motions/forces, etc.

In the course of preparing for the flight of new aircraft, fixed- and, sometimes, moving- base simulations are used to determine initial gains, that are then refined in flight tests. Unfortunately, experience has shown that fixed-base, and even in-flight simulations, have not been generally reliable predictions of the best controlled element gains. Even with conventional inceptors, attempts to set appropriate sensitivities in fixed-base simulators are seldom fruitful. As noted in Ref. 55, "Pilots (particularly fighter pilots) always want a very responsive airplane; however, when real-world motion and visual cues are experienced their opinion frequently is revised..." Typically, the fixed-base simulator

values are too large. For newer inceptors such as side sticks, the simulations are also usually inadequate to address all the major questions listed above. For instance, considering pitch axis control alone without any biodynamic considerations, amplitude nonlinearities found acceptable or even desirable in simulations are often not appropriate in flight, sometimes becoming a factor in PIOs. Further, cross-axis harmonization demands a flight venue even to achieve, much less to validate, satisfactory results. Thus, in the modern era where a wide variety of novel controller inceptors and multiple aircraft control effectors are being considered, flight-based developments are an essential aspect of what previously was a detailed design feature. These developments, however, may not always be simple and straightforward. The adjustments required have generally involved complex ad hoc empirical modifications that must be acceptable to a reasonable cross-section of pilots. For example, Ref. 56 summarizes some aspects of the F-16 side stick controller/roll prefilter development that included a 155 flight, 34 pilot program evaluating 19 different side stick and prefilter configurations in the YF and F-16A aircraft. Of the 155 flights, 74 were devoted to stick displacement, force gradient, and input axis orientation considerations, while 81 considered various roll pre-filter configurations.

The determination of optimum effective aircraft gains, pilot controller gain and frequency shapings, etc. are not the only features that are difficult to evolve reliably in ground-based simulators. Comprehensive simulation studies to gain understanding and detailed examinations of specific aircraft have, as yet, been insufficiently representative of the flight environment to be reliable quantitative predictors of PIO tendencies. Even variable stability aircraft results can be ambiguous because the relationships between acceleration at the pilot's station and attitude are configuration- and speed-specific. A proper match may require that the variable stability aircraft have high authority, high bandwidth force as well as moment producers. Only the USAF Total In-Flight Simulator (TIFS) aircraft is currently in this class for relatively low speeds, and there is nothing available for high speed flight.

C. FACTORS CONTRIBUTING TO CATEGORY II PIOs

I. *Series Rate and Position Limiting*

As shown in Figure 4 rate and position limits are often found throughout a flight control system. The following discussion elaborates on the forward path limit sources that are in series with the linear control system elements. Limits in the feedback path are more complex nonlinear cases that fall into Category III.

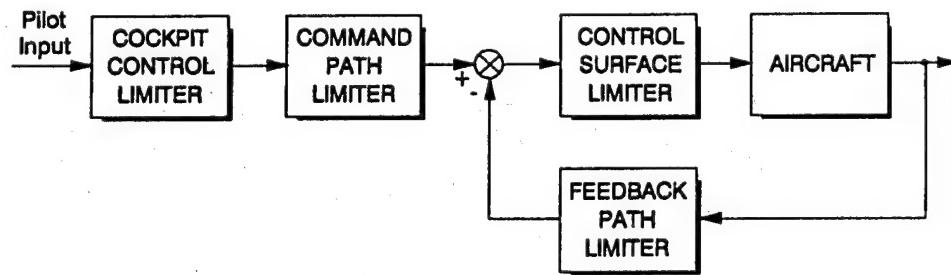


Figure 4. Possible Flight Control System Locations of Rate and Position Limits

Cockpit Control: In the classical case the position limit of the cockpit control (e.g., pitch stick) is reached as the corresponding limit of the control surface (e.g., elevator) is reached. This ensures that maximum maneuvering capability is accessible. Rate limiters are not usually found on fixed-wing aircraft cockpit controls, although they are found on some helicopters. Some designs do incorporate stick dampers that act as an effective limiter. Stick limiters are also being considered as a method to alleviate PIO, though this may come at the price of reduced flying qualities and maneuverability.

Recent fly-by-wire aircraft (i.e., B777) have back-driven cockpit controls that provide enhanced cues to the pilot. These cues include increased stick force near stall and beyond bank angles of 30°. This technology could also be employed as a potential PIO alleviation scheme by providing an actuator valve 'bottoming cue' that signals the onset of actuator rate limiting to the pilot through the back-driven manipulator.

Command Path: Command path limiters define maximum command signals relative to feedback signals. Thus they establish the priority between command and stabilization which protects against degrading effective aircraft dynamics. A specific intent of command path rate limiters is to prevent the pilot from saturating the actuator. If saturation of the command path limiter occurs, however, it will still appear to be surface rate saturation to the pilot. Command path rate limiters are also used to set maximum rolling velocity in order to minimize inertial coupling effects.

Control Surface: Rate and position limits of surfaces are fundamental constraints in the design process. Reaching control surface rate limits is never desirable since this is directly related to Category II PIOs. Constraints on surface rates, however, are essential in sizing hydraulic or electric actuators. Surface position limits, on the other hand, are determined by control power needs (e.g., rotation nose wheel liftoff, maximum lift, time to roll, sideslip constraints, etc.) in the overall surface sizing process. Specific issues related to actuator rate limiting are discussed in the following section.

2. Effector Rate Limiting

A block diagram of a simplified rate limited actuator model is presented in Figure 5. As shown in the figure the input surface command (δ_c) produces an output surface deflection (δ). The output deflection is fed back to the command to produce an error signal, $e = \delta_c - \delta$. In the forward path the error signal serves as the input to the nonlinear saturation block. The saturation block is characterized by two design parameters: 1) a gain equivalent to the linear actuator closed-loop bandwidth or more simply referred to as the linear bandwidth (ω_a) and 2) a saturation value equivalent to the actuator rate limit (V_L). From Figure 5 it is clear that the saturation point (e_L) can be defined in terms of these design parameters by $e_L = V_L/\omega_a$. The output from the saturation block is the surface rate ($\dot{\delta}$). This signal is then integrated to produce the surface deflection (δ).

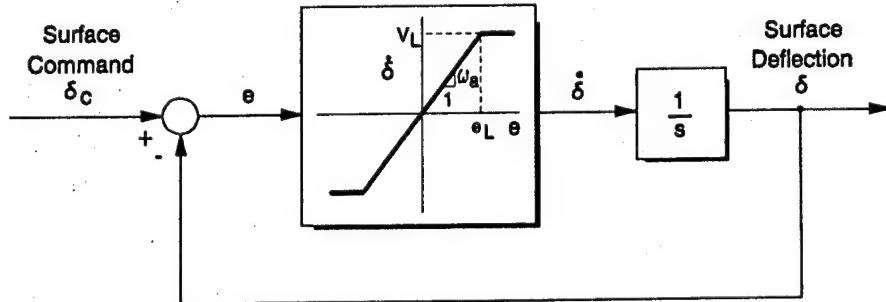


Figure 5. Closed-Loop Surface Actuator System

The model has three distinct operating ranges. First, when $e < e_L$, the model is linear with a closed-loop response characterized by a simple first order lag with a time constant, $T = 1/\omega_a$. These first order features are exemplified in the Bode plot and step time response of Figure 6. Here everything is characterized by the time constant. Interpreted in the frequency domain, T is the inverse of the linear bandwidth (i.e., the frequency at which the output/input is down 3 dB from the value at zero frequency) as shown in Figure 6a. In the time domain the indicial response is governed completely by the time constant, e.g., the Figure 6b exponential response exhibits a series of subtangents that again reflect T . The time constant also corresponds to a "system rise time" of the indicial response that is determined by the time to reach the maximum (final) surface displacement at the maximum output velocity. One or more of these characteristics is fundamentally changed when the input amplitude exceeds the linear region.

The second operating range is the near saturation range that occurs when the maximum error exceeds e_L by a small amount. This region is characterized by a quasi-linear response that is only intermittently rate limited. Thus, the nonlinear amplitude effects in this region are imperceptible to the pilot.

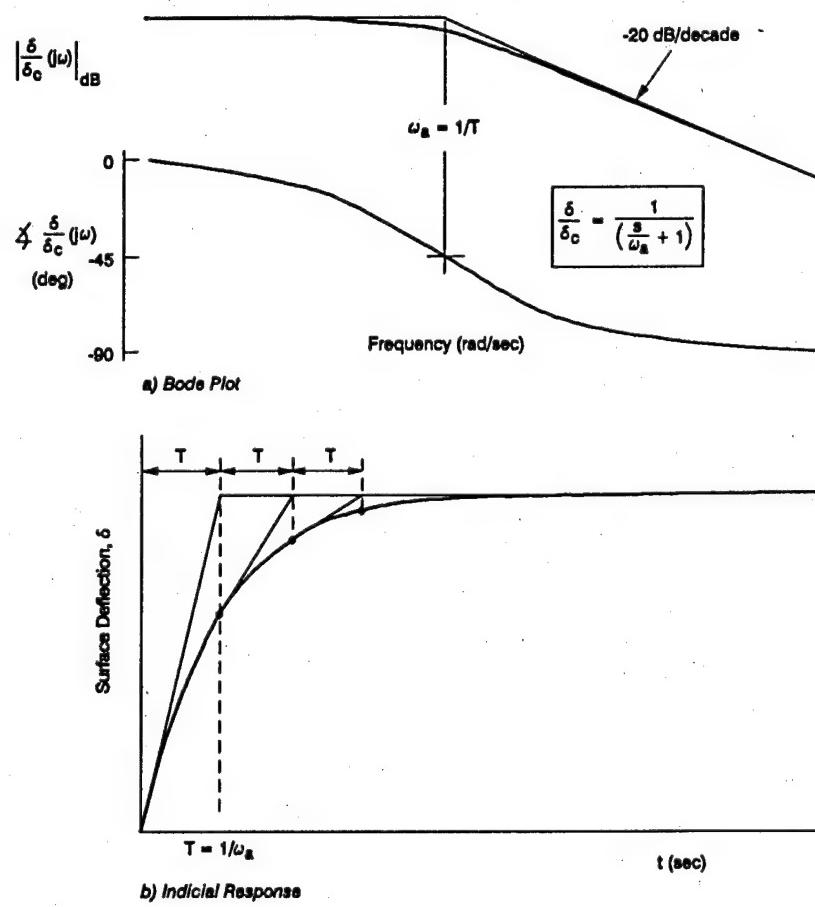


Figure 6. Example Linear Closed-Loop Surface Actuator Response to Command

The third operating range is fully nonlinear and is characterized by an output rate that equals the actuator rate limit, $\dot{\delta} = V_L$, for most of the time. In this highly saturated region the presence of the nonlinearity makes both the frequency and time responses amplitude dependent. For the indicial response, the system rise time (T_{NL}) will be the magnitude of the step input divided by the velocity limit as shown in Figure 7. This defines a step input describing function for the highly saturated case that can be applied to the initial large amplitude inputs that often precede a fully developed PIO. For sinusoidal inputs with amplitudes that are large enough to keep the system velocity at limit values most of the time, the limiter approaches a bang-bang characteristic. As illustrated later, this type of closed-loop system can be characterized by describing functions that can be expressed in simple analytical terms. The bang-bang idealization is a very useful limiting case that is valid when the linear bandwidth is very large when contrasted to the effective bandwidth of the nonlinear system. This "rise time" is completely independent from that for the linear system. Thus, for this fully nonlinear case, the closed-loop frequency and time response characteristics are totally defined by the rate limit and the input amplitude, *independent of the linear system time constant.*

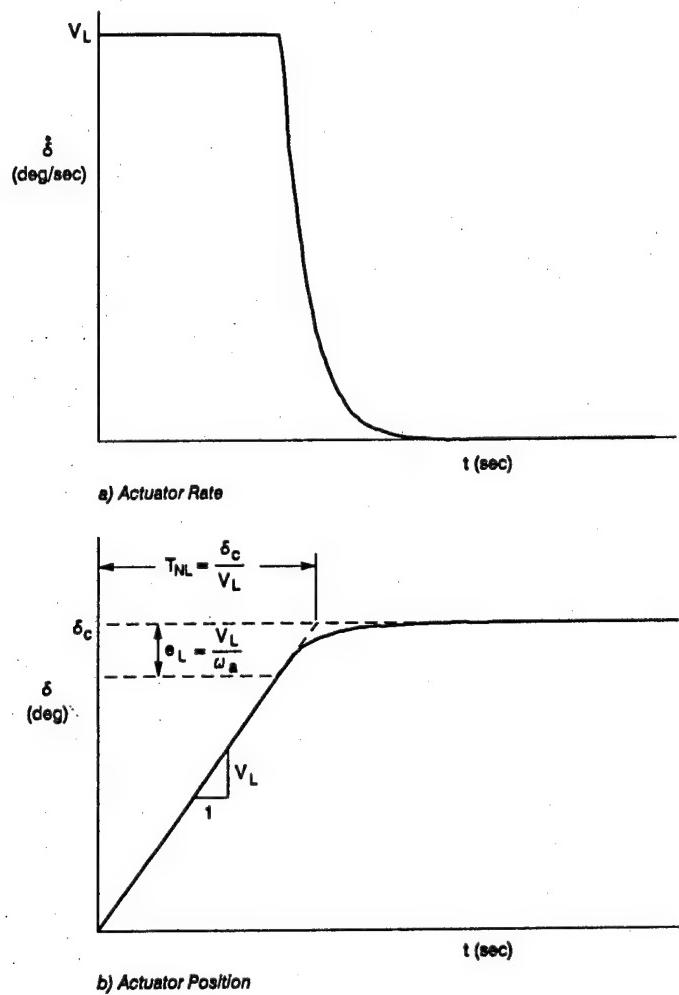


Figure 7. Example Nonlinear Closed-Loop Surface Actuator Response to a δ_c Step

In the transition near saturation regime between the essentially linear and the essentially nonlinear, the system responses will depend on the linear time constant, the velocity limit, and the input amplitude. Although this situation defies a straightforward analytical treatment, the quasi-linear nature of the system response permits the use of nonlinear computer simulation models to generate time responses and with some effort (i.e., FFT techniques applied to the output time histories) corresponding frequency responses.

MatlabTM/SimulinkTM was used to develop a computer simulation of the closed-loop actuator model defined in Figure 5. To implement the Figure 5 system, the input (δ_c) was assumed to be sinusoidal, $\delta_c = A\sin(\omega_i t + \phi_i)$. The many time traces given in Appendix A support this assumption for PIO cases. To exercise the model, nominal values for the design parameters (ω_a and V_L) and the input parameters (A , ω_i and ϕ_i) were first defined. By varying these five parameters systematically, a series of model time responses was obtained.

The following discussion provides three example cases that span the ranges of interest (i.e., linear, near saturation, and highly saturated). For all of these cases the design parameters ω_a and V_L were held constant at 20 rad/sec and 40 deg/sec, respectively. The input sine wave frequency (ω_i) was held constant at 5 rad/sec. Thus the input magnitude of δ_c was varied to obtain responses within the three desired range categories. When the design parameters are held constant at these values the system will not saturate until $e = 2$ deg. It should also be noted that for all cases reported here, the input sine wave phase angle (ϕ_i) was set to zero.

a. Linear Range

Figure 8a presents the closed-loop actuator model time responses for a linear range case with an input magnitude of 5 deg. As shown in the figure the error signal remains below the 2 deg saturation point at all times. The linearity of the response is further exemplified by an actuator rate that is at all times well below the 40 deg/sec rate limit. In Figure 8b the output actuator position is compared to the input command. The noticeable lag in the output response results from the first order closed-loop time constant as previously identified in Figure 6. The phase lag due to the effective first-order time constant is $\tan^{-1}(T\omega)$. For the conditions illustrated this phase lag is well-approximated by the argument. Thus, for input frequencies much less than the bandwidth the output response is shifted from the input by T seconds as indicated in Figure 8b.

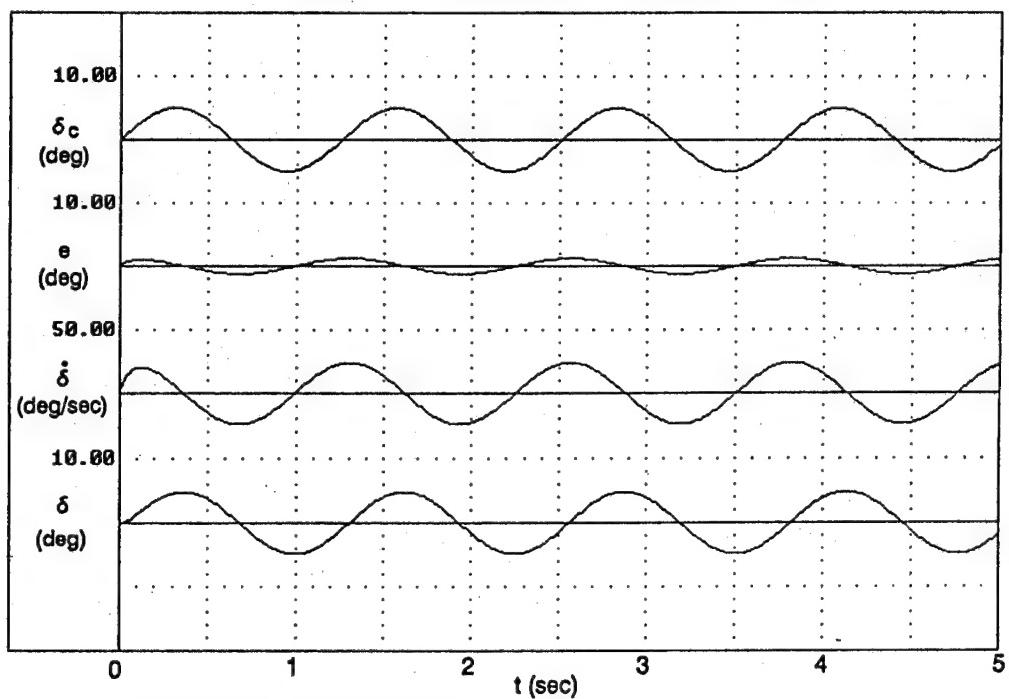
b. Near Saturation

Figure 8c presents the closed-loop actuator model time responses for a near saturation case with an input magnitude of 9 deg. As shown in the figure the error signal intermittently exceeds the 2 deg saturation point. These excursions into the nonlinear range are more evident in the actuator rate response that becomes clipped at the 40 deg/sec rate limit. In Figure 8d the output actuator position is compared to the input command. The figure displays an output position response that remains effectively linear even though the saturation point has been clearly exceeded. The nearly linear nature of the output actuator position is further exemplified by a phase lag that remains consistent with the linear time constant (i.e., $\Delta\phi \approx \omega T$).

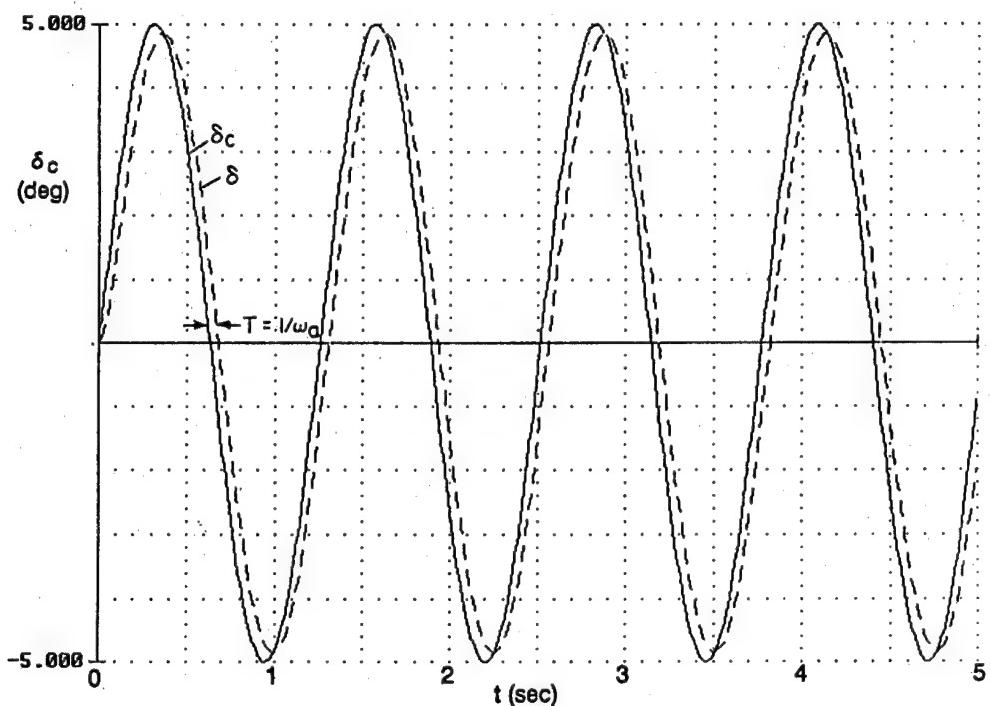
c. Highly Saturated

Figure 8e presents the closed-loop actuator model time responses for a saturation case with an input magnitude of 15 deg. As shown in the figure the error signal generally exceeds the 2 deg saturation point although it still appears more or less sinusoidal. The nonlinear nature is more evident in the actuator rate response that appears "box car-like" for this highly saturated case. Thus the actuator

$$\omega_a = 20 \text{ rad/sec}; V_L = 40 \text{ deg/sec}; \omega_l = 5 \text{ rad/sec}; A = 5 \text{ deg}$$



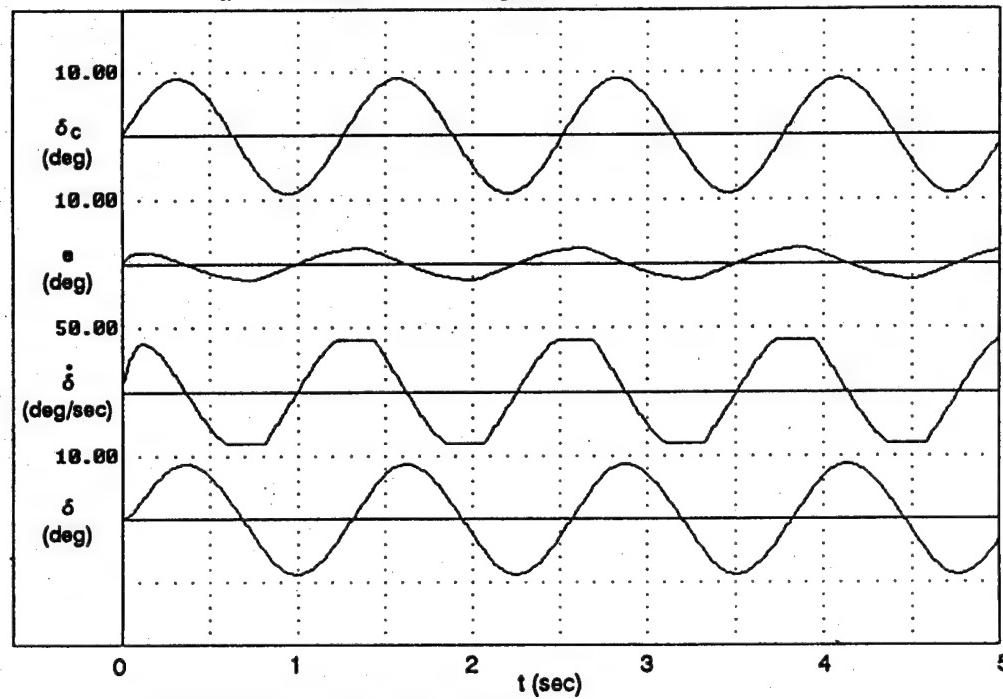
a) Linear System Time Responses



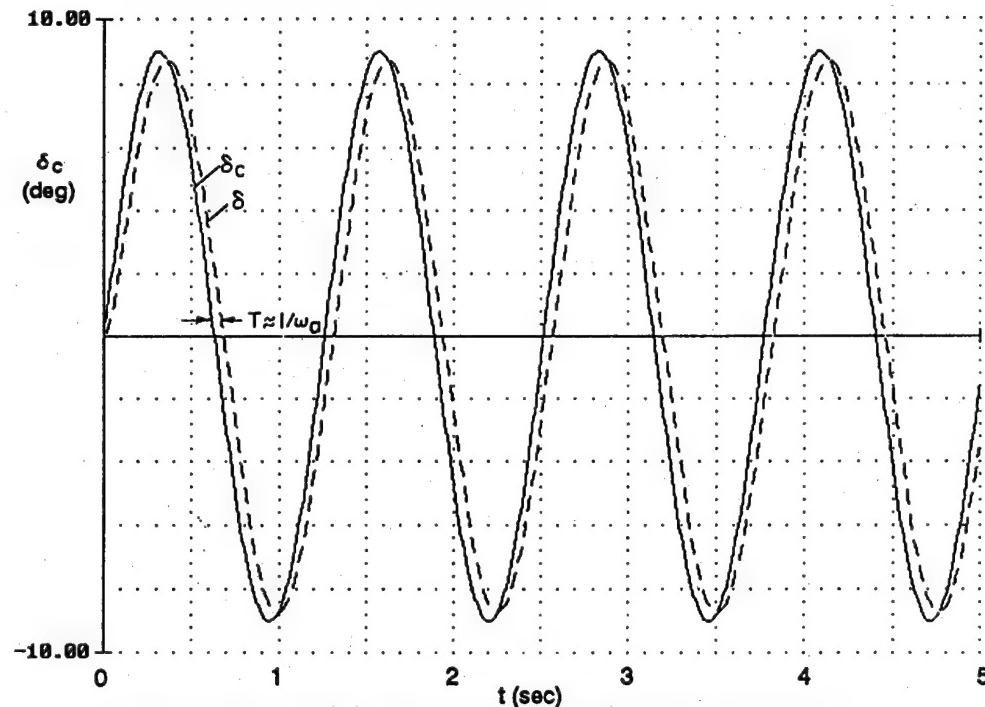
b) Linear System Input and Output Time Response Comparison

Figure 8. Closed-Loop Surface Actuator Model Examples

$$\omega_a = 20 \text{ rad/sec}; V_L = 40 \text{ deg/sec}; \omega_I = 5 \text{ rad/sec}; A = 9 \text{ deg}$$



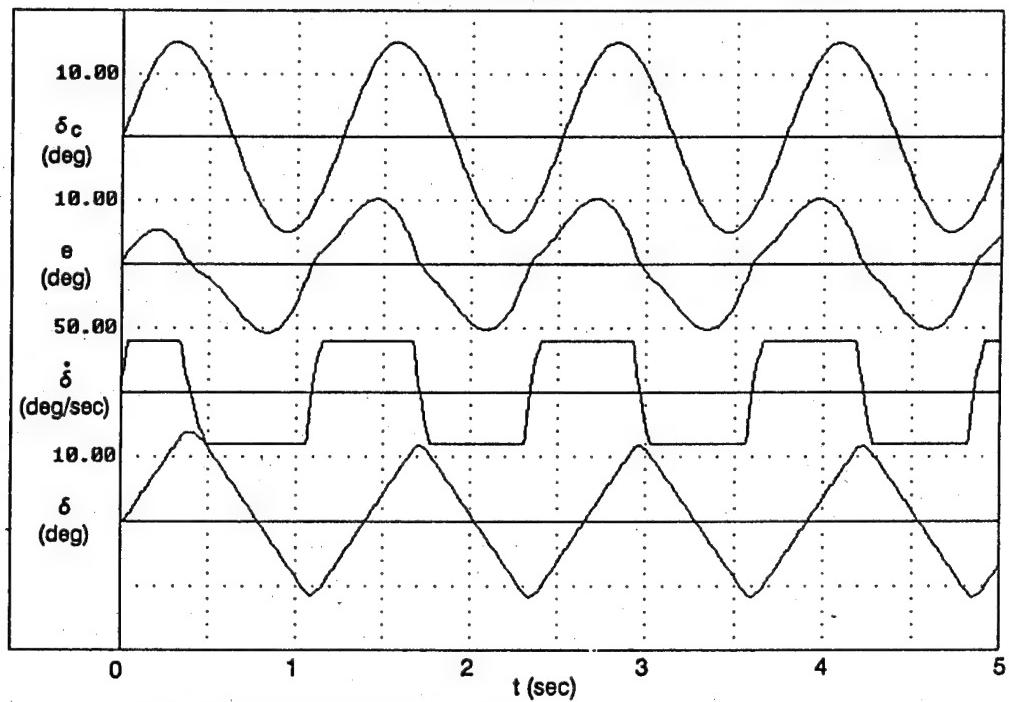
c) Near Saturation System Time Responses



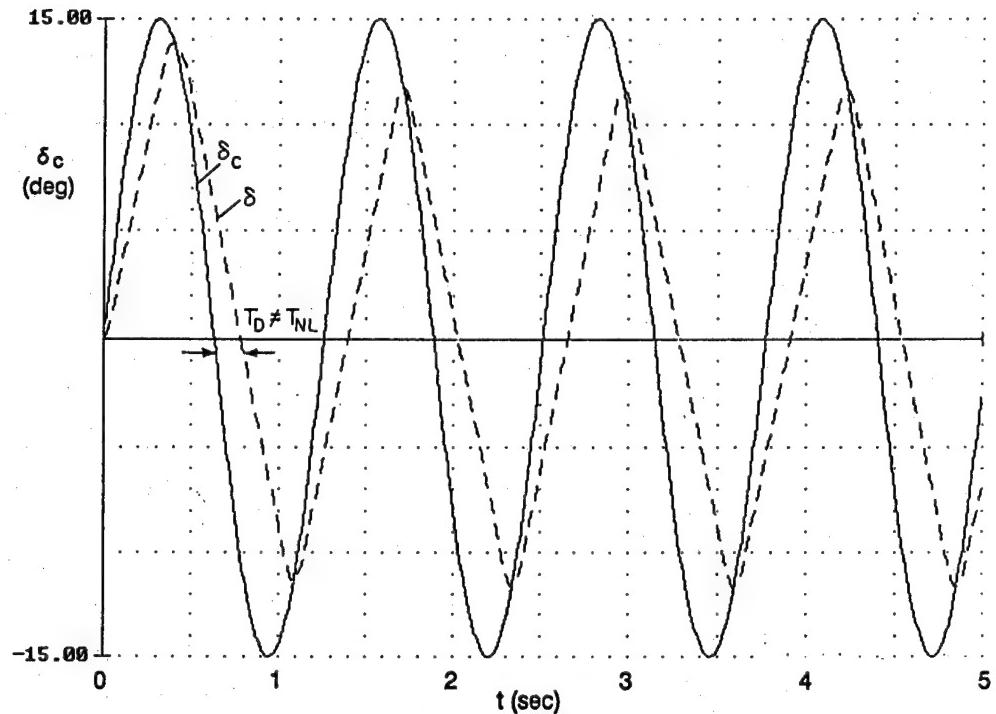
d) Near Saturation System Input and Output Time Response Comparison

Figure 8. Closed-Loop Surface Actuator Model Examples (continued)

$$\omega_a = 20 \text{ rad/sec}; V_L = 40 \text{ deg/sec}; \omega_l = 5 \text{ rad/sec}; A = 15 \text{ deg}$$



e) Highly Saturated System Time Responses



f) Highly Saturated System Input and Output Time Response Comparison

Figure 8. Closed-Loop Surface Actuator Model Examples (concluded)

operates as a bang-bang (i.e., maximum-to-maximum) controller. In Figure 8f the actuator output position is compared to the input command. The figure displays a triangle wave output response that reverses when equal to the input (i.e., when the error signal passes through zero). It should be noted that, unlike the indicial response discussed earlier, the phase lag for this more generalized case is not consistent with T_{NL} (i.e., $\Delta\phi \neq \omega T_{NL}$). In the analyses that follow, however, it is shown that the T_{NL} parameter still plays a significant role in characterizing the nonlinear system.

A survey of the PIO time histories of Appendix A reveals similar actuator position responses for rate limited cases. In Ref. 2 the survey time histories of Appendix A were used to estimate the PIO frequencies of the individual events. These frequencies were found to vary from 1.4 to 25 rad/sec, with the vast majority of the "extended rigid body" events occurring between 1.4 and 8 rad/sec. The most relevant cases for the analysis and prediction of Category II PIOs are, therefore, the highly saturated cases with input command frequencies from 1.4 to 8 rad/sec.

D. FACTORS CONTRIBUTING TO CATEGORY III PIOS

As noted in the definitions of the PIO Categories, the distinction drawn between the Category II and III types of PIO is fundamentally one of complexity of the nonlinearities involved. Category III PIOs can be much more complex in that they intrinsically involve transitions in either the pilot or the effective controlled element dynamics. As discussed earlier, pilot-centered transitions include:

- Shifts in Cues – e.g., from attitude tracking to load-factor;
- Shifts in Behavioral Mode – e.g., from pursuit to compensatory, precognitive to pursuit to compensatory; and
- Shifts in Effective Pilot Equalization Dynamics – e.g., from compensatory to synchronous (pure-gain).

Past experience indicates that the most important are shifts from compensatory to pure gain and, perhaps, the shifts in cues from attitude to load-factor. Such shifts have been found to be especially important for cases involving flexible modes and neuromuscular couplings (e.g., limb-bobweight effects).

The most extensive Category III cases are transitions in the effective vehicle dynamics. As already noted, the transition will be a function of the pilot's output amplitude, flight control system mode changes or other shifts in the effective controlled-element dynamics (e.g., shifts in the effective vehicle propulsion or aerodynamic configuration). The pre-transition controlled element is ordinarily linear, while the post-transition effective controlled element for a modern fly-by-wire system can reflect the influence of a large variety of limiting elements and other nonlinear features. The post-transition effective vehicle dynamics of greatest interest are those that depart most from the pre-transition condition. For these, a comparison of pre- with post-transition potential limit cycle conditions suggests PIO potential. Comparison of the two gives a direct indication of the amount of adaptation needed on the part of the pilot to tolerate the shift.

Past history indicates that Category III PIOs are highly unusual but also very severe events. The post-transition effective vehicle dynamics are almost always unforeseen, as are the triggering possibilities. Thus this type of PIO is particularly insidious because they tend to be unanticipated. That is, in the best modern fly-by-wire designs the pre-transition (i.e., normal) effective aircraft dynamics are designed to have excellent flying qualities. Most of the system nonlinearities (e.g., limiters, faders, mode-switches, etc.) are deliberately introduced to counter anticipated problems. It is only when they act in peculiar, usually unforeseen, ways in the presence of large pilot inputs that the "bad" post-transition vehicle dynamics are created. Yet modern systems are so complex and elaborate that more and more Category III PIOs are likely to occur in the future.

IV. PIO ANALYSIS

Reference 1 presents an in-depth survey and study of severe pilot-induced oscillations as interactions between the human pilot and effective aircraft dynamics. The severe PIOS examined there exhibited a rich variety of highly diverse phenomena in terms of effective aircraft dynamics and pilot behavioral modes. The range of effective aircraft dynamics implicated in particular PIOS included such linear properties as excessive lags and/or inappropriate gain and nonlinear changes or transitions in dynamic form and character. Human pilot response patterns associated with PIOS are similarly diverse, and include transitions from one form to another. Further, the frequency range of the human/aircraft interactions can be very large, extending from the rigid body to flexible mode frequency regimes.

To cope with these pilot and effective aircraft complexities in the analysis of PIOS, three proposed PIO categories have been defined (see Section II) that fit particular PIO possibilities into separate and distinct analysis domains. Although their first purpose is to divide PIOS into groups that can be attacked with viable analysis procedures, they also serve as divisions for PIO classification and criteria development.

The vast majority of past severe PIOS have fallen into Category I or II. The human pilot response and aircraft dynamics data available have permitted a thorough understanding of the closed-loop, fully-developed aspects of Category I PIOS in which attitude control is the dominant factor. Applicable theory has been well-developed and applied for over three decades (see, e.g. Refs. 2, 4, 42, and 48). Further, flight test results (e.g., Ref. 57) have provided a great deal of comprehensive information to validate the theory. The analysis aspects for Category I PIOS are briefly summarized in this section.

Rate limiting in the surface actuators has been a prominent feature of essentially all the severe PIOS for which recordings exist, although their analyses have seldom accounted for the rate-limiting effects as primary governing and/or causative factors. This has not been because of deficiencies in analytical concepts; indeed, analysis of Category II PIOS also has an ancient history (e.g., Refs. 4 and 7). In fact, in these cases the analyses were central to understanding the phenomena. The rate limiting nonlinearity intrinsic to the inner loop of a surface actuator has here-to-fore been approached using approximate describing functions (Ref. 4) or computer simulation techniques (Ref. 7) that have required quite substantial efforts to mount. Such complications, coupled with a lack of data sufficient to develop a complete quantitative story including the PIO amplitude, are the main reasons that more attention has not been paid to Category II situations in spite of their overwhelming importance in practice. One of the major thrusts in this study, therefore, has been to reduce the approximation and complication level needed to treat rate limiting phenomena. And, a major recommendation for future flight test is for data pertinent to severe rate limited PIOS (i.e., the Category II parallel to Ref. 57 for Category I). The analysis aspects for Category II PIOS are developed in detail in this section, and the famous X-15 landing/flare PIO is then used to exemplify these analysis procedures.

Recent flight control technology advances and PIO events suggest that a vast majority of future PIOS may often fall into Category III. Unfortunately, this is the least understood of the three categories. In this section the issues relevant to Category III analysis procedures are discussed. For several famous Category III PIOS including the F-8 DFBW case, the effective vehicle dynamics had poor handling qualities and high PIO susceptibility as predicted by Category I criteria. It may be argued, therefore, that separate analysis procedures are not needed. To counter this argument, the YF-12 Category III PIO is discussed in terms of its linear effective vehicle dynamics which were satisfactory in Category I terms.

Another important consideration for the complete analysis of PIO potential is the effect of high frequency dynamics. These issues are most relevant for large, flexible aircraft (e.g., B777 and the High Speed Civil Transport) that have flexible modes that fall well into the region of closed-loop piloted

control. Because flexible effects can result in any Category of PIO, it is presented as a separate issue in this section.

The section concludes with a step-by-step PIO analysis guide. These steps include the delineation of most likely flight conditions, the determination of effective controlled element dynamics, pure-gain-pilot/vehicle closed-loop system analysis, and closed-loop compensatory pilot/vehicle system analyses.

A. CATEGORY I ANALYSIS

Ordinarily the higher frequency dynamics of the pilot-vehicle system are associated with attitude regulation and control, either as a primary task or as an inner loop closed by the pilot in support of such outer loop functions as path or altitude control. These features are depicted as a single-input, single-output system in Figure 9 (which may be merely a component of a more elaborate system). When the task precision control demands and urgency are very great the pilot adaptively adjusts the pilot-vehicle system operation to maximize the system's precision. This is associated with maximizing the effective closed-loop system bandwidth and with minimization of system errors. These desirable conditions are established by the pilot's adjustment of gain to very high levels that approach, and sometimes exceed, the closed-loop system stability limits. The actual stability limit corresponds to a steady-state pilot-induced oscillation. In the usual situation in which the closed loop pilot-vehicle system is operating to control and regulate aircraft attitude the condition for a Category I pilot-induced oscillation is given by,

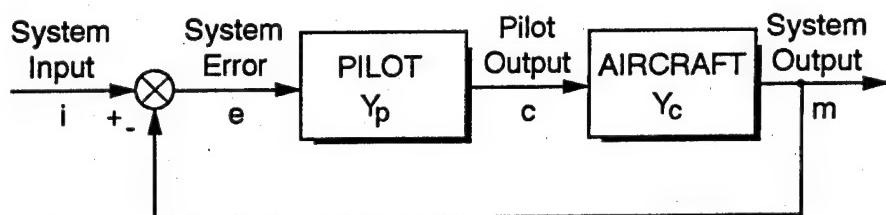
$$Y_p Y_c = -1 \quad (5)$$

where Y_p and Y_c are quasi-linear describing functions representing the actions of the pilot and the effective aircraft. The corresponding amplitude ratio and phase relationships are given as the first entry of Table 2. For the usual attitude-dominant conditions the aircraft describing function will relate attitude (e.g., pitch angle, θ , or bank angle, ϕ) to the pilot's command. If normal acceleration or another aircraft output quantity is the regulation task, the same equation applies to the PIO situation with the definition of Y_c changed appropriately. The describing functions are quasi-linear in that they characterize input-output relationships as approximate linear operations for the particular inputs at hand (Ref. 44). Thus they can change as the inputs change. For PIOS the appropriate quasi-linear operators are sinusoidal-input describing functions. Because the describing functions are input-dependent, the pilot and effective aircraft operators can include amplitude-dependent nonlinearities, such as amplitude-dependent gains. Otherwise, the 1 presents pilot and their use in the analysis of Category I PIOS, together with a large number of examples based and effective aircraft describing functions, and the oscillations defined by Eqn. 5, are time-stationary and essentially linear. Indeed, in the limit for the airplane, its describing function becomes a transfer function as nonlinear terms are removed.

Reference a detailed review of pilot describing functions on severe PIO situations studied in flight and reported in Ref. 57. There are two types of pilot behavioral patterns of interest in closed-loop oscillatory operations, "compensatory" and "synchronous."

In compensatory control the pilot responds primarily to errors in the pilot-vehicle system. The pilot's describing function is adjusted to compensate for the deficiencies of the vehicle dynamics, and is thus vehicle-dynamics-dependent. Compensatory behavior is very well understood based on decades of experimental and pilot modeling research, and the describing function for a specific situation can be accurately defined, in terms of either classical structural-isomorphic or optimal control formulations, over a very wide frequency band if need be (Ref. 41). For most studies of PIOS associated with extended rigid-body effective aircraft characteristics the essence of the compensatory model is provided by an

ELEMENTARY PILOT-VEHICLE FEEDBACK SYSTEM



NECESSARY AND SUFFICIENT CONDITION FOR INSTABILITY

Full Attention -- Transfer Characteristics of Pilot + Effective Aircraft, $Y_p Y_c = -1$

USUAL CONDITIONS OF ONSET

High Gain/Task Urgency -- Often with a Precursor Trigger

TYPICAL TRACKING TASKS WITH HIGH PILOT GAIN/URGENCY

Aerial Refueling

Formation Flying

Precision Tracking

Precision Approaches and Spot Landings (e.g., carrier approach)

Terrain Following

Demanding/Unexpected Transitions

Figure 9. Conditions Associated with PIO

TABLE 2. SUMMARY OF CONDITIONS FOR CATEGORY I PIO

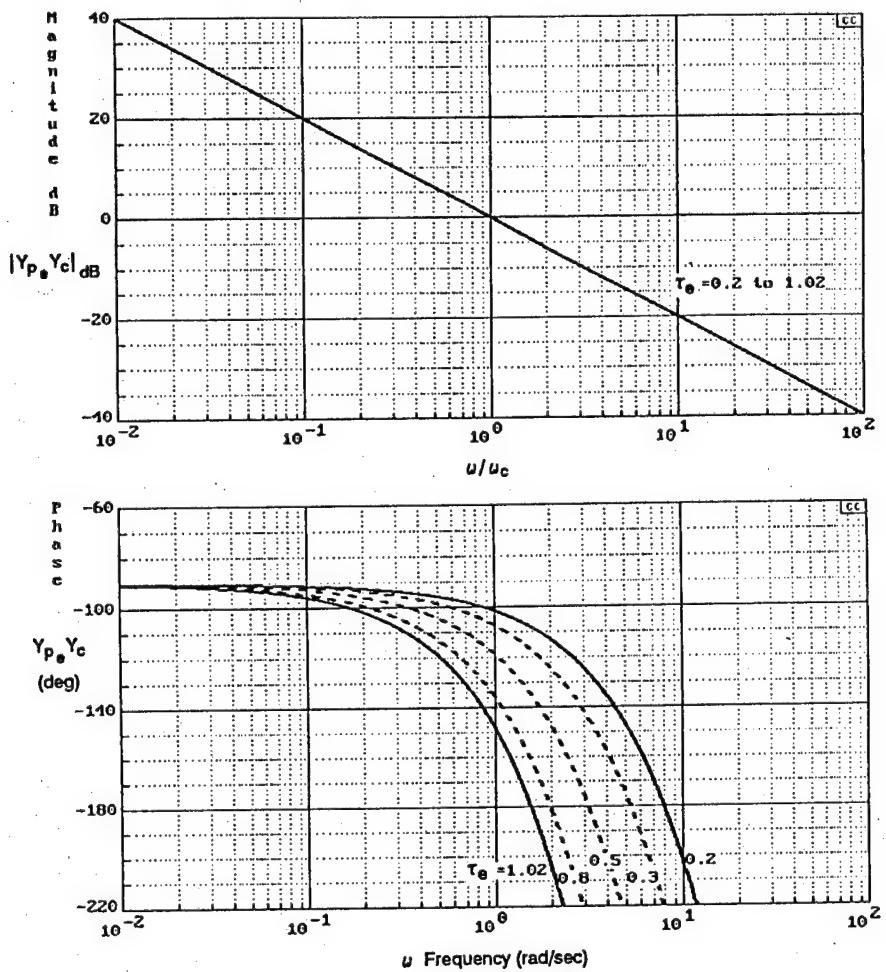
Pilot Behavior Pattern	Open-Loop Describing Function	Phase Margin (rad)	Conditions for PIO	
			Amplitude Ratio	Phase
General	$Y_p Y_c$	$\pi + \angle Y_p(j\omega) Y_c(j\omega)$	$ Y_p(j\omega_u) Y_c(j\omega_u) = 1$ $\omega_c = \omega_u$	$\angle Y_p(j\omega_u) Y_c(j\omega_u) = -\pi$
Compensatory (Crossover Model Approx.)	$Y_p Y_c \approx \frac{\omega_c e^{-j\omega\tau_e}}{j\omega}$	$\frac{\pi}{2} - \tau_e \omega_e$	$\omega_c = \omega_u$	$\omega_u = \frac{\pi}{2\tau_e}$
Synchronous	$Y_p Y_c \approx K_p Y_c(j\omega)$	$\pi + \angle Y_c(j\omega_c)$	$ K_p Y_c(j\omega_u) = 1$	$\angle Y_c(j\omega_u) = -\pi$

approximation valid in the region of the pilot-vehicle system crossover frequency (ω_c), where $|Y_p(j\omega_c) Y_c(j\omega_c)| = 1$. The simplest version is the "crossover model," which is shown as the compensatory entry in Table 2. The effective time delay in the crossover model is a low-frequency approximation valid in the region of pilot-vehicle system crossover. It is a composite that comprises myriad high-frequency lags, delays, and leads from the aircraft and the pilot that, in their details, appear at frequencies well above ω_c .

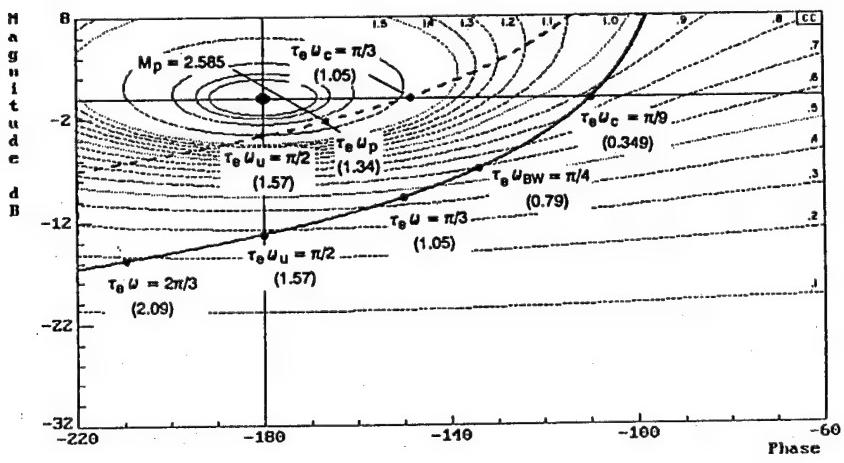
Bode and gain-phase diagrams for the crossover model are shown in Figures 10a and 10b, respectively. These are reproduced from Ref. 1, which contains a review of the crossover, its properties, and descriptions of the detailed nature of the Figure 10 diagrams. Two levels of gain are depicted on the gain-phase plots. In the first (solid line) the crossover frequency is arbitrarily set to occur when the phase is -110° . This follows a convention that will appear again later in connection with flying qualities criteria related to PIO susceptibility. The dashed line version is more representative of normal pilot dynamic behavior wherein the phase margin of 30° lies within the 20° to 40° range typical of full-attention pilot-vehicle system operation (Ref. 41). In the event of a Category I PIO the open-loop gain is raised and the gain-phase locus goes through the 0 dB and minus 180° point at the normalized frequency of $\tau_e \omega_u = \pi/2$. This is the estimate for the frequency of a Category I PIO when the crossover model is an appropriate approximation.

For higher frequency compensatory behavior PIOs the simple crossover model must be replaced by more elaborate pilot models that explicitly incorporate properties of the pilot's neuromuscular actuation system elements (see Ref. 41) as they interact with manipulator (inceptor) characteristics.

For attitude-dominant Category I PIOs the basic compensatory behavior analysis problem is to estimate the system crossover frequency, ω_c , pertinent to full-attention, high-pilot-gain circumstances. When higher frequency flexible modes are not relevant, and when ω_c is the only quantity needed, pilot modeling issues can be simplified. Then the more precise, detailed, and complex pilot models of Ref. 41 are often little better than much simpler and more approximate procedures. With the crossover model, for instance, the problem of estimating the unstable frequency (ω_u) is translated into one of estimating an



a) Bode Diagrams



b) Gain Phase Diagram

Figure 10. Frequency Responses for Crossover Model

effective time delay (τ_e) that provides a lower-frequency approximation to all the above-crossover higher frequency properties of the pilot and effective vehicle. Illustrative examples are given in Ref. 1. An even simpler approach uses the "critical frequency" formula developed in Ref. 48. This is based on empirical data from an extensive fixed-base experimental series for elementary ($Y_c = K_c$, K_c /s , and K_c /s^2) systems. The formula, developed as an extrapolation intended to cover more complex controlled elements, in its current version (Ref. 49) is,

$$\omega_c = 6.0 + 0.24m \quad (6)$$

where m is an average slope in dB/octave (at frequencies defined in Ref. 49) of the effective aircraft dynamics in the crossover region. This expression has been criticized on the bases that: (1) there are instances where the estimates are higher than and others lower than actually observed in flight; (2) " m " is sometimes difficult to determine unambiguously; and (3) the underlying data are for fixed-base, attitude-tracking tasks. Nonetheless, predictions of Category I PIO made using the formula have often proved to be accurate (e.g., Refs. 49 and 57) for some operational aircraft and for the severe PIOs generated in the Ref. 57 "Have PIO" tests. These points are considered in more detail in Section V.

Synchronous behavior is quite different. When sinusoidal signals appear in pilot-vehicle systems the pilot can progress through several behavioral phases adapting to the input. Initially the periodic character is not perceived, and the pilot treats the input as unpredictable and operates off errors only (i.e., compensatory behavior). After intermediate adaptation phases the pilot ultimately recognizes the periodic sinusoidal character and, up to frequencies of about 3 Hz, can duplicate the sinusoid with no phase lag (Ref. 29). If a transfer characteristic is assigned to this "synchronous" mode the pilot describing function will be simply $Y_p = K_p$. Thus in the presence of sustained oscillation the pilot can become phase-locked and, therefore, exhibit very little if any delay or lag.

For many severe, fully-developed PIOs the pilot-vehicle system oscillations start life as compensatory system neutral stability, and then progress to the synchronous state. In these instances the oscillatory condition reduces to the following:

$$\angle Y_c(j\omega) = -\pi \text{ radians (or } -180^\circ\text{)} \quad (7)$$

Thus, when the pilot's behavior is synchronous, the pilot-vehicle closed-loop system oscillatory frequency is governed by the effective vehicle dynamics alone. This is a great simplification for analysis. Because the pilot's actions approximate a pure gain, the unstable frequency will typically be somewhat higher than that for compensatory control where some pilot time delay is included. This is reflected in synchronous pilot estimates for the Ref. 57 PIO flights that are about 10% higher than those of the actual PIOs (Refs. 1 and 58).

The crossover model results described above can be used in a different context as an elementary example to illustrate the estimation of PIO frequency for synchronous operation. The simplest ideal rate-command effective aircraft dynamics have the following attitude to pilot input describing function:

$$Y_c \approx \frac{K_c e^{-ts}}{s} \quad (8)$$

Here the K_c/s is the ideal rate control, while the effective time delay is a low-frequency approximation to the net high frequency lags. This is, of course, identical in form to the crossover model, although it represents only the effective vehicle dynamics and the delay term arises solely from these properties. The PIO frequency for a synchronous pilot will then have the same form as the instability frequency for the crossover model ($\omega_u = \pi/2\tau$). A value of τ that represents the vehicle dynamics alone replaces the effective time delay (τ_e) that represents both pilot and vehicle dynamics in the crossover model itself.

B. RATE AND POSITION LIMITING

When nonlinearities associated with rate and position limiting terms enter the effective vehicle dynamics the PIO analysis picture becomes far more complex. A summary is given in Table 3. The elements from this table will be referred to as the analysis issues for Category II and III PIOS are presented.

3. PIO Situations

TABLE 3. PIO SITUATIONS ASSOCIATED WITH RATE AND POSITION LIMITING

Situation	Conditions for PIO	PIO Category
Series Command Rate Limiter Dominant	$Y_p(j\omega_u)Y_c(j\omega_u) \frac{8K^*}{\pi^2} e^{-j\cos^{-1}(K^*)} = -1$	II
Single Effector Rate Limiting [Actuator $\omega_a \gg \omega_u$]	$Y_p(j\omega_u)Y_c(j\omega_u) \frac{8K^*}{\pi^2} e^{-j\cos^{-1}(K^*)} = -1$	II
Single Effector Rate Limiting with Finite Actuator Bandwidth	$Y_p(j\omega_u)Y_c(j\omega_u)N[j\omega_u, A, V_{L_k}] = -1$ $k = 1 \rightarrow m$ limiters, $N[]$ = actuator + FCS limiters	II
Single Effector Rate & Position Limiting	$Y_p(j\omega_u)Y_c(j\omega_u)N[j\omega_u, A, V_{L_k}, \delta_L] = -1$ $k = 1 \rightarrow m$ limiters	II
Multiple Effector Rate & Position Limiting	$Y_p(j\omega_u)Y_c[j\omega_u, A, V_{L_k} \dots, \delta_{L_i} \dots] = -1$ $k = 1 \rightarrow m$ limiters, $i = 1 \rightarrow n$ effectors	III

Note that K^* is the ratio of the peak amplitude of the output triangular wave to the peak amplitude of the sinusoidal input.

C. DESCRIBING FUNCTIONS FOR SINGLE EFFECTOR RATE LIMITING

With constantly increasing computing power available, simulation remains the tool of choice for analyzing specific nonlinear systems. There are, however, several reasons to employ describing function techniques as well. The most important reason in regards to the analysis of Category II PIOS is that describing functions can be generalized. This is especially important for criterion development. Although powerful, computer simulation results are specific to a particular set of model parameters. The simulation model is, therefore, an important verification tool, but not necessarily the best means to develop criteria. Describing functions also provide extensions of linear graphical procedures. In this section describing functions that apply to the first three listings in Table 3 are developed. The derivations are carried out for the more general finite actuator bandwidth case.

I. Sinusoidal Input Describing Function Approximation

a. Open-Loop

As discussed in Section III, a sinusoidal input (i.e., $\delta_c = A \sin(\omega_i t + \phi_i)$) generally approximates the actuator commands for PIO incidents. This suggests approximating the saturation nonlinearity within the feedback loop with a sinusoidal describing function. Saturation is a "simple" nonlinearity (Ref. 44) such that a sinusoidal describing function is a real number invariant with input frequency. It is given by the ratio of the Fourier fundamental of the output to that of the input. To use this describing function to model the closed-loop system of Figure 5, it must be assumed that the error is approximately sinusoidal. This assumption is justified below. Because of the complex nature of the saturation Fourier fundamental, approximations are necessary to achieve a literal solution. Although some of the material presented in this section is based on analytical work that was originally presented in Ref. 4, it is included here for completeness.

The first step in developing an approximate describing function is to assume that the error signal in Figure 5 can be represented by a sinusoid, $e = E \sin(\omega t + \phi)$. By examining the error signal time response in Figure 8e, a highly saturated case, this is shown to be a reasonable assumption. In the linear range up to the saturation point ($E \leq e_L$), the effective gain of the nonlinearity is ω_a . Further, ω_a sets the bandwidth of the linear closed-loop δ/δ_c response. In the highly saturated range, however, the effective gain of the saturation nonlinearity with the feedback loop open is related to the saturation Fourier fundamental by the following equation¹ as defined in Figure 4-10c of Ref. 44:

$$\omega_a' = \frac{2\omega_a}{\pi} \left[\sin^{-1}\left(\frac{e_L}{E}\right) + \left(\left[\frac{e_L}{E}\right]\right) \sqrt{1 - \left(\frac{e_L}{E}\right)^2} \right] \quad (9)$$

One can see that as the magnitude of the input to the nonlinear element (E) increases, the effective nonlinear gain (ω_a') further decreases with respect to the linear bandwidth (ω_a). In fact $\omega_a'/\omega_a \rightarrow 0$ as $E/e_L \rightarrow \infty$.

By using series expansions for the arcsine and square root terms in Eqn. 9 and by retaining only the linear terms, the following approximation is obtained:

$$\omega_a' = \frac{4}{\pi} \frac{V_L}{E} \left[1 - \frac{1}{6} \left(\frac{V_L}{\omega_a E} \right)^2 - \dots \right] \approx \frac{4}{\pi} \frac{V_L}{E} \quad (10)$$

As shown in Ref. 4, the first order approximation of Eqn. 10 represents an approximation of the saturation output with a square wave. Such a square wave will have a fundamental $4/\pi$ times the saturation rate. By examining the rate signal of Figure 8e, it is evident that the square wave approximation is appropriate for the highly saturated range.

In the near saturation range an approximation of the effective nonlinear gain is made by the following equation:

$$\omega_a' \approx \frac{V_L}{E} \quad (11)$$

Eqn. 11 represents the case displayed in Figure 8c where the slightly clipped output rate is still represented by a sinusoid whose amplitude is approximated by the magnitude of the rate limit.

¹ Note that the Ref. 44 equation was written in terms of the $e_L = V_L/\omega_a$ substitution.

The three effective gains from Eqns. 9, 10, and 11 are compared in Figure 11. As shown in the sketch, the two approximations bound the exact result. This feature is further revealed in Figure 12 where the describing function approximations of Eqns. 10 and 11 are compared to the exact describing function of Eqn. 9 for the open-loop case. Specifically, the plots are the nonlinear open-loop gain normalized by the linear closed-loop bandwidth (ω_a) versus the error amplitude normalized by the saturation point. To obtain the displayed hyperbolic curves substitute $V_L = \omega_a e_L$ in Eqns. 10 and 11 and then solve in terms of the normalized parameters. The linear range is represented by a normalized gain value of 1 for $E/e_L \leq 1$. As illustrated previously in Figure 11, the nonlinear bandwidth decreases as the actuator rate limit becomes more highly saturated. In the near saturation region the Eqn. 11 describing function provides an adequate representation of the normalized gain as E/e_L approaches 1^+ . The normalized gain for the highly saturated describing function, on the other hand, remains at a value of 1 until $E/e_L = 4/\pi$. Thus it provides a poor approximation in the near saturation range. For $E/e_L \gg 1$, however, the highly saturated describing function provides an excellent approximation of the open-loop nonlinear bandwidth.

b. Closed-Loop

To obtain a closed-loop sinusoidal describing function, the approximations for the nonlinear bandwidths (i.e., Eqns. 10 and 11) must be defined in terms of the system input and output variables, δ_c and δ , respectively. First, block diagram algebra is used with Figure 5 to define an error signal transfer function in terms of the input command (for $e \leq e_L$):

$$\frac{e(s)}{\delta_c(s)} = \frac{1}{1 + \frac{\omega_a}{s}} \quad (12)$$

The next step is to substitute $j\omega$ for s and ω_a' for ω_a in Eqn. 12 and then solve for the describing function magnitude. This yields the following equation:

$$\left| \frac{e(j\omega)}{\delta_c(j\omega)} \right| = \frac{\omega}{\sqrt{\omega^2 + (\omega_a')^2}} = \frac{E}{A} \quad (13)$$

At this point either Eqn. 10 or 11 can be used to provide a substitution for E in Eqn. 13. Eqn. 10 is used here since the highly saturated range is more relevant to the analysis of Category II PIOs. Thus the next step is to substitute the following relation for E , obtained from Eqn. 10, into Eqn. 13:

$$E = \frac{4 V_L}{\pi \omega_a} \quad (14)$$

The final step is to then solve for ω_a' . After performing some algebra, the following equation is obtained:

$$\omega_a' = \frac{1}{\sqrt{\left(\frac{\pi A}{4 V_L}\right)^2 - \left(\frac{1}{\omega}\right)^2}} \text{ or } \frac{\omega}{\sqrt{\left(\frac{\pi A \omega}{4 V_L}\right)^2 - 1}} \quad (15)$$

The closed-loop response for the linear, near saturation, and highly saturated regions is determined from basic block diagram relationships to be:

$$\frac{\delta_c(j\omega)}{\delta(j\omega)} = \frac{1}{\frac{j\omega}{\omega_a} + 1} \quad (16)$$

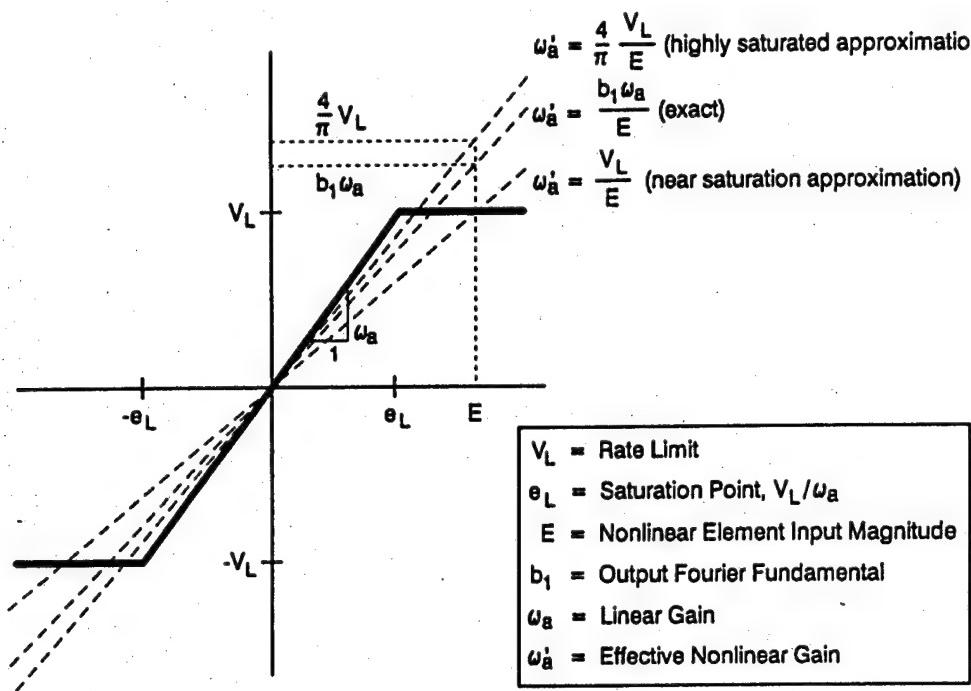


Figure 11. Effective Nonlinear Gain for the Open-Loop Saturation Nonlinearity

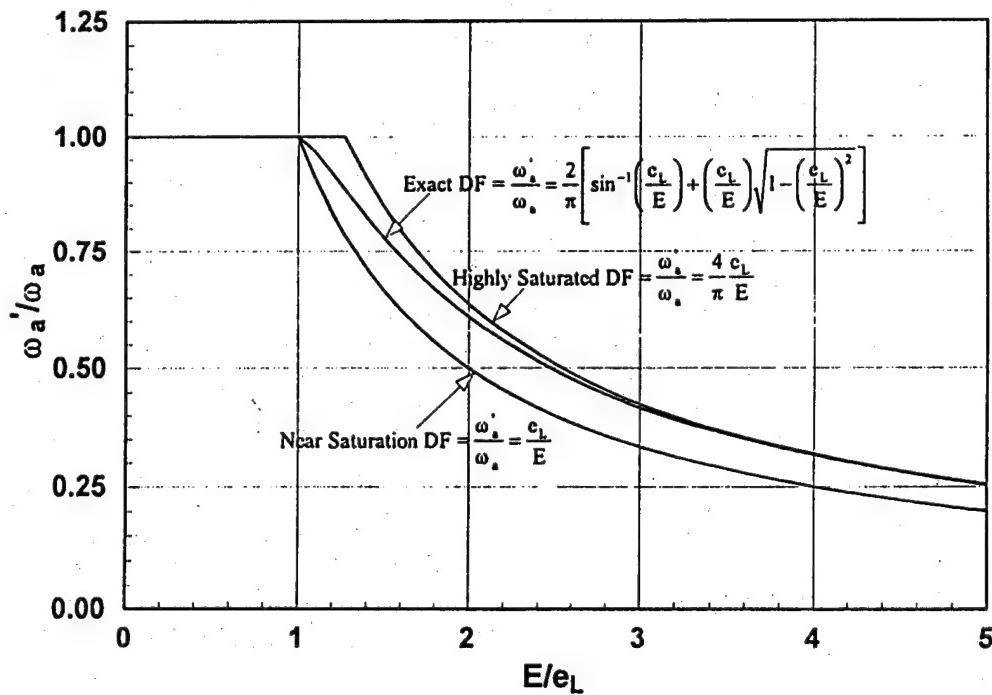


Figure 12. Open-Loop Describing Function Representations of the Nonlinear Gain

In the linear range, where $\omega_a' = \omega_a$, Eqn. 16 reduces to the simple first order lag in Figure 6.

Magnitude $\left(\sqrt{\frac{1}{1 + (\omega / \omega_a)^2}} \right)$ and phase $(-\tan^{-1}(\omega / \omega_a))$ responses for the approximate closed-loop system describing function are determined by substituting ω_a' as defined in Eqn. 15 into Eqn. 16. For the highly saturated case this yields the following:

$$\left| \frac{\delta(j\omega)}{\delta_c(j\omega)} \right| = \frac{4}{\pi} \frac{V_L}{A\omega} \quad (17a)$$

$$\angle \frac{\delta(j\omega)}{\delta_c(j\omega)} = -\tan^{-1} \left[\sqrt{\left(\frac{\pi}{4} \frac{A\omega}{V_L} \right)^2 - 1} \right] \quad (17b)$$

When the near saturation approximation of Eqn. 11 is used in the previous derivation the following frequency response equations are obtained:

$$\left| \frac{\delta(j\omega)}{\delta_c(j\omega)} \right| = \frac{V_L}{A\omega} \quad (18a)$$

$$\angle \frac{\delta(j\omega)}{\delta_c(j\omega)} = -\tan^{-1} \left[\sqrt{\left(\frac{A\omega}{V_L} \right)^2 - 1} \right] \quad (18b)$$

c. Closed-Loop Frequency Response

As defined in Eqn. 9, the effective gain, from which the near saturation and highly saturated describing function approximations were derived, only applies in the post saturation region. Thus to obtain the complete rate limited actuator frequency response approximation, a combination of the linear, near saturation, and highly saturated region results must be employed. In the *linear* region the magnitude and phase as a function of normalized frequency (ω/ω_a) is given by:

$$\left| \frac{\delta(j\omega)}{\delta_c(j\omega)} \right| = \sqrt{\frac{1}{(\omega / \omega_a)^2 + 1}} \quad (19a)$$

$$\angle \frac{\delta(j\omega)}{\delta_c(j\omega)} = -\tan^{-1}(\omega / \omega_a) \quad (19b)$$

For constant input amplitude and constant actuator design parameters, there is a specific frequency at which the actuator just saturates. A literal form for the saturation frequency (ω_s) is obtained from Eqn. 13 by substituting $e_L = E$ (at saturation) and then solving for frequency. This results in the following:

$$\omega_s = \frac{\omega_a}{\sqrt{\left(\frac{A}{e_L}\right)^2 - 1}} \quad (20)$$

This result is further reduced by substituting $e_L = V_L/\omega_a$, and then solving for a normalized saturation frequency as shown by:

$$\frac{\omega_s}{\omega_a} = \frac{1}{\sqrt{\left(\frac{A\omega_a}{V_L}\right)^2 - 1}} = \frac{1}{\sqrt{\left(\frac{T_{NL}}{T}\right)^2 - 1}} \quad (21)$$

In Figure 13 the normalized saturation frequency is plotted as a function of the time constant ratio (T/T_{NL}) with identified linear and post saturation regions. This curve indicates that, as expected, the frequency required to saturate becomes larger as the time constant ratio approaches 1. The Figure 13 result is, therefore, used to establish if the system has saturated for a given time constant ratio.

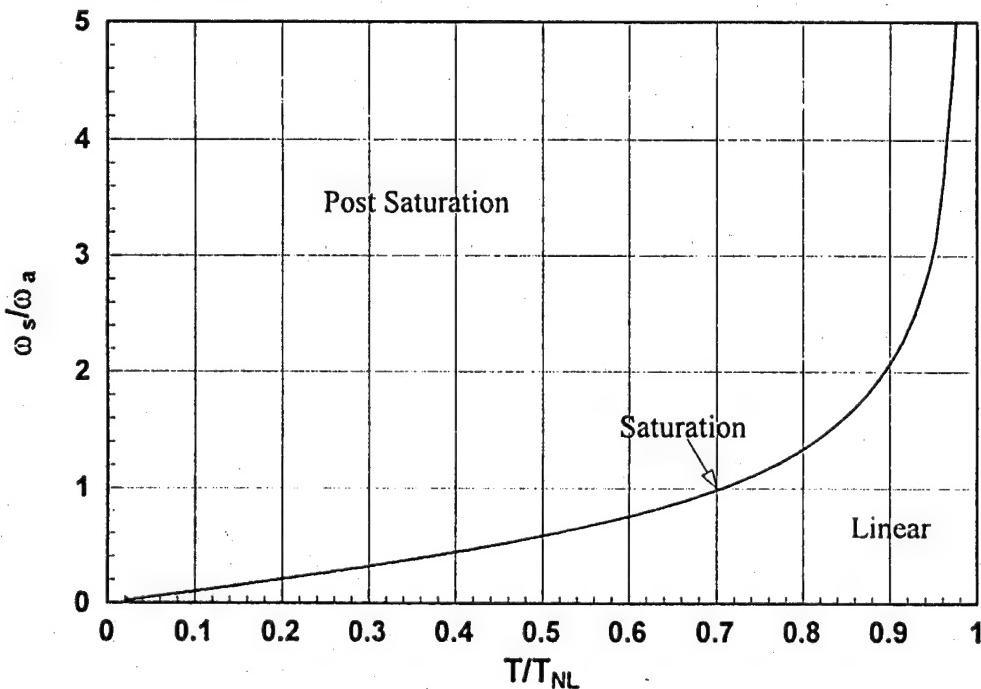


Figure 13. Saturation Frequency as a Function of the Time Constant Ratio

For time constant ratios of 1, the *near saturation* describing function (Eqn. 18) applies as given by the following normalized frequency magnitude and phase equations:

$$\left| \frac{\delta(j\omega)}{\delta_c(j\omega)} \right| = \frac{V_L}{A\omega_a} \frac{1}{(\omega / \omega_a)} = \frac{T}{T_{NL}} \frac{1}{(\omega / \omega_a)} \quad (22a)$$

$$\angle \frac{\delta(j\omega)}{\delta_c(j\omega)} = -\tan^{-1} \left[\sqrt{\left(\frac{T_{NL}}{T} \frac{\omega}{\omega_a} \right)^2 - 1} \right] \quad (22b)$$

Note that when Eqn. 22a applies, the resulting magnitude variation with frequency takes the form of a minus 20 dB/decade "k/s-like" asymptotic slope.

For inverse time constant ratios approximately greater than 2, the *highly saturated* describing function approximation applies as given by the following normalized frequency magnitude and phase equations:

$$\left| \frac{\delta(j\omega)}{\delta_c(j\omega)} \right| = \frac{4}{\pi} \frac{T}{T_{NL}} \frac{1}{(\omega / \omega_a)} \quad (23a)$$

$$\angle \frac{\delta(j\omega)}{\delta_c(j\omega)} = -\tan^{-1} \left[\sqrt{\left(\frac{\pi}{4} \frac{T_{NL}}{T} \frac{\omega}{\omega_a} \right)^2 - 1} \right] \quad (23b)$$

Note that when Eqn. 23a applies, the resulting magnitude also falls along a minus 20 dB/decade asymptotic slope.

A survey comparison of the near saturation and highly saturated describing function approximations and actual nonlinear system phase angle frequency responses is shown in Figures 14 and 15, respectively. The curves are displayed with the time constant ratio (T/T_{NL}) as a parameter. It should be noted that a crossplot of the saturation boundary of Figure 13 on Figures 14 and 15 would lie on the upper envelope, $T/T_{NL} = 1.0$, curve. The curves that depart from this upper boundary, therefore, are in the post saturation region per Figure 13 and thus guaranteed to meet the $\omega > \omega_s$ requirement. Several key features of the approximations are evident in the figures. As shown in Figure 14 the near saturation describing function only provides a good match for $T/T_{NL} \geq 0.8$. Each of the near saturation approximation curves asymptotically approaches a frequency equivalent to its time constant ratio as the phase approaches zero. The highly saturated describing function, on the other hand, provides its best match for the $T/T_{NL} = 0.4$. As the time constant ratio becomes smaller, the approximation gradually diverges from the nonlinear simulation line. Since for a given curve the approximation predicts a larger than actual phase lag, the divergence is conservative. In contrast to the near saturation approximation, each of the Figure 15 curves asymptotically approaches a frequency equivalent to $4/\pi$ times its time constant ratio as the phase approaches zero.

2. Sinusoidal Input/Triangle Output Describing Function Approximation

A describing function approximation between δ_c and δ for a highly saturated rate limited actuator can be obtained by assuming a sinusoidal input/triangle output rate limiting element as was done by Hanke in Ref. 59 following a suggestion from A'Harrah (Ref. 67). Unlike the derivation described

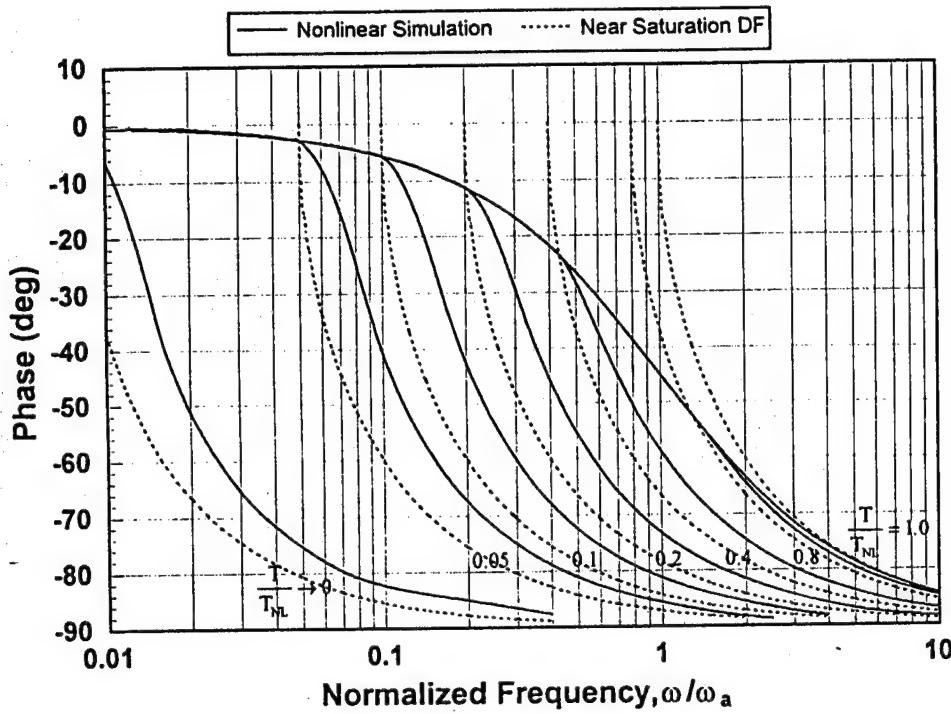


Figure 14. Rate Limiting Actuator Phase Angle Frequency Response Comparison Between the Near Saturation Describing Function Approximation and the Nonlinear Simulation

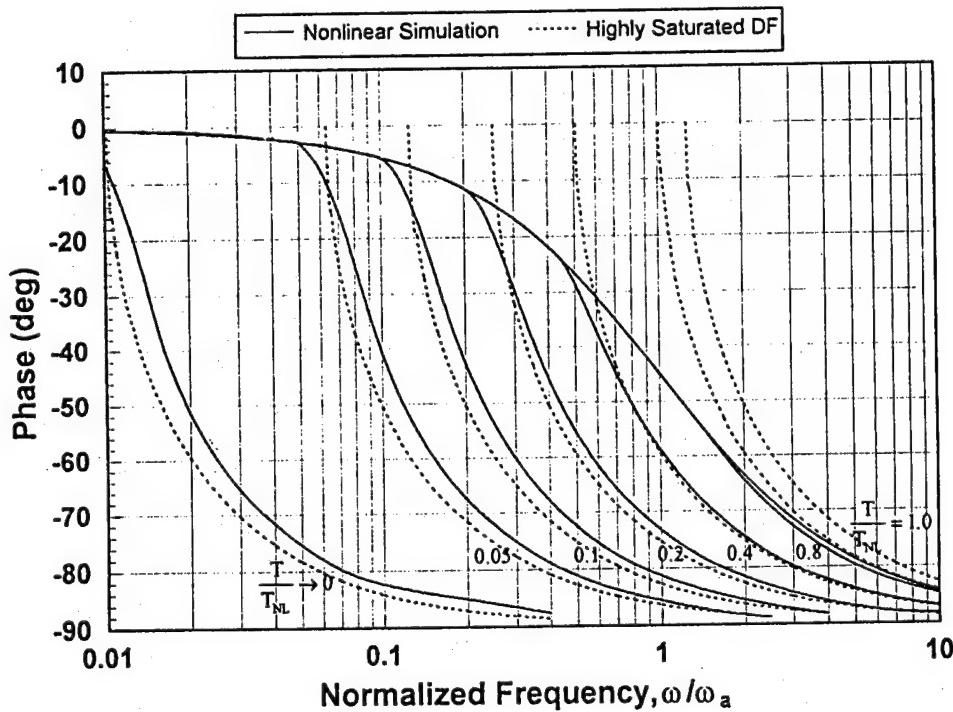


Figure 15. Rate Limiting Actuator Phase Angle Frequency Response Comparison Between the Highly Saturated Describing Function Approximation and the Nonlinear Simulation

above, this method does not consider the servo loop explicitly, since only the wave forms of the input and output of the rate limiting element are considered. It does, however, implicitly take into account the servo loop by requiring a reversal of the output whenever the servo error, $e = x_i - x_o$, becomes zero. This nonlinear element model is exact when applied to a flight control system (FCS) software limiter that contains no dynamics. It is also used here to approximate an infinite bandwidth actuator (i.e., $\omega_a \gg \omega$). Input and output time responses for the Ref. 59 model are shown in Figure 16 with the variables related

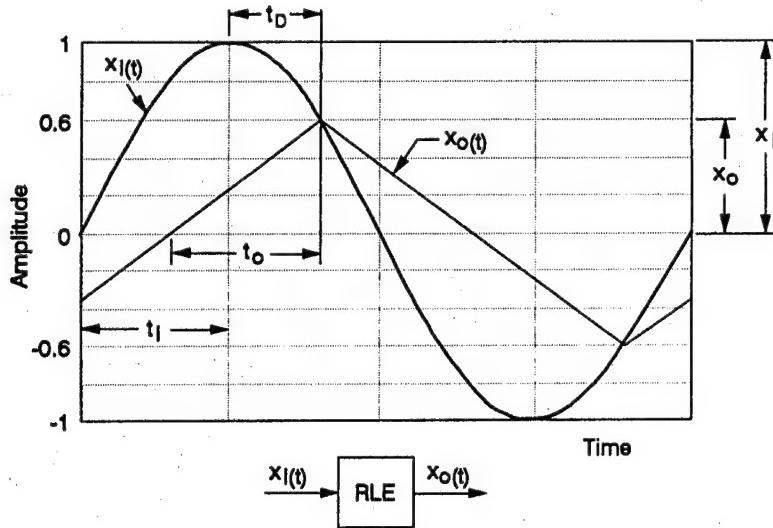


Figure 16. Rate Limiting Element (RLE) Time Response for a Sinusoidal Input
(from Ref. 59 and 67)

to this derivation identified. Since the periods for the input and output are the same in the steady state, the times to peak amplitude or quarter periods (t_i and t_o , respectively) are also equivalent. The sinusoidal input (i.e., command position) is defined by the following equation:

$$x_i(t) = x_{i_{\max}} \sin(\omega t) \quad (24)$$

and the input rate is therefore:

$$\dot{x}_i(t) = x_{i_{\max}} \omega \cos(\omega t) \quad (25)$$

Eqn. 25 can be written in terms of t_i by substituting $\omega = 2\pi/T$, where the period $T = 4t_i$. The maximum input rate (i.e., $\cos(\omega t) = 1$) is thus:

$$\dot{x}_{i_{\max}} = \frac{\pi}{2} \frac{x_{i_{\max}}}{t_i} \quad (26)$$

The peak magnitude of the triangle wave output is equal to x_o . The constant output rate is therefore:

$$\dot{x}_o = \pm \frac{x_o}{t_0} \quad (27)$$

The actual output/input magnitude is defined by taking the ratio of the constant output to maximum input rates and then solving for $x_o/x_{i_{\max}}$. Defining K as $x_o/x_{i_{\max}}$, this yields the following result:

$$K^* = \frac{x_o}{x_{i_{max}}} = \frac{\pi}{2} \frac{\dot{x}_o}{\dot{x}_{i_{max}}} \quad (28)$$

This result can be written in terms of the Figure 5 variables, as shown in Eqn. 29, by recognizing that the output rate when saturated is V_L and the maximum input rate is $A\omega$:

$$K^* = \frac{\pi}{2} \frac{V_L}{A\omega} \quad (29)$$

The K^* parameter is next used to define the describing function magnitude and phase. The describing function magnitude is obtained by multiplying K^* , which represents the actual peak magnitude of the triangle wave, by the Fourier fundamental of the triangle wave (i.e., $8/\pi^2$) as shown by:

$$\left| \frac{\delta(j\omega)}{\delta_c(j\omega)} \right| = \frac{8}{\pi^2} K^* = \frac{4}{\pi} \frac{V_L}{A\omega} \quad (30)$$

Note that this is identical to the highly saturated sinusoidal input describing function approximation magnitude (Eqn. 17a) with the same "k/s-like" frequency response.

The time difference between the output and input is represented by t_D in Figure 16. It is also noted in the figure that the input and output amplitudes are equal at $t = t_i + t_D$. Thus to obtain t_D , set the input relation of Eqn. 24 equal to the output and use the above substitution for t to produce the following:

$$x_i \sin[\omega(t_i + t_D)] = x_o \quad (31)$$

Equation 31 is simplified by substituting K^* for $x_o/x_{i_{max}}$, expanding $\sin[\omega(t_i + t_D)]$ and noting that $\omega t_i = \pi/2$. This results in,

$$\cos(\Delta\phi) = K^* \quad (32)$$

where $\Delta\phi = \omega t_D$ is the phase angle between the input and output. Finally, the phase difference ($\Delta\phi$) is obtained by solving for the argument in Eqn. 32:

$$\Delta\phi = \cos^{-1}(K^*) \quad (33)$$

Thus, using basic trigonometric relations, the phase angle² for the describing function is given simply by:

$$\angle \frac{\delta(j\omega)}{\delta_c(j\omega)} = -\Delta\phi = -\cos^{-1}(K^*) = -\tan^{-1} \left[\sqrt{\left(\frac{1}{K^*} \right)^2 - 1} \right] \quad (34)$$

From Eqn. 30, $K^* = \frac{\pi}{2} \frac{T}{T_{NL}} \frac{\omega_a}{\omega}$. Thus, the magnitude and phase can be written in terms of the normalized frequency and time constant ratio as follows:

$$\left| \frac{\delta(j\omega)}{\delta_c(j\omega)} \right| = \frac{4}{\pi} \frac{T}{T_{NL}} \frac{1}{(\omega / \omega_a)} \quad (35a)$$

² The minus sign comes from the describing function phase lag definition.

$$\angle \frac{\delta(j\omega)}{\delta_c(j\omega)} = -\tan^{-1} \left[\sqrt{\left(\frac{2}{\pi} \frac{T_{NL}}{T} \frac{\omega}{\omega_a} \right)^2 - 1} \right] = -\cos^{-1} \left(\frac{\pi}{2} \frac{T}{T_{NL}} \frac{\omega_a}{\omega} \right) \quad (35b)$$

Eqn. 35b was used to generate a survey comparison of the sinusoidal input/triangle output describing function approximation and actual nonlinear system phase angle frequency responses as shown in Figure 17. Once again the curves are displayed as a function of the time constant ratio (T/T_{NL}). Several key features of the approximations are evident in the figure. First, as expected, the approximation does poorly in the near saturation region, $T/T_{NL} \geq 0.8$. In the highly saturated region, on the other hand, the approximation provides an excellent match for $T/T_{NL} \leq 0.1$. In the $0.2 \geq T/T_{NL} \geq 0.4$ region, the match is good, however, it is not conservative in that for a given normalized frequency it predicts a smaller than actual phase lag. Each of the Figure 17 curves asymptotically approaches a frequency equivalent to $\pi/2$ times its time constant ratio as the phase approaches zero.

3. Approximate Describing Function Comparison

Two approximate describing function derivations were shown in the previous sections. The sinusoidal input describing function approximation provided both a near saturation and a highly saturated result, while the sinusoidal input/triangle output approximation only provides a highly saturated region result. To best compare results of these two methods refer to the magnitude and phase equations written in terms of the normalized frequency and time constant ratio (i.e., Eqns. 22, 23, and 35). The sinusoidal input/triangle output describing function formulation assumes that the output is a perfect triangular wave. This could only occur if ω_a were infinite (i.e., the bandwidth of the servo in the linear range were infinite). Thus, this approximation would not be expected to exactly match the earlier approximate describing function developments. In the highly saturated region, both approximations result in the same magnitude, but the phase angles, however, differ by an $8/\pi^2$ factor. These two approximations are compared in the time domain with the nonlinear simulation in Figure 18. The results indicate that the two describing functions have comparable phase offset errors for this example case.

A more insightful comparison is made by reviewing the approximate describing function and nonlinear simulation phase angle frequency plots shown in Figures 14, 15, and 17. Basically, each describing function has a region in which it provides the best match to the nonlinear simulation. These results are summarized as follows:

- $T/T_{NL} \geq 0.8$: sinusoidal input near saturation approximation;
- $0.2 \leq T/T_{NL} < 0.8$: sinusoidal input highly saturated approximation; and
- $T/T_{NL} < 0.2$: sinusoidal input/triangle output approximation.

Although both highly saturated approximations provide essentially equivalent matches in the $0.2 \leq T/T_{NL} < 0.8$ region, the sinusoidal input result was selected because it provided the more conservative phase estimate and an excellent match to the 0.4 time constant ratio curve.

4. Exact Sinusoidal Describing Function

The limitations of the literal describing functions, as described above, are their inability to provide an exact phase match to the nonlinear result for the full range of frequencies and time constant ratios. To yield this desired match numerically, an exact sinusoidal describing function is obtained by first computing the Fourier integrals for the input and output fundamentals as defined in Ref. 44 by the following equations:

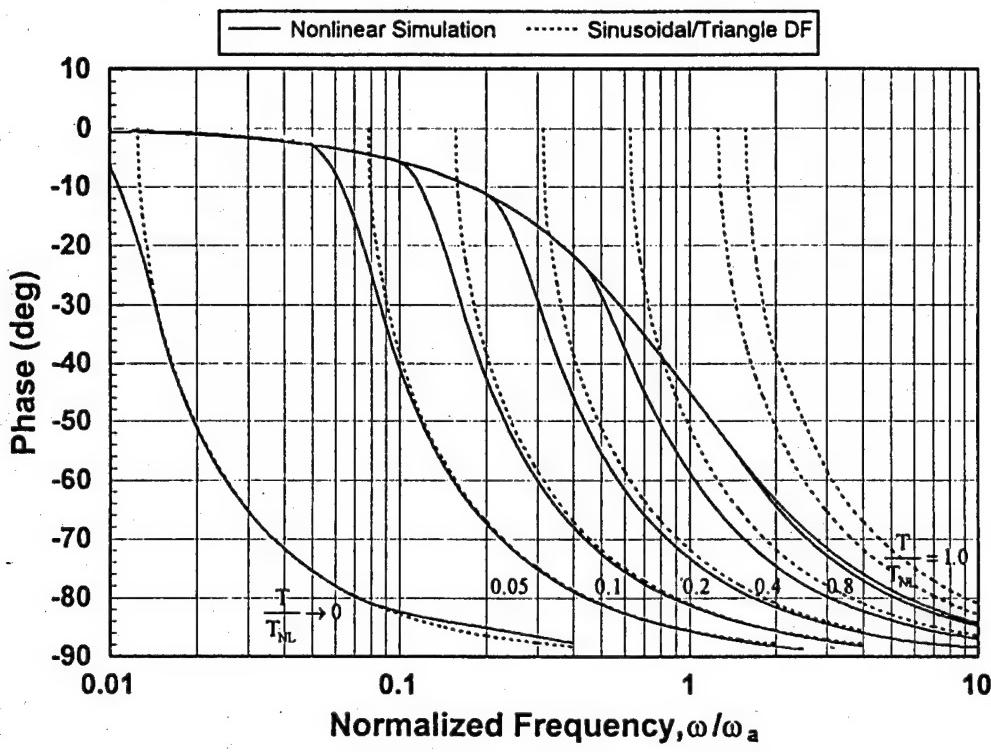


Figure 17. Rate Limiting Actuator Phase Angle Frequency Response Comparison Between the Sinusoidal Input/Triangle Output Describing Function Approximation and the Nonlinear Simulation

$$\omega_a = 20 \text{ rad/sec}; V_L = 40 \text{ deg/sec}; \omega_l = 5 \text{ rad/sec}; A = 15 \text{ deg}$$

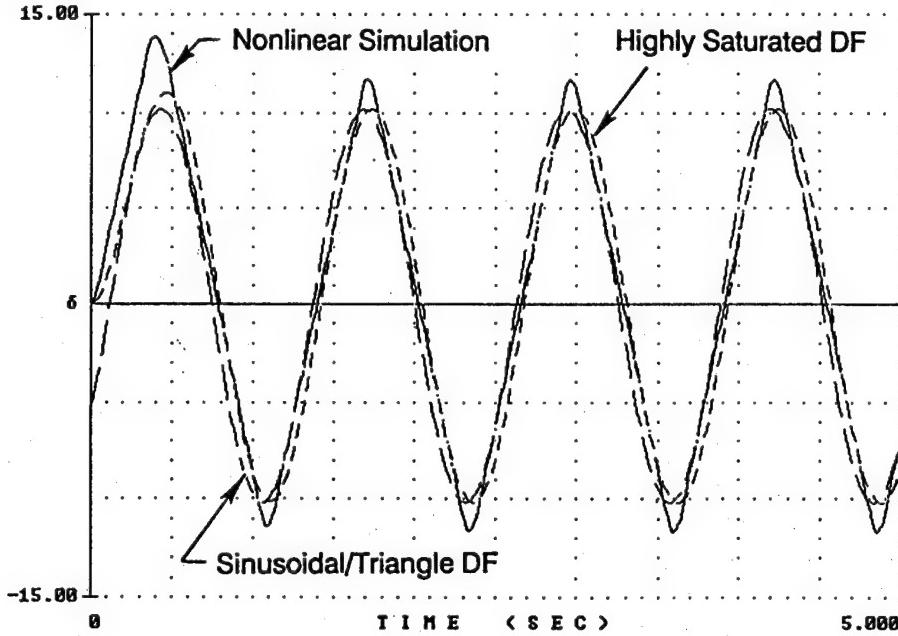


Figure 18. Approximate Describing Function Time Response Comparison to the Nonlinear Simulation

$$a_1 = \frac{2}{P} \int_{-P/2}^{P/2} f(t) \cos(\omega_{in} t) dt \quad (36a)$$

$$b_1 = \frac{2}{P} \int_{-P/2}^{P/2} f(t) \sin(\omega_{in} t) dt \quad (36b)$$

In the preceding equations, $f(t)$ is the input or output periodic forcing function that for this case is a sine wave of period P . For sinusoidal input describing functions the a_1 term for the input is always zero. Thus the a and b terms of Eqn. 36 are then used to define the describing function magnitude and phase from Ref. 44 as shown by:

$$\left| \frac{\delta(j\omega)}{\delta_c(j\omega)} \right| = \frac{\sqrt{a_{1_{out}}^2 + b_{1_{out}}^2}}{b_{1_{in}}} \quad (37a)$$

$$\angle \frac{\delta(j\omega)}{\delta_c(j\omega)} = -\tan^{-1} \left(\frac{a_{1_{out}}}{b_{1_{out}}} \right) \quad (37b)$$

The nonlinear simulation of the Figure 5 system was amended to compute the Fourier integrals of Eqn. 36 and the magnitude and phase from Eqn. 37. In Figure 19 the exact sinusoidal describing function is compared with the nonlinear simulation for the highly saturated example case of Figure 8f. As shown

$$\omega_a = 20 \text{ rad/sec}; V_L = 40 \text{ deg/sec}; \omega_i = 5 \text{ rad/sec}; A = 15 \text{ deg}$$

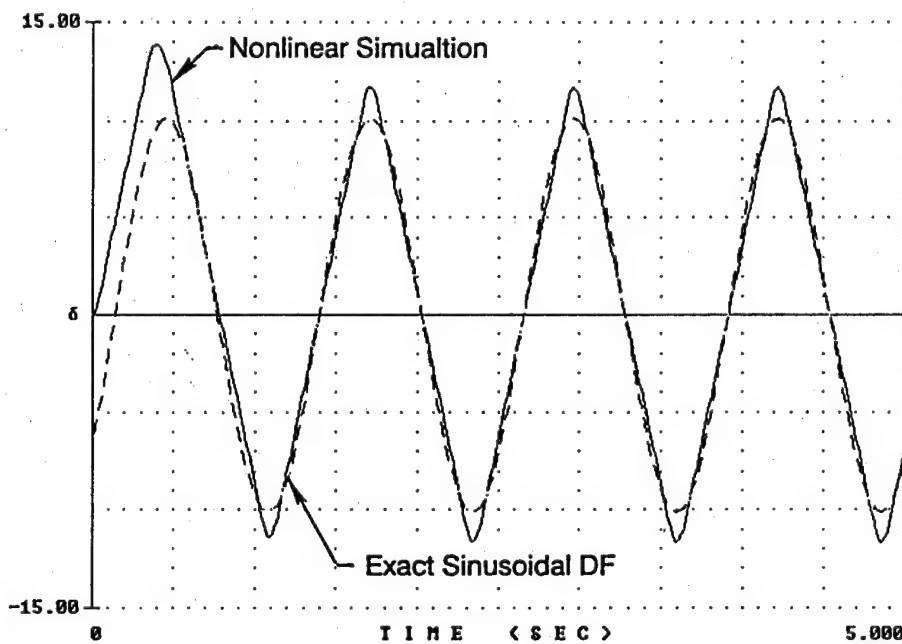


Figure 19. Exact Sinusoidal Describing Function Comparison with the Nonlinear Simulation

in the figure the describing function provides an exact phase match to the simulation result once the initial transient has passed. This exact phase match occurs because for a sinusoidal input, only the Fourier fundamental is required to completely define the input and output phase. That is, the higher harmonic terms all share the same phase with the fundamental. The magnitude, however, will in general not be matched unless the remnant harmonic terms are also included. In the Figure 19 example the describing function peak magnitude falls short of the true nonlinear magnitude by approximately 15%. For full saturation, when the output wave is triangular, the peak of the complete output will be simply $\pi^2/8$ that of the fundamental. It should be noted that the actual peak values of the output wave is irrelevant for stability analyses, whereas the fundamental is essential.

Equation 36 was evaluated numerically to generate the magnitude and phase curve families displayed in Figure 20. Both sets of curves are plotted as a function of a normalized frequency (ω/ω_a) and the linear to nonlinear time constant ratio (T/T_{NL}). Thus the two plots display the describing function magnitude and phase of the nonlinear system in terms of the actuator design parameters (V_L and ω_a) and the input parameters (A and ω_i), all known quantities. There are several observations to note from the plots. First, the $T/T_{NL} = 1$ curve represents the linear case. A second observation is that the more highly saturated cases are represented by the smaller time constant ratio curves; these curves depart from the linear curve at a normalized frequency that is equivalent to their time constant ratio. For example, the $T/T_{NL} = 0.1$ curve departs from the linear curve at a normalized frequency of 0.1.

Another more significant result is that known design and input parameters can be used to exactly³ identify the added phase lag due to a rate limiting actuator. The magnitude and phase plots of Figures 21a and 21b, respectively, represent the difference between the exact sinusoidal describing function and the linear system. As expected, the more highly saturated cases have larger phase differences. It should also be noted that since the maximum first order phase lag is minus 90°, $\Delta\phi \rightarrow 0$ for all of the curves as $\omega/\omega_a \rightarrow \infty$.

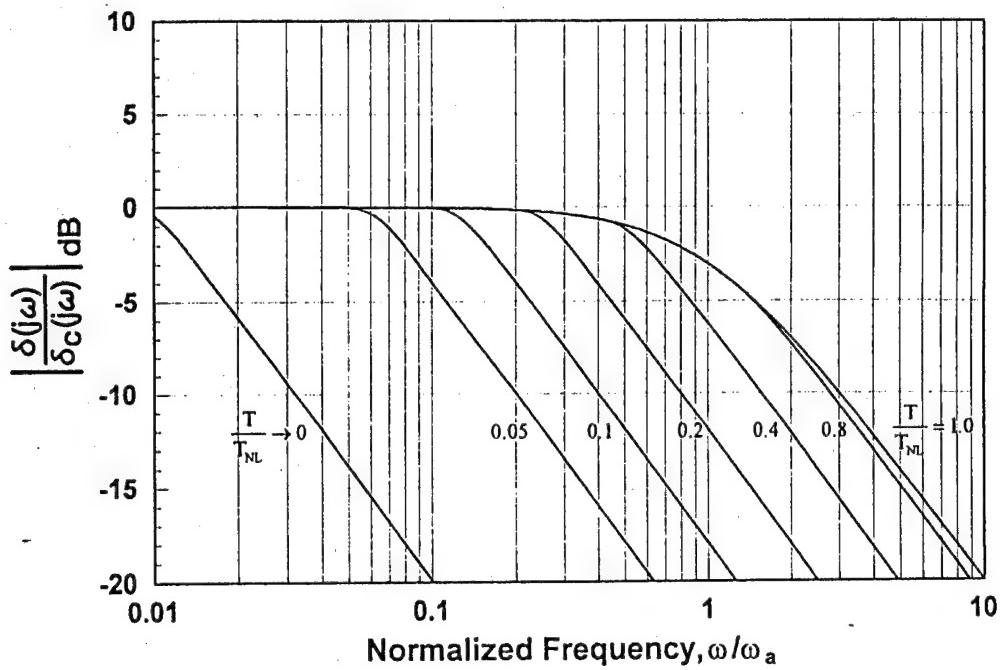
5. Nonlinear Bandwidth

A primary interest in the frequency responses of the describing functions is a search for a useful extension of the linear system bandwidth metrics to the nonlinear case. For the linear first order case the asymptotic breakpoint of $|\delta/\delta_c|$, ω_a , is a common linear system bandwidth metric. Equation 16 suggests that even the nonlinear cases can be characterized by a first order form. Thus ω_a becomes an obvious candidate for a nonlinear bandwidth metric. As shown in Figure 20a, the magnitude frequency response curves for the exact sinusoidal describing function display a "first order-like" character in that there is a distinct break frequency defined by the intersection of high (-20 dB/decade) and low (0 dB/decade) frequency asymptotes. This break frequency is near ω_a . From the figure it is also evident that ω_a decreases as T/T_{NL} decreases, and $\omega_a' = \omega_a$ for the $T/T_{NL} = 1$ (i.e., linear) case.

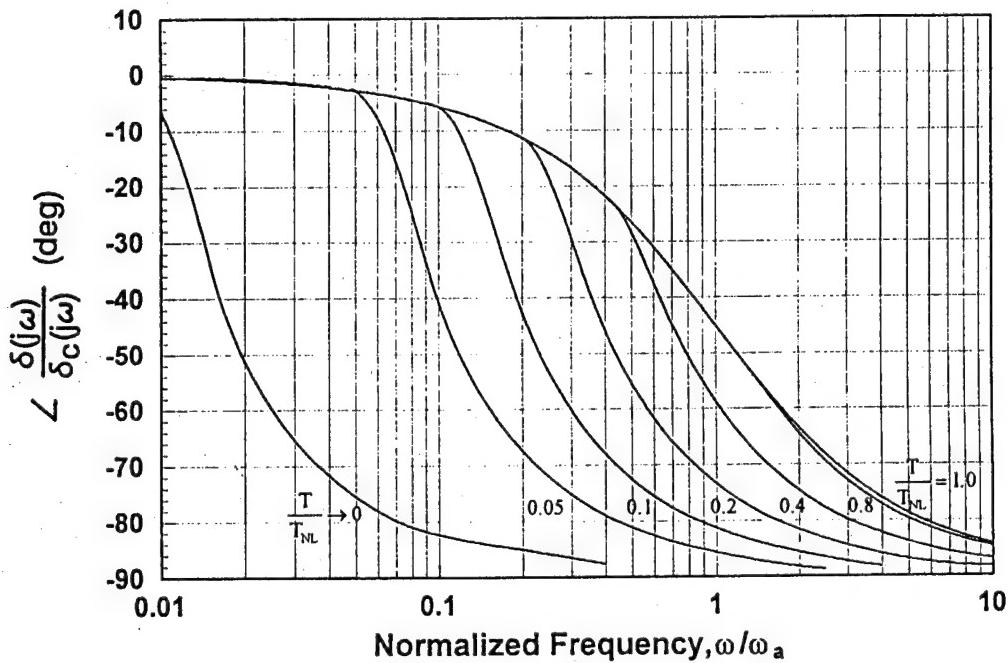
To obtain a literal rather than a graphical representation for the nonlinear bandwidth, the describing function approximations must be used. As stated earlier, however, the nonlinear magnitude responses of Eqns. 22a and 23a have "k/s-like" frequency responses that do not allow for a first order lag bandwidth to be defined. This occurs because Eqns. 22a and 23a are effectively high frequency approximations that are only valid for $\omega > \omega_s$. The corresponding nonlinear phase relations of Eqns. 22b and 23b do not, however, have the flat character of a "k/s-like" frequency response and thus do provide a basis for defining the nonlinear bandwidth.

In the following discussion approximations are given for the nonlinear closed-loop actuator bandwidth (ω_a') that are based on the previously developed sinusoidal input describing function

³ It is exact in relation to the system defined in Figure 5.

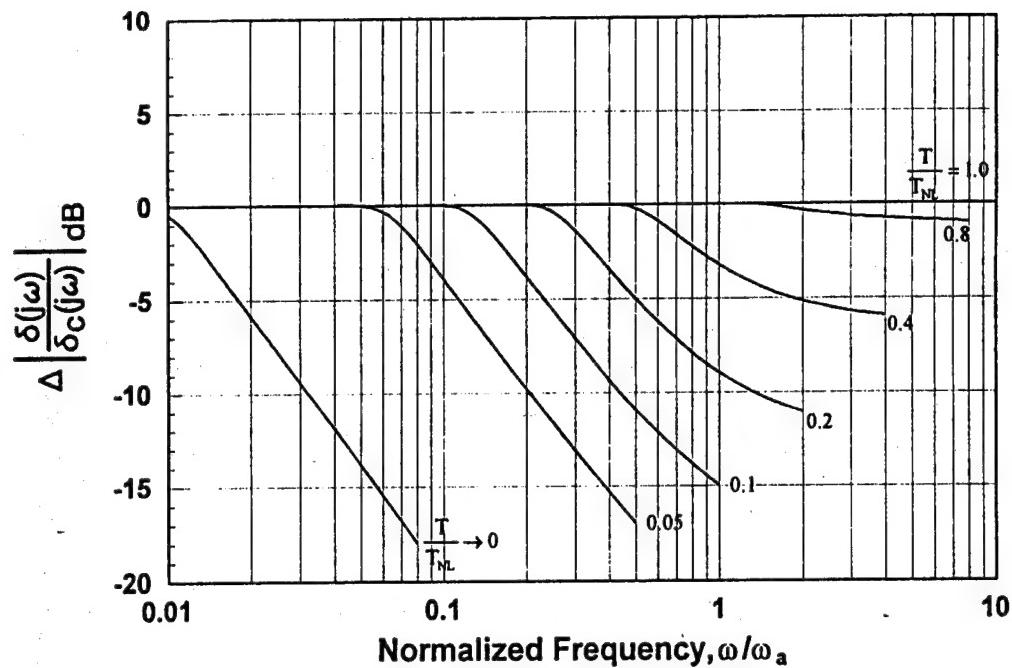


a) *Magnitude*

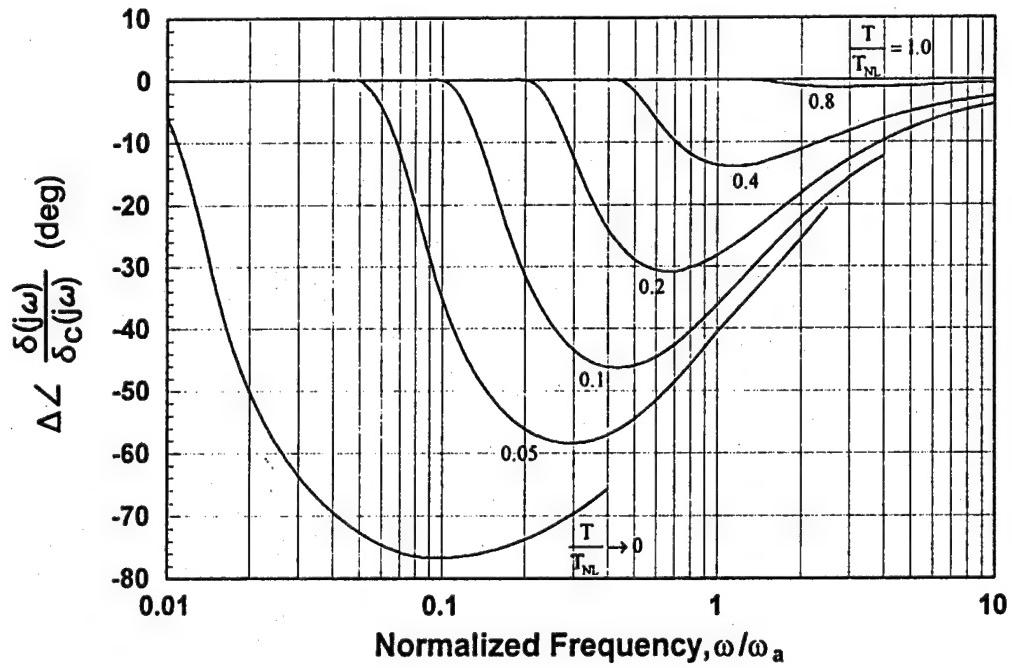


b) *Phase*

Figure 20. Exact Sinusoidal Describing Function Frequency Response



a) *Magnitude*



b) *Phase*

Figure 21. Frequency Response Difference Between the Exact Sinusoidal Describing Function and the Linear Response

approximations. As shown by Eqn. 8 the rate limited actuator is approximated in the highly saturated region by a first order system with a nonlinear bandwidth that was defined in Eqn. 15. This equation can be written in terms of the normalized frequency and the time constant ratio as shown by:

$$\frac{\omega_a}{\omega_a} = \frac{\omega / \omega_a}{\sqrt{\left(\frac{\pi}{4} \frac{T_{NL}}{T} \frac{\omega}{\omega_a}\right)^2 - 1}} \approx \frac{4}{\pi} \frac{T}{T_{NL}} \quad (38)$$

The simplified form of Eqn. 38 applies when the inverse of the time constant ratio (T_{NL}/T) is much greater than 1 ($T_{NL}/T \gg 1$). By applying the $\omega_a = 1/T$ identity to the simplified form of Eqn. 38, the nonlinear bandwidth is shown to be approximated by a constant with a value near 1 ($4/\pi = 1.273$) times the inverse of the nonlinear time constant. Thus in the highly saturated region, there is still an analogy to the linear case (i.e., $\omega_a \approx \frac{1}{\pi T_{NL}}$)

A similar result is obtained for the near saturation region case when the Eqn. 11 approximation is used to define the nonlinear bandwidth. This results in the following equation when the inverse of the time constant ratio approaches 1, $T_{NL}/T \rightarrow 1^+$:

$$\frac{\omega_a}{\omega_a} = \frac{\omega / \omega_a}{\sqrt{\left(\frac{T_{NL}}{T} \frac{\omega}{\omega_a}\right)^2 - 1}} \approx \frac{T}{T_{NL}} \text{ or } \omega_a = \frac{1}{T_{NL}} \quad (39)$$

Since $T_{NL}/T \approx 1$, the simplified form given in Eqn. 39 applies when $\omega/\omega_a \gg 1$. As shown by a review of the Figure 20a magnitude plot, this corresponds to near saturation cases that fall along the high frequency asymptote. By applying the $\omega_a = 1/T$ identity to the simplified form of Eqn. 39, the nonlinear bandwidth is shown to be approximated by the inverse of the nonlinear time constant. Thus, as expected in this region, there is a direct analogy to the linear case.

The saturation frequency defined in Eqn. 21 can also be written in terms of the nonlinear bandwidth as shown by the following:

$$\frac{\omega_s}{\omega_a} = \frac{1}{\sqrt{\left(\frac{T_{NL}}{T}\right)^2 - 1}} \frac{1}{\left(\omega_a / \omega_a\right)} \quad (40)$$

Since the highly saturated case is of most interest here, the simplified form of Eqn. 38 can be substituted into Eqn. 40 for $T_{NL}/T \gg 1$ to yield:

$$\frac{\omega_s}{\omega_a} = \frac{\pi}{4} \quad (41)$$

Thus when highly saturated, the nonlinear bandwidth is approximated by a constant factor of $4/\pi$ times the saturation frequency.

As described above the nonlinear actuator model displays a "first order-like" character. Thus the nonlinear bandwidth can be defined graphically in terms of classical first order system measures. In addition to the intersection of the high and low frequency asymptotes, these also include the frequency at a phase of -45° and at a magnitude of -3 dB. For a linear system these measures, of course, all yield the same bandwidth frequency. As shown in Figure 22, this is not the case for nonlinear systems. The

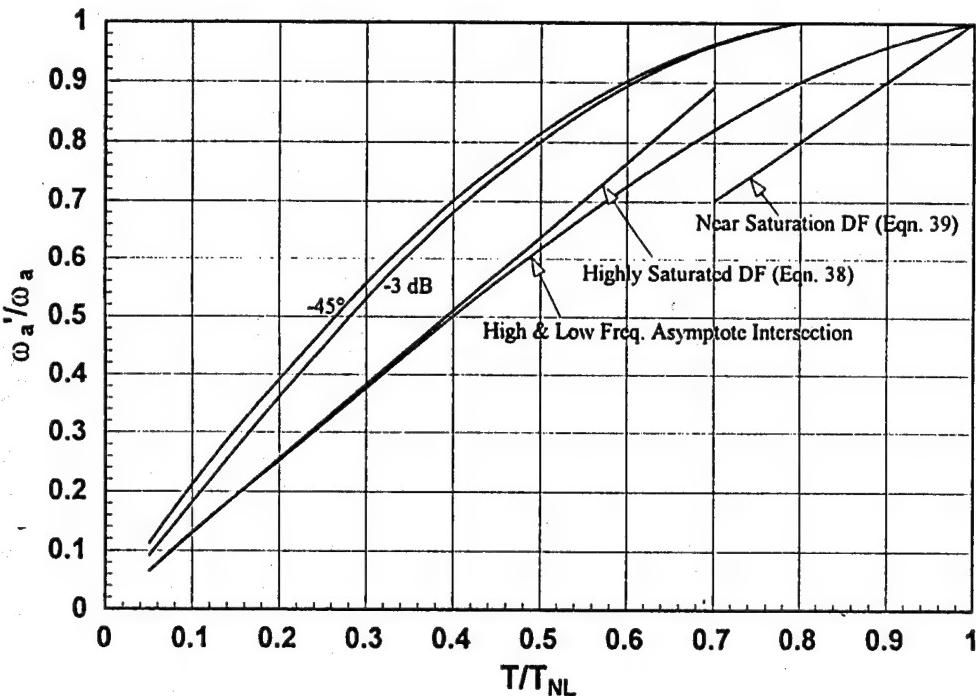


Figure 22. Nonlinear Bandwidth Variation

Figure 20 exact sinusoidal describing function plots were used to obtain the bandwidth frequencies as a function of T/T_{NL} for the above three measures. The resulting curves are shown in the figure along with the highly saturated and near saturation nonlinear bandwidth approximations of Eqns. 38 and 39. The figure reveals that the nonlinear bandwidths indicated by the -45° and -3 dB curves are nearly identical and larger than those indicated by the asymptote intersection curve. The figure also reveals that the nonlinear bandwidth approximations (Eqns. 38 and 39) bound the asymptote intersection curve. When the approximations are directly compared to the asymptote intersection curve, the highly saturated approximation provides an excellent match for $T/T_{NL} \leq 0.4$ and a good match for $0.4 < T/T_{NL} \leq 0.6$. The near saturation approximation, on the other hand, provides a reasonable match to the asymptote intersection curve for $T/T_{NL} \geq 0.9$. There may be some debate as to which curve appropriately defines the nonlinear bandwidth. Since the asymptote intersection yields a lower frequency, it is the conservative case. Thus in the appropriate T/T_{NL} regions the approximations can be used to attain a conservative estimate of the nonlinear bandwidth.

D. ANALYSIS OF CATEGORY II SITUATIONS

The approximate and exact describing functions for rate limiting developed above provide a complete tool kit for the analysis of Category II PIOs. Their use will be illustrated below in a series of examples beginning with the simple and proceeding to more complex situations. For the simplest example the open-loop linear system transfer characteristic, $K e^{-Ts}/s$, will again be used. This simultaneously serves as a specific elementary idealized controlled element with synchronous pilot control, as a generalized compensatory system that obeys the crossover model, and is a common thread throughout this study.

For more complex examples a database for series rate limiting similar to that of Ref. 57 would be desired. Unfortunately this does not yet exist. There are, however, a few single point examples. One in particular is the landing/flare PIO experienced on the first flight of the X-15. Because a sufficient data set exists for this vehicle, it will serve as the basis for a variety of Category II case studies.

The theme from simple to complex parallels the range of describing functions from elementary series rate limiting through to the most complete and exact simulation-based describing functions.

I. Analytical Preliminaries and X-15 Case Study Data

a. Inverse Describing Function Techniques

A key motivation for developing the describing functions (approximate and exact) defined above is to predict closed-loop limit cycles (Ref. 4) referred to here as Category II PIOs. A synchronous pilot longitudinal closed-loop system with a rate limited actuator nonlinear element in series with linear elements is given in Figure 23. As discussed earlier, when sinusoidal inputs appear in pilot-vehicle systems, a pilot can essentially duplicate the sinusoid with no phase lag up to frequencies of about 3 Hz (about 20 rad/sec). Thus, as shown in the block diagram, the pilot can be represented by a pure gain (K_p). The criterion for a neutrally damped oscillation is simply that the open-loop amplitude ratio is 1.0 (0 dB) and the phase is -180° . For an oscillation to persist in the Figure 23 example, the synchronous pilot system with a series nonlinear element(s) must satisfy the following equation:

$$G(j\omega)N(j\omega, A) = -1 \quad (42a)$$

or

$$G(j\omega) = \frac{-1}{N(j\omega, A)} \quad (42b)$$

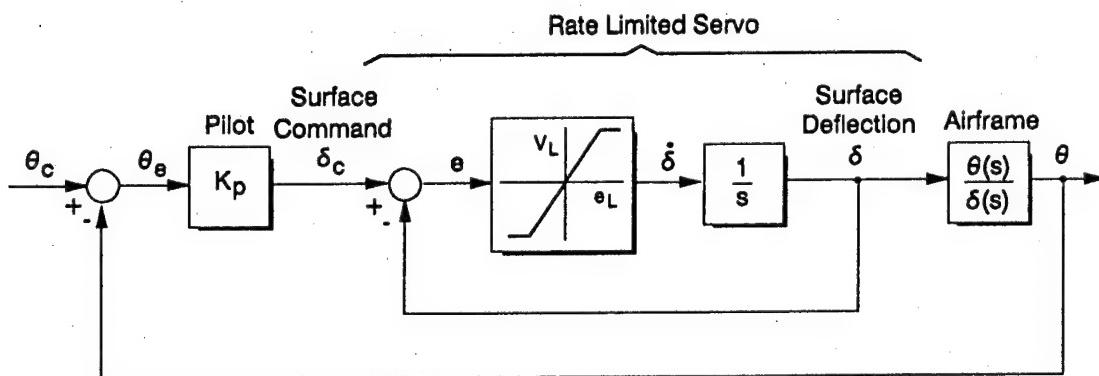


Figure 23. Synchronous Pilot Closed-Loop System

In the equation $G(j\omega)$ represents the frequency dependent linear elements (K_p and θ/δ in Fig. 23) and $N(j\omega, A)$ represents the frequency and amplitude dependent nonlinear element(s) (the describing function δ/δ_c in Fig. 23).

A simple analysis technique is possible when the describing function can be separated from the linear elements as in the Figure 23 example. First, the negative inverse describing function (i.e., the right hand side of Eqn. 42b) is plotted on a standard Nichols or gain-phase chart. The linear portion (i.e., the left hand side of Eqn. 42b) is then plotted. An intersection of the two curves satisfies Eqn. 42b and provides the frequency and amplitude of the limit cycle.

The most straightforward version of this kind of analysis for rate limiting conditions applies for series command rate limiters or single effectors where $\omega_a \gg \omega_u$, since the nonlinearity is only a function of K' . In this case the inverse describing function magnitude and phase are defined from Eqns. 29 and 34, respectively. The Nichols chart plot for this case is shown in Figure 24. Once again, the limit cycle frequency is defined by an intersection of the linear transfer function with the Figure 24 curve.

When ω_a is not necessarily much larger than ω_u , a more elaborate procedure is required. In Figure 25 the inverse exact sinusoidal describing function curves are plotted on a Nichols chart for various time constant ratios. It should be noted that each curve is a function of amplitude (δ_c / V_L), time constant ratio (T/T_{NL}), and normalized frequency (ω/ω_a) as indicated on the plots. (It should be noted that $\dot{\delta}_c = A\omega$.) Thus to find the appropriate intersection, the normalized limit cycle frequency, defined by the linear transfer function, must match the normalized frequency of the inverse describing function. The details of applying these methods are illustrated by the examples below.

b. X-15 Data for the Case Studies

The X-15 landing/flare PIO occurred on 8 June 1959 with pilot Scott Crossfield. This first flight (designated as Flight 1-1-5) was an unpowered glide flown with the side-located controller and pitch damper off. Additional details of the flight and subsequent changes to the aircraft are provided in Ref. 3. As shown in the flare time history traces of Figure 26, severe longitudinal oscillations developed near the end of the flap cycle and rate limiting is clearly evident in the horizontal stabilizer angle (δ_h) trace. The "triangle-wave" response of the δ_h time trace in the PIO region indicates that the actuator was operating in the highly saturated region. From the pitch rate (q) trace, a PIO frequency of approximately 3.3 rad/sec is estimated. For this flight the control surface rate was limited to 15 deg/sec.

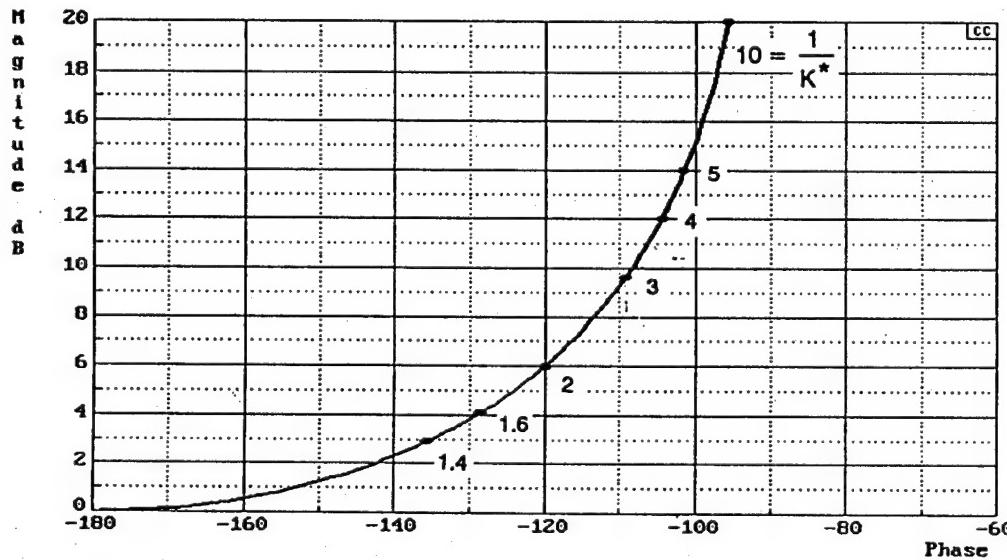
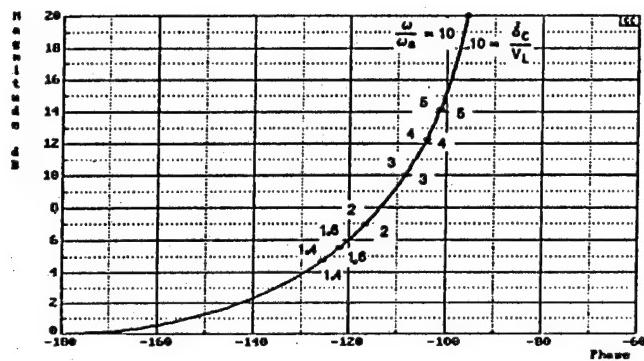
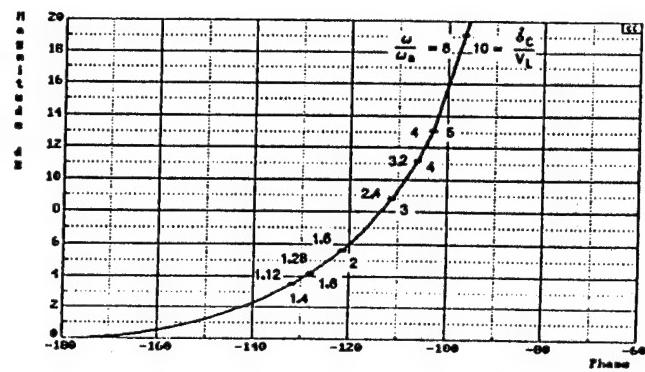


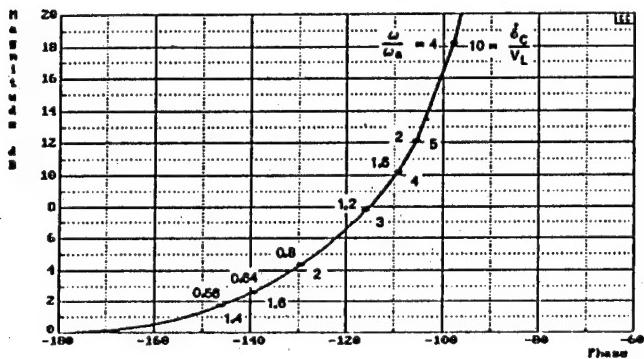
Figure 24. Sinusoidal Input/Triangle Output Inverse Describing Function



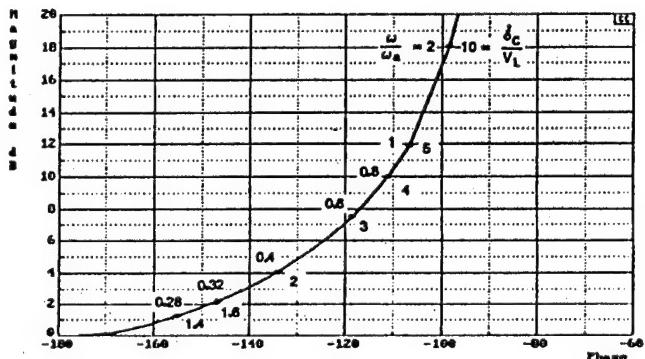
$$a) \frac{T}{T_{NL}} = 1.0$$



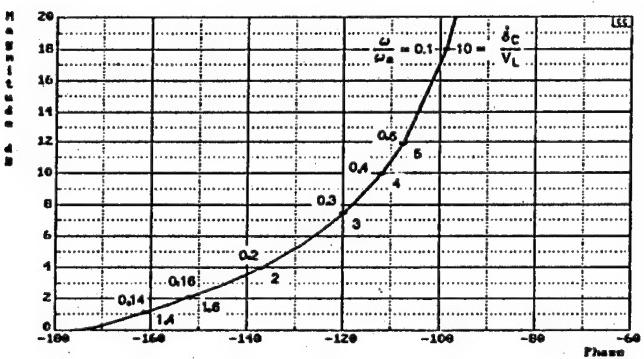
$$b) \frac{T}{T_{NL}} = 0.8$$



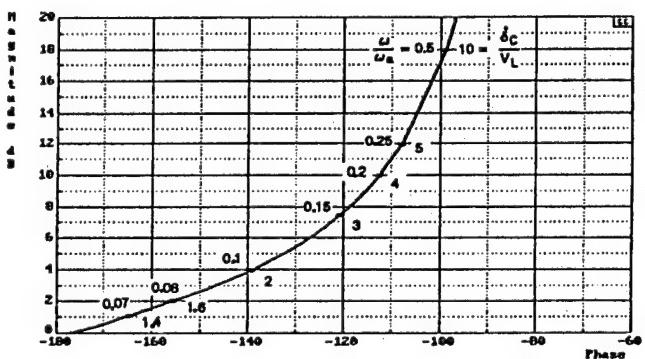
$$c) \frac{T}{T_{NL}} = 0.4$$



$$d) \frac{T}{T_{NL}} = 0.2$$



$$e) \frac{T}{T_{NL}} = 0.1$$



$$f) \frac{T}{T_{NL}} = 0.05$$

Figure 25. Exact Sinusoidal Inverse Describing Function

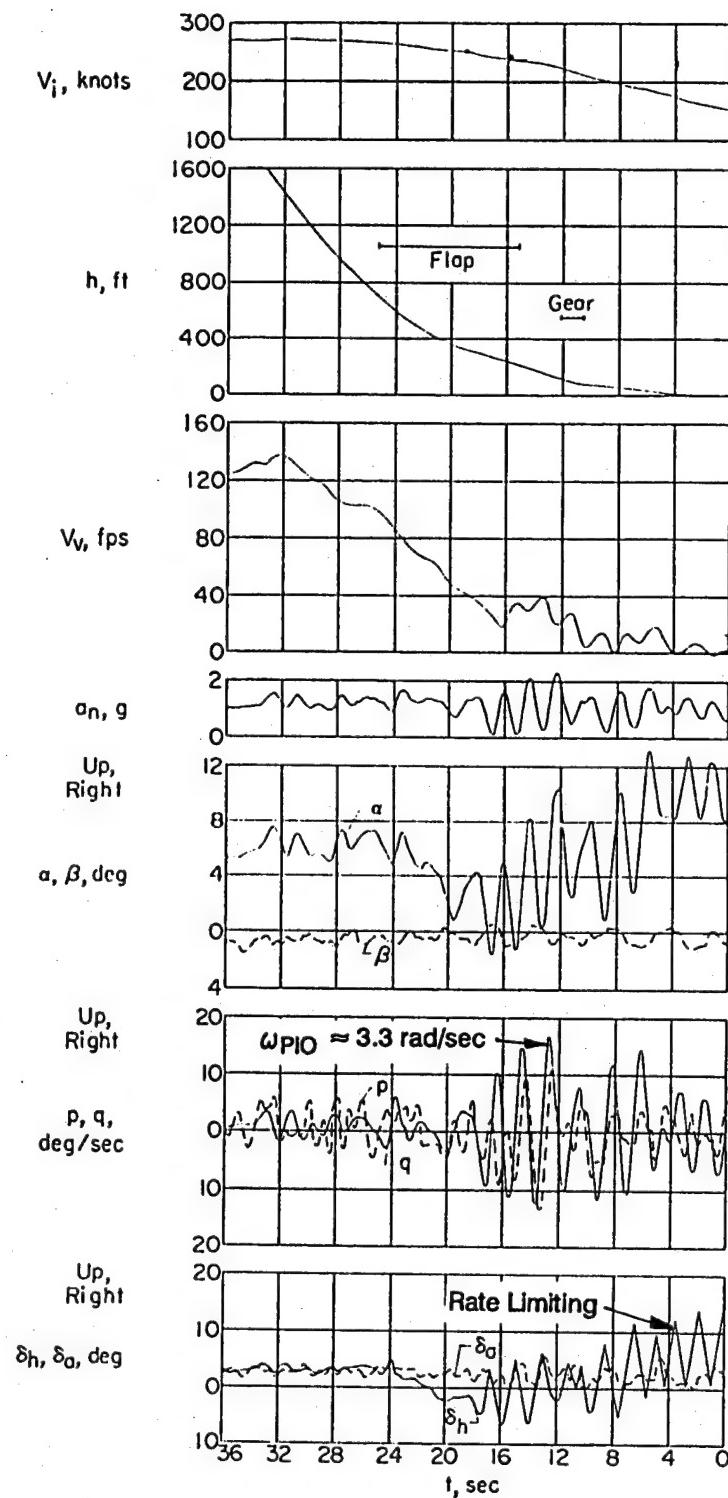


Figure 26. Time History of the Landing Flare on X-15 Flight 1-1-5
(from Ref. 5)

Since the PIO occurred with the pitch SAS off, the X-15 bare airframe data of Ref. 60 could be used to generate relevant longitudinal transfer functions. Corrections to the Ref. 60 data were made to accommodate the PIO flight condition and aircraft weight. A first order model for the horizontal stabilizer actuator ($\omega_a = 25$ rad/sec) was obtained from Ref. 61. Using these data the Bode and Nichols frequency response survey of Figure 27 for the θ/δ_h transfer function was generated. It should be noted that the transfer function gain was arbitrarily set so that the frequency response would pass through 0 dB at -110° of phase. Several key Category I PIO indicators (e.g., bandwidth frequency, phase delay, and average phase rate) are identified on the plots, while a more complete accounting of these indicators is given in Appendix B. As indicated in Table B1 of Appendix B, not only do all of the applied Category I criteria indicate that the X-15 would not be susceptible to PIO but also the aircraft was found to be Level 1 for most of the applied handling qualities measures. Figure 27 also indicates that the instability frequency for the linear system with a synchronous pilot loop closure is 5.31 rad/sec. This is almost twice that of the observed PIO frequency of 3.3 rad/sec.

2. Elementary Series Rate Limiting

a. Analysis for Elementary $Y_c = K_c e^{-ts}/s$ or for the Crossover Model

The simplest situation occurs with the insertion of a rate limiter into the pilot's command path in a pilot-vehicle system that is basically single-input, single-output in nature (i.e., *Series Command Rate Limiter Dominant* in Table 3). In this case the limiter describing function is simply inserted in series with the open-loop describing functions of the pilot and the effective vehicle dynamics. As developed in Ref. 59 and described in the preceding section, a sinusoidal input/triangular output describing function for the limiter is,

$$N_{RL} = K^* e^{-j\phi(K^*)} \quad (43)$$

where $K^* = (\text{triangular output peak amplitude})/(\text{peak amplitude of the input sinusoid})$ and the phase lag $\phi(K^*)$ is $\cos^{-1}(K^*)$. Note that, in terms of the usual sinusoidal input describing function the amplitude ratio K^* must be multiplied by $8/\pi^2$ to convert from the triangular wave of the output to the fundamental. Thus, in this simplest of rate-limited situations, the pilot and effective vehicle dynamics have the same quasi-linear forms as for Category I PIOS, but the results become amplitude sensitive due to the rate limit. A PIO analysis thus yields both an estimate for PIO frequency, as with Category I, and an amplitude.

The same description also applies to the second entry in Table 3, *Single Effector Rate Limiting*, when the effector actuator bandwidth is much larger than the PIO frequency ($\omega_a \gg \omega_u$).

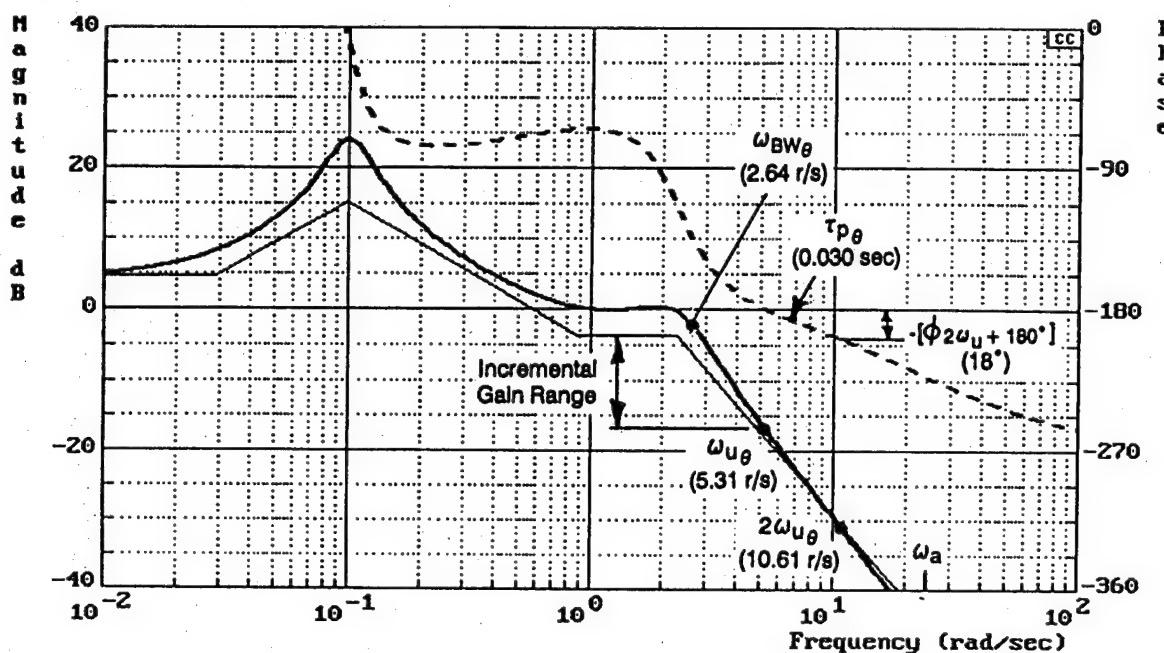
As a simple illustration we will again use the idealized rate-command effective vehicle dynamics of Eqn. 8, and assume that the pilot dynamics are synchronous. The phase angle then becomes:

$$\phi = -\pi/2 - \omega\tau - \cos^{-1}(K^*) \quad (44)$$

For neutral stability the phase angle, $\phi = -\pi$. The condition for a limit cycle then becomes:

$$K^* = \cos\left(\frac{\pi}{2} - \tau\omega_u\right) \quad (45a)$$

$$\text{or, } \tau\omega_u = \sin^{-1}(K^*) \quad (45b)$$



$$\frac{\theta}{\delta} = \frac{86.9 (.0292)(.883)}{[.19, .1][.366, 2.3](25)}$$

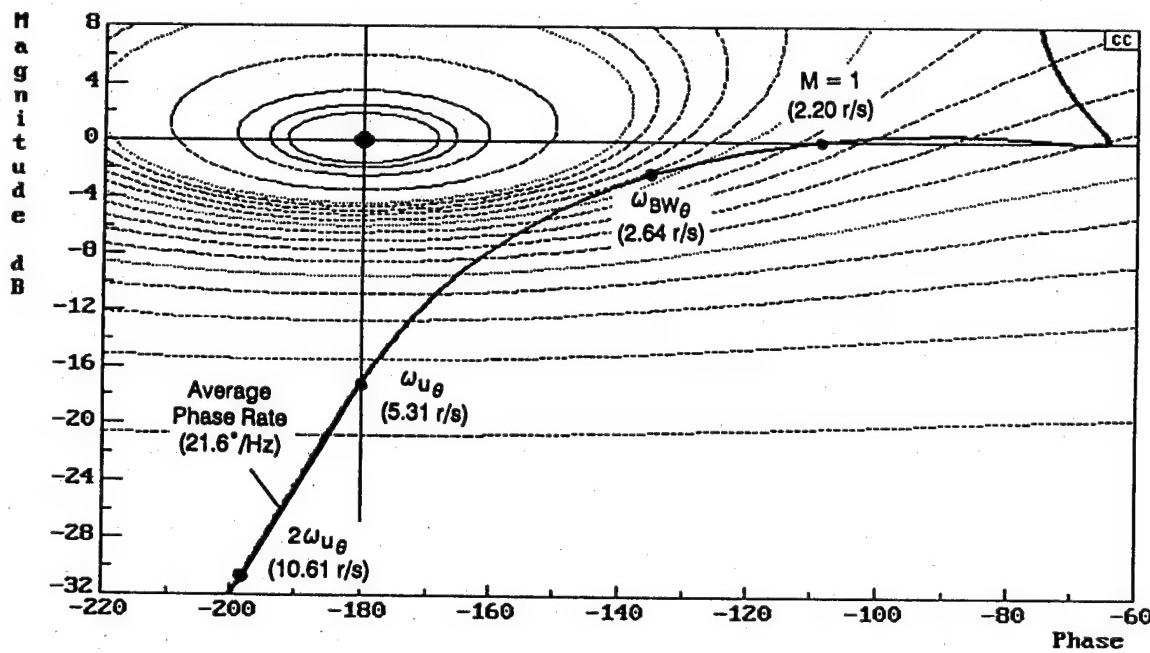


Figure 27. X-15 Pitch Attitude (θ/δ) Frequency Response at the Flight 1-1-5 Landing Flare Condition

This relationship is shown in Figure 28. The limit cycle amplitude is represented by the amplitude ratio K^* , and the frequency is normalized by the effective time delay τ . Equation 45 reduces to the linear system result for $K^* = 1$.

The conditions for a Category I PIO are given by the following:

$$\tau \omega_{u_{\text{linear}}} = \frac{\pi}{2} \quad (46)$$

The ratio of nonlinear Category II to linear Category I is therefore:

$$\frac{\omega_{u_{\text{nonlinear}}}}{\omega_{u_{\text{linear}}}} = \frac{\sin^{-1}(K^*)}{\pi/2} \quad (47)$$

There is thus a monotonic decrease in PIO frequency as rate limiting becomes more severe. Because the rate limiting describing function is $8K^*/\pi^2$, the pilot gain (K_p) must increase as

$$K_{p_u} = \frac{\pi^2}{8K_c K^*} \quad (48)$$

in order to create an oscillation. For example if $K^* = \sqrt{2}/2$,

$$\frac{\omega_{u_{\text{nonlinear}}}}{\omega_{u_{\text{linear}}}} = \frac{1}{2} \quad (49a)$$

and

$$\frac{K_{p_{u_{\text{nonlinear}}}}}{K_{p_{u_{\text{linear}}}}} = \frac{1}{K^*} = \frac{2}{\sqrt{2}} = 3 \text{ dB} \quad (49b)$$

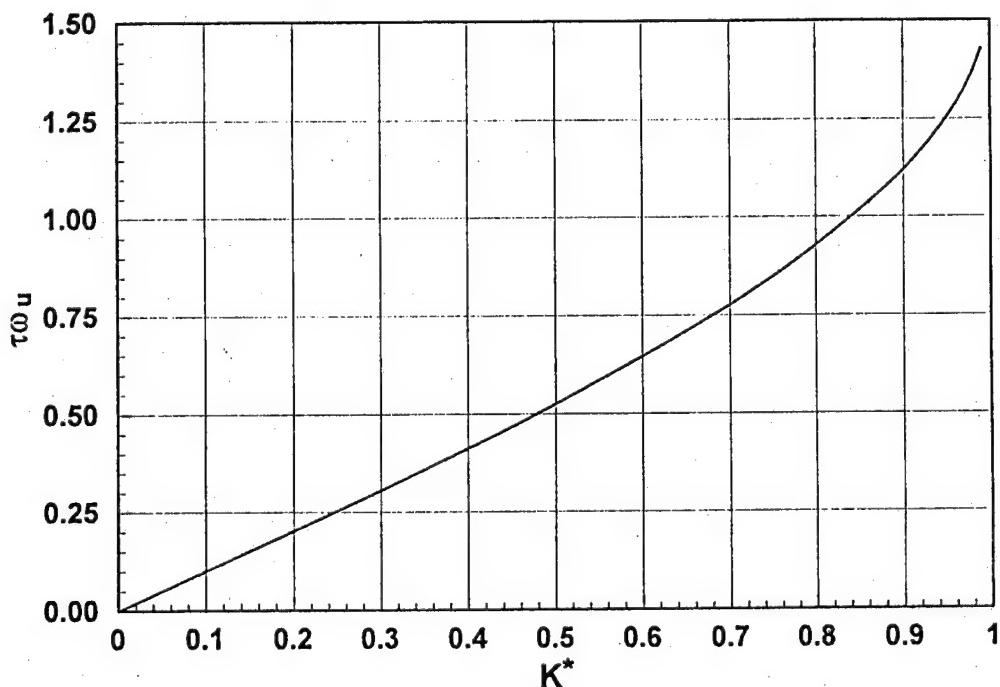


Figure 28. Normalized Limit Cycle Frequency for Elementary Series Rate Limiting

The system for this example, as described, comprises a synchronous pilot and idealized rate control vehicle attitude dynamics. It also applies to the much more general situation of compensatory operations as approximated by the crossover model when the effective time delay is modified to reflect both the pilot and the effective vehicle properties.

b. Analysis for X-15 Example

Inverse describing function techniques are used for single effector series nonlinearities to predict limit cycle frequencies and associated added phase lags and magnitude reductions. The X-15 example will be used here to demonstrate the technique. As mentioned above, the sinusoidal input/triangle output describing function applies for series rate limiting elements and for cases where the effector actuator bandwidth is much larger than the PIO frequency. Because this describing function is only a function of K , a significant simplification exists when one of the these conditions is met. The X-15 has a 25 rad/sec actuator bandwidth, so it is reasonable to assume that this frequency will be significantly larger than limit cycle frequencies that, as discussed earlier, typically vary from 1.4 to 8 rad/sec.

Figure 24 displays the sinusoidal input/triangle output inverse describing function on a Nichols chart with specific values of $1/K$ called out. To determine the limit cycle frequency, the gain of the bare airframe X-15 transfer function is adjusted (this assumes a synchronous pilot model) until the curve is just tangent with the inverse describing function curve. The end result is shown in Figure 29. At the tangency point a limit cycle frequency of 2.73 rad/sec is identified. This is within 20% of the actual PIO frequency (as compared to 60% for the previous linear analysis), and clearly demonstrates that the rate limiting effects are in the right direction. At the tangency point the nonlinearity provides an added phase lag of -47° and a magnitude reduction of -3.3 dB. This process is easily automated with control system software analysis programs such as Program CCTM or MatlabTM.

To provide additional insight, an effective aircraft transfer function at (or near) the PIO condition is developed. The added phase lag and limit cycle frequency are first used to define a first order lag representing the rate limited actuator. Then this lag is combined with the bare airframe X-15 dynamics to define a new effective vehicle. A Bode frequency response for the "new" vehicle is shown in Figure 30. When this response is compared with the linear response of Figure 27, there is significant reduction in bandwidth, a large increase in phase delay, and the unstable frequency is, as expected, equal to the limit cycle frequency.

3. *Single Effector Rate Limiting with Finite Actuator Bandwidth*

a. Analysis Issues

For the third entry in Table 3 the rate limiter is contained within the actuator closed-loop system and, unlike the second entry, the actuator bandwidth is not necessarily very large compared with the PIO frequency. This situation corresponds to conventional primary aircraft controls in which mechanical linkages or cables are connected to fully-powered surface actuating systems. It also applies to fly-by-wire flight controls if the first rate limits to appear are those intrinsic to the actuator. Rate limiting in actuators is much more complicated than the simpler rate limiting considered above. Instead of merely changing the amplitude ratio and phase lag in series with the pilot and effective vehicle dynamics, the actuator bandwidth is also affected.

b. Analysis for X-15 Example

Inverse describing function techniques are again used for single effector with finite bandwidth series nonlinearities to predict limit cycle frequencies and associated added phase lags and magnitude

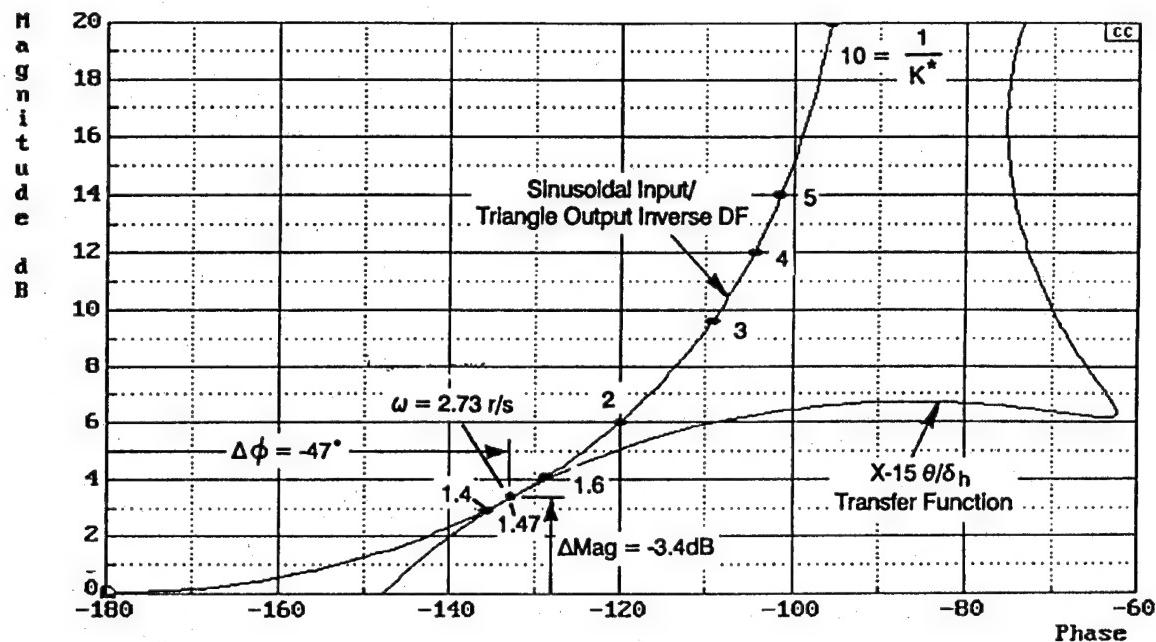


Figure 29. Limit Cycle Frequency Identification Using the Sinusoidal Input/Triangle Output Inverse Describing Function with the X-15 Example Case.

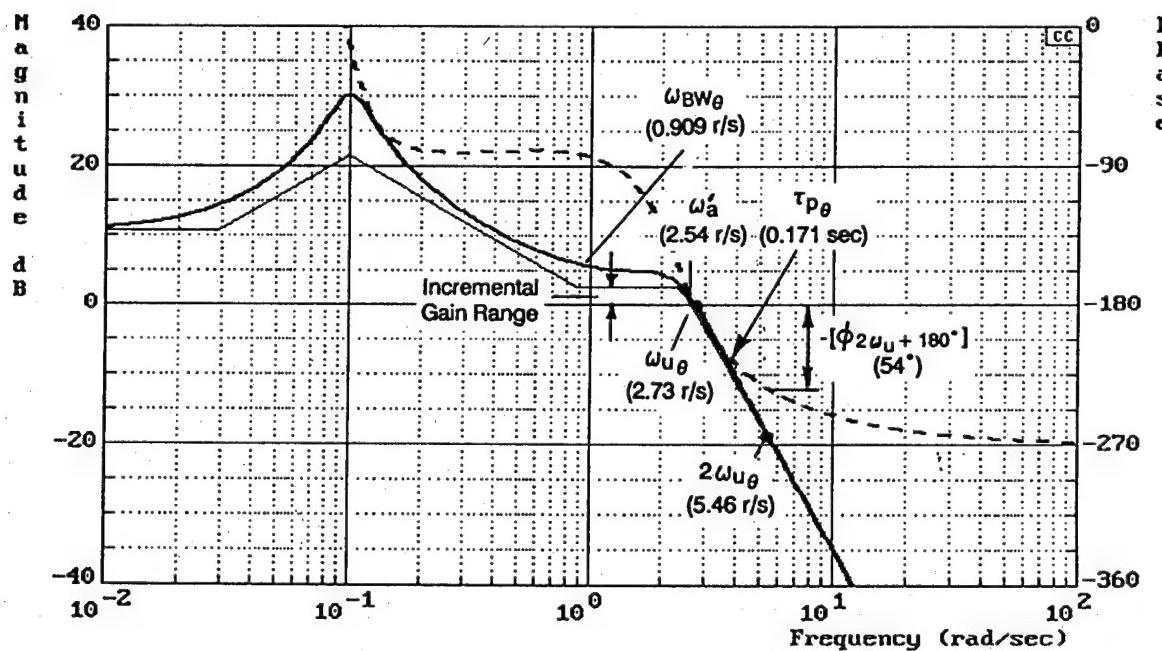


Figure 30. Frequency Response Bode Plot of the X-15 Example Case with First Order Lag Representation of Single Effector Rate Limiting

reductions. As discussed earlier, there is an added complication for the finite bandwidth case, however, in that the inverse describing function is a function of not only amplitude but also the normalized frequency and time constant ratio (see Figure 25). Several describing functions were defined earlier in this section to represent series effector rate limiting finite bandwidth. To recap, the most accurate representation of the nonlinearity is attained with the exact sinusoidal input describing function. This describing function, however, has to be evaluated numerically (this is a simple chore once the describing function is mechanized in a simulation model). More direct results can be obtained with the literal describing function approximations. In this example, the exact sinusoidal describing function will be used first, and then the procedure will be repeated with the appropriate describing function approximation as determined by the time constant ratio.

The X-15 example is again used to demonstrate the technique. For the previous analysis example it was assumed that the linear 25 rad/sec actuator bandwidth of the X-15 was significantly larger than the limit cycle frequency. This assumption reduced the problem to a single curve that was only a function of amplitude (K'). For the current example the methods apply regardless of the linear actuator bandwidth. The first step is to identify the normalized frequency variation on a Nichols chart for the θ/δ_h transfer function. To accommodate possible intersections with the inverse describing function, it is only necessary to identify normalized frequencies for phase angles less than -90° as shown in Figure 31. These normalized frequencies correspond most closely to the $T/T_{NL} = 0.05$ curve from Figure 25. To determine the limit cycle frequency, the gain of the X-15 transfer function is adjusted until the curve is just tangent with the inverse describing function curve. The end result is shown in Figure 32. At the tangent point a limit cycle frequency of 2.74 rad/sec is identified via the linear transfer function and corresponding values of added phase lag (-46°) and magnitude reduction (-4.8 dB) are read from the plot.

To provide a transfer function interpretation of the oscillatory system, a first order lag is again defined to represent the rate limiting actuator and this lag is then combined with the bare airframe X-15 dynamics to define a new effective vehicle. A Bode frequency response for this vehicle is shown in Figure 33. As was the case in the previous analysis example, there is a significant reduction in bandwidth, a large increase in phase delay, and the unstable frequency is, as intended, equal to the limit cycle frequency.

The literal describing function approximations can also be used to estimate the limit cycle frequency. These describing functions are referred to as approximations since various simplifications were made to develop the literal representations of the finite bandwidth series effector. As identified earlier, the sinusoidal input/triangle output finite bandwidth describing function approximation (i.e., Eqn. 35) should be applied to a $T/T_{NL} = 0.05$ case. The only difference between the Eqn. 35 form of this describing function and the form used in the previous example is that the magnitude has been modified by the $\pi^2/8$ factor. As discussed earlier the inclusion of this factor defines the magnitude response in terms of the Fourier fundamental. Following the same procedures outlined for the exact sinusoidal inverse describing function results in a limit cycle frequency of 2.73 rad/sec, an added phase lag of -47° , and a magnitude reduction of -5.2 dB as identified in Figure 34. A summary of the results obtained with the three inverse describing function methods is provided below.

4. Category II X-15 Analysis Summary

In the previous analysis examples, three inverse describing function methods were used to estimate an initial limit cycle frequency for the X-15 PIO condition. In Table 4 the results of the three methods are compared with a nonlinear simulation result. Since the nonlinear simulation can not be used to directly determine the initial limit cycle frequency, the value attained via the exact sinusoidal input describing function was used to set the simulation input sine wave frequency. Two of the three parameters listed in Table 4, the limit cycle frequency and the added phase lag, are in clear agreement for

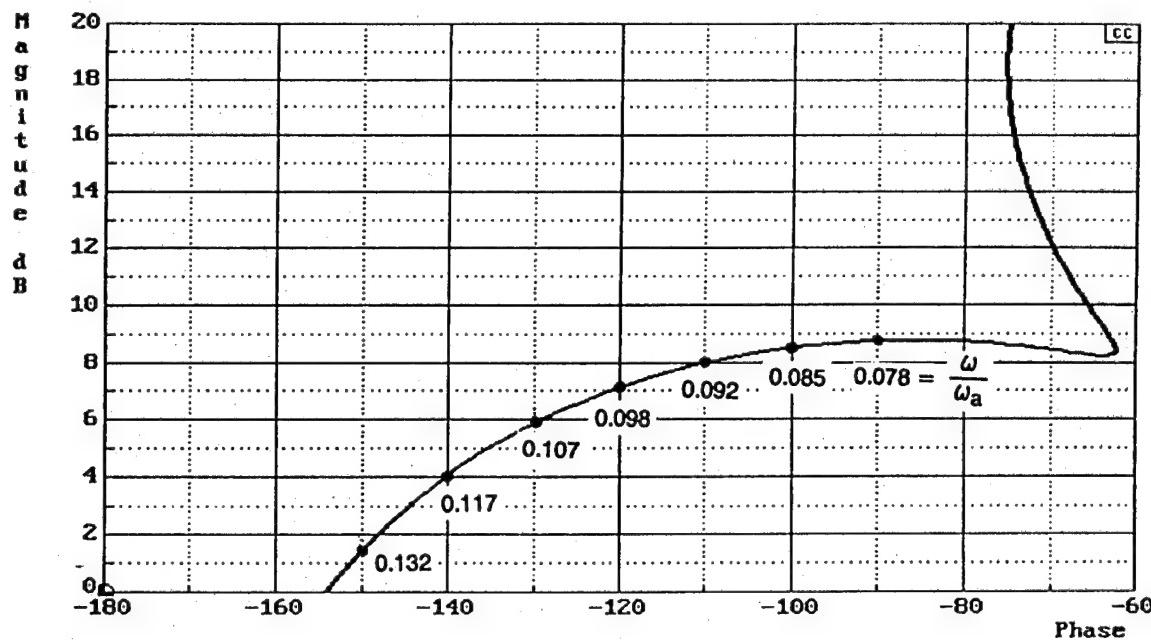


Figure 31. Normalized Frequency Variation for the X-15 θ/δ_h Transfer Function

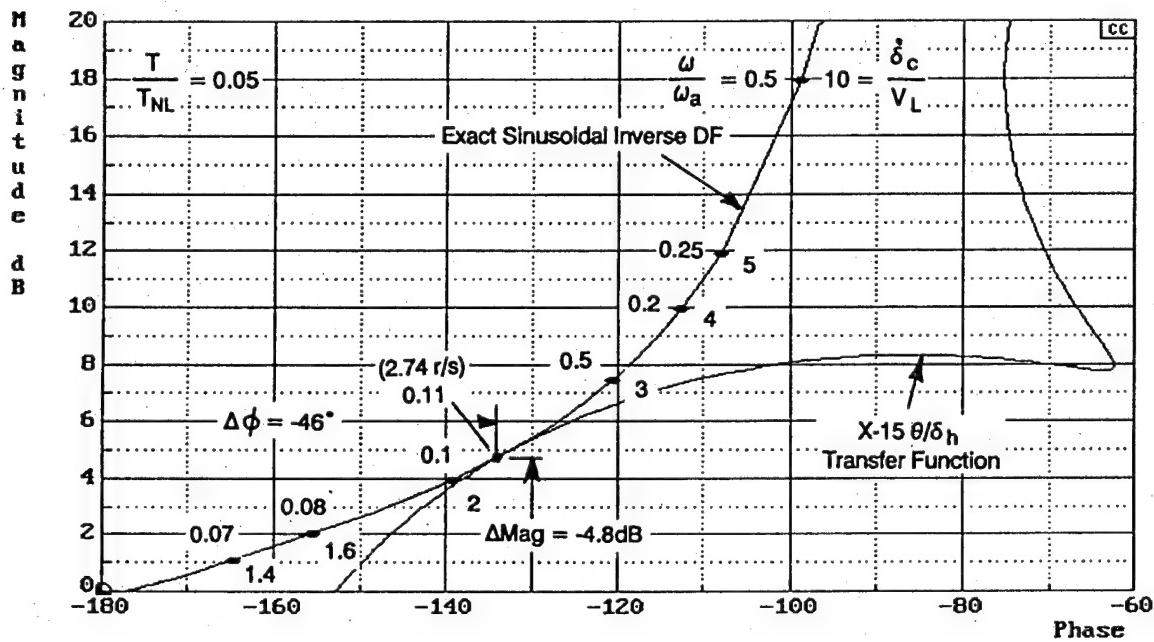


Figure 32. Limit Cycle Frequency Identification Using the Exact Sinusoidal Inverse Describing Function with the X-15 Example Case

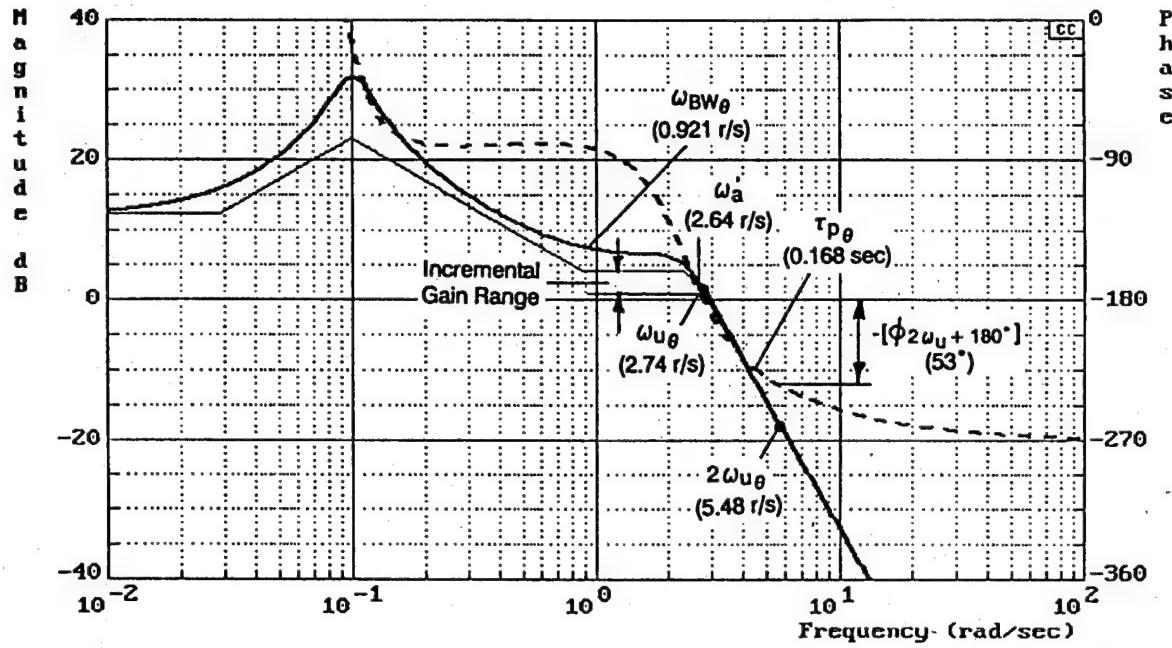


Figure 33. Frequency Response Bode Plot of the X-15 Example Case with First Order Lag Representation of Single Effector Rate Limiting with Finite Bandwidth

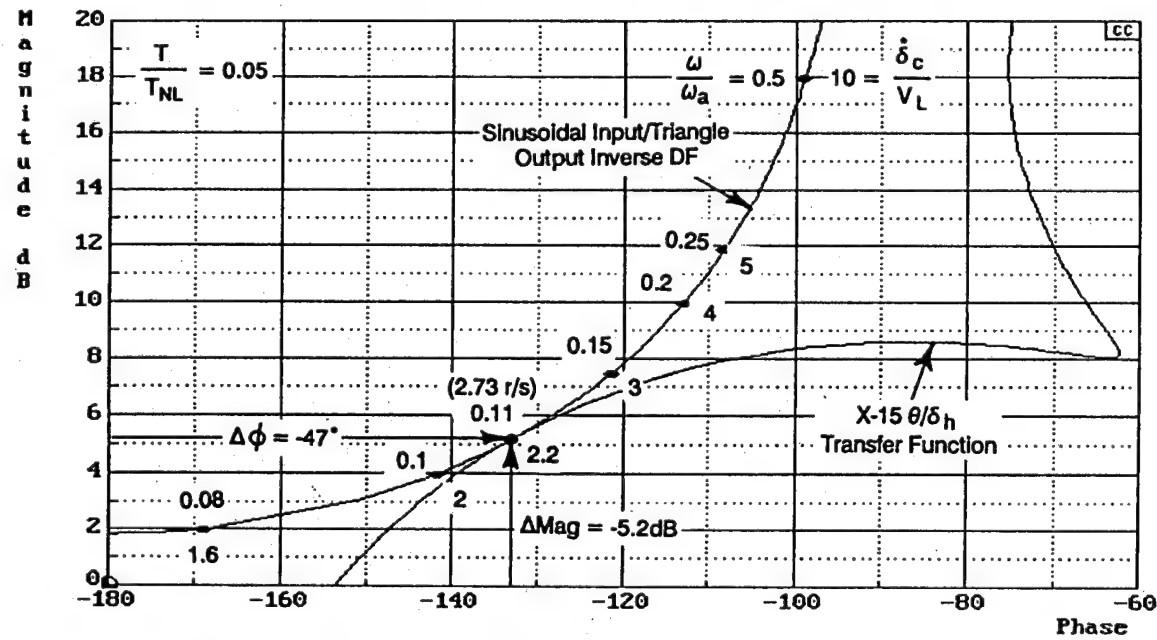


Figure 34. Limit Cycle Frequency Identification Using the Sinusoidal Input/Triangle Output Finite Bandwidth Inverse Describing Function Approximation with the X-15 Example Case

this example. This is not a surprising result when several factors are taken into account. First, the assumption that $\omega_a \gg \omega_{PIO}$ was clearly valid for this case. Thus the single effector rate limiting method based on the sinusoidal input/triangle output rate limiting element describing function could be confidently applied. Second, the exact describing function method provides by definition an accurate representation for any series effector rate limiting case with finite bandwidth. Finally, Figure 17 indicates that the sinusoidal input/triangle output describing function approximation provides an excellent match to the nonlinear result for the finite bandwidth $T/T_{NL} = 0.05$ curve.

There are, however, differing results in the estimated magnitude reductions due to the rate limiting. The sinusoidal input/triangle output describing function magnitude is defined in terms of the peak magnitude of the triangle wave. The exact sinusoidal input describing function magnitude, on the other hand, is defined by an exact computation of the Fourier fundamental for the finite bandwidth case. From previous discussions it was stated that the only difference between finite the bandwidth sinusoidal input/triangle output describing function result and the result obtained with the single effector rate limiting method is the $\pi^2/8$ factor. This difference is reflected in Table 4 (i.e., $\pi^2/8 \cdot 0.55 = 0.68$). Since only the limit cycle frequency and the added phase lag are used to define the first order lag representation of the rate limiting element, these magnitude differences do not enter into the determination of PIO susceptibility.

TABLE 4. INVERSE DESCRIBING FUNCTION RESULTS

Method	ω_{PIO} (rad/sec)	$\Delta\phi$ (deg)	Δ Magnitude (dB)
Nonlinear Simulation	2.74	-46	-3.1
<u>Single Effector Rate Limiting</u> Sinusoidal Input/Triangle Output Describing Function (Fig. 29)	2.73	-47	-3.4 (0.68)
<u>Single Effector Rate Limiting</u> <u>with Finite Bandwidth</u> Exact Sinusoidal Input Describing Function (Fig. 32)	2.74	-46	-4.8 (0.58)
<u>Single Effector Rate Limiting</u> <u>with Finite Bandwidth</u> Sinusoidal Input/Triangle Output Describing Function Approximation (Fig. 34)	2.73	-47	-5.2 (0.55)

5. Increasing Pilot Gain

Inverse describing function analysis provides a limit cycle frequency at the point of tangency. As the pilot gain is increased beyond this point, several intersections can occur as shown in Figure 35, however, only the intersections that result in stable limit cycles (i.e., sustained oscillations) are of interest when evaluating PIO susceptibility. The question then arises as to how to determine the stability at the point of intersection. (A complete discussion of limit cycle stability is provided in Ref. 44.) First, identify the direction of increasing frequency on the linear transfer function and increasing amplitude on

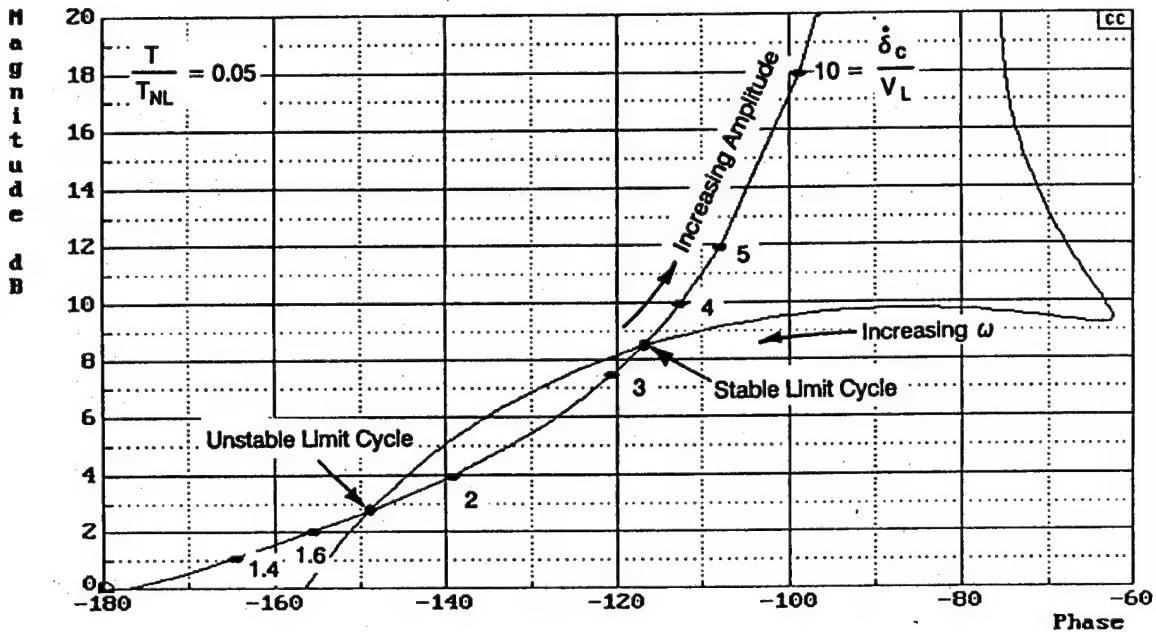


Figure 35. Determining Limit Cycle Stability

the inverse describing function. Next, place yourself as an observer moving along the linear curve in the direction of increasing frequency. As you pass through the point of intersection, if the direction of increasing amplitude along the inverse describing function is toward your right, the limit cycle is stable. If, on the other hand, the direction of increasing amplitude is toward your left, then the limit cycle is unstable. This method was used to identify the stability of the two intersections shown in Figure 35.

The tangent intersection of the linear and inverse describing function curves provides the minimum pilot gain limit cycle frequency. Figure 35 indicates that stable limit cycles can occur for pilot gains beyond this minimum value. In Figure 36 stable limit cycle normalized frequencies are plotted versus normalized pilot gain ($K_p/K_{p\min}$) for the X-15 example case. For this example the limit cycle frequency decreases with increasing pilot gain. This result is intuitive in that the system unstable frequency is expected to decrease as gain is increased.

6. Multiple Rate Limits

As discussed in Ref. 59, the flight control systems of modern aircraft may employ several rate limiters in series. A common example is a software limit placed in series with an actual hardware (i.e., actuator) limit. The software limit will in general be lower to ensure that it will always limit first. In this way the actuator hardware will in theory never limit. The goal is to protect the hardware from routinely reaching its physical constraints. If, however, the first limit has an equal or larger saturation point then cases will exist where both limiters are functioning at the same time. This results in a cascade effect that produces additional magnitude reductions and phase lags.

E. CATEGORY III ANALYSIS

1. Analysis Issues

Several quite recent PIO examples (e.g. JAS 39, YF-22, some early B777 tests) suggest that the introduction of the more elaborate and sophisticated system possibilities made possible by the full

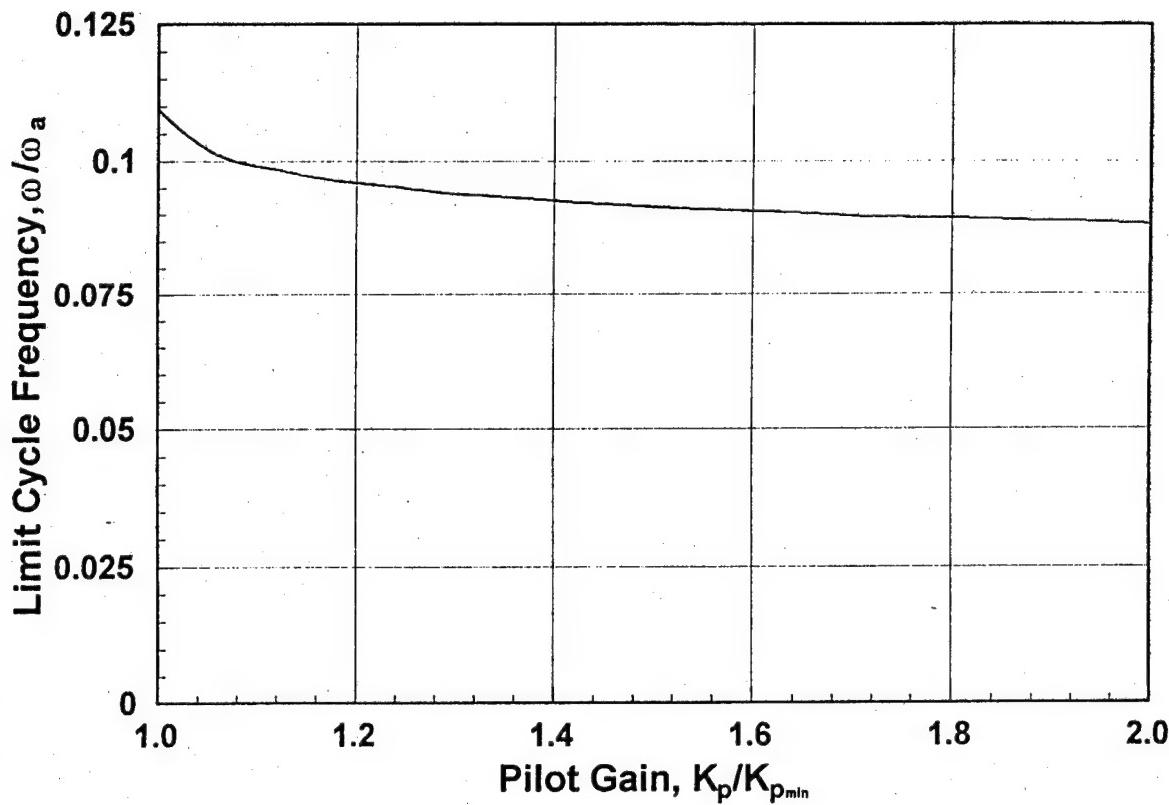


Figure 36. Stable Limit Cycle Frequency Variation with Increasing Pilot Gain for the X-15 Example Case

exploitation of fly-by-wire flight control systems can sometimes produce new PIO possibilities as well. In general these come about because the effective controlled element dynamics may have several manifestations in the course of a PIO sequence. That is, the pilot may be confronted with a variety of different effective aircraft within the oscillation. The simplest of these is, of course, the rate-limiting case covered above. There, for the series limiters, the analysis of the nonlinear conditions is well-handled by a describing function characterizing the nonlinear features acting in series with the quasi-linear pilot and aircraft dynamics. The nonlinear features themselves are readily parameterized by a very small set of quantities, e.g. values of an input amplitude, and of rate limits in series. When these become more extensive, such as when series position limits are introduced in addition, the describing functions of the nonlinear elements may still be capable of being represented in series with effective vehicle dynamics. These describing functions, however, then become much more elaborate functions of several variables, as represented by the fourth entry in Table 3.

When there are multiple effectors (e.g. canards, elevators, flaps, thrust vectoring, etc.) operating with high actuator bandwidths to create a number of coordinated flight control system control loops, the rate and position limiting possibilities are multiplied. In these cases the effective vehicle dynamics can no longer be represented by a linear transfer function and a series describing function. Consider, as an example, an aircraft augmented using both elevator, maneuvering flap, and thrust vectoring, all with high bandwidth control loops. Within the linear range, the effective vehicle dynamics will be essentially linear in character. For large amplitude maneuvers and system inputs, however, one of these loops will limit before another. At this instant, the effective vehicle dynamics presented to the pilot will be changed from those present for smaller inputs. And, more importantly from the analysis standpoint, the situation can no

longer be represented as a nonlinear element in series with a linear one. Instead, the effective airplane itself becomes a highly nonlinear element consisting of a large variety of different effective vehicle dynamics that depend on just what limits are acting. The effective vehicle dynamics may, in this example, "transition" from one to another in the course of a particular maneuver or oscillatory sequence. This is, perhaps, the simplest of the Category III situations in that it involves only limiting elements in the control system, but it is a complicated variety nonetheless. It is represented by the last entry in Table 3.

Category III PIOs can arise from many other "transitions" in effective controlled element dynamics. For instance, the impact on the effective vehicle dynamics of sudden changes in thrust, flap settings, stores release, flight control system modes, etc., or the rapid but somewhat less sudden changes such as increased mass introduced in refueling, drastic trim changes in sudden decelerations, etc. can lead to major changes in the effective controlled element dynamics. These can create great challenges for pilot adaptive behavior especially when they occur as surprises. These kinds of transitions in effective controlled-element dynamics have become more prevalent as advances in flight control system technology have made possible new modes intended to improve overall performance.

For at least some of the Category III PIOs that have been encountered to date, it appears that the aircraft were very likely susceptible to Category I PIOs. For these, the suggestion has been made that the PIOs encountered were initially Category I, then diverged to rate-limiting amplitudes (becoming Category II), and then finally advanced to a stage where a full-blown Category III analysis was needed to "explain" the PIO. This suggestion brings up the basic question as to whether Category III PIO considerations are fundamental to the avoidance and/or prediction of such PIOs, or whether they can be avoided by assuring that the assumed initial Category I stage is made highly unlikely.

Unfortunately, there are as yet very little data available to subject this conjecture to definitive scrutiny. The origin of the Category III concept was the famous T-38 PIO (Refs. 1 and 43) in which the limiting cases of effective vehicle dynamics were associated with the feel system bobweight "in" or "out." As the "triggering" event for this PIO was failure of a stability augmenter, the pre-PIO effective aircraft dynamics were not Level 1.

To understand PIOs that are initiated by a post-transition retention of pre-transition pilot dynamics requires an appreciation of the pre-transition pilot characteristics, Y_{p1} . In pre-transition situations where the pilot is exerting full-attention, high-gain closed-loop control, the pilot dynamics can be estimated using the procedures of Ref. 41. As a simple example, presume that the pre-transition effective aircraft dynamics in the region of pilot-vehicle crossover approximate K_{c1}/s (i.e., rate control) closely enough to require no compensating pilot lead in order to satisfy the crossover model. This will typically be the case for normal operations with many modern stability augmentation systems. Then the pilot's amplitude ratio will be a pure gain, and the pre-transition pilot transfer characteristic will be $K_{p1}e^{-\tau_h s}$. The value of the pilot's effective time delay can be estimated from Table 3 of Ref. 41. For this example, this will be about 0.25 sec. When this form of the pilot's dynamics is combined with the effective aircraft, the calculation of the neutral stability frequency for the pre-transition case is straightforward. Then, to determine the pilot gain, K_{p1} , the crossover frequency must be estimated. For the case with no pilot lead, Ref. 41 indicates that the ratio of the crossover to the neutral stability frequency, ω_c/ω_n , will be 0.78, from which the crossover frequency emerges directly, providing the basis for determination of K_{p1} . The stability of the post-transition retention phase can then be examined by combining the pre-transition pilot dynamics (in this example, $K_{p1}e^{-\tau_h s}$) with the post-transition effective aircraft dynamics, Y_{c2} .

2. YF-12 Case Study

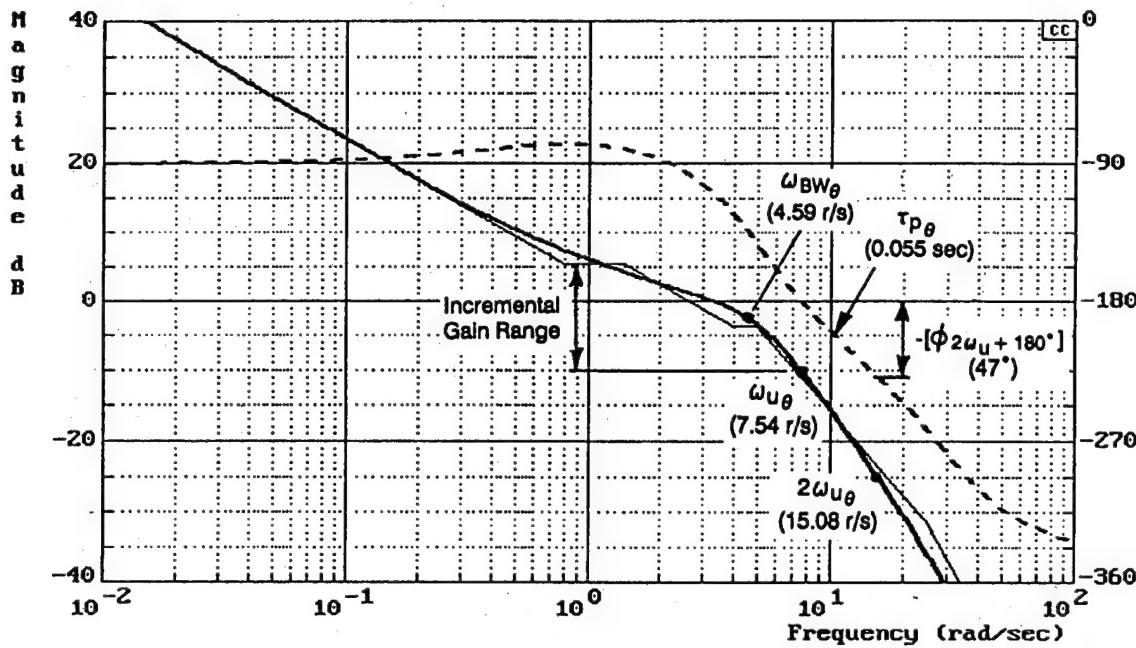
A major Category III PIO was the severe 1 Hz, -1g to 3g, PIO of the YF-12. Reference 7 conclusively demonstrated that a Category III explanation was needed to duplicate the details of this event. In the process, the analysis procedure, using a computer simulation that was quite elaborate for the time to develop appropriate and highly complex describing functions, sets the agenda for Category III PIO analysis even today. Since few other examples are available (e.g., F-8 DFBW), it is fortunate that this still exemplifies the process.

Reference 7 did not, however, examine the properties of the YF-12 as to PIO susceptibility prior to the onset of the SAS rate limiting associated with the PIO. Unlike the series rate limiters involved in Category II PIOs, the SAS rate and position limits appear in the feedback loop of the effective aircraft dynamics, and thereby add both a phase lag and an amplitude ratio increase to these dynamics as seen by the pilot. The question posed above as to the nature of the low-input-amplitude effective vehicle dynamics will therefore be addressed here. Basically, was the YF-12 pre-PIO deficient or not in terms of Category I considerations and criteria?

There are several methods currently available to determine flying qualities and Category I PIO tendencies (Refs. 1 and 2). Of these, Bandwidth/Phase Delay/Dropback (Ref. 2), Smith-Geddes (Ref. 49), and Average Phase Rate (Ref. 50) were selected to assess the PIO tendencies of the YF-12. To complete the assessment, specific information and data were needed corresponding to the touchstones of the selected evaluation criteria. As a starting point a YF-12 short period approximation transfer function was developed from information presented in Appendix E of Ref. 7 for the rigid body only, SAS-on case. Bode and Nichols plots of these transfer functions are shown in Figure 37. Note that the gain has been arbitrarily adjusted to pass through 0 dB at -110° . The bandwidth, phase delay, and average phase rate for this configuration are called out on the plots. These and other parameters relevant to determining Category I PIO susceptibility have been tabulated in Appendix B. The results indicate that the YF-12 would not be labeled PIO susceptible for the refueling flight condition. In fact, the aircraft also met most of the Level 1 handling qualities requirements associated with these criteria.

As the YF-12 is a long-range interceptor, the greatest percentage of its mass when fully loaded is fuel. For the aerial refueling flight condition where the PIOs occurred, the majority of the initial fuel load presumably had been expended, and the aircraft was, therefore, nearly empty. This reduction in mass would yield a lower moment of inertia, a general stiffening of the aircraft, and perhaps improved handling qualities. The SAS also improved the handling qualities by stiffening and damping the short period. Also, as can be seen in Figure 37, the SAS shaping (i.e., T5 from Appendix E of Ref. 7) creates a lag-lead that preserves a "K/s-like" characteristic in the region of crossover, thus avoiding the Bode magnitude shelf associated with PIO syndrome.

From this example it would appear that Category III PIOs exist as separate and independent PIOs that need their own criteria, since Category I criteria, whatever they may be, do not reveal the PIO susceptibility.



$$\frac{\theta}{\delta} = \frac{10000 (.8)(4)[.671, 50.5]}{(0)(1.42)[.587, 4.95](24.7)[.647, 39.7](40.5)}$$

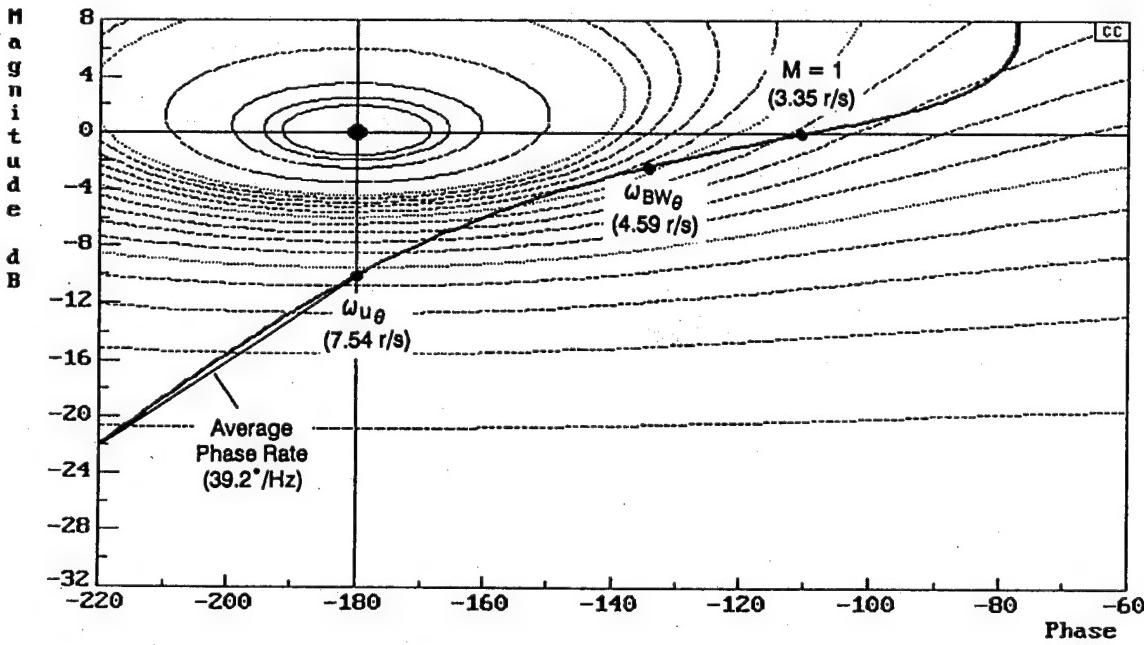


Figure 37. YF-12 Pitch Attitude Frequency Response for an Aerial Refueling Flight Condition

F. HIGH FREQUENCY PIO ANALYSIS

1. Analysis Issues

a. Minimization of Remnant Excitation of Flexible Modes

Pilot-induced noise can be an important excitation source for the lower frequency flexible modes. This is because there can be significant pilot remnant power to about 2 Hz. The effects of remnant excitation are minimized in the following ways:

- crossover region, thereby reducing the pilot equalization dependent remnant source;
- Provide appropriate manipulator (e.g., control column, side stick, etc.) force/displacement characteristics;
- Provide appropriate filtering of the pilot command inputs; and
- Increase the damping of the flexible modes that reside within the remnant bandwidth.

These procedures are very much dependent on specific detailed characteristics of the vehicle's primary control system and higher frequency dynamic properties.

b. Minimization of Pilot Closed-Loop Excitation of Flexible Modes

In the high frequency region of piloted control, θ/δ_p can be approximated by the following equation:

$$\frac{\theta}{\delta_p} = \frac{K \prod_i [\zeta_N, \omega_N]_i}{s \prod_j [\zeta_D, \omega_D]_j} e^{-\tau_e s}, \omega > \omega_b, \quad (50)$$

Pilot control action can drive the closed-loop pilot-vehicle system roots starting at the ω_D 's toward the ω_N 's. In the best of circumstances, the frequency region over which the pilot can exert effective closed-loop control is less than 1 Hz, so the flexible modes that may be involved with this type of control activity will be very low. For sinusoidal signals, however, the pilot can track to much higher frequencies (i.e., within the 1 to 3 Hz range). For any flexible modes in or near the region where pilot control action may have an interactive effect, the relative pole zero orders should be properly adjusted.

c. Reduction of Vibration Feedthrough

Another component of pilot control action is direct feedthrough of lightly damped oscillatory motions within the relevant frequency range. This is illustrated for a stiff stick manipulator in Figure 38 from Ref. 62. As can be appreciated from these data and Refs. 38 and 63, the amount of feedthrough can be substantial to frequencies as high as 10 Hz. The phasing and amplitude of this "biodynamic feedthrough" may be adverse so that it tends to destabilize flexible modes that have undamped natural frequencies in this range. Figure 38 also shows that pilot response to a vibratory environment can excite the resonant modes in the frequency region up to nearly 10 Hz simply because the remnant may be increased by the flexible modes impinging on the pilot.

The design requirements are vehicle specific, and in this case they are specific to the flexible modes at the pilot station. The primary means to minimize vibration feedthrough and excessive remnant include:

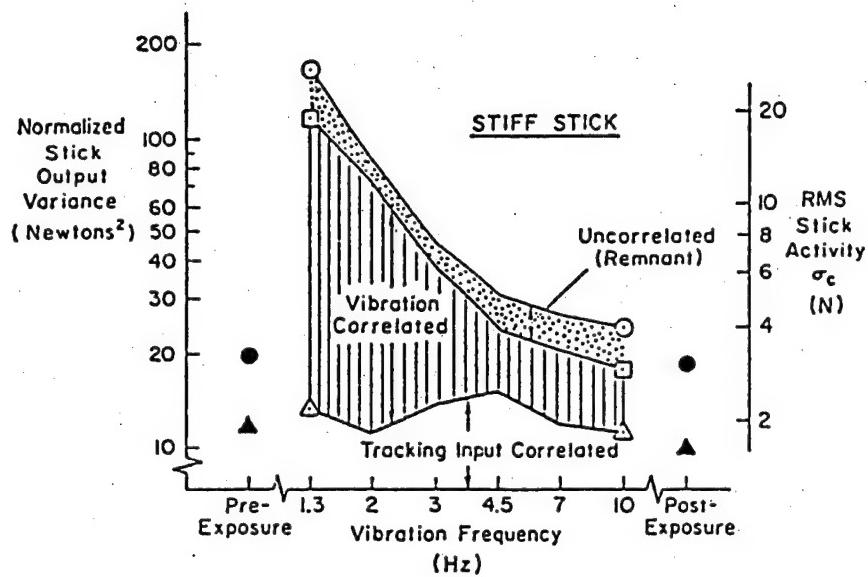


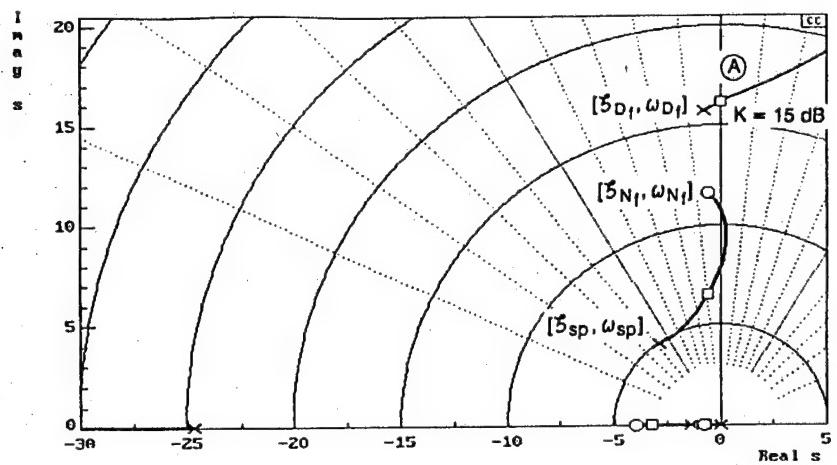
Figure 38. Stick Output Variance Components for Vibratory Forcing (from Ref. 62)

- Use of proper force/displacement loading on the manipulator (e.g., no stiff sticks or columns, include finite breakout forces, etc.);
- Reduce the vibration environment at the pilot station by seat design, arm support, etc.;
- Increase the flexible mode damping and/or reduce the modal response for all modes that have significant amplitudes at the pilot station in the 0 to 10 Hz range; and
- Consider the residual excitation (after all of the above steps have been taken to the extent possible) in the design of command input element filters.

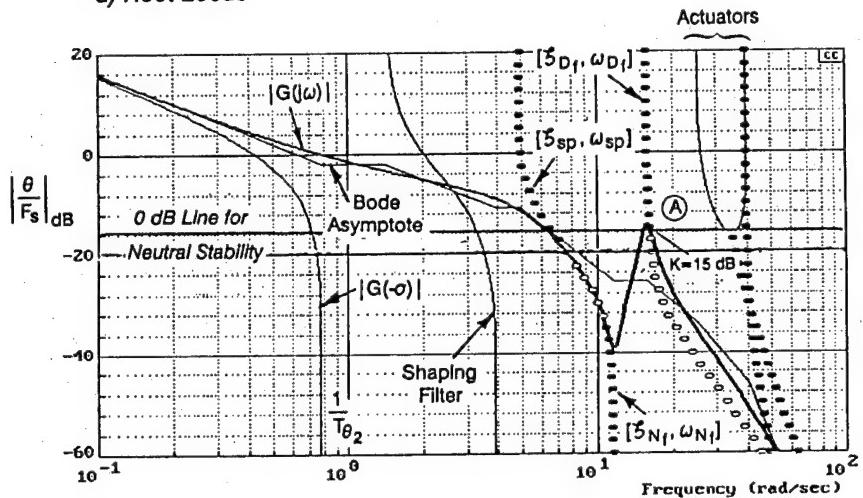
2. Analysis Examples

a. YF-12

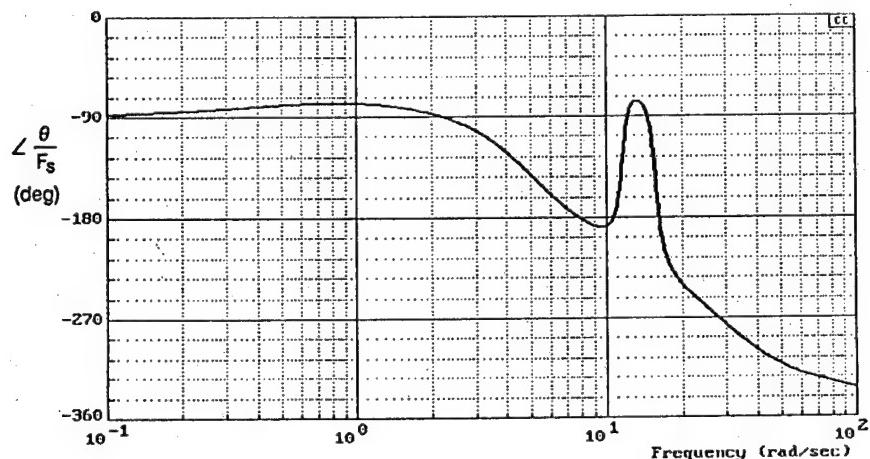
In addition to the severe Category III PIO that occurred with the YF-12 during aerial refueling, smaller amplitude PIOs (see Appendix A) that resulted from pilot interaction with the flexible modes were also reported. In Ref. 7 these PIOs were attributed by the pilot to the bobbling motion of the cockpit that is caused by the flexing of the aircraft. A system survey of the pitch attitude to stick force rigid body plus first flexible mode model of the YF-12 (from Ref. 7) is displayed in Figure 39. This survey consists of a root locus, a Bode-siggy, and a Bode-phase plot. A Bode-siggy plot, the elements of which are completely defined in Ref. 64, directly displays the effects of gain for various loop closures on a Bode magnitude plot. As shown in Figure 39a, the flexible mode dipole has a favorable zero location that should produce a phase stable closure for a pure gain (synchronous) pilot. The short period mode, however, couples with this zero, and the flexible mode departs into the right half plane. As indicated by point A on both the root locus and Bode-siggy plots, there is a gain margin of 15 dB if a synchronous pilot closure is assumed. This gain margin would be more than sufficient for most piloted tasks, however, in aerial refueling tight attitude tracking is required by the pilot. Thus, as concluded in Ref. 7, the combination of the bobbling of the flexible aircraft which served as a trigger and a high gain closed-



a) Root Locus



b) Bode-Siggy



c) Bode Phase

Figure 39. YF-12 System Survey of the Pitch Attitude to Stick Force Transfer Function
(from Ref. 7) at the Aerial Refueling Flight Condition

loop task resulted in the observed PIOs. One possible way to alleviate the undesired coupling is to develop a control scheme that would take advantage of the favorable pole-zero combination of the flexible mode. In this way the damping of the flexible mode would be perhaps significantly increased and any interactions with the short period would be removed.

b. Large Helicopter

For the YF-12 case described above, pilot interaction with the first body bending flexible mode resulted in a nuisance (i.e., small amplitude) PIO. In contrast, several severe PIOs were encountered on a modern large cargo helicopter due to pilot coupling with higher frequency flexible modes. The task was a high pilot gain, precision hover. Specific events resulted in loss of aircraft and/or cargo. In Figure 40 a system survey consisting of a root locus and Bode plot for the closed-loop pitch rate to longitudinal cyclic (q/δ_B) response (Ref. 11) at hover is shown. For a synchronous pilot, the root locus indicates that the second flexible mode (ω_{F_2}) is the first mode drawn into the right-half (unstable) plane. This behavior is indicated in the Bode magnitude plot in that the smallest high frequency gain margin is associated with this mode. (This excludes the smaller margin shown for the mode that falls beyond the data bandwidth.) To rectify the coupling problem, a command path desensitizer filter was added to the flight control system. Figure 41 presents a Bode plot comparison of the q/δ_B response with and without the desensitizer. By attenuating the frequency response in the flexible mode region, the system with the desensitizer provides enhanced gain margins and thus reduces the possibility of high frequency PIO.

G. ANALYSIS GUIDE

As detailed in the above discussions, Category I analysis techniques are in a mature state, although further refinements are conceivable. Specific Category II analysis techniques have been proposed in this effort, however, more data are needed to validate and refine the methods. Because of the complex nature of Category III PIOs and a shortage of data, available analysis techniques have not been fully developed. Thus, to investigate the PIO potential of a given configuration, the current state-of-the-art is encompassed in the analysis steps that are detailed in this section. These steps include:

- Delineation of Most Likely Flight Conditions;
- Determination of Effective Controlled Element Dynamics;
- Pure-Gain-Pilot/Vehicle Closed-Loop System Analysis and Associated Considerations; and
- Closed-Loop Compensatory Pilot/Vehicle System Analyses.

A minimum data set is needed to completely carry out the above steps for a given configuration. This set includes the following items:

- Complete System Dynamics - Frequency response plots (preferably from flight) of the effective controlled element at PIO critical flight conditions;
- Bare Airframe Dynamics - Frequency response plots, stability derivatives and/or attitude, rate, and acceleration transfer functions defined for PIO critical flight conditions (inertial and aeroelastic bending effects should be included when appropriate);
- Actuator Dynamics - Control output/input frequency response and describing function with rate and position limits defined;

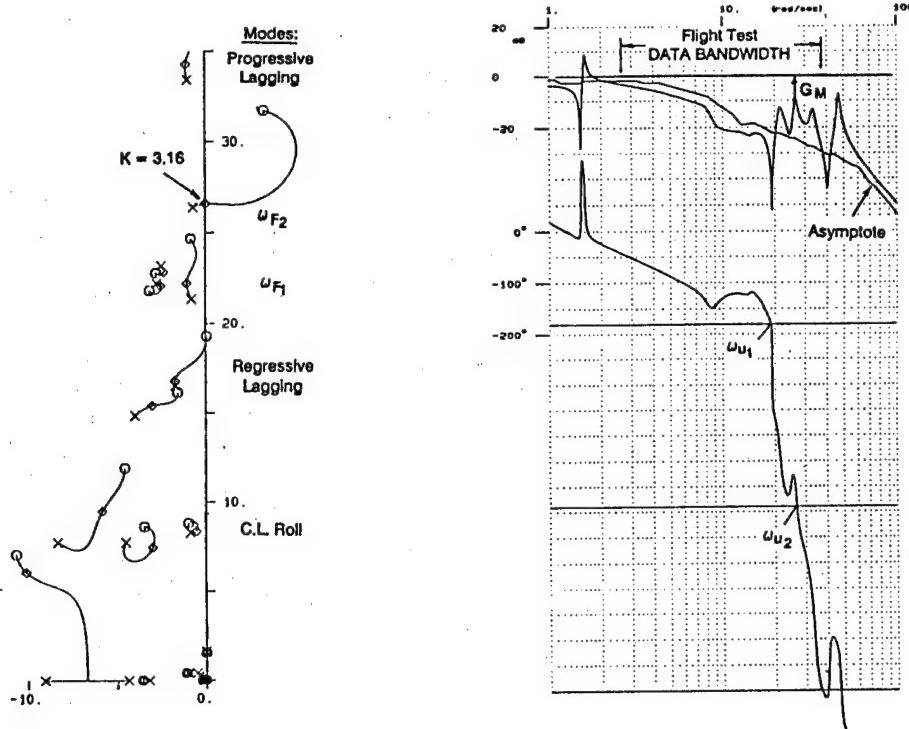


Figure 40. Large Helicopter q/δ_B Response with All SAS Loops Closed

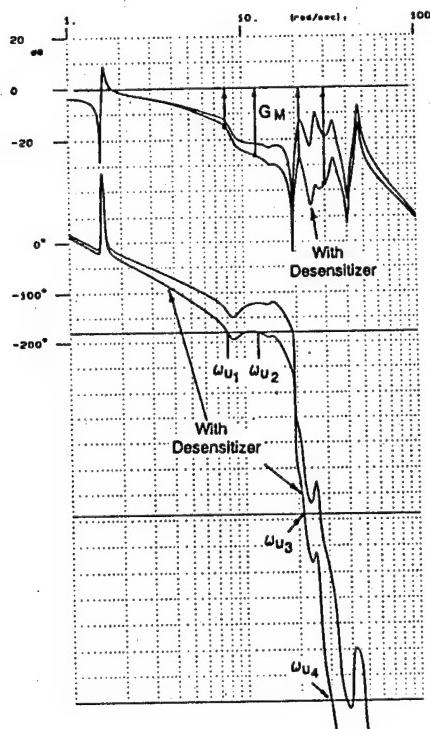


Figure 41. Comparison of Large Helicopter q/δ_B Response with All SAS Loops Closed with and without Desensitizer

- Feel System Dynamics - Frequency response and describing function for manipulator force or position with limits, gearing, and other nonlinearities defined;
- Augmentation - Flight control system block diagram with limits, thresholds, mode switching, and other nonlinearities defined;
- Displays - Type of presentation, instrument dynamics, and kinematics of visual field; and
- PIO Specifics - Time histories, pilot commentary and ratings, flight reports, etc.
- If elements in the above list are not available, which is often the case, proceed through the following steps within the constraints of the available data.

1. Delineation of Most Likely Flight Conditions

As the first step, the most likely flight conditions for PIO are identified. These are flight situations or mission-task-elements (MTEs) that require full pilot attention and have a high degree of task urgency (i.e., demanding a high pilot gain). Typically these include such tracking tasks as:

- Precision approaches and spot landings;
- Conditions inducing or requiring major and sudden configuration changes e.g., wave offs, stores release, LAPES operations, etc.;
- Aerial refueling;
- Formation flying;
- Precision tracking;
- Terrain following; and
- Conditions of major upset, from either external or internal forces, ranging from unexpected events, evasive maneuvers, shifting of pilot attention, etc.

For each of these conditions, a list (usually expanding during analysis) is made of conceivable upsetting external and internal events/forces that might serve as a triggering precursor. A good start on such a vehicle-specific catalog is available from past experience, as reflected in the details of the discussion of PIO triggers in Section III, and by the specifics of the faders and other details of the flight control system being considered. The mode switching and configuration change sequences in the flight control system, and the impact of sudden configuration changes on the vehicle, are often extremely fertile ground.

2. Determination of Effective Controlled Element Dynamics

The second step is to develop the effective vehicle dynamics, including nonlinearities and the lower frequency flexible modes if available and appropriate, representative of the more critical of the flight situations defined above. An important facet in this stage is the selection of the possible transitional sets of effective controlled element dynamics that might be presented to the pilot depending on the amplitude of pilot output. In older aircraft this could be fairly simple; for example, with the T-38 (see Ref. 4):

- Very low pilot output amplitude - "bobweight-out," i.e. aircraft dynamics without any bobweight feedback;
- Intermediate pilot output amplitudes - "bobweight-in," i.e. aircraft dynamics as modified by bobweight feedback; and
- Large pilot output amplitudes - "bobweight-in plus surface rate limiting."

With modern fly-by-wire, multi-mode, task-tailored flight control systems the number of effective controlled elements corresponding to: different positions of mode switches, fader circuits, and aircraft configuration shifts; SAS rate and position limits; primary surface actuator rate and position limits; other limiting and nonlinear features in the system (e.g., limits on integrator outputs, alpha limiters, etc.); can be large. The set of transitional possibilities can be even more extensive.

Keeping in mind all the possibilities identified above, transfer characteristics are found for the following, as a minimum:

Longitudinal

- Pitch attitude/pilot input (force and/or displacement, as appropriate for the artificial feel system);
- Acceleration at the pilot station/pilot input;

Lateral-Directional

- Bank angle/pilot input(s);
- Lateral acceleration at the pilot station/pilot input(s); and

Nonlinearities

- Describing functions of actuator rate and position limiting (for SAS and surface actuators), multi-purpose surface position limiting priorities, stick command nonlinearities, etc.

The longitudinal and lateral-directional effective controlled elements to be considered at this stage should include those that are present for extreme pilot amplitudes (i.e., small and very large).

3. Pure-Gain-Pilot/Vehicle Closed-Loop System Analysis and Associated Considerations

a. Category I

The first closed-loop analysis of pilot-vehicle characteristics can be performed at this point by finding the various instability conditions for the synchronous (pure gain) pilot model. This is appropriate both for a fully-developed PIO for all cases, and for high-frequency vibration feedthrough for PIOS associated with flexible modes. A linear analysis delivers the possible oscillatory frequencies and the pilot gain ranges consistent with stable operations (a key assessment feature). Next, examine the effective vehicle characteristics in the light of experimental data from past in-flight simulations and actual PIO experiences in an attempt to establish close parallels with any of the properties of the airplane being assessed. This step also includes the examination of the aircraft relative to the existing and proposed specifications and all available Category I criteria for PIO considerations as well as particular conditions such as "PIO Syndrome" (Refs. 1 and 4), unfavorable numerator/denominator (ω_n/ω_d) characteristics (Ref. 4), and other related effects.

b. Category II

The effect of series nonlinearities (i.e., software or actuator rate limits) on the effective vehicle dynamics can be determined as follows. First, the frequency of any projected limit cycles can readily be determined via inverse describing function analysis. Having determined a limit cycle frequency, describing functions are then used to estimate the added phase lag due to the series rate limit. The most accurate phase lag estimate is generated from the exact sinusoidal input describing function. If appropriate numerical simulation tools are not available, the phase frequency response curves of Figure 20b can be used to obtain the desired value. The approximate describing functions may also be used to accurately estimate the added phase lag. Here the best result is obtained, as discussed previously, by selecting the approximate describing function based on the saturation region of interest.

c. Category III

More extensive nonlinearities require more elaborate analyses. For example, the YF-12 severe PIO (Ref. 7) involved, as a limiting case, controlled element transitions between a well-damped set of augmented longitudinal characteristics and a higher-gain airplane with a lightly damped natural short period. Both amounted to linear conditions. The nonlinear feature important to the pilot was the transition between the two sets as a function of pilot output amplitude. The large-input amplitude effective vehicle dynamics themselves were associated with the several limiting features in the SAS. The central elements were the SAS actuator rate limit (that was less than the limit for the surface actuator) and position limits (Ref. 7). In determining just where the pilot-effective vehicle dynamics lie between the two extreme positions, describing function analysis procedures are still appropriate, although they are more elaborate than a simple series rate limit. Interestingly, the basic PIO problem in this type of transition is revealed, at least qualitatively, by considering only the two extremes, both linear (the fully-augmented, no-limits-operating and the effectively non-augmented, limits-operating, cases). Similar considerations are valuable to focus on the more important transitional situations to be considered with modern fly-by-wire systems.

4. *Closed-Loop Compensatory Pilot/Vehicle System Analyses*

The fourth step is to perform assessments of pilot-vehicle characteristics for compensatory tracking. This requires the use of the pilot models and guidelines given in Ref. 41. Just as with the synchronous pilot, the instability points and total ranges of available pilot gain are determined. For these compensatory conditions, however, the crossover frequency for a nominal pilot closure is also obtained to provide an indicator of the closed-loop system maximum operational bandwidth available to support the command or regulation responses to extreme inputs or disturbances. Again, the effects of the more important nonlinearities can be taken into account to estimate the amplitudes of any oscillations that progress to limit cycles.

V. CONSIDERATION OF CRITERIA FOR ASSESSMENT OF PIO POTENTIAL

In this section criteria that have been proposed for the assessment of PIO potential will be examined from the perspective of pilot-vehicle analysis. To establish a basis for this examination, a discussion of desirable features for such criteria (i.e., some general "criteria" for criteria) is given. From this perspective, short reviews are then presented for some of the major suggested criteria that have received recent attention. All of these are specifically addressed to Category I PIOS, as there are no available criteria (as contrasted with analysis procedures) for Category II and III PIOS in general. It should be noted from the start that the most fundamental of all Category I PIO criteria are the handling qualities requirements that currently reside in MIL-STD-1797A (Ref. 45). In other words, Category I PIO potential is fundamentally reduced by providing Level 1 handling qualities. Any PIO specific criteria, therefore, should compliment existing requirements.

A. "CRITERIA" FOR CRITERIA

For an assessment and predictive criterion to be of use it must satisfy three prerequisites: *validity; selectivity; and ready applicability*.

1. *Validity*

Validity implies that the criterion is associated with properties and characteristics that define the environment of interest. For severe PIOS, this translates into a need for the criterion to be *connected with closed-loop, high-gain and urgent, piloted control behavior*. The connection can be either explicit or implicit; but it must derive, in some sense, from a fundamental appreciation that pilot actions combine with aircraft actions to result in a PIO. At a more subtle level, these actions should be unusual in that they very seldom occur. This recognizes that *severe PIOS are very unusual events*. A logical assumption is that the effective airplane dynamics will be designed to provide good flying qualities in normal flight maneuvers. Further, "good flying qualities" must be understood to include very small high-frequency effective lags and other features that are directly associated with exceptional pilot-aircraft properties in high-gain tracking-like situations. The rarity of severe PIOS can also be associated with an infrequency of triggering events (i.e., out-of-the-norm system forcing functions or disturbances). Thus, a valid criterion is likely to imply no PIO for normal maneuvers and small inputs, but may raise the question of a "flying qualities' cliff" in more extreme and unusual circumstances. For these reasons, the most useful valid criterion will be more than simply *go/no go*. It should explicitly provide additional information about such aspects as conditions of validity (and hence, situations of maximum risk), frequency and bounding amplitudes of oscillation (which lead to an indication of potential severity), etc. Simple indications of *go/no go and the likely circumstances* are, of course, often quite adequate. They can indicate some of the other, more detailed and descriptive features that should be examined by applying the analysis procedures described in Section IV.

2. *Selectivity*

Selectivity demands that the criterion differentiate sharply between "good" systems and those that are merely "acceptable." A sharp differentiation at the level of acceptability assures that there be no question at all about selecting between "good" and "bad" per se. In the context of PIO prediction the most important selectivity feature is the capability to distinguish between configurations that may be susceptible to *severe PIOS* from those that are not.

3. Ready Applicability

Ready Applicability simply requires that the criterion be easily and conveniently applied. Its expression in terms of readily available system parameters should be compact; procedures for its analytical evaluation should be convenient; and it should be easily measured in terms of either simulation models and/or empirical operations on the actual airplane and its systems.

B. PROMINENT CATEGORY I PIO ASSESSMENT CRITERIA

The most prominent criteria or partial criteria that have been proposed for Category I PIO assessment include:

- Attitude-Dominant Smith-Geddes Type III (Refs. 48 and 49);
- Neal-Smith (original version - Ref. 65 and updated version - Ref. 45);
- Bandwidth/Phase Delay (Ref. 2);
- Gain/Phase Template, Including Average Phase Rate (Refs. 50 and 52); and
- Dropback.

The theoretical bases for these criteria can all be associated with closed-loop pilot-vehicle system considerations, albeit some more directly than others. Smith-Geddes Type III and Neal-Smith are explicitly based on pilot models related to compensatory control. At the other extreme, Dropback as a measure of closed-loop pilot-vehicle actions may appear to be a bit of a stretch because, strictly, it is an open-loop aircraft response. Dropback for K_c /s vehicle dynamics, however, is zero and becomes larger the greater the effective vehicle dynamics depart from a K_c /s character. This can thus be interpreted as a time-domain indicator of the degree of "K/s-ness" exhibited by a particular set of effective aircraft attitude dynamics. Then, to the extent that an ideal PIO-insensitive aircraft has dynamics approximating K/s over a suitably prescribed frequency regime, the dropback parameter can serve as some sort of measure of PIO susceptibility.

The Bandwidth/Phase Delay and Gain/Phase Templates occupy a middle ground. The Gain/Phase Templates including Average Phase Rate are explicitly associated with closed-loop pilot-vehicle system operations when the pilot's behavior is synchronous. The Bandwidth/Phase Delay measures are chosen to reflect closed-loop pilot-vehicle system characteristics in terms of vehicle properties, as are such major features of the Gain/Phase Templates as Average Phase Rate. Boundaries in terms of these parameters are established to encompass pilot-rating data appropriate to given flying qualities levels or other pilot rating-based concerns. Because the pilot ratings are sensitive measures of the dynamics of the pilot that are required to exert appropriate control in closed-loop tasks, the ratings will intrinsically reflect both pilot and vehicle dynamics. The actual boundary lines for a given purpose, such as PIO potential or flying qualities levels, can then be drawn to reflect the qualities desired. In principle, the boundaries could be different for different closed-loop task scenarios (e.g., precision tracking closed-loop maneuvers, large amplitude corrective maneuvers and tight regulation, general flying qualities levels, etc.) and for different types of pilot behavior.

The emphasis below will be placed on PIO assessment criteria for Category I PIOS. Currently, only three of the items on the above list can be considered to offer complete or nearly complete criteria for this purpose. Neal-Smith, although solidly based on closed-loop operations, has boundaries that are connected with flying qualities levels rather than PIO potential per se. In this context, PIO-proneness will be one factor that leads to a non-Level 1 airplane, but may not be the only reason. Thus, Neal-Smith, as presently constituted, is not *selective* for PIO per se. With suitable modifications to the boundaries perhaps Neal-Smith could be adjusted to serve such needs. Similarly, the dropback parameter is

insufficiently quantified to serve the PIO purpose. It can, however, be useful as a supplementary tool, as can Neal-Smith.

1. Bandwidth/Phase Delay (Including Average Phase Rate)

Popular and effective measures that have been successfully applied for flying qualities purposes are the Bandwidth and Phase Delay (see e.g., Ref. 66). These satisfy the *validity* criterion in that they are intimately related to closed-loop pilot-vehicle control, and the *ready-applicability* criterion in that they are ordinarily easy to assess from analyses, simulations, flight test data, etc. The airplane attitude bandwidth, ω_{BW} , is a measure of the frequency extent: (1) over which a pilot can exert good closed-loop control without the need to develop excessive compensation; and (2) within which the aircraft dynamics are consistent with the system need to accommodate major adjustments of pilot gain to reflect control precision demands. Thus, within the frequency band defined by the aircraft bandwidth, the effective aircraft dynamics are such as to tolerate either high or low pilot gain and demand very little lead or other pilot equalization. The common ideal controlled element satisfying these desires for single-loop pilot-vehicle systems is $Y_c = K_c / s$. As already described, these controlled element dynamics require no pilot lead equalization to close the loop, and they permit a very large range of pilot-vehicle system crossover frequencies and associated pilot-gain-adjustment possibilities.

Well-designed aircraft and flight control systems can produce effective aircraft attitude dynamics that approximate the ideal K_c / s form in the region of crossover well enough to require very little pilot lead and to permit large variations in pilot gain. The higher frequency effective aircraft dynamics, however, contribute a variety of lags and leads that impact the available crossover region in both quantitative and qualitative ways. These higher frequency dynamics have a first-order effect on the airplane attitude bandwidth measure that, for "good" airplanes, is invariably determined by the frequency where $\angle Y_c = -135^\circ$. There is a second-order effect on the pilot-vehicle system closure possibilities that is determined by how fast the phase is changing at frequencies somewhat higher than the bandwidth frequency. Thus, a phase that changes slowly with frequency above ω_{BW} permits a larger, smoother, and better graded increase in pilot gain without undue changes in the closed-loop system characteristics than is possible with a more rapidly changing phase. The pilot is confronted with less of a "cliff" when operating with maximum gain levels. At the limits of control encountered with high pilot gains these effects are significant, so aircraft bandwidth alone is not a sufficient measure. Consequently, a measure of the higher frequency phase has been added to take these higher-frequency features into account. The measure adopted is the "phase delay," τ_p (Ref. 66). This emphasizes the phase changes in the region of the unstable frequency for the effective aircraft plus synchronous pilot system. Accordingly, it should be particularly sensitive to synchronous pilot Category 1 PIOs although not confined to this variety. The "average phase rate," (ϕ_{ω}) is a direct multiple of the "phase delay" (by 720 when in $^{\circ}/\text{Hz}$). This measure is a primary PIO indicator in the "Gain/Phase Template" criteria set, so it can be treated here along with the phase delay.

As an elementary example of the application of bandwidth/phase delay considerations to PIO predictions consider, as a minimum ideal form, the single-loop controlled element dynamics approximated by the following:

$$Y_c = \frac{K_c e^{-j\omega\tau_c}}{j\omega} \quad (51)$$

Table 5 presents a cross-section of closed-loop system characteristics for this idealized rate-command controlled element and a synchronous pilot. References 51 and 52 suggest an average phase rate of less than 100 deg/Hz as a boundary associated with PIO potential, while Ref. 2 suggests that an aircraft will be susceptible to PIOs if $\tau_p \geq 0.19$ for Category A flight and $\tau_p \geq 0.15$ sec for Categories B and C flight. The 100 deg/Hz corresponds to a τ_p of 0.14 sec, so the statements are compatible for Categories B and C. In terms of the Table 5 cases, these criteria would imply that idealized rate-command effective vehicle characteristics with an effective time delay parameter greater than 0.35 sec for Category A flight or 0.30 sec for Categories B and C are likely to be PIO prone on a synchronous control basis.

TABLE 5. CLOSED-LOOP CHARACTERISTICS FOR SYNCHRONOUS PILOT AND IDEALIZED RATE-COMMAND CONTROLLED ELEMENTS

τ_e (sec)	ω_{BW_0} (rad/sec)	τ_{p_0} (sec)	ω_u (rad/sec)	ϕ_{ω_u}	
				(deg/rad/sec)	(deg/Hz)
0.10	7.85	0.05	15.7	5.73	36
0.15	5.24	0.075	10.5	8.60	54
0.20	3.93	0.10	7.85	11.46	72
0.25	3.14	0.125	6.28	14.32	90
↓ PIO Potential					
0.30	2.62	0.15	5.23	17.19	108
0.35	2.24	0.175	4.49	20.06	126
0.40	1.96	0.20	3.92	22.92	144

As outlined at the beginning of this section, the particular boundaries in the airplane bandwidth/phase delay space depend on the experimental pilot-rating and other pilot-vehicle system data they are drawn to include/exclude. Thus, when boundaries connected with flying qualities levels are appropriate, the critical data sets may include high-gain tracking tasks (where compensatory and pursuit pilot operations and control are important) as well as precision maneuvers where combined open-loop, closed-loop pilot operations are important (where pursuit and precognitive operations may be major discriminators). For PIOs, data sets appropriate for either or both compensatory and synchronous high pilot-gain operations are relevant. PIO-specific boundaries would incorporate Level 1 flying qualities boundaries as a subset because a PIO-prone aircraft can never be considered to possess Level 1 flying qualities.

The application of bandwidth and phase delay concepts to Category 1 PIO assessment is examined in detail in Ref. 2 where bandwidth and phase delay boundaries pertinent to PIO prediction are developed that take into account most of the available data. The Categories B and C boundaries are shown in Figure 42. The basic non-PIO prone region is the rectangle defined by $1 \leq \omega_{BW} \leq 6$ rad/sec and $0 \leq \tau_p \leq 0.15$. (An appeal to other considerations, such as dropback, is made in Ref. 2 to expand the PIO-prone space on an ad hoc basis.) In Figure 43 the Appendix B operational and test aircraft examples are plotted against these basic boundaries. The results show that the boundaries are generally very good in distinguishing between the severe PIOs of the Ref. 57 (Have PIO) configurations and their baseline conditions. (Indeed, these data had much to do in establishing the boundaries). The ALT-5 case is shown

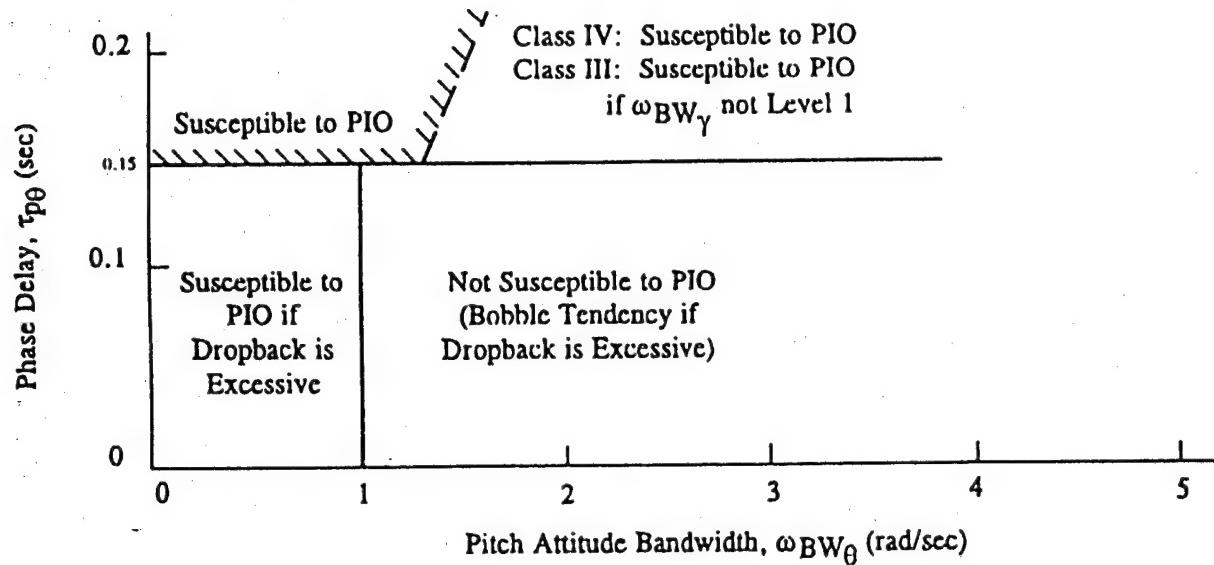


Figure 42. Categories B and C Bandwidth/Dropback Requirements for PIO Resistance
(from Ref. 2)

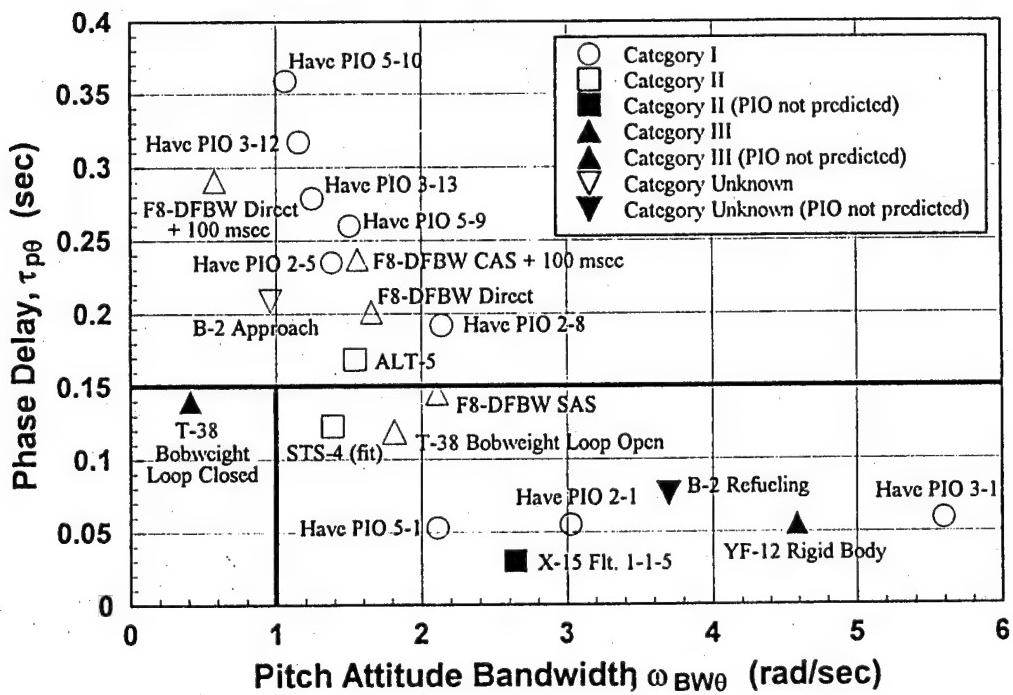


Figure 43. Prediction of PIO Susceptibility with Bandwidth/Phase Delay for Example Operational and Test Aircraft

as PIO prone, although it is close to the upper boundary of non-PIO prone configurations. The F-8 DFBW PIO case can be traced through its various sequences from CAS + 100ms to Direct + 100ms to Direct to SAS. The very limited Category II and III situations are generally not well covered by the Bandwidth/Phase Delay boundaries per se.

The Gain/Phase Template criterion of 100 deg/Hz can be considered in conjunction with the Bandwidth/Phase delay boundaries by noting that 100 deg/Hz corresponds to a phase delay of 0.14 sec. This slight reduction in the phase delay upper bound in Figure 43 makes all of the F-8 DFBW configurations marginal. Further, as would be expected, it gives no insight into the potential for Category II and III PIOs for aircraft such as YF-12 and X-15 that show up well within bounds in their linear manifestations.

Neither the Bandwidth/Phase Delay nor the Average Phase Rate indicators provide an explicit estimate for a likely PIO frequency. The synchronous pilot ($Y_p = K_p$) pilot-aircraft system neutral stability frequency, ω_u , is evident in the effective open-loop pilot/attitude-control gain/phase diagram associated with the Gain/Phase Template, and is also involved in the calculation of the phase delay. This frequency is not, however, always called out as part of the PIO assessment information. When it is, and to the extent that the PIO is associated with open-loop pilot characteristics that approximate a pure gain at the PIO frequency, ω_u is an estimate for ω_{PIO} . This discussion of PIO frequency estimates in no way implies that the suggested Bandwidth/Phase Delay boundaries for PIO shown in Figures 40 and 41 rest upon a synchronous pilot assumption.

For most extended rigid body effective aircraft dynamics where the higher frequency flexible modes do not significantly affect the phase or amplitude ratio plots at frequencies below or near $2\omega_u$, the bandwidth and phase delay measurements are normally straightforward. Otherwise, as with the YF-12 with flexible modes considered, uncertainties and ambiguities appear. These measures could also be confounded in applications to roll attitude control situations if ω_p/ω_d effects are prominent near ω_{BW} , ω_u , or $2\omega_u$.

2. *Smith-Geddes Attitude-Dominant Type III*

The application of the Smith-Geddes criterion for attitude dominant PIOs has already been covered in the discussion of Category I PIO analyses in Section IV. As the fundamental basis for this criterion, Smith developed a very simple linear formula for the crossover frequency from an extensive fixed-base experimental series for a cross-section of elementary systems. Repeating Eqn. 6 here, the formula is,

$$\omega_c = 6.0 + 0.24m \quad (52)$$

where m is an average slope in dB/octave of the effective aircraft dynamics in the crossover region. This formula does not explicitly depend on the phase. It provides an estimate for the crossover frequency of a compensatory pilot-vehicle system for controlled element dynamics other than those on which the equation is based. The elementary system dynamics ($Y_c = K_c$, K_c/s , and K_c/s^2) used to develop the empirical data base had no higher frequency net lags. Therefore, in its essence this crossover frequency is appropriate to the crossover model for those conditions where high-frequency lags and leads beyond the crossover region are not included. For such systems Eqn. 52, in company with the crossover model, is a simple (and essentially complete) pilot-vehicle system model. When such lags are included the nominally positive phase margins associated with these system types may be consumed if the same crossover characteristics are maintained. The Smith-Geddes Type III criterion for attitude dominant PIOs is a straightforward test of whether or not a positive phase margin exists when the actual effective aircraft dynamics are examined at the crossover frequency. That is, an attitude-dominant, compensatory system, single-loop PIO is predicted if the following condition is met:

$$\angle \frac{\theta}{F_{es}}(j\omega) \leq -180^\circ \quad (53)$$

Although this criterion explicitly involves only the effective aircraft dynamics, the pilot characteristics are present via the definition of the crossover frequency.

If the Smith-Geddes criterion is applied to the elementary example of an idealized rate-command effective aircraft (i.e., $Y_c = K_c e^{-j\omega\tau_e} / j\omega$) the criterion frequency, ω_c will be,

$$\omega_c = 6.0 + 0.24m = 6.0 + 0.24(-6 \text{ dB/oct}) = 4.56 \text{ rad/sec} \quad (54)$$

The effective time delay, τ_e , corresponding to a predicted PIO condition will then be,

$$4.56\tau_e = \frac{\pi}{2}, \text{ or } \tau_e = 0.344 \text{ sec} \quad (55)$$

This corresponds to a phase delay, τ_p , of 0.172 sec and an average phase rate of 124 deg/Hz. These are close to, but somewhat larger than, the bandwidth/phase delay estimate of 0.15 sec and the average phase rate of 100 deg/Hz cited above.

As a PIO predictor the Smith-Geddes Type III criterion shows up very well for the essentially linear Category I severe PIOS from the Ref. 57 Have PIO data, showing good selectivity between the "good" baselines and their severe PIO subsets. It has also delivered predictions that a variety of aircraft were PIO prone (e.g., see Ref. 49) which, in the event, proved to be the case. The criterion was also effective in accurately showing PIO tendencies for configurations in the Neal-Smith data base (Ref. 2). Table 6 summarizes the Smith-Geddes Type III based estimates for attitude dominant PIO susceptibility for the operational and test aircraft documented in Appendix B and the severe PIOS from the Have PIO data base. As noted in Table 6, the Shuttle ALT-5 and the F-8 DFBW, as well as the Have PIO data are well-covered by the criterion. For these, and other reasons, the criterion has been proposed to be added to the MIL-STD-1797A (Ref. 45) along with features of the Gain/Phase Template.

TABLE 6. PREDICTION OF PIO SUSCEPTIBILITY WITH SMITH-GEDDES ATTITUDE-DOMINANT TYPE III CRITERION FOR OPERATIONAL AND TEST AIRCRAFT

Aircraft	ω_{PIO} (rad/sec)	ω_c (rad/sec)	$\phi(\theta/F_{\text{cs}})$ (deg)	Type III PIO Prone
Have PIO 2-1 (Baseline)	No PIO	4.37	-161.0	No
Have PIO 2-5	2.7	3.18	-211.6	Yes
Have PIO 2-8	3.8	4.33	-201.5	Yes
Have PIO 3-1 (Baseline)	No PIO	5.06	-127.9	No
Have PIO 3-12	2.2	3.26	-225.6	Yes
Have PIO 3-13	3.2	3.97	-223.9	Yes
Have PIO 5-1 (Baseline)	No PIO	3.77	-167.6	No
Have PIO 5-9	3.5	3.56	-216.9	Yes
Have PIO 5-10	2.7	3.14	-229.5	Yes
X-15 Flight 1-1-5	3.3	4.14	-170.9	No
T-38 Bobweight Closed	7.8	5.52	-66.0	No
T-38 Bobweight Open	7.8	5.45	-108.4	No
YF-12 Rigid Body Only	3.5	4.97	-142.6	No
Shuttle ALT-5	3.4	3.84	-193.1	Yes
F-8 DFBW CAS + 100 msec	3.1	4.10	-215.2	Yes
F-8 DFBW Direct + 100 msec	3.1	3.65	-232.5	Yes
F-8 DFBW Direct	3.1	3.65	-211.6	Yes
F-8 DFBW SAS	3.1	4.15	-179.8	Borderline
B-2 Off Nominal Approach	2.7	3.21	-210.0	Yes
B-2 Aerial Refueling	3.8	5.05	-158.0	No

On the other hand, the Ref. 2 review of research aircraft data gathered subsequent to the original development of Ref. 48 indicates that the criterion can be very conservative (i.e., more configurations are predicted to be susceptible to PIOs than actually exhibit them). Of the 51 cases examined in Ref. 2, the Smith-Geddes predictions indicated that 48 should be susceptible to PIO, but only 17 actually exhibited PIOs. All configurations with a PIOR of 3 or greater were in the latter group, whereas many of the others indicated as PIO-prone had PIORs of 1 and did not exhibit such tendencies. Thus, meeting the Type III criterion indicates a very low probability of encountering an attitude-dominant, PIO, although failing it does not necessarily mean that PIO will occur. Accordingly, the criterion as it stands is not sufficiently selective to serve as a go/no go test.

An important aspect of PIO assessment is an estimate of the likely PIO frequency. For Smith-Geddes Type III the crossover frequency of Eqn. 52 is the estimated PIO frequency. This can be tested with the Ref. 57 Have PIO data. These are recapitulated as part of Table 6. A linear regression for the six severe PIO cases gives,

$$\omega_{\text{PIO}} = -0.05 + 0.86\omega_c, \quad r = 0.97 \quad (56)$$

This is shown in Figure 44, which also contains the other data from Table 6. [Interestingly, the Category II X-15 PIO and the Category III YF-12 PIOs have frequencies in the neighborhood of those for Have PIO (as do those for the F-8 DFBW cases). None of these essentially nonlinear cases were used in the linear regression.] In general, Figure 44 demonstrates that the existing formula for ω_c delivers an estimate for a Category I PIO frequency which is higher than actually observed.

Because the phase lag of θ/F_{es} usually increases with frequency, the phase lag will generally be larger for higher criterion frequencies. This is surely one reason for the lack of selectivity with the criterion as it stands. There are a variety of underlying reasons that Eqn. 52 gives a high value for ω_c . These include the very high performance levels trained into the subjects for the basic experiments (which were conducted 30 years ago) on which the formula is based, the very good, no lag manipulator used, etc. The Eqn. 52 formula could probably be refined to provide better *selectivity* using the much more extensive data now available and documented in Ref. 41. These would give less conservative coverage, and could also be adjusted to account for specific manipulators, experimental scenarios such as fixed-, moving-, or in-flight simulations, etc.

An important feature pertinent to *ready applicability* is the manner in which the amplitude ratio slope, m , is computed. The fitting of a frequency response amplitude ratio with a straight line in the crossover region is seldom as unambiguous as it is with the idealized rate control system. Ref. 18 provides an example that shows that the criterion will not account for the B-2 PIOs without modification to the details of the computation of m .

Alternatives to the estimation of the PIO frequency abound. One way is to use Eqn. 56 directly. This is suggested not only from the good way it fits the Have PIO data but also by the (possible) coincidence that it's not too far off for the other aircraft represented in Figure 44. Such a purely empirical equation could perhaps be greatly refined using other PIO data. Another is to apply the pilot modeling routines of Ref. 41 to find the neutral stability frequency from specific pilot model estimates for particular effective aircraft dynamics. Although this is more complicated than the use of Eqn. 52, it is a straightforward application and can also provide considerable additional information about pilot dynamic behavior, including pseudo ratings if needed. Some appreciation for the potential accuracy of this procedure can be gained from the estimates of the estimated attitude control resonant frequency, ω_R , developed by Bjorkman in Ref. 57 for the Have PIO data. From Ref. 1, the linear regression is,

$$\omega_{\text{PIO}} = 0.02 + 1.01\omega_r, \quad r = 0.97 \quad (57)$$

This is an excellent correlation, which is essentially right on for this restricted data set. It also suggests that the Have PIO Category I PIOs were fundamentally compensatory in nature.

Another easy way to make an estimate for the PIO frequency is to connect ω_{PIO} with the neutral stability frequency for the synchronous pilot pitch-attitude control system. Ref. 1 gives this relationship for the Have PIO severe PIO data as,

$$\omega_{\text{PIO}} = 0.13 + 1.11\omega_{u_0}, \quad r = 0.97 \quad (58)$$

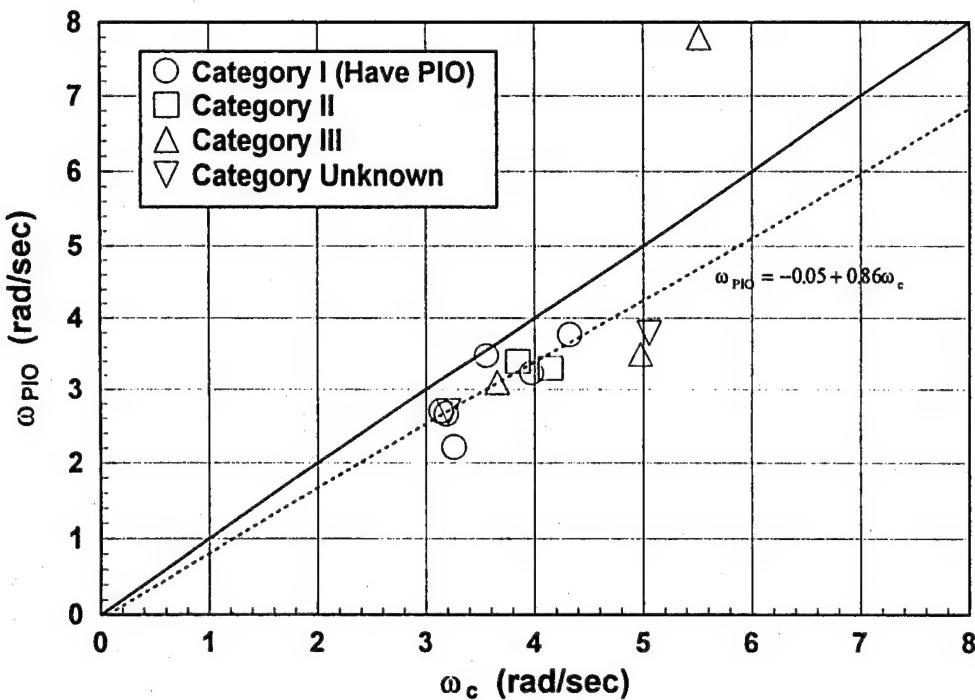


Figure 44. PIO Frequencies of Operational, Test, and Have PIO Data as a Function of Smith-Geddes Criterion Frequency

Thus, if this is capable of generalization, the estimated PIO frequency would nominally be about 11% higher than the frequency that would be predicted for a synchronous pilot interacting with the airplane's attitude dynamics. This has some interesting implications. For example, if operating primarily on attitude cues the pilot must be providing a phase advance at the PIO frequency which more than offsets all of his internal lags. An alternative explanation could be that the dominant cues in the PIO are pitch rate or another aircraft output variable that leads attitude oscillations, thereby permitting nominal pilot lags. There is insufficient data to carry such speculations further, although some time traces in Refs. 68 and 69 indicate that pilot switching on rate cues appears to be present in some cases. For the present, one can interpret Eqns. 56 and 57 as statements that the Smith-Geddes ω_c estimate is higher than, and the ω_{u_0} neutral stability frequency for attitude is lower than, the actual PIO frequency. If these correlations had any generality they could serve as useful, very easily calculated, bounds on the Category I PIO frequency. Summing Eqns. 56 and 57,

$$\omega_{PIO} = 0.04 + 0.55\omega_{u_0} + 0.43\omega_c \quad (59)$$

Eqn 59 implies that an estimate for Category I ω_{PIO} is not far from the mean of ω_{u_0} and the Smith-Geddes ω_c . In using this, the ancient principle of caveat emptor should be remembered!

3. Summary Conclusions

From the above review it would appear the Bandwidth/Phase Delay, the Average Phase Rate aspect of Gain/Phase Templates, and the Smith-Geddes Attitude-Dominant Type III all have something to offer for Category I PIOS. Bandwidth/Phase Delay and Average Phase Rate measures are the easiest to determine unambiguously if flexible modes appear well above $2\omega_u$. They also appear to be the most appropriate for straight go/no go application in that they offer a sharper discrimination between aircraft

likely to suffer Category I PIOs and those that do not. Bandwidth/Phase Delay boundaries are also easily amenable to adjustment to accommodate new data. Smith-Geddes in its current formulation tends to be overly conservative, sometimes warning of PIO susceptibility when it's quite unlikely. On the other hand, an aircraft that clears both the Bandwidth/Phase Delay and Smith-Geddes Criteria will almost certainly be satisfactory from a Category I PIO standpoint.

Although the slope "m" for Smith-Geddes sometimes requires an artistic interpretation, the Smith-Geddes formula may provide a useful upper bound on PIO frequency. Similarly, the synchronous pilot based frequency may provide a lower bound. As a further practical matter, it is currently prudent to: (1) consider more elaborate analyses if either approach shows marginal PIO potential; and (2) be particularly aware that all of the above applies only to Category I PIOs!

C. CONSIDERATIONS FOR EXTENSIONS TO TREAT CATEGORY II SITUATIONS

The current status of PIO theory and knowledge is excellent for understanding and analysis. Unfortunately, empirical data suitable for the development of Category II and III criteria are generally unavailable. Coverage of Category II situations is vastly superior to Category III in that straightforward analyses can be made that permit the estimation of possible frequencies and amplitudes if a Category II PIO is to occur. This is a very great advantage, for it offers some bases for defining conditions and likely consequences, although no estimation of probabilities. The consideration of Category III possibilities is so dependent on the specifics of the flight control systems and possible flight modes involved as to make almost any generalized criteria unlikely.

1. Conjectures Based on $Y_c = K_c e^{-\tau_s s}$

First-order adjustments to the airplane bandwidth/phase delay and the Type III Smith-Geddes measures due to rate limiting are possible. These provide some insight but, in the absence of data, no criteria. To illustrate, consider yet again the idealized effective aircraft dynamics, $Y_c = e^{-j\omega\tau_e} / j\omega$.

a. Bandwidth/Phase Delay

In the linear (Category I) case the unstable frequency $\omega_{u_{linear}}$ and phase delay are given by the following:

$$\omega_{u_{linear}} = \frac{\pi}{2\tau_e} \quad (60a)$$

and

$$\tau_p = \frac{\tau_e}{2} \quad (60b)$$

When the simplest form of rate limiting is present, the open-loop phase angle of the effective aircraft dynamics plus the series rate limiting is given by,

$$\angle NY_c = -\pi/2 - \tau_e \omega - \cos^{-1}(K^*) \quad (61)$$

The instability frequency in the presence of the nonlinearity will then become,

$$\omega_{u_{\text{nonlinear}}} = \frac{\pi}{2\tau_e} \left[1 - \frac{2\cos^{-1}(K^*)}{\pi} \right] \quad (62a)$$

or

$$\frac{\omega_{u_{\text{nonlinear}}}}{\omega_{u_{\text{linear}}}} = \left[1 - \frac{2\cos^{-1}(K^*)}{\pi} \right] \quad (63b)$$

This relationship can be useful for first-order estimates of the rate limiting amplitude ratio K^* in limited data circumstances. For example, with the X-15 PIO the available time traces reproduced here in Figure 26 did not include the input to the actuator, so the input end of K^* is unknown. Equation 63b can be written in the following form:

$$K^* = \cos \left[\frac{\pi}{2} \left(1 - \frac{\omega_{u_{\text{nonlinear}}}}{\omega_{u_{\text{linear}}}} \right) \right] \quad (64)$$

Some appreciation for the adequacy of this much oversimplified estimating procedure can be obtained by its application to the X-15 analyses of Section IV. There, the estimated PIO frequency was $\omega_{u_{\text{nonlinear}}} = 2.73$ rad/sec, the estimated linear instability frequency was $\omega_u = 5.31$ rad/sec (see Figure 27), and K^* was 0.68 (see Figure 29). For these conditions the simplified system formula (Eqn. 64) gives $K^* = 0.72$.

The attitude bandwidth is the frequency at which the phase angle is -135° or $-3\pi/4$ radians. For the linear system this is $\pi/4\tau_e$, or just one-half the linear instability frequency. For the nonlinear system the rate-limiting-dependent bandwidth will be,

$$\omega_{BW_{\text{nonlinear}}} = \frac{\pi}{4\tau_e} \left[1 - \frac{4\cos^{-1}(K^*)}{\pi} \right] \quad (65a)$$

or,

$$\frac{\omega_{BW_{\text{nonlinear}}}}{\omega_{BW_{\text{linear}}}} = \left[1 - \frac{4\cos^{-1}(K^*)}{\pi} \right] \quad (65b)$$

Figure 45 shows Eqns. 63b and 65b as a function of the nonlinear parameter K^* . The aircraft bandwidth will thus be "used up" or reduced to zero when K^* is 0.707. From Eqn. 63 the corresponding oscillation frequency will occur at the linear system attitude bandwidth frequency. Satisfaction of the open-loop amplitude ratio condition for an oscillation requires that the describing function magnitude, $|N|$, which is $(8/\pi^2)$ times K^* , be 0.573. This would require the pilot gain to increase by $1/0.573 = 1.745$ or 4.84 dB. Interestingly, the phase delay is unchanged for this elementary example because the incremental phase, $\cos^{-1}(K^*)$, due to the rate limiting appears in both the phase at ω_u and that at $2\omega_u$. It therefore cancels out and τ_p remains at its linear value of $\tau_e/2$.

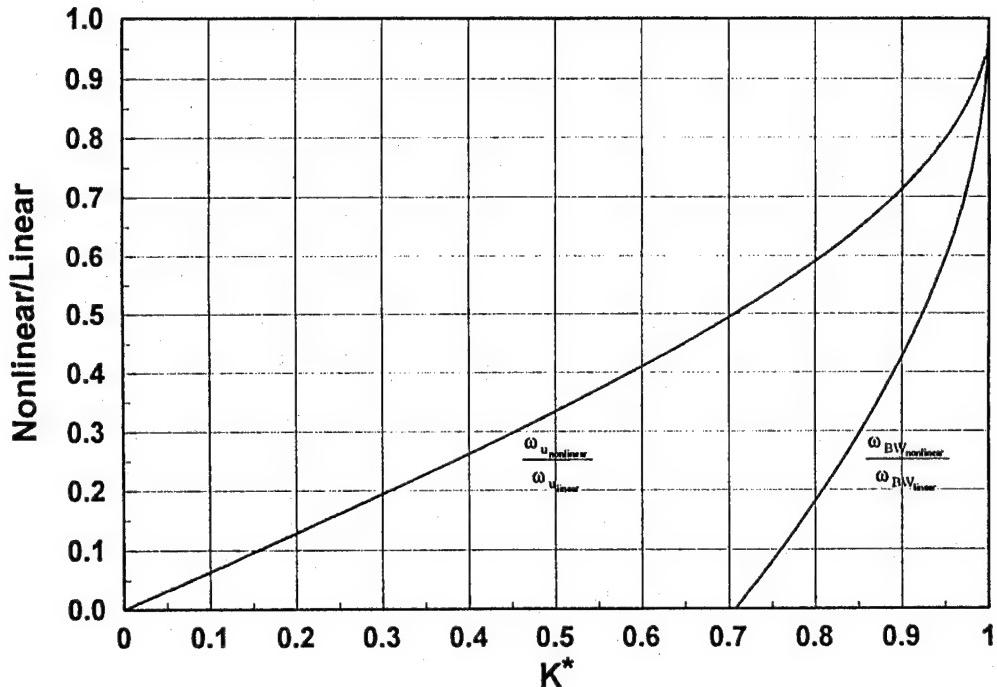


Figure 45. Ratio of Nonlinear to Linear Bandwidth and Unstable Frequencies as a Function of K^*

This example is instructive in that it indicates the general effect of series rate limiting as a reduction of the aircraft attitude bandwidth available for use, and the reduction of a rate-limited PIO frequency from that of the Category I linear situation.

b. Smith-Geddes

The Smith-Geddes criterion when applied to the same illustrative example yields some other interesting results. First, the phase condition for instability can be shown to be,

$$\tau_e \omega_c = \sin^{-1}(K^*) \quad (66)$$

This expression has already appeared in the analysis of PIOs with rate limiting, albeit with the unstable frequency ω_u in the place of the crossover frequency ω_c . But in the Smith-Geddes context, the crossover frequency is the predicted PIO frequency, so this is no anomaly. A plot showing this variation with the degree of rate limiting is given in Figure 28. The oscillation frequency will remain at the crossover frequency. Thus, to the extent that there is some transfer from the linear to the nonlinear case, this will be 4.56 rad/sec from the formula for ω_c . The limit cycle amplitude is represented within K^* , that will then be,

$$K^* = \sin(4.56\tau_e) \quad (67)$$

This result depends on the fundamental assumption that the crossover frequency will be maintained in the presence of the nonlinearity. In some famous PIOs the fully developed PIO is close to the initial frequency, while in other cases it is somewhat reduced. There are very few if any examples where the PIO frequency is markedly reduced as the PIO develops. The bandwidth/phase delay considerations for this exemplary vehicle would suggest that a fairly significant reduction (a factor of 2

in this example) might be present, while the projection of the Category I Smith-Geddes crossover frequency relationship into the rate-limited domain implies only minor change if any.

The Smith-Geddes criterion frequency permits the development of an equivalent delay time due to a given amount of rate limiting. In general, the delay associated with rate limiting is,

$$t_d = \frac{\cos^{-1}(K^*)}{\omega_i} \quad (68)$$

where ω_i is the frequency of the sinusoidal input to the rate limiting nonlinearity. For the Smith-Geddes case this frequency is the crossover frequency, and is therefore a given in the problem. The time delay is thus,

$$t_d = \frac{\cos^{-1}(K^*)}{4.56} \quad (69)$$

This ranges from 0 to 0.22 sec as the pilot's input to the rate-limiting feature varies from the small and essentially linear to the large and fundamentally nonlinear.

2. Possibilities Based on X-15 Analyses

A key to understanding the X-15 PIO lies with the severe 15 deg/sec rate limit. That is, the added phase lag ($\Delta\phi$) from the rate limiting was an essential ingredient in this event. Thus it is hypothesized that existing Category I criteria can be applied to a new effective vehicle transfer function that has been modified to include this added phase lag. To estimate the added phase lag with the describing functions developed in the previous section, it is necessary to define the normalized frequency (ω_{PIO}/ω_a) and the time constant ratio (T/T_{NL}) for the PIO condition. From the information available on the X-15 PIO the normalized frequency is easily defined, however, a longitudinal stick or actuator command time trace is needed to define the maximum actuator command input (A) and hence the time constant ratio. To examine the effect of this unknown, the exact sinusoidal describing function was used to estimate the added phase lag for a range of actuator command values (i.e., $A = 3^\circ, 6^\circ, 9^\circ, 12^\circ$, and 15°). Using these estimated phase lags and the PIO frequency, a linear first order lag of time constant T was then defined for each amplitude ($T = \tan(\Delta\phi)/\omega_{PIO}$). This first order lag, therefore, represents the rate limited actuator at the PIO frequency.

For this case study the Bandwidth/Phase Delay portion of the Bandwidth/Dropback requirements for PIO resistance (Ref. 2) as shown in Figure 42 were used as representative Category I criteria. These are the boundaries shown in Figure 46. To apply the requirements, an effective vehicle transfer function was defined for each case using the bare airframe dynamics and the first order lag representation of the rate limited actuator. Then bandwidths and phase delays were computed and plotted as shown in Figure 46. For $A = 3^\circ$ the actuator does not saturate ($\omega_s = 5.1$ rad/sec for this case), and thus the linear bandwidth and phase delay values result. The remaining cases, on the other hand, move from near saturation ($A = 6^\circ$) to the more highly saturated ($A = 9^\circ, 12^\circ$, and 15°). Notice that there is also a large reduction in bandwidth between the $A = 9^\circ$ to 12° cases that results from a shift in the bandwidth definition from phase margin to gain margin. The most significant result, however, is that two of the highly saturated cases ($A = 12^\circ$ and 15°) fall distinctly in the *Susceptible to PIO* region, while the third ($A = 9^\circ$) falls near the *Susceptible to PIO* boundary. (It is actually on a $\tau_{p_0} = 0.14$ sec boundary corresponding to an average phase rate of 100 deg/Hz.) Thus this X-15 case study suggests that Category II cases involving series rate limits can be studied using existing Category I criteria if the series rate limiting element (e.g., software or actuator limits) is properly accounted for in terms of the added phase

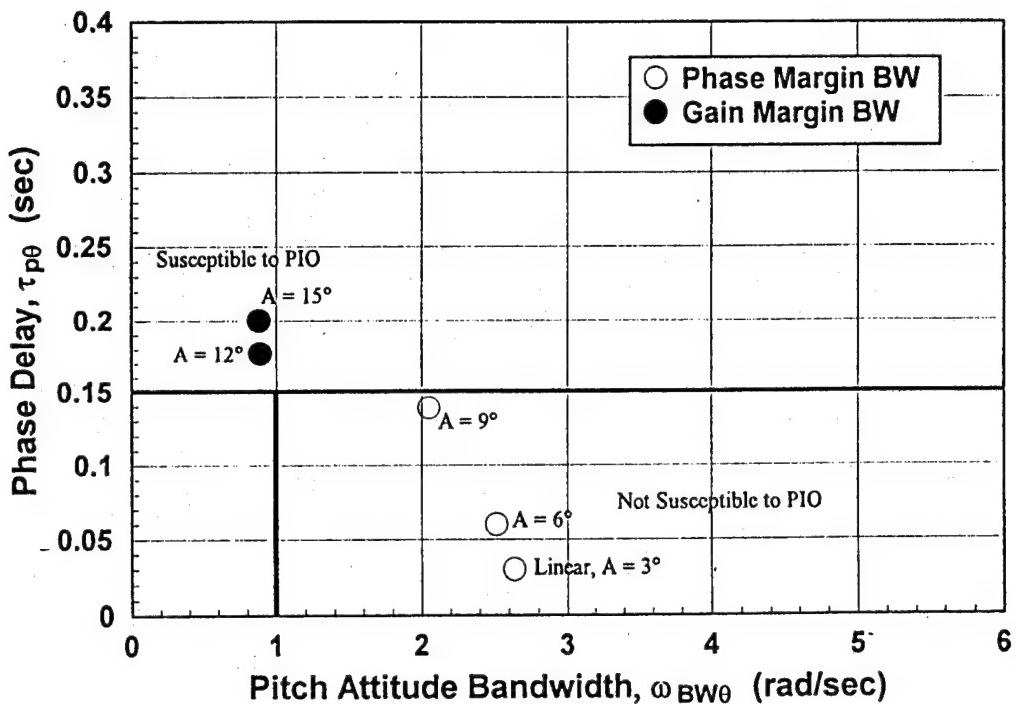


Figure 46. Bandwidth/Phase Delay Requirements for PIO Resistance Applied to X-15 Example Cases

lag. It must be stated, however, that this single point example is only an indicator. The method must be verified with an appropriate database that has yet to be established.

In this example the rate limited actuator was represented by a first order lag. The describing function results (e.g., the exact sinusoidal describing function displayed in Figure 20) indicate that this is an appropriate representation. Since the time constant is defined in terms of the added phase lag of the rate limited element and the limit cycle frequency, the linear first order lag provides an exact match to the nonlinear phase lag at that frequency. There is a question, however, as to how effectively this lag represents the magnitude reduction of the nonlinear element. In Figure 47 a comparison is made between the magnitude of the first order lag at the limit cycle frequency for the X-15 example cases and the actual nonlinear actuator magnitude ratio as computed with the simulation model. There is clearly excellent agreement between the two results. Only the near saturation case ($A = 6^\circ$) does not fall directly upon the 1 to 1 line.

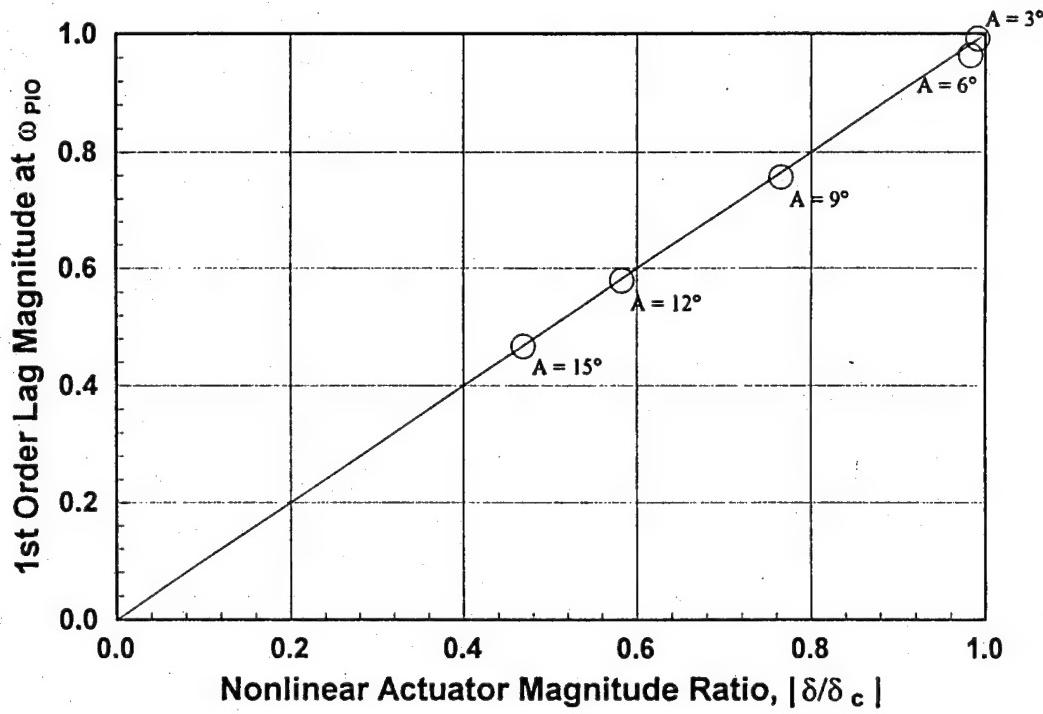


Figure 47. Comparison of a First Order Lag Representation of the Magnitude Reduction Due to Rate Limiting with the Nonlinear Result for the X-15 Example Cases

VI. SUMMARY COMMENTS AND CONCLUSIONS

A. PIO CONSTITUENTS

The fundamental elements involved in severe PIOS are: effective aircraft dynamics; pilot dynamics; and triggering or precursor events. Some distinguishing features for these constituents pertinent to PIO are summarized below.

1. Aircraft Dynamics Frequency Range

Extended Rigid-Body – effective rigid-body vehicle dynamics + actuators, SAS, etc. Most “famous” PIOS are of this variety.

Flexible Modes Inclusive – extended rigid-body + flexible modes + actuators, SAS, etc. Notable instances include YF-12 high frequency PIO, CH-53E and V-22 PIOS and two types of 3 Hz interactions with the B777 during development.

2. Pilot Behavioral Dynamics

Compensatory - conventional high-gain, error-reduction, closed-loop control. Pilot adapts dynamic characteristics (e.g. adjusts gain and lead) as needed to offset effective aircraft deficiencies. Applicable to most extended rigid body PIOS for which sufficient data are available for discriminating analysis (e.g., Shuttle and Have PIO).

Pursuit - combined open-loop (feed-forward), closed-loop (compensatory) operations. Because the closed-loop system stability is the same as for compensatory control, this pilot behavioral mode is more important as the initial stage in a pilot transition that can serve as a trigger. Transition examples include shifting to a “spotting the deck” mode in carrier approach, “tunneling” to a restricted field of view (losing the “surround” references) in response to unexpected events such as runway incursions, probe-and-drogue refueling with a KC-135 tanker wherein the pilot’s visual field is sometimes insufficient to view both the basket and tanker, thereby losing the reference cues needed to support the pursuit feedforward, etc.

Synchronous – Pilot dynamics approach pure-gain, pilot “locked-in.” Also works fairly well for the Have PIO severe cases; required for the T-38 PIO.

3. Triggers

Triggers induce major corrective inputs that start severe PIO. Because of their extensive variety, systematic searches for and elimination of triggers tend to be under-emphasized by the flying qualities community. Yet, after PIO encounters great emphasis is placed on discovering the specific triggering events as “causes” and then, more often than not, these are the specific items “fixed” after PIO encounters.

B. PROPOSED PIO CATEGORIES

Category I – Essentially linear and time stationary.

Examples: Reference 57 (Have PIO) flight experiment data; beginning phases of many PIOS initiated by large corrective inputs that subsequently introduce velocity limiting into corrective actions.

Category II – Linear and time stationary except for specific series nonlinearities (e.g., rate limiting).

Examples: Rate limiting introduces amplitude sensitive phase lags, that both aggravate the effective time delay and limit most fully-developed PIOs (e.g., X-15 and Shuttle Alt-5)

Category III – Complex nonlinearities are central and the closed-loop situation is often non-stationary. These commonly involve either pilot-amplitude induced aircraft dynamics changes or transitions in either the effective aircraft or pilot dynamics. Pre- and post-transition effective dynamics are often effectively linear, just different. Aircraft dynamics changes include: deliberate mode switches (SAS or aircraft configuration shifts); input-amplitude-dependent effective vehicle dynamics shifts (e.g., incremental opening/closing of SAS loops, usually due to one loop saturating before another; amplitude-sensitive gains, etc.). Changes in the pilot's system organization include pursuit to compensatory; compensatory to synchronous; shifts in dominant control variable such as attitude to normal acceleration, etc.

Examples: YF-12 mid-frequency PIO and early B777 as effective aircraft changes; YF-16 "first flight" as an example of pilot dynamic changes.

C. STATUS OF ASSESSMENT CAPABILITY

I. *Category I*

Analysis – For either synchronous or compensatory pilot dynamics the analysis of PIO possibilities with either attitude or normal acceleration control with extended rigid body effective vehicle dynamics is in good shape (i.e. pilot behavior, including rating and pseudo commentary estimates). Applicable pilot models for flexible-mode-inclusive attitude control and vibration-feedthrough modes exist, although action threshold data and connections with pilot ratings are not available.

Criteria – Several criteria have a high degree of fundamental applicability for *attitude control dominant tasks*, especially with effective vehicle dynamics (with near-optimum controlled element gain) that are dominated by excessive lags and/or highly limited ranges for pilot gain adjustment/variation but which are otherwise adequate. These include:

- Smith-Geddes Type III (phase at ω_c); and
- Bandwidth/Phase Delay (and Average Phase Rate).

Although all these criteria require only effective aircraft dynamics data to apply, they are *based on tight closed-loop piloted control* in one way or another. The critical frequency for Smith-Geddes Type III derives fundamentally from compensatory control data, and most of the pilot rating data used to establish Bandwidth/Phase Delay boundaries have compensatory operations as major entries in the data base. The specific numerical values were based on data available at the time the criteria were evolved, and all are subject to adjustment and fine tuning as new data emerge. The latest versions of these criteria forms are, in consensus, adequate for Category 1 PIO circumstances with extended rigid-body effective aircraft dynamics. Data from several sources and correlations developed here suggest that the current Smith-Geddes formula provides an estimate for ω_c that is too high. Further, the results of the Ref. 2 study indicate that the Smith-Geddes predictions tend to be overly conservative in the *go/no go* determination of PIO susceptibility. Both criteria forms are subject to ambiguities. An example for Smith-Geddes is the definition of the slope "m." For phase delay and average phase rate, high frequency dipole pairs may contaminate the estimate. No criteria yet include off-optimum controlled element gain situations or explicitly provide assessments of available pilot gain ranges.

Criteria for flexible-mode-inclusive situations are not yet available.

2. Category II

Analysis – The effects of actuator rate limiting on PIO frequency and amplitude are readily analyzed with either applications of the wide array of describing functions developed in this report or with computer simulations. The fundamental effect of a series rate limiter is to add an amplitude-sensitive phase lag (in the simplest version, $\phi = \cos^{-1}(K^*)$, where $K^* = x_o / x_i$) to the effective aircraft dynamics, thereby lowering the PIO frequency from that of a neutrally stable linear system. Rate limits in actuators approach this same describing function when the actuator bandwidth is very large, but otherwise have more profound effects including major reductions in effective actuator bandwidth.

Criteria – There are currently no applicable criteria. There is some hope that Category I criteria might be extended to cover rate limiting if a data base were established. Possibly pertinent Category I criteria for extension include:

- Smith-Geddes Type III (by adding the incremental phase lag due to rate-limiting). The PIO frequency will continue to be ω_c and the PIO amplitude would be given by the value of x_o/x_i needed to make the total phase lag -180 degrees; and
- Bandwidth/Phase Delay (by adding the incremental phase lag due to rate-limiting). The PIO frequency will be lower than that for the linear system. The primary effect of rate limiting is to reduce the airplane bandwidth (effectively, the bandwidth becomes a function of the rate limit/input ratio) and increase the phase delay.

Criteria for flexible-mode-inclusive situations are not available.

3. Category III

Analysis – Complex describing functions derived from elaborate simulations of the effective controlled element dynamics can cover those Category III situations where the pilot's input amplitude is the major variable. These cases include effective controlled element changes due to various SAS loops saturating at different levels, other SAS-internal nonlinearities, etc. Controlled-element-transitions within the SAS can be treated as pre- and post-transition situations. Other Category III possibilities are more subtle, in that they are difficult to identify or discover without an elaborate search.

Criteria – No universally applicable criteria exist; satisfaction of Category I criteria does not necessarily insure against Category III PIOs (e.g., YF-12). Smith-Geddes Type I criteria are based on the hypothesis that the pilot transitions from attitude to normal acceleration control, so these may be relevant to such specific Category III transitions.

D. FUNDAMENTAL CONCLUSIONS AND RECOMMENDATIONS

1. In view of the complexities and different features involved in the several categories of PIOs one *cannot expect to achieve quantitative criteria applicable to all*. Some Category I situations for longitudinal (and lateral) attitude control of extended rigid-body aircraft dynamics are in good shape, while Category II situations, which have been prominent in severe operational PIOs, and Category III cases, the emerging major threat associated with (FBW/FBL) applications, as well as higher frequency PIOs are devoid of criteria and destitute of data. Sufficient data and criteria currently exist to cover with a high degree of confidence Category I PIOs for extended rigid-body effective vehicle dynamics (with optimized effective aircraft gains) in longitudinal attitude control. Further, Category I and II PIOs usually have a common origin in the effective dynamics that exist at the lower amplitude levels where the aircraft dynamics are essentially linear. Thus Category I criteria are, in this sense, basic. Category II criteria can include the Category I baselines (as suitable for the linear

cases) and can, perhaps, be supplemented with extended versions. Category III PIOs are quite idiosyncratic, although it may be possible to develop sets of criteria applicable to particular element-combinations, ideally criteria sets that build on each other.

2. There is an *urgent need* for systematic experimental data for Category II (i.e., rate limited) situations. These should be addressed in both simulators and in-flight programs in parallel.
3. There is an *urgent need* for the development of simulation fidelity requirements, protocols, and procedures (e.g., pilot inputs, system excitation, appropriate maneuvering complexes), etc. for fixed, moving, and in-flight simulation assessments of PIO potential for all Categories for both extended rigid body and flexible-mode-inclusive situations. This will not only respond to and enhance understanding of current problem areas, but will also expedite the gathering of data for Category II and III situations.
4. Because rate limiting associated PIOs appear to be ubiquitous in connection with FBW aircraft, there is an *urgent need* for well-developed and understood fixes. Thus, the more promising alleviation schemes should be brought to a higher level of maturity. Some "alternate control schemes" (Ref. 70) have already been flight tested (Refs. 71 to 73) and at least one is currently applied operationally (on the JAS 39); others, e.g. cueing of rate limits in backdrives, should be evaluated as elements in proposed test programs.
5. The vast majority of past severe PIOs are of the Category I and/or II varieties. For new aircraft equipped with high-technology cockpits and FBW/FBL flight control systems the PIO of the future is likely to be Category III. *Detailed examinations of existing FBW/FBL systems should be conducted to discover specific sources and gain better appreciation of the likely range of Category III possibilities.* Within this context, analysis and manned simulation studies should then be conducted to develop the data and more complete understanding needed. Urgent emphasis should be placed on those aircraft coming into the inventory.
6. Fine tuning of Category I criteria should be continued. This could include consideration of modern data to tune Smith-Geddes Type III, and refinement of Bandwidth, Phase Delay, and Average Phase Rate to encompass broader data bases as they become available. Consideration should also be given to quantification of the "available pilot-gain range" as a major factor in the PIO picture. In addition, the criteria need to be modified to handle the presence of higher frequency modes.
7. A major deficiency for Category I is the lack of data on effective controlled element gain as a major variable for novel inceptors.

VII. REFERENCES

1. McRuer, Duane T., *Pilot-Induced Oscillations and Human Dynamic Behavior*, NASA CR-4683, Dec. 1994.
2. Mitchell, David G., and Roger H. Hoh, *Development of a Unified Method to Predict Tendencies for Pilot-Induced Oscillations*, WL-TR-95-3049, June 1995.
3. Matranga, Gene J., *Analysis of X-15 Landing Approach and Flare Characteristics Determined from the First 30 Flights*, NASA TN D-1057, July 1961.
4. Ashkenas Irving L., Henry R. Jex, and Duane T. McRuer, *Pilot-Induced Oscillations: Their Causes and Analysis*, Northrop-Norair Rept., NOR 64-143, June 1964.
5. Taylor, Lawrence W., Jr., *Analysis of a Pilot-Airplane Lateral Instability Experienced with the X-15 Airplane*, NASA TN D-1059, Nov. 1961.
6. Smith, John W., *Analysis of a Lateral Pilot-Induced Oscillation Experienced on the First Flight of the YF-16 Aircraft*, NASA TM-72867, Sep. 1979.
7. Smith, John W., and Donald T. Berry, *Analysis of Longitudinal Pilot-Induced Oscillation Tendencies of YF-12 Aircraft*, NASA TN D-7900, Feb. 1975.
8. Teper, Gary L., Richard J. DiMarco, Irving L. Ashkenas, and Roger H. Hoh, *Analysis of Shuttle Orbiter Approach*, NASA CR 163108, July 1981.
9. Johnston, Donald E., and Raymond E. Magdaleno, *Independent Assessment of C/MH-53E Technical Evaluation Program (TEP)*, Systems Technology, Inc., TR-1251-1R, Sep. 1990.
10. Kaplita, Thaddeus T., Joseph T. Driscoll, Myron A. Diftler, and Steven W. Hong, "Helicopter Simulation Development by Correlation with Frequency Sweep Flight Data," *American Helicopter Society 45th National Forum Proceedings*, Boston, MA, May 1989.
11. Aponso, Bimal L., Donald E. Johnston, Walter A. Johnson, and Raymond E. Magdaleno, "Identification of Higher-Order Helicopter Dynamics Using Linear Modeling Methods," *American Helicopter Society 47th Annual Forum Proceedings*, May 1991, pp 137 to 153.
12. Richards, Dick, and C. D. Pilcher, "F/A-18A Initial Sea Trials," *Technical Review of the Society of Experimental Test Pilots*, Vol. 16, No. 1, 1981, pp. 10 to 22.
13. Stowe, Steve, and Gary Jennings, "F-15E Initial Flight Test Results," *Thirty-first Symposium Proceedings of the Society of Experimental Test Pilots*, Sep. 1987, pp. 171 to 186.
14. Parham, Tom, Jr., and David Popelka, "V-22 Pilot-in-the-Loop Aeroelastic Stability Analysis," presented at the *American Helicopter Society 47th Annual Forum*, Phoenix, AZ, 6 to 8 May 1991.
15. Niewoehner, Rob, and Steve Minnich, "F-14 Dual Hydraulic Failure Flying Qualities Evaluation," *Thirty-fifth Symposium Proc. of the Society of Experimental Test Pilots*, Sep. 1991, pp. 4 to 15.
16. Dornheim, Michael A., "Report Pinpoints Factors Leading to YF-22 Crash," *Aviation Week and Space Technology*, 9 Nov. 1992, pp. 53 to 54.
17. *Aircraft Accident Report PB 93-910408*, National Transportation Safety Board, NTSB/AAR-93/07, Washington, D.C., 27 Oct. 1993.
18. Givens, Margo L., *Evaluation of B-2 Susceptibility to Pilot-Induced Oscillations*, Northrop Grumman, B-2 Division, White Paper 120-4, 1 March 1994.
19. Dornheim, Michael A., and David Hughes "Boeing Corrects Several 777 PIOS," *Aviation Week and Space Technology*, 8 May 1995, p. 32.
20. Johnston, D. E., and D. T. McRuer, *Investigation of Interactions Between Limb-Manipulator Dynamics and Effective Vehicle Roll Control Characteristics*, NASA CR-3983, May 1986.

21. Johnston, D. E., and B. L. Aponso, *Design Considerations of Manipulator and Feel System Characteristics in Roll Tracking*, NASA CR-4111, Feb. 1988.
22. Mitchell, D. G., B. L. Aponso, D. H. Klyde, *Effects of Lateral Stick Characteristics on Handling Qualities and Pilot Dynamics*, NASA CR-4443, June 1992.
23. Norton, William J., Captain, USAF, "Aeroelastic Pilot-in-the-Loop Oscillations," *Flight Vehicle Integration Panel Workshop on Pilot-Induced Oscillations*, AGARD-AR-335, Feb. 1995.
24. Ashkenas, I. L., R. E. Magdaleno, and D. T. McRuer, *Flight Control and Analysis Methods for Studying Flying and Ride Qualities of Flexible Transport Aircraft*, NASA CR-172201, Aug. 1983. (A shorter summary appears as "Flexible Aircraft Flying and Ride Qualities," in *NASA Aircraft Controls Research 1983*, NASA Conference Publication 2296, October 25-27, 1983, Gary P. Beasley, Compiler).
25. McRuer, Duane and Ezra Krendel, *Dynamic Response of Human Operators*, WADC-TR-56-524, Oct. 1957. (Also, "The Human Operator as a Servo System Element," *J. Franklin Inst.*, Vol. 267, No. 5, May 1959, pp. 381-403 and No. 6, June 1959, pp. 511-536).
26. Krendel, Ezra S., and Duane T. McRuer, "A Servomechanisms Approach to Skill Development," *J. Franklin Inst.*, Vol. 269, No. 1, Jan. 1960, pp. 24-42.
27. McRuer, D. T., and H. R. Jex, "A Review of Quasi-Linear Pilot Models," *IEEE Trans. Human Factors in Electronics.*, Vol. HFE-8, No. 3, Sept. 1967, pp. 231-249.
28. Young, L. R., "Human Control Capabilities," J.F. Parker and V.R. West (eds.), 2nd Edition, *Bioastronautics Data Book*, Chapter 16, NASA SP-3006, 1973, pp. 751-806.
29. McRuer, D. T., and E. S. Krendel, *Mathematical Models of Human Pilot Behavior*, AGARDograph No. 188, Jan. 1974.
30. McRuer, D. T., "Human Dynamics in Man-Machine Systems," *Automatica*, Vol. 16, No. 3, May 1980, pp. 237-253.
31. Krendel, E. S., and D. T. McRuer, "Psychological and Physiological Skill Development - A Control Engineering Model," in A. S. Iberall and J. B. Reswick, (eds.), *Technical and Biological Problems of Control - A Cybernetic View; Proc. of IFAC Conference*, Instrument Society of America, Pittsburgh, PA, 1970, pp. 657-665; also in *Proc. of Fourth Annual NASA-University Conference on Manual Control*, NASA SP-192, Mar. 1968, pp. 275-288.
32. Allen, R. Wade, and Duane T. McRuer, "The Man/Machine Control Interface - Pursuit Control," *Automatica*, Vol. 15, No. 6, Nov. 1979, pp. 683-686.
33. Jagacinski, Richard J. and Sehchang Hah, "Progression-Regression Effects in Tracking Repeated Patterns," *J. Experimental Psychology: Human Perception and Performance*, Vol. 14, No. 1, 1988, pp. 77-88.
34. Magdaleno, R. E., and D. T. McRuer, *Effects of Manipulator Restraints on Human Operator Performance*, AFFDL-TR-66-72, Dec. 1966.
35. McRuer, D. T., and R. E. Magdaleno, *Human Pilot Dynamics with Various Manipulators*, AFFDL-TR-66-138, Dec. 1966.
36. Graham, Dunstan, *Research on the Effect of Nonlinearities on Tracking Performance*, AMRL-TR-67-9, July 1967.

37. Magdaleno, R. E., D. . McRuer, and G. P. Moore, *Small Perturbation Dynamics of the Neuromuscular System in Tracking Tasks*, NASA CR-1212, Dec. 1968.
38. Jex, H. R., and R. E. Magdaleno, "Biomechanical Models for Vibration Feedthrough to Hands and Head for a Semisupine Pilot," *Aviation, Space and Environ. Med.*, Vol. 49, No. 1, Jan. 1978, pp. 304-316.
39. Hess, Ronald A., "A Model-Based Investigation of Manipulator Characteristics and Pilot/Vehicle Performance," *J. Guidance and Control*, Vol. 6, No. 5, Oct. 1983.
40. Ellson, J. I. and F. Gray, *Frequency Responses of Human Operators Following a Sine Wave Input*, USAF AMC Memo Rept MCREXD-694-2N, 1948.
41. McRuer, Duane T., Warren F. Clement, Peter M. Thompson and Raymond E. Magdaleno, *Minimum Flying Qualities. Volume II: Pilot Modeling for Flying Qualities Applications*, WRDC-TR-89-3125, Vol. II, Jan. 1990.
42. Smith, R. H. *A Theory for Longitudinal Short-Period Pilot-Induced Oscillations*, AFFDL-TR-77-57, June 1977.
43. Smith, Ralph H., *Notes on Lateral-Directional Pilot-Induced Oscillations*, AFWAL TR-81-3090, Mar. 1982.
44. Graham, Dunstan and Duane McRuer, *Analysis of Nonlinear Control Systems*, John Wiley and Sons, Inc., New York, 1961. (Also Dover, 1971).
45. *Military Standard, Flying Qualities of Piloted Aircraft*, MIL-STD-1797A, 30 Jan. 1990.
46. Davenport, Otha, *Aircraft Digital Flight Control Technical Review Final Briefing*, AFMC/EN, 26 Oct. 1992.
47. *Draft MIL-STD-1797A Update*, ASC/ENFT, Flight Technology Branch, Flight Systems Engineering Division, Wright-Patterson Air Force Base, Ohio, 4 Nov. 1993.
48. Smith, Ralph H., and Norman D. Geddes, *Handling Quality Requirements for Advanced Aircraft Design Criteria for Fighter Airplanes*, AFFDL-TR-78-154, Aug. 1979.
49. Smith, R. H., "The Smith-Geddes Criteria," presented at the SAE Aerospace Control and Guidance Systems Committee meeting, Reno NV, 11 Mar. 1993.
50. Gibson, J. C., "The Prevention of PIO by Design," in *Active Control Technology: Applications and Lessons Learned*, AGARD CP-560, Jan. 1995.
51. Gibson, John C., "Piloted Handling Qualities Design Criteria for High Order Flight Control Systems," *Criteria for Handling Qualities of Military Aircraft*, AGARD CP-333, Apr. 1982.
52. Buchacker, E., H. Galleithner, R. Kohler, and M. Marchand, "Development of MIL-8785C Into a Handling Qualities Specification for a New European Fighter Aircraft," in *Flying Qualities*, AGARD CP-508, Quebec City, Canada, 15-18 Oct. 1990.
53. Cooper, George E. and Robert P. Harper, Jr., *The Use of Pilot Rating in the Evaluation of Aircraft Handling Qualities*, NASA TN D-5153, Apr. 1969.
54. McRuer Duane, "Estimation of Pilot Rating via Pilot Modeling," *Flying Qualities*, AGARD CP-508, 15-18 Oct. 1990, Quebec City, Canada.

55. Kempel, Robert W., Weneth D. Painter, and Milton O. Thompson, *Developing and Flight Testing the HL-10 Lifting Body: A Precursor to the Space Shuttle*, NASA Reference publication 1332, Apr. 1994.
56. Garland, Michael P., Michael K. Nelson, and Richard C. Patterson, *F-16 Flying Qualities with External Stores*, AFFTC-TR-80-29, Feb. 1981.
57. Bjorkman, Eileen A., Captain, USAF, *Flight Test Evaluation of Techniques to Predict Longitudinal Pilot Induced Oscillations*, Thesis AFIT/GAE/AA/86J-1, Air force Institute of Technology, Wright-Patterson Air force Base, Ohio, Dec. 1986.
58. Mitchell, David G., Roger H. Hoh, Bimal L. Aponso, and David H. Klyde, "The Measurement and Prediction of Pilot-in-the-Loop Oscillations," AIAA-94-3670, *Proceedings of the AIAA Guidance and Control Conference*, Scottsdale, AZ, 1-3 Aug. 1994.
59. Hanke, Dietrich, "Handling Qualities Analysis on Rate Limiting Elements in Flight Control Systems," *Flight Vehicle Integration Panel Workshop on Pilot Induced Oscillations*, AGARD-AR-335, February 1995.
60. Heffley, Robert K., and Wayne F. Jewell, *Aircraft Handling Qualities Data*, NASA CR-2144, Dec. 1972.
61. Taylor, Lawrence W., Jr., and John W. Smith, *An Analysis of the Limit-Cycle and Structural-Resonance Characteristics of the X-15 Stability Augmentation System*, NASA TN D-4287, Dec. 1967.
62. Teper, G. L., H. R. Jex, D. T. McRuer, and W. A. Johnson, *A Study of Fully-Manual and Augmented-Manual Control Systems for Saturn V Booster Using Analytical Pilot Models*, NASA CR-1079, July 1968.
63. Allen, R. W., and R. E. Magdaleno, *Manual Control Performance and Dynamic Response During Sinusoidal Vibration*, AMRL-TR-73-78, Oct. 1973.
64. McRuer, Duane, Irving Ashkenas, and Dunstan Graham, *Aircraft Dynamics and Automatic Control*, Princeton University Press, Princeton, New Jersey, 1973.
65. Neal, T. Peter, and Rogers E. Smith, *An In-Flight Investigation to Develop Control System Design Criteria for Fighter Aircraft*, AFFDL-TR-70-74, Volume I, Dec. 1970.
66. Mitchell, David G., Roger H. Hoh, Bimal L. Aponso, and David H. Klyde, *Proposed Incorporation of Mission-Oriented Flying Qualities into MIL-STD-1797A*, WL-TR-94-3162, Oct. 1994.
67. A'Harrah, Ralph C., "Communique with DLR and Others," NASA Headquarters, Washington D.C., 14 July 1992.
68. Gibson, J. C., "Looking for the Simple PIO Model," in *Flight Vehicle Integration Panel Workshop on Pilot Induced Oscillations*, AGARD AR-335, Feb. 1995.
69. Chalk, C., "Calspan Experience of PIO and the Effects of Rate Limiting," in *Flight Vehicle Integration Panel Workshop on Pilot Induced Oscillations*, AGARD AR-335, Feb. 1995.
70. A'Harrah, Ralph C., "An Alternate Control Scheme for Alleviating Aircraft-Pilot Coupling," AIAA-94-3673, *Proceedings of the AIAA Guidance and Control Conference*, Scottsdale, AZ, 1-3 Aug. 1994.
71. Deppe, P. R., *Flight Evaluation of a Software Rate Limiter Concept*, Calspan Final Report No. 8091-1, Calspan Advanced Technology Center, March 1993.

72. Ohmit, E. E., *NT-33A In-Flight Investigation into Flight Control System Rate Limiting*, Calspan Final Report No. 7738-24, Calspan Advanced Technology Center, Feb. 1994.
73. Deppe, P. R., C. R. Chalk, M. Shafer, *Flight Evaluation of an Aircraft with Side and Centerstick Controllers and Rate-Limited Ailerons*, Calspan Final Report No. 8091-2, Calspan Advanced Technology Center, April 1994.

APPENDIX A

A CATALOG OF PIO TIME HISTORIES FOR OPERATIONAL, EXPERIMENTAL, AND RESEARCH AIRCRAFT

APPENDIX A

A CATALOG OF PIO TIME HISTORIES FOR OPERATIONAL, EXPERIMENTAL, AND RESEARCH AIRCRAFT

This Appendix, a joint effort between Systems Technology, Inc. and Hoh Aeronautics, Inc., presents the results of a literature search undertaken as part of Wright Laboratories' Unified Pilot-Induced Oscillation (PIO) Theory program. The material compiled here includes a table summary of specific PIO events as identified in Refs. A-1 through A-32 followed by corresponding time traces reproduced from the same references. Since many of the time traces have been obtained from decades old reports or have been copied from copies, the quality of the reproductions is not always ideal. The search was limited initially to the STI library which contains a comprehensive but not complete collection of data. There is no attempt here to analyze these PIOs. The intent is simply to initiate a library of documented PIO events.

A list of PIO events originally compiled in Ref. A-14 and enhanced by the Air Force was used as a starting point for the literature search. Unfortunately, the authors were unable to locate information on many of the PIO events listed. Documentation for over thirty specific events, however, was found and compiled in Table A-1. These events include PIOs, pitch and roll high frequency ratchet, and some "bubbles." The table includes only operational or flight test PIOs. Other known PIOs (e.g. the F-4B Sageburner PIO) were not included in the table because time histories were not available. In Table A-1 "PIO Date" is either the specific date the event occurred or the date on the time history. If neither of these is available, the date is listed as January of the year the report was published. When multiple events came from the same report, they are entered as having occurred on the first, then the second, and so on. It should be noted that the "PIO Axis" column is only intended to be a general axis designation (e.g., a "pitch" axis PIO may be pitch or flight path). Figures A-1 through A-32 display the time histories for the Table A-1 events.

Flight research PIOs (e.g., USAF NT-33A or TIFS events) with documented time histories are given in Table A-2. Since the flight condition details for these cases are well defined in the corresponding references, this information has not been included here. Figures A-33 through A-117 display the time histories for the Table A-2 events. Table 3 lists specific PIO events for which time traces were not available. An addendum to the original search was made from material collected during the independent STI and HAI research efforts that includes 8 flight test PIOs (Refs. A-33 to A-36) and 8 flight research PIOs (Refs. A-37 and A-38). The additional material follows Figure A-117. The events are listed in Tables A-4 and A-5, respectively, and the corresponding time traces are shown in Figures A-118 through A-133.

Table A-1 PIO Events with Documented Time Histories

Fig. No.	Aircraft	PIO Date	Ref. No.	Flight Condition	Mach	A/S (KIAS)	Altitude (ft)	PIO Axis
A-1	C-97	12/25/54	A-1	GCA Approach	0.2	130	500	Pitch
A-2	F-101B	01/01/58	A-2	CR (Rolls)	0.776		10,040	Roll
A-3	F-101B	01/02/58	A-2	CR (Rolls)	0.87		10,680	Roll
A-4	B-52G	01/01/59	A-3	AR	0.76	268	33,000	Pitch
A-5	B-52G	01/02/59	A-3	AR	0.76	268	33,000	Roll
A-6	F-104B	01/02/59	A-4	CR	0.80	3,600	Yaw	
A-7	YF-5A	01/02/59	A-5	SB Extension	0.881		11,690	Pitch
A-8	YF-5A	01/02/59	A-5	TO		130	1	Pitch
A-9	X-15	06/08/59	A-6	L (Aug. off)		200	0	Pitch
A-10	T-38A	01/26/60	A-7	CR	0.91		6,500	Pitch
A-11	M2-F2 (Flt. 1)	01/01/71	A-8	Turn to final	0.48		5,500	Roll/Yaw
A-12	M2-F2 (Flt. 10)	01/02/71	A-8	All. pulse (aug. off)	0.61		19,000	Roll/Yaw
A-13	M2-F2 (Flt. 16)	01/03/71	A-8	Turn to final	0.48		8,577	Roll/Yaw
A-14	YF-16	01/20/74	A-9	TO		130	0	Roll
A-15	YF-16	12/13/74	A-10	CR (Rolls)	0.8		10,600	Roll
A-16	YF-12	01/01/75	A-11	AR	0.77		25,000	Pitch
A-17	YF-12	01/02/75	A-11	AR	0.77		25,000	Pitch
A-18	YA-7D DIGITAC	06/01/76	A-12	CR (Roll)	0.75	348	20,340	Roll
A-19	Shuttle Orbiter	11/26/77	A-13	L	0.3		0	Pitch/Roll
A-20	F-8 DFBW	04/11/78	A-14	L		190	1	Pitch
A-21	F-15A	05/01/79	A-15	HQDT (4g)	0.86		10,000	Pitch
A-22	F-15C	08/30/79	A-16	HQDT (3g)	0.95		15,000	Pitch
A-23	F-15C	08/30/79	A-16	HQDT (CAS off)	0.95		15,000	Pitch
A-24	F-15C	08/30/79	A-16	HQDT (CAS off)	0.95		15,000	Roll
A-25	F/A-18A	01/01/81	A-17	Carrier Ldg		140	50	Roll
A-26	F/A-18 (w/o eddy damper)	01/01/82	A-18	CR	0.8		20,000	Roll
A-27	F-15E (CAS off)	01/01/87	A-19	CR	0.9		20,000	Pitch
A-28	F-14A (Dual Hyd Fail)	01/01/91	A-20	AR	200	0	Pitch	
A-29	F-14A (Dual Hyd Fail)	01/02/91	A-20	AR (Tracking)	250	0	Pitch	
A-30	YF-22A	04/25/92	A-21	Fly-By	200	0	Pitch	
A-31	B-2	01/01/94	A-22	L (Off Nom.)		0	Pitch	
A-32	B-2	01/02/94	A-22	AR (Disconnect)		0	Pitch	

Table A-2 Research PIO Events with Documented Time Histories

Fig. No.	Aircraft	Configuration	Ref. No.	Flight Condition	PIO Axis
A-33	X-15		A-23	CR	Roll/Yaw
A-34	NT-33A	1G	A-24	Pitch Tracking	Pitch
A-35	NT-33A	4D	A-24	Pitch Tracking	Pitch
A-36	NT-33A	6E	A-24	Pitch Tracking	Pitch
A-37	NT-33A	14	A-25	Pitch Tracking	Pitch
A-38	NT-33A	1-3	A-26	L	Pitch
A-39	NT-33A	2-4	A-26	L	Pitch
A-40	NT-33A	2-4	A-26	L	Pitch
A-41	NT-33A	2-9	A-26	L	Pitch
A-42	NT-33A	4-10	A-26	L	Pitch
A-43	NT-33A	4-10	A-26	L	Pitch
A-44	NT-33A	5-3	A-26	L	Pitch
A-45	NT-33A	6-1 (YF-17)	A-26	L	Pitch
A-46	NT-33A	6-1 (YF-17)	A-26	L	Pitch
A-47	NT-33A	P5-1	A-27	L	Pitch
A-48	NT-33A	P10D	A-27	L	Pitch
A-49	NT-33A	P11	A-27	L	Pitch
A-50	NT-33A	P12	A-27	L	Pitch
A-51	NT-33A	P12A	A-27	L	Pitch
A-52	NT-33A	P12B	A-27	L	Pitch
A-53	NT-33A	P13A	A-27	L	Pitch
A-54	NT-33A	P14	A-27	L	Pitch
A-55	NT-33A	P15	A-27	L	Pitch
A-56	NT-33A	P16	A-27	L	Pitch
A-57	NT-33A	P16A	A-27	L	Pitch
A-58	NT-33A	L8	A-27	L	Roll
A-59	NT-33A	L8B	A-27	L	Roll
A-60	NT-33A	L10	A-27	L	Roll
A-61	NT-33A	L11C	A-27	L	Roll
A-62	NT-33A	L11D	A-27	L	Roll
A-63	NT-33A	L14B	A-27	L	Roll
A-64	NT-33A	L16A	A-27	L	Roll
A-65	NT-33A	5-2	A-28	Lat. HUD Tracking	Roll
A-66	TIFS	X-29A -AR/PA	A-29	PA	Roll
A-67	TIFS	5 + 200ms	A-30	L	Pitch
A-68	TIFS	5 + 200ms	A-30	L	Pitch
A-69	TIFS	11	A-30	L	Pitch
A-70	TIFS	11	A-30	L	Pitch
A-71	TIFS	11	A-30	L	Pitch
A-72	TIFS	11	A-30	L	Pitch
A-73	TIFS	12	A-30	L	Pitch
A-74	TIFS	12	A-30	L	Pitch
A-75	TIFS	13	A-30	L	Pitch
A-76	TIFS	13	A-30	L	Pitch
A-77	TIFS	14	A-30	L	Pitch
A-78	TIFS	14	A-30	L	Pitch
A-79	TIFS	21	A-30	L	Pitch
A-80	TIFS	21	A-30	L	Pitch
A-81	TIFS	21	A-30	L	Pitch
A-82	TIFS	21	A-30	L	Pitch
A-83	TIFS	22	A-30	L	Pitch
A-84	TIFS	22	A-30	L	Pitch
A-85	TIFS	22	A-30	L	Pitch
A-86	TIFS	22	A-30	L	Pitch

Table A-2 Research PIO Events with Documented Time Histories

Fig. No.	Aircraft	Configuration	Ref. No.	Flight Condition	PIO Axis
A-87	TIFS	22A	A-30	L	Pitch
A-88	TIFS	22A	A-30	L	Pitch
A-89	TIFS	27	A-30	L	Pitch
A-90	TIFS	27	A-30	L	Pitch
A-91	TIFS	27	A-30	L	Pitch
A-92	TIFS	27	A-30	L	Pitch
A-93	TIFS	27	A-30	L	Pitch
A-94	TIFS	27	A-30	L	Pitch
A-95	TIFS	27	A-30	L	Pitch
A-96	TIFS	27	A-30	L	Pitch
A-97	TIFS	28	A-30	L	Pitch
A-98	TIFS	28	A-30	L	Pitch
A-99	TIFS	28	A-30	L	Pitch
A-100	TIFS	28	A-30	L	Pitch
A-101	TIFS	28A	A-30	L	Pitch
A-102	TIFS	28A	A-30	L	Pitch
A-103	NT-33A	2-B	A-31	L	-Pitch
A-104	NT-33A	2-5	A-31	L	Pitch
A-105	NT-33A	2-7	A-31	L	Pitch
A-106	NT-33A	2-8	A-31	L	Pitch
A-107	NT-33A	3-1	A-31	L	Pitch
A-108	NT-33A	3-6	A-31	L	Pitch
A-109	NT-33A	3-8	A-31	L	Pitch
A-110	NT-33A	3-12	A-31	L	Pitch
A-111	NT-33A	3-13	A-31	L	Pitch
A-112	NT-33A	5-9	A-31	L	Pitch
A-113	NT-33A	5-10	A-31	L	Pitch
A-114	NT-33A	5-11	A-31	L	Pitch
A-115	NT-33A	141F (10)	A-32	Gun Tracking	Roll
A-116	NT-33A	141F (10)	A-32	LATHOS Tracking	Roll
A-117	NT-33A	143P (18)	A-32	LATHOS Tracking	Roll

Table A-3 Additional Known PIO Cases

Aircraft	PIO Description
Douglas A3D	Yaw PIO at low altitude, transonic flight
Douglas A4D-2	Pitch PIO at low altitude, transonic flight
Grunman A-6	Lateral-directional PIO
NASA AD-1 Oblique Wing	Multi-axis PIO
Douglas XB-19	Pitch PIO during landing approach
Convair B-38	Lateral-directional PIO
Sikorsky CH-53E	Multi-axis PIO in precision hover with heavy sling loads
Convair XF2Y-1	Pitch PIO during takeoff
McDonnell Douglas F-4B	Pitch PIO at low altitude, high-speed flight condition
Northrop XF-89A	Pitch PIO during dive recovery
North American F-86D	Pitch PIO during formation flying while pulling g's
North American F-100C	Pitch PIO during tight maneuvering
McDonnell Douglas F-101B	Pitch PIO
General Dynamics F-16	Roll ratchet, directional PIO with asymmetric store, and supersonic lateral-directional PIO
General Dynamics AFTI/F-16	Roll ratchet, roll PIO during power approach, Dutch roll PIO, PIO during aerial refueling, low altitude PIO
Gruumman F-14A	Multi-axis PIO at high α with some β
Republic F-105	Lateral PIO during aerial refueling
Lockheed XF-104A	Pitch PIO
Convair F-106A	Pitch PIO
Northrop F-5A	Lateral-directional boresight oscillations
McDonnell Douglas F-15A	Pitch PIO
McDonnell Douglas F-15 SMTD	Pitch PIO in power approach
McDonnell Douglas F-15E	Pitch PIO up and away with CAS off
Saab JAS 39	Multi-axis PIO during power approach and during low altitude demonstration
Israeli Aircraft Industries Lavi	Lateral PIO in crosswind landings
Panavia MRCA	Pitch PIO during short takeoff
Parasev	Lateral rocking during ground tow
Curtiss SB2C-1	Pitch PIO
General Dynamics F-111	Lateral control coupling with sustained underwing heavy store limit cycle oscillation
Voyager	Pilot coupling with symmetric wing bending
Bell/Boeing V-22	Lateral oscillation on gear, antisymmetric mode destabilized by aileron, and symmetric mode destabilized by collective
Bell X-5	Multi-axis PIO
Bell XS-1	Pitch PIO during approach and landing

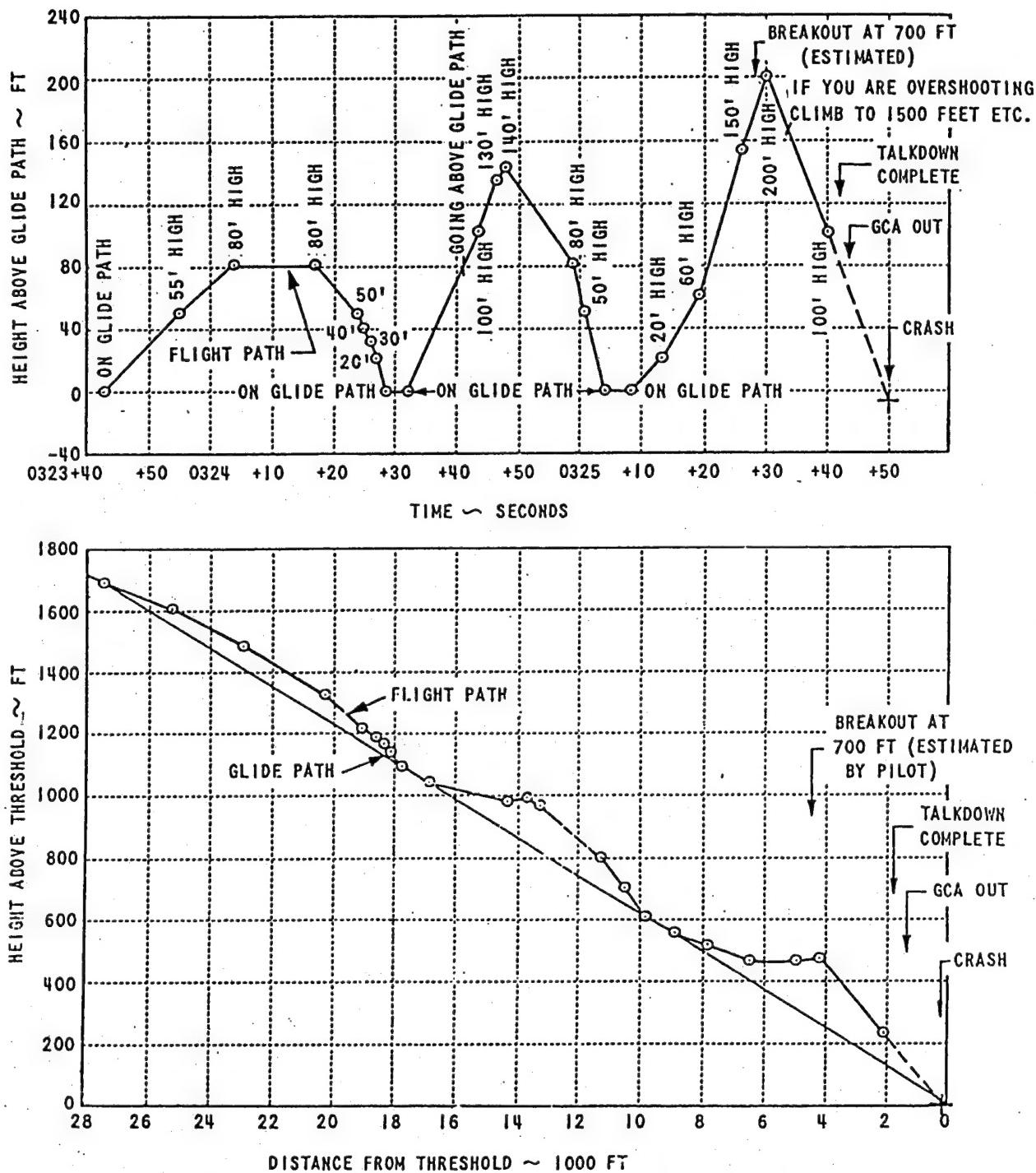


FIGURE I GCA POSITION REPORTS WITH RESPECT TO GLIDE PATH OF
BOAC STRATOCRUISER G-ALSA ACCIDENT 25 DECEMBER 1954
PRESTWICK, SCOTLAND

WADC TR 57-650

Figure A-1. C-97 (Ref. A-1)

Figure No. 54
AILERON ROLLS
F-101B USAF S/N 56-0233
Cruise Configuration

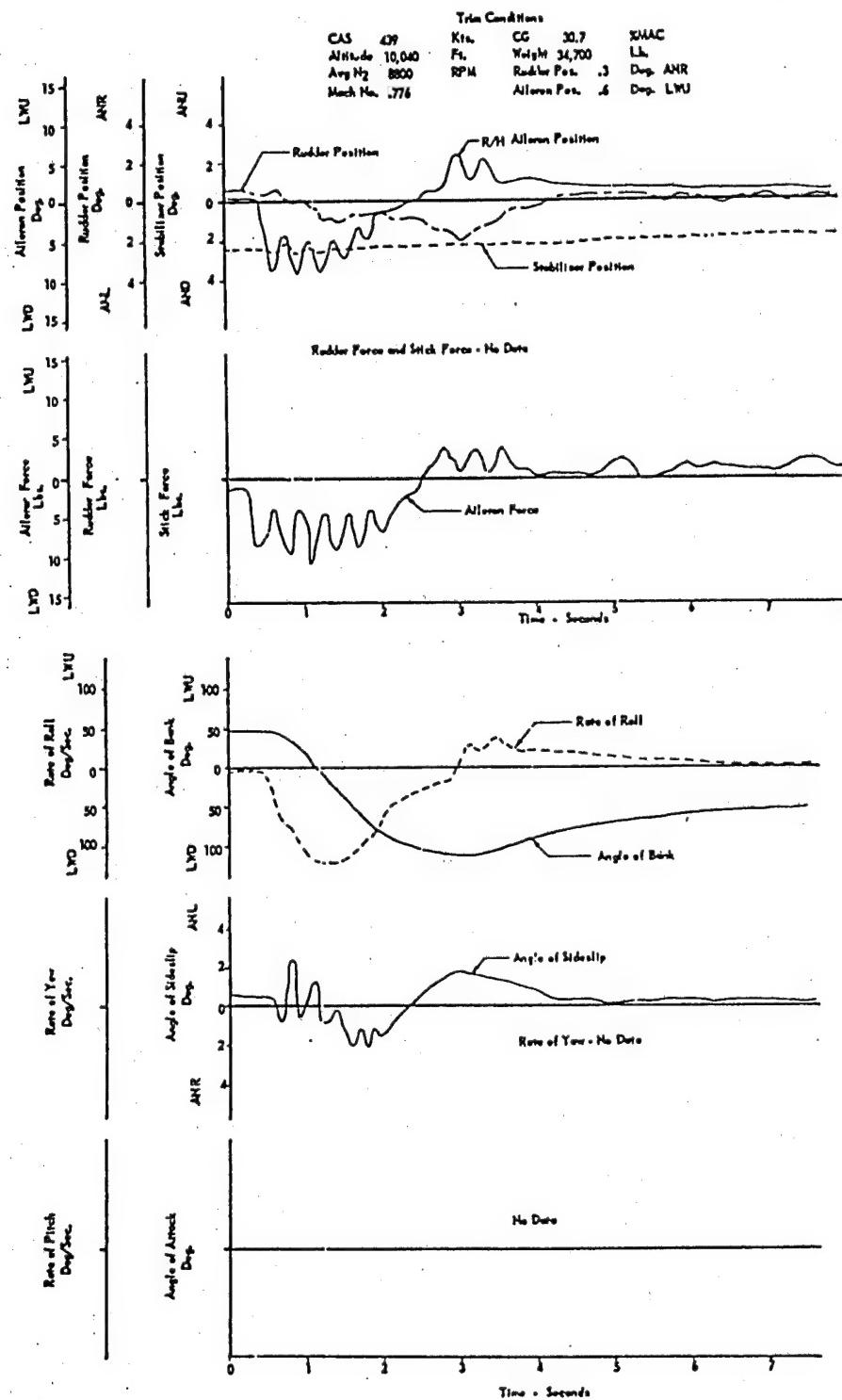


Figure A-2. F-101B (Ref. A-2)

Figure No. 55
AILERON ROLLS
F-101B USAF S/N 56-0233
Cruise Configuration

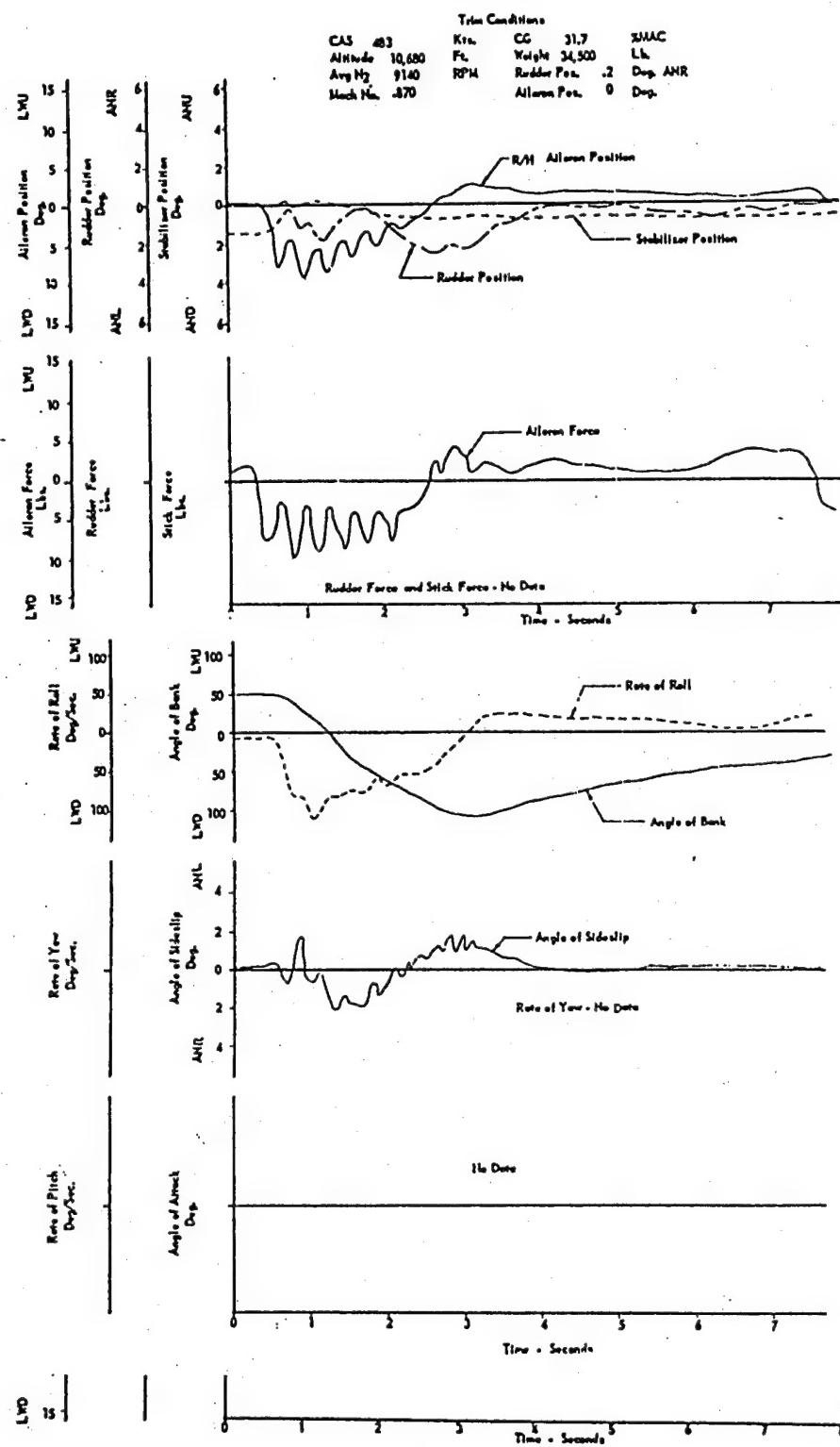


Figure A-3. F-101B (Ref. A-2)

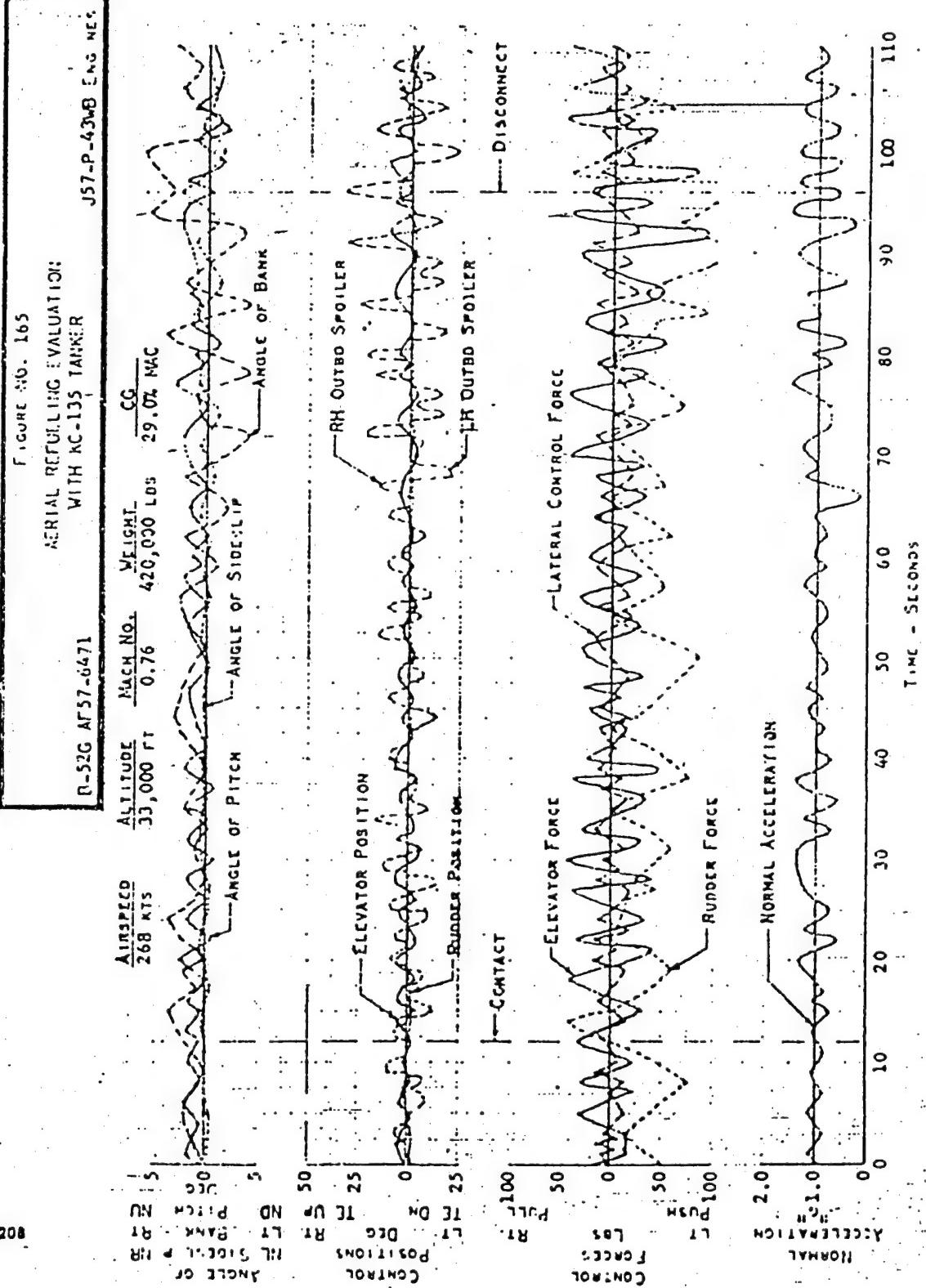


Figure A-4. B-52G (Ref. A-3)

208

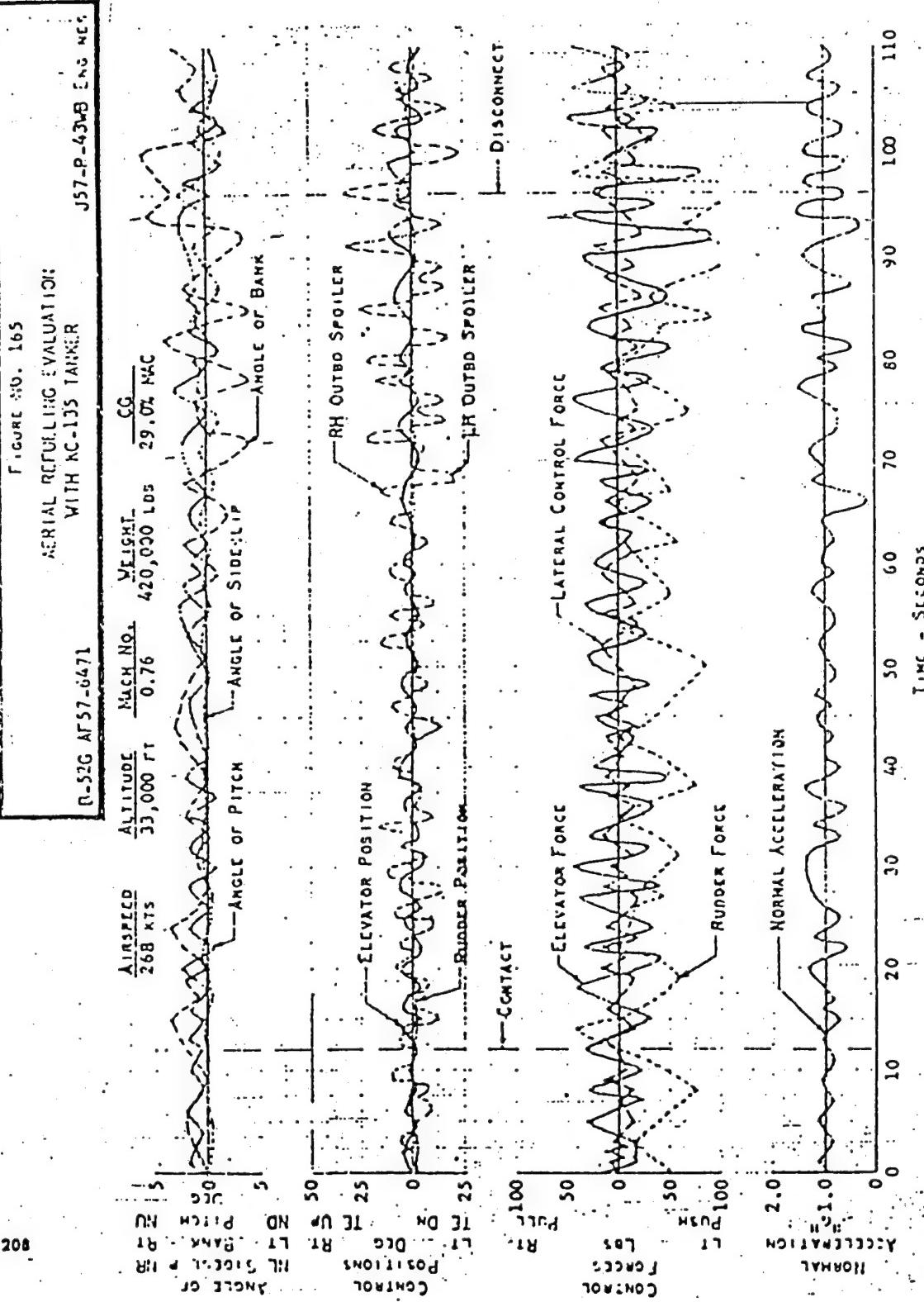


Figure A-5. B-52G (Ref. A-3)

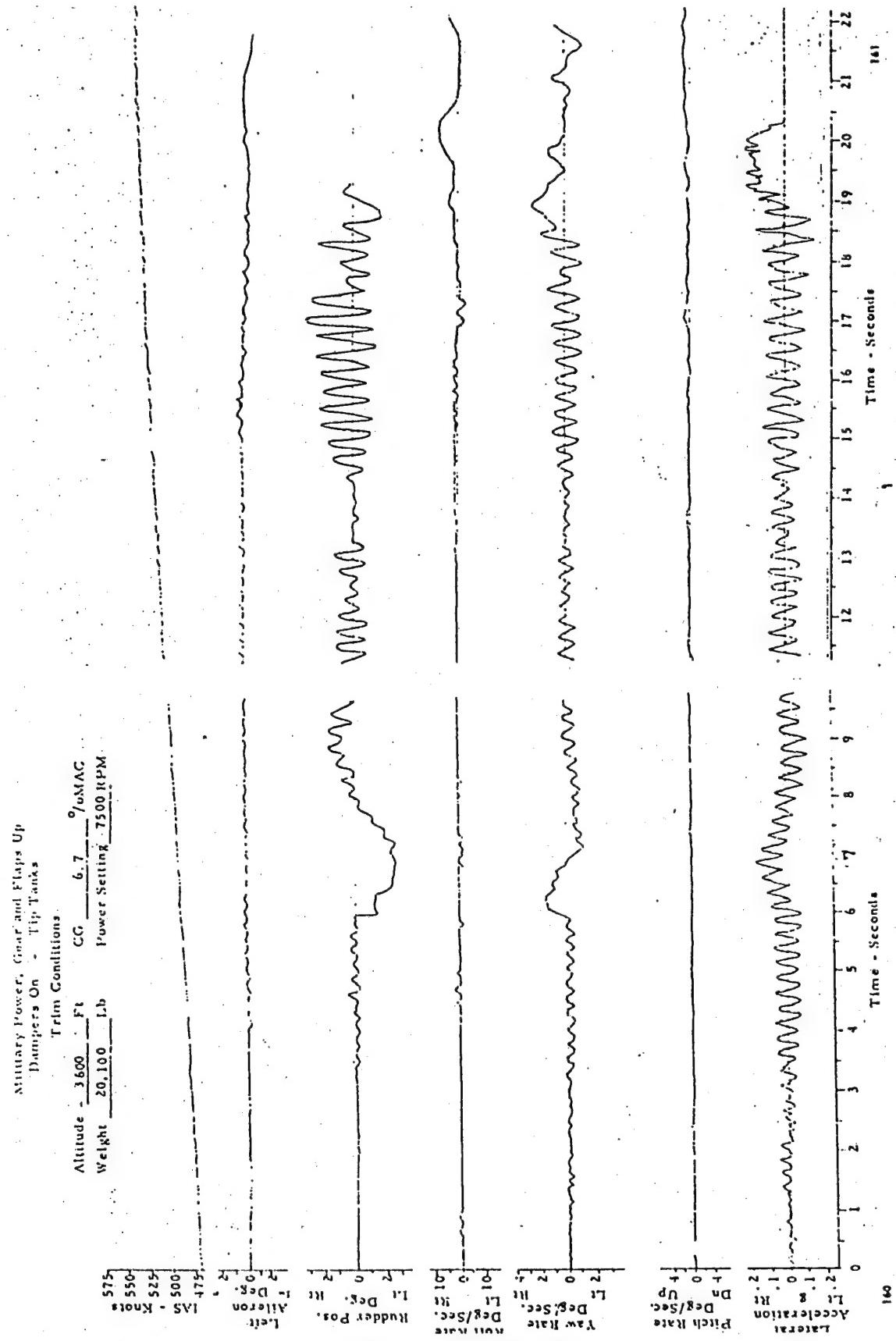


Figure A-6. F-104B (Ref. A-4)

TR-1313-1

A-12

Limited Distribution (see Reference for Time Trace)

Figure A-7. YF-5A (Ref. A-5)

Limited Distribution (see Reference for Time Trace)

Figure A-8. YF-5A (Ref. A-5)

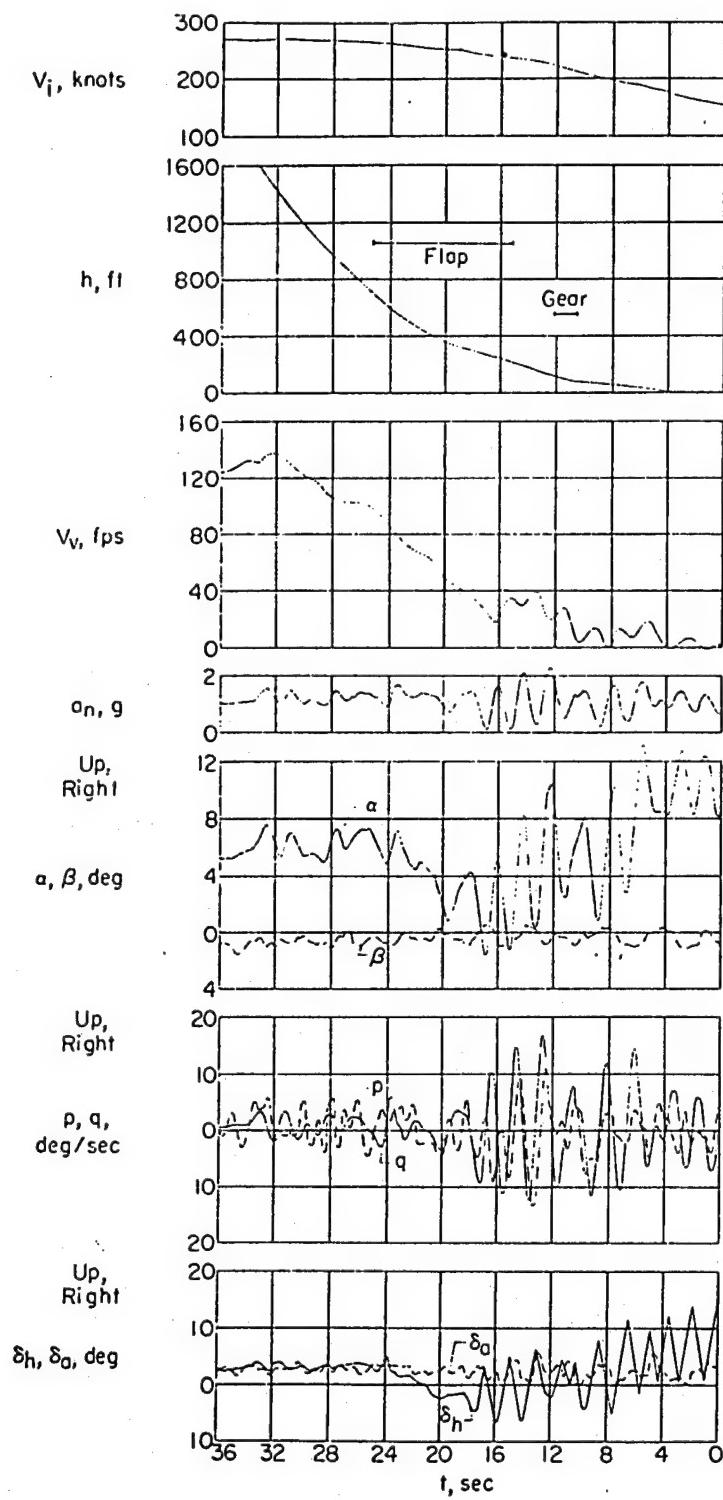


Figure 10.- Time history of the flare on X-15 flight 1-1-5.

Figure A-9. X-15 (Ref. A-6)

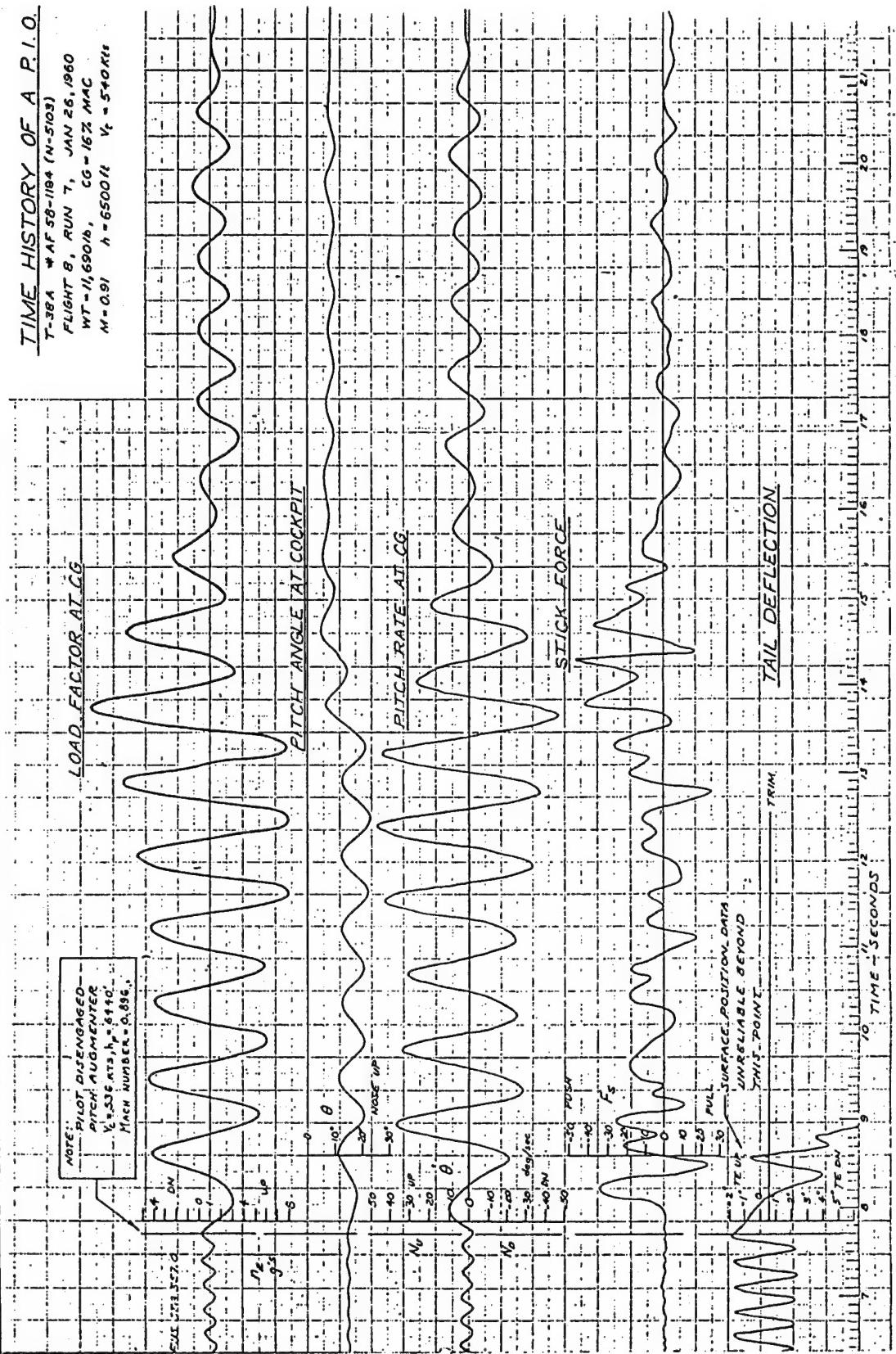
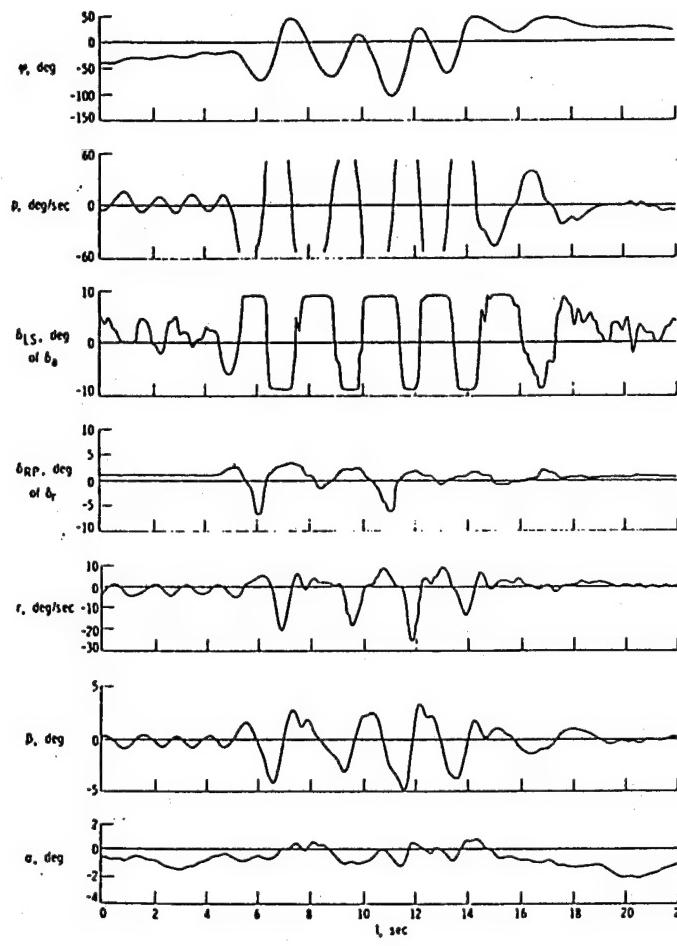
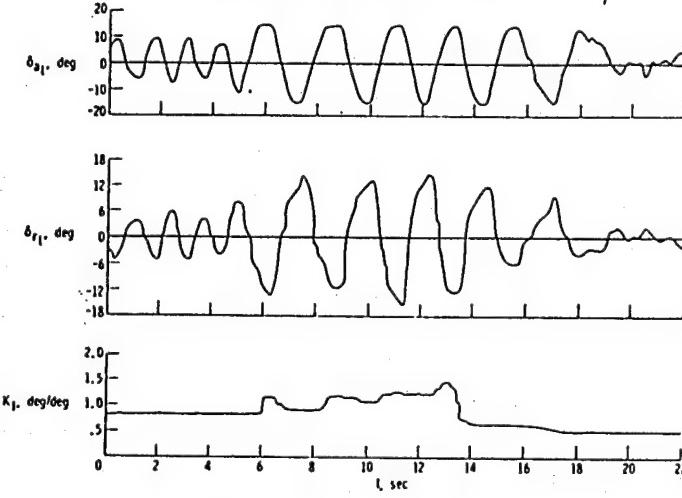


Figure A-10. T-38A (Ref. A-7)



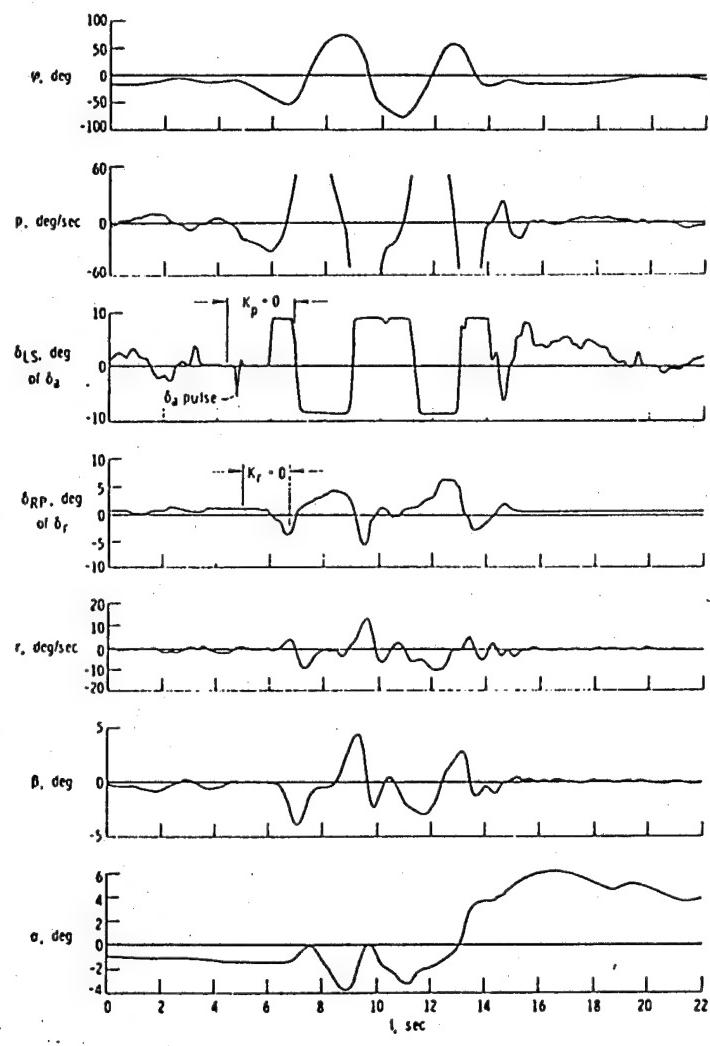
(a) Pilot's input and vehicle response.



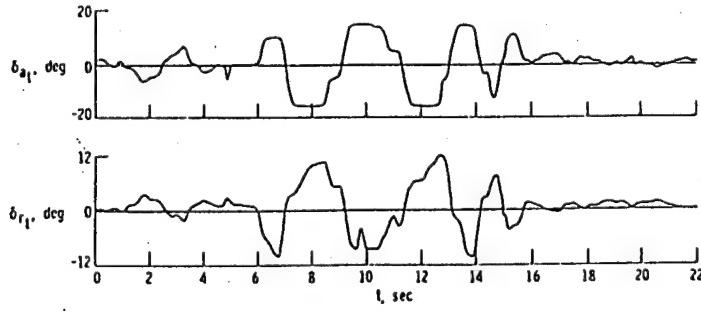
(b) Control and interconnect inputs.

Figure 8. Time history of pilot-induced lateral-directional oscillation on M2-F2 flight 1. $M = 0.48$; $h = 2830$ m (9275 ft) to 1678 m (5500 ft); $K_p = 0.6$; $K_r = 0.6$.

Figure A-11. M2-F2, Flight 1 (Ref. A-8)



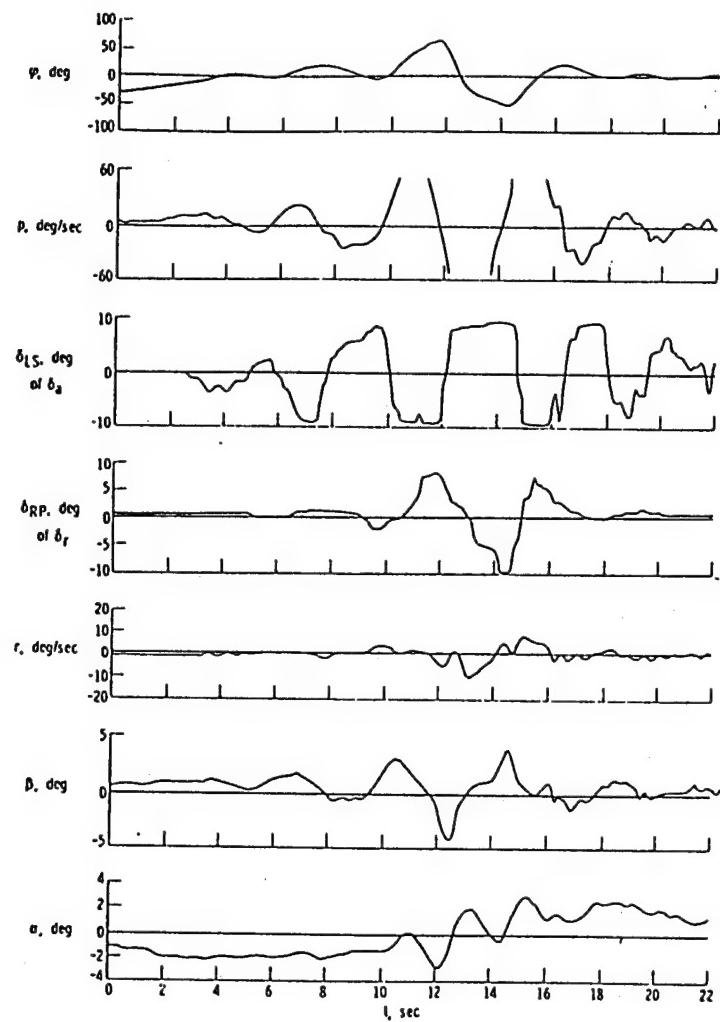
(a) Pilot's input and vehicle response.



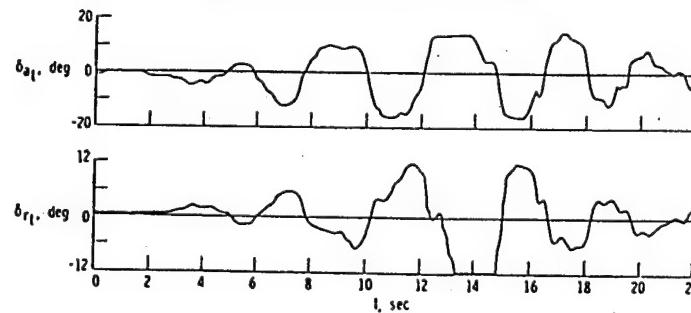
(b) Control inputs.

Figure 10. Time history of pilot-induced lateral-directional oscillation on M2-F2 flight 10. $M = 0.61$; $h = 7020 \text{ m}$ (23,000 ft) to 5500 m (19,000 ft); $K_p = 0.4$ and $K_f = 0.6$ except as noted; $K_f = 0.49$.

Figure A-12. M2-F2, Flight 10 (Ref. A-8)



(a) Pilot's input and vehicle response.



(b) Control inputs.

Figure 11. Time history of pilot-induced lateral-directional oscillation on M2-F2 flight 16. $M = 0.48$; $h = 2620 \text{ m}$ (8577 ft); $V = 159.5 \text{ m/sec}$ (523 ft/sec); $q = 12,100 \text{ N/m}^2$ (253 lb/ft²); $K_p = 0.2$; $K_r = 0.4$; $K_f = 0.45$.

Figure A-13. M2-F2, Flight 16 (Ref. A-8)

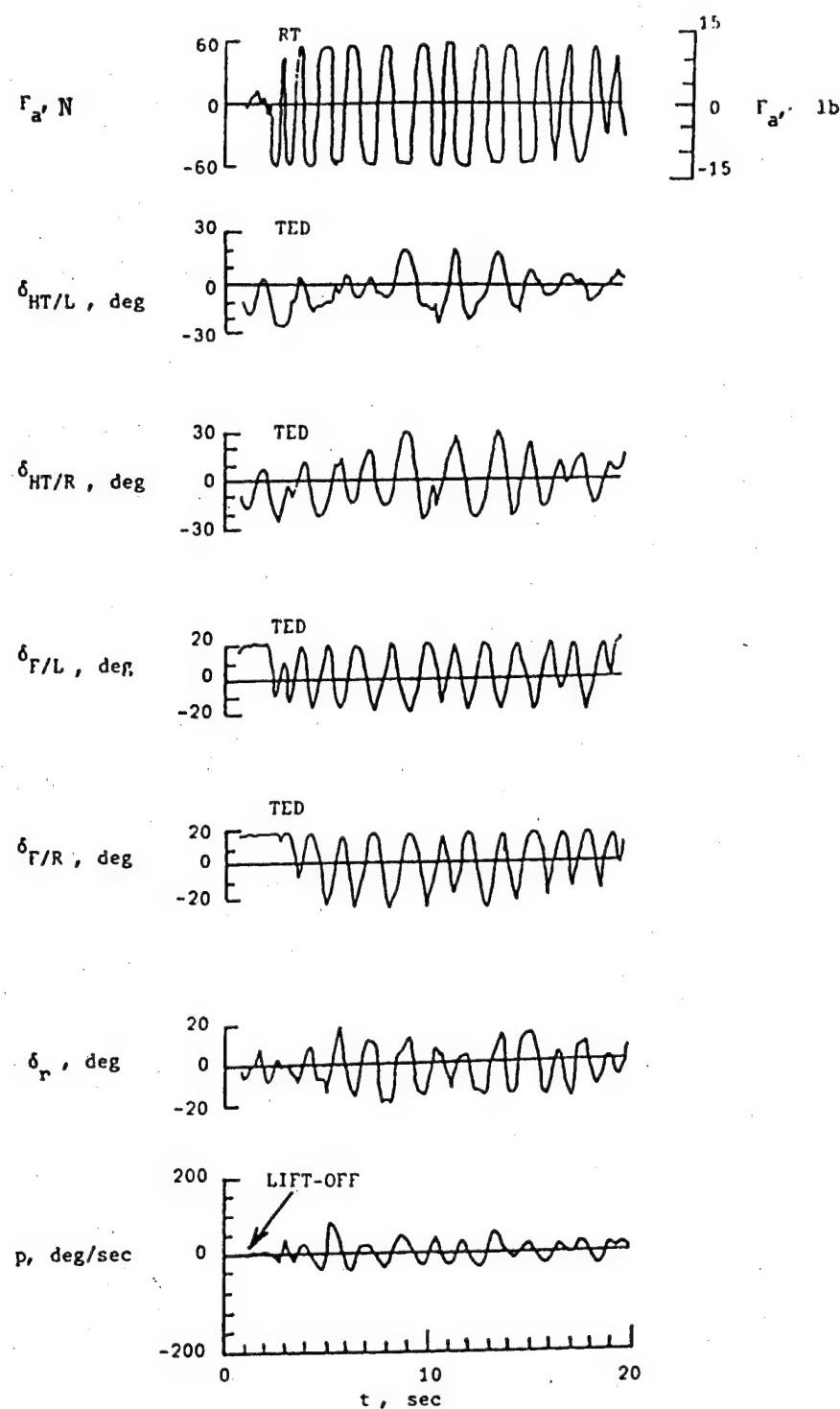


Figure 3. YF-16 pilot induced oscillation experienced on the first flight.

Figure A-14. YF-16 (Ref. A-9)

Limited Distribution (see Reference for Time Trace)

Figure A-15. YF-16 (Ref. A-10)

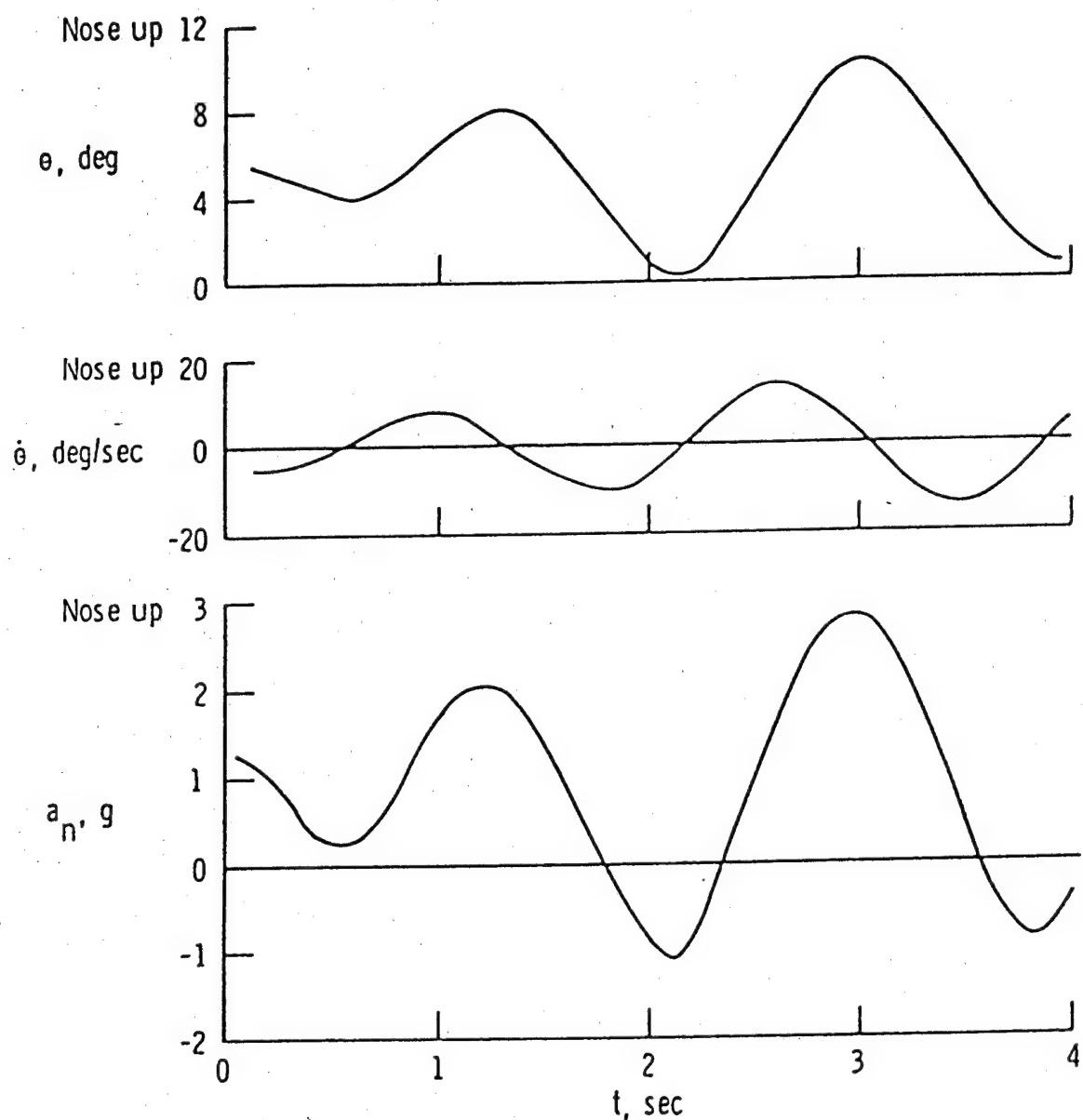
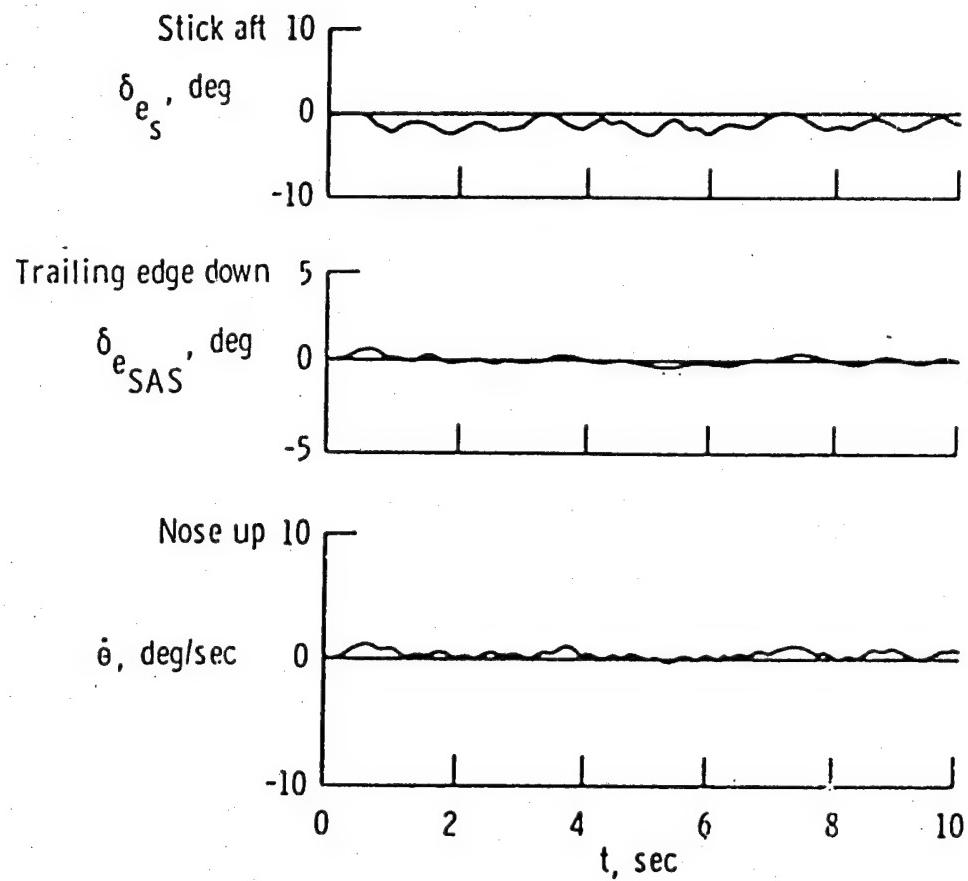


Figure 3. Large-amplitude PIO time history.

Figure A-16. YF-12 (Ref. A-11)



*Figure 2. Time history during refueling.
Typical of small-amplitude PIO tendency.*

Figure A-17. YF-12 (Ref. A-11)

Limited Distribution (see Reference for Time Trace)

Figure A-18. YA-7D Digitac (Ref. A-12)

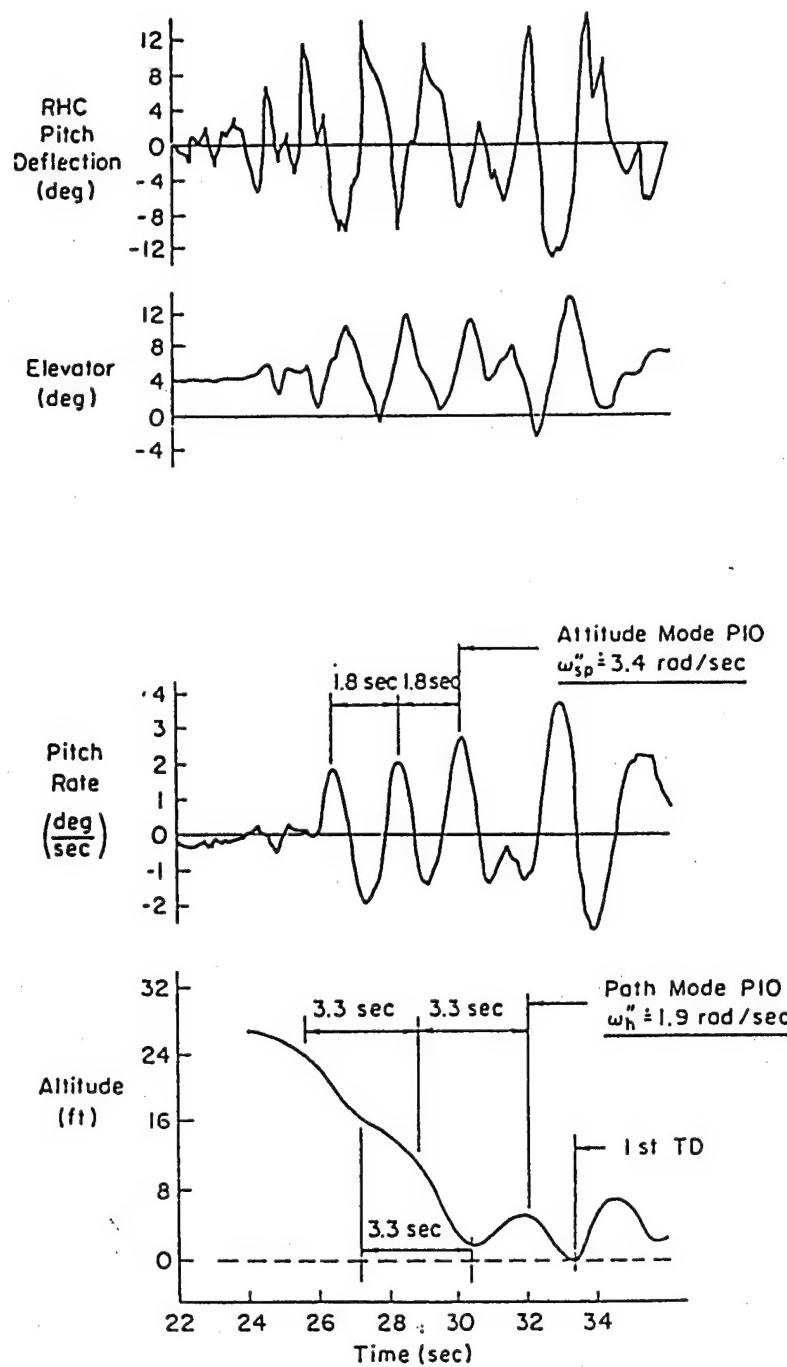


Figure 1. FF5 Flight Evidence of PIO

Figure A-19. Shuttle Orbiter (Ref. A-13)

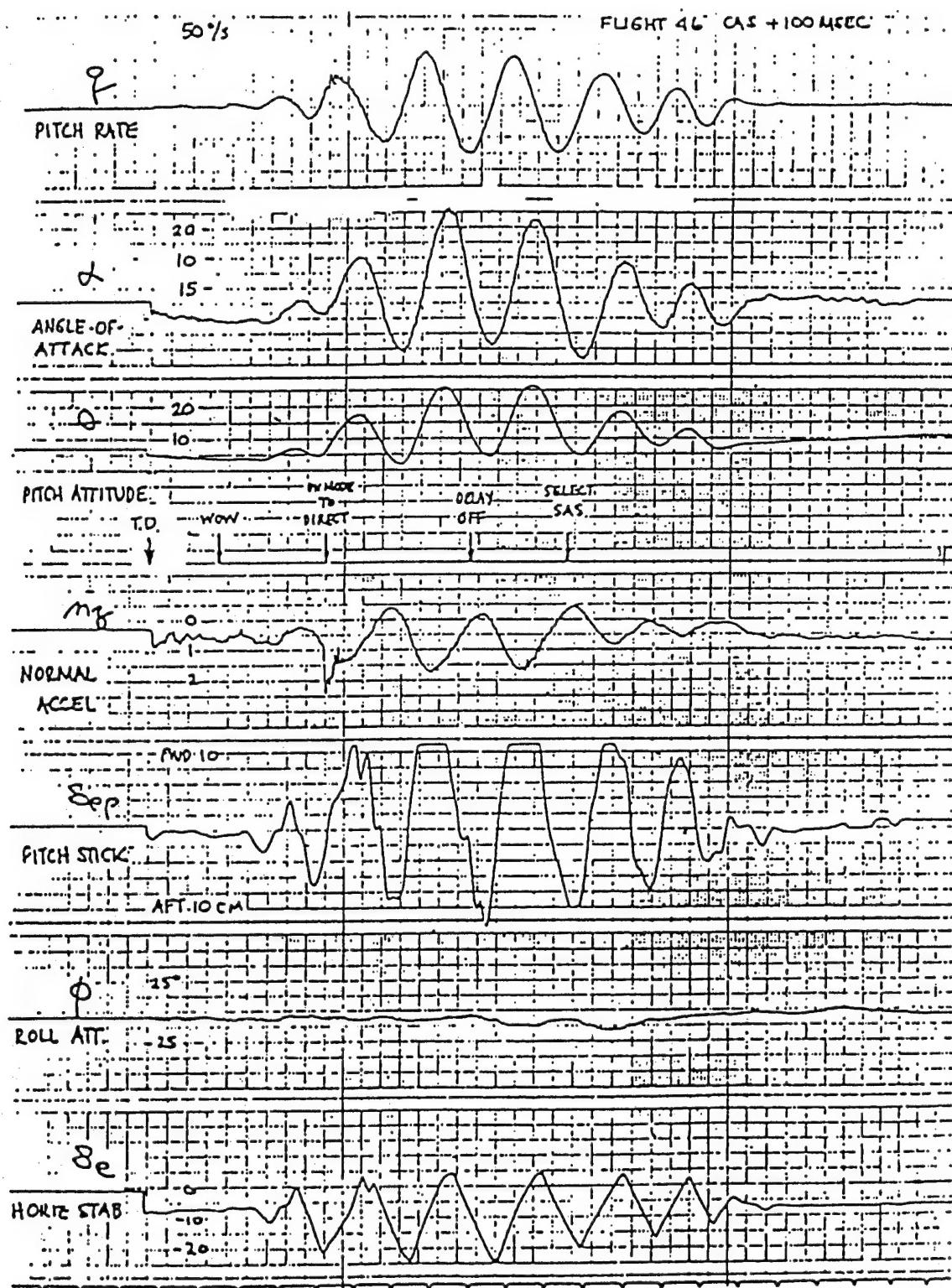


Fig. 17 Flight Recording of F-8 DFBW PIO
(NASA Ames/Dryden Flight Research Facility)

Figure A-20. F-8-DFBW (Ref. A-14)

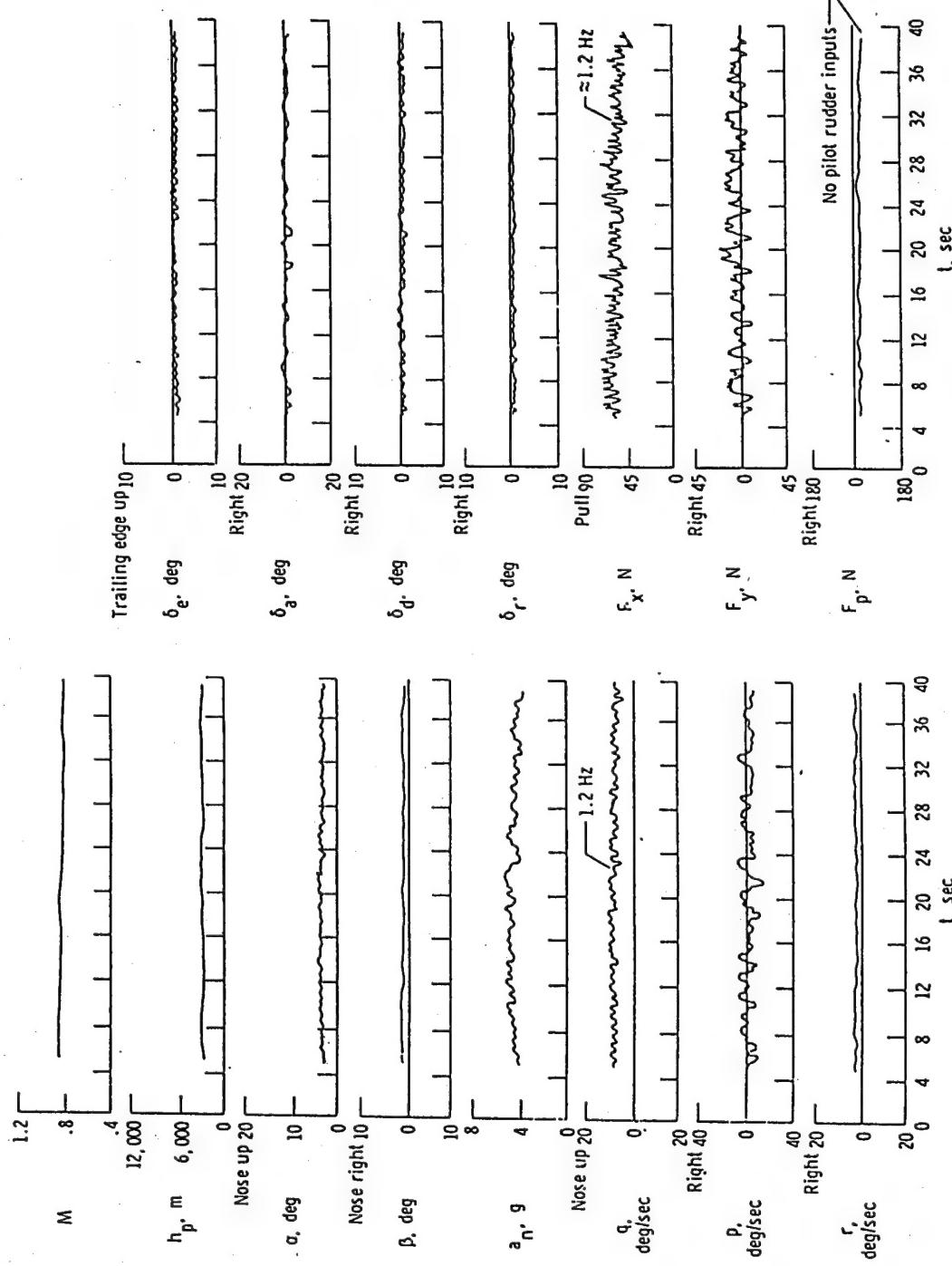


Figure A-21. F-15A. (Ref. A-15)

Figure 8. Constant g tracking time history illustrating pitch sensitivity. $M = 0.86$; $h_p = 3200 \text{ m}$; CAS on.

(b) Airplane control parameters.

Limited Distribution (see Reference for Time Trace)

Figure A-22. F-15C (Ref. A-16)

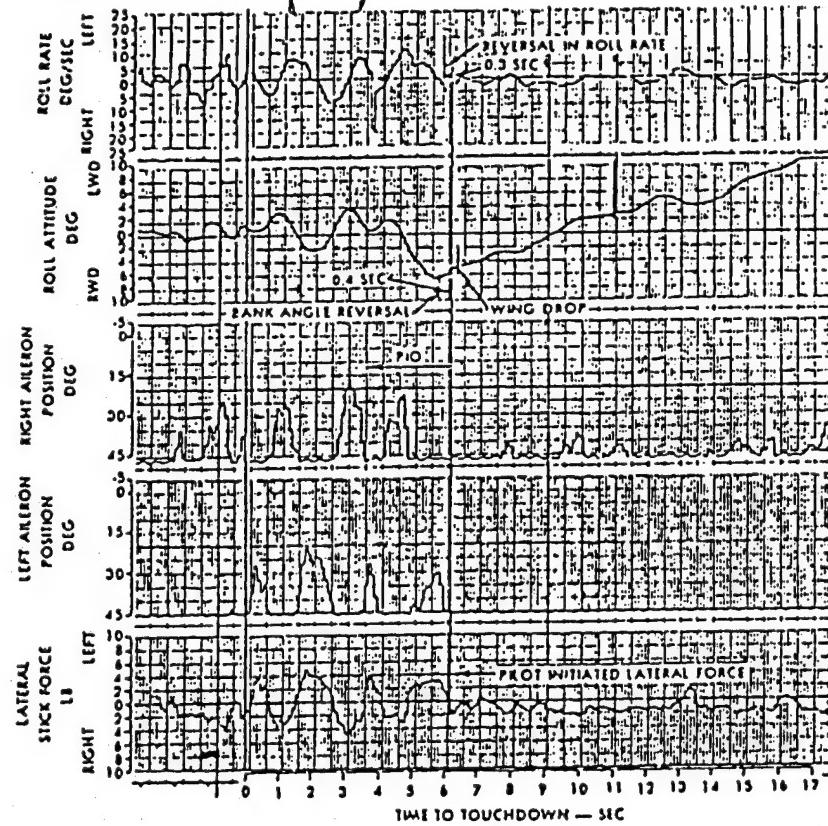
Limited Distribution (see Reference for Time Trace)

Figure A-23. F-15C (Ref. A-16)

Limited Distribution (see Reference for Time Trace)

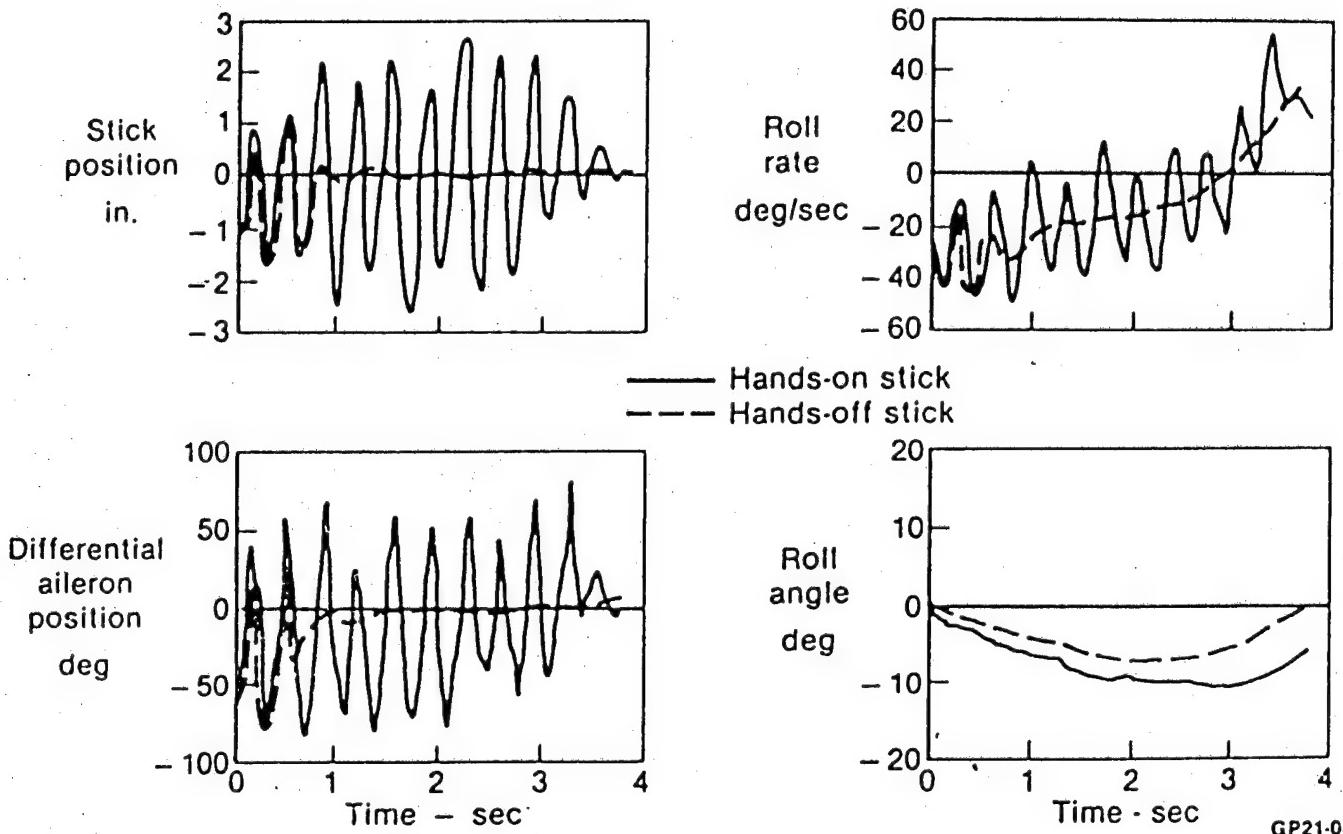
Figure A-24. F-15C (Ref. A-16)

TIME HISTORY OF LATERAL PILOT INDUCED OSCILLATION



Page 20 — The Society of Experimental Test Pilots

Figure A-25. F/A-18A (Ref. A-17)



GP21-0889-1

**Figure 10. Lateral Monkey-Induced-Oscillations
Stick Rap Without Eddy Current Damper**

Figure A-26. F/A-18, without eddy damper (Ref. A-18)

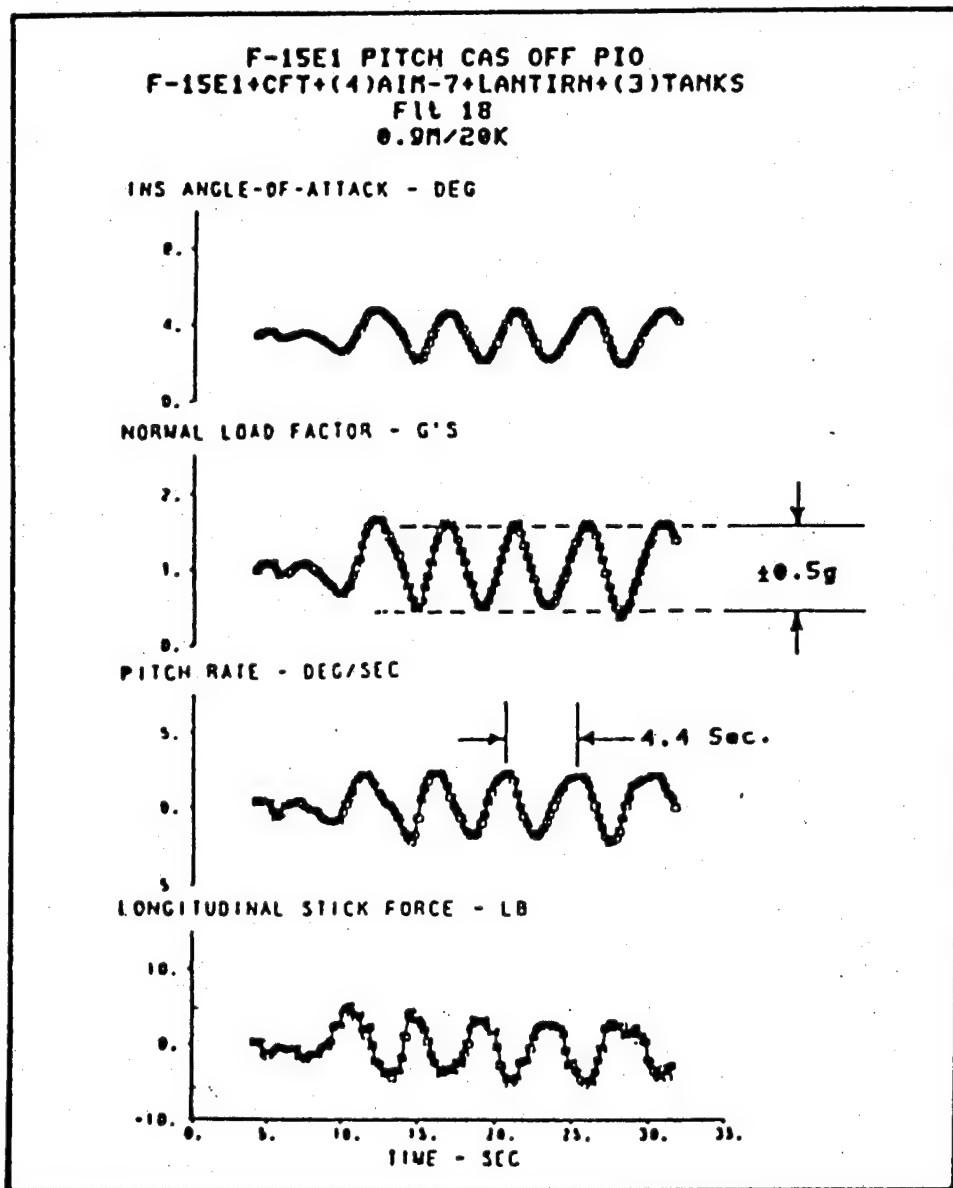


Figure A-27. F-15E (CAS off) (Ref. A-19)

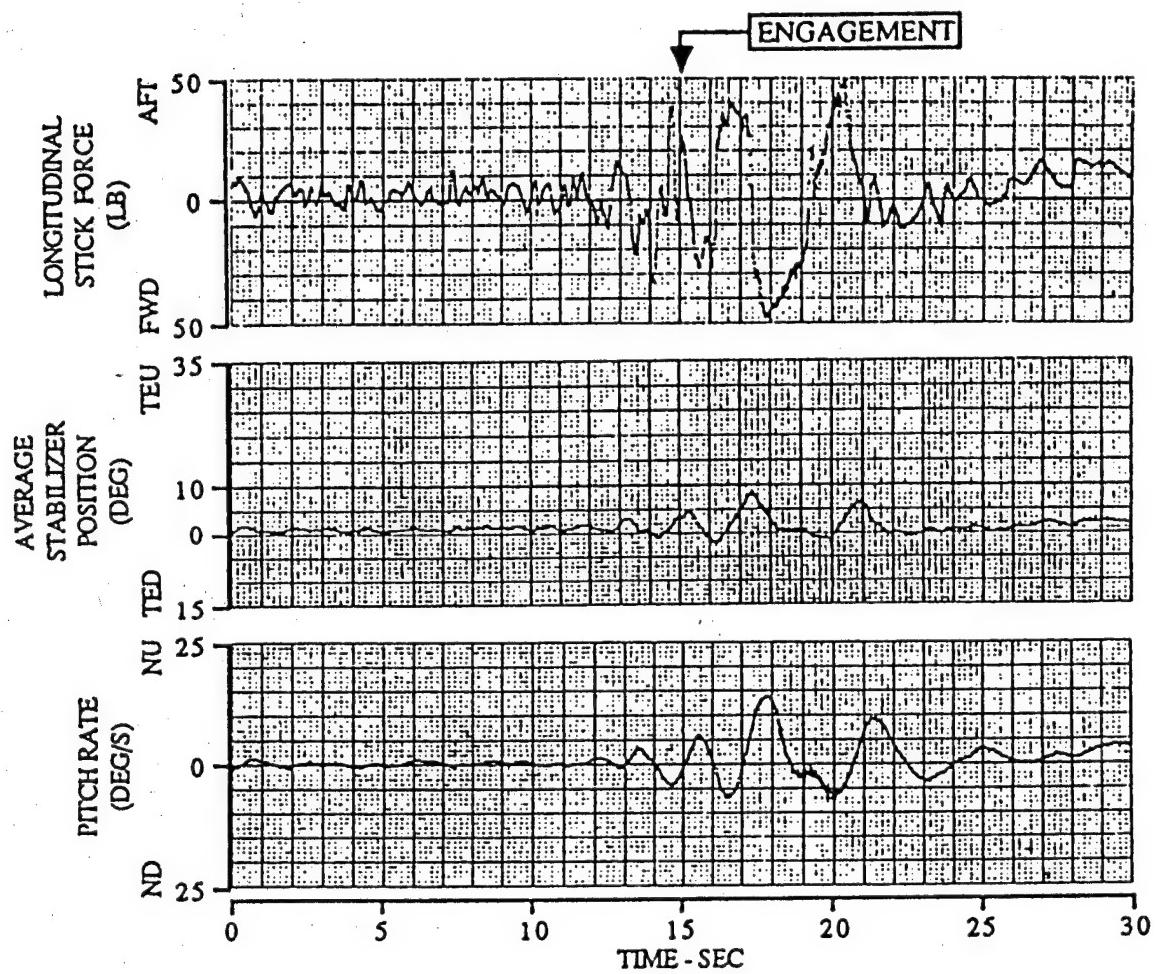


Figure 1
RATE LIMITING OF THE LONGITUDINAL CONTROL SYSTEM

Figure A-28. F-14A, Dual Hydraulic Failure (Ref. A-20)

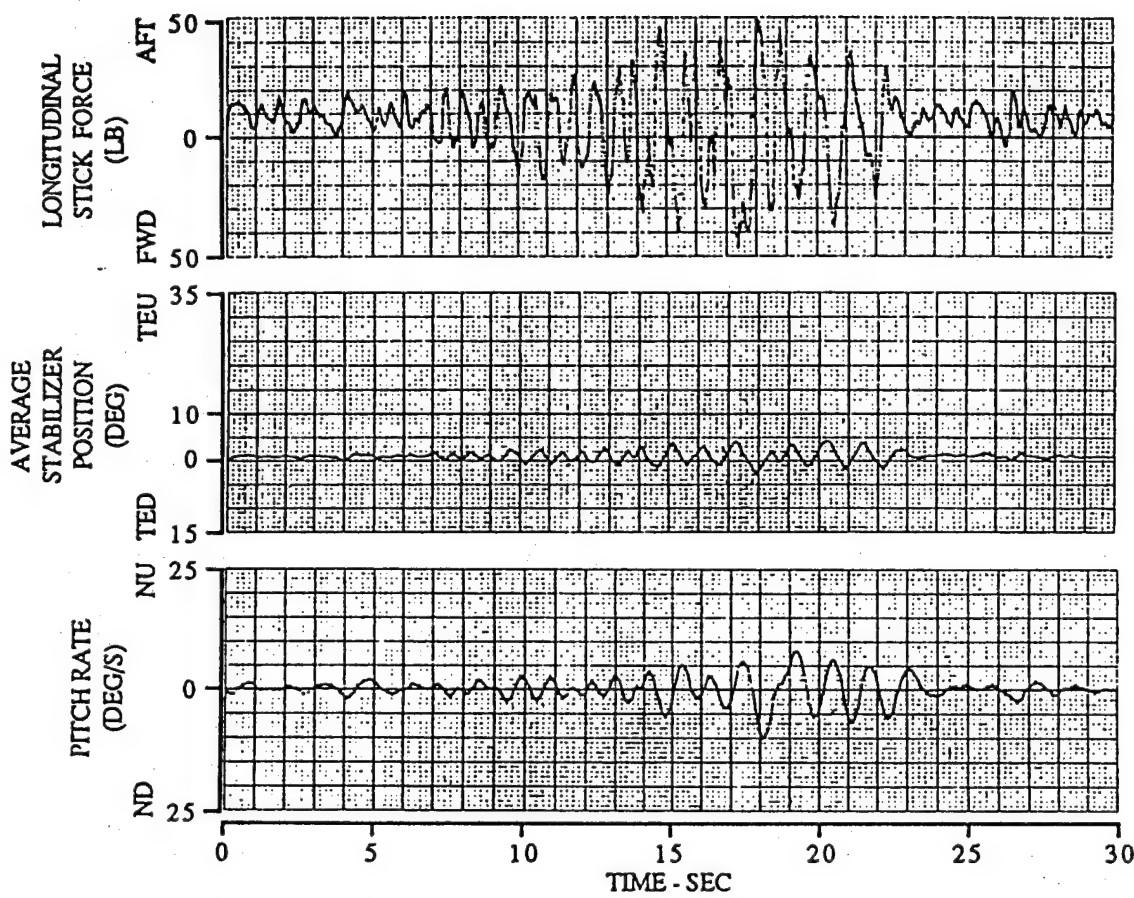


Figure 2
PIO DURING TRACKING DRILL

Figure A-29. F-14A, Dual Hydraulic Failure (Ref. A-20)

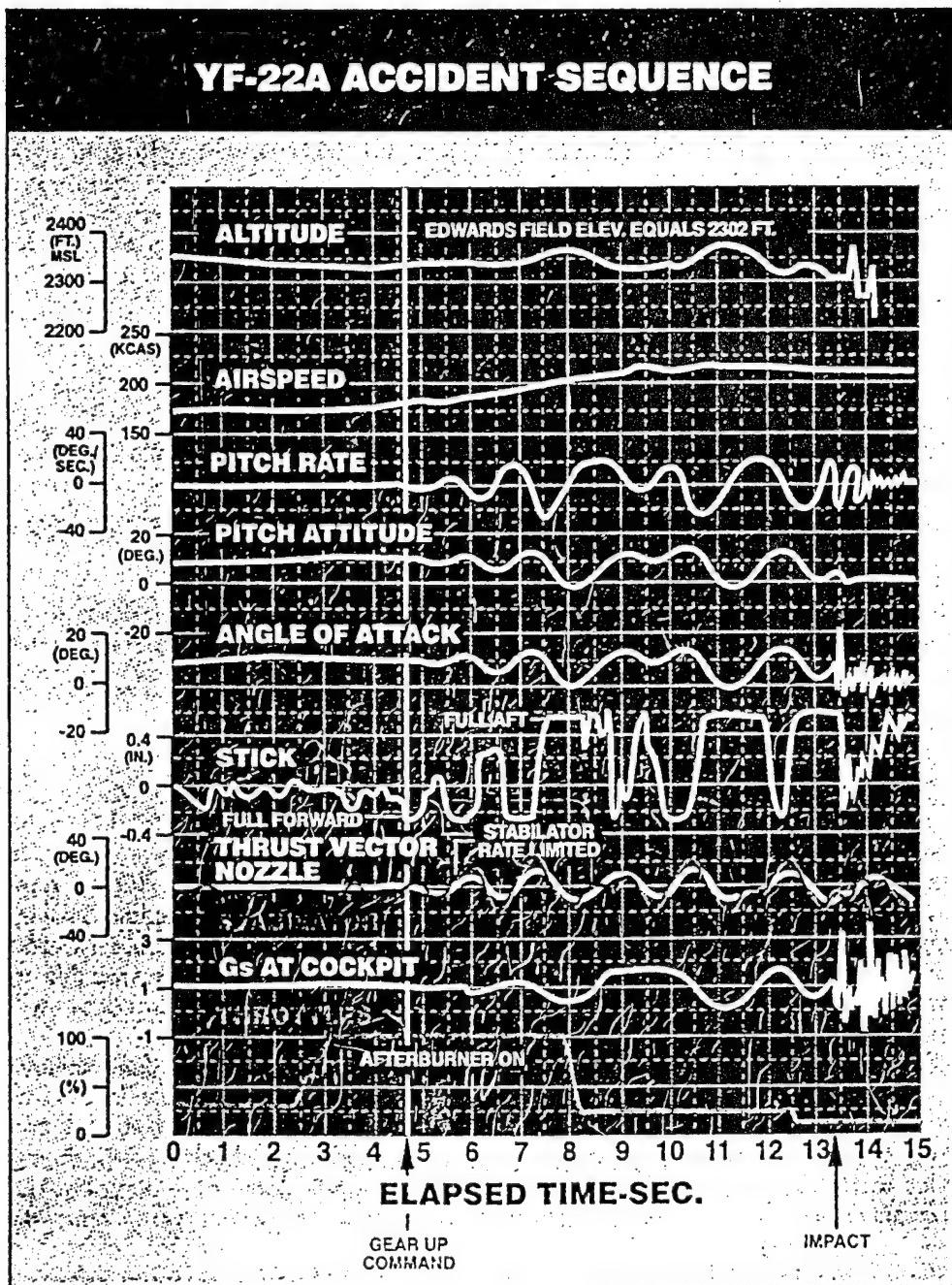


Figure A-30. YF-22A (Ref. A-21)

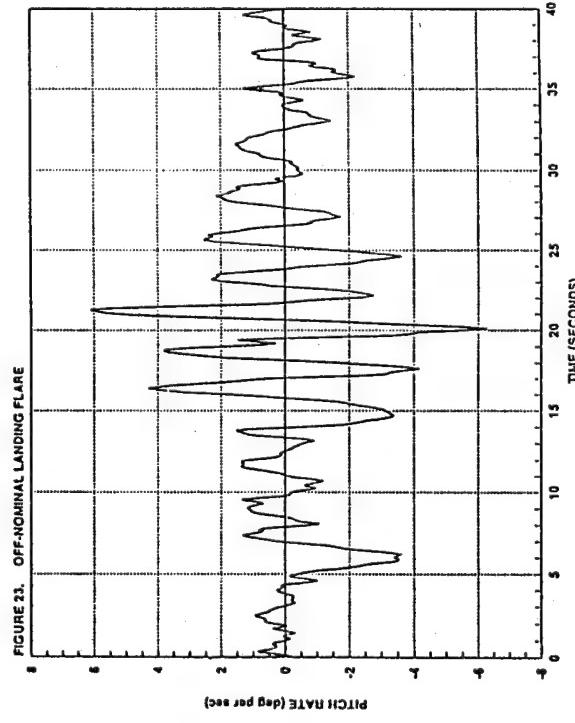
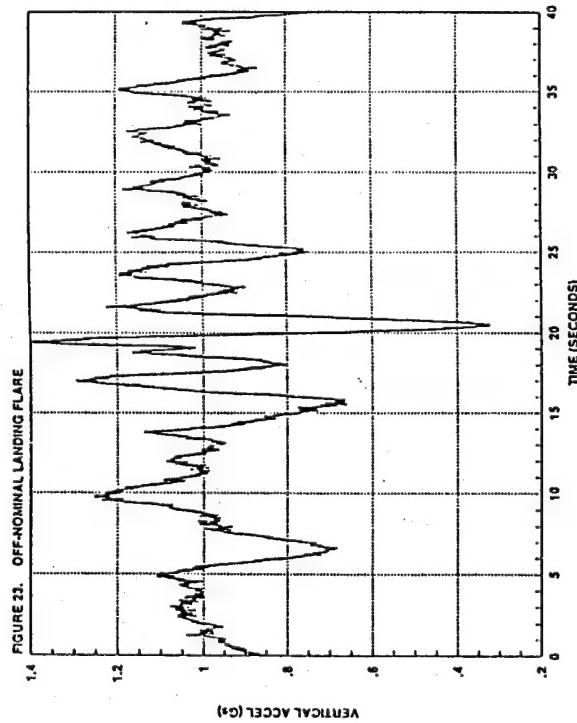
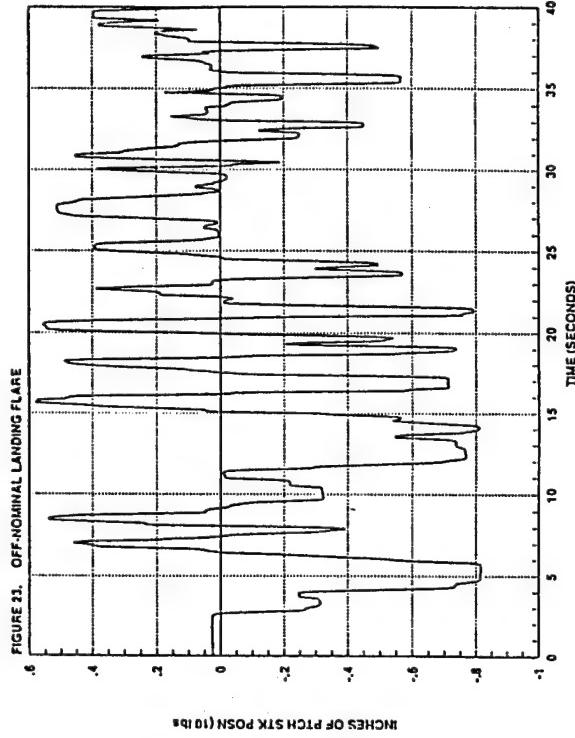
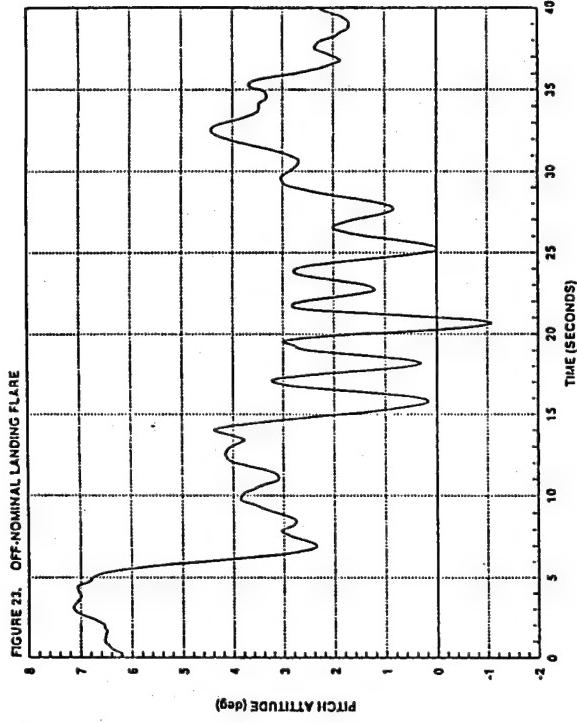


Figure A-31. B-2 (Ref. A-22)

FIGURE 25. REFUELING

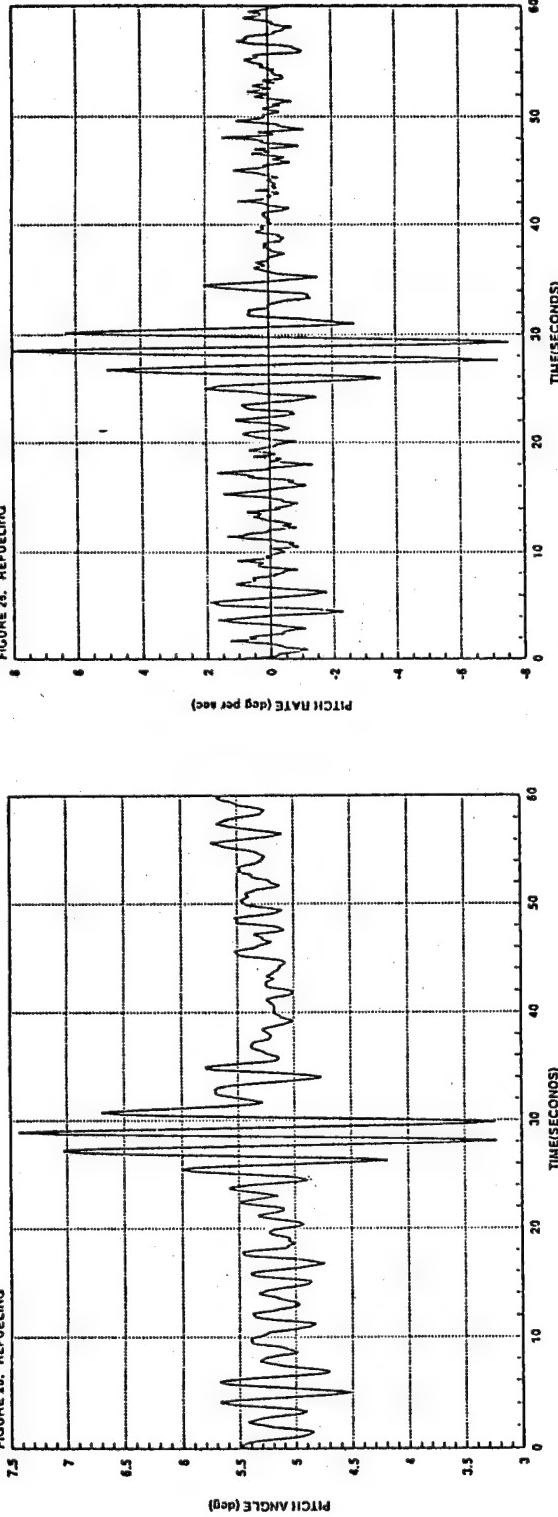


FIGURE 25. REFUELING

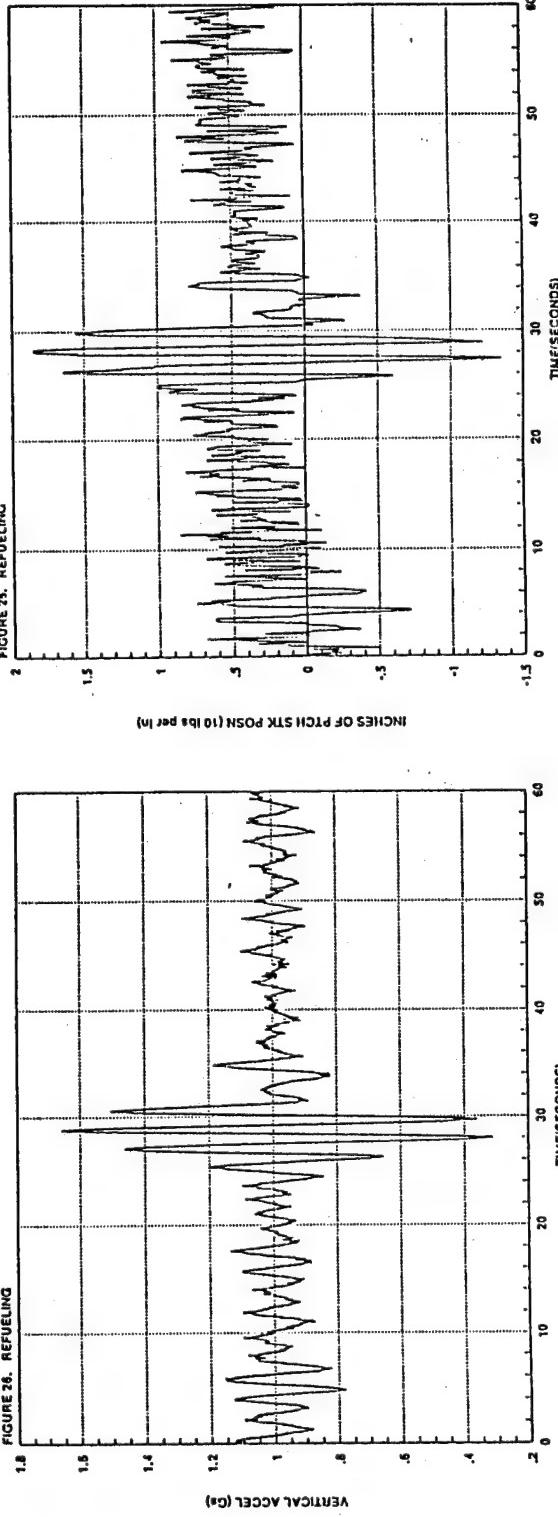


Figure A-32. B-2 (Ref. A-22)

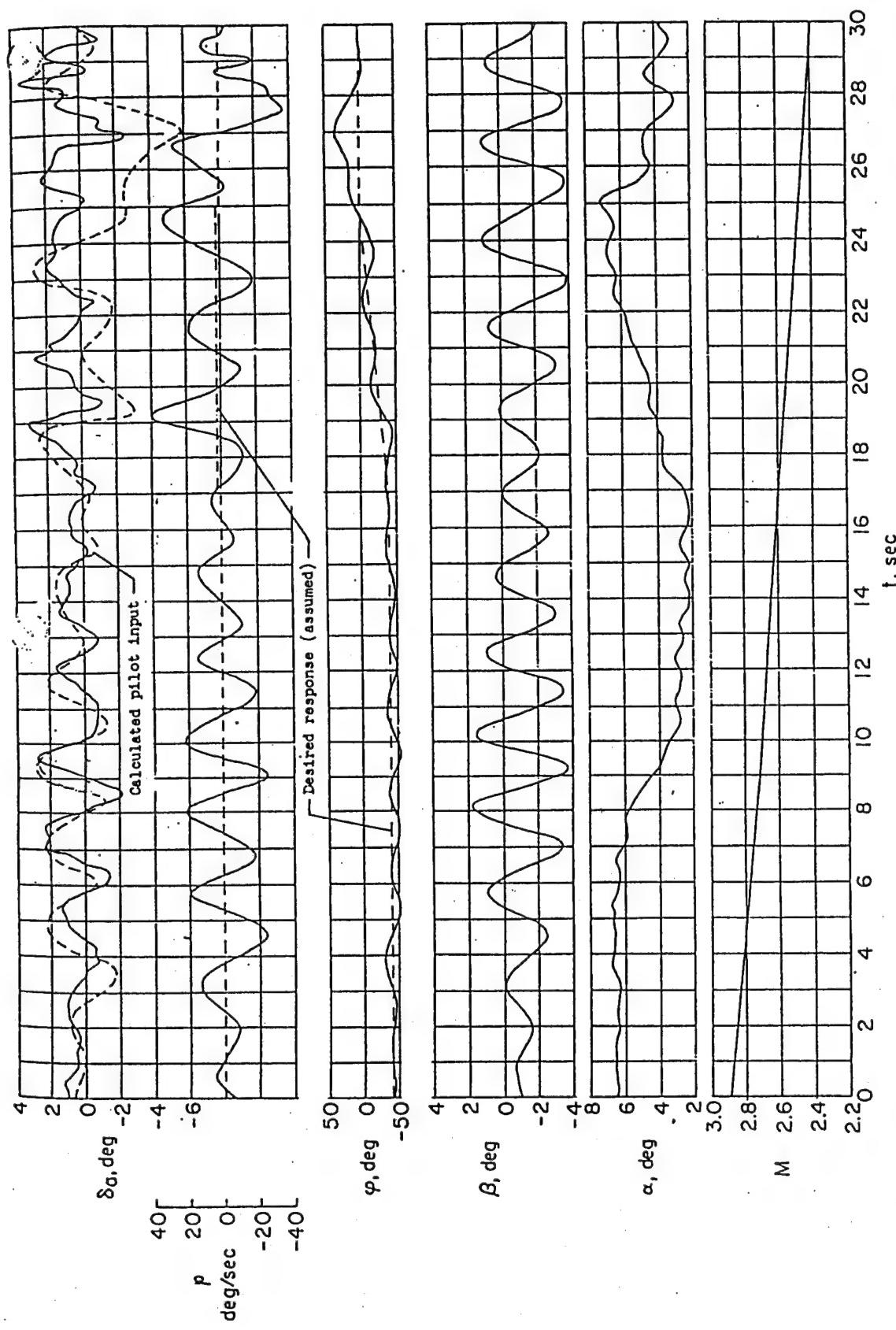


Figure A-33. X-15 (Ref. 23)

TR-1313-1

A-39

Figure 3.- Time history of an X-15 flight near the lateral-controllability limit.

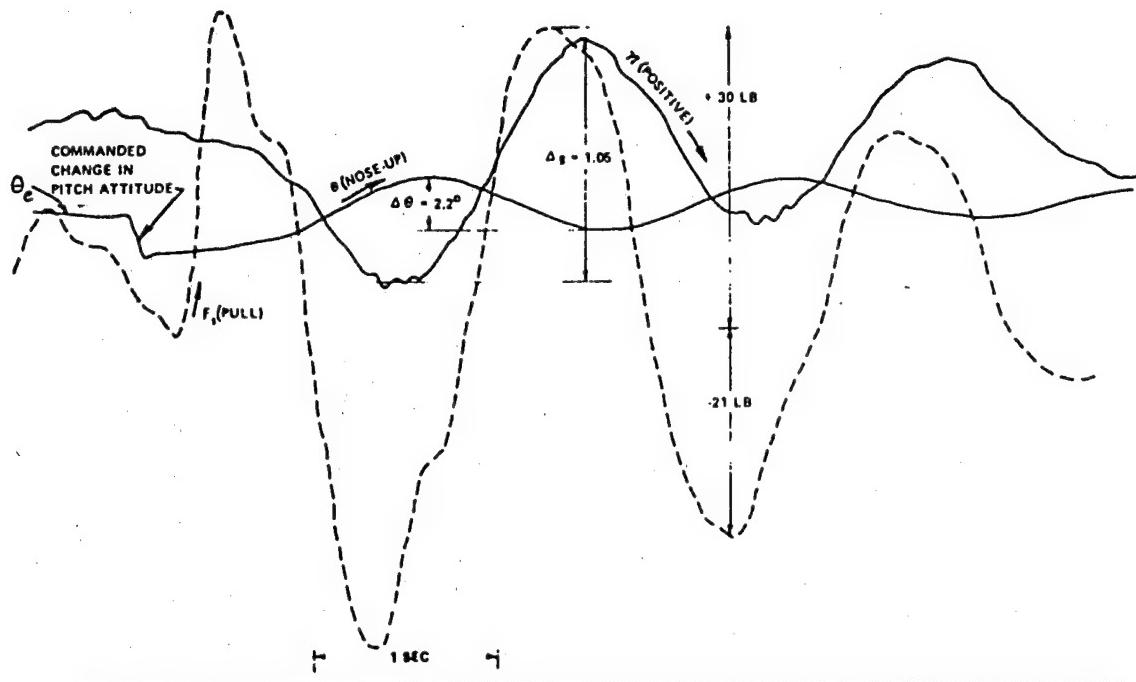


Figure 38. In-Flight Record of a PIO Occurring During Discrete Error Tracking Task.
(Configuration 1G, Flight 1061)

Figure A-34. NT-33A, Configuration 1G (Ref. A-24)

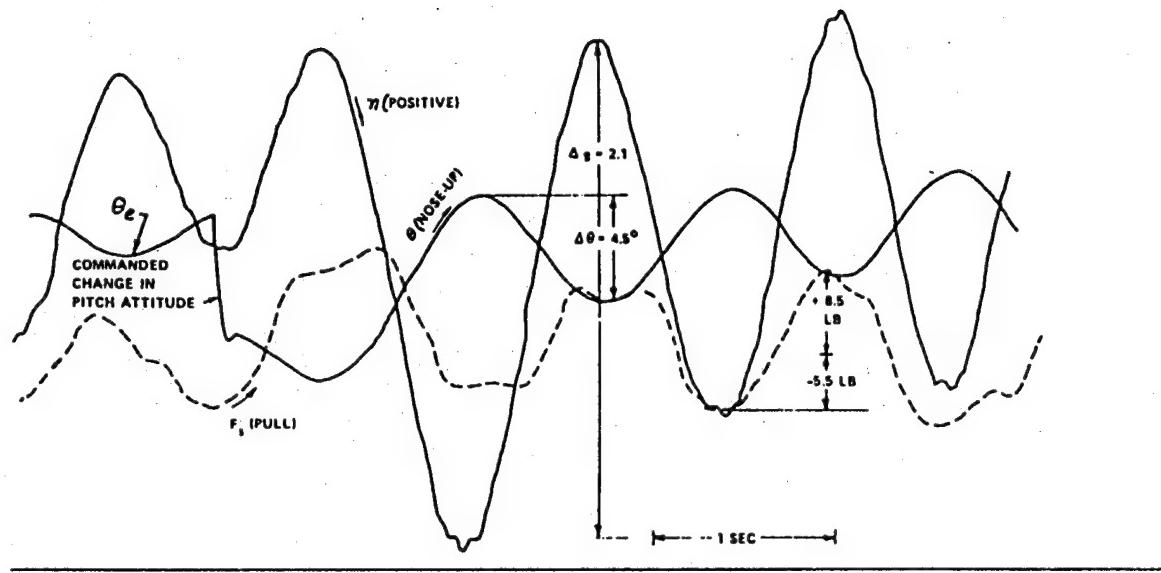


Figure 40. In-Flight Record of a PIO Occurring During Discrete-Error Tracking Task (Configuration 4D, Flight 1057)

Figure A-35. NT-33A, Configuration 4D (Ref. A-24)

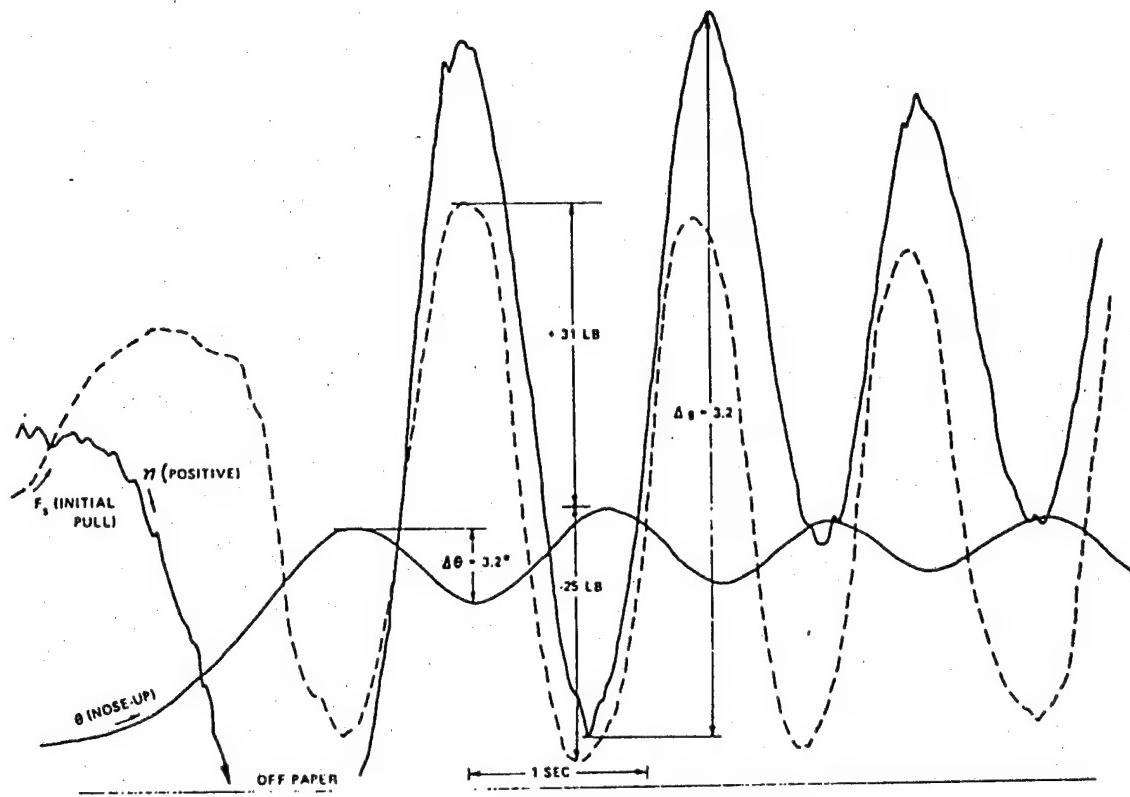


Figure 41. In-Flight Record of a PIO Occurring During Visual Tracking (Configuration 6E, Flight 1071)

Figure A-36. NT-33A, Configuration 6E (Ref. A-24)

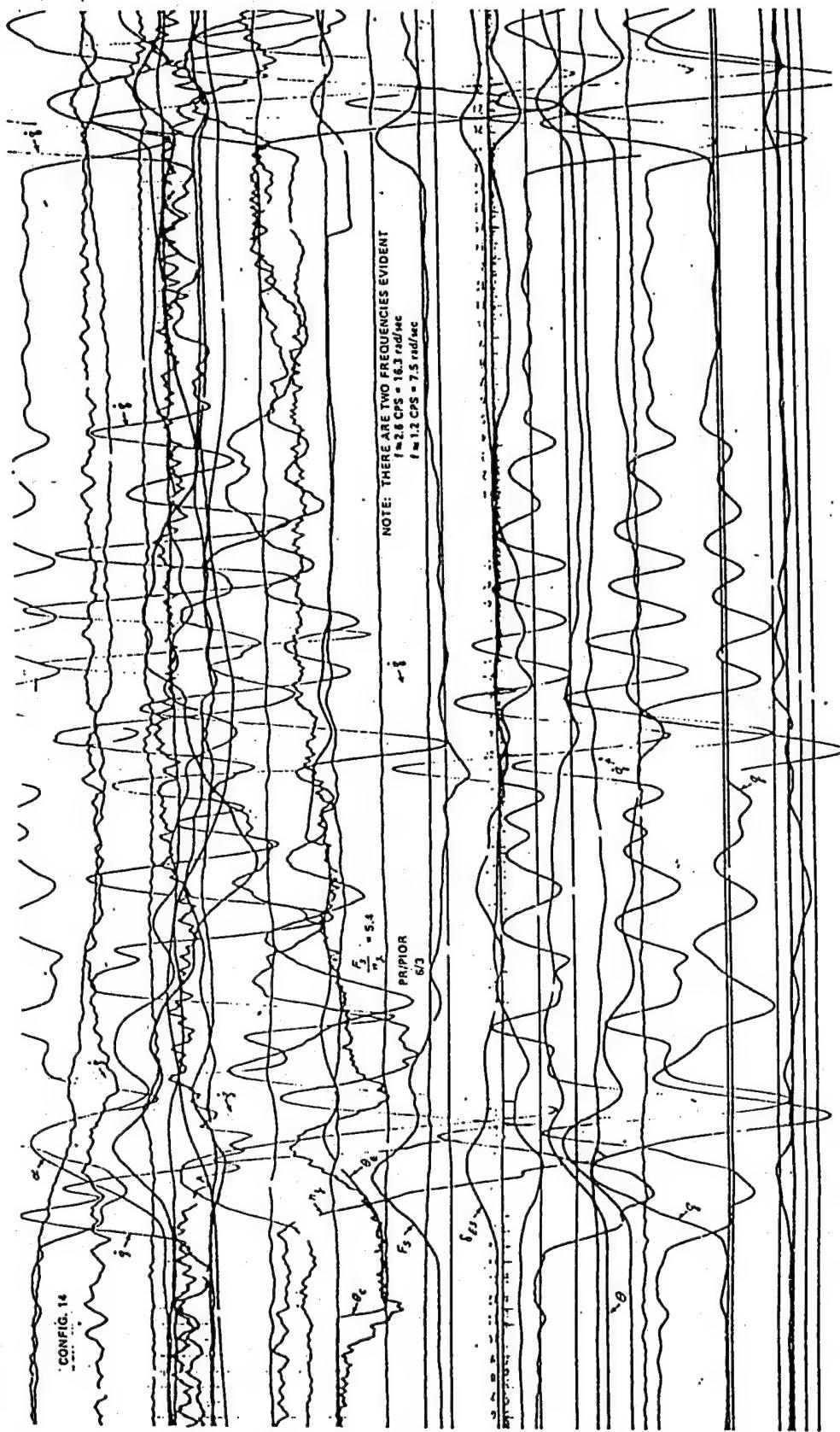


Figure A-37. NT-33A, Configuration 14 (Ref. A-25)

TR-1313-1 -

A-43

Figure 40 TIME HISTORY OF CONFIGURATION 14
 (REFERENCE 8)

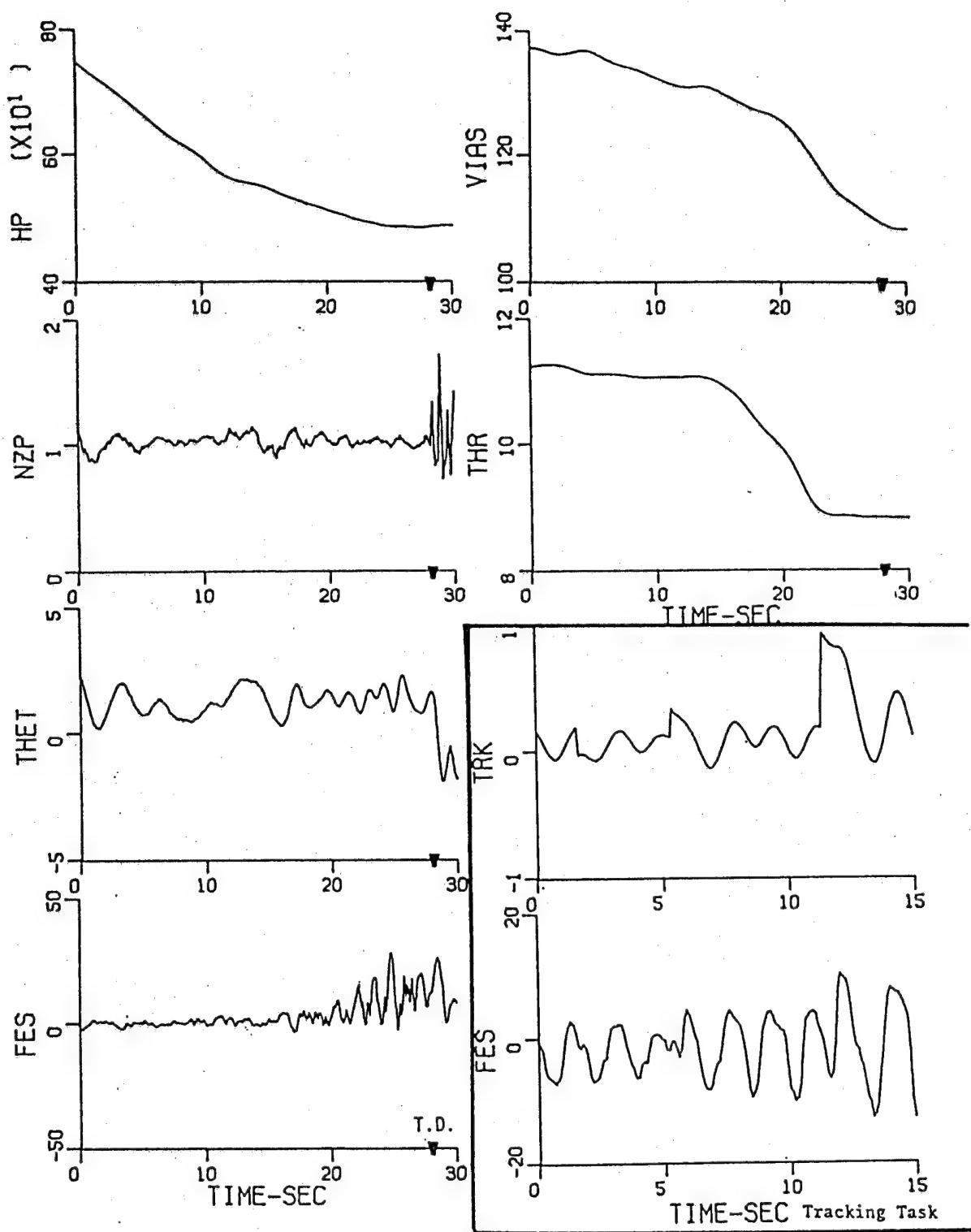


Figure 13: CONFIG. 1-3, PILOT B/1892, VISUAL TASK AND TRACKING TASKS, PR:10--

Figure A-38. NT-33A, Configuration 1-3 (Ref. A-26)

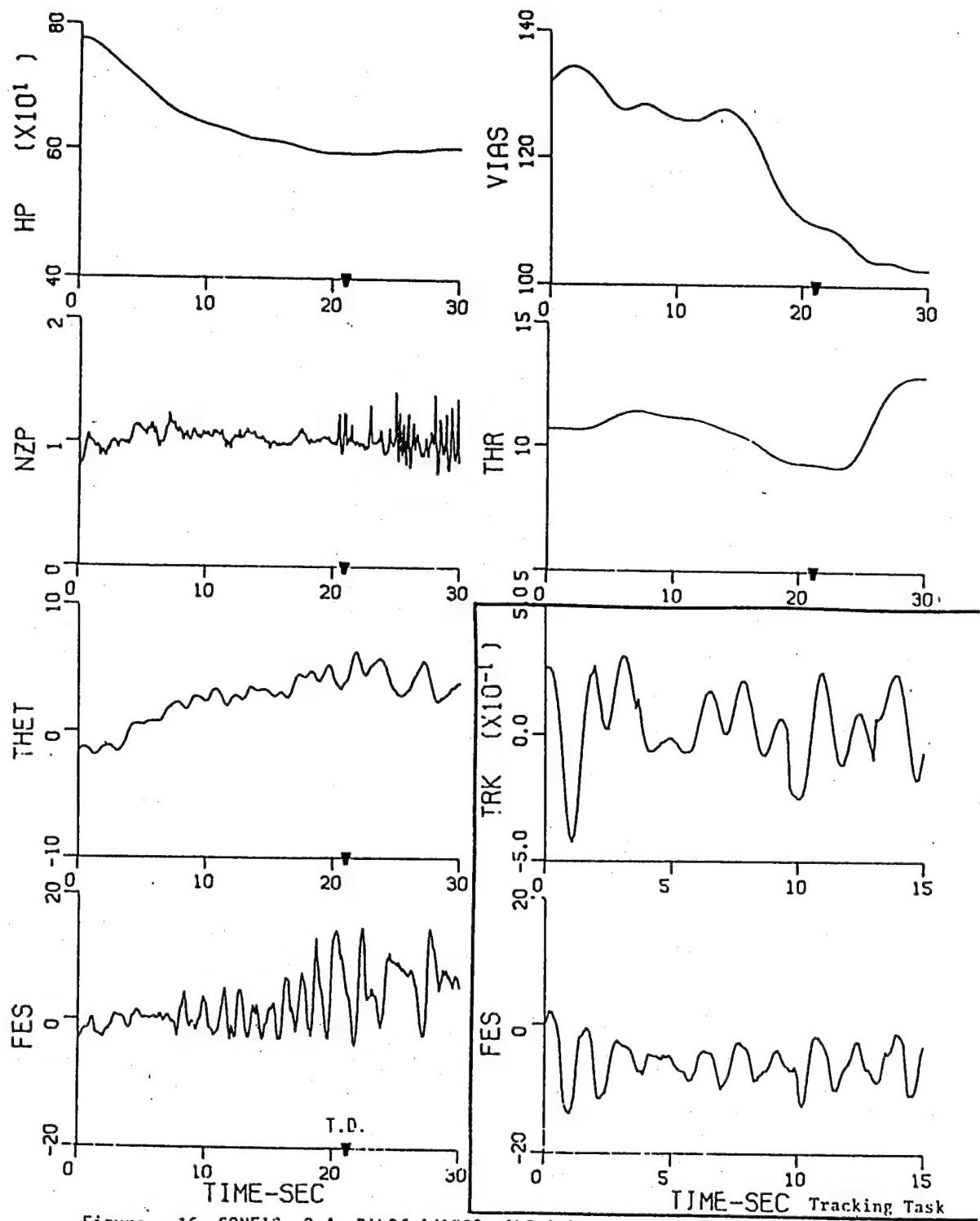


Figure 16: CONFIG. 2-4, PILOT A/1088, ILS AND TRACKING TASKS, PR: 9/--

Figure A-39. NT-33A, Configuration 2-4 (Ref. A-26)

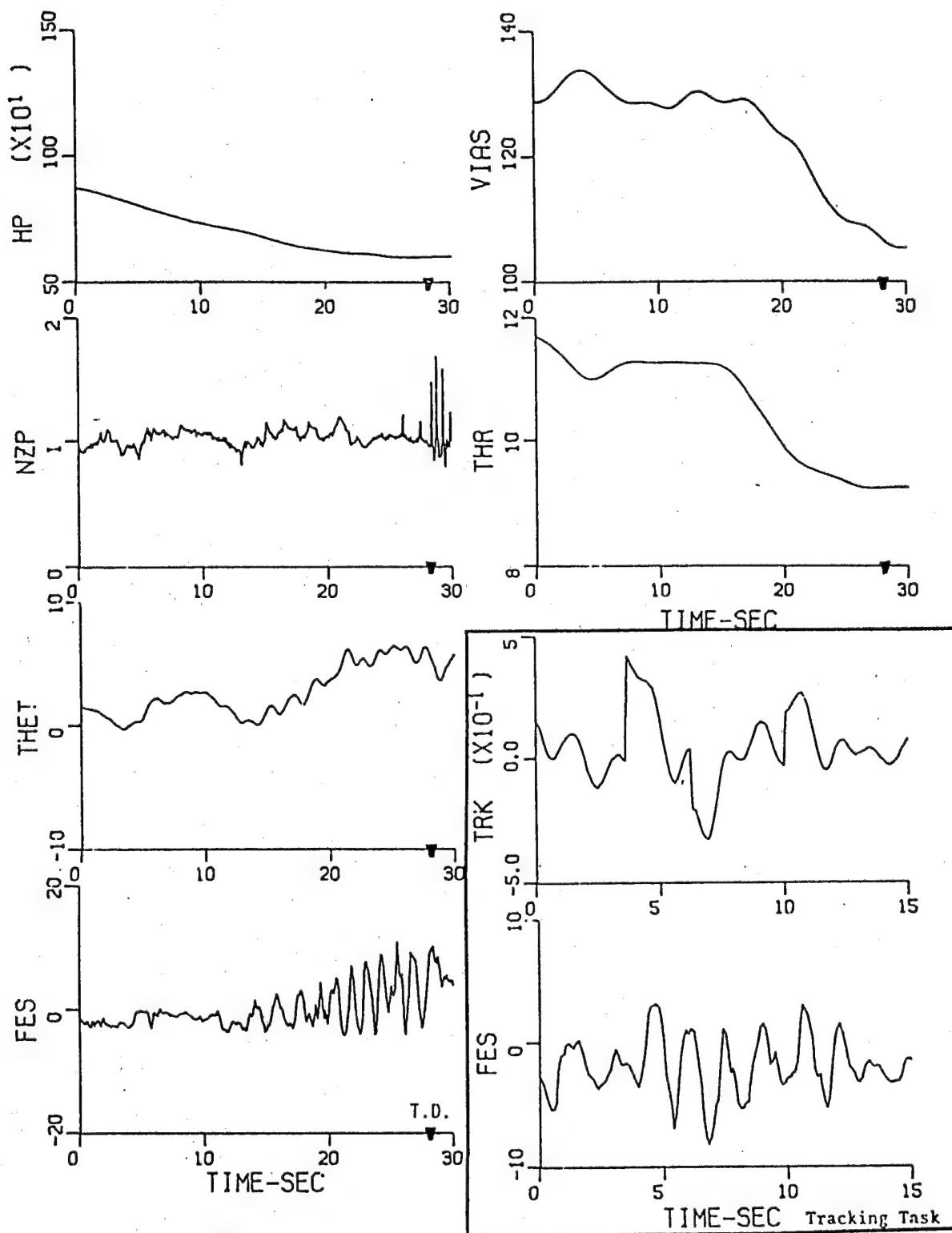


Figure 17: CONFIG. 2-4, PILOT A/1888, VISUAL TASK AND TRACKING TASKS, PR:9/--

Figure A-40. NT-33A, Configuration 2-4 (Ref. A-26)

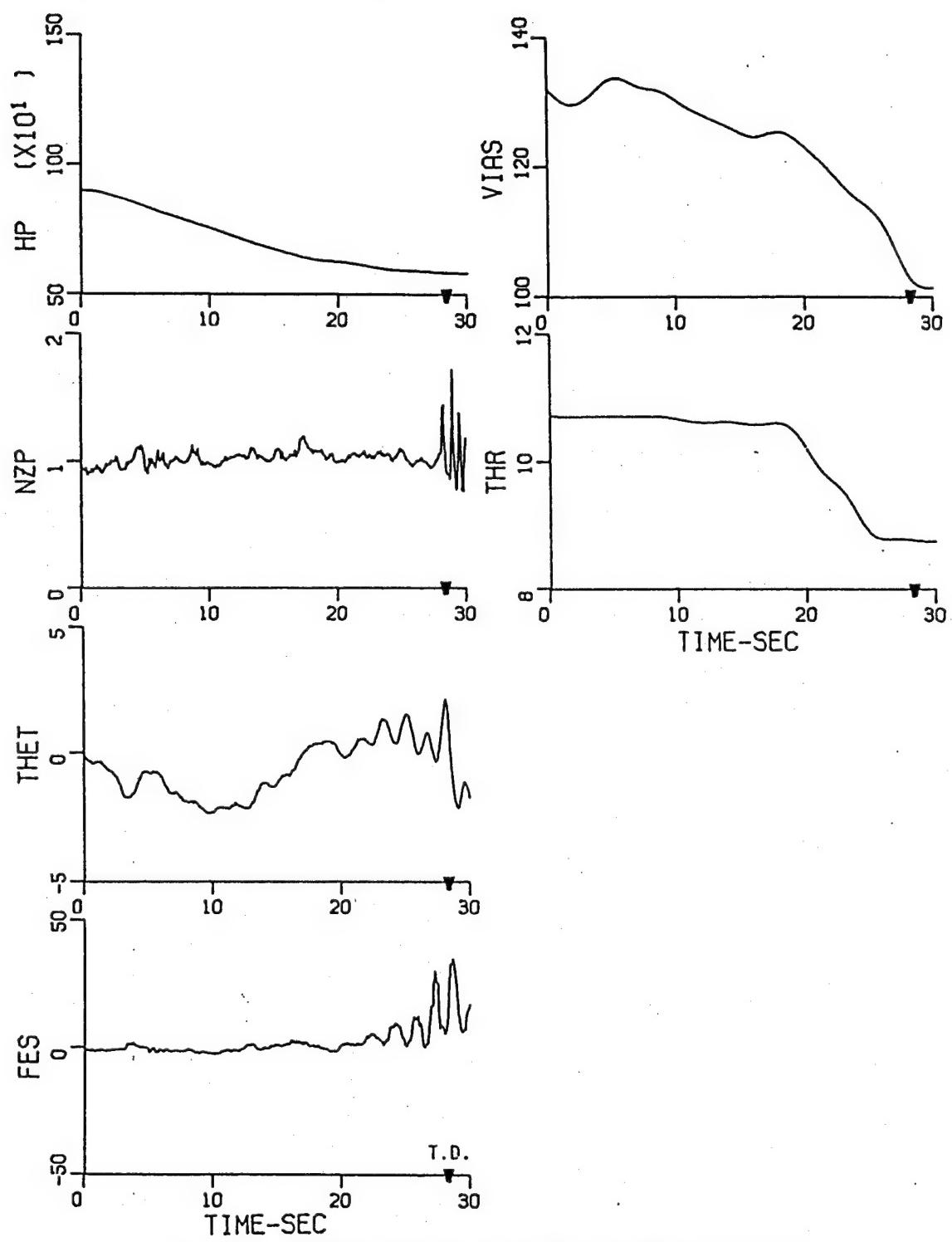


Figure 21: CONFIG. 2-9, PILOT B/1895, ILS TASK PR: 10/5

Figure A-41. NT-33A, Configuration 2-9 (Ref. A-26)

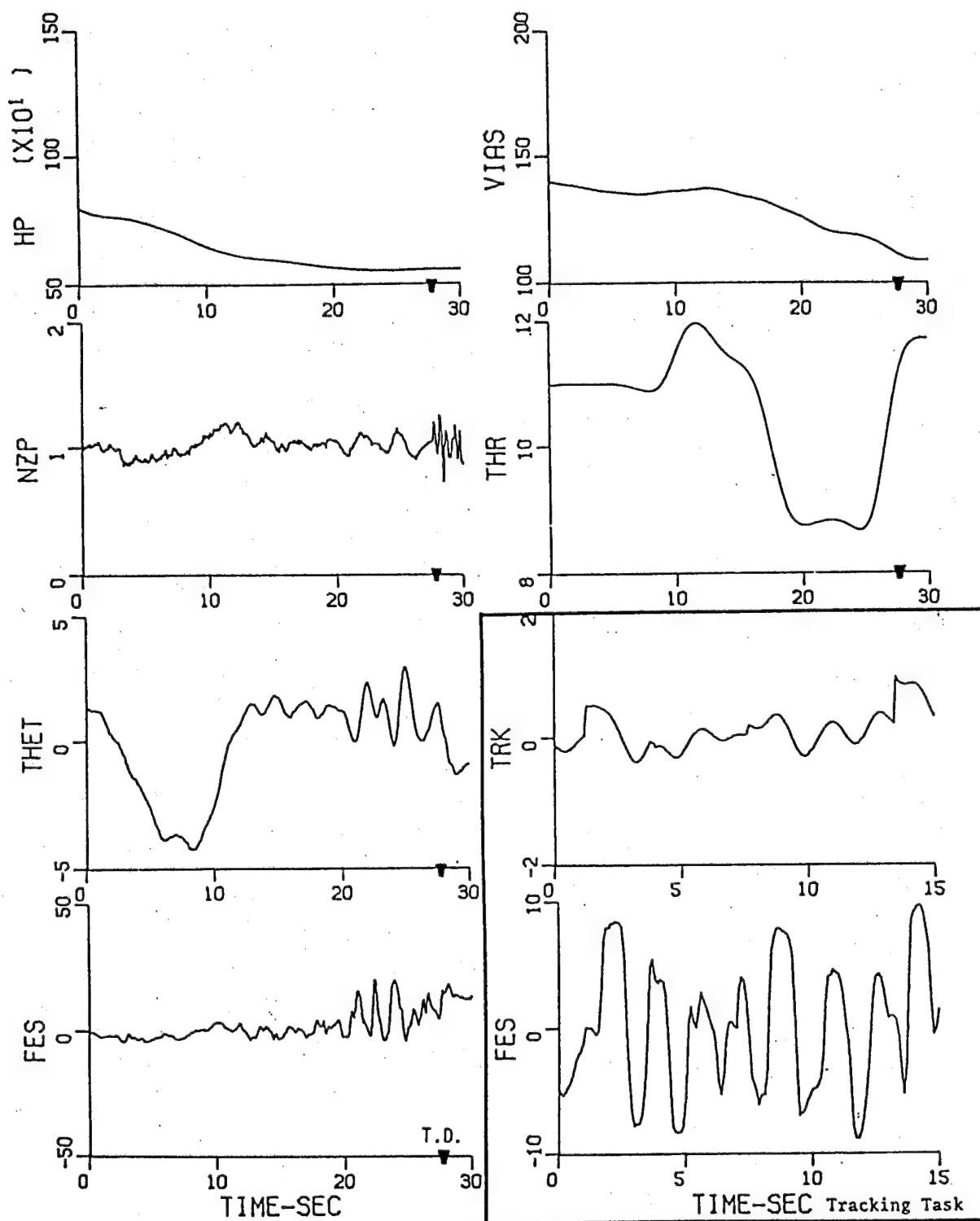


Figure 26: CONFIG. 4-10, PILOT A/1893, ILS AND TRACKING TASKS, PR: 9/6

Figure A-42. NT-33A, Configuration 4-10 (Ref. A-26)

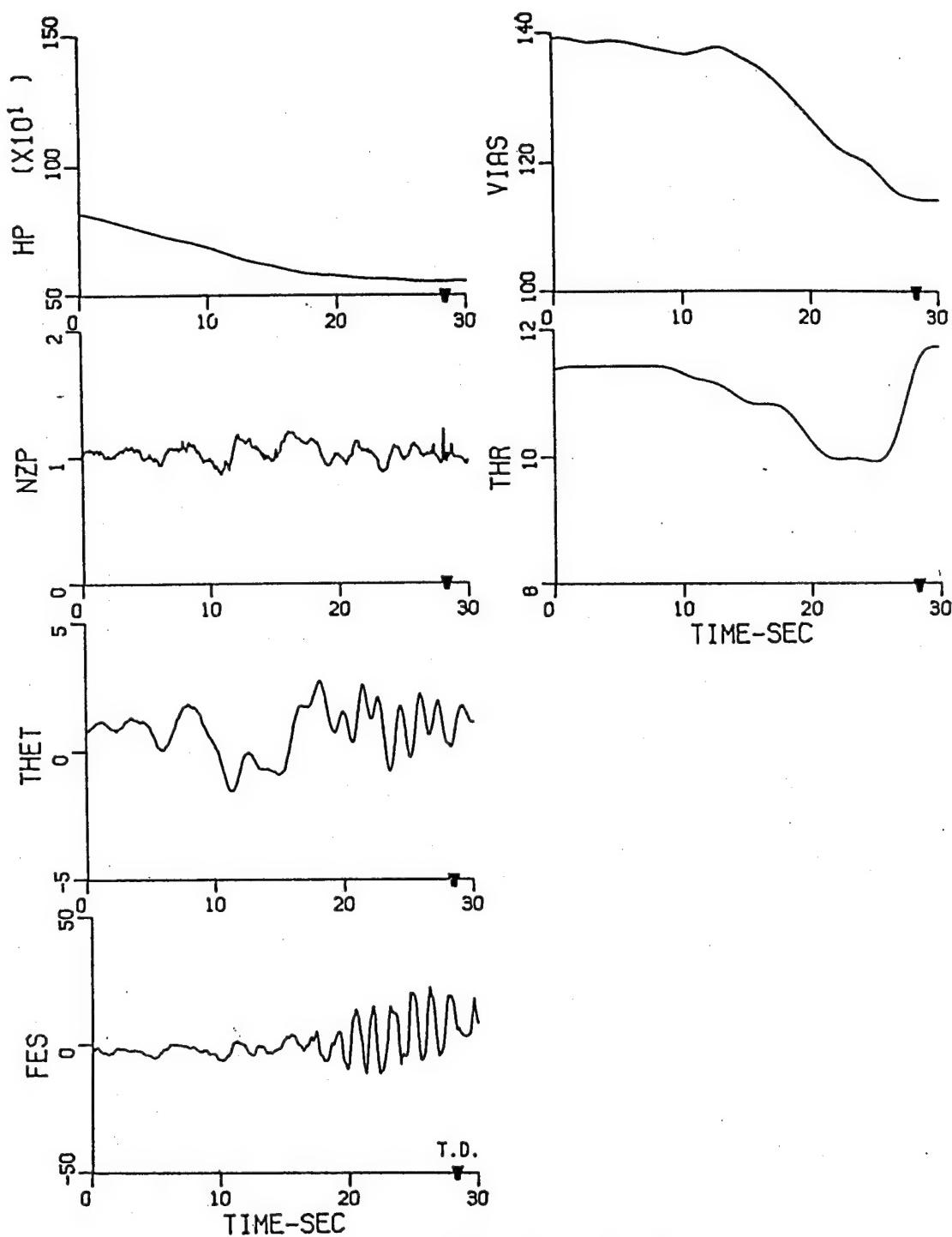


Figure 27: CONFIG.4-10, PILOT A/1893, VISUAL TASK, PR: 9/6

Figure A-43. NT-33A, Configuration 4-10 (Ref. A-26)

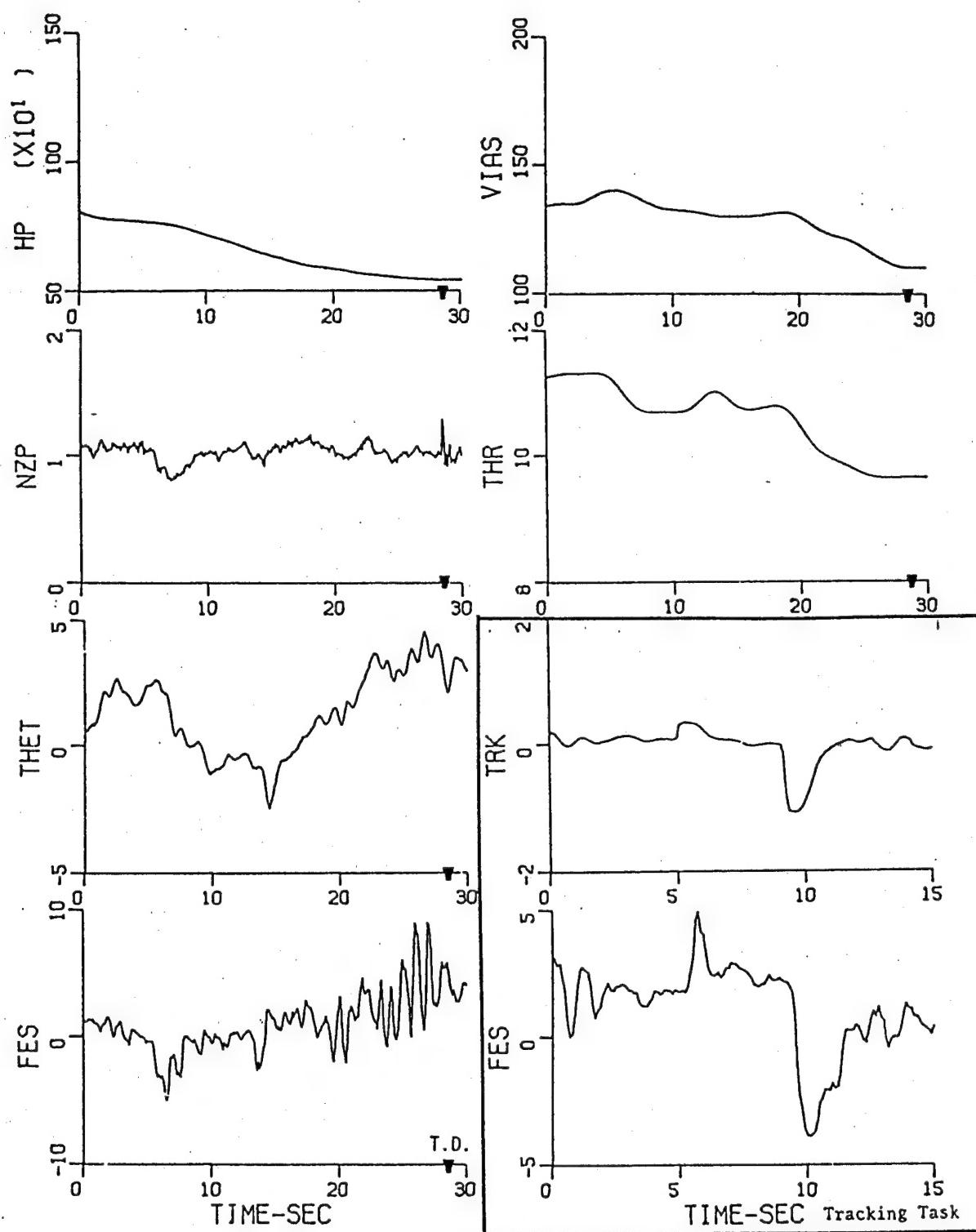


Figure 28: CONFIG. 5-3, PILOT A/1886, ILS AND TRACKING TASKS, PR: 8--

Figure A-44. NT-33A, Configuration 5-3 (Ref. A-26)

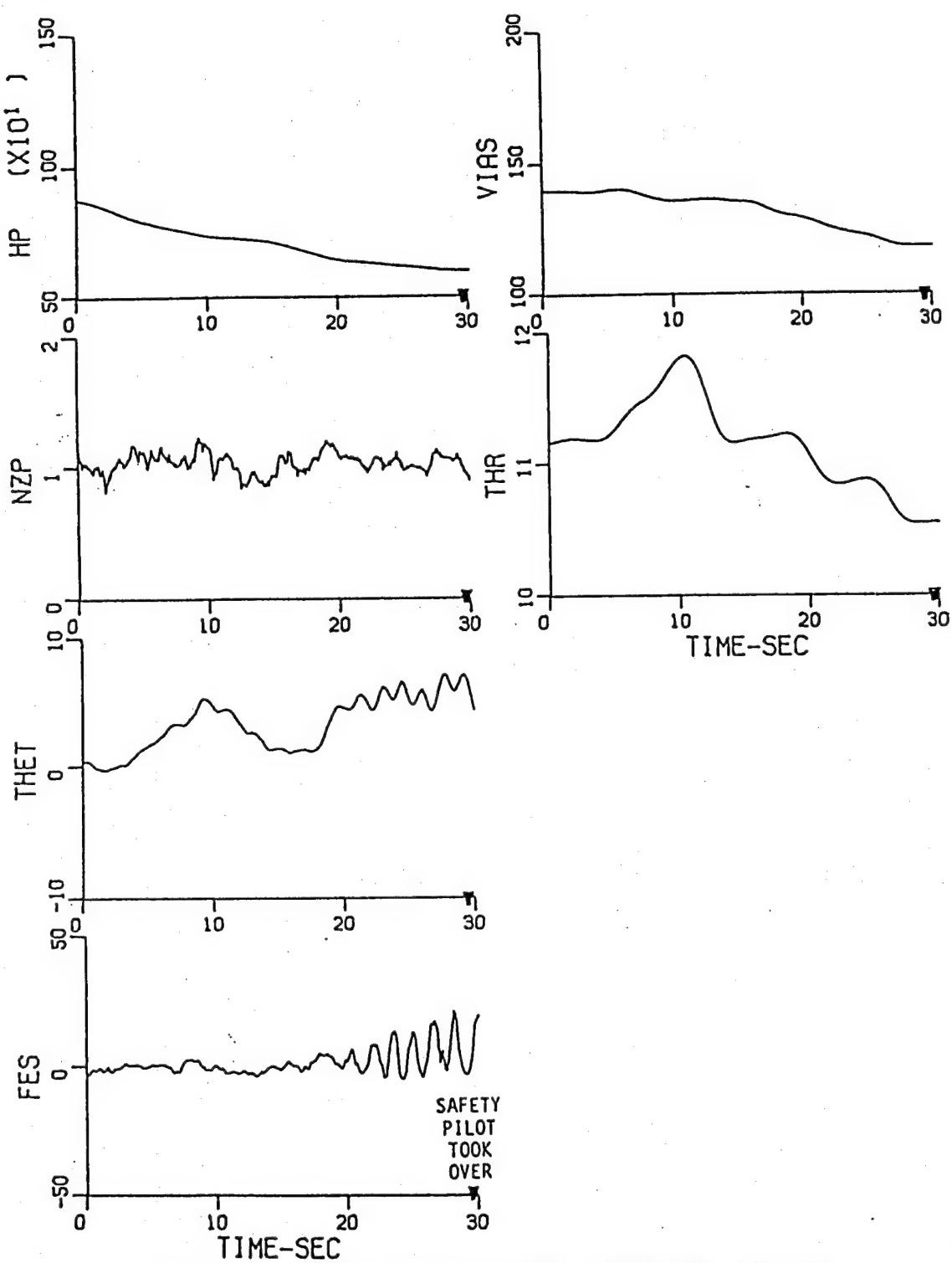


Figure 30: CONFIG. 6-1, PILOT A/1888, VISUAL TASK, PR: 10--

Figure A-45. NT-33A, Configuration 6-1, YF-17 (Ref. A-26)

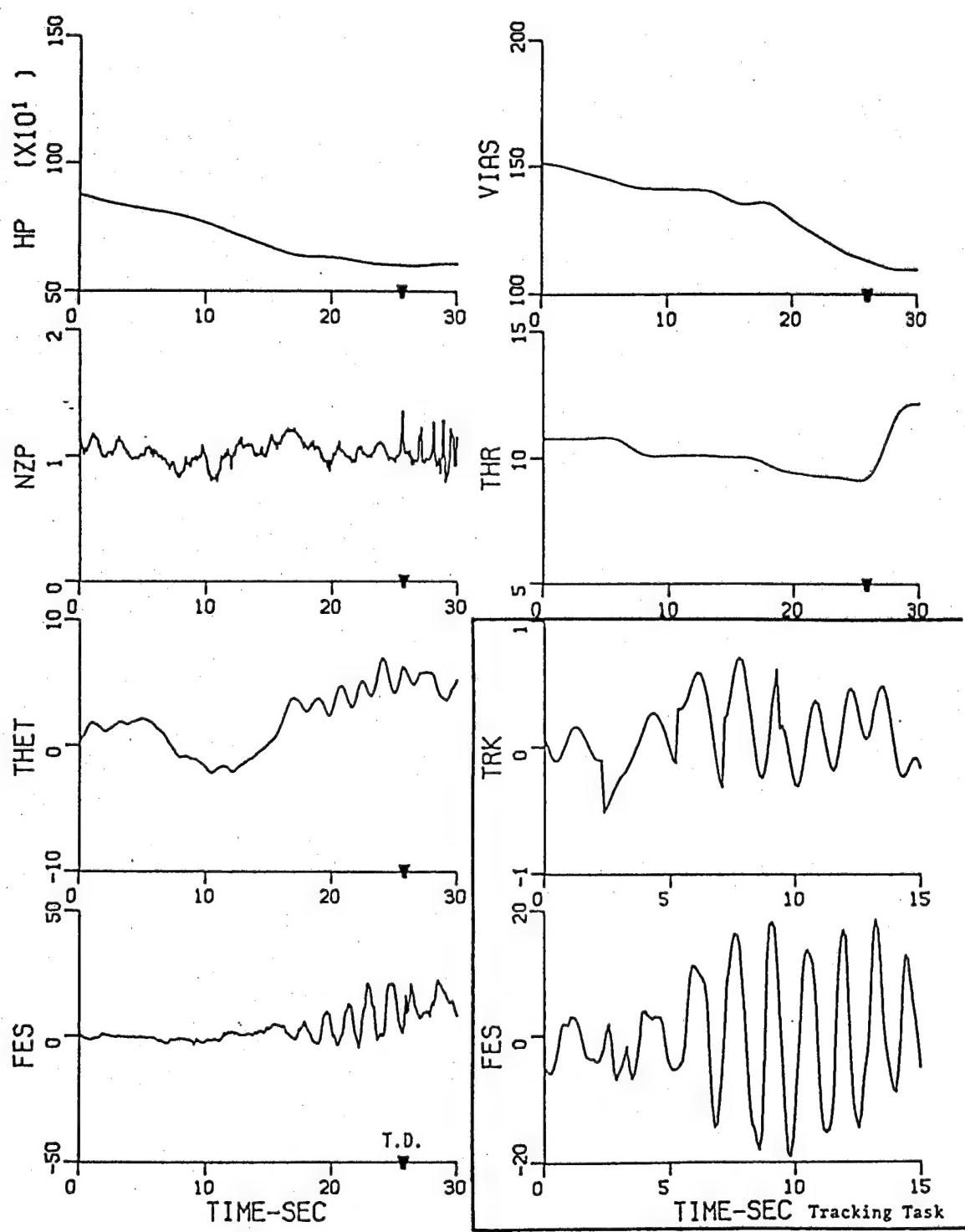
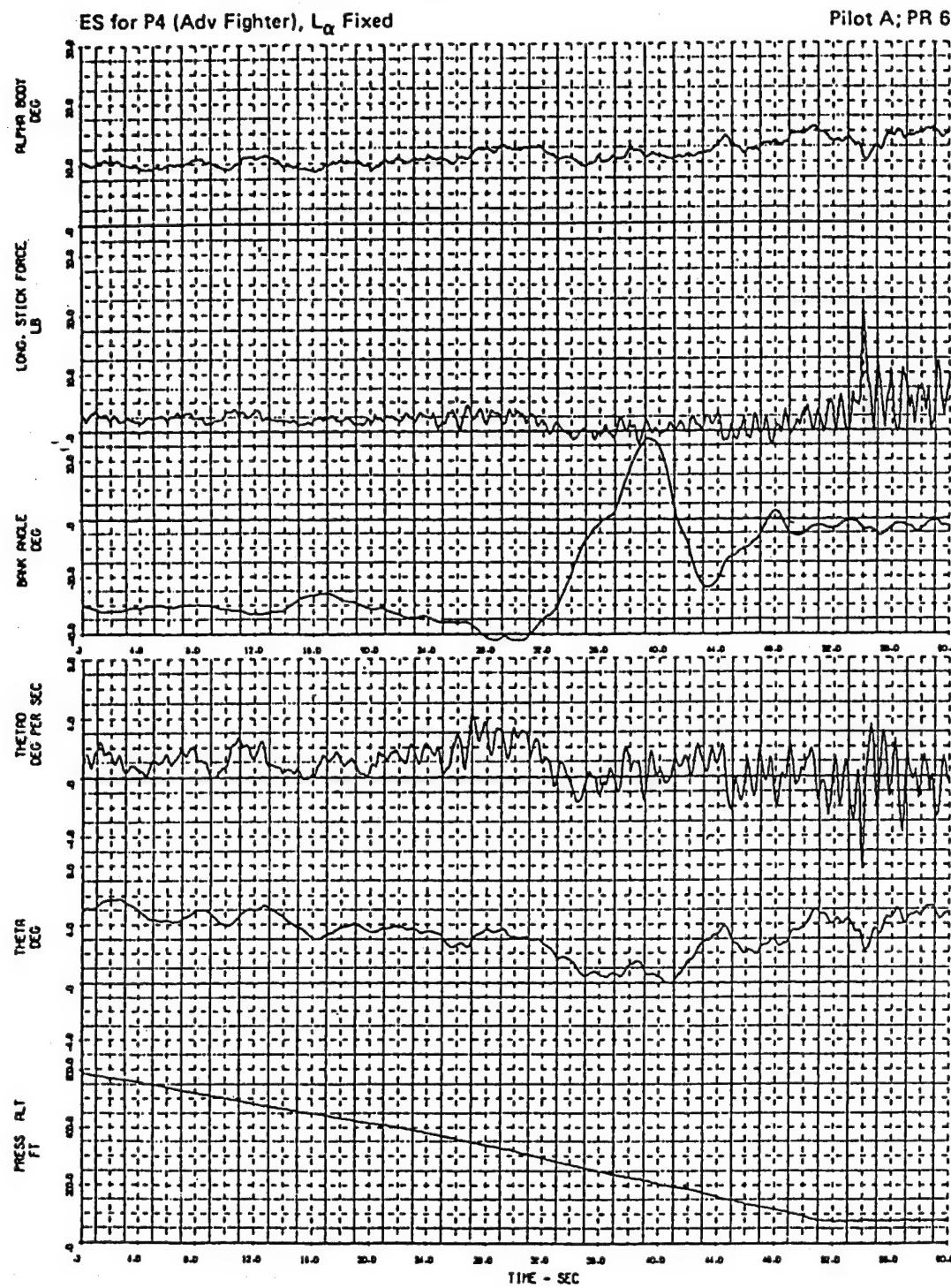


Figure 31: CONFIG. 6-1, PILOT A/1888, ILS AND TRACKING TASKS. PR: 10/--

Figure A-46. NT-33A, Configuration 6-1, YF-17 (Ref. A-26)

CONFIG PS-1 -LANDING NO. 2 FLT 2071 REC NO. 14



GP13-0824-40

Figure E-2a. Flight Characteristics - Time History

Figure A-47. NT-33A, Configuration P5-1 (Ref. A-27)

CONFIG P100 -LANDING NO. 2 FLT 2070 REC NO. 18

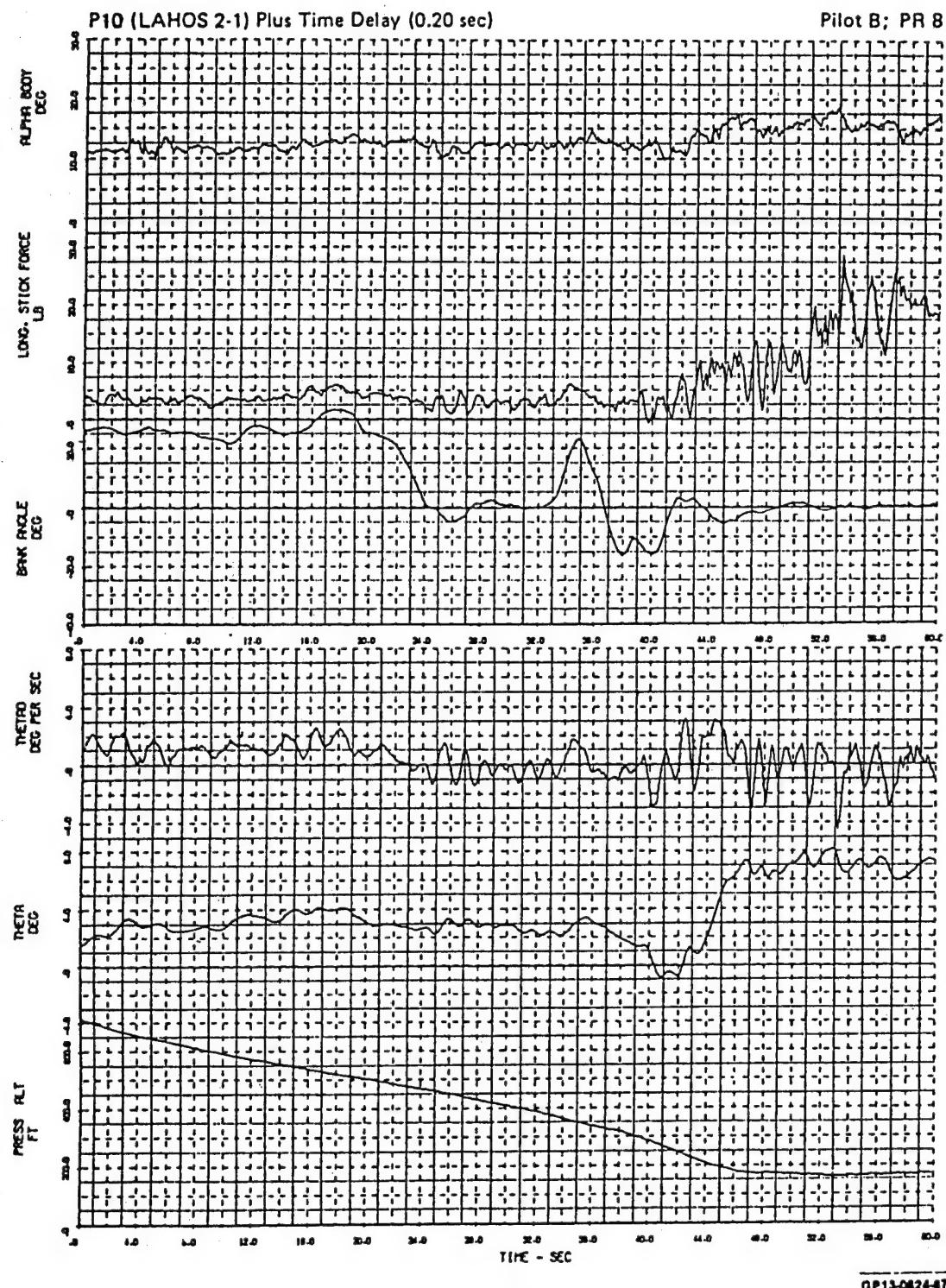


Figure E-15a. Flight Characteristics - Time History

Figure A-48. NT-33A, Configuration P10D (Ref. A-27)

CONFIG P11 - LANDING NO. 2 FLT 2062 REC NO. 7

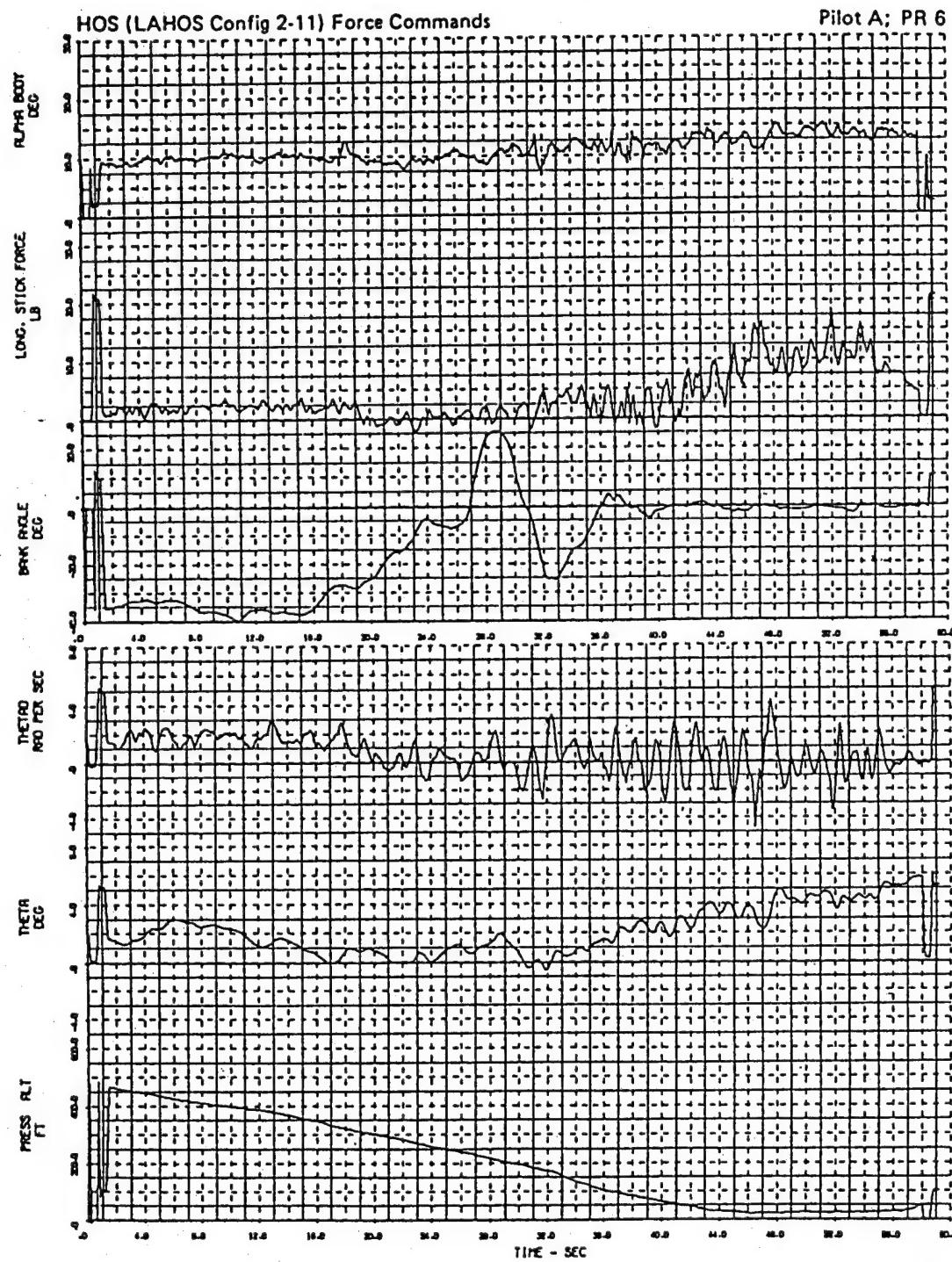


Figure E-16a. Flight Characteristics - Time History

QP13-0824-49

Figure A-49. NT-33A, Configuration P11 (Ref. A-27)

CONFIG P12 - LANDING NO. 3 FLT 2069 REC NO. 4

Pilot A; PR 9

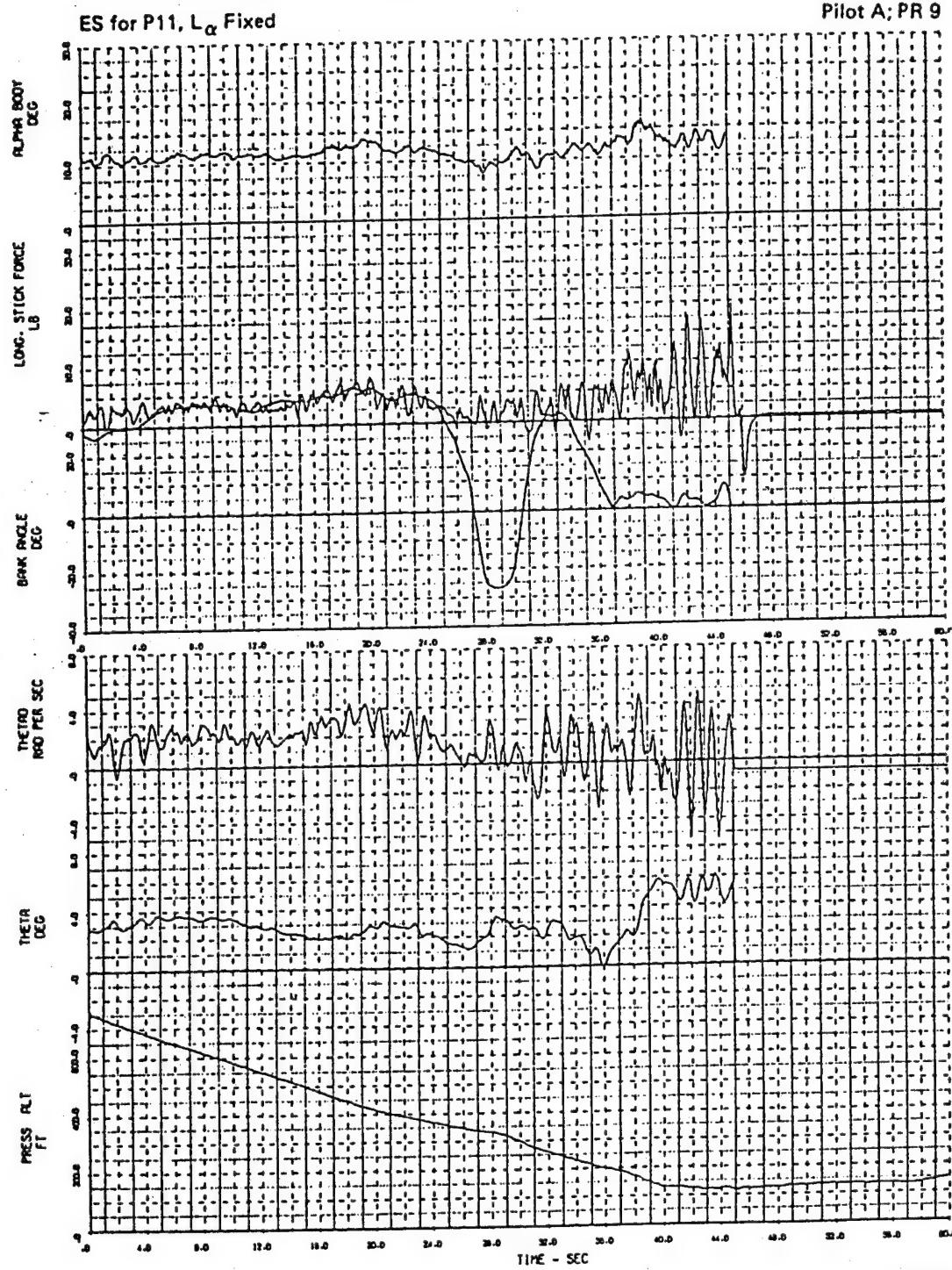


Figure E-20a. Flight Characteristics - Time History

Figure A-50. NT-33A, Configuration P12 (Ref. A-27)

CONFIG P12A - LANDING NO. 1 FLT 2069 REC NO. 15

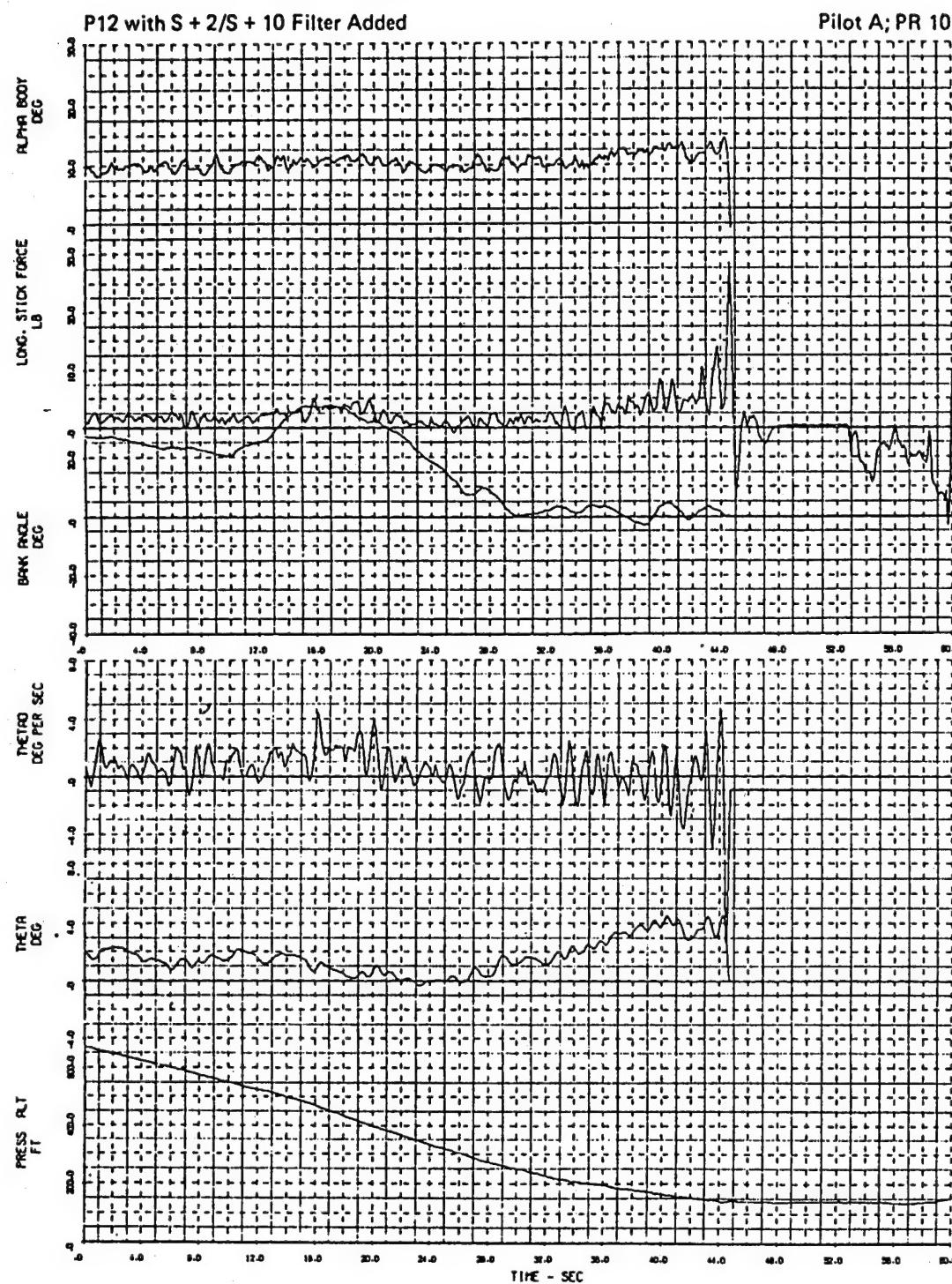


Figure E-23a. Flight Characteristics - Time History

GP13-0824-83

Figure A-51. NT-33A, Configuration P12A (Ref. A-27)

CONFIG P12B - LANDING NO. 2 FLT 2072 REC NO. 25

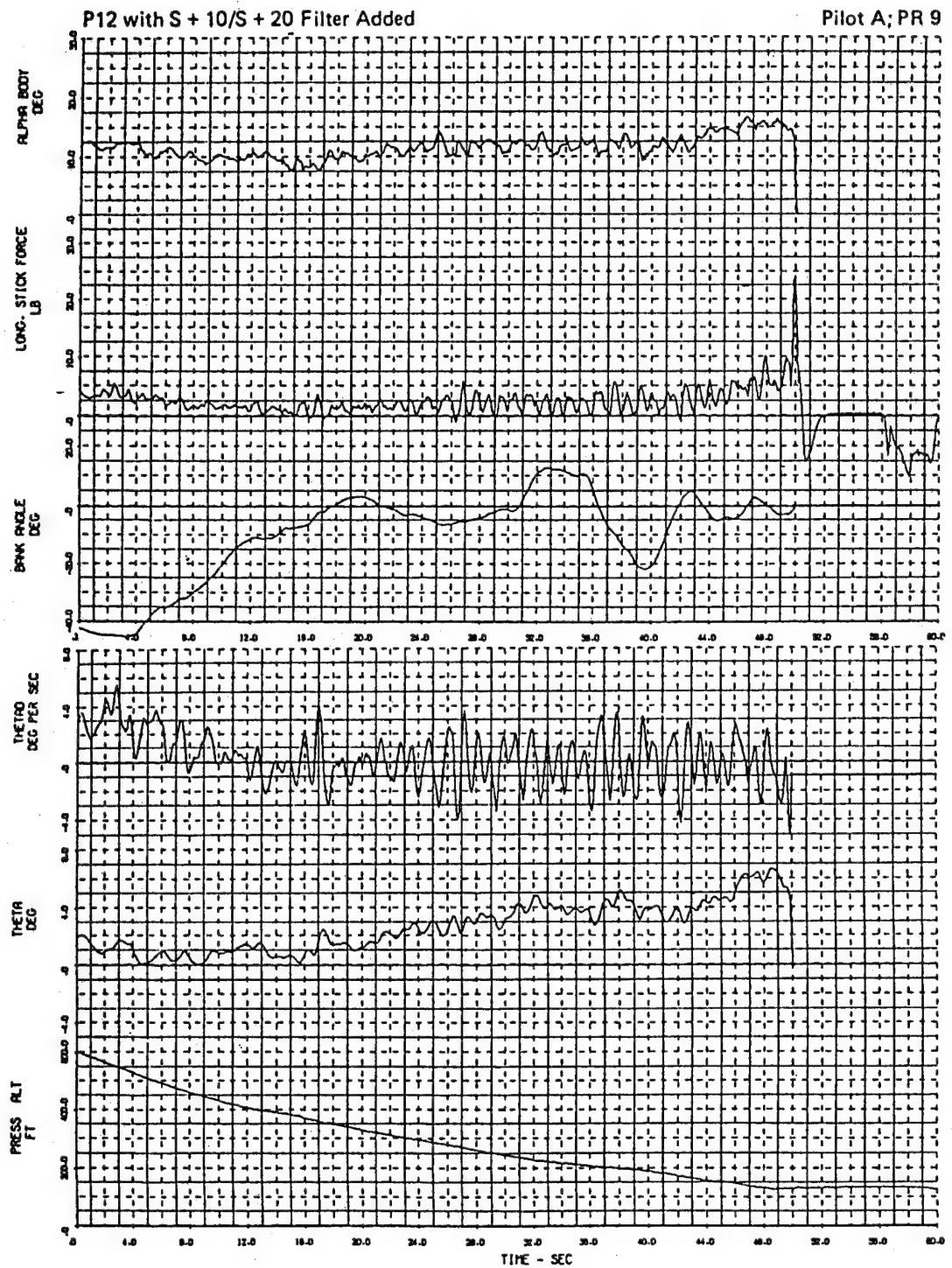


Figure E-24a. Flight Characteristics - Time History

QP13-0824-85

Figure A-52. NT-33A, Configuration P12B (Ref. A-27)

CONFIG P13A- LANDING NO. 2 FLT 2064 REC NO 19

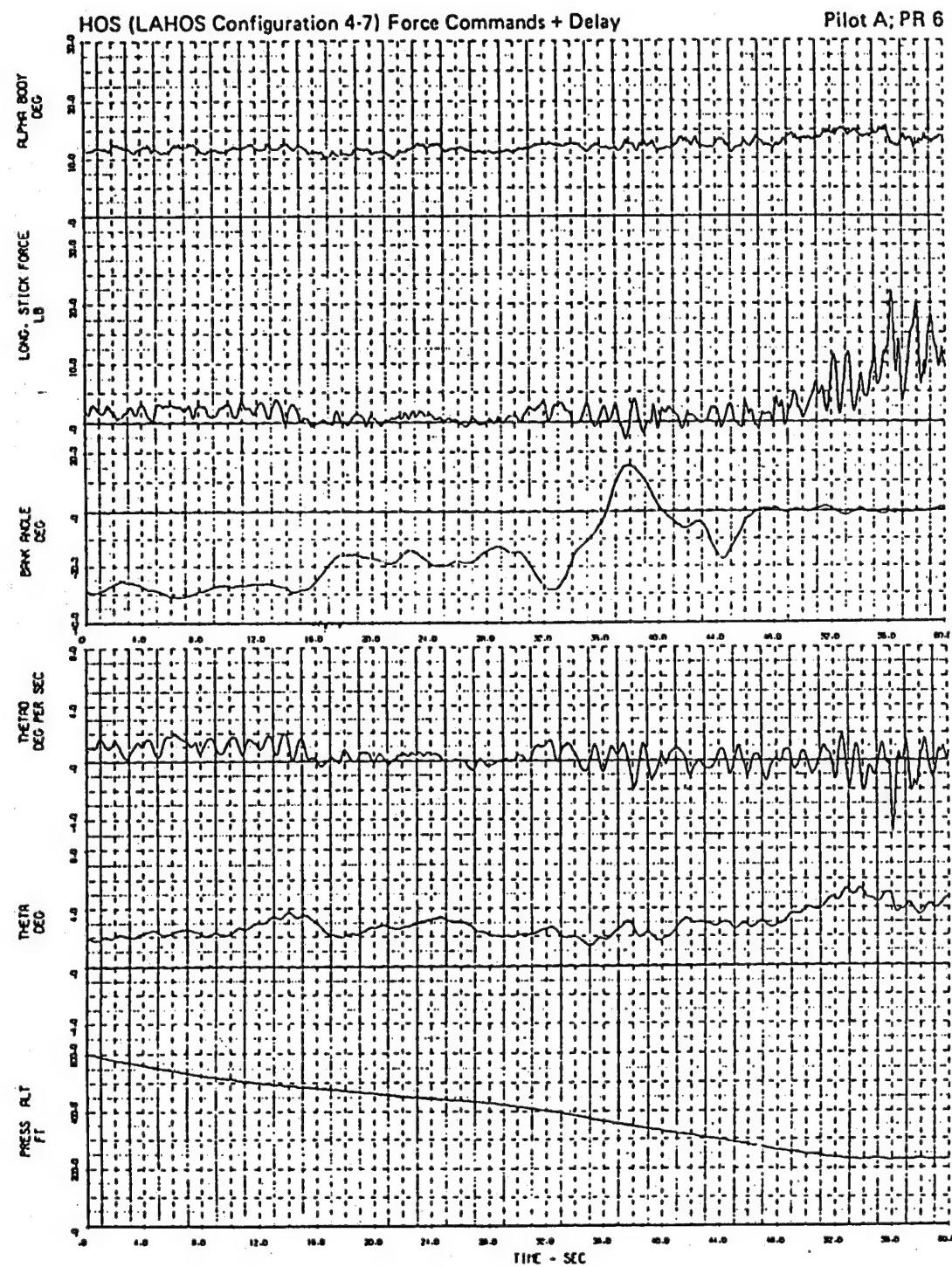


Figure E-27a. Flight Characteristics - Time History

Figure A-53. NT-33A, Configuration P13A (Ref. A-27)

CONFIG P 14- LANDING NO. 2 FLT 2054 REC NO. 12

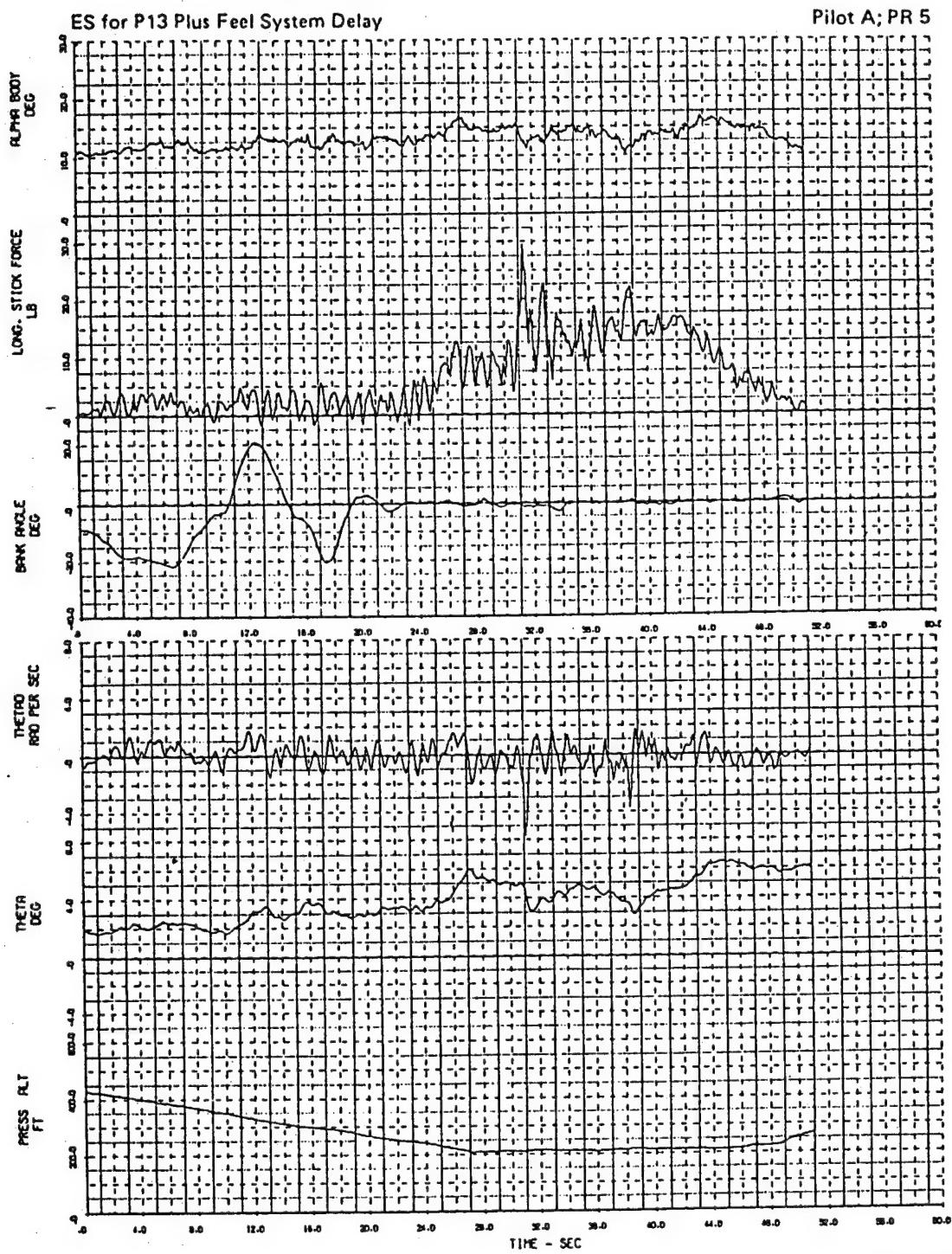
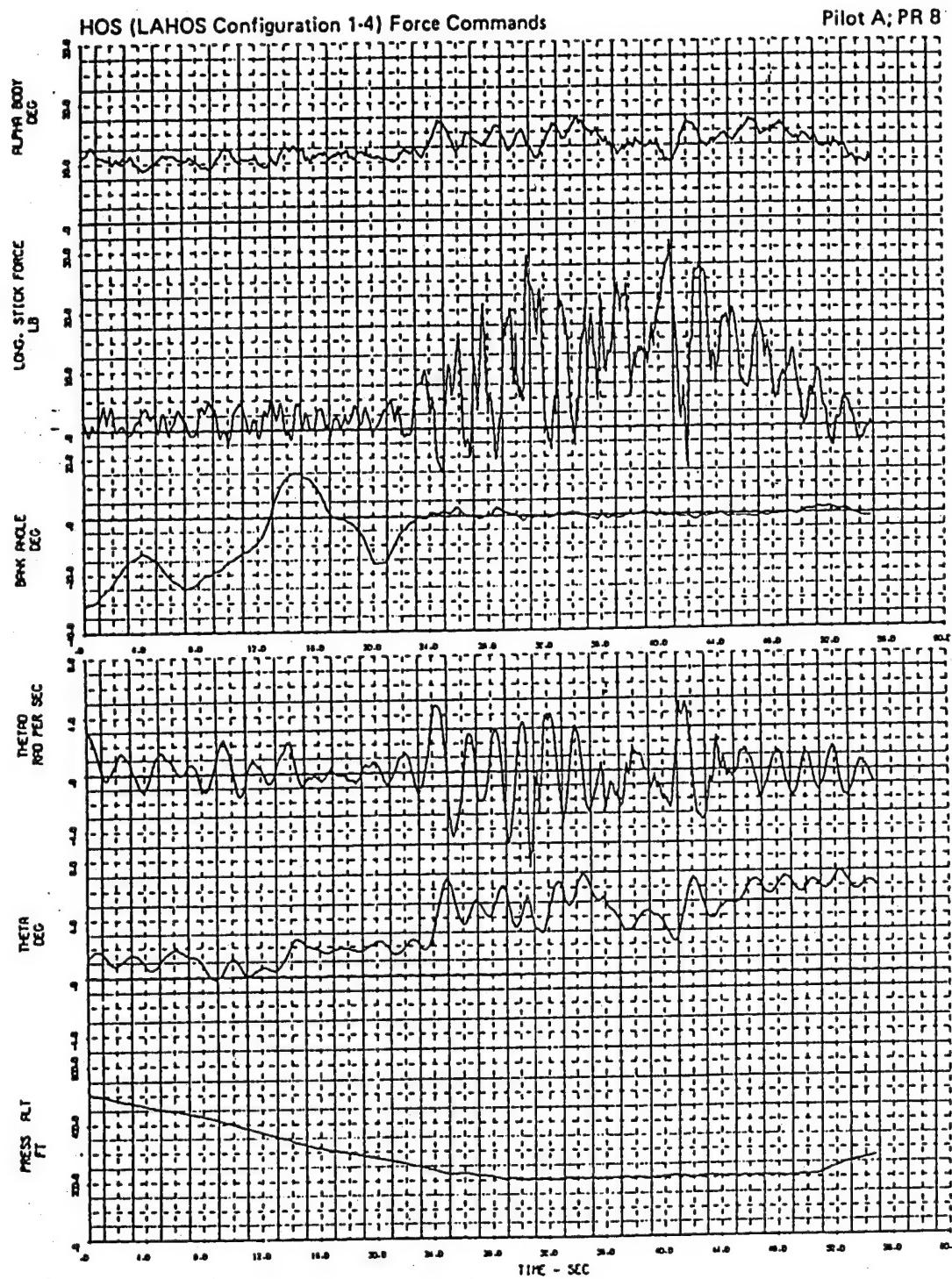


Figure E-28a. Flight Characteristics - Time History

Figure A-54. NT-33A, Configuration P14 (Ref. A-27)

CONFIG P15 - LANDING NO. 2 FLT 2064 REC NO. 7

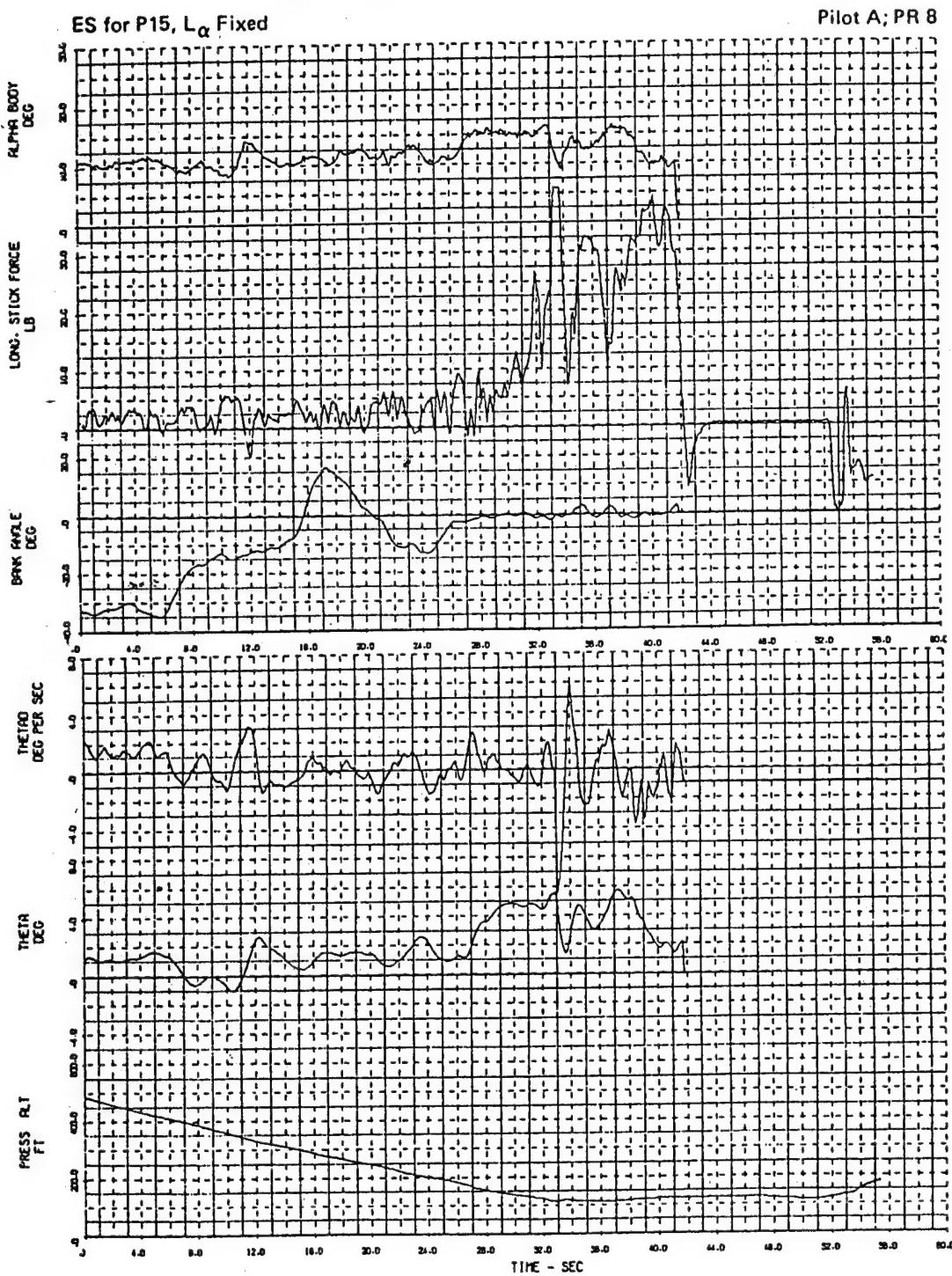


GP13-0824-95

Figure E-28a. Flight Characteristics - Time History

Figure A-55. NT-33A, Configuration P15 (Ref. A-27)

CONFIG P16 - LANDING NO. 2 FLT 2072 REC NO. 8

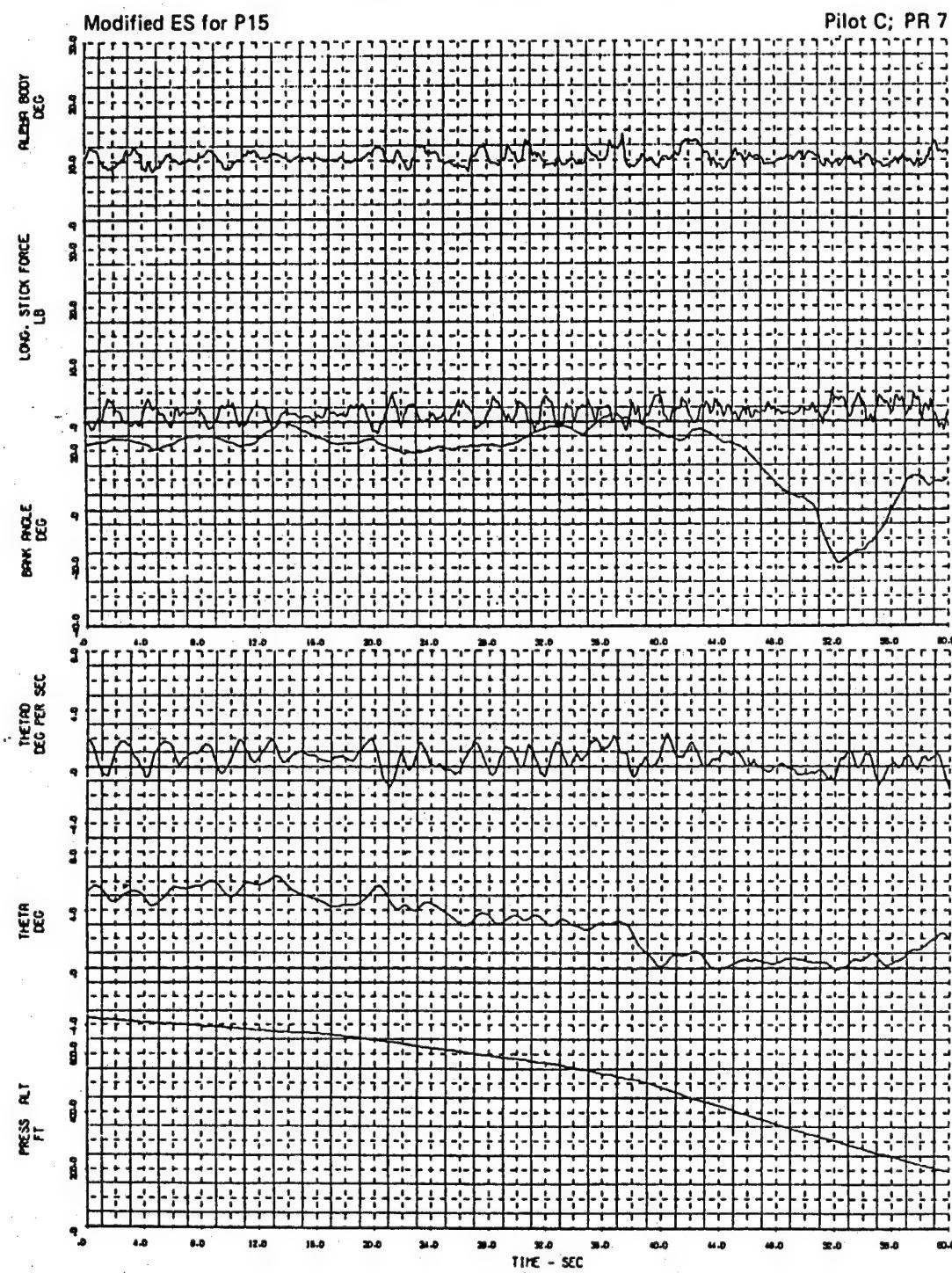


QP13-0824-97

Figure E-30a. Flight Characteristics - Time History

Figure A-56. NT-33A, Configuration P16 (Ref. A-27)

CONFIG P16A - LANDING NO. 2 FLT 2068 REC NO. 10



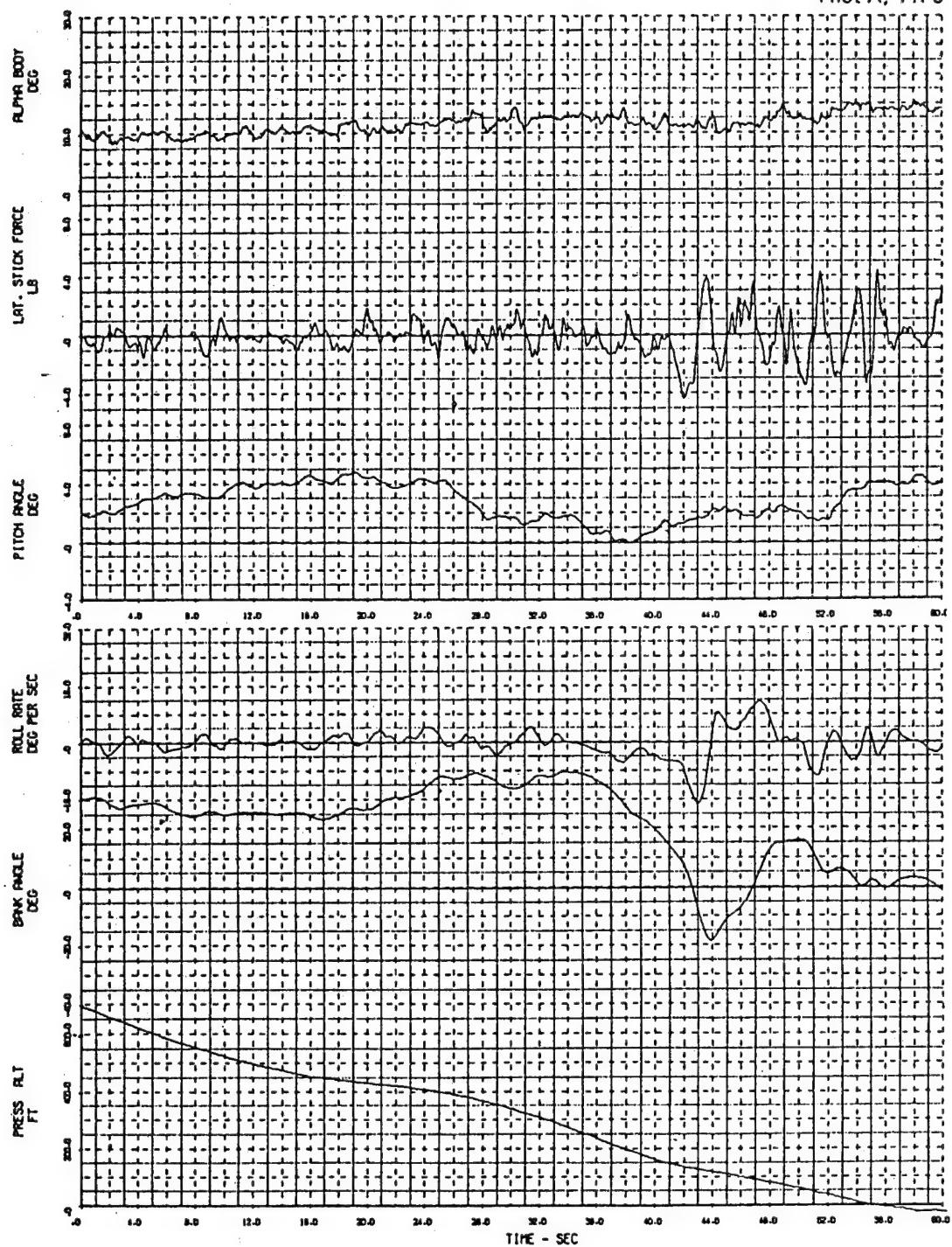
GP13-0824-101

Figure E-32a. Flight Characteristics - Time History

Figure A-57. NT-33A, Configuration P16A (Ref. A-27)

CONFIG L8 - LANDING NO. 2 FLT 207B REC NO. 3

Pilot A; PR 5



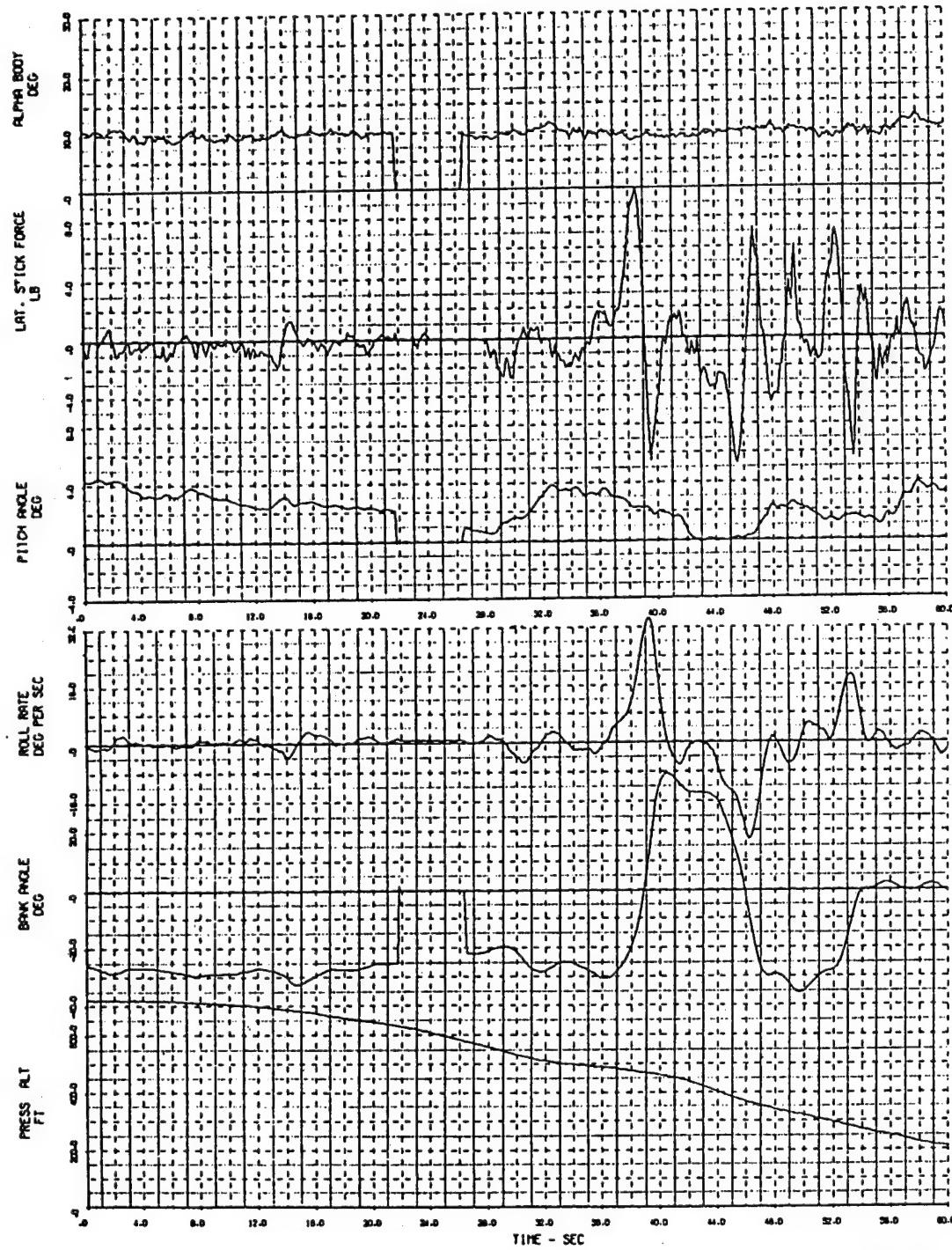
OP13-0824-113

Figure E-38a. Flight Characteristics - Time History

Figure A-58. NT-33A, Configuration L8 (Ref. A-27)

CONFIG L8B - LANDING NO. 2 FLT 2086 REC NO. 21

Pilot A; PR 9



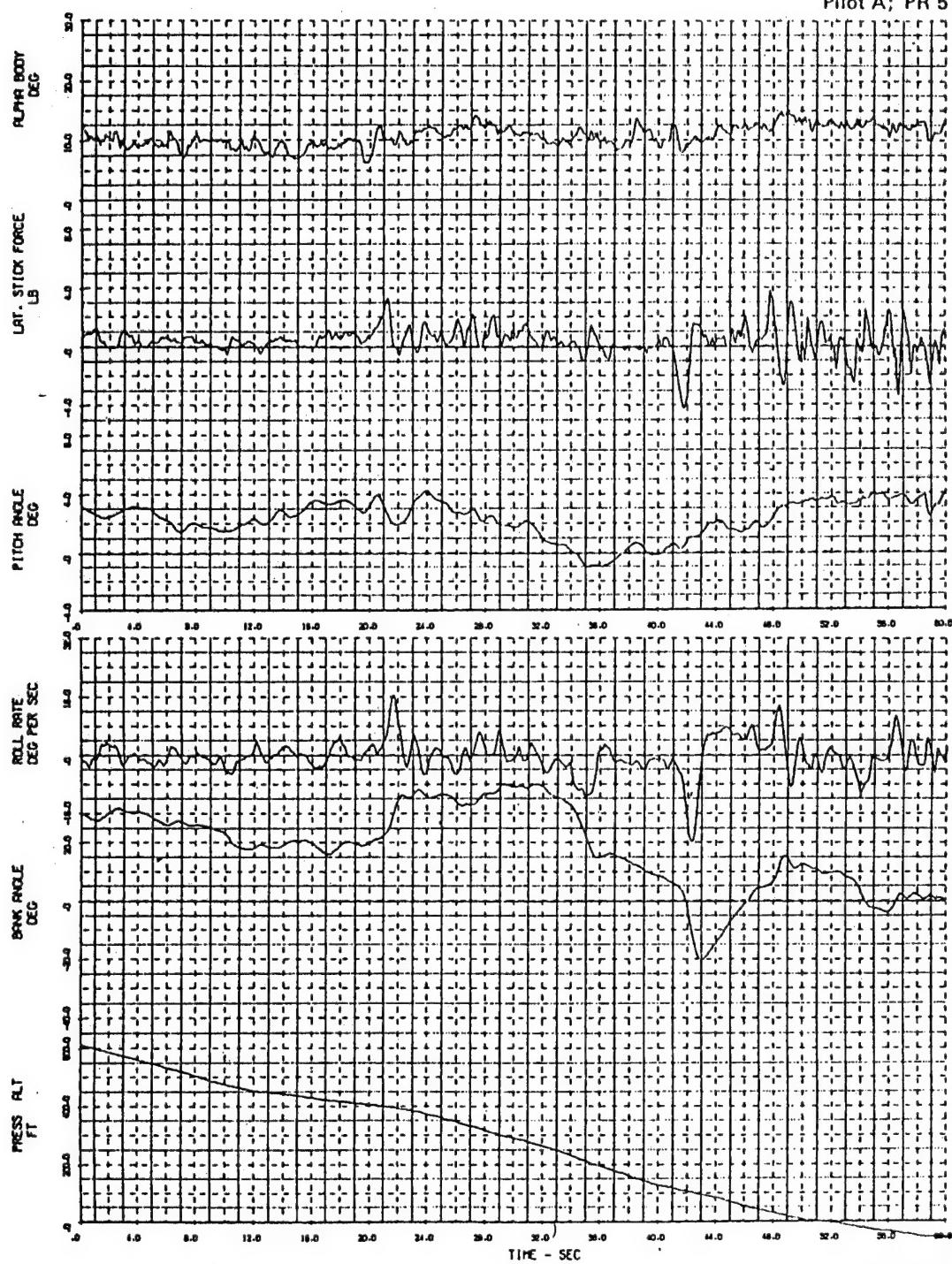
QP13-0824-117

Figure E-40a. Flight Characteristics - Time History

Figure A-59. NT-33A, Configuration L8B (Ref. A-27)

CONFIG L10 -LANDING NO. 2 FL1 2077 REC NO. 17

Pilot A; PR 5



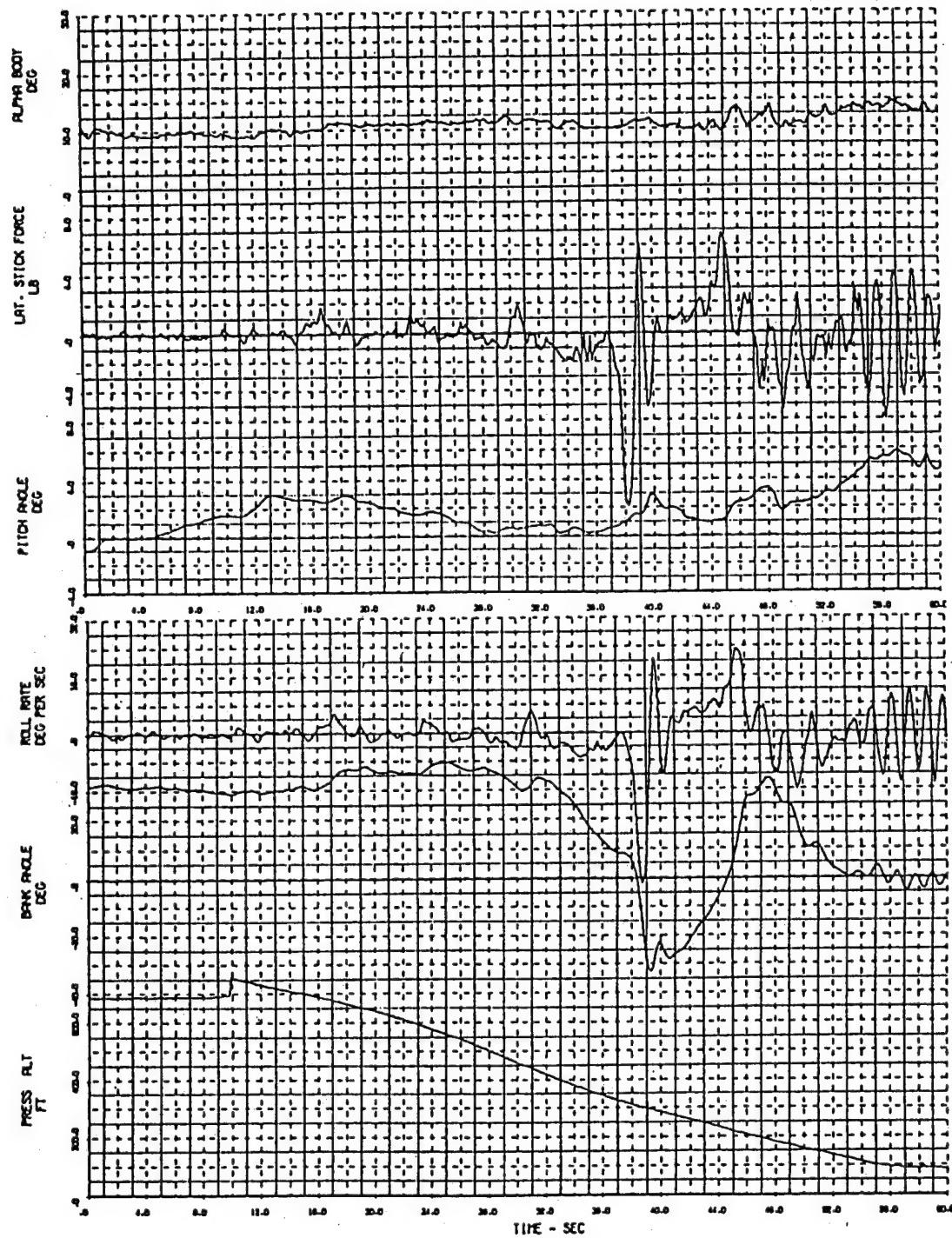
QP13-0824-121

Figure E-42a. Flight Characteristics - Time History

Figure A-60. NT-33A, Configuration L10 (Ref. A-27)

CONFIG L11C - LANDING NO. 2 FLT 2003 REC NO. 15

Pilot A; PR 9



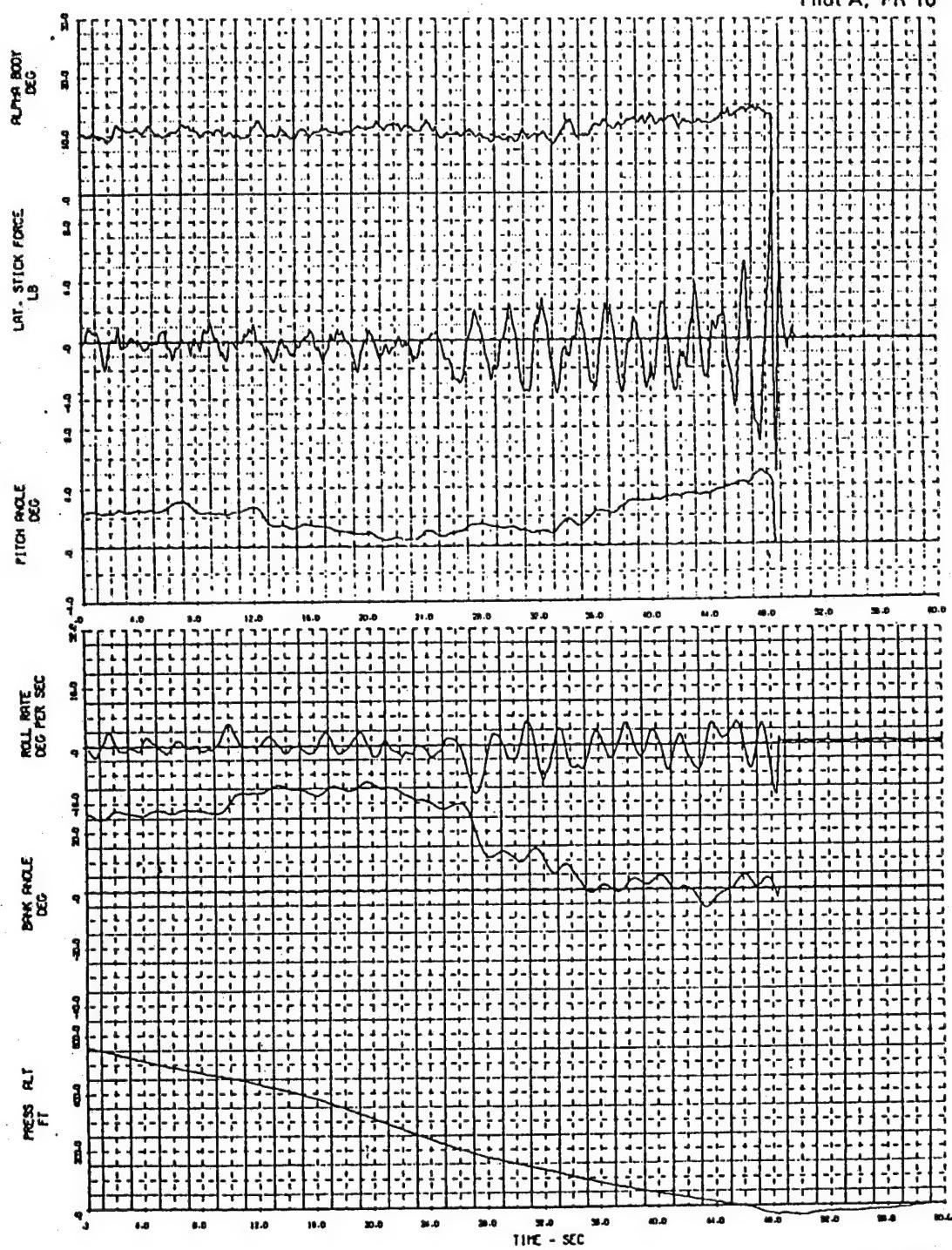
GP13-0624-123

Figure E-43a. Flight Characteristics - Time History

Figure A-61. NT-33A, Configuration L11C (Ref. A-27)

CONFIG L11D-LANDING NO. 1 FLT 2070 REC NO. 7

Pilot A; PR 10



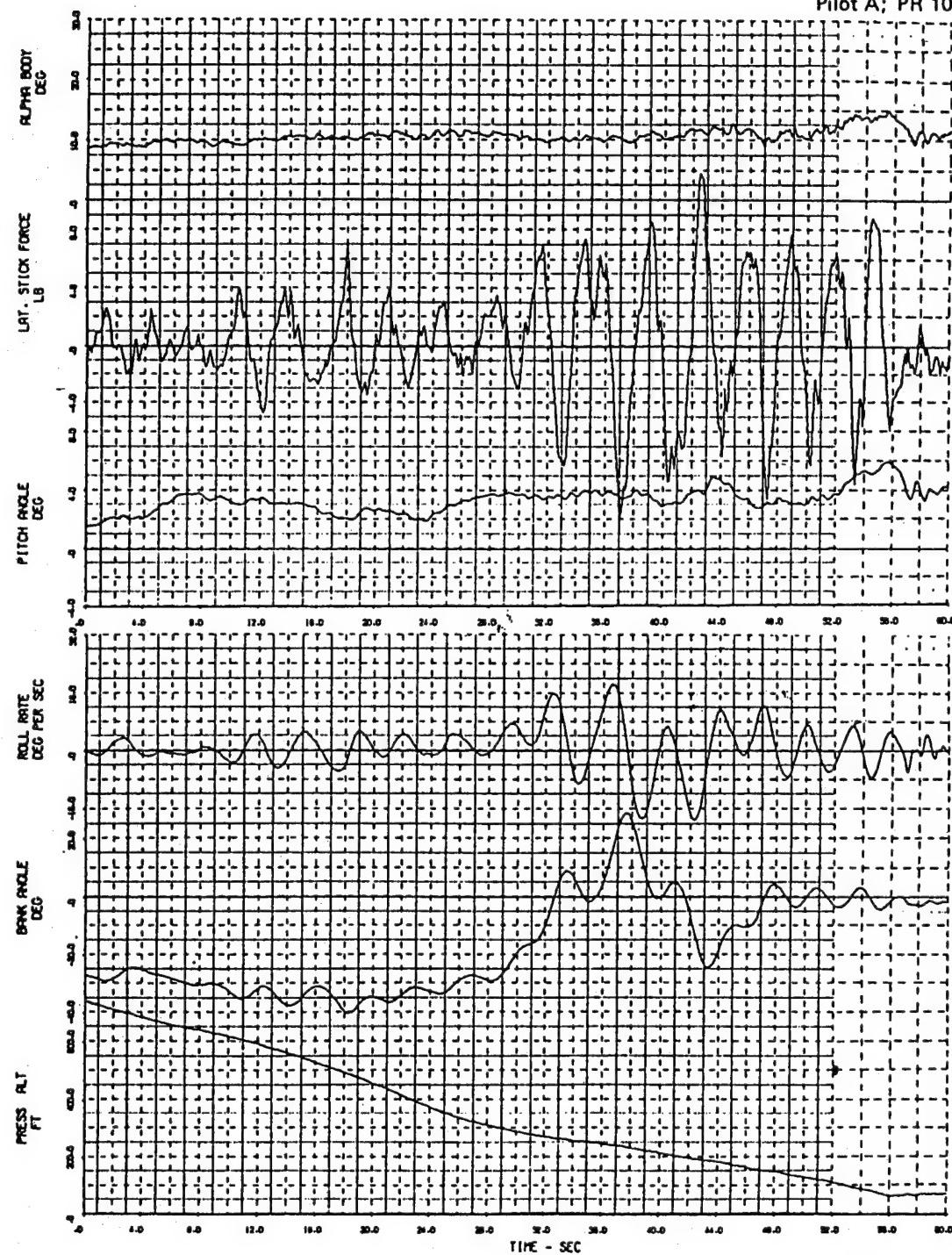
GP13-0824-128

Figure E-44a. Flight Characteristics - Time History

Figure A-62. NT-33A, Configuration L11C (Ref. A-27)

CONFIG L14B - LANDING NO. 2 FLT 2083 REC NO. 4

Pilot A; PR 10



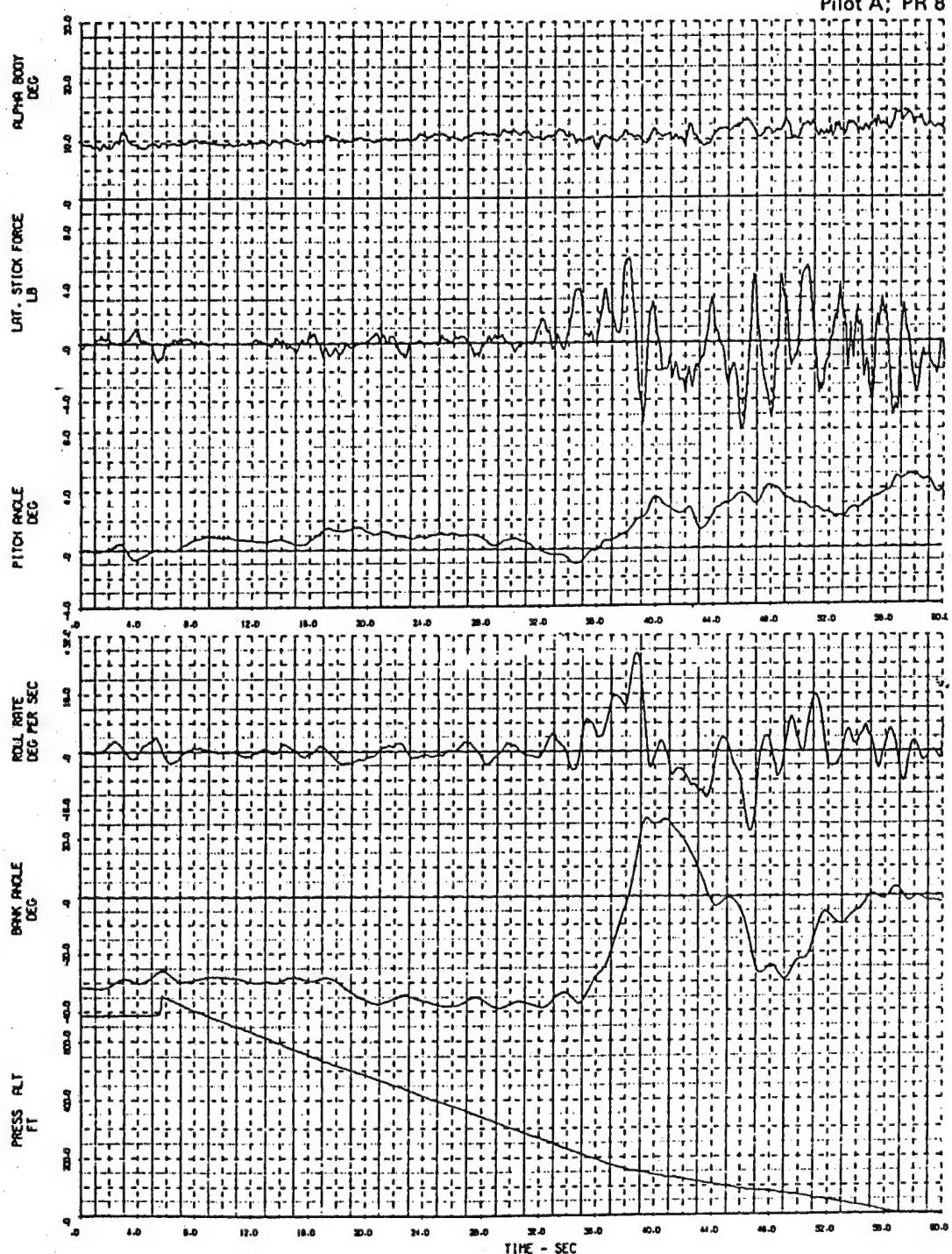
QP13-0024-131

Figure E-47a. Flight Characteristics - Time History

Figure A-63. NT-33A, Configuration L14B (Ref. A-27)

CONFIG L16A - LANDING NO. 2 FLT 2080 REC NO. 14

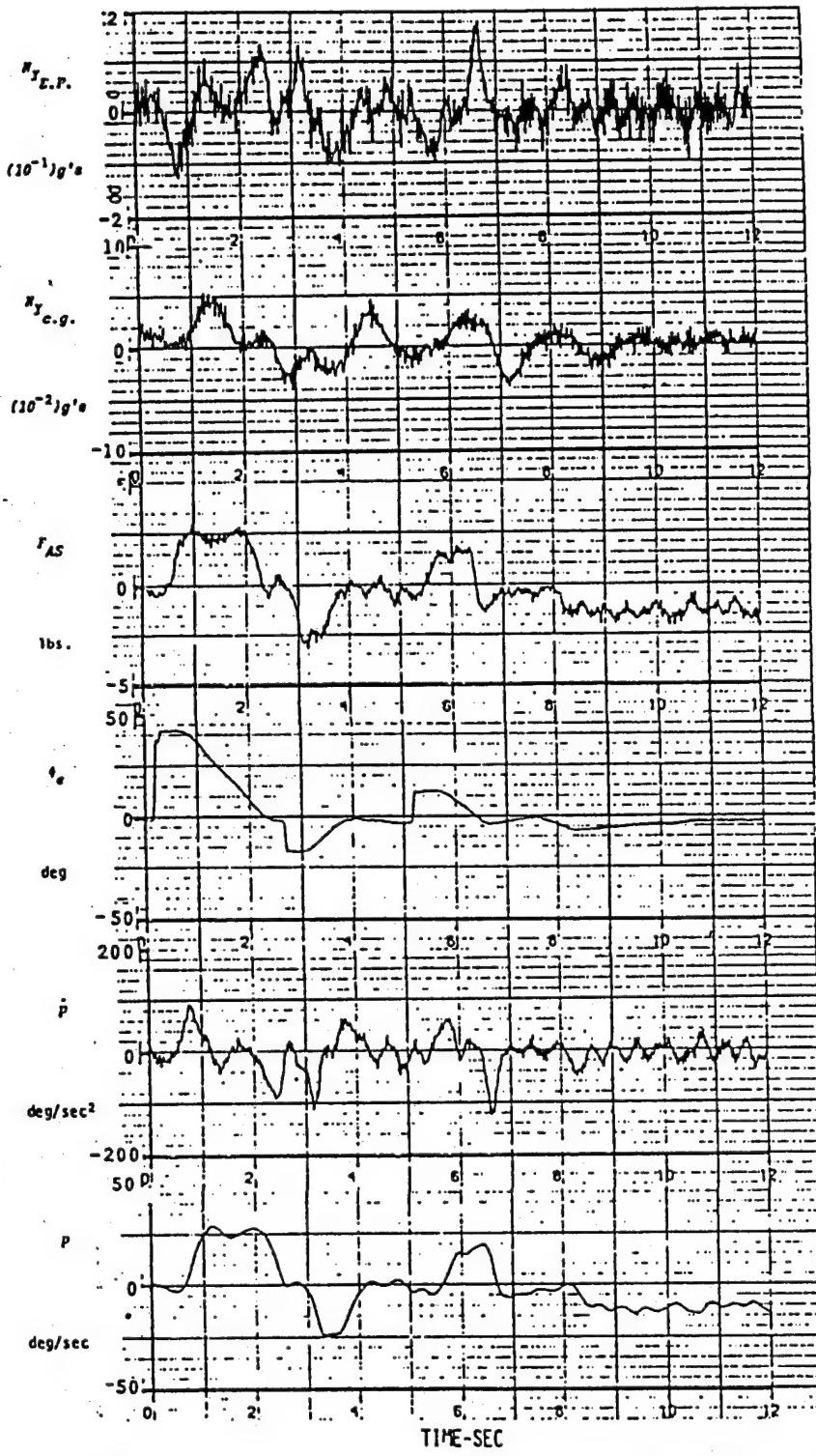
Pilot A; PR 8



GP13-0824-133

Figure E-48a. Flight Characteristics - Time History

Figure A-64. NT-33A, Configuration L16A (Ref. A-27)



HUD TRACKING TASK RECORD, CONFIGURATION 5-2 (EVALUTION NO. 12) "ROLL RATCHETING"

Figure A-65. NT-33A, Configuration 5-2 (Ref. A-28)

**Lateral Pilot Induced Oscillation;
AR/PA Mode; TIFS III**

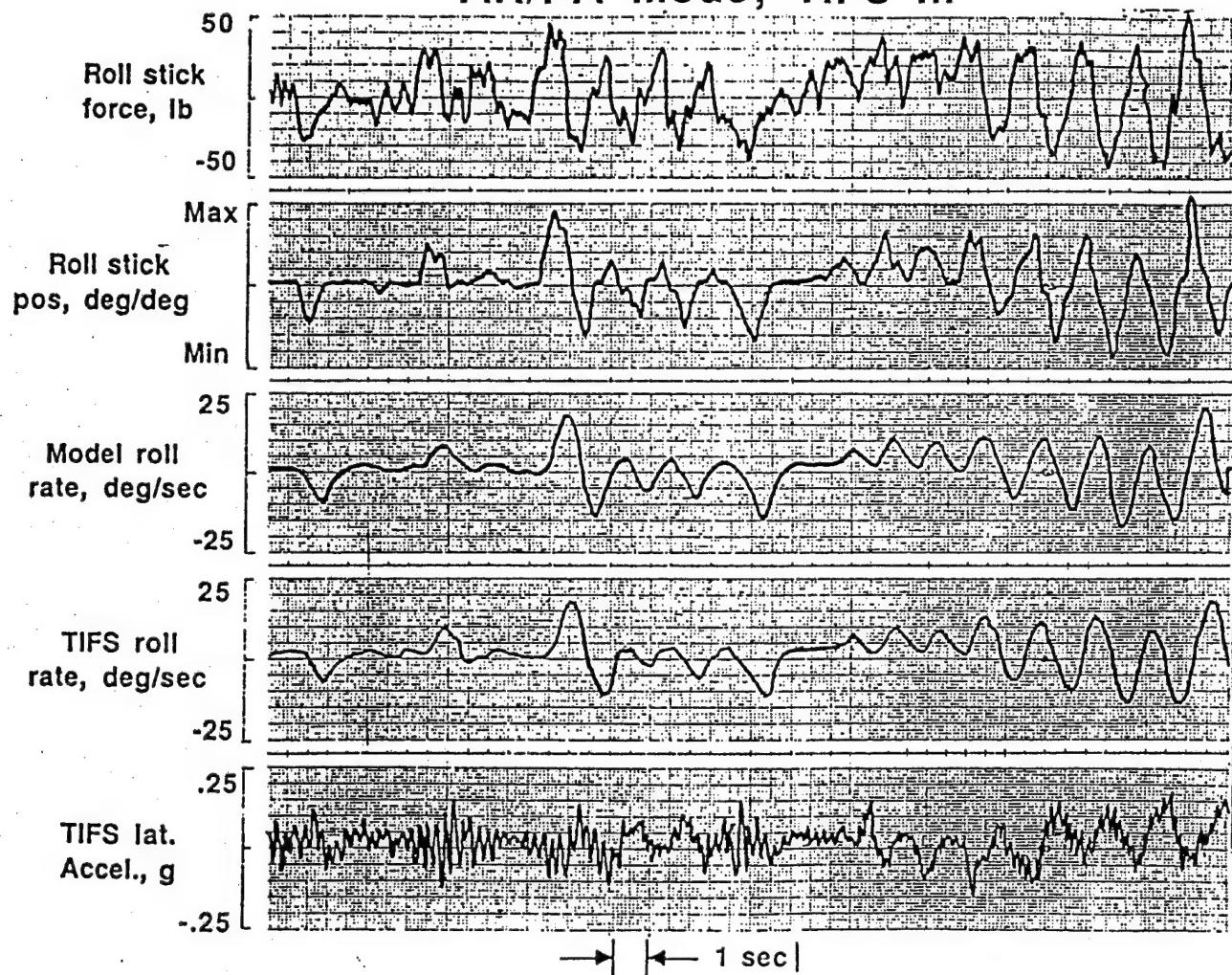


Figure A-66. TIFS, Configuration X-29A - AR/PA (Ref. A-29)

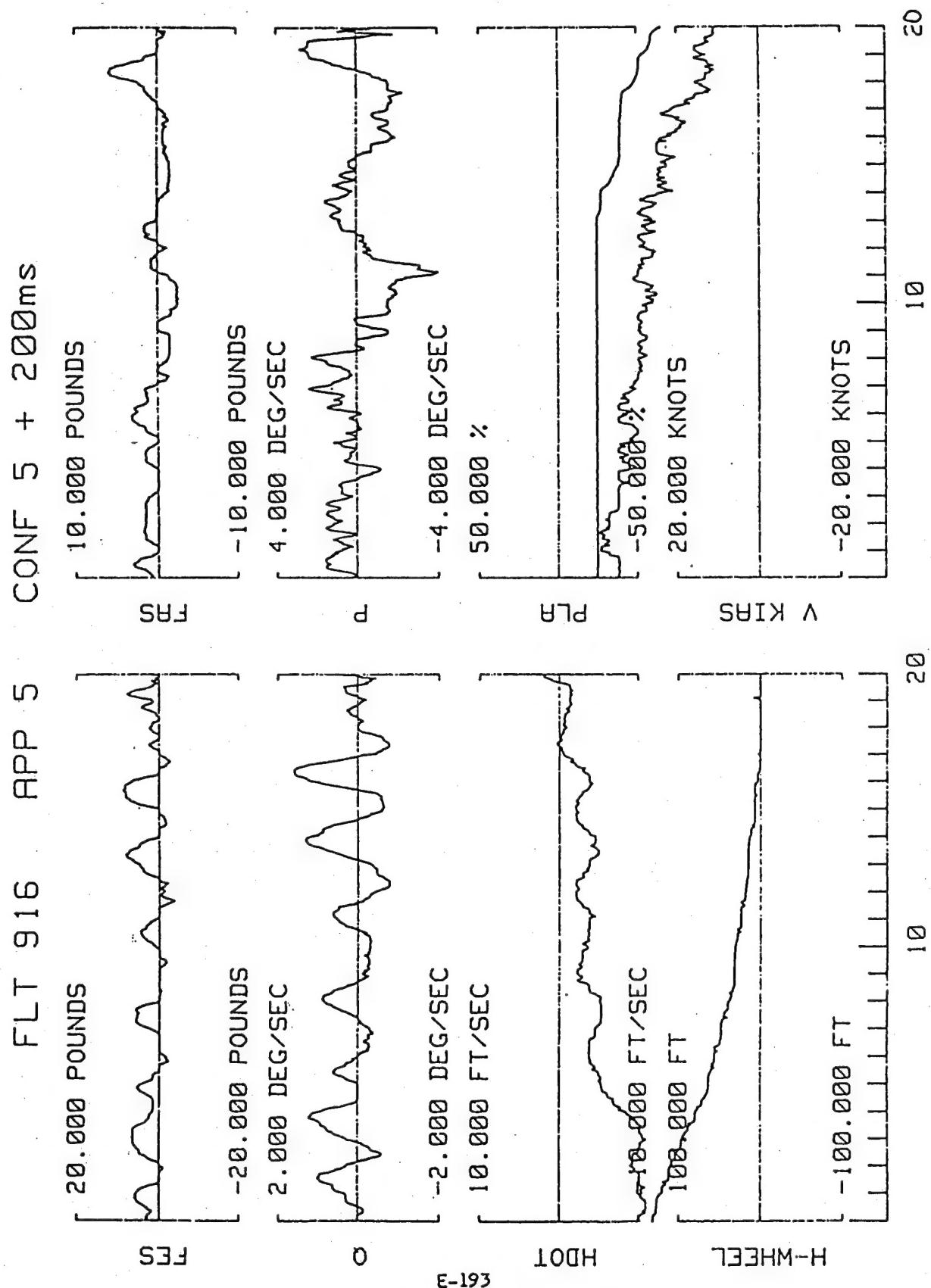


Figure A-67. TIFS, Configuration 5 + 200ms (Ref. A-30)

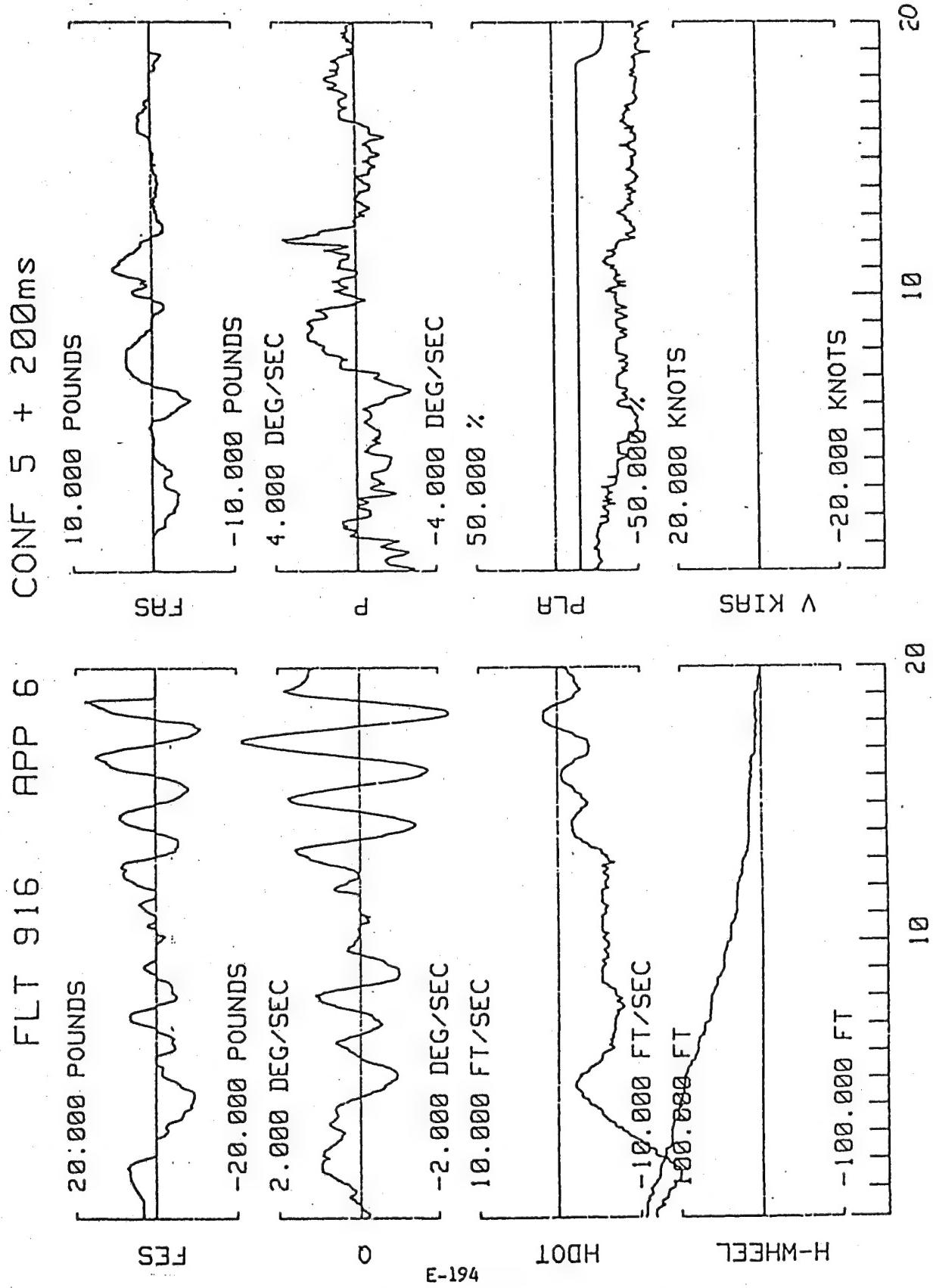


Figure A-68. TIFS, Configuration 5 + 200ms (Ref. A-30)

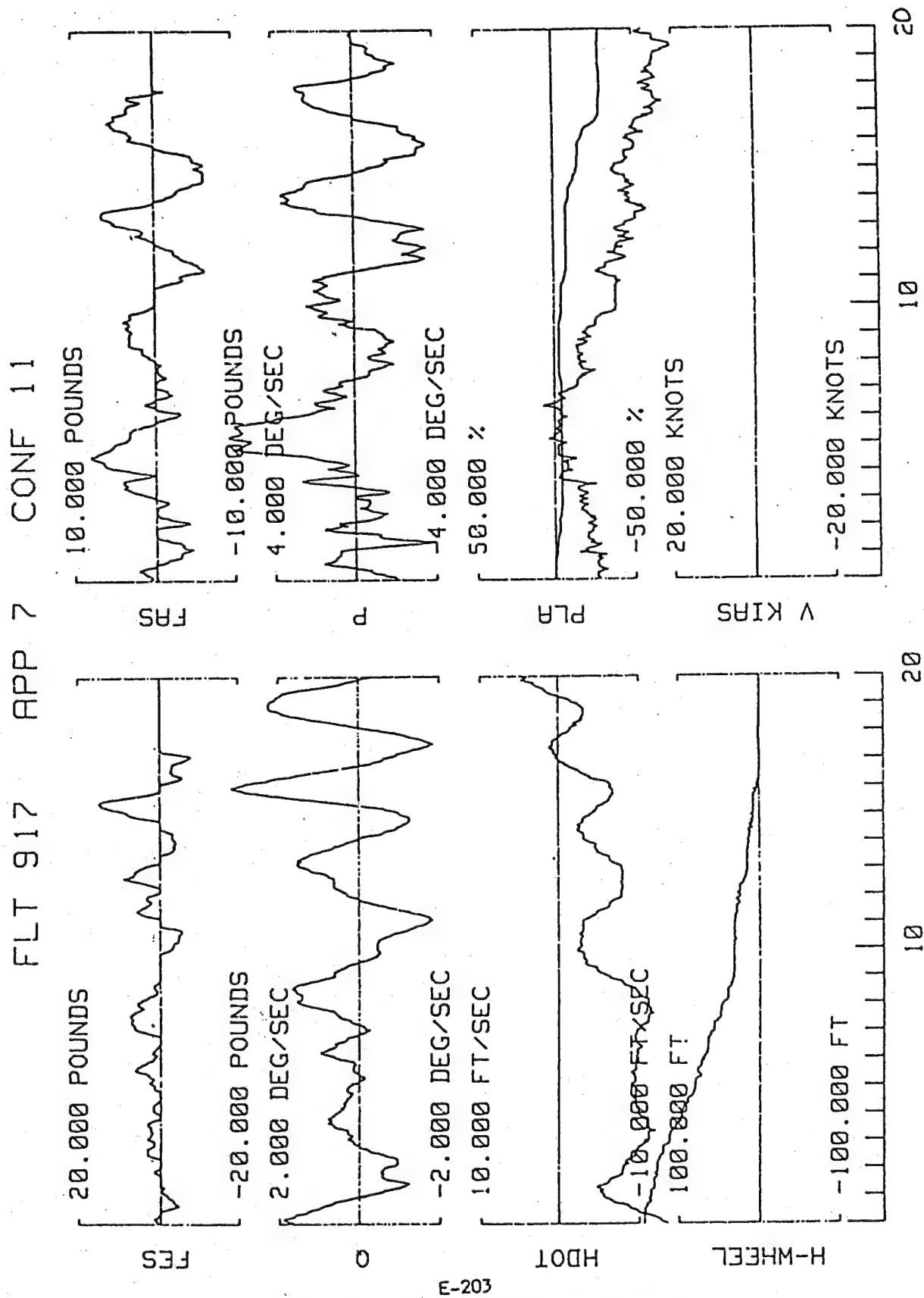


Figure A-69. TIFS, Configuration 11 (Ref. A-30)

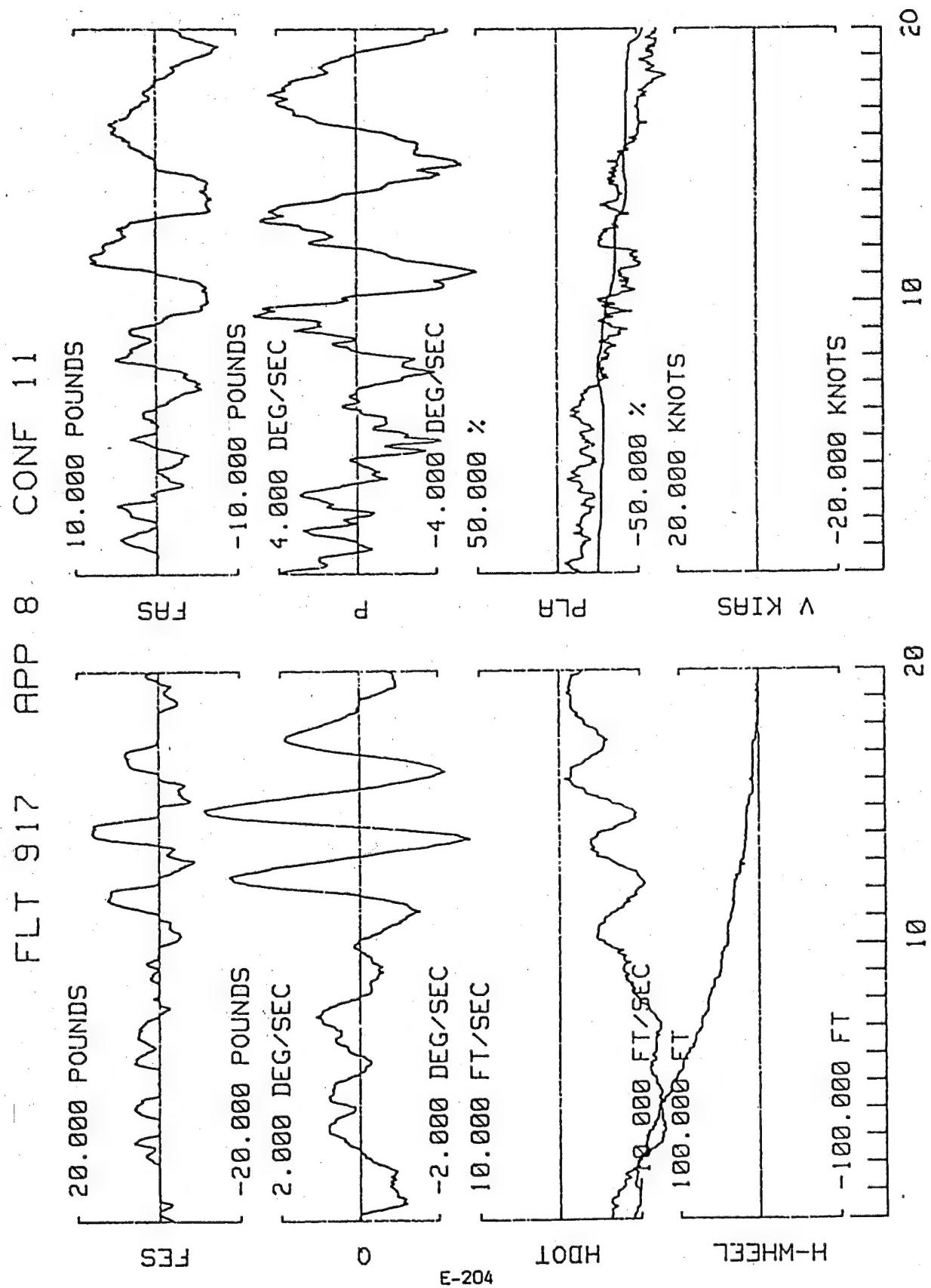


Figure A-70. TIFS, Configuration 11 (Ref. A-30)

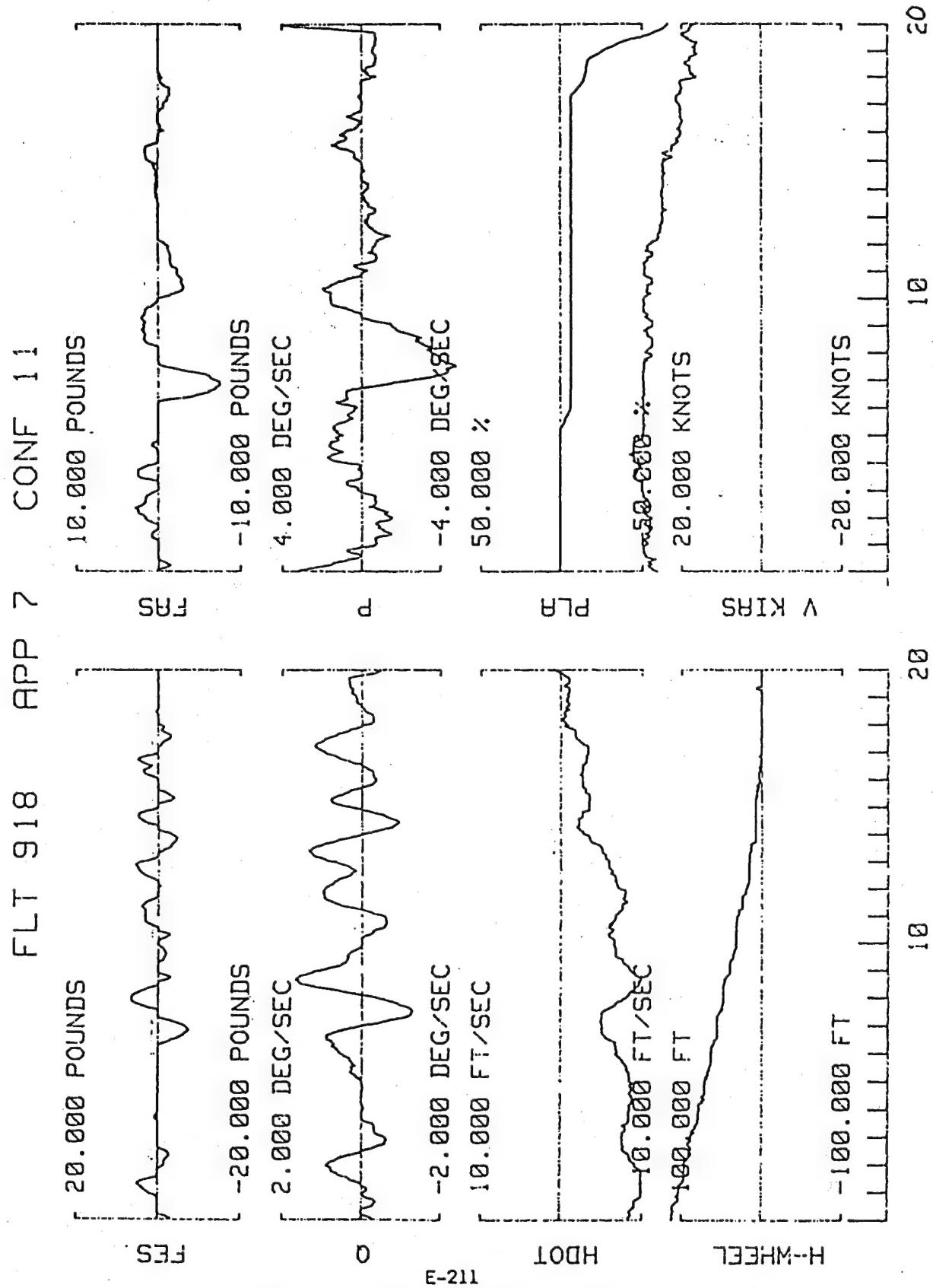


Figure A-71. TIFS, Configuration 11 (Ref. A-30)

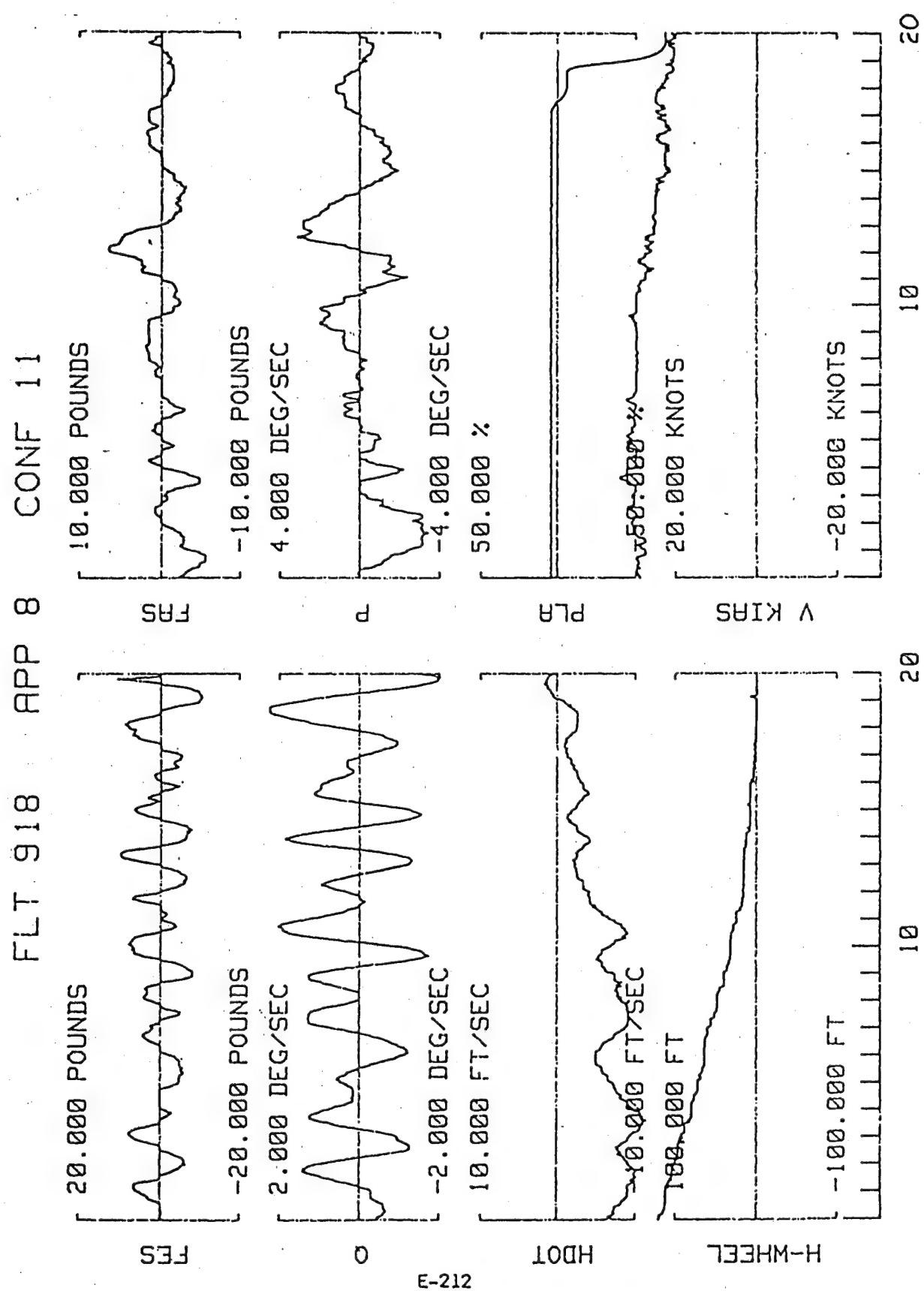


Figure A-72. TIFS, Configuration 11 (Ref. A-30)

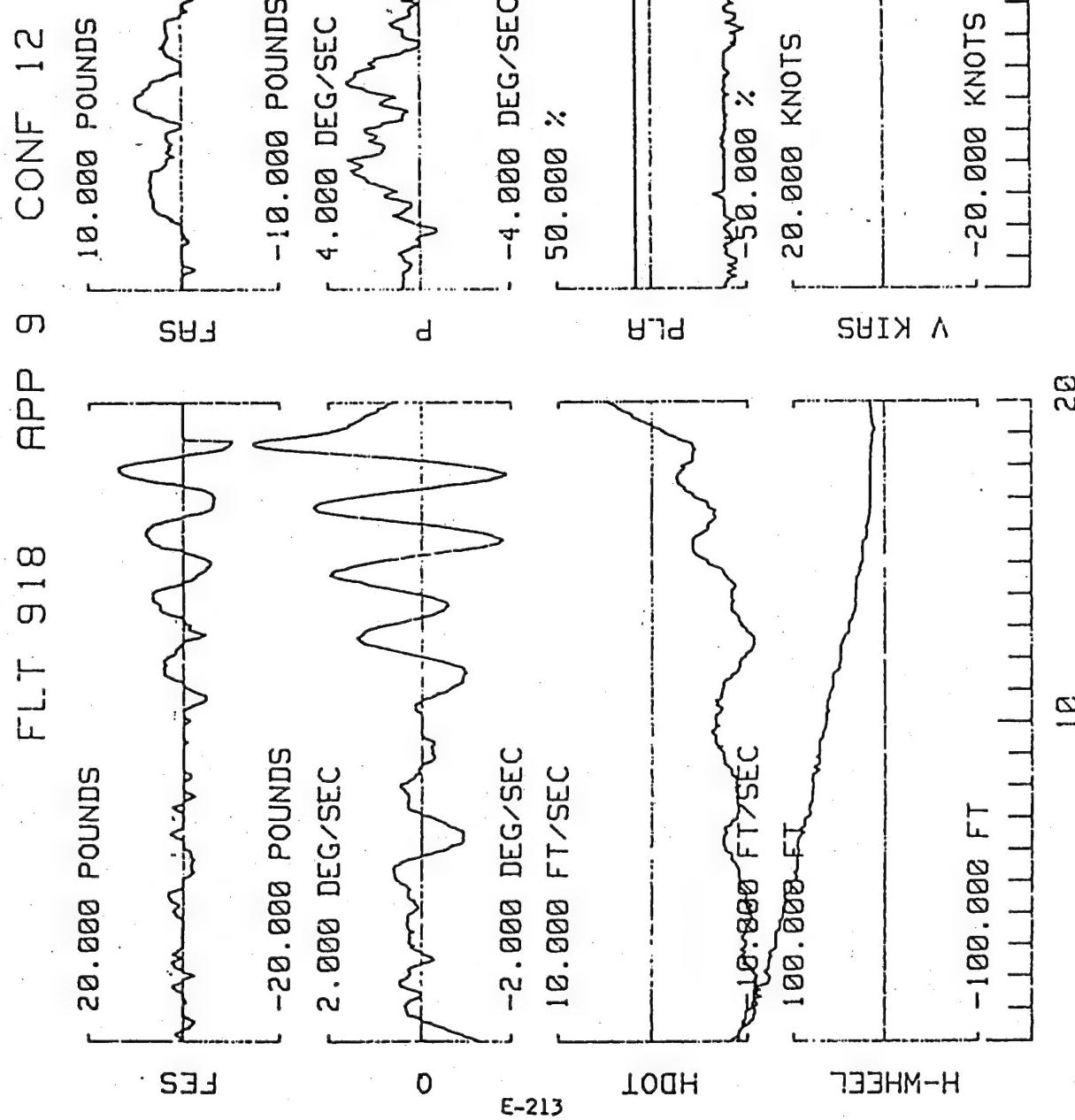


Figure A-73. TIFS, Configuration 12 (Ref. A-30)

FLT 918 APP 10 CONF 12

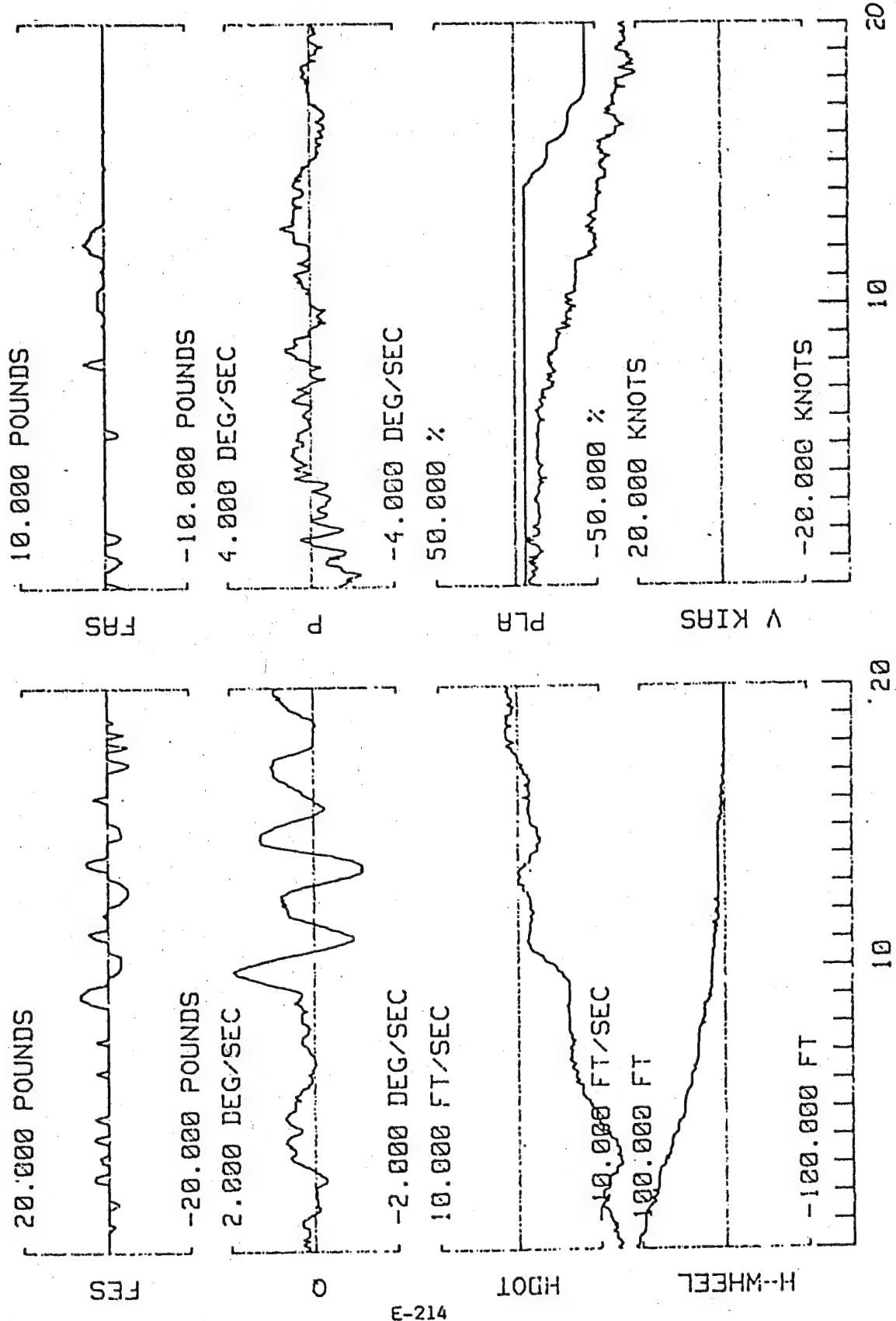


Figure A-74. TIFS, Configuration 12 (Ref. A-30)

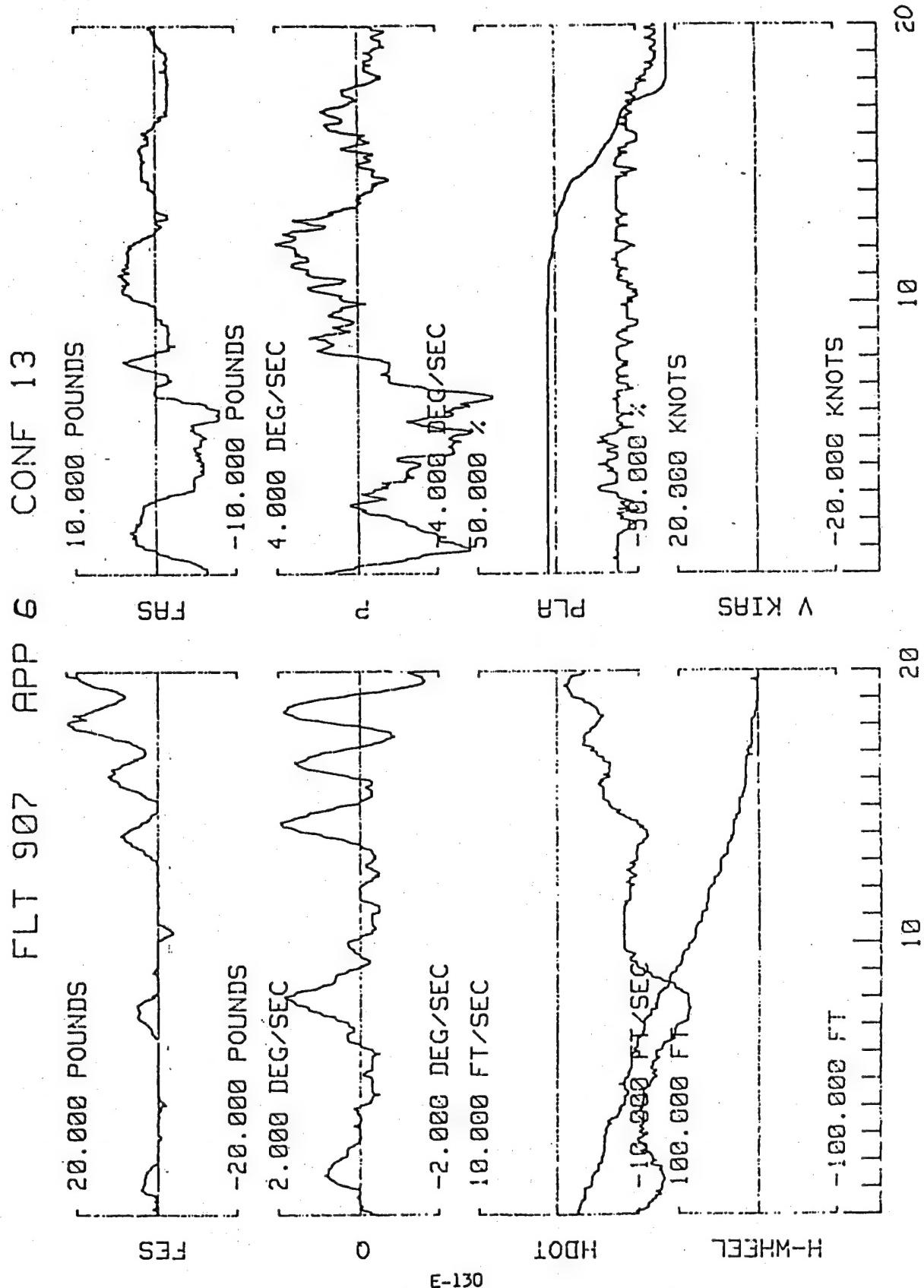


Figure A-75. TIFS, Configuration 13 (Ref. A-30)

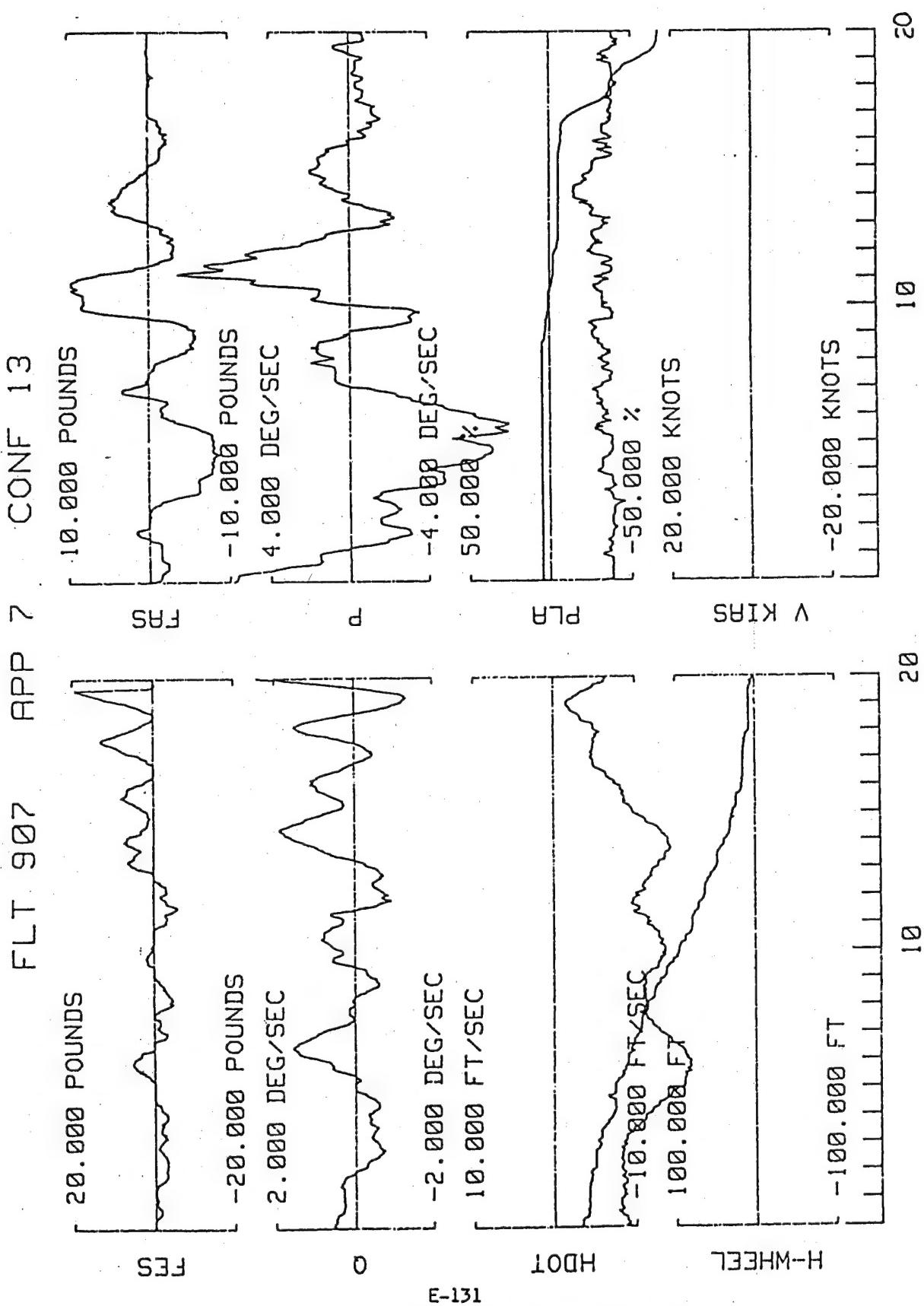


Figure A-76. TIFS, Configuration 13 (Ref. A-30)

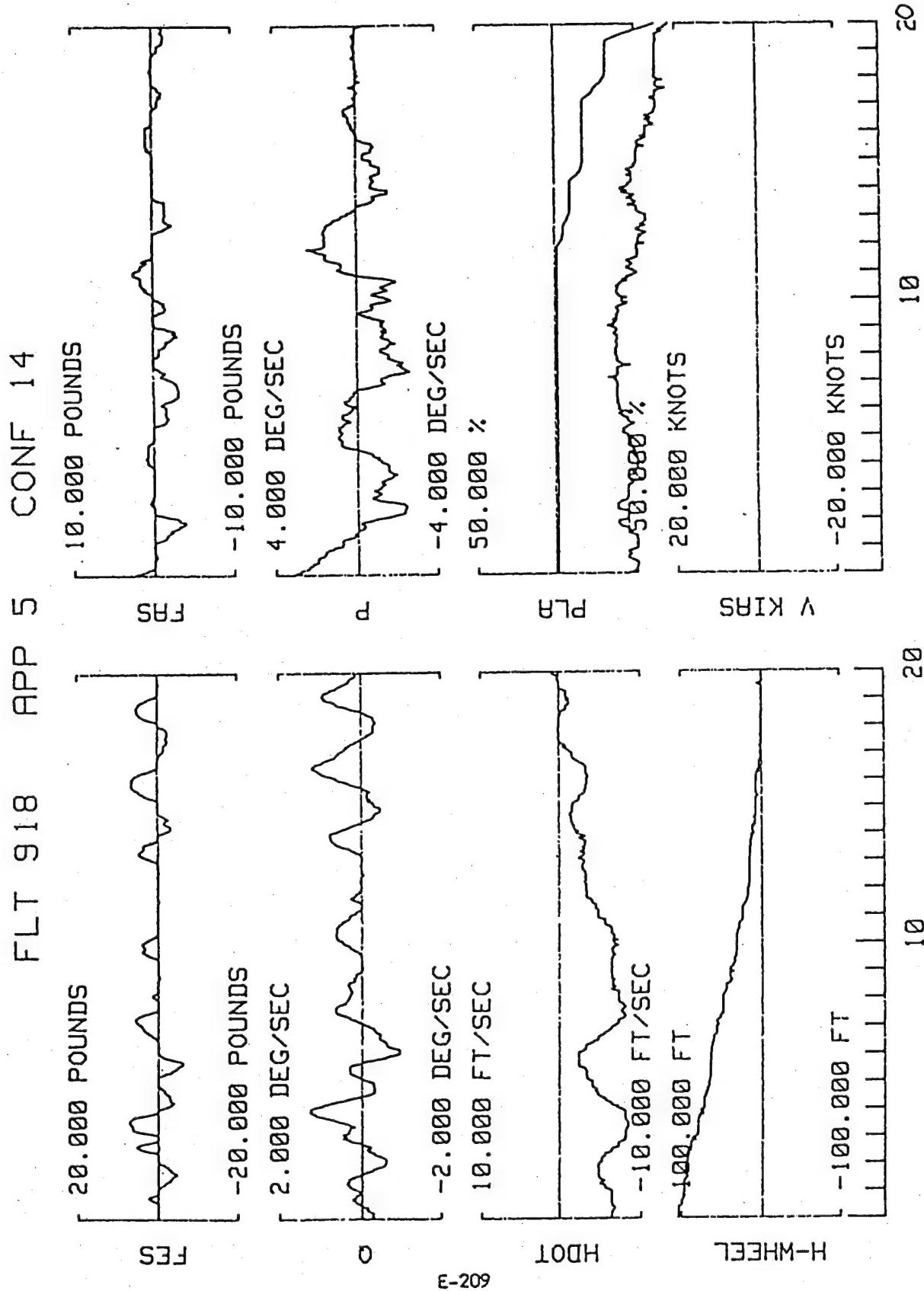


Figure A-77. TIFS, Configuration 14 (Ref. A-30)

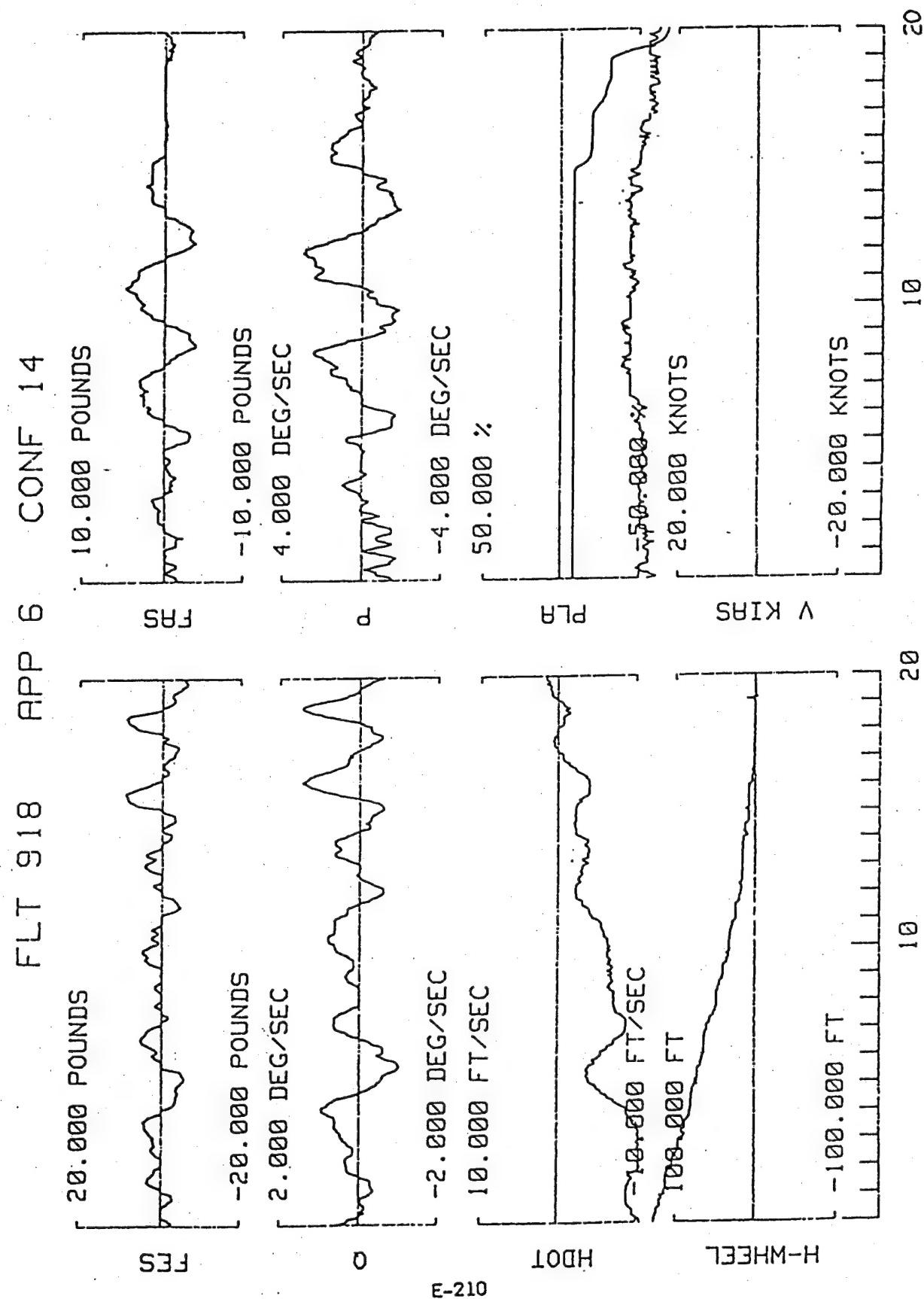


Figure A-78. TIFS, Configuration 14 (Ref. A-30)

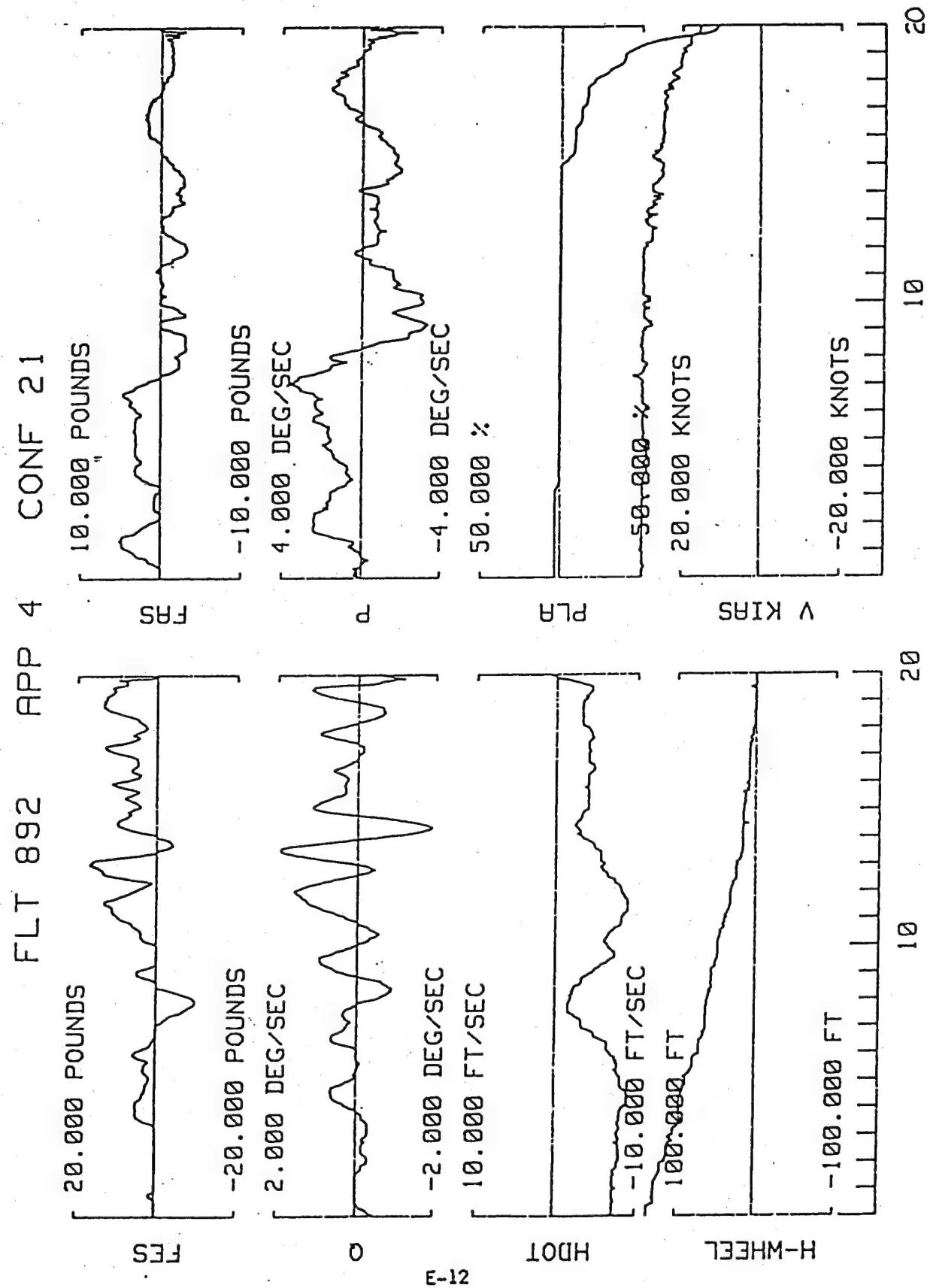


Figure A-79. TIFS, Configuration 21 (Ref. A-30)

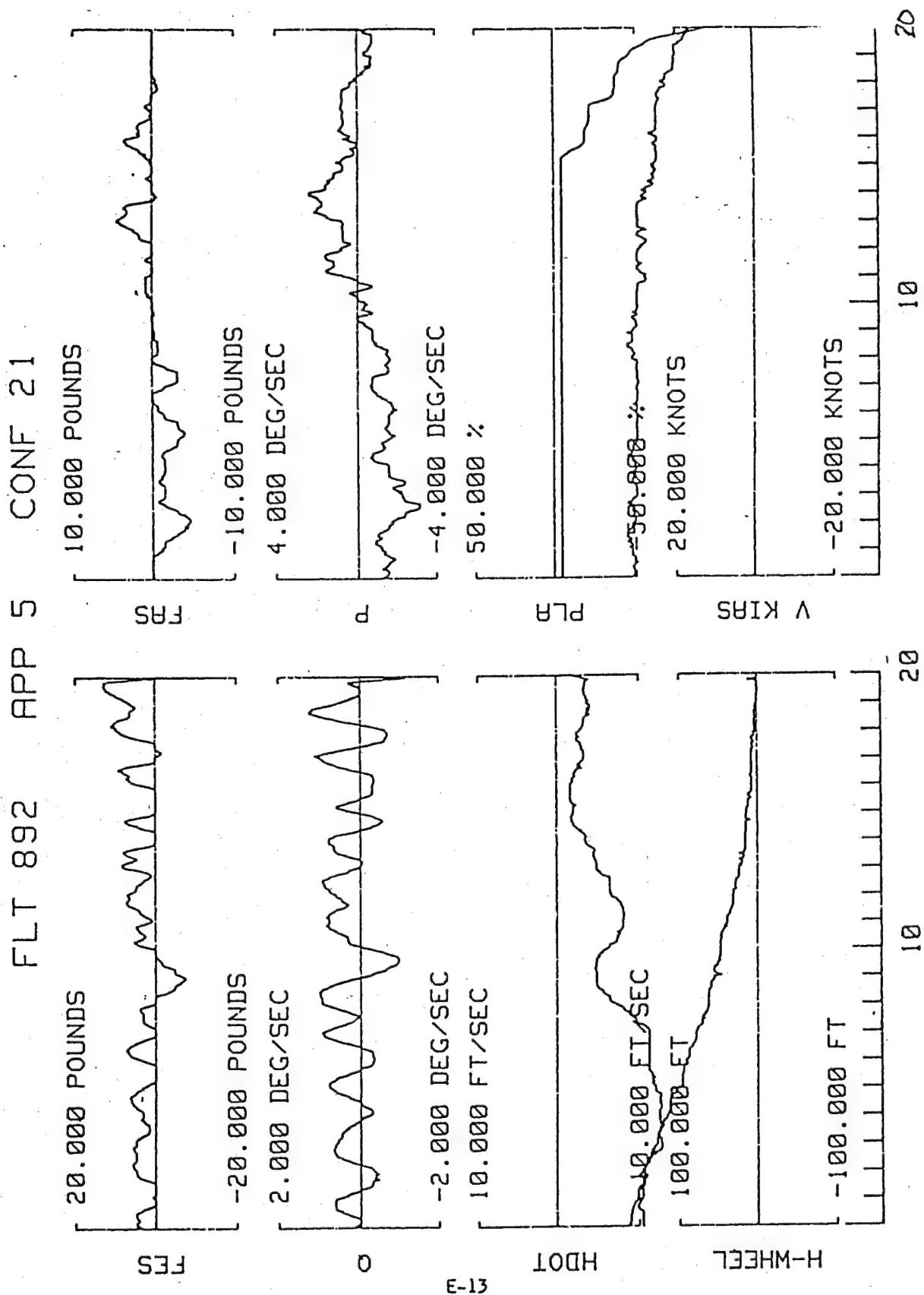


Figure A-80. IIFS, Configuration 21 (Ref. A-30)

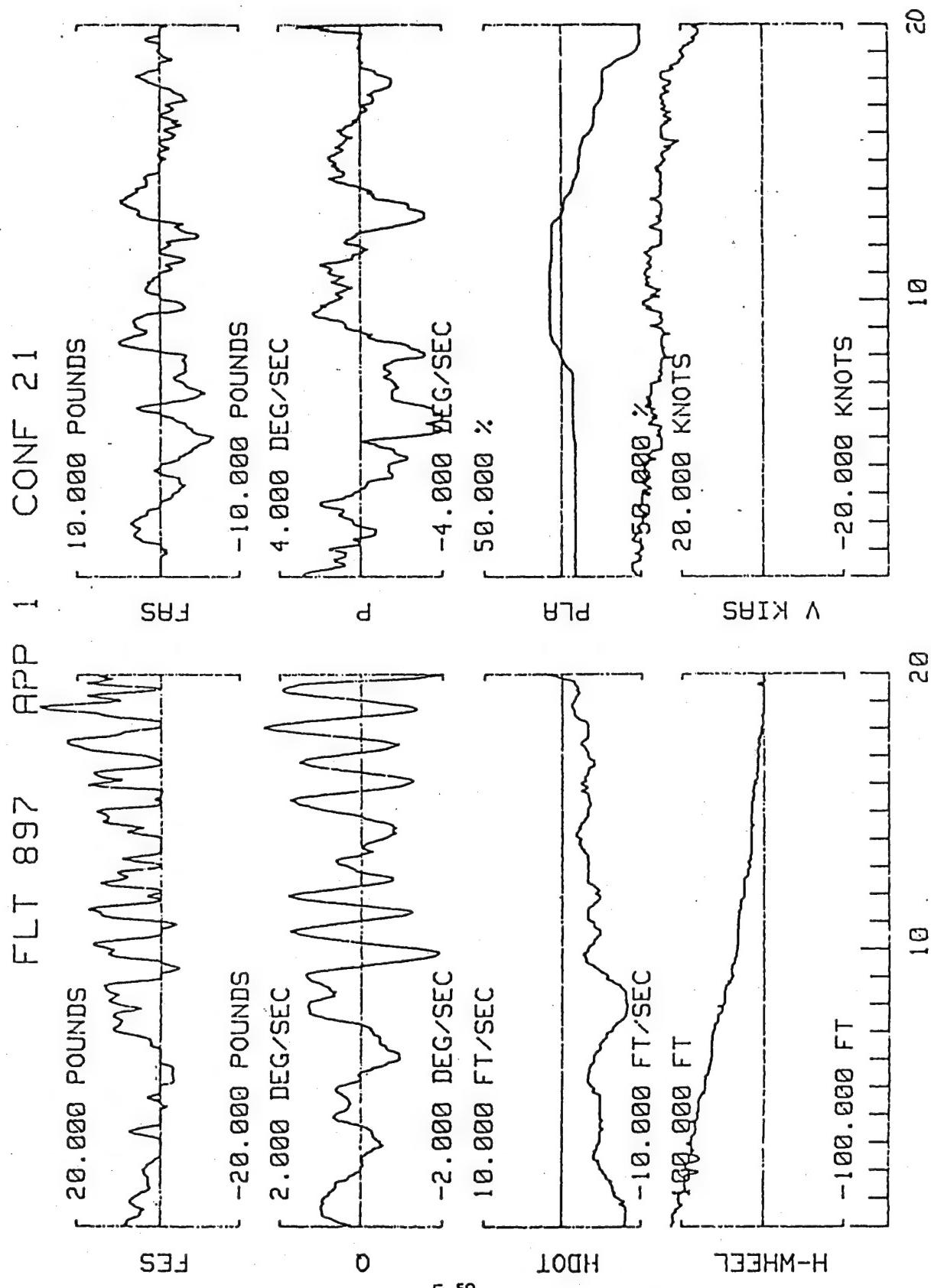


Figure A-81. TIFS, Configuration 21 (Ref. A-30)

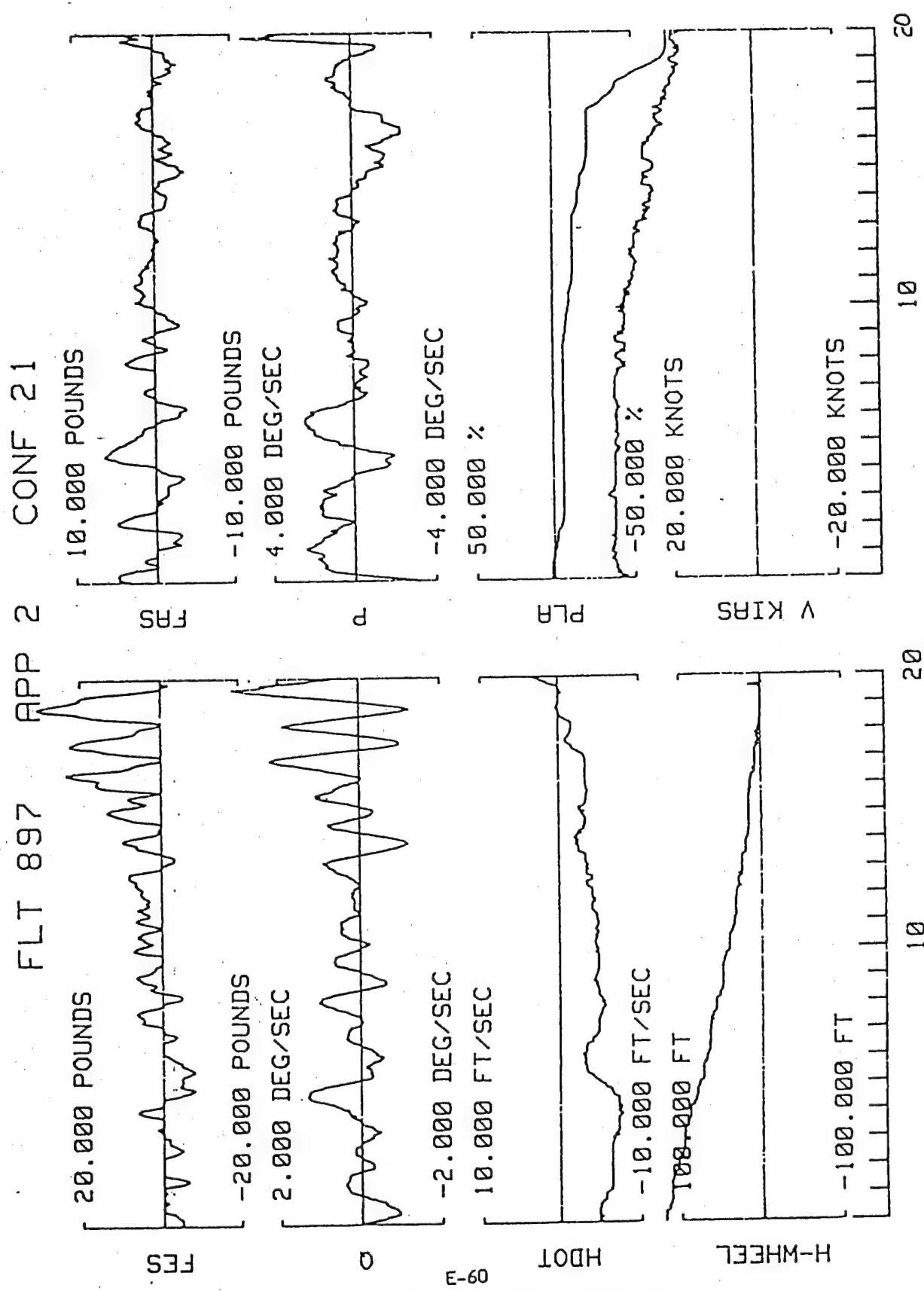


Figure A-82. TIFS, Configuration 21 (Ref. A-30)

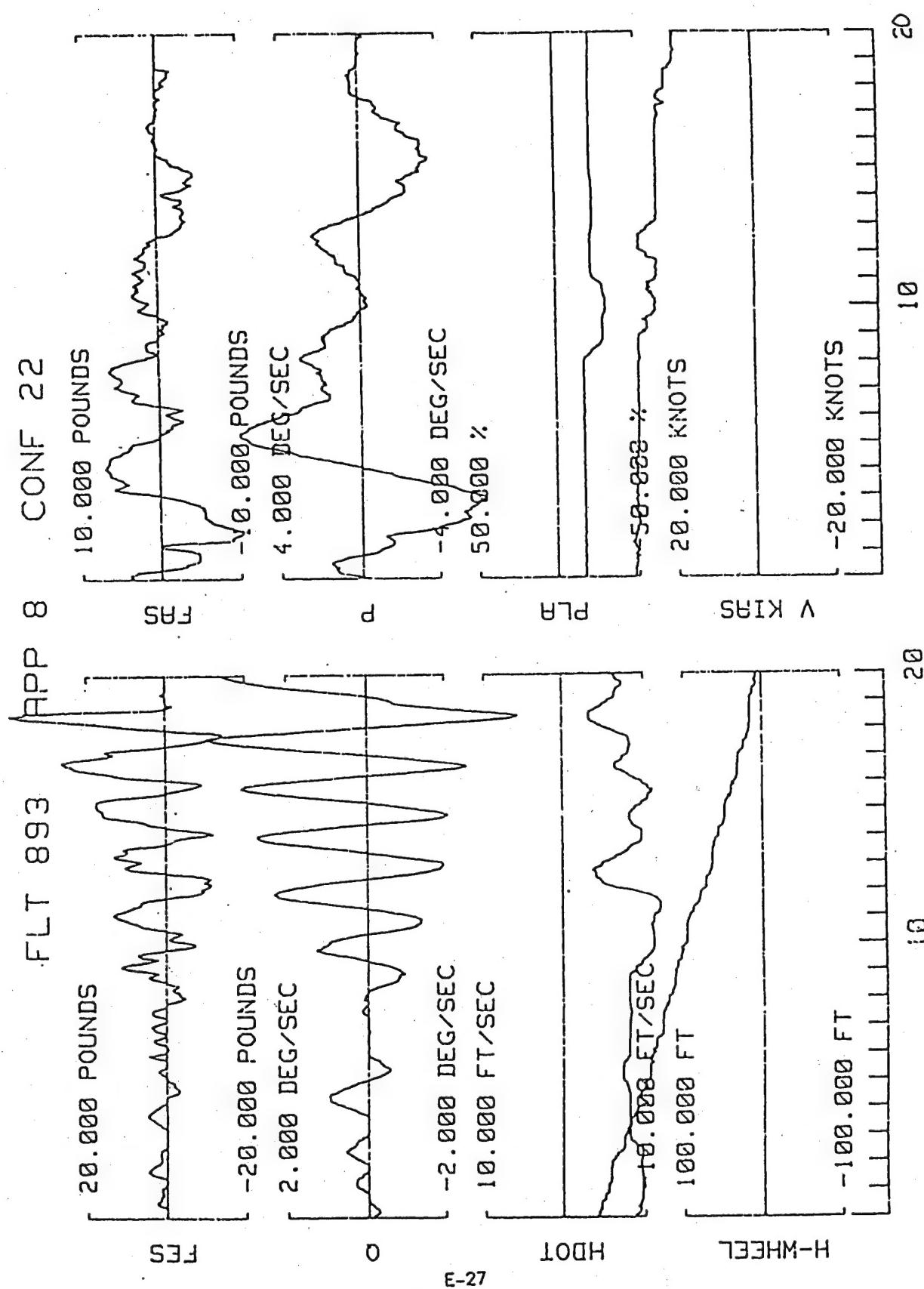


Figure A-83. TIFS, Configuration 22 (Ref. A-30)

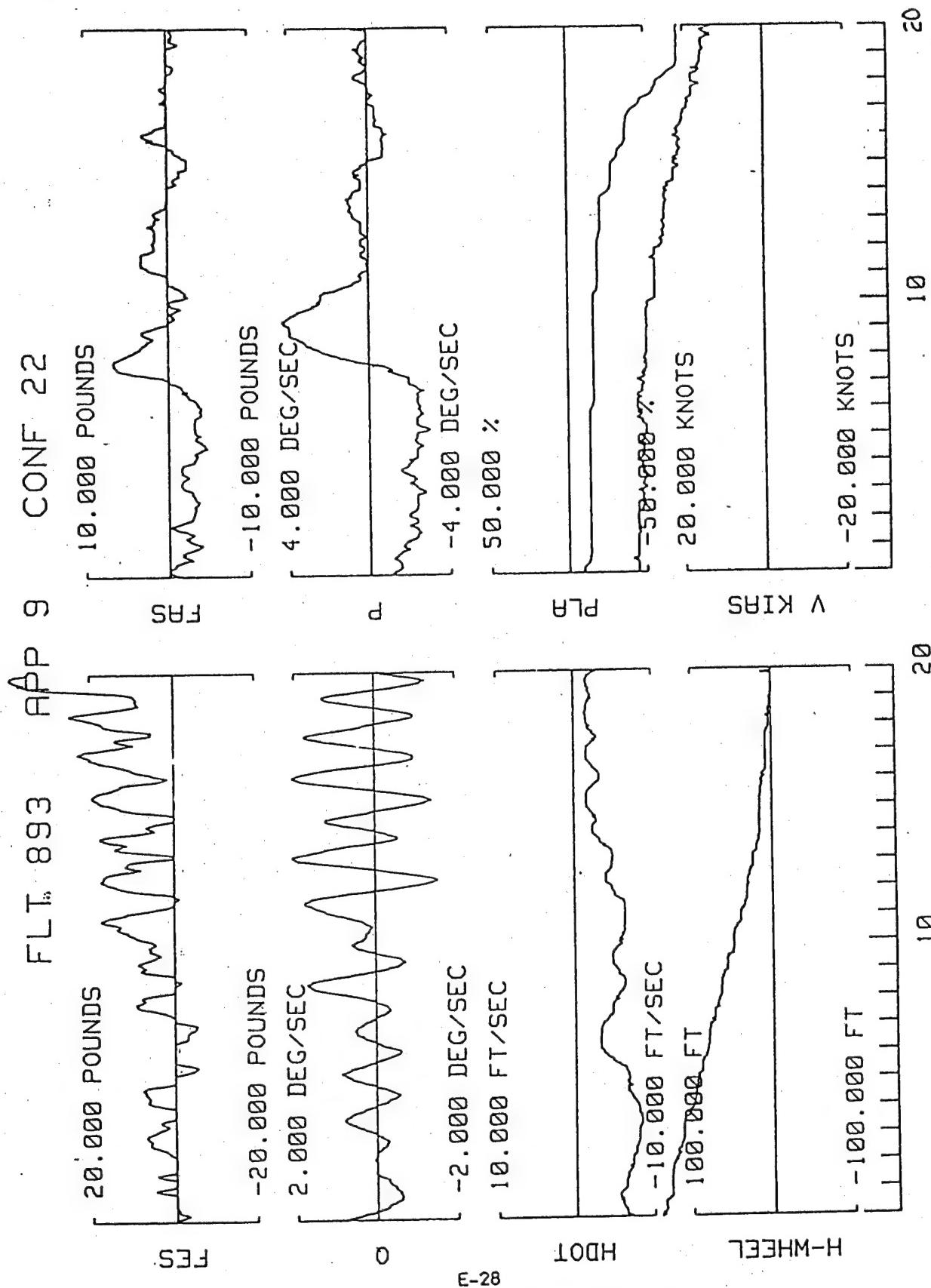


Figure A-84. TIFS, Configuration 22 (Ref. A-30)

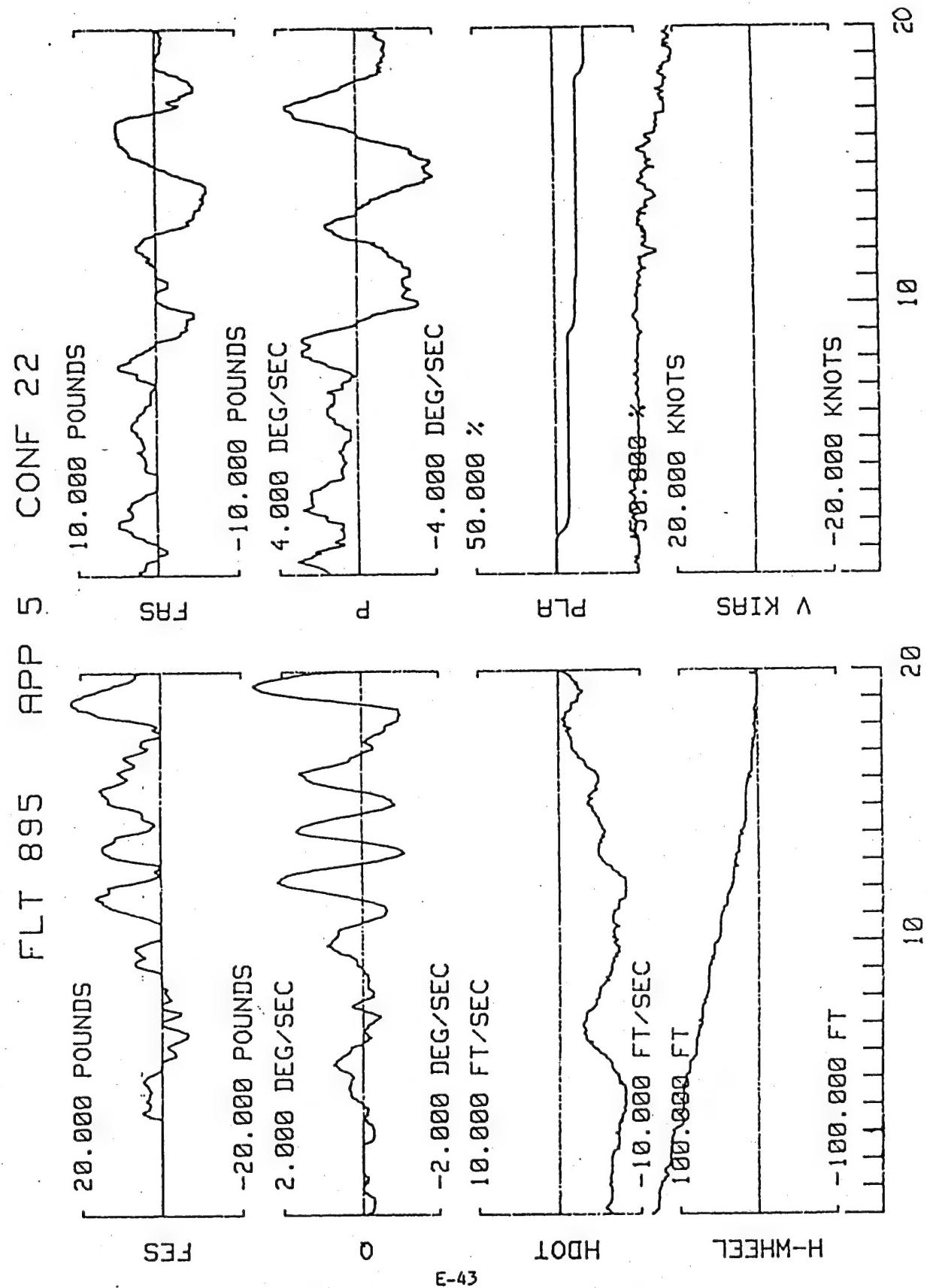


Figure A-85. TIFS, Configuration 22 (Ref. A-30)

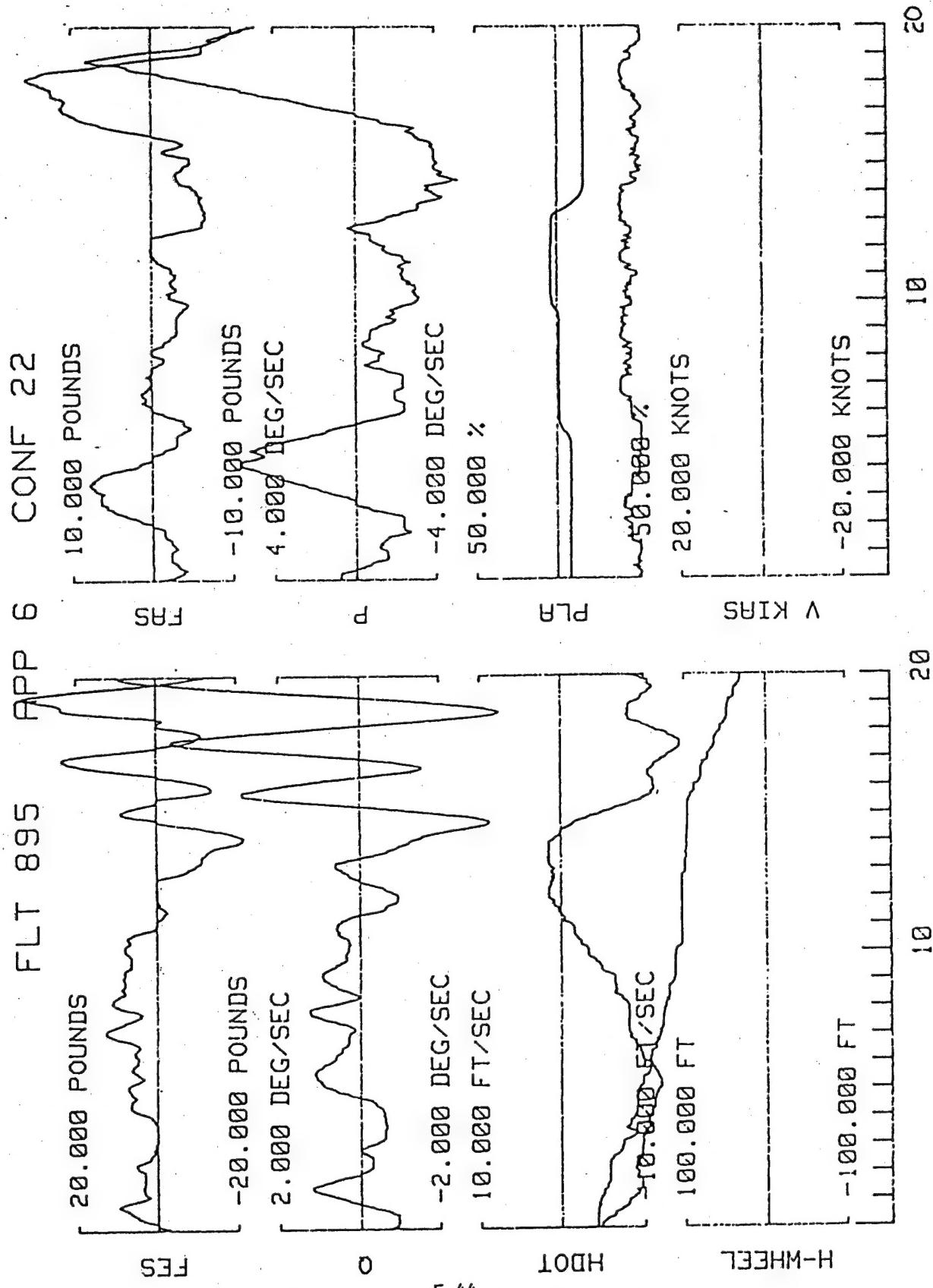


Figure A-86. TIFS, Configuration 22 (Ref. A-30)

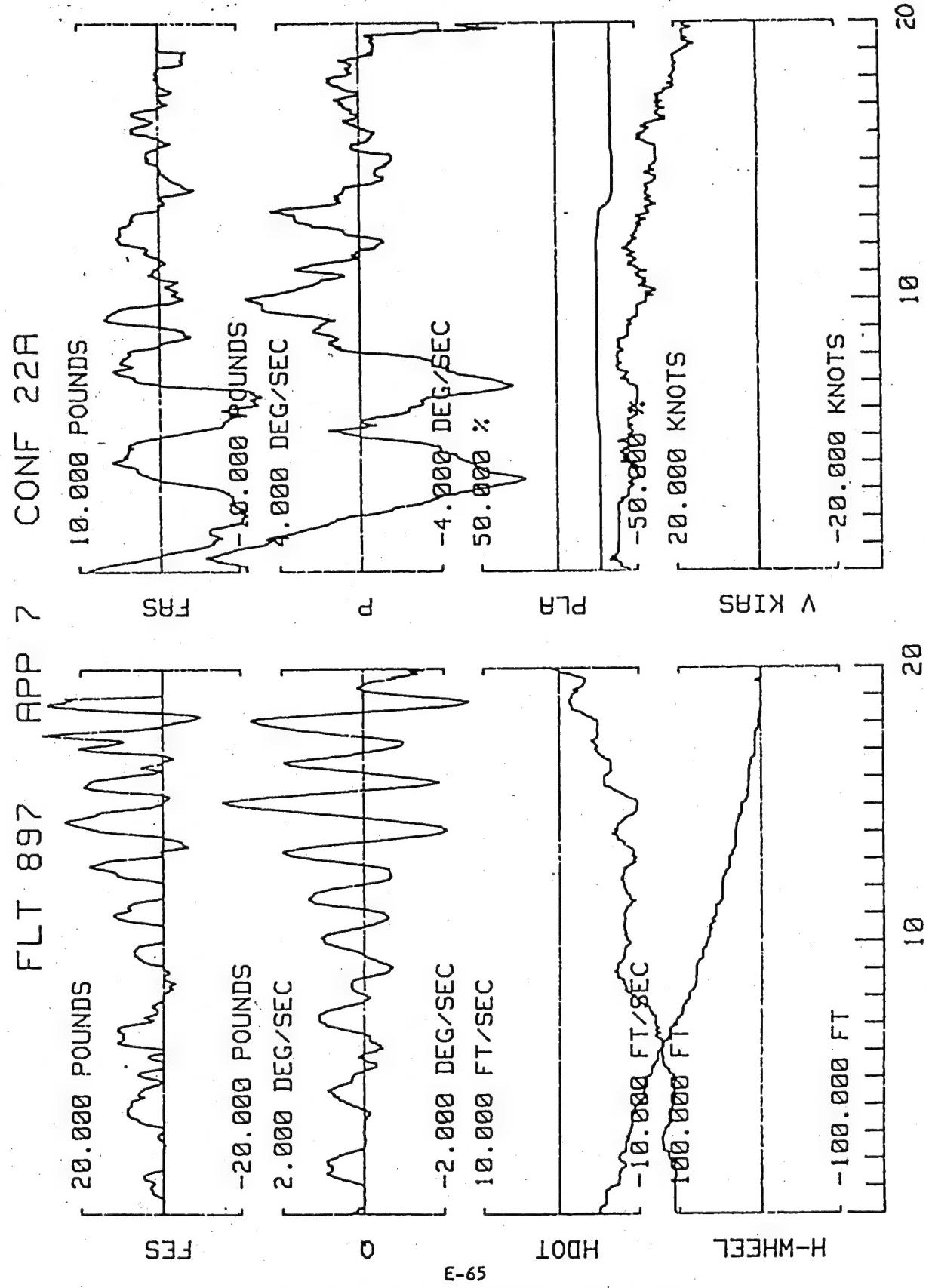


Figure A-87. TIFS, Configuration 22A (Ref. A-30)

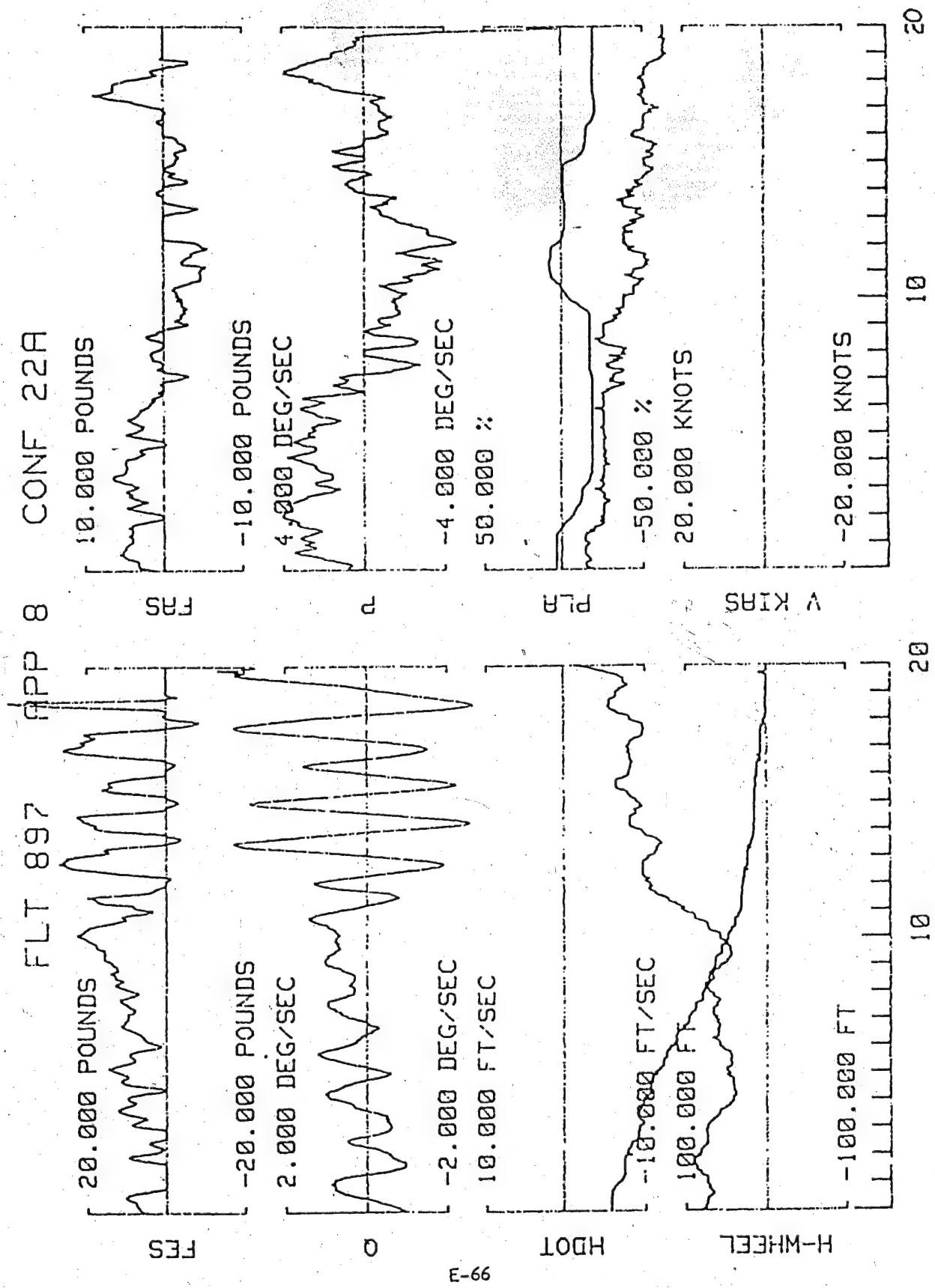


Figure A-88. TIFS, Configuration 22A (Ref. A-30)

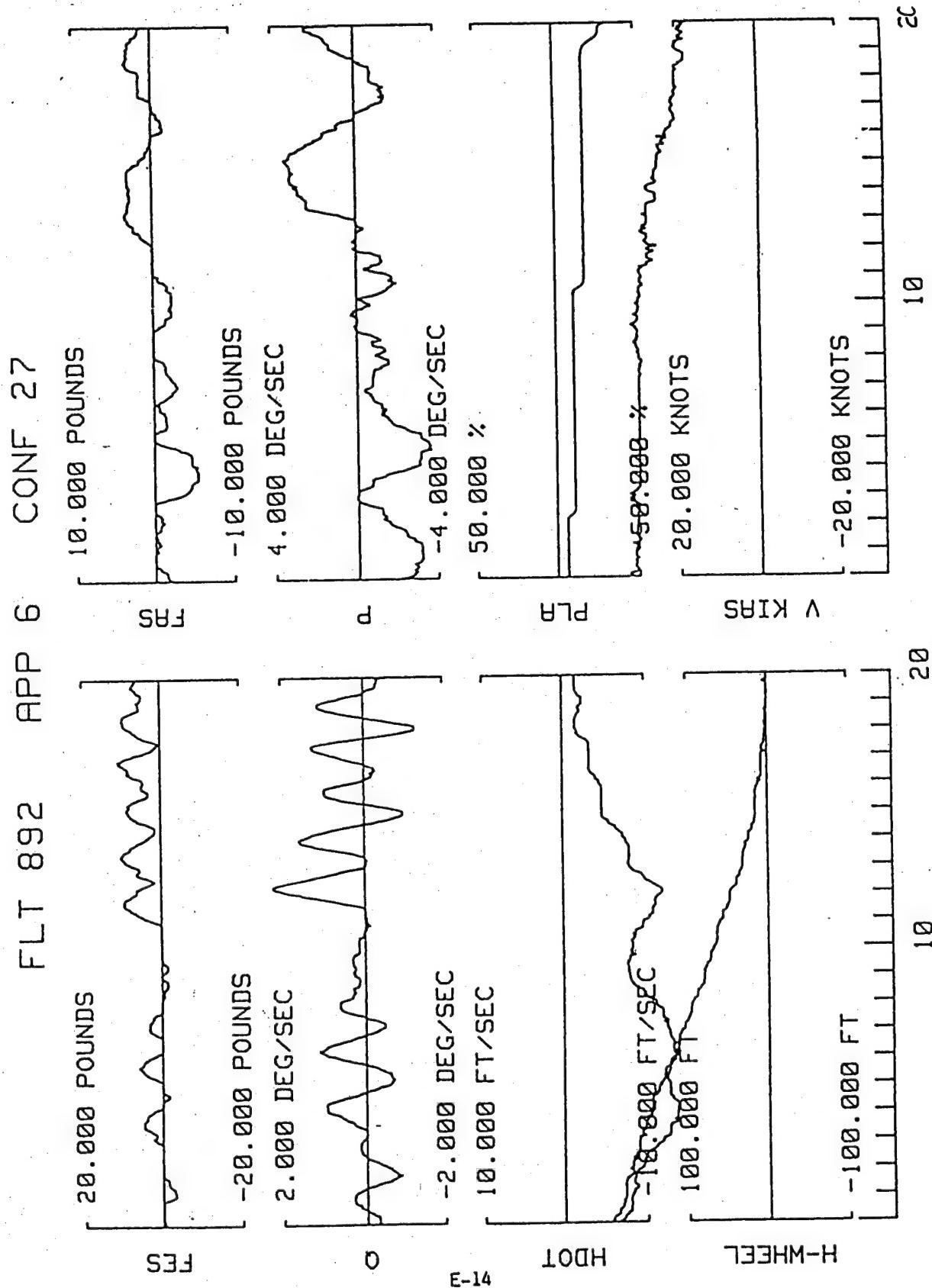


Figure A-89. TIFS, Configuration 27 (Ref. A-30)

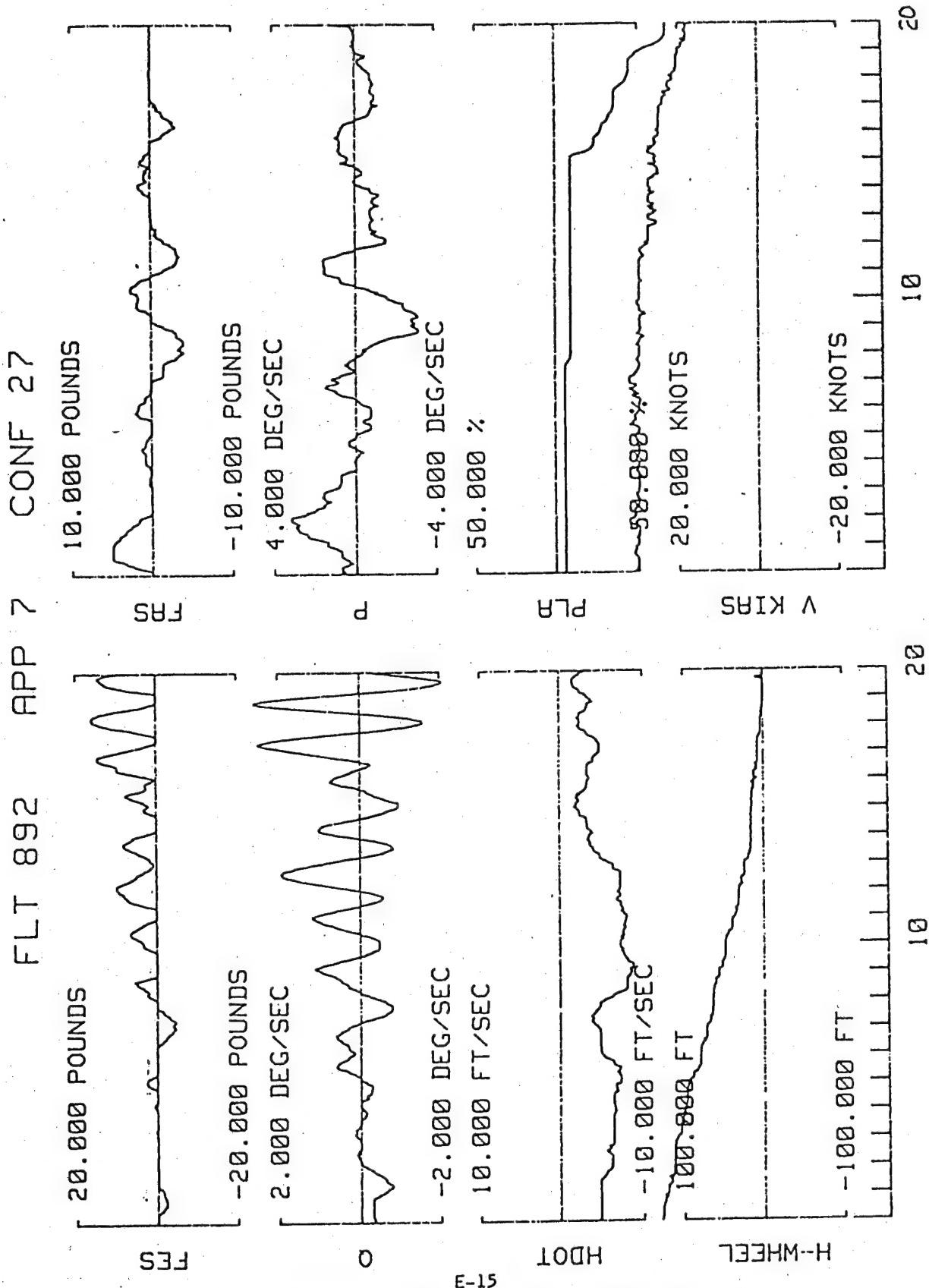


Figure A-90. TIFS, Configuration 27 (Ref. A-30)

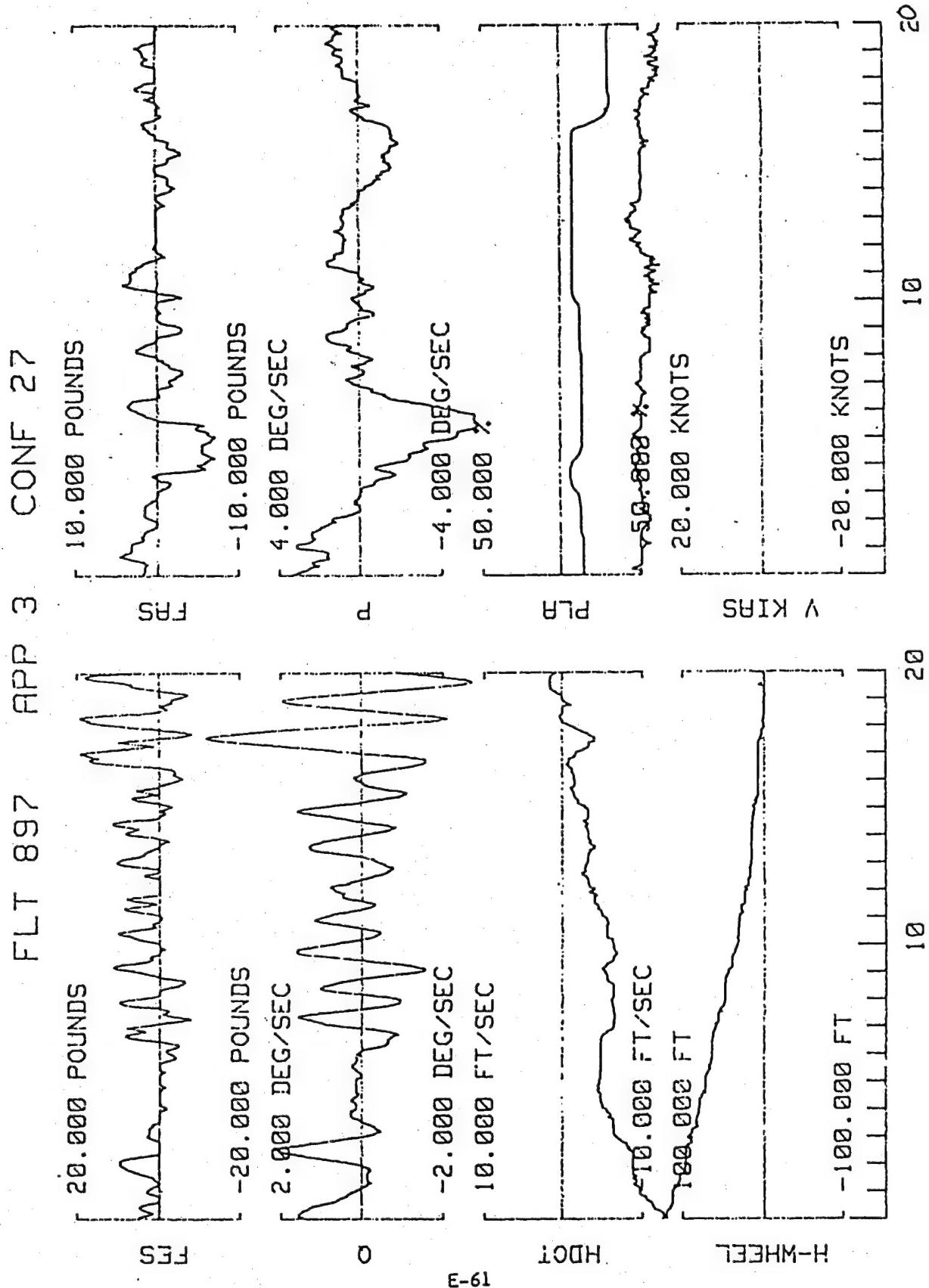


Figure A-91. TIFS, Configuration 27 (Ref. A-30)

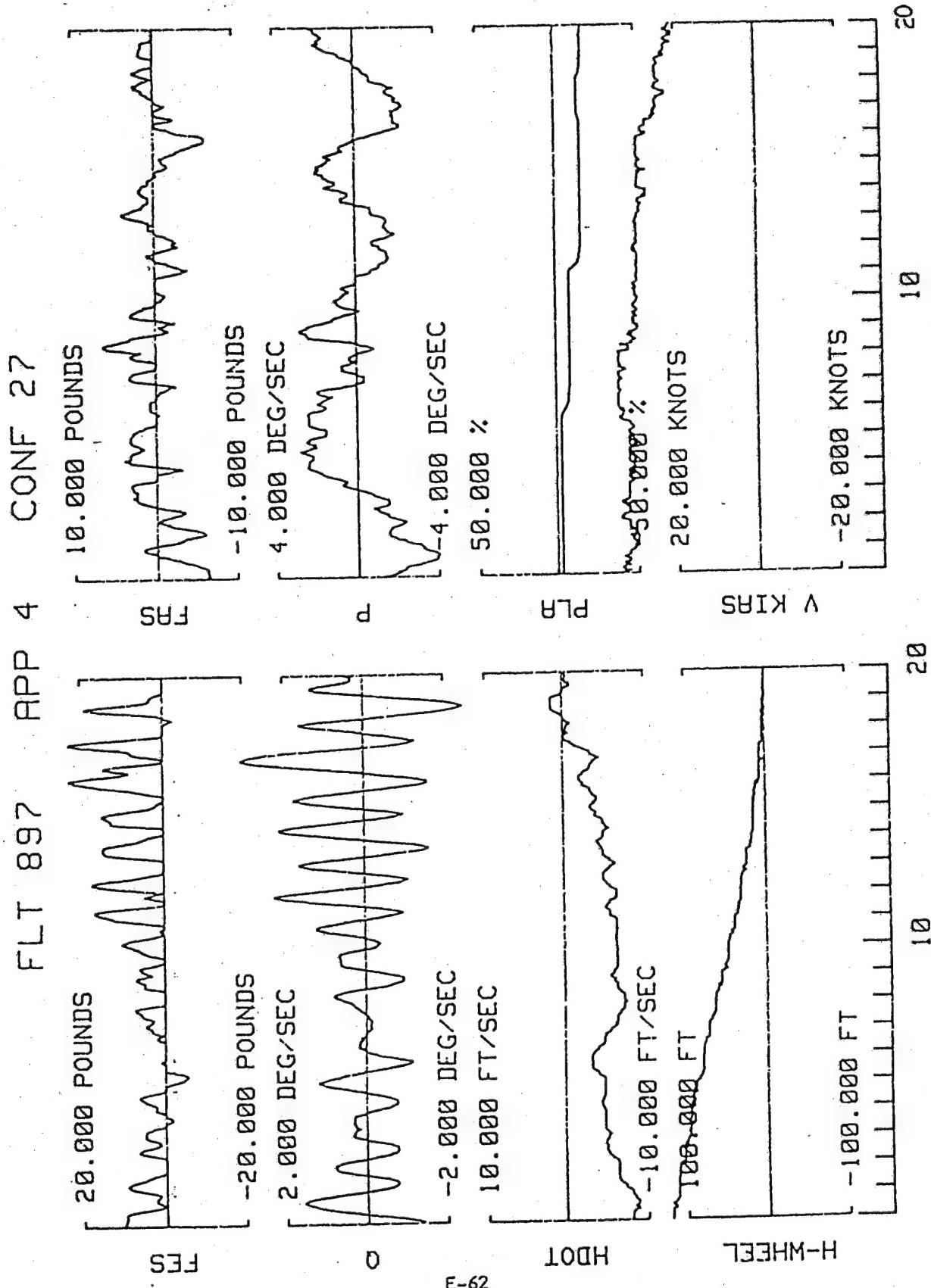


Figure A-92. TIFS, Configuration 27 (Ref. A-30)

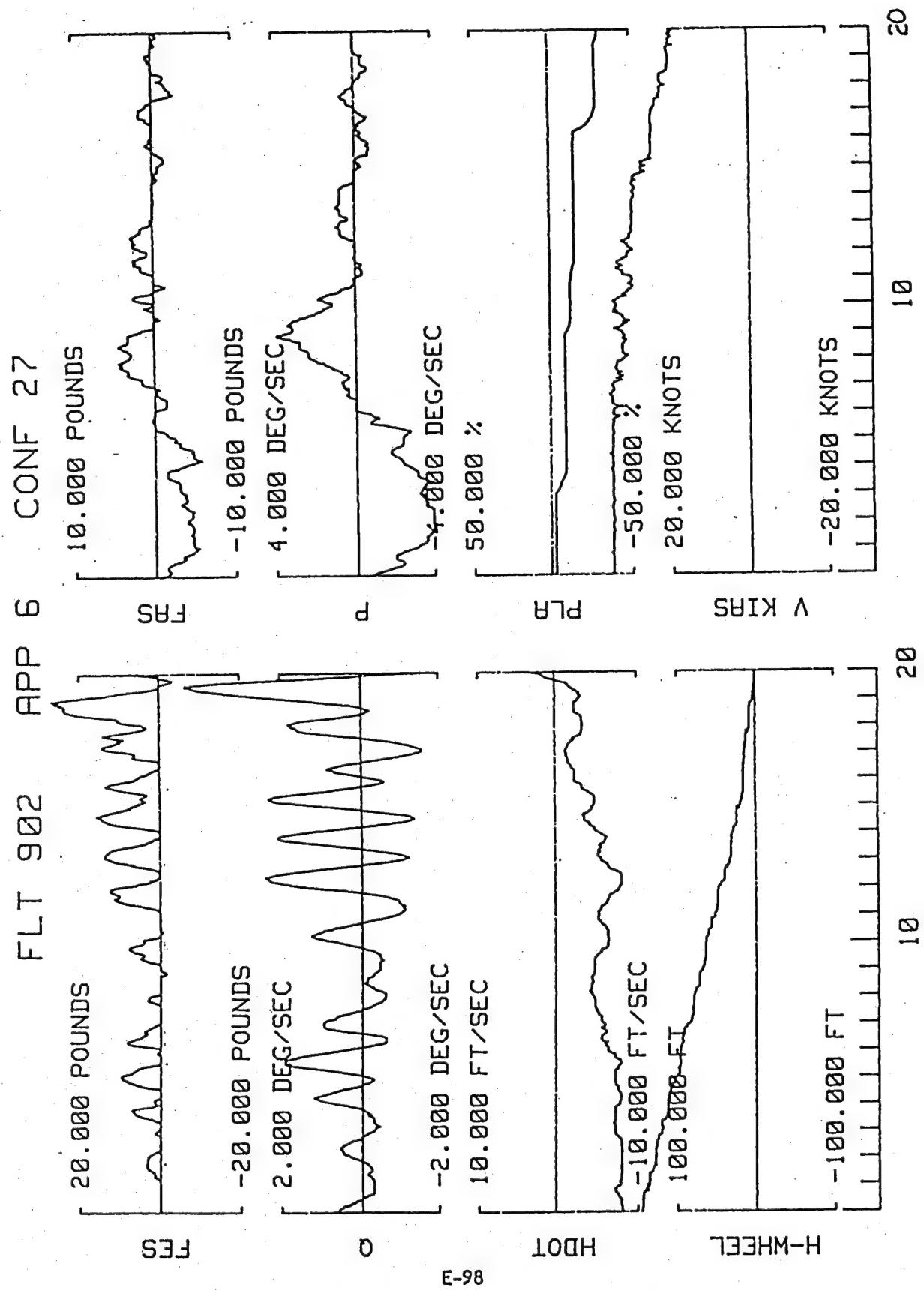


Figure A-93. TIFS, Configuration 27 (Ref. A-30)

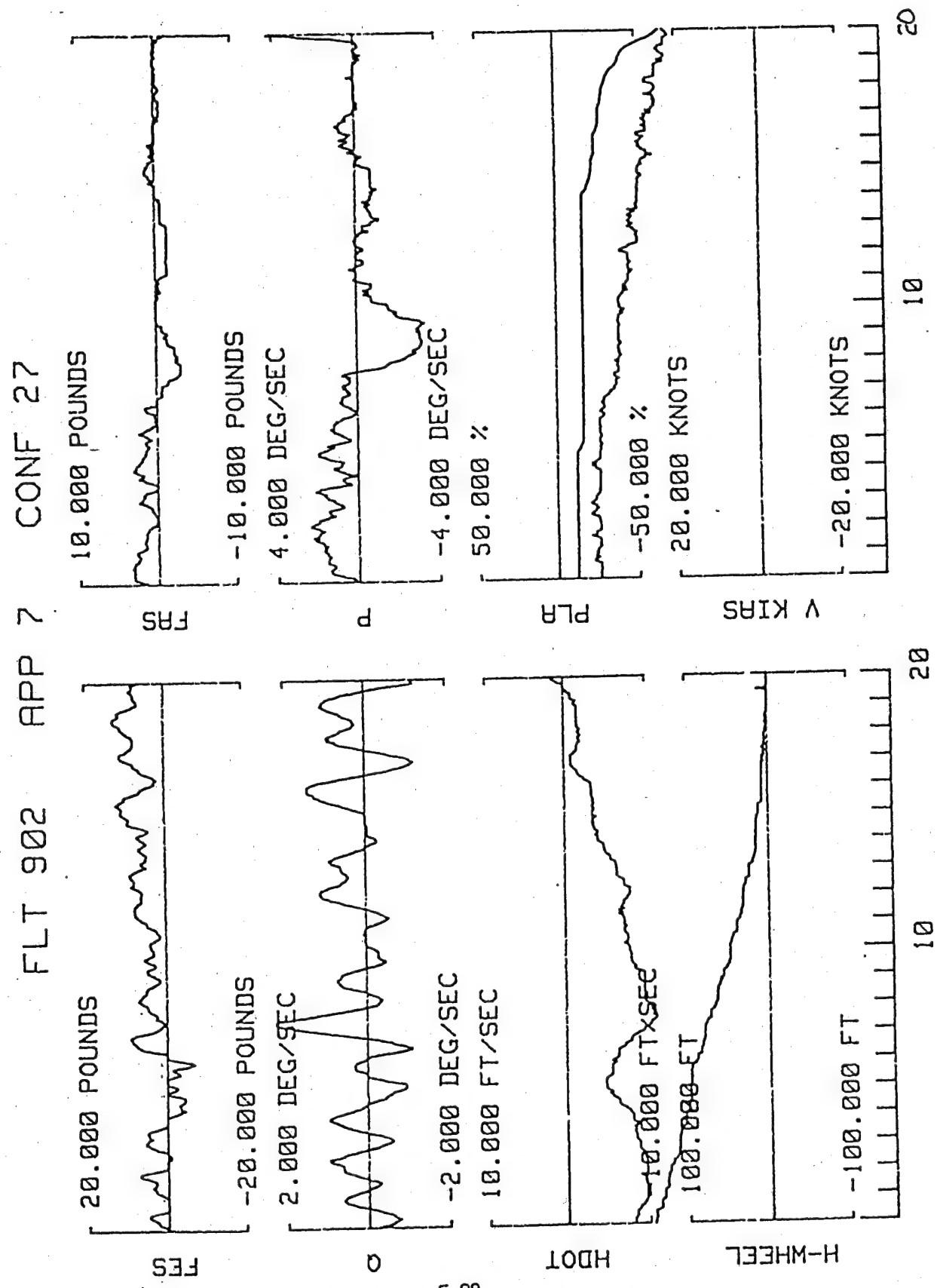


Figure A-94. TIFS, Configuration 27 (Ref. A-30)

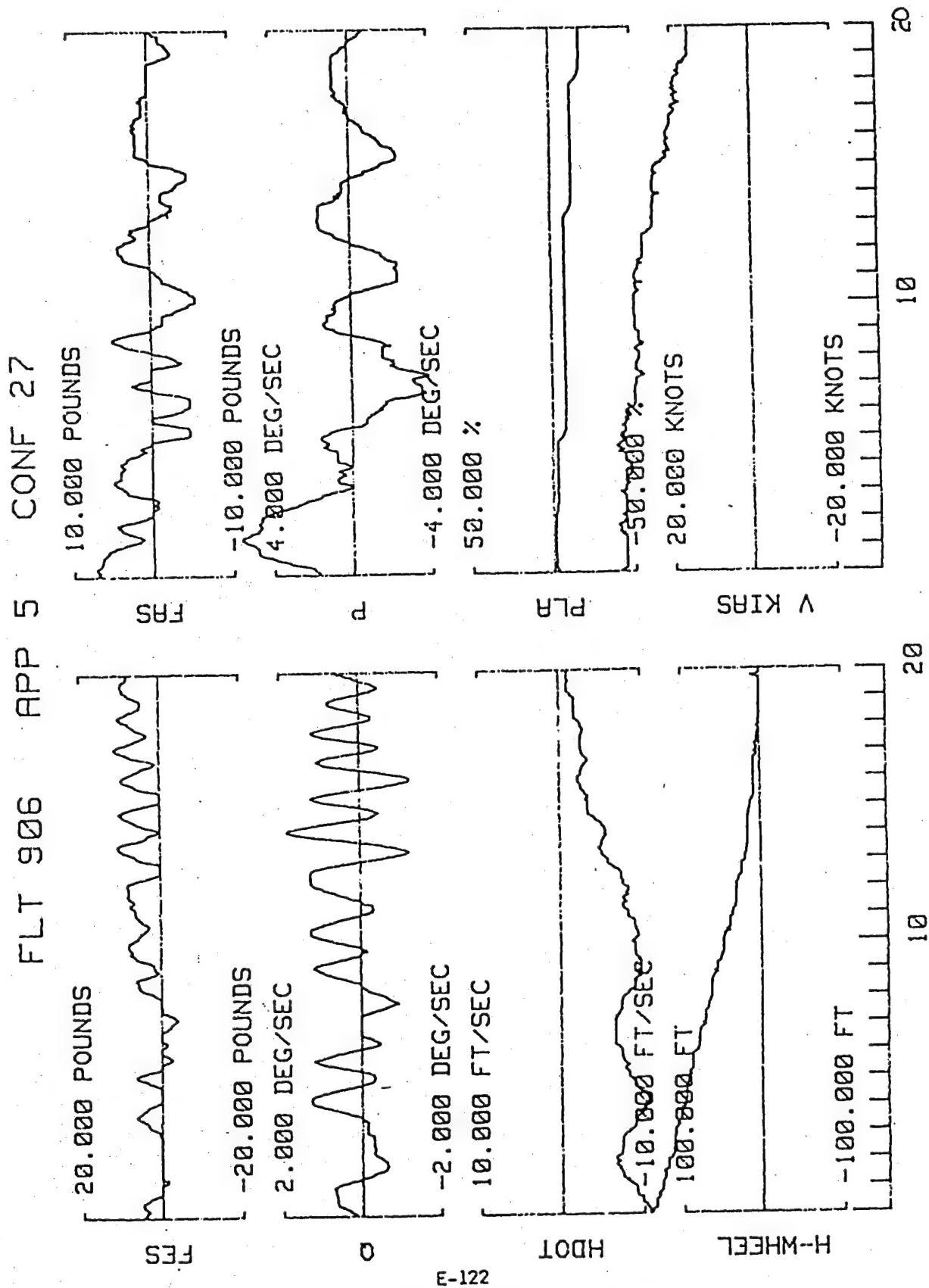


Figure A-95. TIFS, Configuration 27 (Ref. A-30)

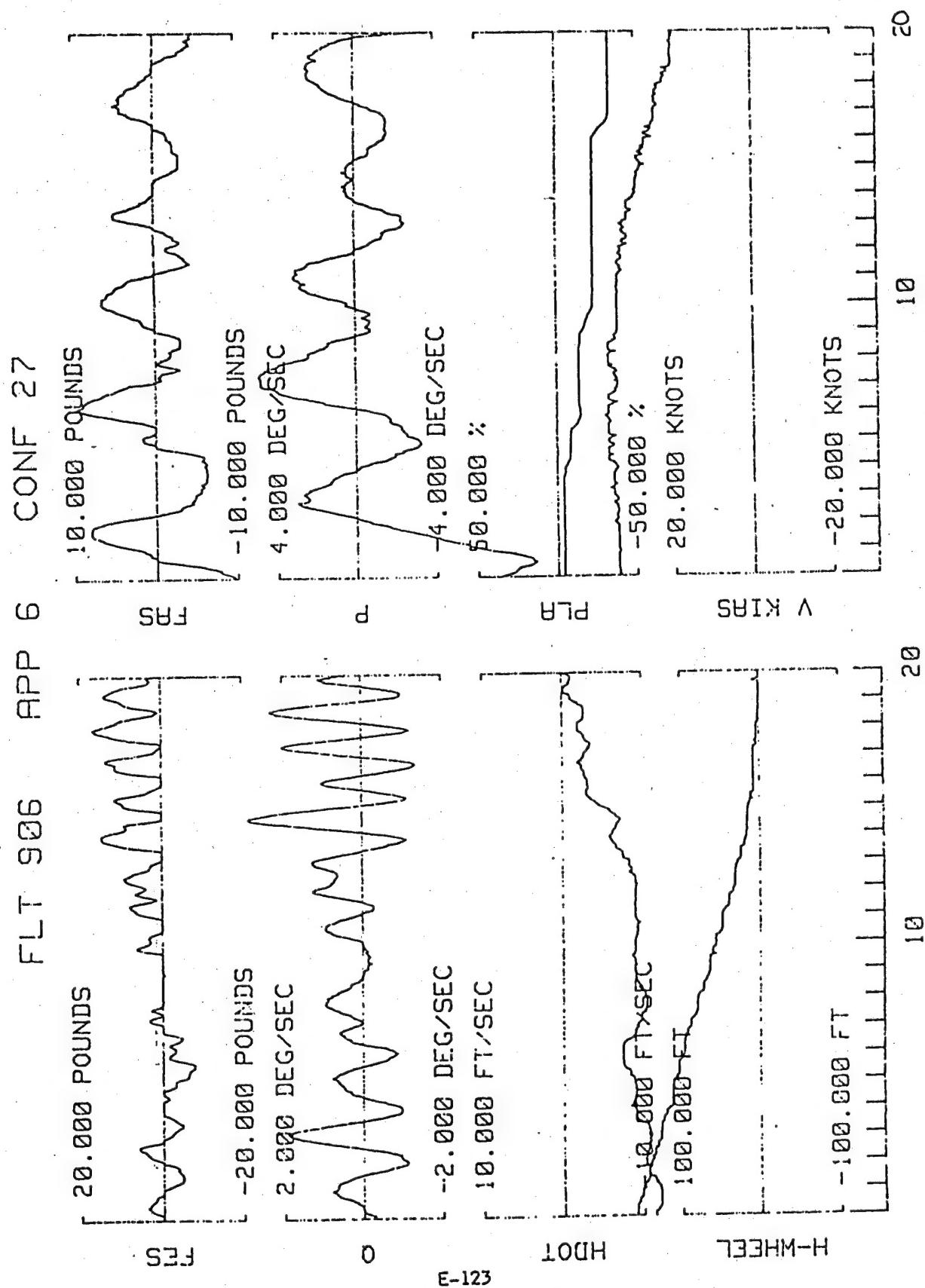


Figure A-96. TIFS, Configuration 27 (Ref. A-30)

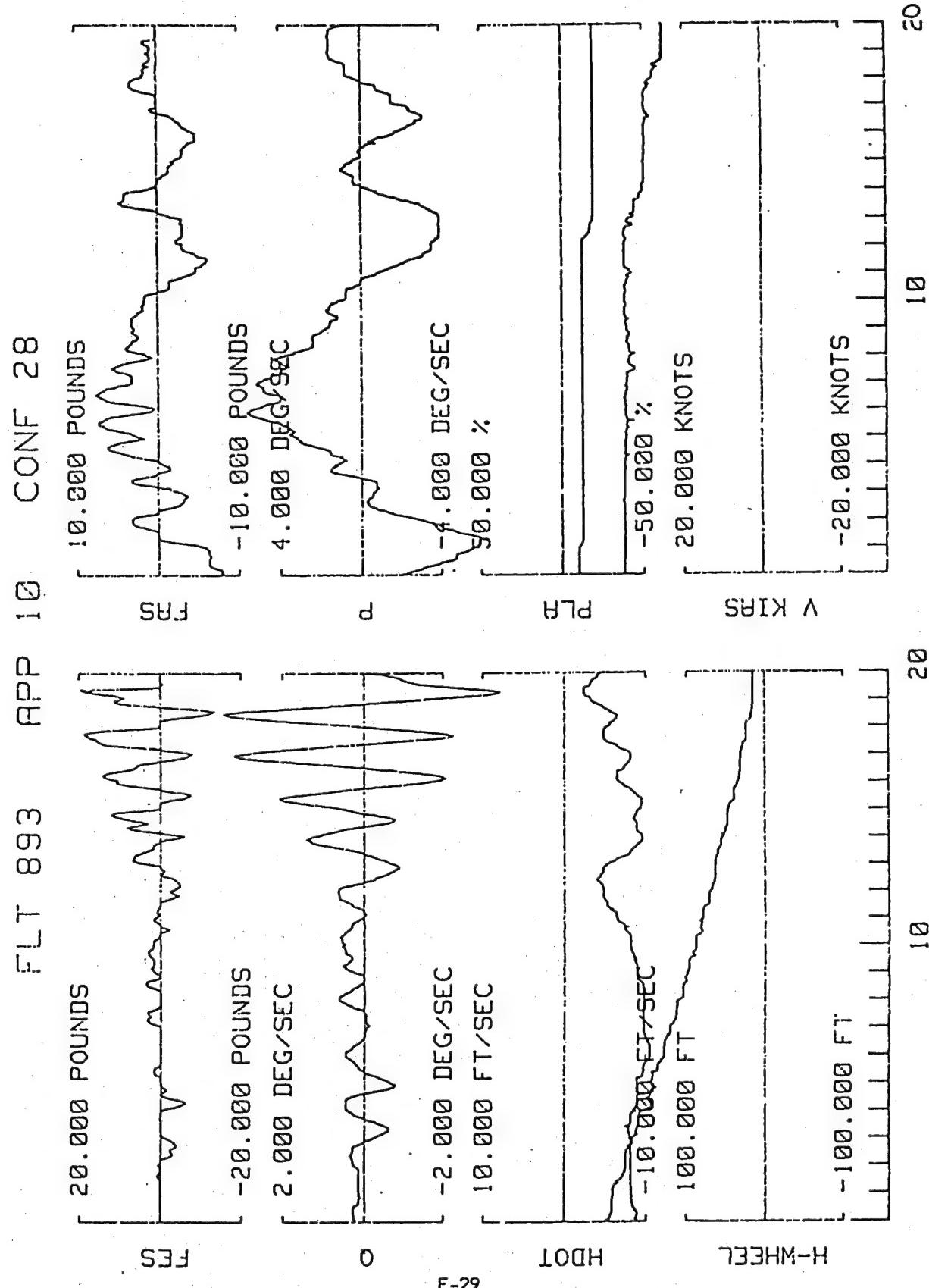


Figure A-97. TIFS, Configuration 28 (Ref. A-30)

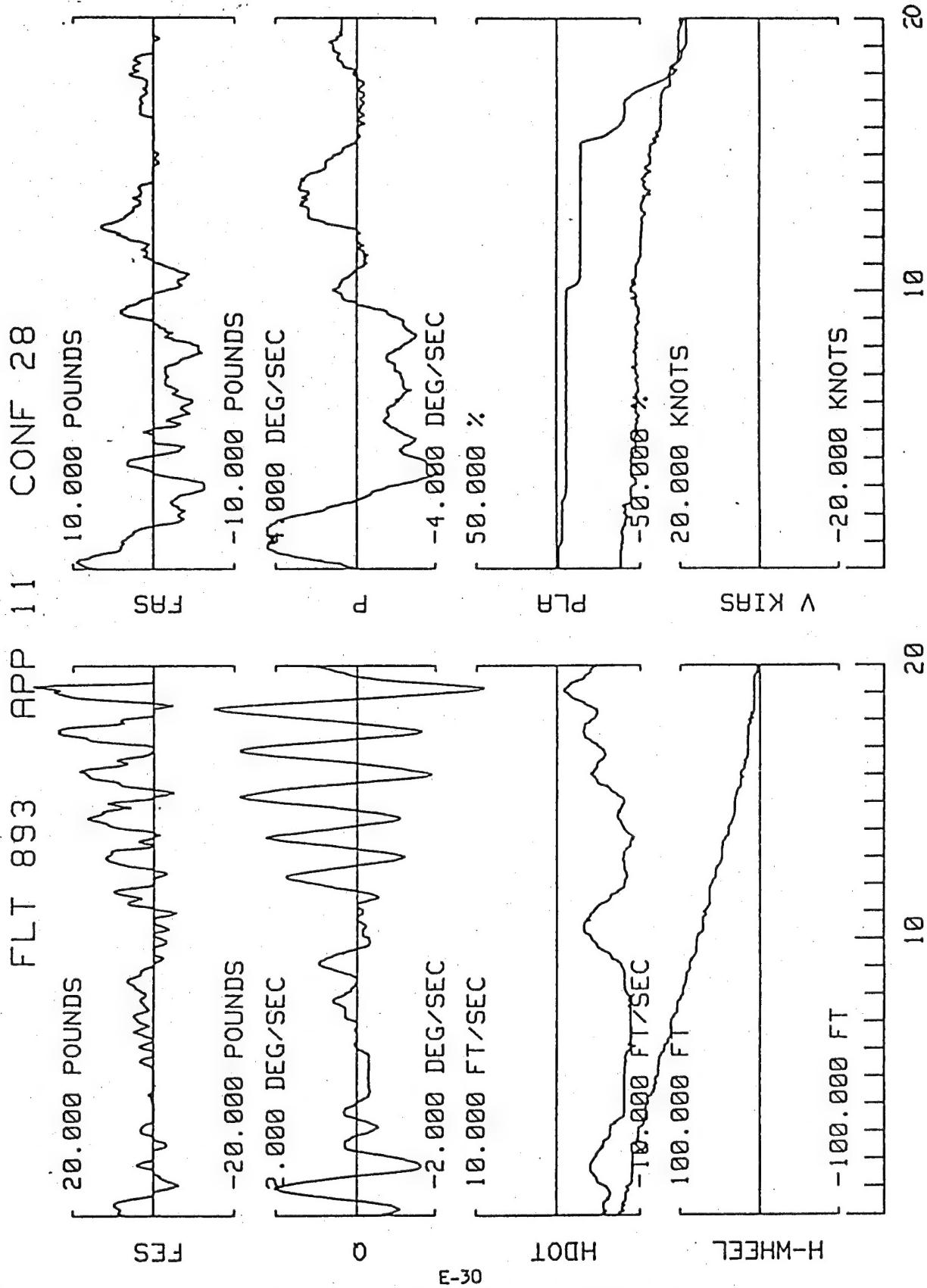


Figure A-98. TIFS, Configuration 28 (Ref. A-30)

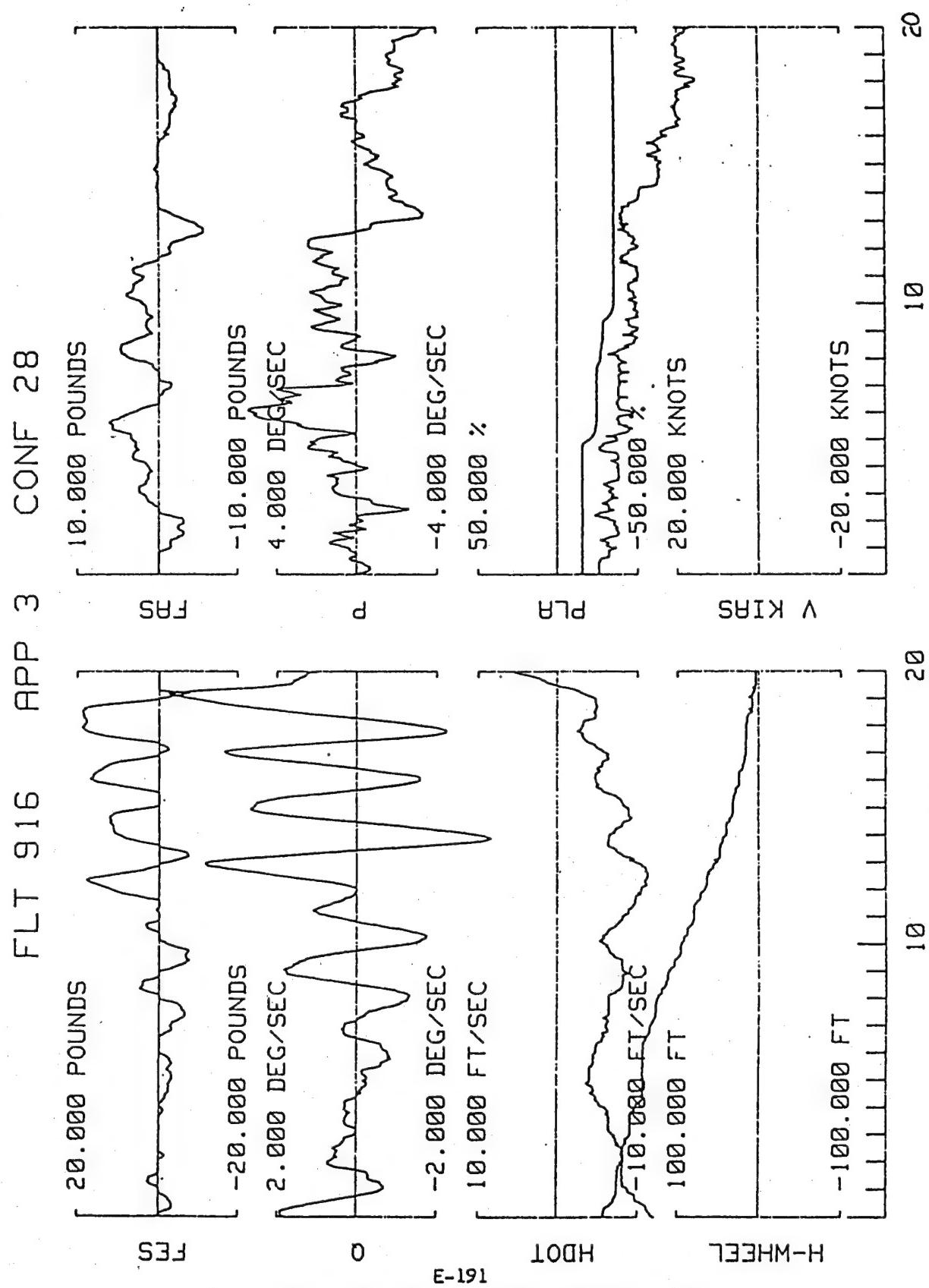


Figure A-99. TIFS, Configuration 28 (Ref. A-30)

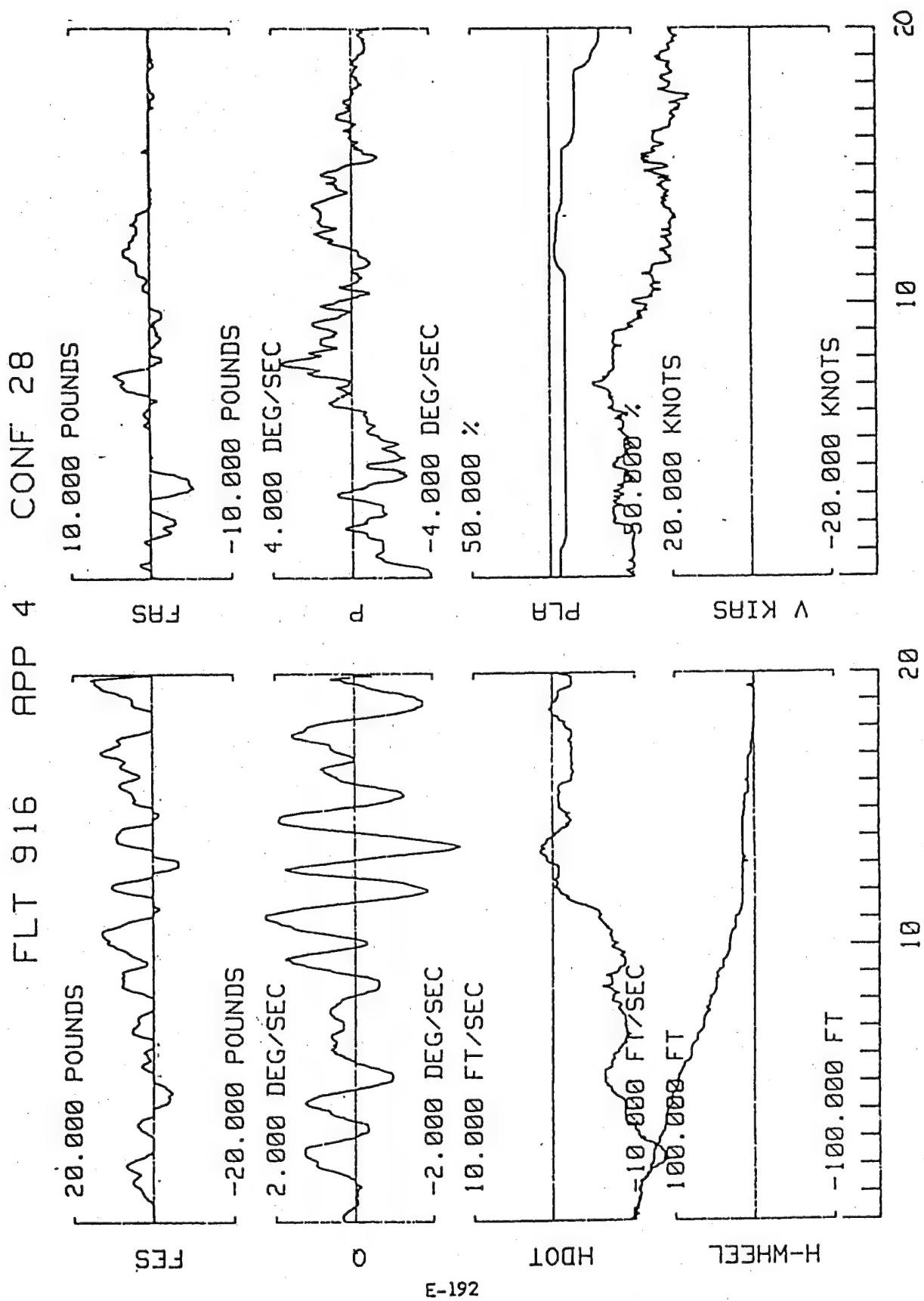


Figure A-100. TIFS, Configuration 28 (Ref. A-30)

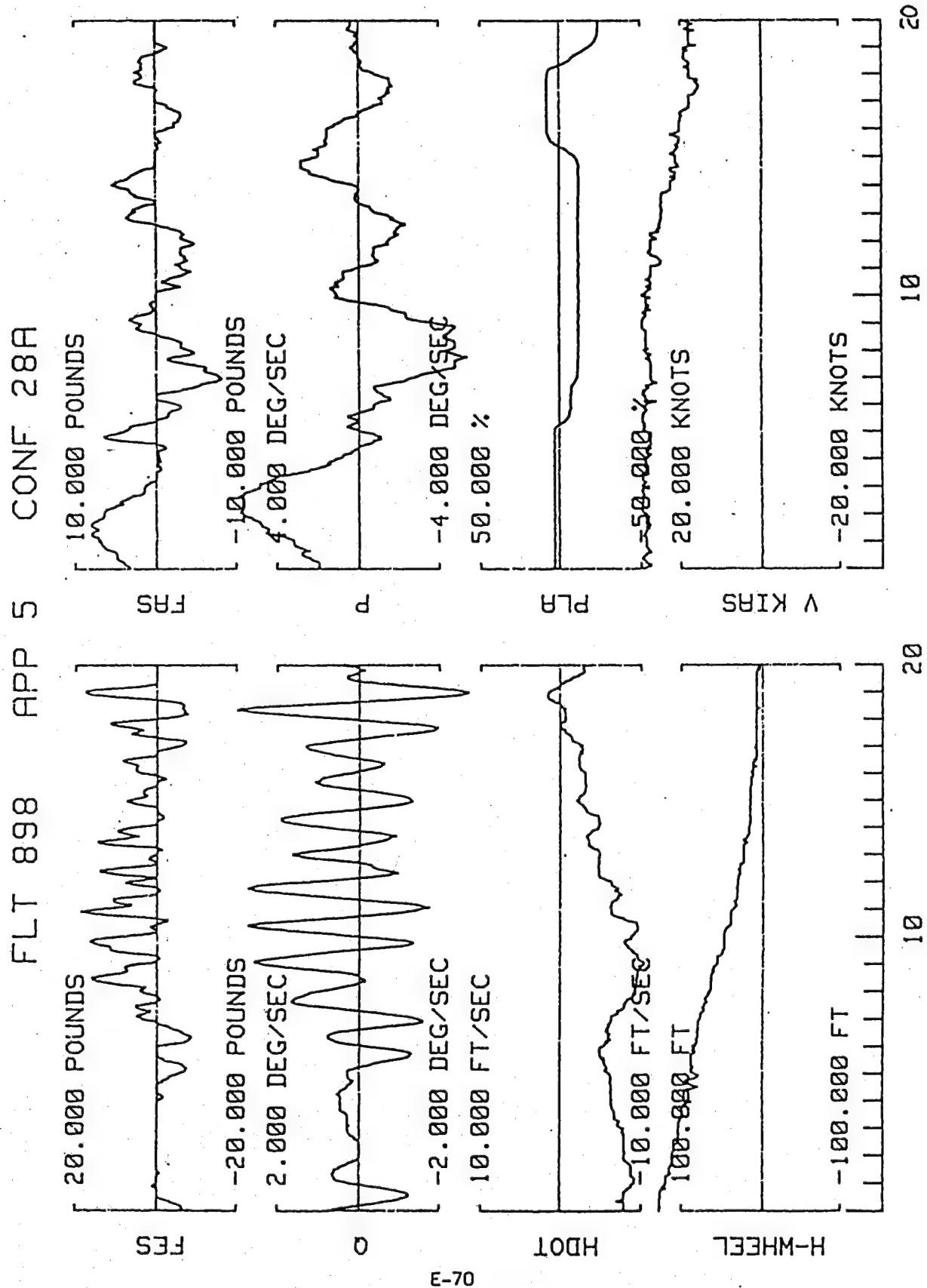


Figure A-101. TIFS, Configuration 28A (Ref. A-30)

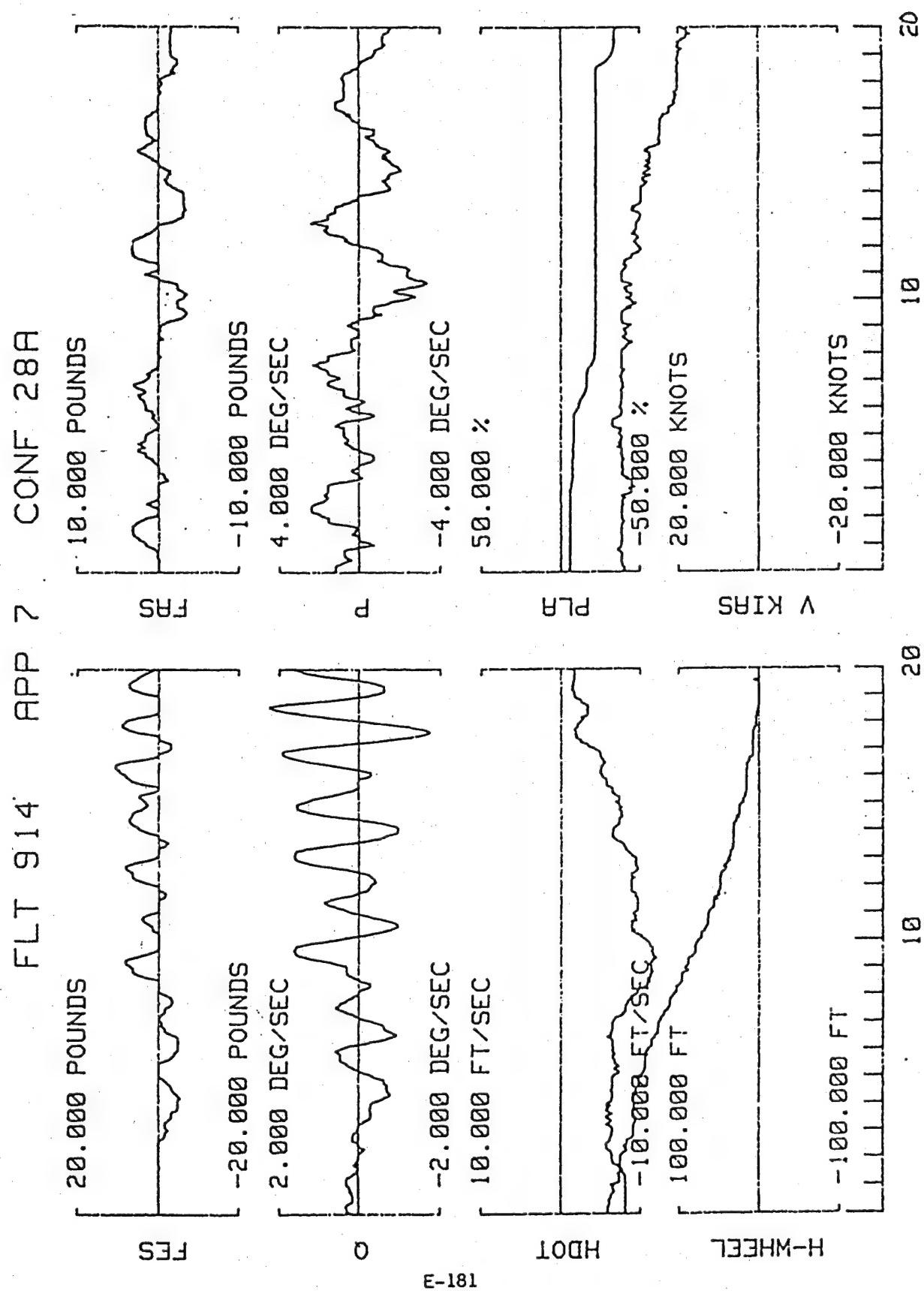


Figure A-102. TIFS, Configuration 28A (Ref. A-30)

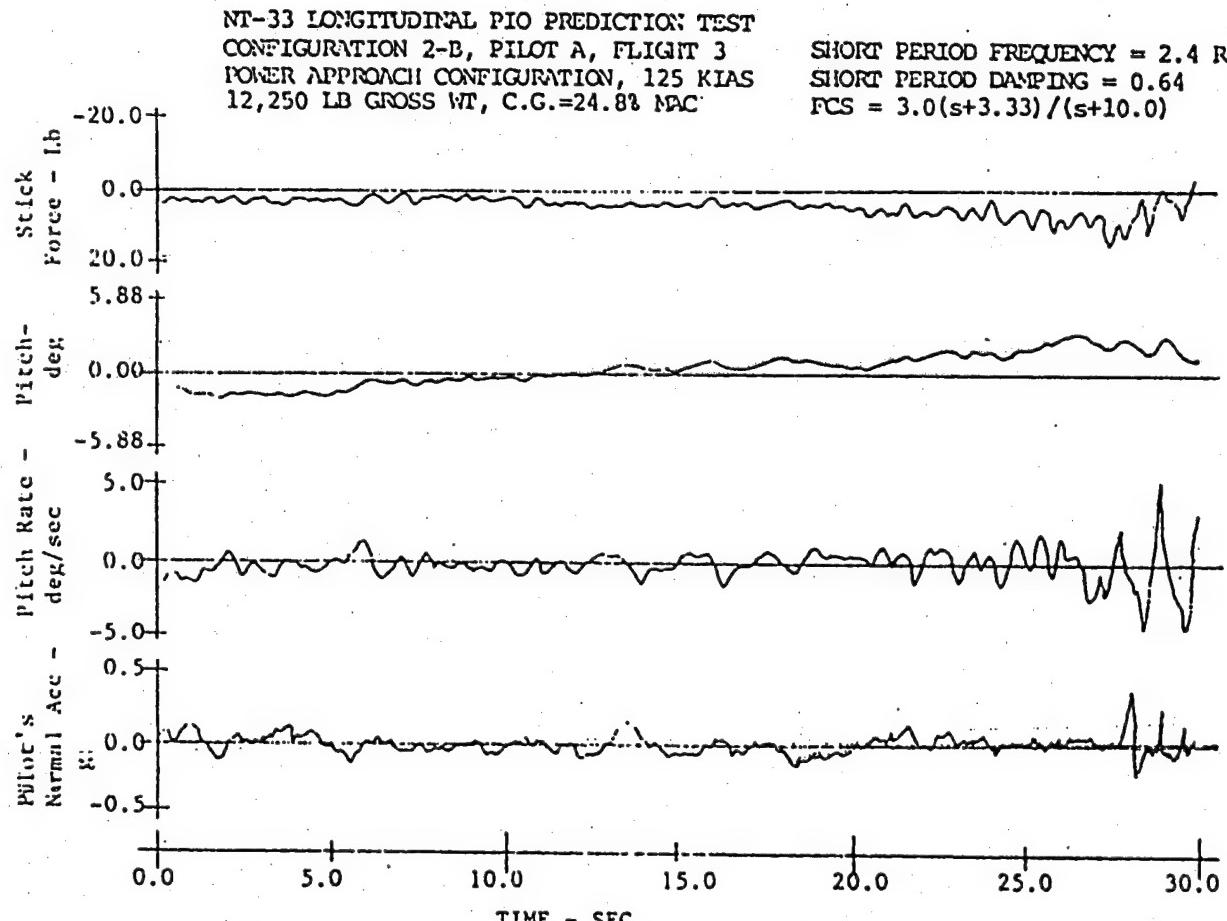


Figure 31. Selected Parameter Time Histories, Configuration 2-B

Figure A-103. NT-33A, Configuration 2-B (Ref. A-31)

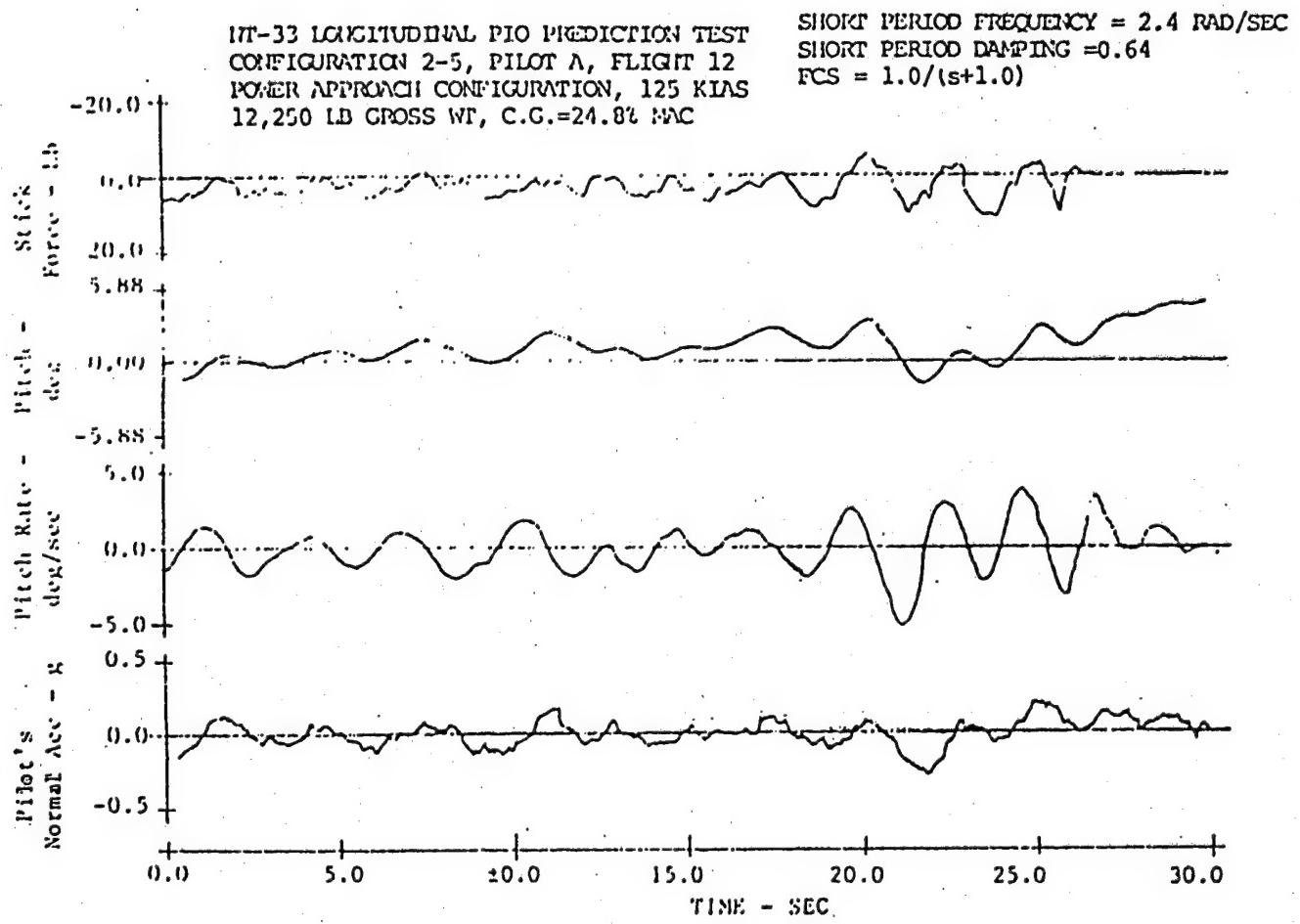


Figure 33. Selected Parameter Time Histories, Configuration 2-5

Figure A-104. NT-33A, Configuration 2-5 (Ref. A-31)

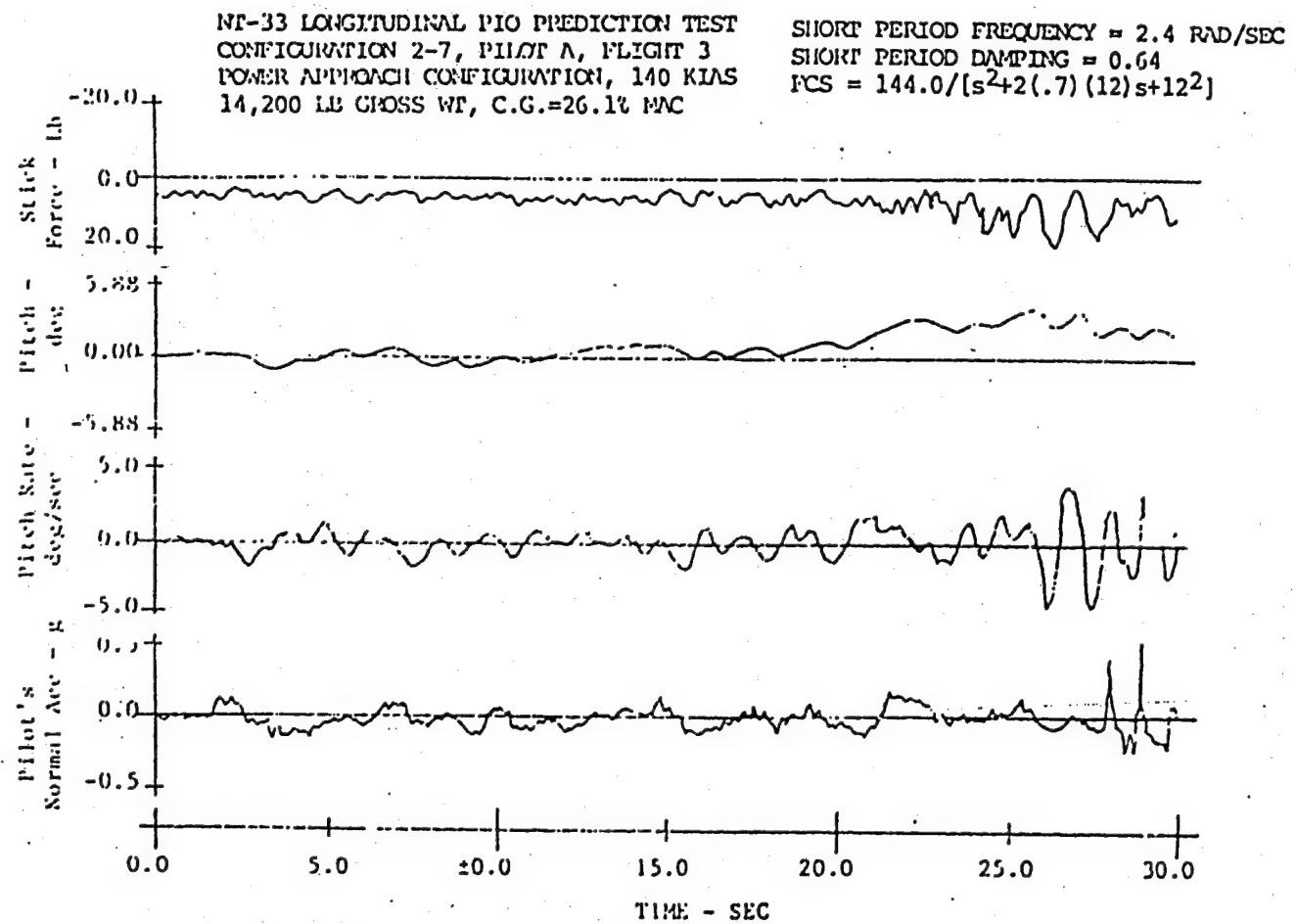


Figure 34. Selected Parameter Time Histories, Configuration 2-7

Figure A-105. NT-33A, Configuration 2-7 (Ref. A-31)

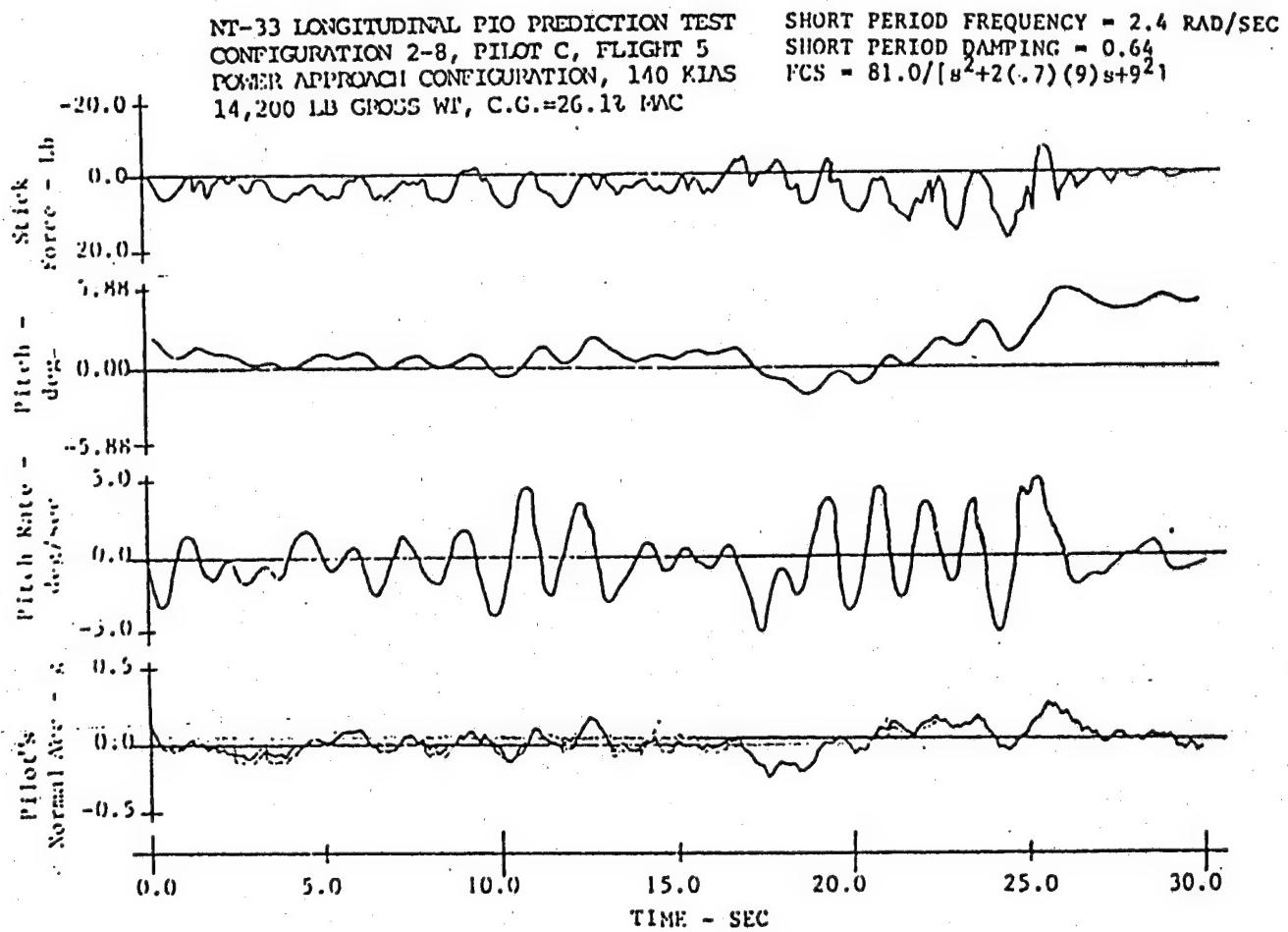


Figure 35. Selected Parameter Time Histories, Configuration 2-8

Figure A-106. NT-33A, Configuration 2-8 (Ref. A-31)

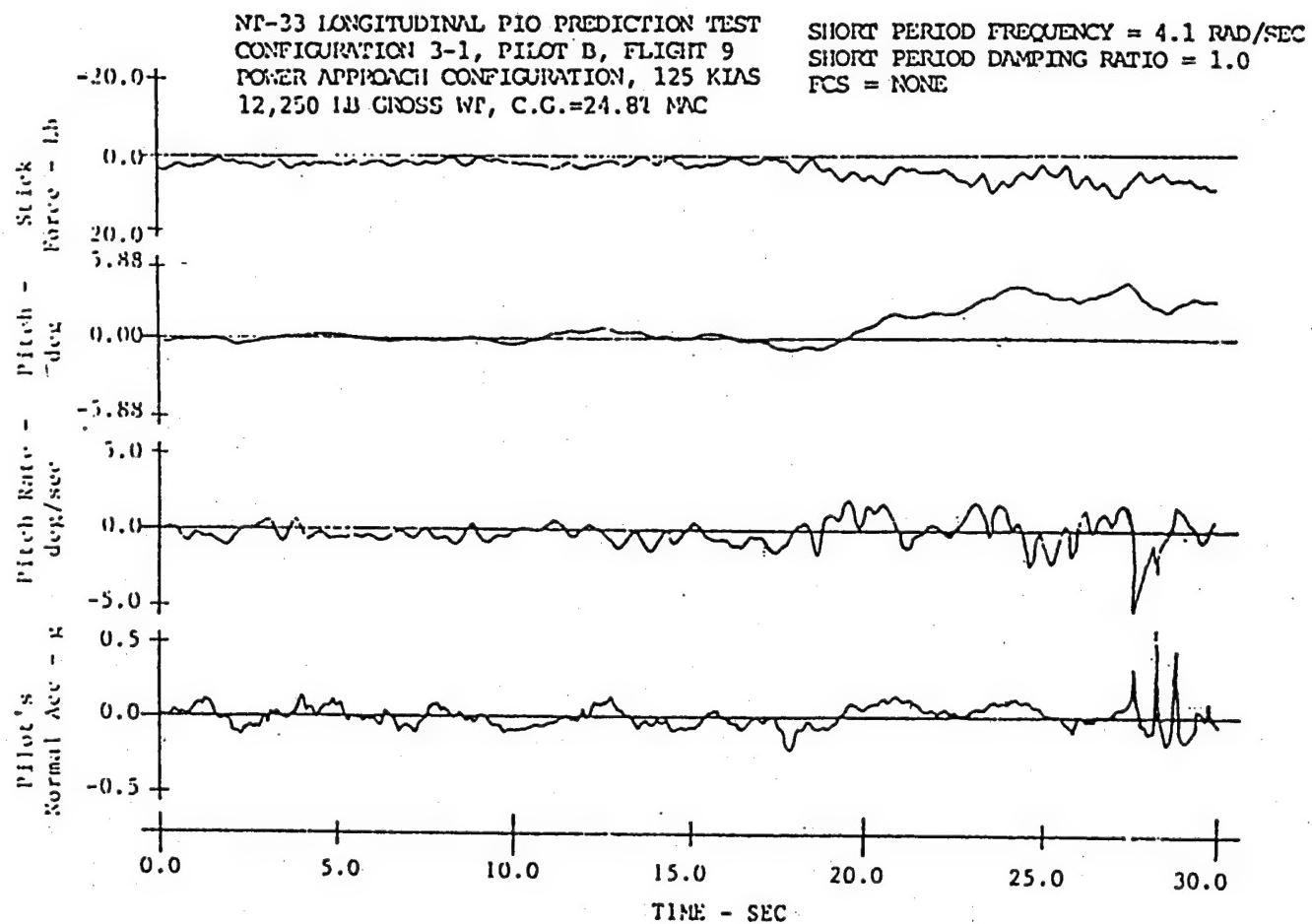


Figure 37. Selected Parameter Time Histories, Configuration 3-1

Figure A-107. NT-33A, Configuration 3-1 (Ref. A-31)

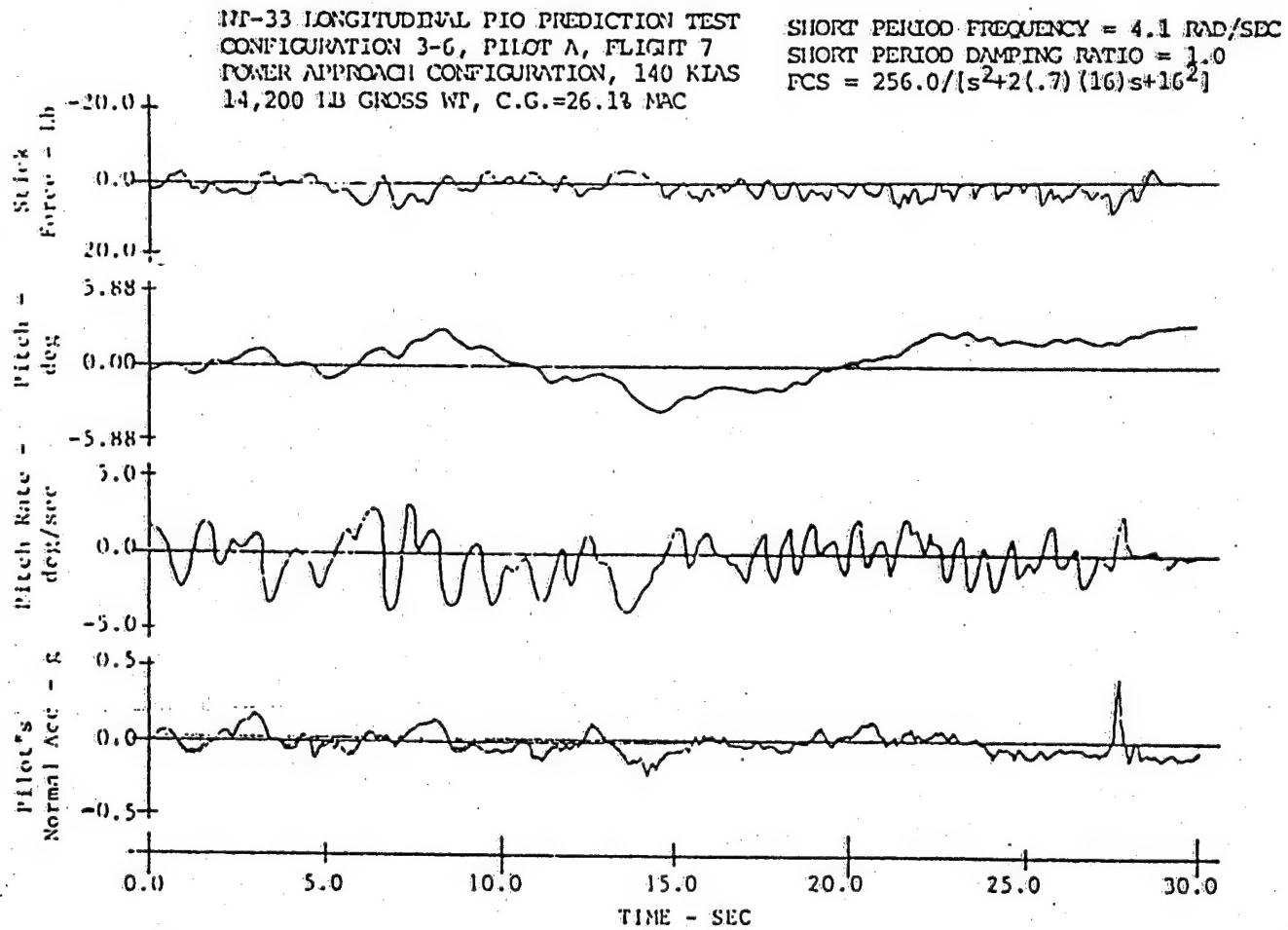


Figure 39. Selected Parameter Time Histories, Configuration 3-6

Figure A-108. NT-33A, Configuration 3-6 (Ref. A-31)

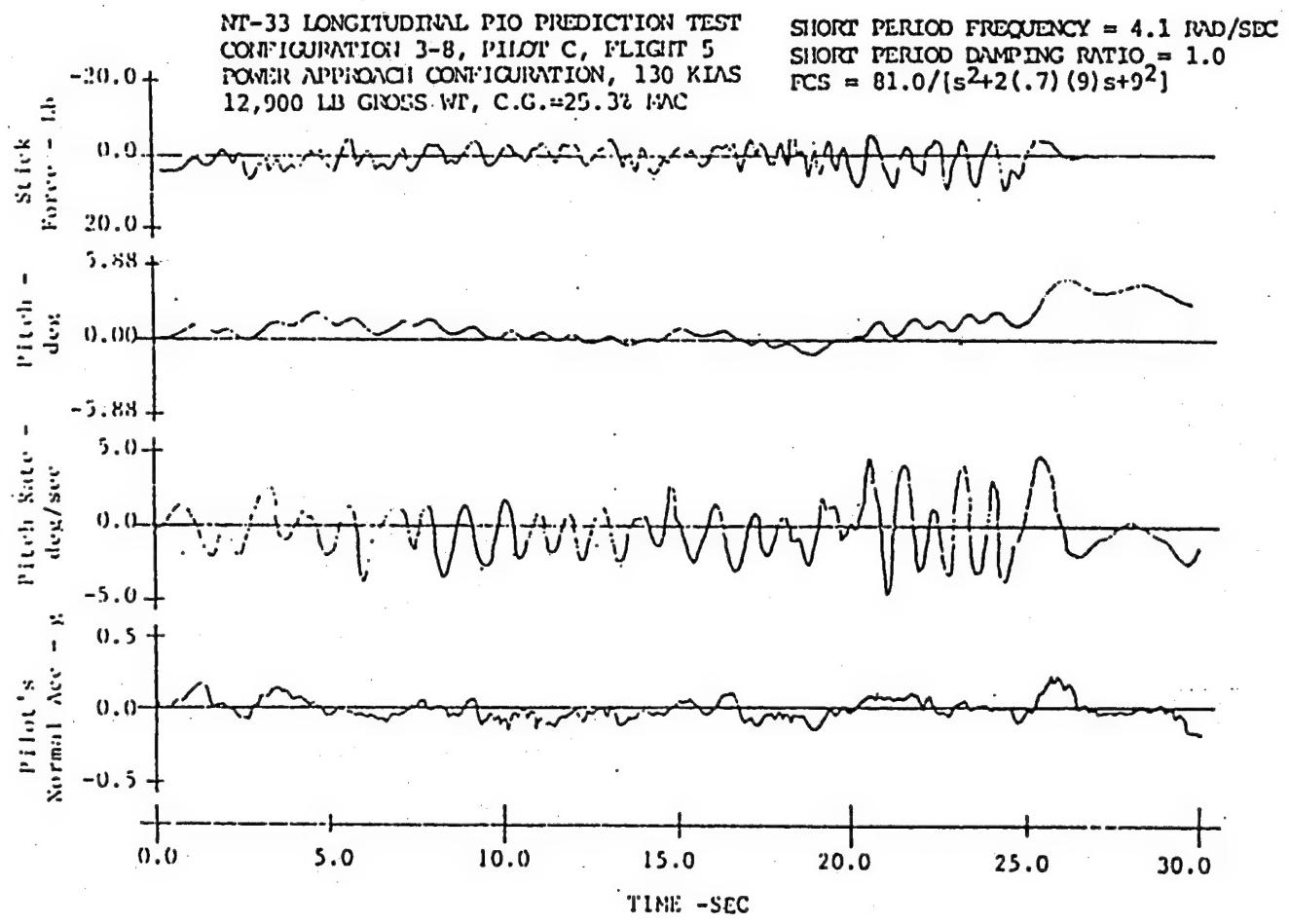


Figure 40. Selected Parameter Time Histories, Configuration 3-8

Figure A-109. NT-33A, Configuration 3-8 (Ref. A-31)

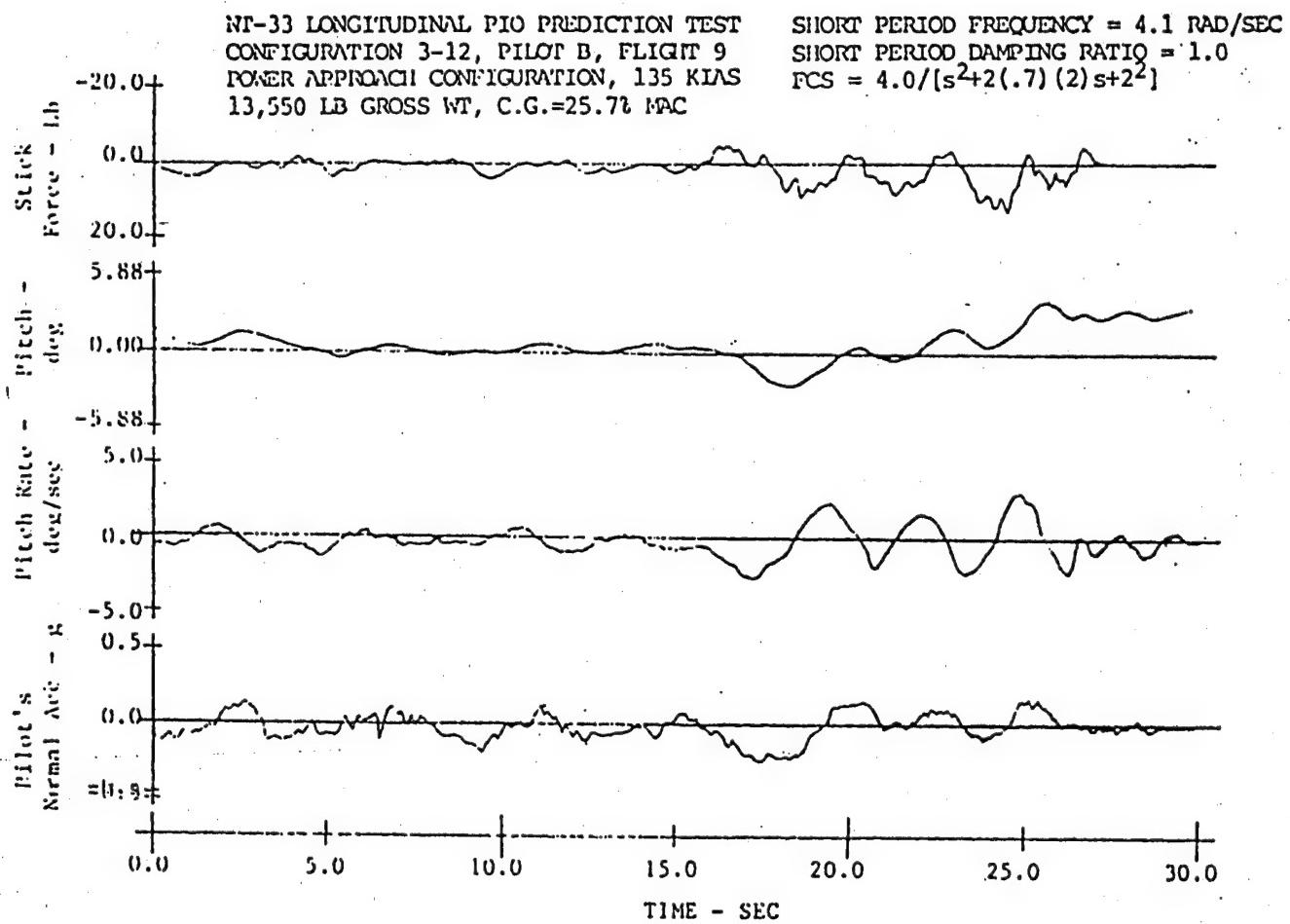


Figure 41. Selected Parameter Time Histories, Configuration 3-12

Figure A-110. NT-33A, Configuration 3-12 (Ref. A-31)

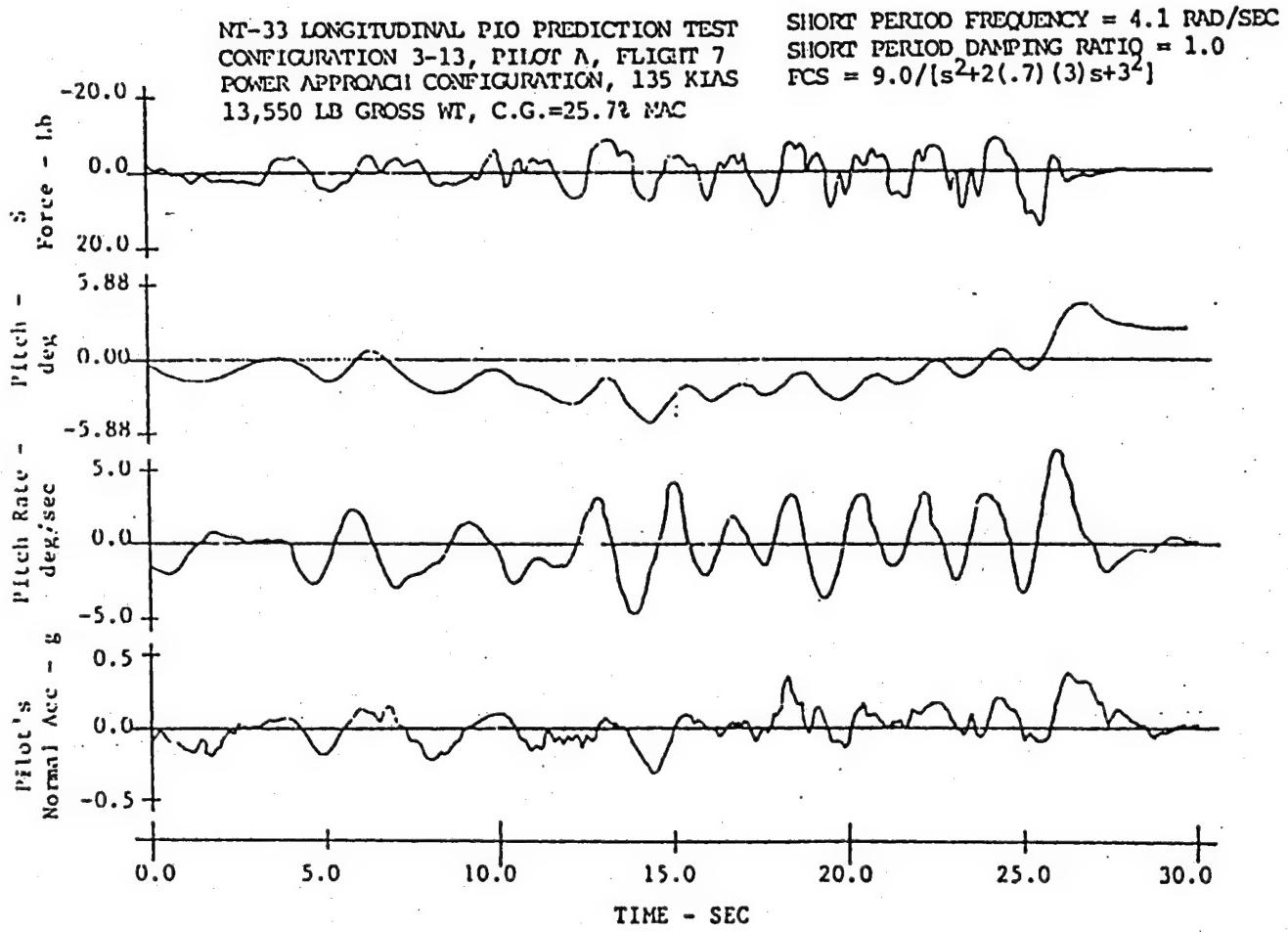


Figure 42. Selected Parameter Time Histories, Configuration 3-13

Figure A-111. NT-33A, Configuration 3-13 (Ref. A-31)

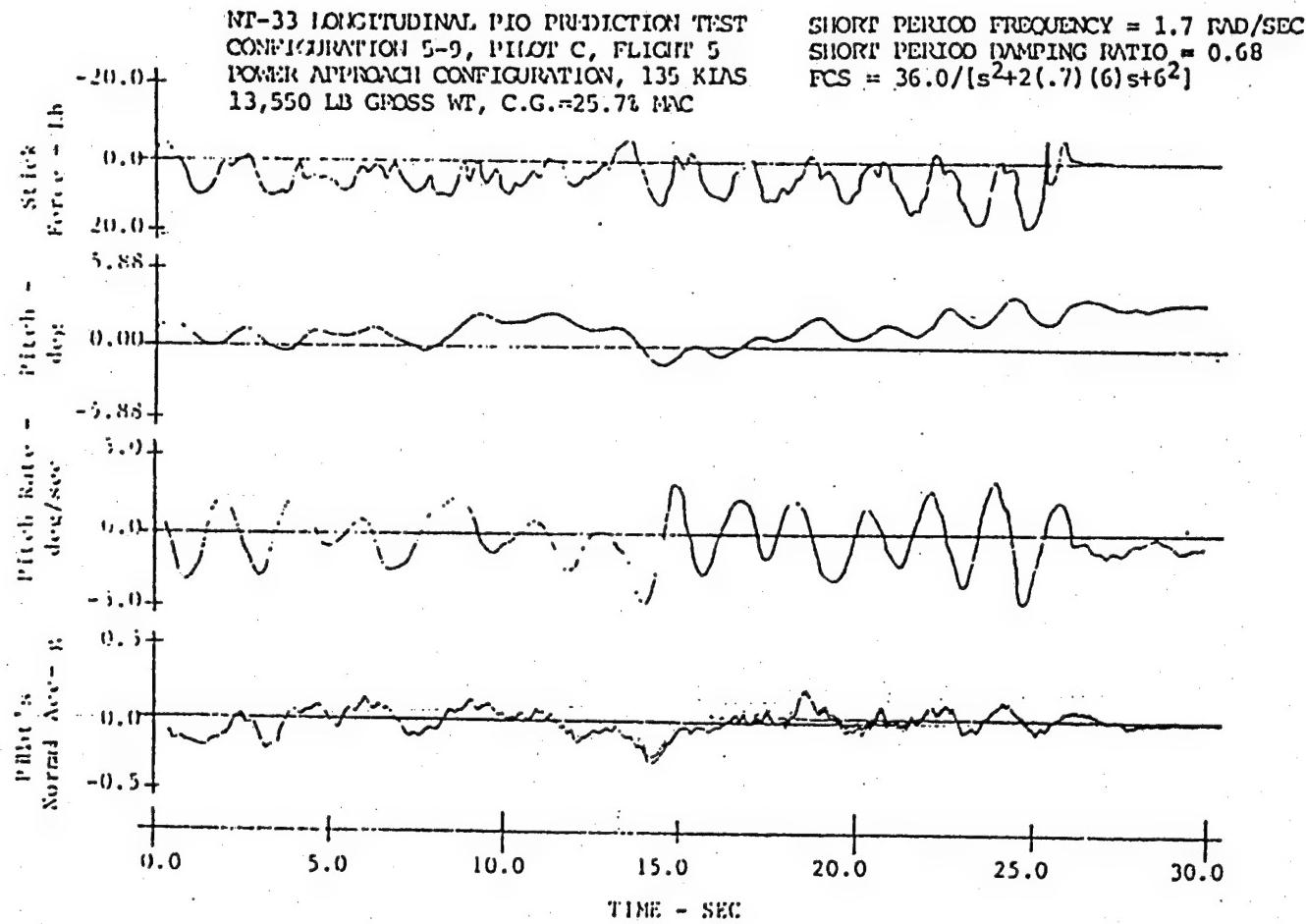


Figure A6. Selected Parameter Time Histories, Configuration 5-9

Figure A-112. NT-33A, Configuration 5-9 (Ref. A-31)

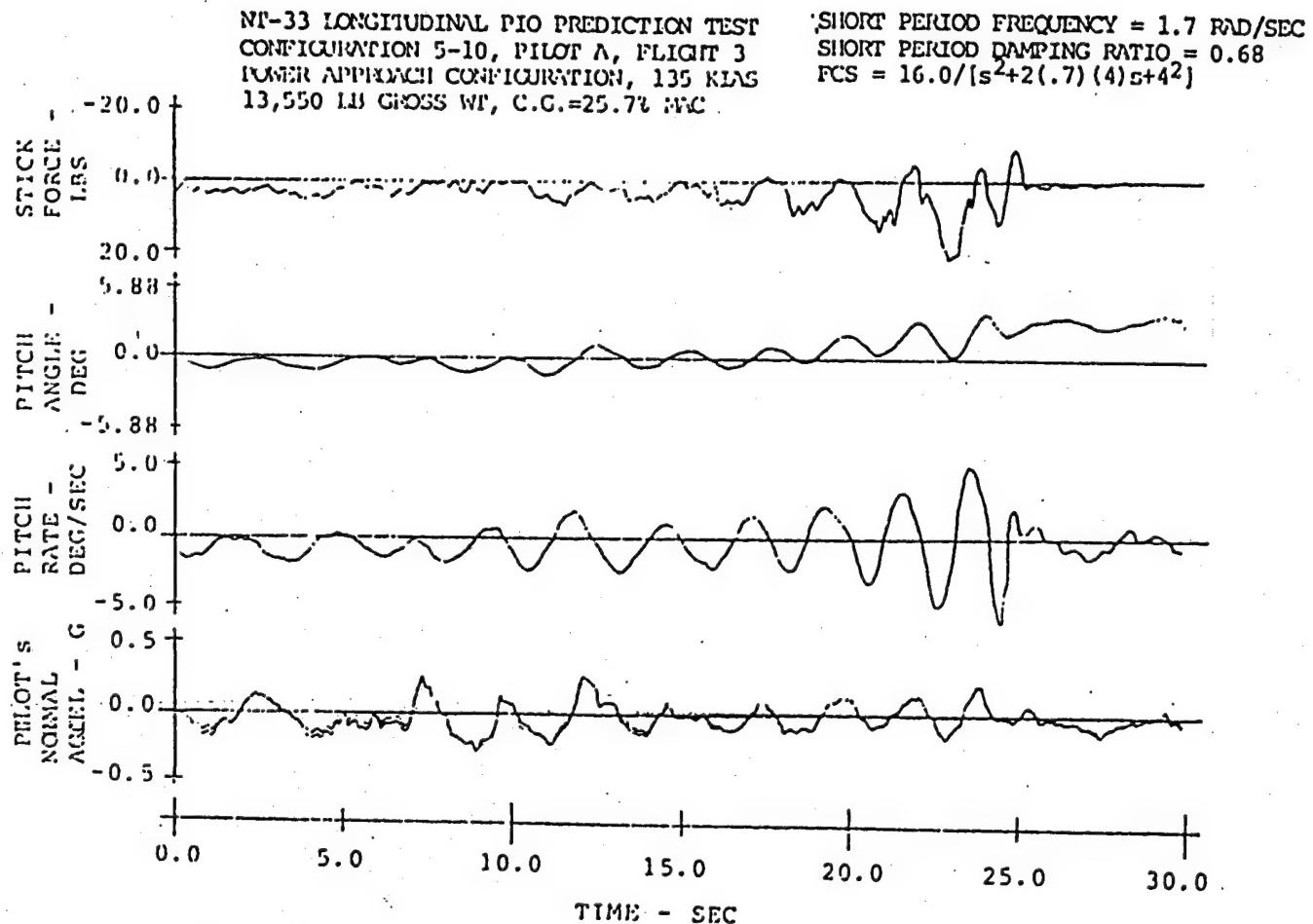


Figure 47. Selected Parameter Time Histories, Configuration 5-10

Figure A-113. NT-33A, Configuration 5-10 (Ref. A-31)

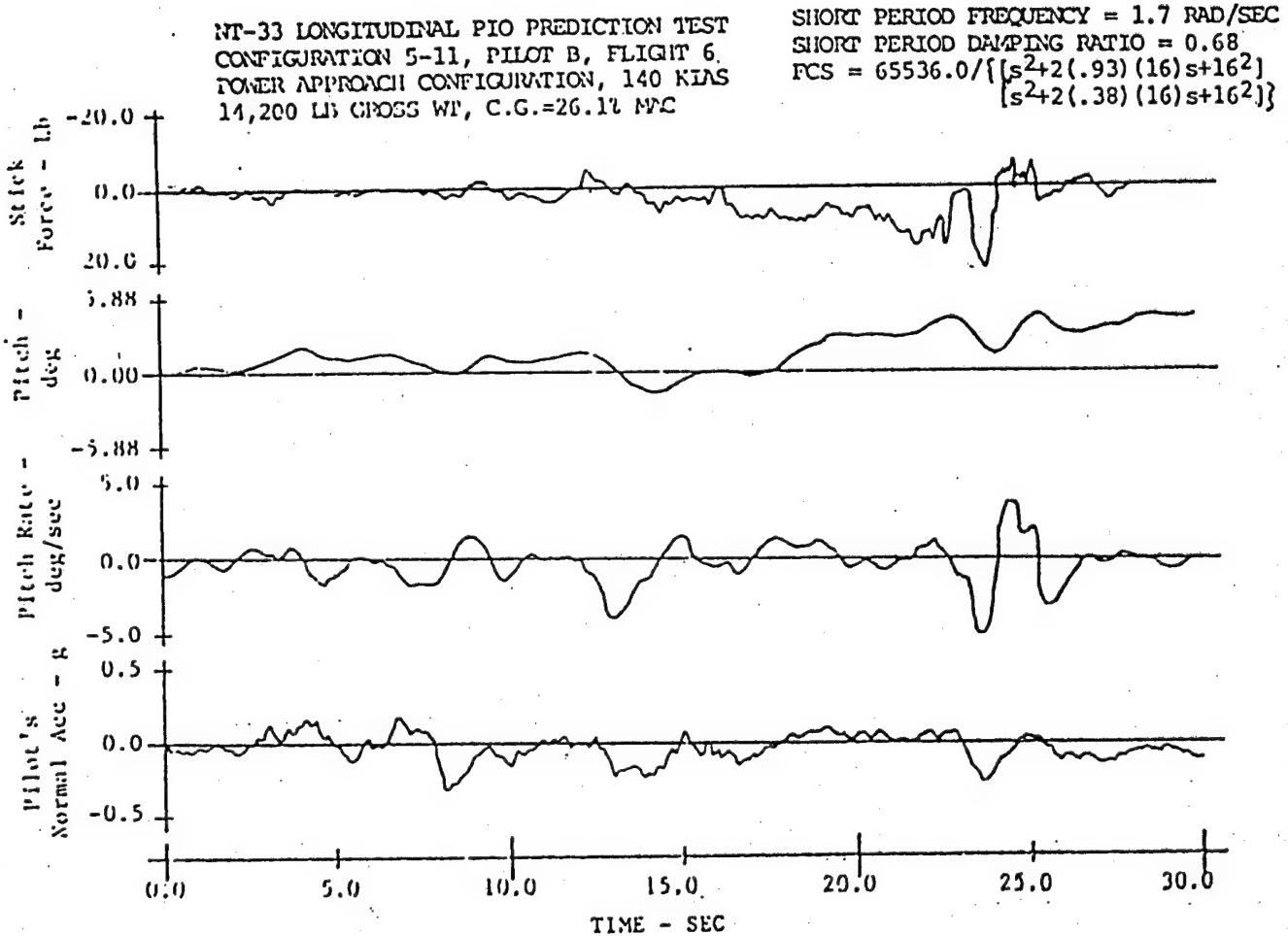


Figure 48. Selected Parameter Time Histories, Configuration 5-11

Figure A-114. NT-33A, Configuration 5-11 (Ref. A-31)

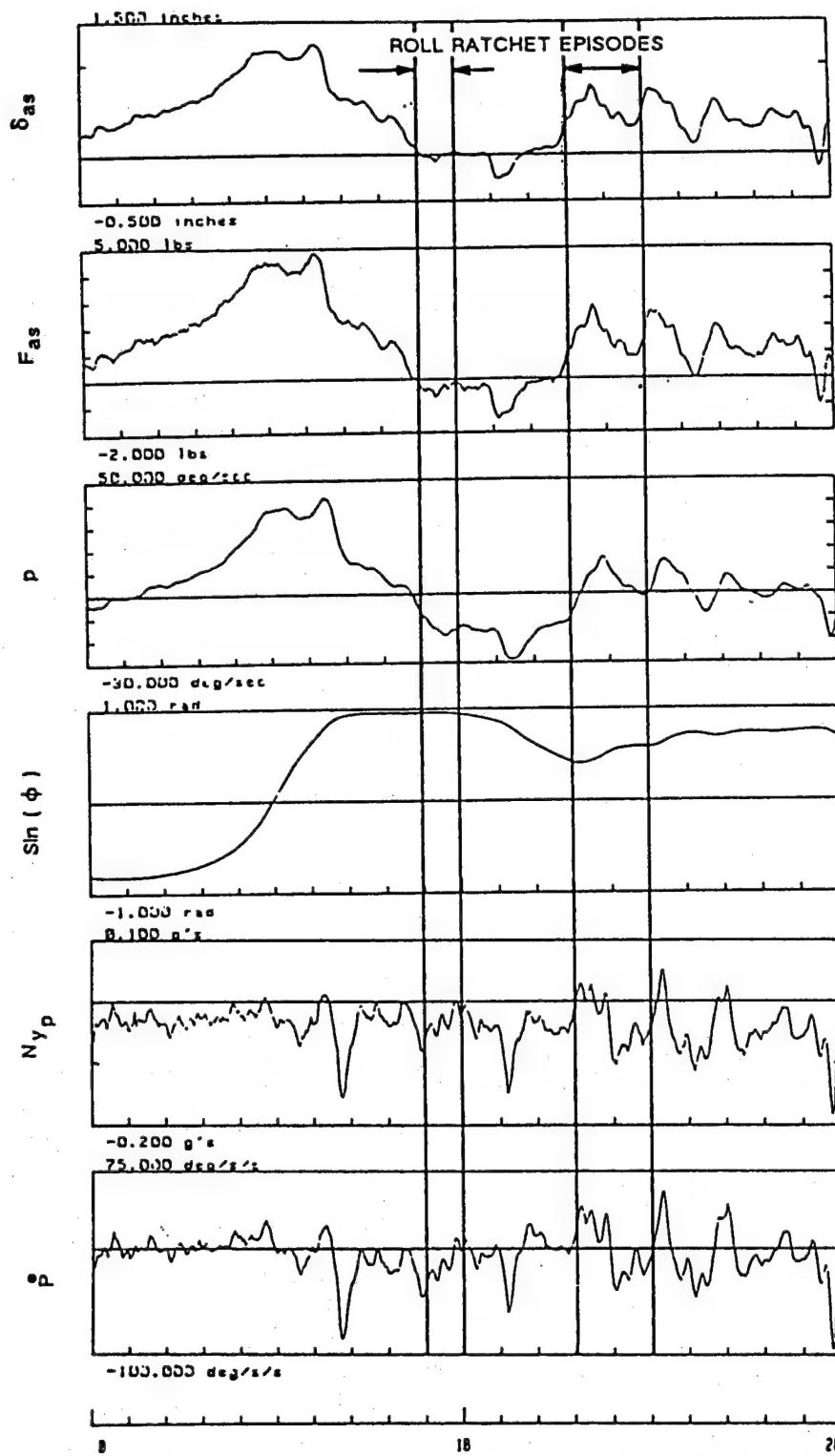


Figure 40 FLIGHT #4069, REC #10; CONFIG: 141F (10), GUN TRACKING BY PILOT A

Figure A-115. NT-33A, Configuration 141F (10) (Ref. A-32)

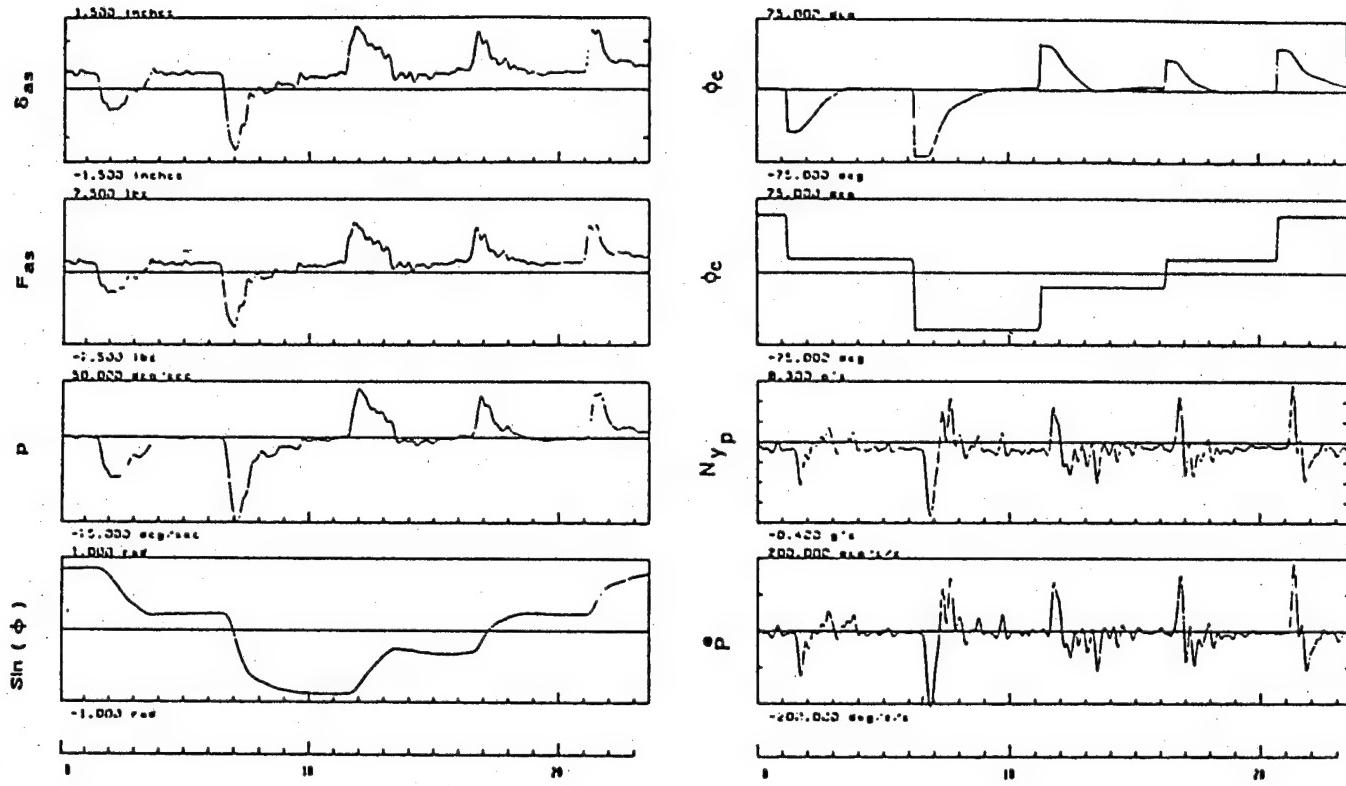


Figure 41 FLIGHT #4069, REC #12; CONFIG: 141F (10), LATHOS TRACKING

Figure A-116. NT-33A, Configuration 141F (10) (Ref. A-32)

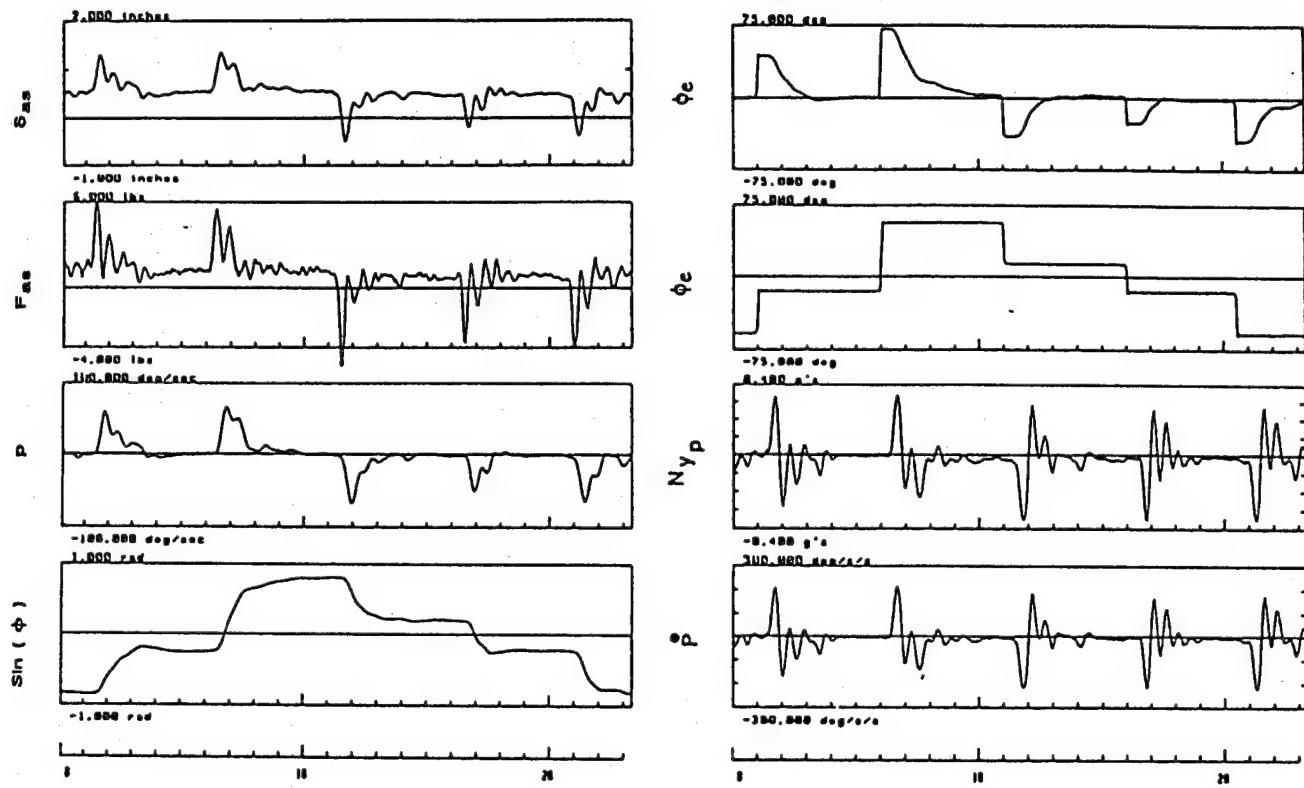


Figure 56 FLIGHT #4176, RECORD #16; CONFIGURATION 143P (18); LATHOS TRACKING

Figure A-117. NT-33A, Configuration 143P (18) (Ref. A-32)

Table A-4 Addendum to PIO Events with Documented Time Historics

Fig. No.	Aircraft	PIO Date	Ref. No.	Flight Condition	Mach	Alt/S (KIAS)	Altitude (ft)	PIO Axis
A-118	C-5A	01/01/75	A-33	AR		237		Pitch
A-119	F-8 DFBW	01/01/80	A-34	AR/FF				Pitch
A-120	F-8 DFBW	01/01/86	A-35	L		260	4,800	Roll
A-121	F-8 DFBW	01/02/86	A-35	AR/FF				Roll
A-122	Tornado	01/01/95	A-36	L				Pitch
A-123	Tornado	01/02/95	A-36	L				Pitch
A-124	Tornado	01/03/95	A-36	Short TO				Pitch
A-125	Tornado	01/04/95	A-36	L				Roll

Table A-5 Addendum to Research PIO Events with Documented Time Histories

Fig. No.	Aircraft	Configuration	Ref. No.	Flight Condition	PIO Axis
A-126	NT-33A	A(F)-5(1)	A-37	Altitude Tracking	Pitch
A-127	NT-33A	A(F)-5(1)	A-37	Pitch Tracking	Pitch
A-128	NT-33A	C(F)-5(2.5)	A-37	Altitude Tracking	Pitch
A-129	NT-33A	C(F)-5(2.5)	A-37	Pitch Tracking	Pitch
A-130	NT-33A	LA(F)-5(1)	A-37	Altitude Tracking	Pitch
A-131	NT-33A	LA(F)-5(1)	A-37	Pitch Tracking	Pitch
A-132	NT-33A	LA(F)-5(1)	A-37	L	Pitch
A-133	TIFS	Short Aft Tail	A-38	L	Pitch

C-5A FLIGHT TEST DATA

BOOM INDICATED A/S: 237 KIAS
BOOM INDICATED ALT: 21965 FT
G.W.: 180,700 LB
C.G.: 29.98% MAC
(STICK FORCE NOT AVAILABLE)

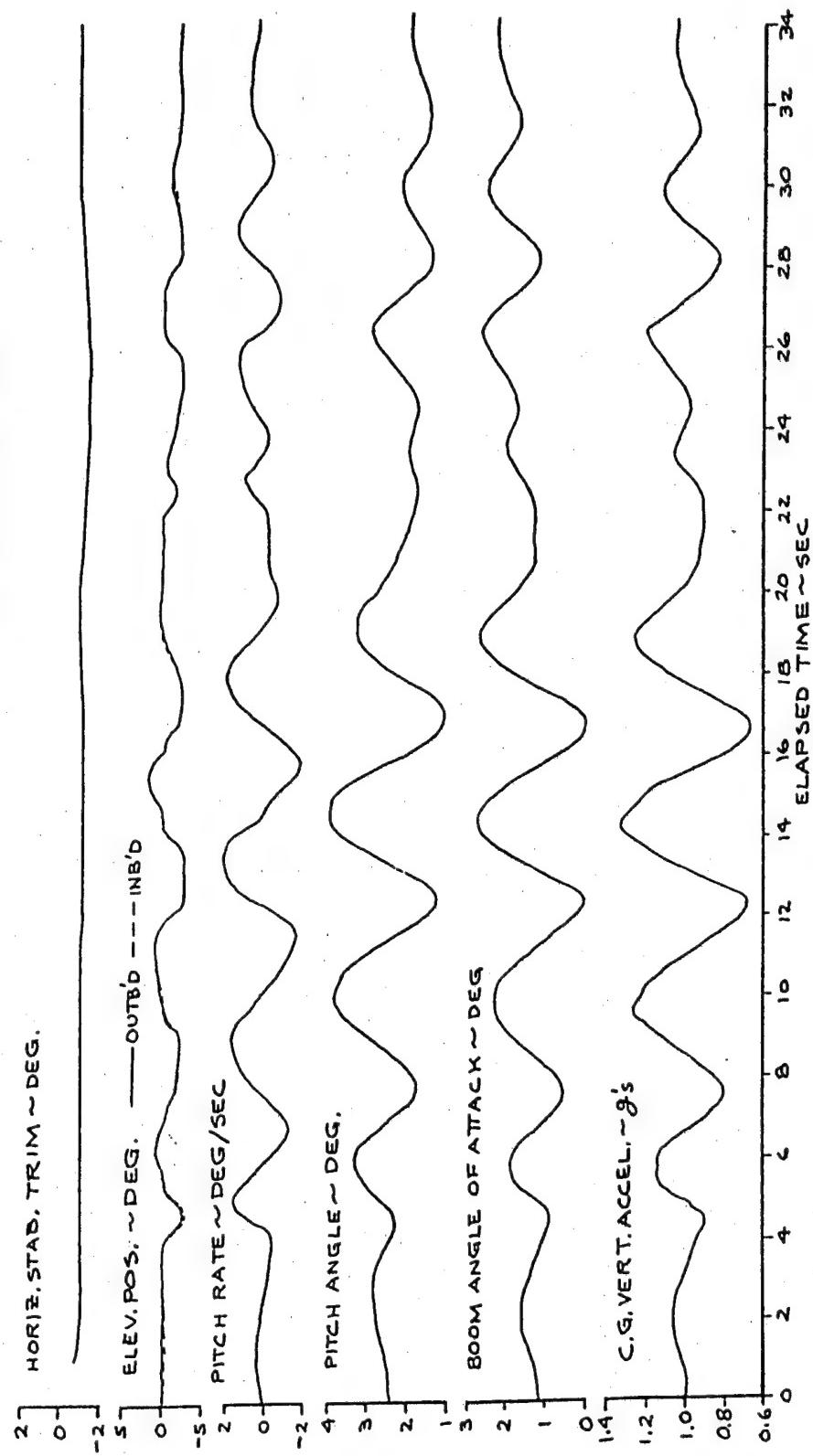


Figure A-118. C-5A (Ref. A-33)

A-126

TR-1313-1

FIGURE NO.1(3,2,2,3) INFLIGHT REFUELING CHARACTERISTICS

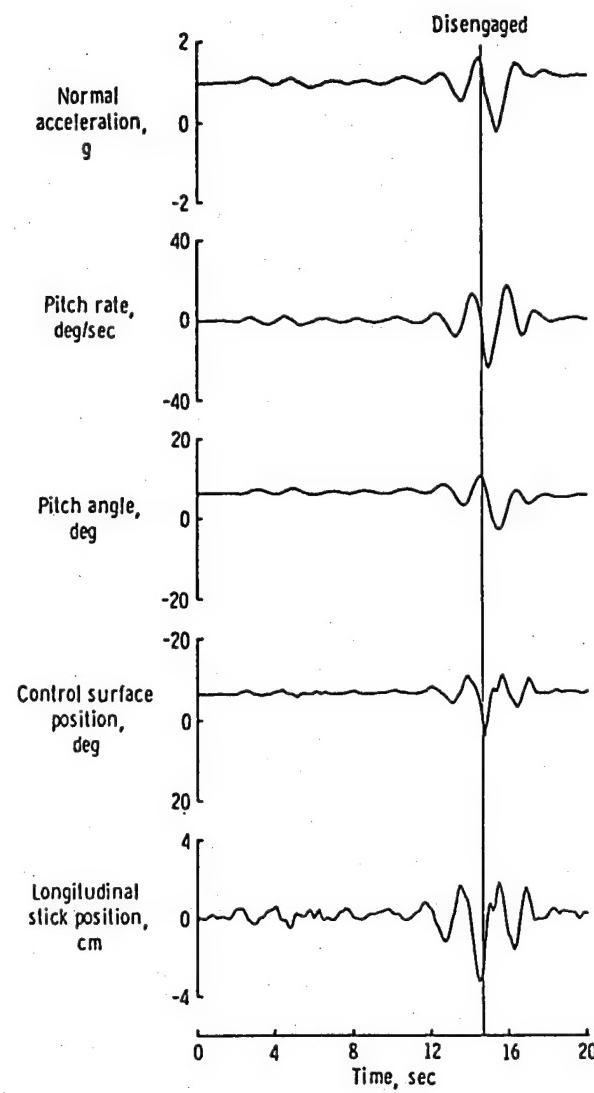


Fig. 11. Flight data for aerial refueling formation flying with P10. Direct mode; 0.20 sec incremental time delay.

Figure A-119. F-8 DFBW (Ref. A-34)

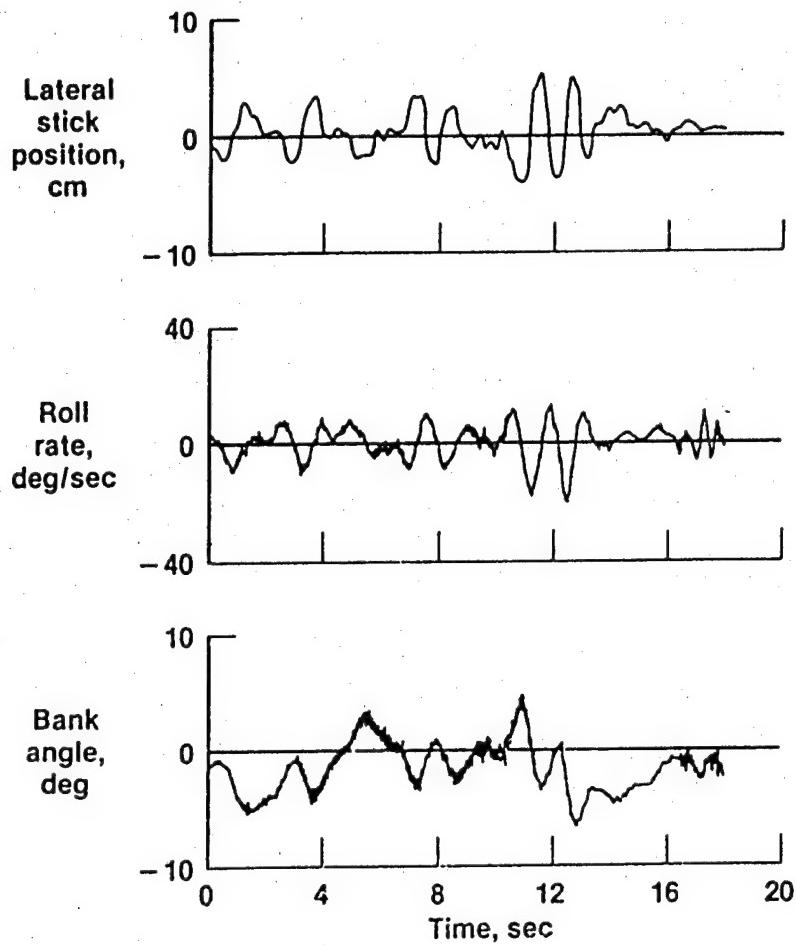


Fig. 7 Roll PIO during the landing approach (time delay = 60 ms).

Figure A-120. F-8 DFBW (Ref. A-35)

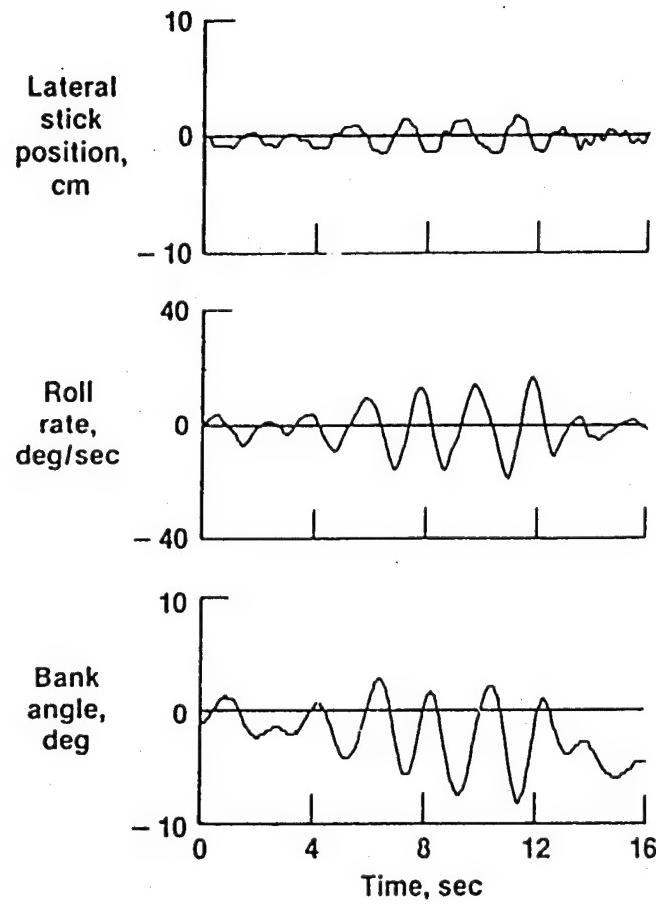


Fig. 8 Roll PIO during formation flying (time delay = 140 ms).

Figure A-121. F-8 DFBW (Ref. A-35)

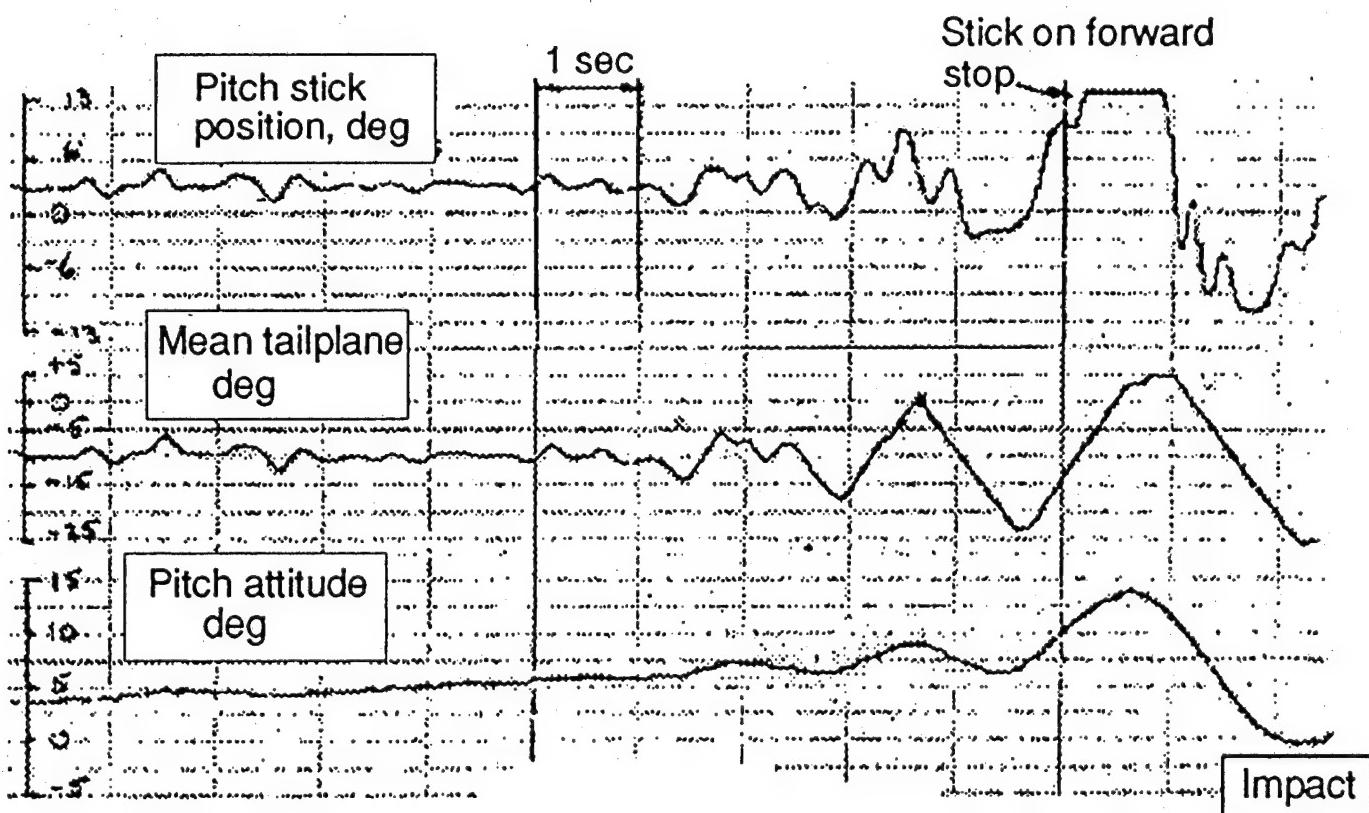


Figure 2 Landing PIO
(Tornado, initial FCS)

Figure A-122. Tornado (Ref. A-36)

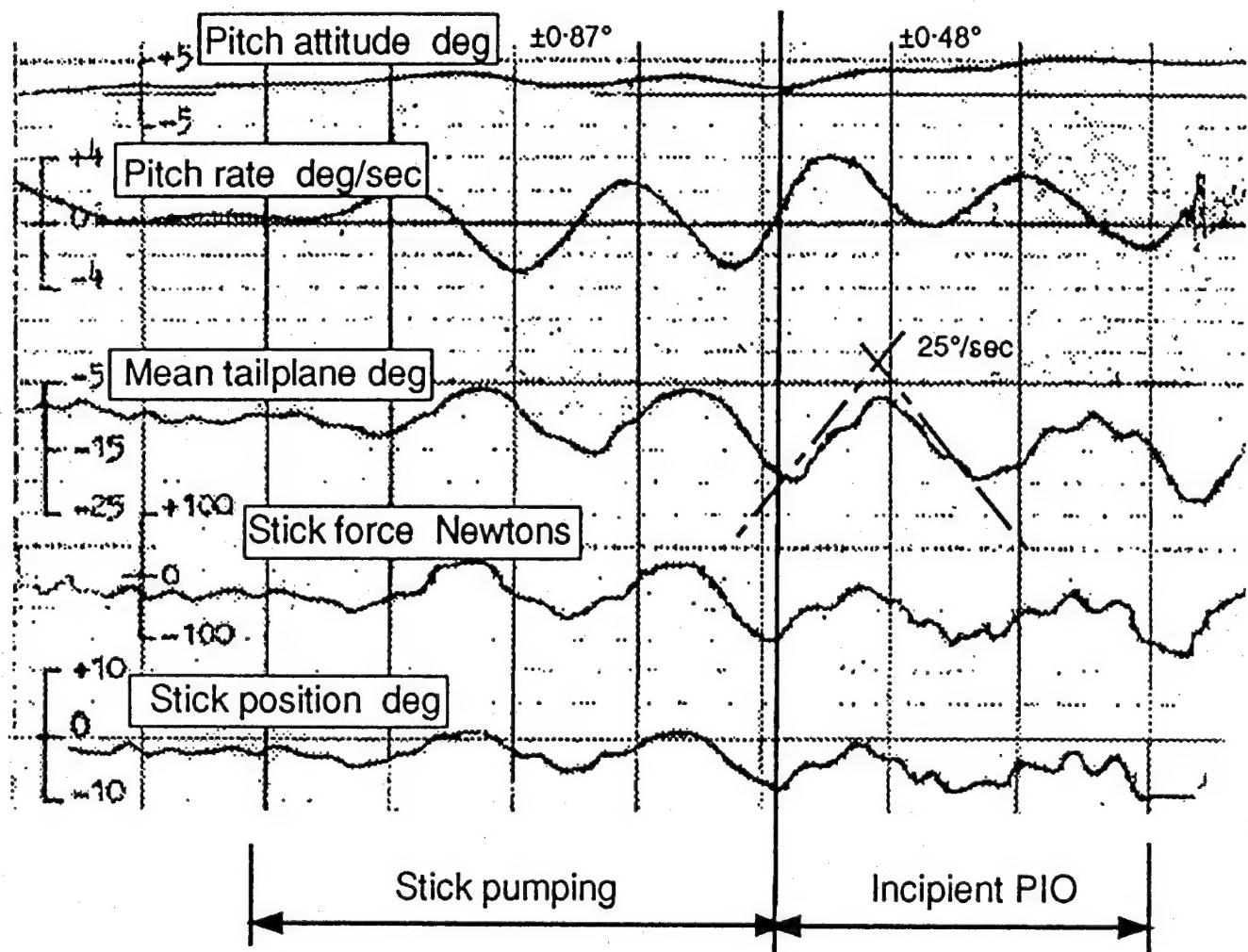


Figure 3 Incipient landing PIO
(Tornado, intermediate FCS)

Figure A-123. Tornado (Ref. A-36)

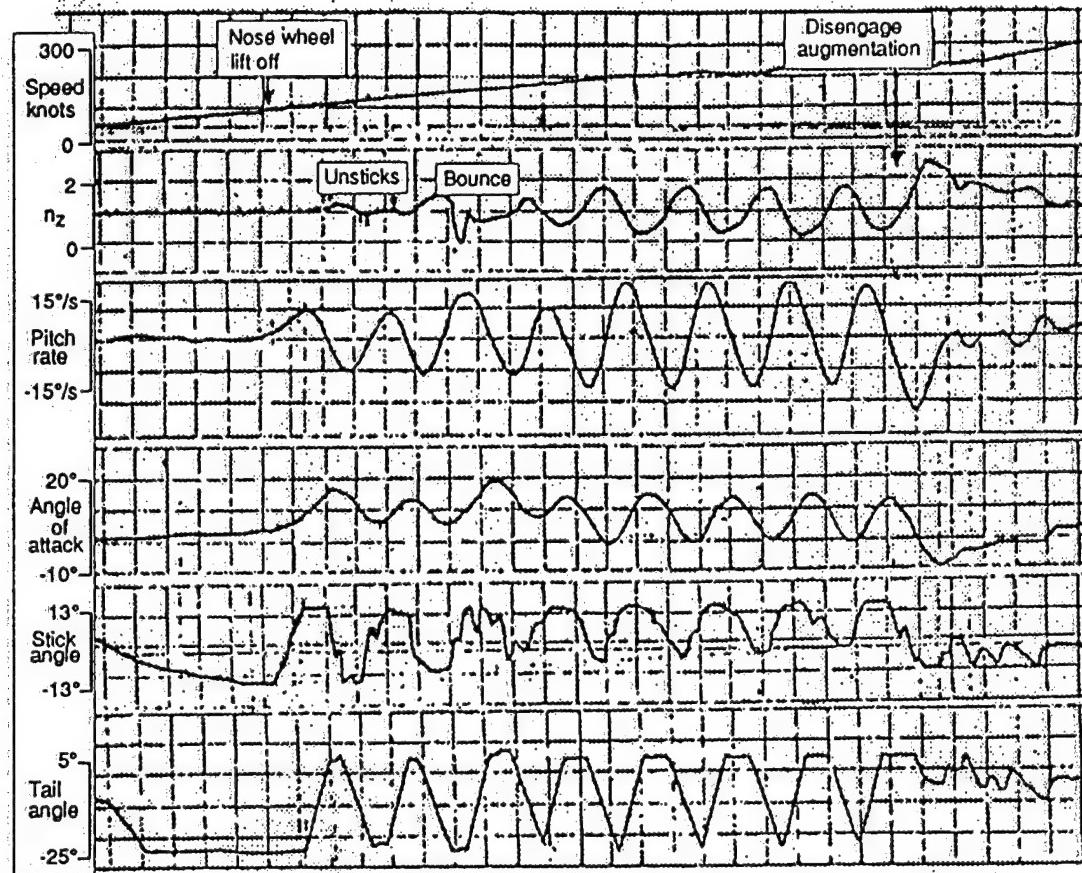


Figure 4 Tornado short take-off PIO

Figure A-124. Tornado (Ref. A-36)

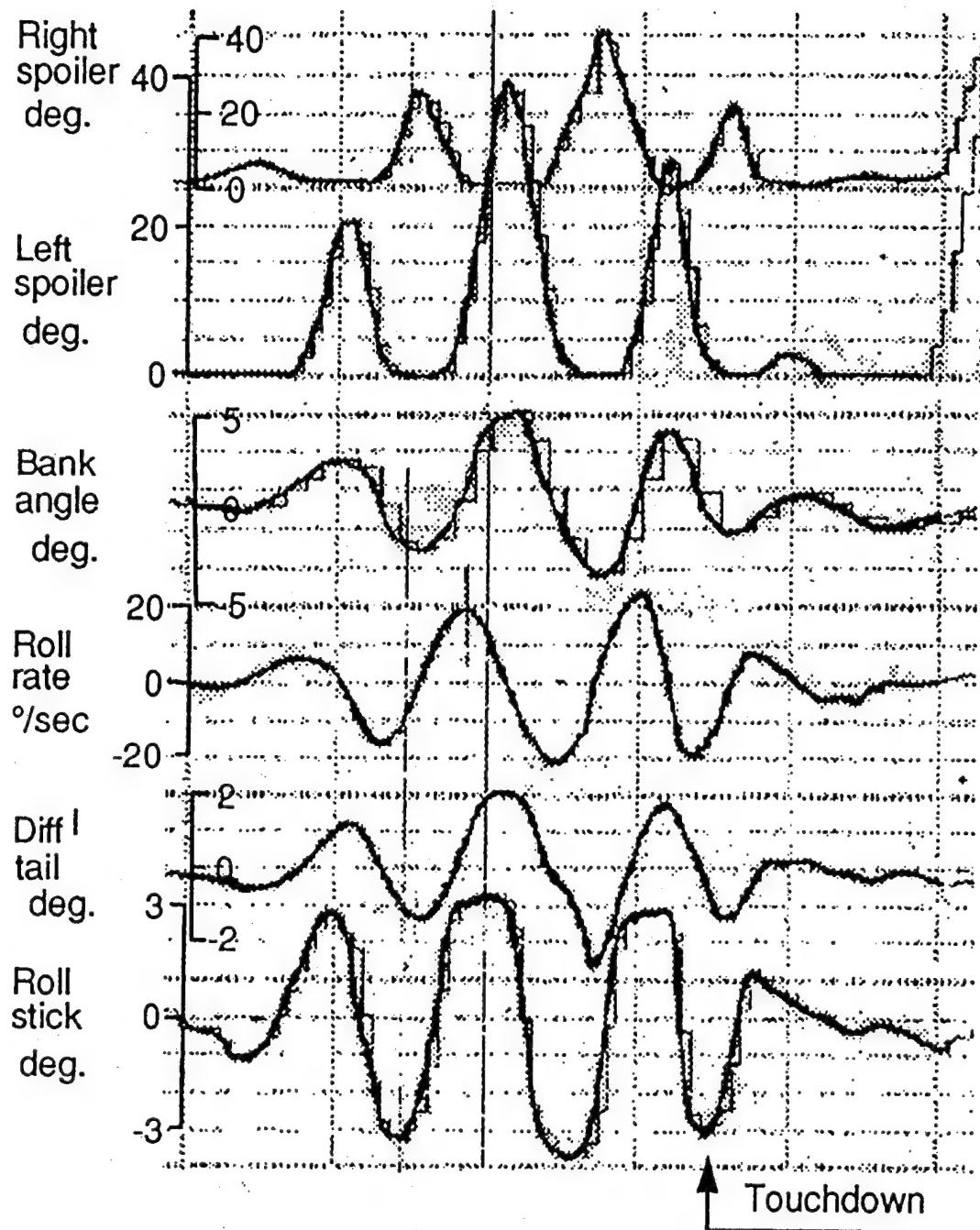


Figure 7 Early Tornado landing roll PIO

Figure A-125. Tornado (Ref. A-36)

CHARACTERISTICS:

$$F_{ES}/\eta_2 = 8.82 \text{ LB/g}$$

$$a_{Lr} = .587 \text{ SEC}$$

$$\alpha_r/\rho_E = .246$$

$$\phi_{cs} = 94^\circ$$

$$PR = 10$$

$$PIOR = 6$$

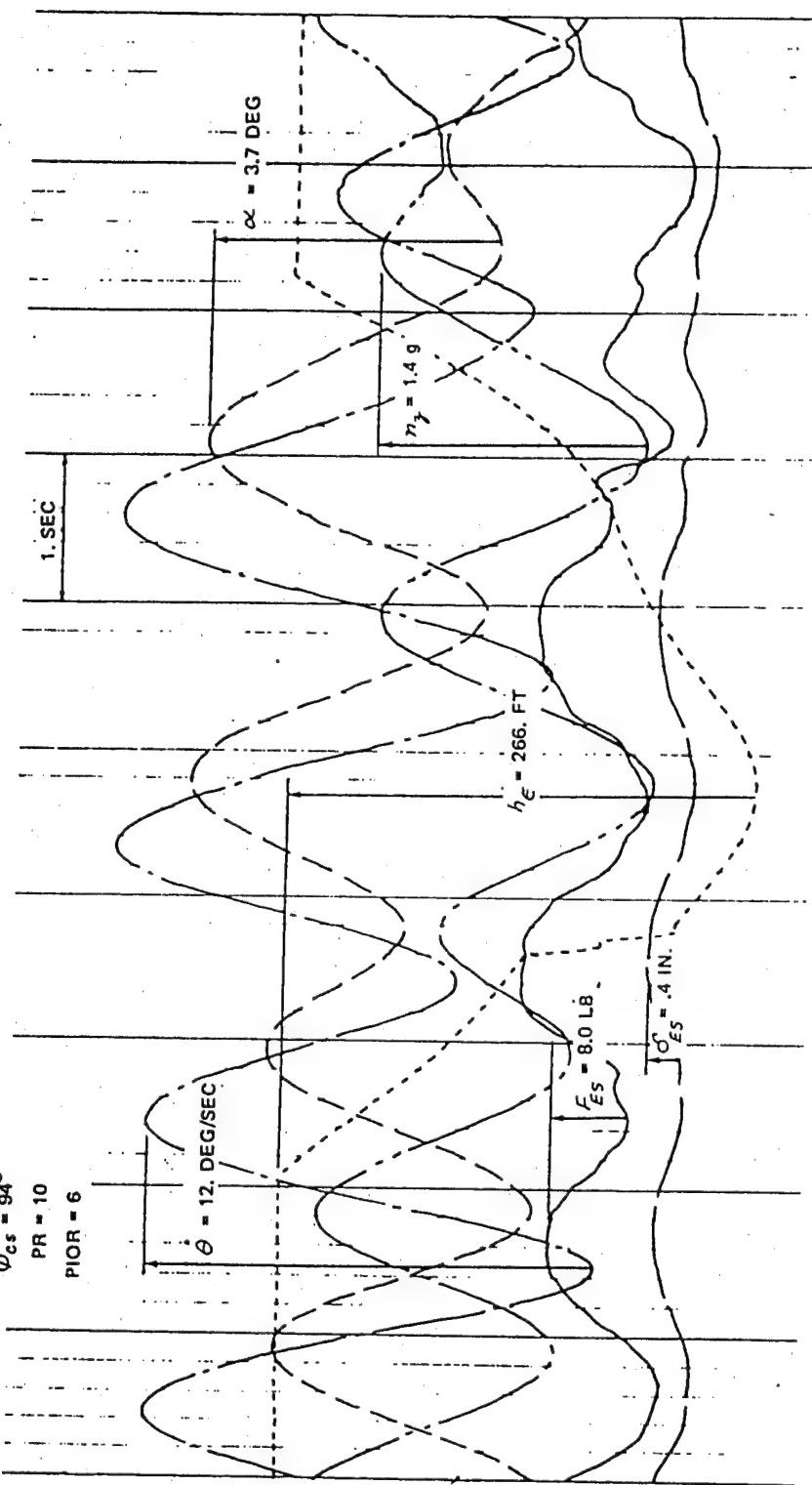


Figure A-126. NT-33A, Configuration A(F)-5(1) (Ref. A-37)

Figure 34 VFR ALTITUDE TRACKING TASK PERFORMANCE OF PILOT H DURING SIMULATION OF CONFIGURATION A(F)-5(1) ON FLIGHT 850

CHARACTERISTICS:

F_{ES}/η_3	= 8.82 LB/g
a_{rf}	.587 SEC.
a_{rf}/ρ_E	.246
θ_c/ϕ_{cs}	94°
PR	U9
PIOR	5

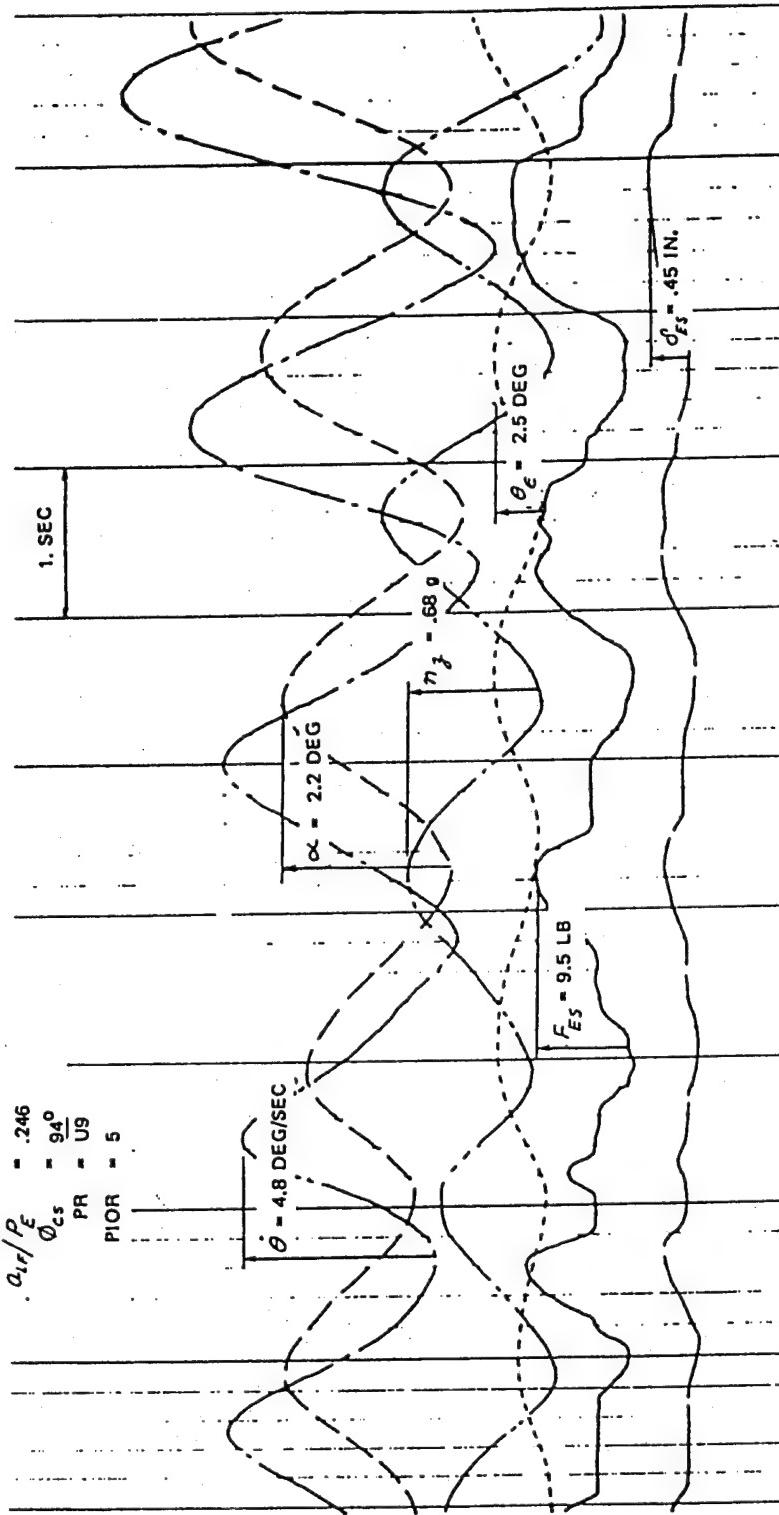


Figure A-127. NT-33A, Configuration A(F)-5(1) (Ref. A-37)

Figure 35 IFR PITCH ATTITUDE TRACKING TASK PERFORMANCE OF PILOT H
DURING SIMULATION OF CONFIGURATION A(F)-5(1) ON FLIGHT 850

CHARACTERISTICS:

$$F_{es}/\eta_2 = 8.04 \text{ LB/g}$$

$$\alpha_{lf} = .283 \text{ SEC}$$

$$\alpha_{lf}/\rho = .223$$

$$\phi_{cs} = 86^\circ$$

$$PR = 10$$

$$PIOR = 6$$

$$\theta = 5.1 \text{ DEG/SEC}$$

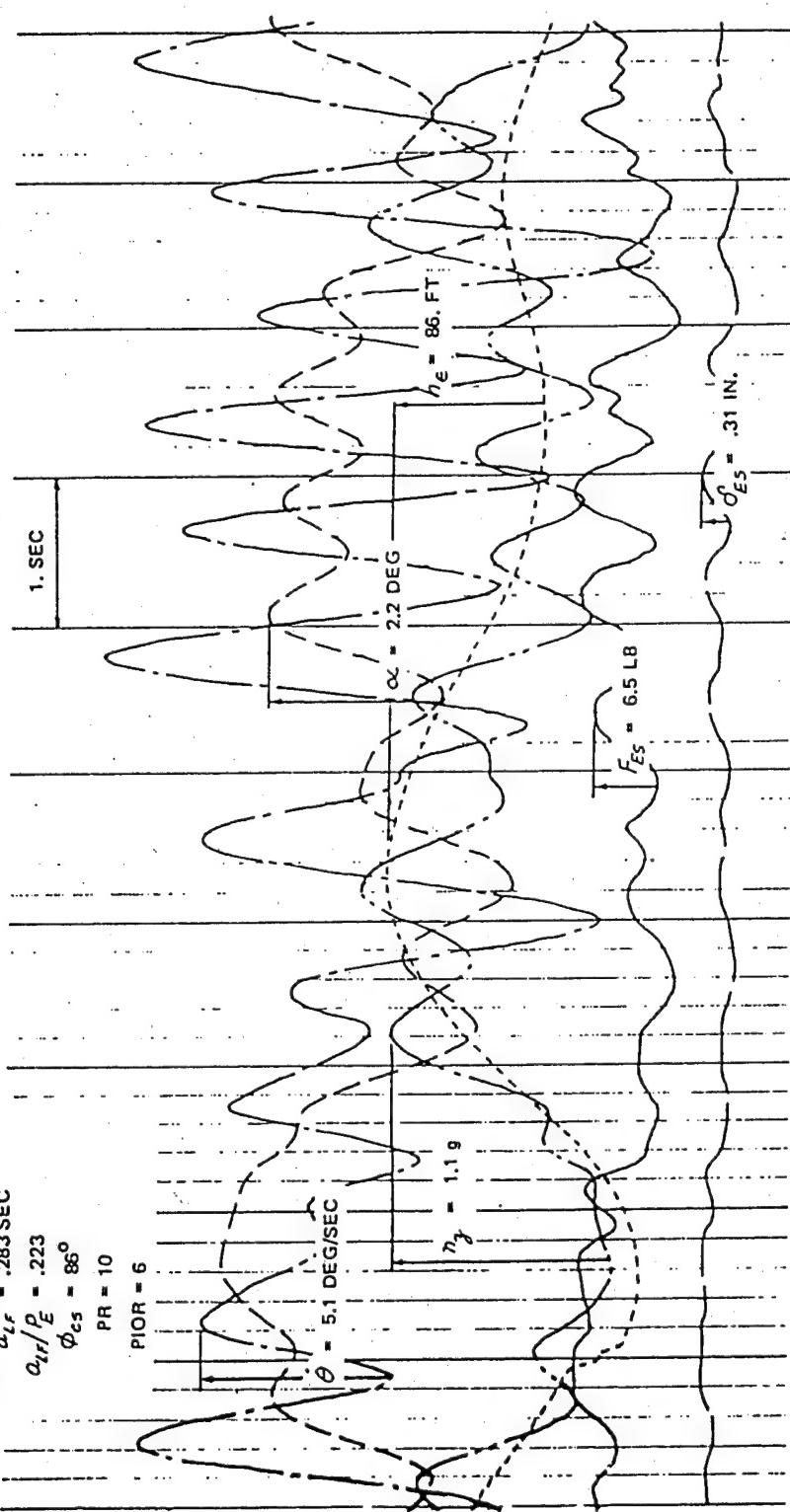


Figure A-128. NT-33A, Configuration C(F)-5(2.5) (Ref. A-37)

Figure 36 VFR ALTITUDE TRACKING TASK PERFORMANCE OF PILOT H
DURING SIMULATION OF CONFIGURATION C(F)-5(2.5) ON FLIGHT 851

CHARACTERISTICS:

$F_{ES}/\eta_F = 17.8 \text{ LB/g}$
 $\alpha_{LF} = .613 \text{ SEC.}$
 $\alpha_{LE}/P_E = .194$
 $\phi_{es} = 68^\circ$
 $PR = U9$
 $Pior = 5$

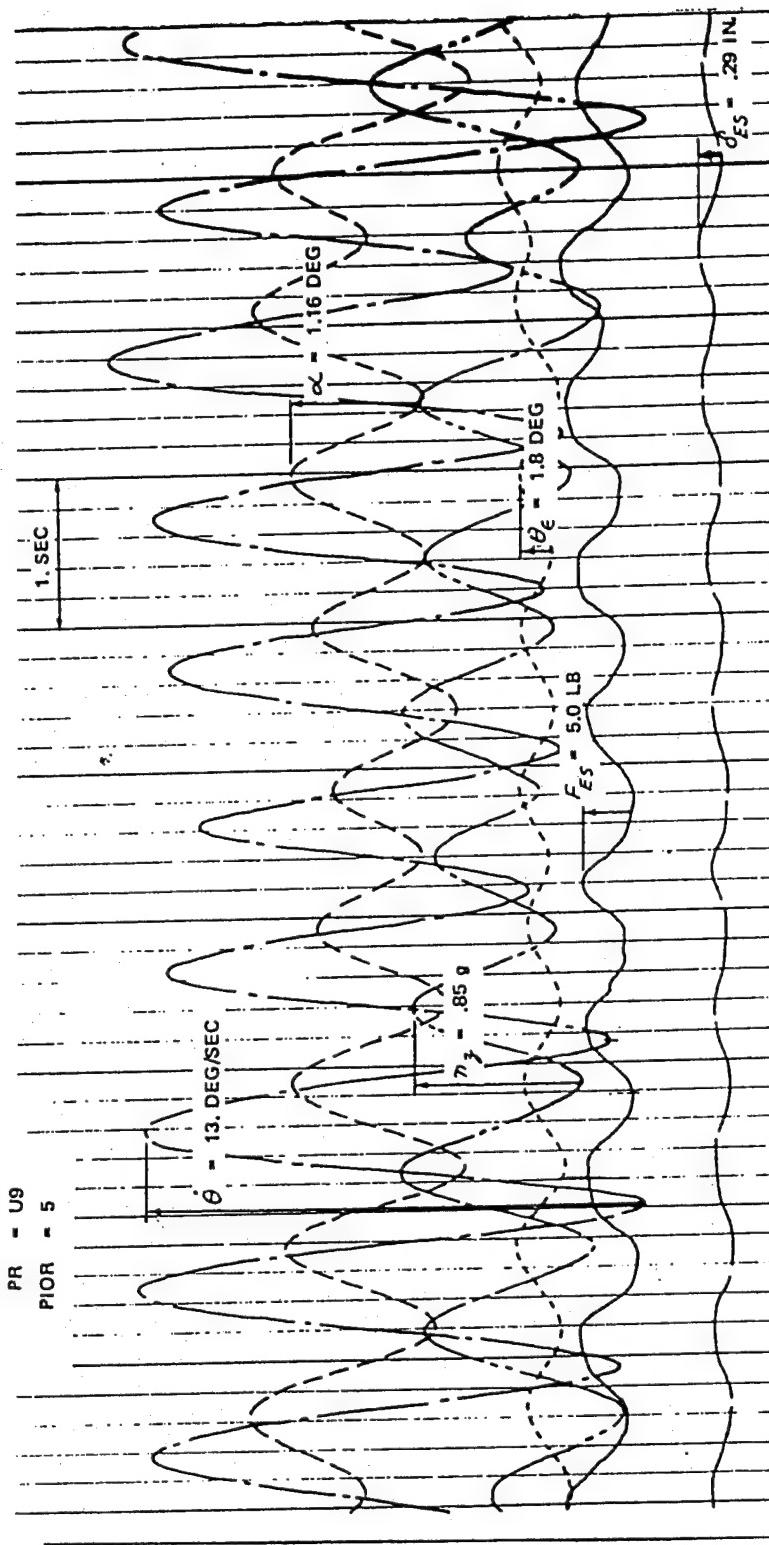


Figure A-129. NT-33A, Configuration C(F)-5(2.5) (Ref. A-37)

Figure 37 IFR PITCH ATTITUDE TRACKING TASK PERFORMANCE OF PILOT H DURING SIMULATION OF CONFIGURATION C(F)-5(2.5) ON FLIGHT 851

CHARACTERISTICS:

$$F_{es}/m_y = 8.04 \text{ LB/g}$$

$$a_{lf} = .283 \text{ SEC}$$

$$a_{rf}/\rho_e = .223$$

$$\phi_{cs} = 86^\circ$$

$$PR = 10$$

$$PIOR = 6$$

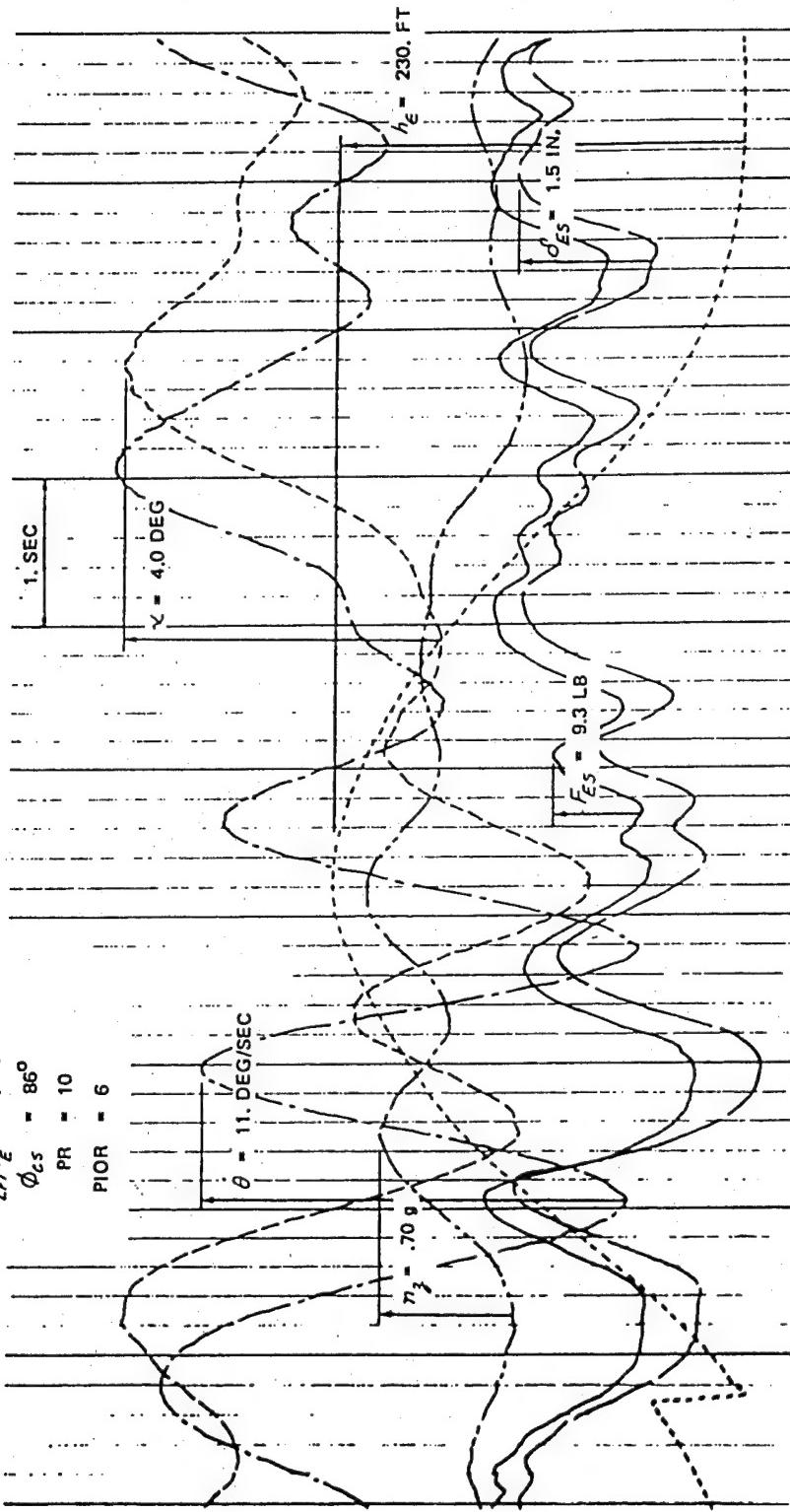


Figure A-130. NT-33A, Configuration LA(F)-5(1) (Ref. A-37)

TR-1313-1

A-138

Figure 38 VFR ALTITUDE TRACKING TASK PERFORMANCE OF PILOT H DURING SIMULATION OF CONFIGURATION LA(F)-5(1) ON FLIGHT 846

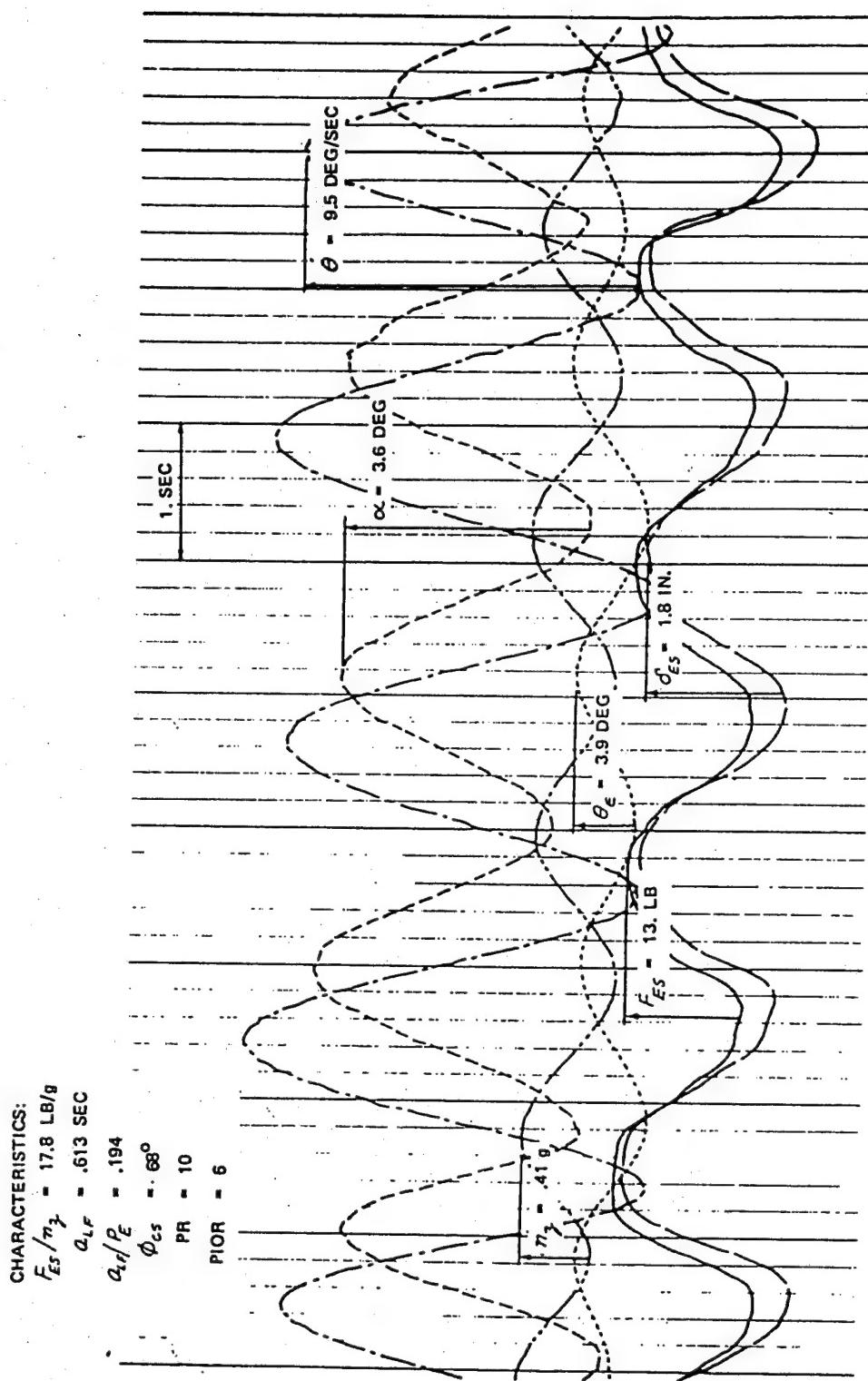


Figure A-131. NT-33A, Configuration LA(F)-5(1) (Ref. A-37)

TR-1313-1

A-139

Figure 39 IFR PITCH ATTITUDE TRACKING TASK PERFORMANCE OF PILOT H DURING SIMULATION OF CONFIGURATION LA(F)-5(1) ON FLIGHT 846

CHARACTERISTICS:

$F_{ES}/\eta_2 = 17.8 \text{ LB/g}$
 $\alpha_{L,F} = .613 \text{ SEC}$
 $\alpha_{L,F}/\rho_F = .194$
 $\phi_{cs} = 68^\circ$
 $PR = 10$

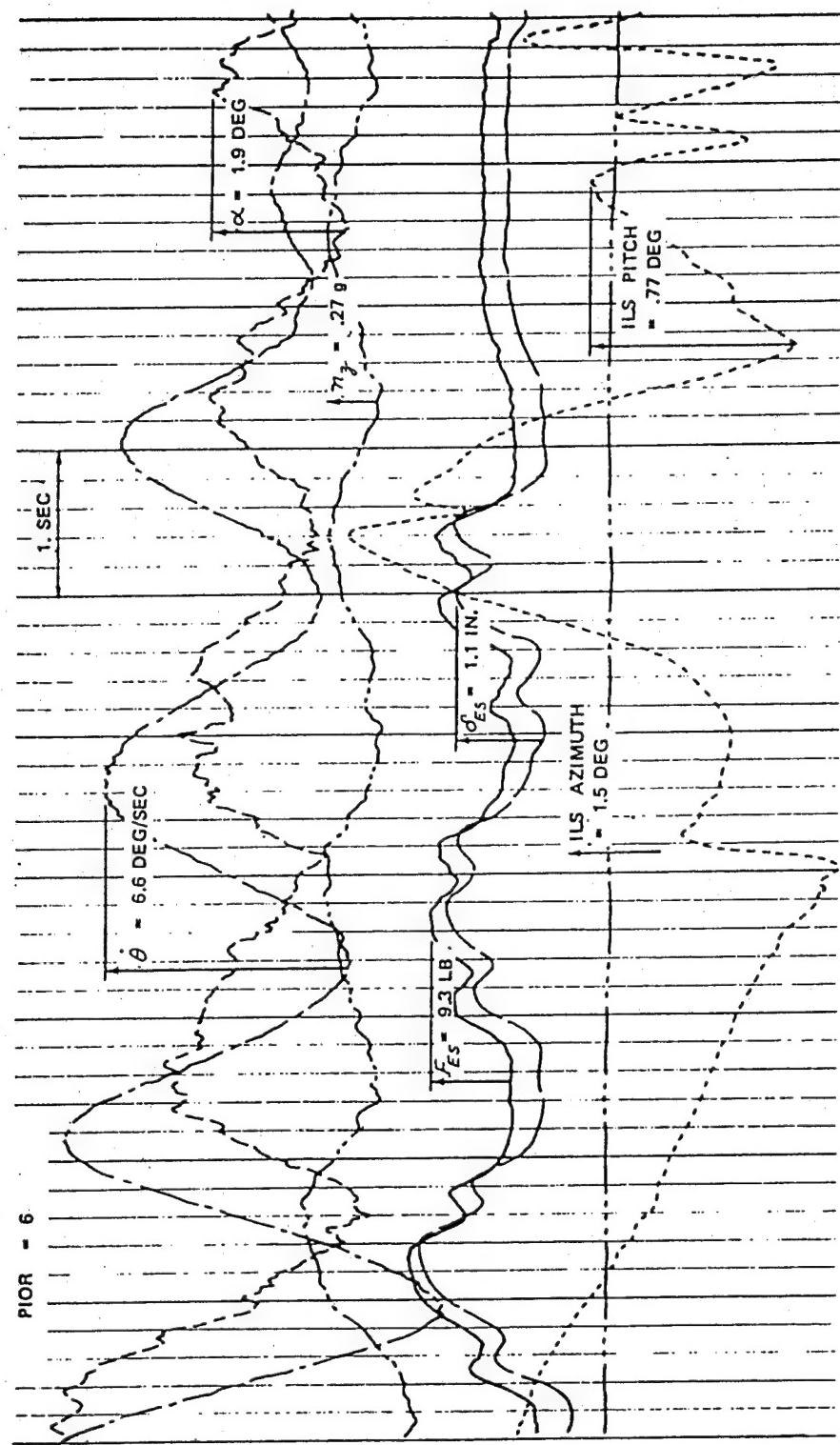


Figure A-132. NT-33A, Configuration LA(F)-5(1) (Ref. A-37)

Figure 40 PERFORMANCE OF PILOT H DURING ILS APPROACH DURING SIMULATION OF CONFIGURATION LA(F)-5(1) ON FLIGHT 846

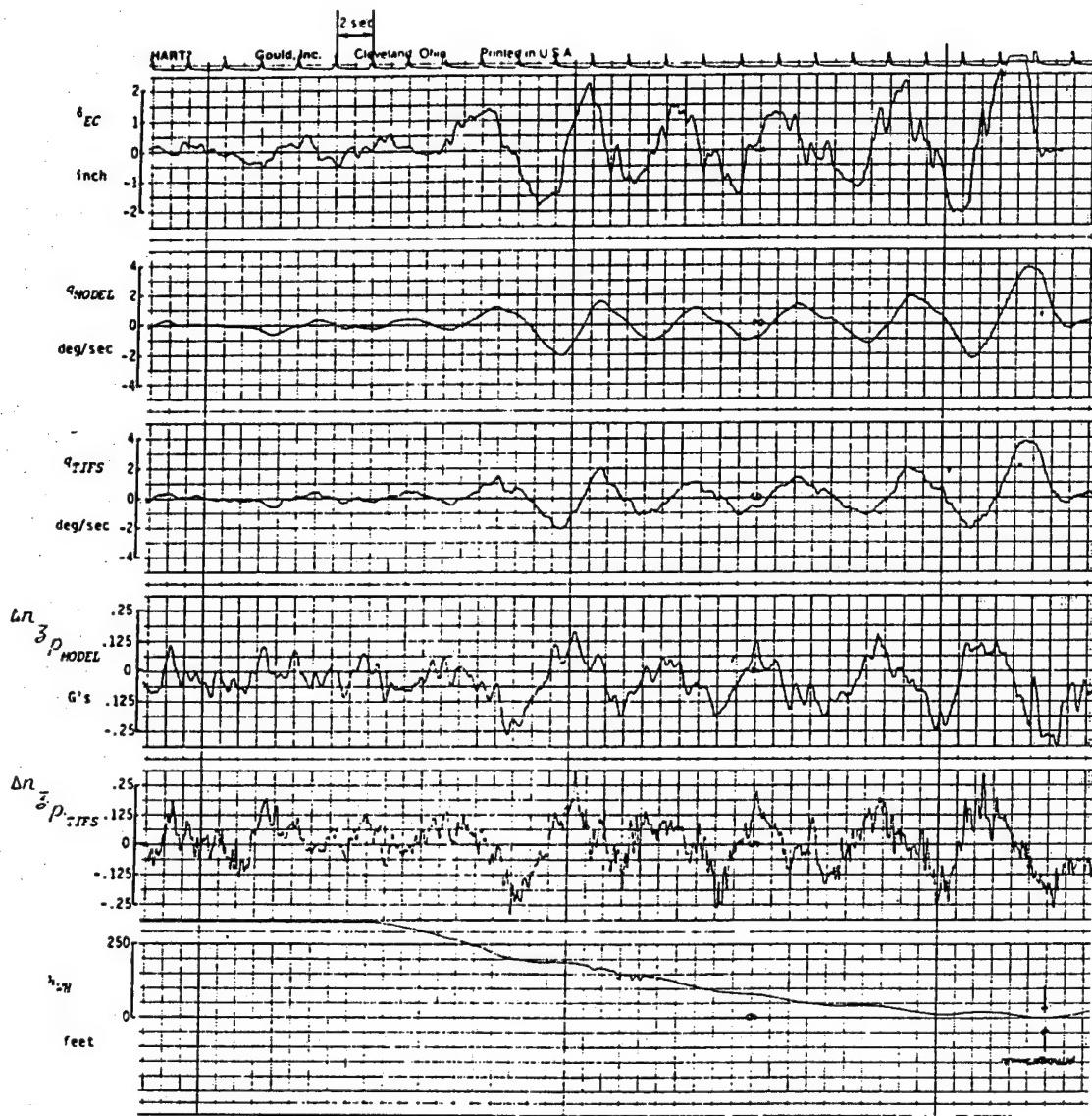


Figure 18. MODEL FOLLOWING - LONGITUDINAL ON APPROACH (INCLUDES PIO)
SHORT AFT TAIL, MED α , $T_1 = B$, FLT 615, REC 31

Figure A-133. TIFS, Short Aft Tail Configuration (Ref. A-38)

REFERENCES

- A-1. Newell, Fred, *Investigation of Phugoid Effects on GCA Landings*, WADC TR 57-650, Dec. 1957.
- A-2. Simmons, Carl D., and Donald M. Sorlie, *F-101B Air Force Stability and Control Evaluation*, Air Force Flight Test Center, TR 58-11, May 1958.
- A-3. Conley, Philip J., Jr., and John M. Carlson, *B-52G Category II Performance, Stability and Control Tests*, Air Force Flight Test Center, TR 59-34, Dec. 1959.
- A-4. Schweikhard, William, and Robert Rushworth, *F-104B Category II Performance and Stability Evaluation*, Air Force Flight Test Center, TR 59-32, Dec. 1959.
- A-5. Mitchell, John F., and Robert K. Parsons, *F-5A Category II Stability and Control Test*, Air Force Flight Test Center, FTC-TR-65-6, June 1965.
- A-6. Matranga, Gene J., *Analysis of X-15 Landing Approach and Flare Characteristics Determined from the First 30 Flights*, NASA TN D-1057, July 1961.
- A-7. Ashkenas Irving L., Henry R. Jex, and Duane T. McRuer, *Pilot-Induced Oscillations: Their Causes and Analysis*, Northrop-Norair Rept., NOR 64-143, June 1964.
- A-8. Kempel, Robert W., *Analysis of a Coupled Roll-Spiral Mode. Pilot-Induced Oscillation Experienced with the M2-F2 Lifting Body*, NASA TN D-6496, Sept. 1971.
- A-9. Smith, John W., *Analysis of a Lateral Pilot-Induced Oscillation Experienced on the First Flight of the YF-16 Aircraft*, NASA TM-72867, Sept. 1979.
- A-10. Eggers, James A., and William F. Bryant, Jr., *Flying Qualities Evaluation of the YF-16 Prototype Lightweight Fighter*, Air Force Flight Test Center, AFFTC-TR-75-15, July 1975.
- A-11. Smith, John W., and Donald T. Berry, *Analysis of Longitudinal Pilot-Induced Oscillation Tendencies of YF-12 Aircraft*, NASA TN D-7900, Feb. 1975.
- A-12. Wood, Richard A., Roger O. Hanson, Stephen D. Peterson, John A. Harris, *Flight Test Development and Evaluation of a Multimode Digital Flight Control System Implemented in an A-7D (DIGITAC)*, Air Force Flight Test Center, AFFTC-TR-76-15, June 1976.
- A-13. Teper, Gary L., Richard J. DiMarco, Irving L. Ashkenas, and Roger H. Hoh, *Analysis of Shuttle Orbiter Approach*, NASA CR 163108, July 1981.
- A-14. McRuer, Duane T., *Pilot-Induced Oscillations and Human Dynamic Behavior*, NASA CR-4683, Dec. 1994.
- A-15. Sisk, Thomas R., and Neil W. Matheny, *Precision Controllability of the F-15 Airplane*, NASA TM 72861, May 1979.
- A-16. Shaner, Keith L., and Robert W. Barham, *F-15C Flying Qualities Air Force Development Test and Evaluation*, Air Force Flight Test Center, AFFTC-TR-80-23, Nov. 1980.
- A-17. Richards, Dick, and C. D. Pilcher, "F/A-18A Initial Sea Trials," *Technical Review of the Society of Experimental Test Pilots*, Vol. 16, No. 1, 1981, pp. 10-22.

- A-18. Walker, Laurence A., and William J. LaManna, "Development of the F/A-18 Handling Qualities Using Digital Flight Control Technology," *Twenty-sixth Symposium Proceedings of the Society of Experimental Test Pilots*, Sept. 1982, pp. 41-67.
- A-19. Stowe, Steve, and Gary Jennings, "F-15E Initial Flight Test Results," *Thirty-first Symposium Proceedings of the Society of Experimental Test Pilots*, Sept. 1987, pp. 171-186.
- A-20. Niewoehner, Rob, and Steve Minnich, "F-14 Dual Hydraulic Failure Flying Qualities Evaluation," *Thirty-fifth Symposium Proceedings of the Society of Experimental Test Pilots*, Sept. 1991, pp. 4-15.
- A-21. Dornheim, Michael A., "Report Pinpoints Factors Leading to YF-22 Crash," *Aviation Week and Space Technology*, 9 Nov. 1992, pp. 53-54.
- A-22. Givens, Margo L., *Evaluation of B-2 Susceptibility to Pilot-Induced Oscillations*, Northrop Grumman, B-2 Division, White Paper 120-4, 1 March 1994.
- A-23. Taylor, Lawrence W., Jr., *Analysis of a Pilot-Airplane Lateral Instability Experienced with the X-15 Airplane*, NASA TN D-1059, Nov. 1961.
- A-24. Neal, T. Peter, and Rogers E. Smith, *An In-flight Investigation to Develop Control System Design Criteria for Fighter Airplanes*, AFFDL-TR-70-74, Volume I, Dec. 1970.
- A-25. Chalk, Charles R., Dante A. DiFranco, J. Victor Lebacqz, and T. Peter Neal, *Revisions to MIL-F-8785B (ASG) Proposed by Cornell Aeronautical Laboratory Under Contract F33615-71-C-1254*, AFFDL-TR-72-41, April 1973.
- A-26. Smith, R. E., *Effects of Control System Dynamics on Fighter Approach and Landing Longitudinal Flying Qualities*, AFFDL-TR-78-122, Volume I, Mar. 1978.
- A-27. Smith, Rogers, John Hodgkinson, and Richard C. Snyder, *Equivalent System Verification and Evaluation of Augmentation Effects on Fighter Approach and Landing Flying Qualities*, AFWAL-TR-81-3116, Volume II-Program Plan, Test Data and Analysis, Sept. 1981.
- A-28. Monagan, Stephen J., Rogers E. Smith, and Randall E. Bailey, *Lateral Flying Qualities of Highly Augmented Fighter Aircraft*, AFWAL-TR-81-3171, Volume I, March 1982.
- A-29. Gera, Joe, and Fred Schaefer, "X-29A Flight Controls Experience," *X-29A Symposium Proc.*, NASA Ames Research Center, 17-19 Sept. 1985.
- A-30. Weingarten, Norman C., Charles J. Berthe, Jr., Edmund G. Rynaski, and Shahan K. Sarrafian, *Flared Landing Approach Flying Qualities, Volume II-Appendices*, NASA CR-178188, Dec. 1986.
- A-31. Bjorkman, Eileen A., *Flight Test Evaluation of Techniques to Predict Longitudinal Pilot Induced Oscillations*, AFIT/GAE/AA/86J-1, Dec. 1986.
- A-32. Bailey, R. E., and L. H. Knotts, *Interaction of Feel System and Flight Control System Dynamics on Lateral Flying Qualities*, NASA CR-179445, Dec. 1990.
- A-33. Lockheed-Georgia Company, *Evaluation of the Flying Qualities Requirements of MIL-F- 8785B (ASG) Using the C-5A Airplane*, AFFDL-TR-75-3, 20 March 1975.

- A-34. Berry, Donald T., Bruce G. Powers, Kenneth J. Szalai, and R. J. Wilson, "A Summary of an In-Flight Evaluation of Control System Pure Time Delays During Landing Using the F-8 DFBW Airplane," AIAA Paper No. 80-1626, presented at the *AIAA Atmospheric Flight Mechanics Conference*, Danvers, MA, 11 to 13 Aug. 1980.
- A-35. Berry, Donald T., "In-Flight Evaluation of Incremental Time Delays in Pitch and Roll," published in *J. Guidance*, Vol. 9, No. 5, Sept.- Oct. 1986. pp. 573 to 577.
- A-36. Gibson, John C., "Looking for the Simple PIO Model," *Flight Vehicle Panel Workshop on Pilot Induced Oscillations*, AGARD-AR-335, Feb. 1995.
- A-37. DiFranco, Dante A., *In-Flight Investigation of the Effects of Higher-Order Control System Dynamics on Longitudinal Handling Qualities*, AFFDL-TR-68-90, Aug. 1968.
- A-38. Weingarten, Norman C., and Charles R. Chalk, *In-Flight Investigation of Large Airplane Flying Qualities for Approach and Landing*, AFWAL-TR-81-3118, Sept. 1981.

APPENDIX B

CATEGORY I PIO DATA COMPILATION

APPENDIX B

CATEGORY I PIO DATA COMPILATION

This Appendix contains a compilation of Category I PIO data for the operational and test aircraft PIO events for which the effective aircraft dynamics have been made available. The baseline and PIO prone *Have PIO* configurations (Ref. B-1) have also been included in this compilation, since they represent the available research aircraft data that specifically addressed PIO. (Any of the Ref. B-1 configurations that received PIO ratings ≥ 4 were considered PIO prone.) Various categories of data have been compiled in Table B-1. These categories include a PIO description, pilot ratings if available, Bode plot parameters, Bandwidth/Phase Delay/Dropback parameters (Ref. B-11), Smith-Geddes Criteria parameters (Ref. B-12), and Gibson Phase Rate parameters (Ref. B-13). Blanks in the table indicate that the effective aircraft dynamics necessary to compute the parameter were not available. For the YF-12 Rigid Body + Flex case, the presence of the flexible mode created ambiguities in the definition of certain parameters (i.e., phase delay and average phase rate). Following the table are Bode and Nichols chart system surveys for each of the configurations. It should be noted that the transfer function gains have been adjusted so that the magnitude passes through 0dB at a phase angle of -110°.

Table B-1. Category I PIO Data for Operational and Test Aircraft

Configuration	Ref. #	PIO Description			Pilot Ratings			Bode Plot Parameters		
		Flt. Cat.	ω_{PIO}	PIO Cat.	HQR	PIOR	ω_{180°	(rad/sec)	ω_{180°	(Hz)
Have PIO 2-1 (baseline)	B-1	C	No PIO		2/2/3	1/1/1	6.166	0.981	12.332	-218.6
Have PIO 2-5	B-1	C	2.66	I	10/7/10	4/4/5	2.332	0.371	4.664	-242.8
Have PIO 2-8	B-1	C	3.77	I	8/10/8	4/4/4	3.538	0.563	7.076	-257.9
Have PIO 3-1 (baseline)	B-1	C	No PIO		5/3/4	3/2/2	10.190	1.622	20.380	-249.3
Have PIO 3-12	B-1	C	2.21	I	7/9	4/5	2.226	0.354	4.452	-261.0
Have PIO 3-13	B-1	C	3.23	I	10/10	4/5	2.887	0.459	5.774	-272.4
Have PIO 5-1 (baseline)	B-1	C	No PIO		2/5	1/1	5.049	0.804	10.098	-210.5
Have PIO 5-9	B-1	C	3.48	I	7/7	4/4	2.471	0.393	4.942	-253.6
Have PIO 5-10	B-1	C	2.70	I	10/10	5/5	2.010	0.320	4.020	-266.3
X-15 Flt. 1-1-5	B-2 to B-4	C	3.3	II			5.307	0.845	10.614	-198.3
T-38 Bobweight Closed	B-5	B	7.8	III			10.083	1.605	20.166	-342.1
T-38 Bobweight Open	B-5	B	No PIO				9.032	1.437	18.064	-303.3
YF-12 Rigid Body Only	B-6	C	3.5	III			7.538	1.200	15.076	-227.1
YF-12 Rigid Body + Flex	B-6	C	3.5	III			7.894	1.256	15.788	-155.7
Shuttle Alt-5	B-7	C	3.4	II			3.228	0.514	6.456	-242.6
Shuttle STS-4 (Fit)	B-8	C	No PIO				2.849	0.453	5.698	-220.1
F-8 DFBW CAS + 100 msec	B-9	C	3.1	III	7.5-8		3.016	0.480	6.032	-262.0
F-8 DFBW Direct + 100 msec	B-9	C	3.1	III	7.5-8		2.324	0.370	4.648	-257.4
F-8 DFBW Direct	B-9	C	3.1	III	10		2.599	0.414	5.198	-239.9
F-8 DFBW SAS	B-9	C	No PIO	3			4.159	0.662	8.318	-249.0
B-2 Off-Nominal Approach	B-10	C	2.7	?			2.500	0.398	5.000	-240.0
B-2 Refueling	B-10	C	3.8	?			6.000	0.955	12.000	-232.0

Table B-1. Category I PIO Data for Operational and Test Aircraft (continued)

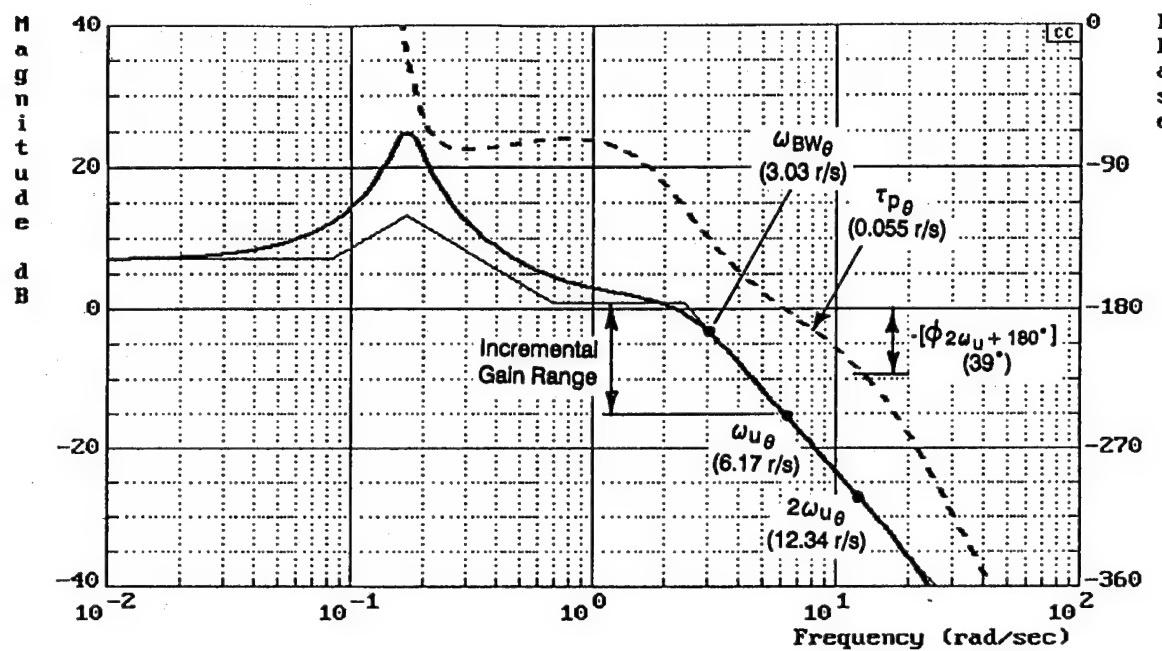
Configuration	ω_{BW0} (rad/sec)	$\tau_{p\theta}$ (sec)	FQ Level	q_{pk} (deg/sec)	Bandwidth/Phase Delay/Dropback							
					q_{ss} (deg/sec)	q_{pk}/q_{ss}	θ_{pk} (deg)	θ_{ss} (deg)	$\Delta\theta$ (deg)	$\Delta\theta/q_{ss}$ (sec)	FQ Level	PIO Prone
Have PIO 2-1 (baseline)	3.028	0.055	1	1.671	0.779	2.145	8.548	7.786	0.762	0.978	1	No
Have PIO 2-5	1.382	0.235	3	0.801	0.623	1.286	6.495	6.267	0.228	0.366	1	Yes
Have PIO 2-8	2.140	0.192	3	1.457	0.672	2.168	7.370	6.721	0.649	0.966	1	Yes
Have PIO 3-1 (baseline)	5.596	0.059	1	3.140	1.207	2.601	13.273	12.072	1.201	0.995	2	No
Have PIO 3-12	1.156	0.317	3	0.972	0.606	1.604	6.493	6.062	0.431	0.711	1	Yes
Have PIO 3-13	1.247	0.279	3	1.328	0.696	1.908	7.528	6.959	0.569	0.818	1	Yes
Have PIO 5-1 (baseline)	2.112	0.053	2	1.211	0.750	1.615	8.086	7.505	0.581	0.775	1	No
Have PIO 5-9	1.508	0.260	3	0.994	0.609	1.632	6.566	6.095	0.471	0.773	1	Yes
Have PIO 5-10	1.067	0.359	3	0.928	0.568	1.634	6.114	5.684	0.430	0.757	1	Yes
X-15 Flt. 1-1-5	2.639	0.030	1	1.372	0.599	2.290	6.523	5.984	0.539	0.900	1	No
T-38 Bobweight Closed	0.412	0.140	2	3.238	0.780	4.151	8.056	7.803	0.253	0.324	3	Yes
T-38 Bobweight Open	1.813	0.119	2	4.535	1.839	2.466	18.881	18.389	0.492	0.268	1	No
YF-12 Rigid Body Only	4.588	0.055	1	2.865	1.490	1.923	15.797	14.901	0.896	0.601	1	No
YF-12 Rigid Body + Flex	4.640			3.388	1.546	2.191	16.375	15.461	0.914	0.591	1	Yes
Shuttle Alt-5	1.545	0.169	1/2	0.872	0.748	1.166	7.699	7.513	0.186	0.249	1	Yes
Shuttle STS-4 (Fit)	1.386	0.123	1/2	0.780	0.704	1.108	7.145	7.044	0.101	0.143	1	No
F-8 DFBW CAS + 100 msec	1.561	0.237	3	0.995	0.656	1.517	6.876	6.563	0.313	0.477	1	Yes
F-8 DFBW Direct + 100 msec	0.580	0.291	3	1.100	0.552	1.993	5.998	5.513	0.485	0.879	1	Yes
F-8 DFBW Direct	1.659	0.201	3	1.111	0.558	1.991	6.061	5.570	0.491	0.880	1	Yes
F-8 DFBW SAS	2.106	0.145	2	0.836	0.700	1.194	7.236	7.003	0.233	0.333	1	No
B-2 Off-Nominal Approach	0.960	0.209	2/3								Yes	
B-2 Refueling	3.700	0.076	1								No	

Table B-1. Category I PIO Data for Operational and Test Aircraft (continued)

Configuration	Smith-Geddes											
	slope	FQ	ω_c	$\phi(\theta/F_{\text{ext}})$	FQ Level	PIO Prone	$\phi(n_p/F_{\text{ext}})$	$\Phi(j\omega_c)$	FQ Level	PIO Prone	t_q	
(dB/oct)	Level	(rad/sec)	(deg)	Type III	Type III	(deg)	(deg)	Type I	Type II	(sec)	Level	
Have PIO 2-1 (baseline)	-6.775	1	4.374	-161.0	2	No	-158.5	-221.1	3	No	Yes	0.687
Have PIO 2-5	-11.729	1	3.185	-211.6	3	Yes	-202.2	-247.8	3	Yes	Yes	1.514
Have PIO 2-8	-6.977	1	4.326	-201.5	3	Yes	-198.8	-260.6	3	Yes	Yes	0.827
Have PIO 3-1(baseline)	-3.937	1	5.055	-127.9	2	No	-174.3	-246.6	2	No	Yes	0.334
Have PIO 3-12	-11.434	1	3.256	-225.6	3	Yes	-240.8	-287.4	3	Yes	Yes	1.408
Have PIO 3-13	-8.440	1	3.974	-223.9	3	Yes	-250.7	-307.5	3	Yes	Yes	1.056
Have PIO 5-1 (baseline)	-9.303	1	3.767	-167.6	3	No	-157.1	-210.9	3	Yes	Yes	1.056
Have PIO 5-9	-10.181	1	3.556	-216.9	3	Yes	-205.6	-256.5	3	Yes	Yes	1.285
Have PIO 5-10	-11.922	1	3.138	-229.5	3	Yes	-216.5	-261.4	3	Yes	Yes	1.479
X-15 Flt. 1-1-5	-7.726	1	4.146	-170.9	3	No				Yes	Yes	0.783
T-38 Bobweight Closed	-2.014	1	5.517	-66.0	1	No	-33.2	-112.1	1	No	Yes	0.290
T-38 Bobweight Open	-2.293	1	5.450	-108.4	1	No	-76.0	-153.9	1	No	Yes	0.317
YF-12 Rigid Body Only	-4.274	1	4.974	-142.6	2	No				No	Yes	0.466
YF-12 Rigid Body + Flex	-4.681	1	4.876	-139.6	2	No				Yes	Yes	0.546
Shuttle Alt-5	-8.988	1	3.843	-193.1	3	Yes	-178.4	-233.3	3	Yes	No	1.496
Shuttle STS-4 (Fit)	-10.366	1	3.512	-192.0	3	Yes				No	Yes	1.743
F-8 DFBW CAS + 100 msec	-7.095	1	4.103	-215.2	3	Yes				No	Yes	1.030
F-8 DFBW Direct + 100 msec	-9.780	1	3.653	-232.5	3	Yes				No	Yes	1.259
F-8 DFBW Direct	-9.780	1	3.653	-211.6	3	Yes				No	Yes	1.162
F-8 DFBW SAS	-7.723	1	4.146	-179.8	3	Borderline				No	Yes	1.337
B-2 Off-Nominal Approach	-11.642	1	3.206	-210.0	3	Yes	-220	-265.8	3	Yes		
B-2 Refueling	-3.948	1	5.052	-158.0	2	No	-180	-252.2	3	No		

Table B-1. Category I PIO Data for Operational and Test Aircraft (concluded)

Configuration	Avg. Phase Rate (deg/rad/sec)	Avg. Phase Rate (deg/Hz)	ϕ_{180° (Hz)	Phase Rate FQ Level	Gibson Phase Rate
Have PIO 2-1 (baseline)	6.27	39.37	0.981	1	
Have PIO 2-5	26.91	169.07	0.371	>3	
Have PIO 2-8	22.02	138.36	0.563	2	
Have PIO 3-1 (baseline)	6.80	42.74	1.622	1	
Have PIO 3-12	36.37	228.49	0.354	>3	
Have PIO 3-13	31.99	200.99	0.459	>3	
Have PIO 5-1 (baseline)	6.05	37.99	0.804	1	
Have PIO 5-9	29.77	187.05	0.393	>3	
Have PIO 5-10	42.94	269.80	0.320	>3	
X-15 Flt. 1-1-5	3.44	21.62	0.845	1	
T-38 Bobweight Closed	16.08	101.01	1.605	2	
T-38 Bobweight Open	13.65	85.76	1.437	2	
YF-12 Rigid Body Only	6.25	39.25	1.200	1	
YF-12 Rigid Body + Flex			1.256		
Shuttle Alt-5	19.40	121.89	0.514	2	
Shuttle STS-4 (Fit)	14.07	88.41	0.453	2	
F-8 DFBW CAS + 100 msec	27.20	170.89	0.480	3	
F-8 DFBW Direct + 100 msec	33.31	209.29	0.370	>3	
F-8 DFBW Direct	23.05	144.81	0.414	3	
F-8 DFBW SAS	16.59	104.23	0.662	2	
B-2 Off-Nominal Approach	24.00	150.80	0.398	3>3	
B-2 Refueling	8.67	54.45	0.955	1	



$$\frac{\theta}{\delta} = \frac{2.46E+07 (.0845)(.699)}{[.15, .17][.63, 2.41][.6, 26][.7, 75]}$$

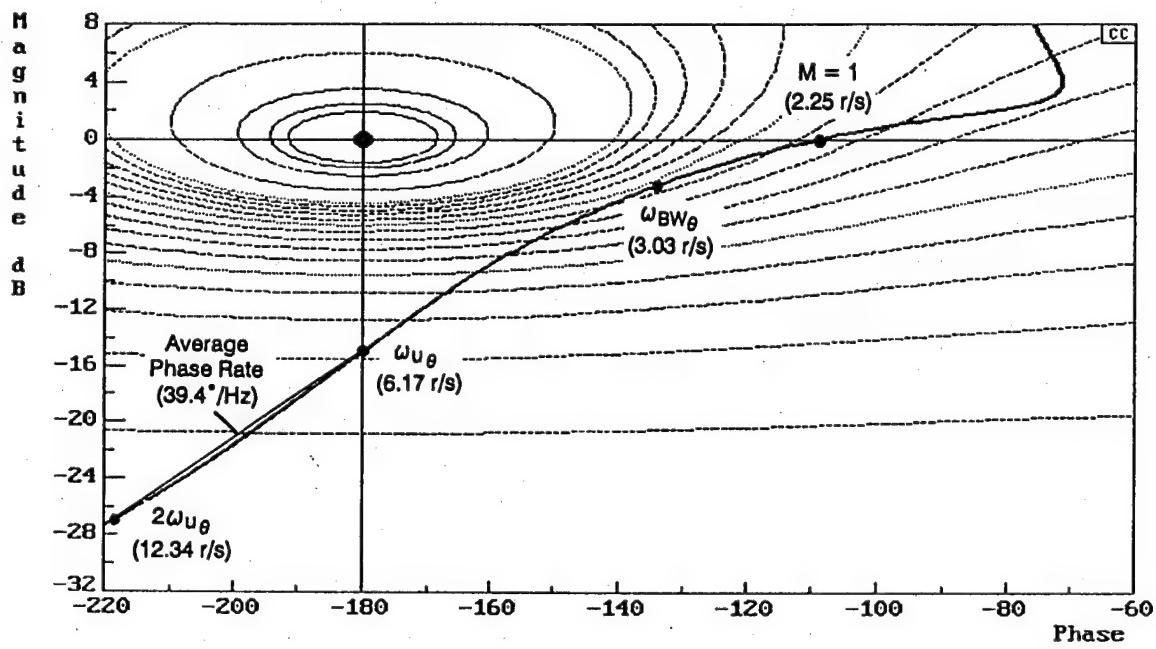
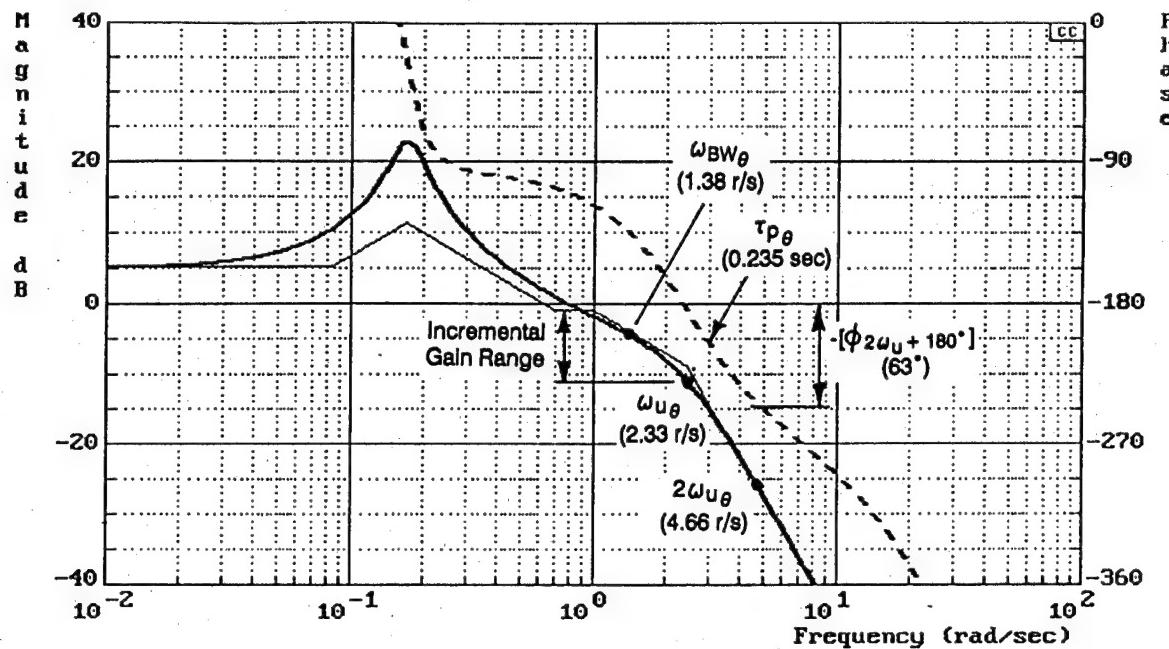


Figure B-1. Have PIO Configuration 2-1 (Baseline)



$$\frac{\theta}{\delta} = \frac{1.98E+07 (.0845)(.699)}{[.15, .17](1)[.63, 2.41][.6, 26][.7, 75]}$$

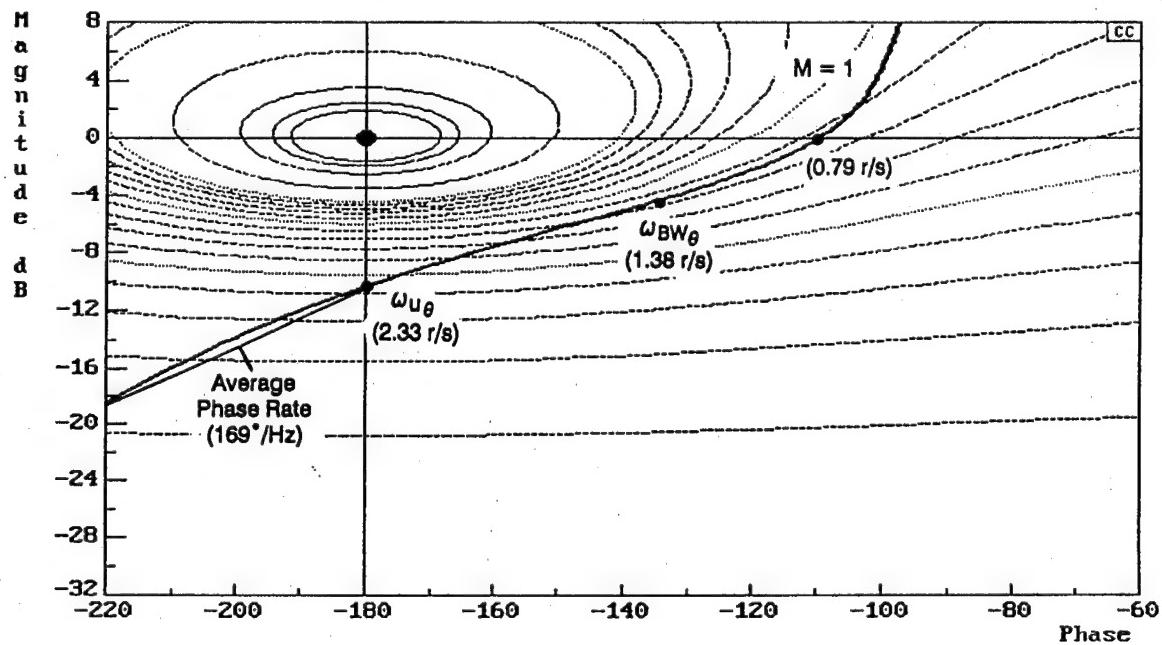
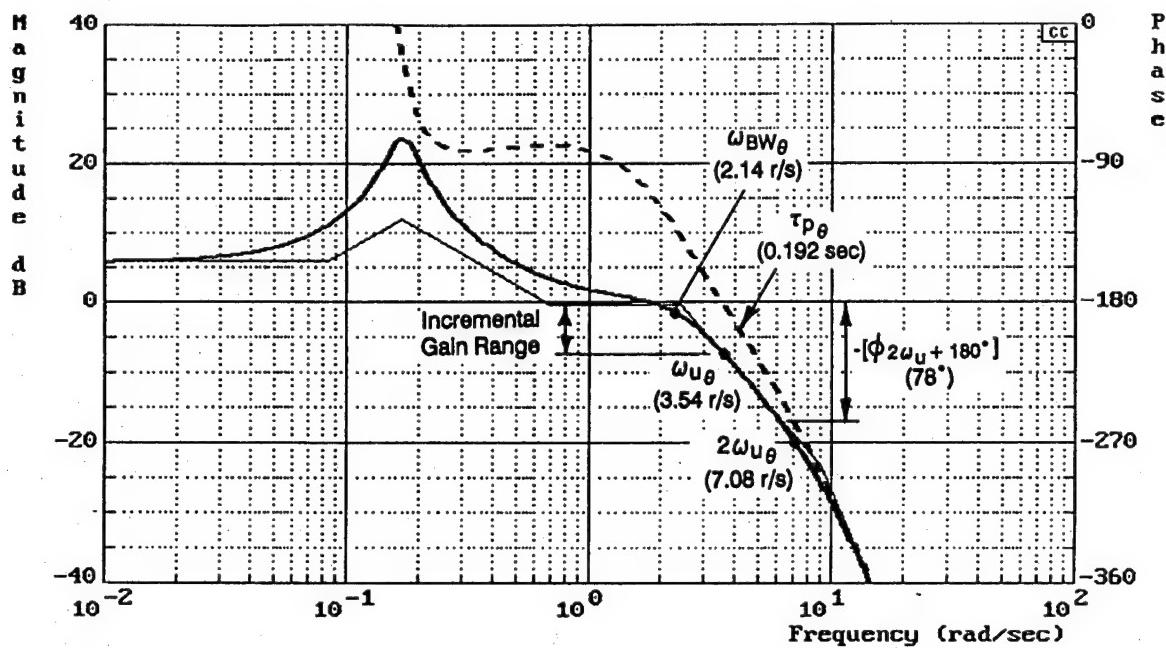


Figure B-2. Have PIO Configuration 2-5



$$\frac{\theta}{\delta} = \frac{1.72E+09 (.0845)(.699)}{[.15, .17][.63, 2.41][.7, 9][.6, 26][.7, 75]}$$

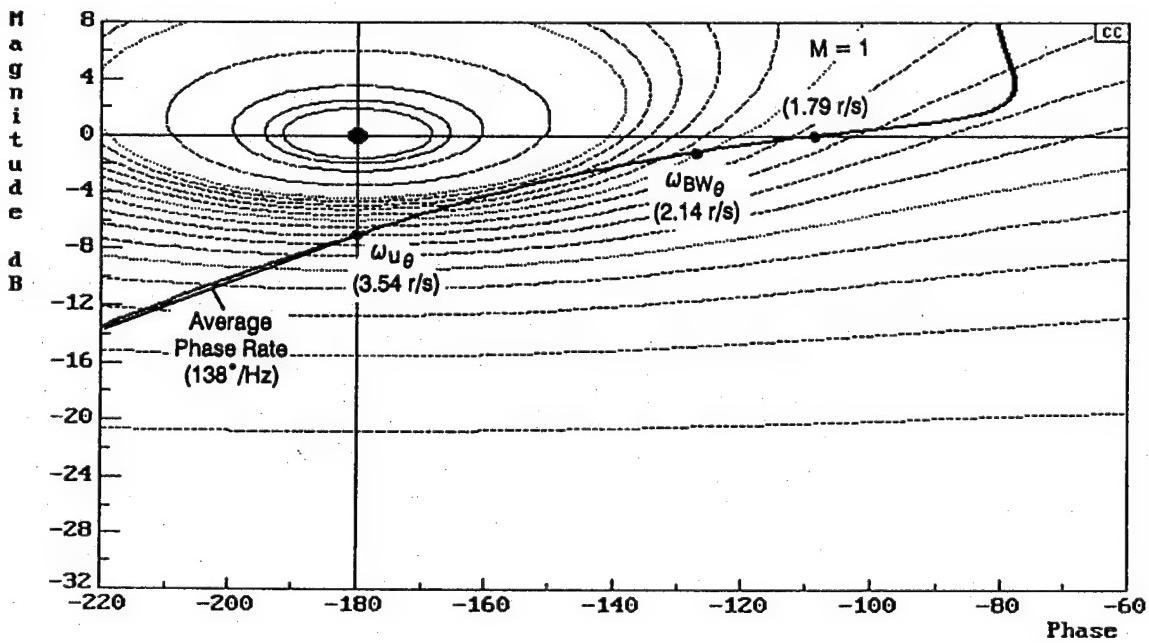
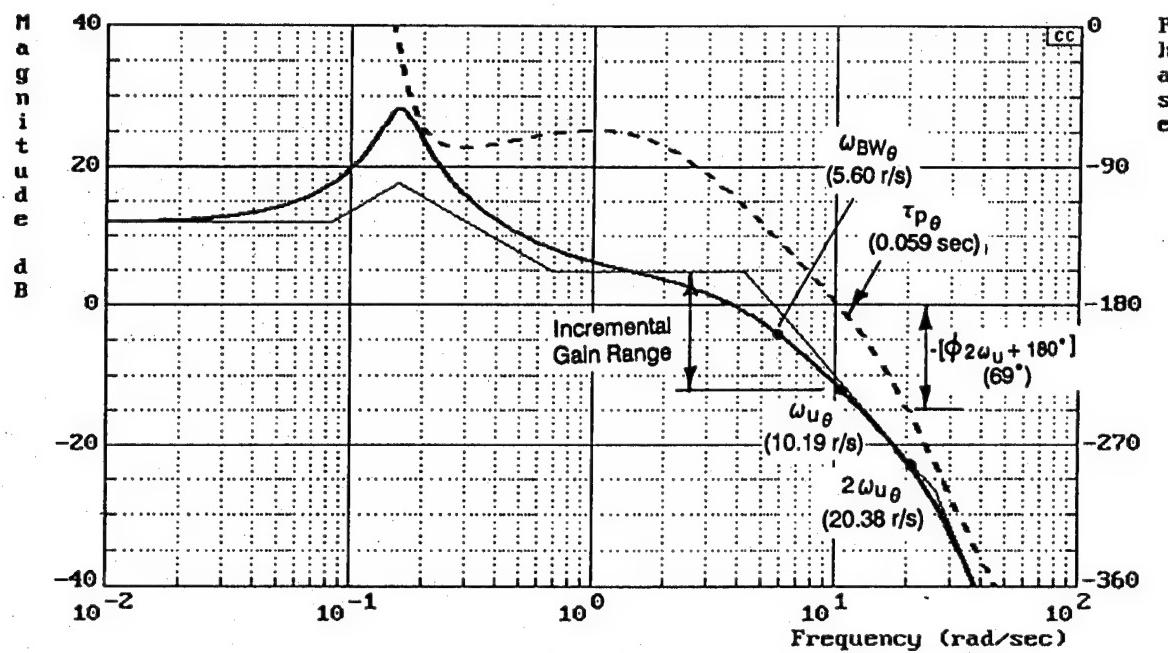


Figure B-3. Have PIO Configuration 2-8



$$\frac{\theta}{\delta} = \frac{1.17E+08 (.0847)(.699)}{[.17, .16][.97, 4.22][.6, 26][.7, 75]}$$

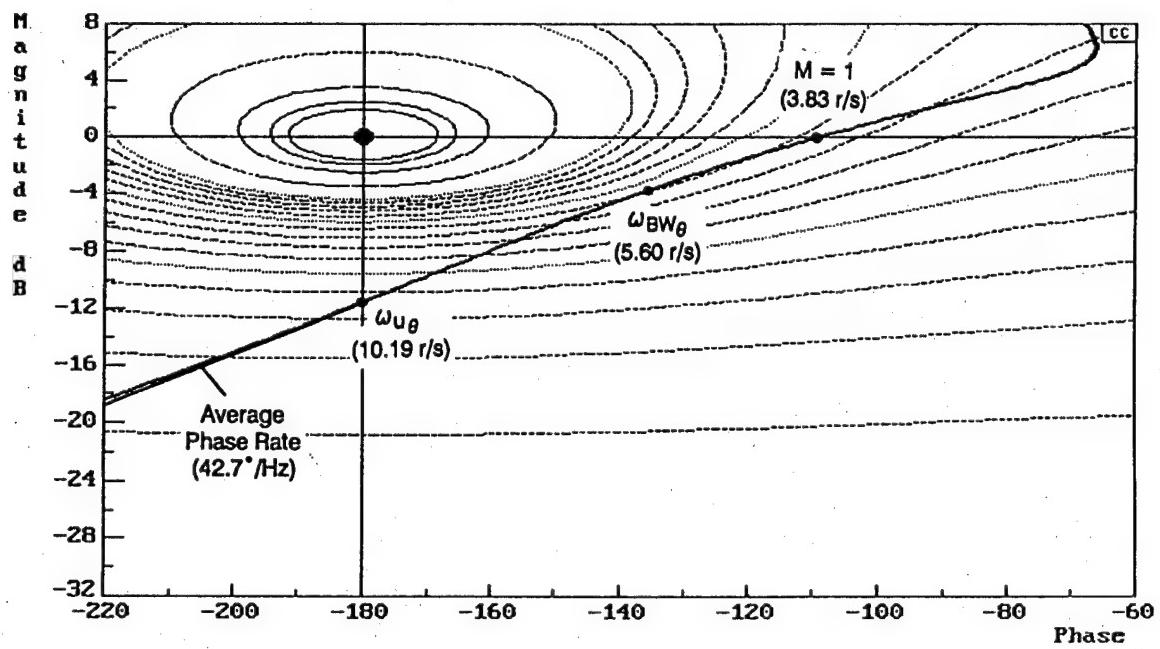
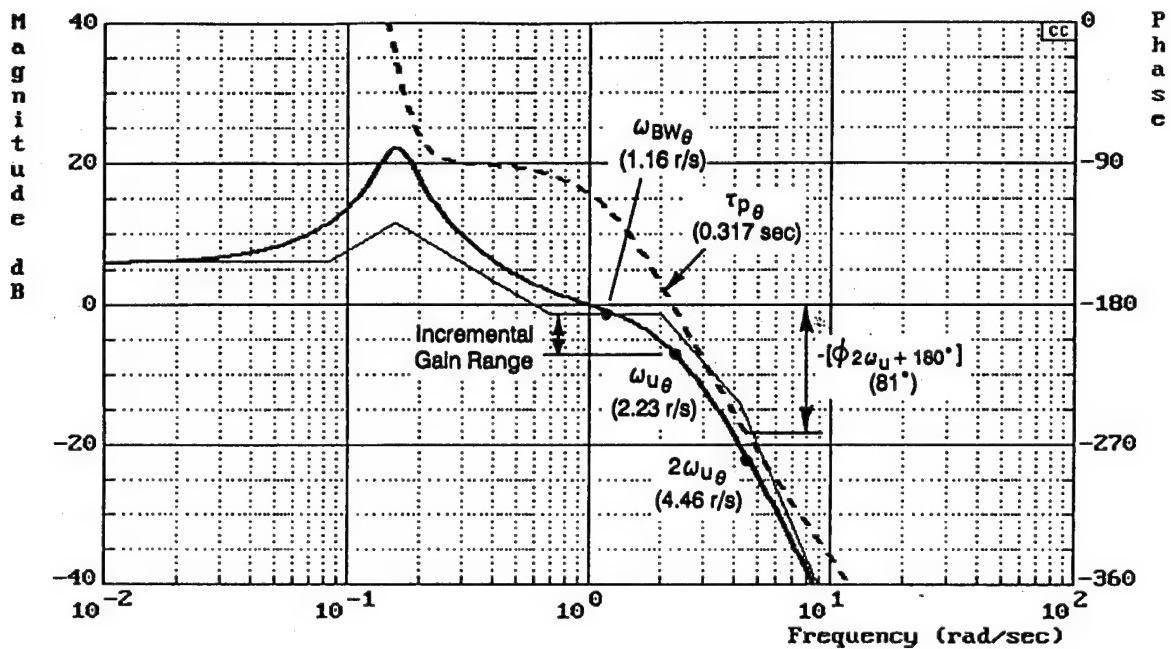


Figure B-4. Have PIO Configuration 3-1 (Baseline)



$$\frac{\theta}{\delta} = \frac{2.35E+08 (.0847)(.699)}{[.17, .16][.7, 2][.97, 4.22][.6, 26][.7, 75]}$$

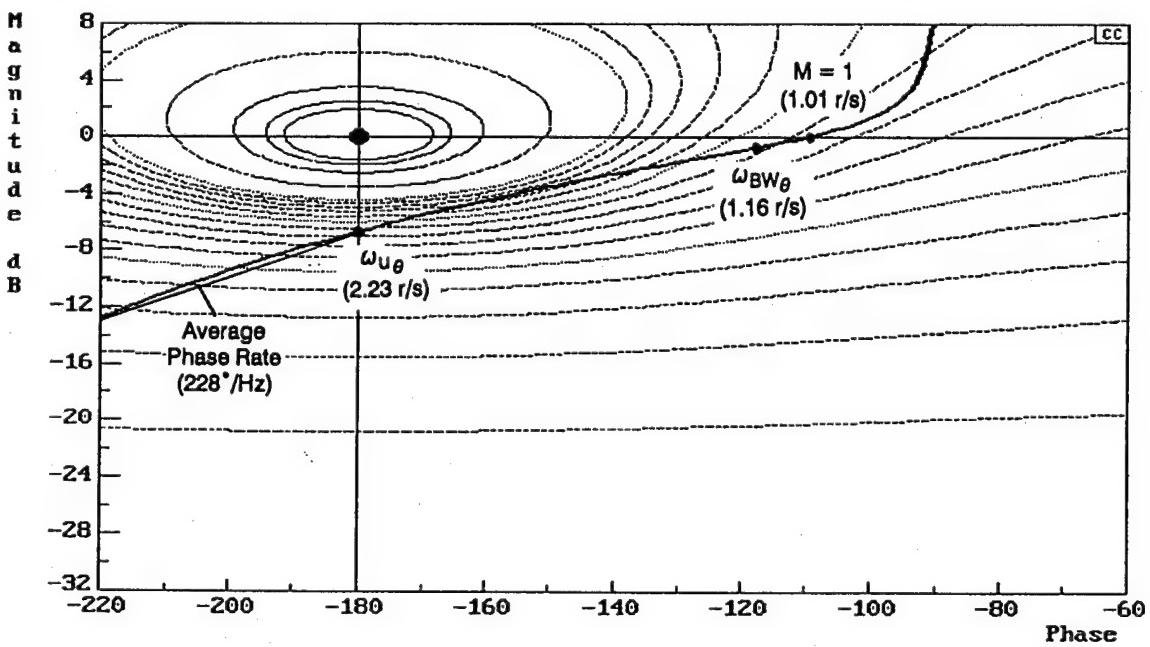
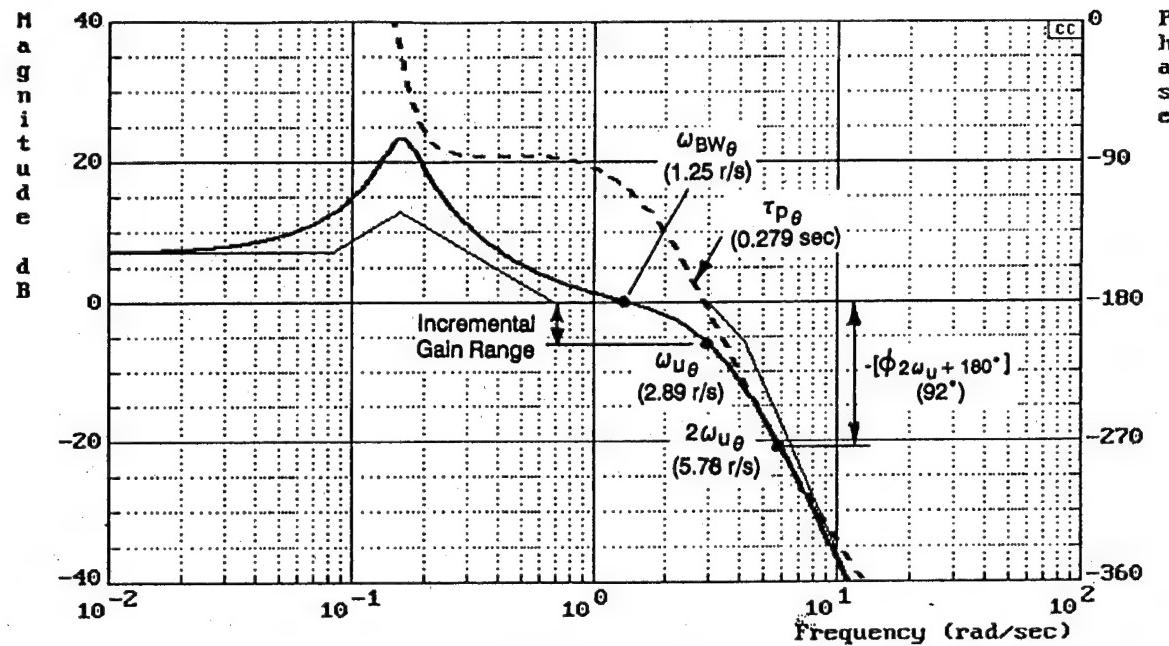


Figure B-5. Have PIO Configuration 3-12



$$\frac{\theta}{\delta} = \frac{6.07E+08 (.0847)(.699)}{[.17, .16][.7, 3][.97, 4.22][.6, 26][.7, 75]}$$

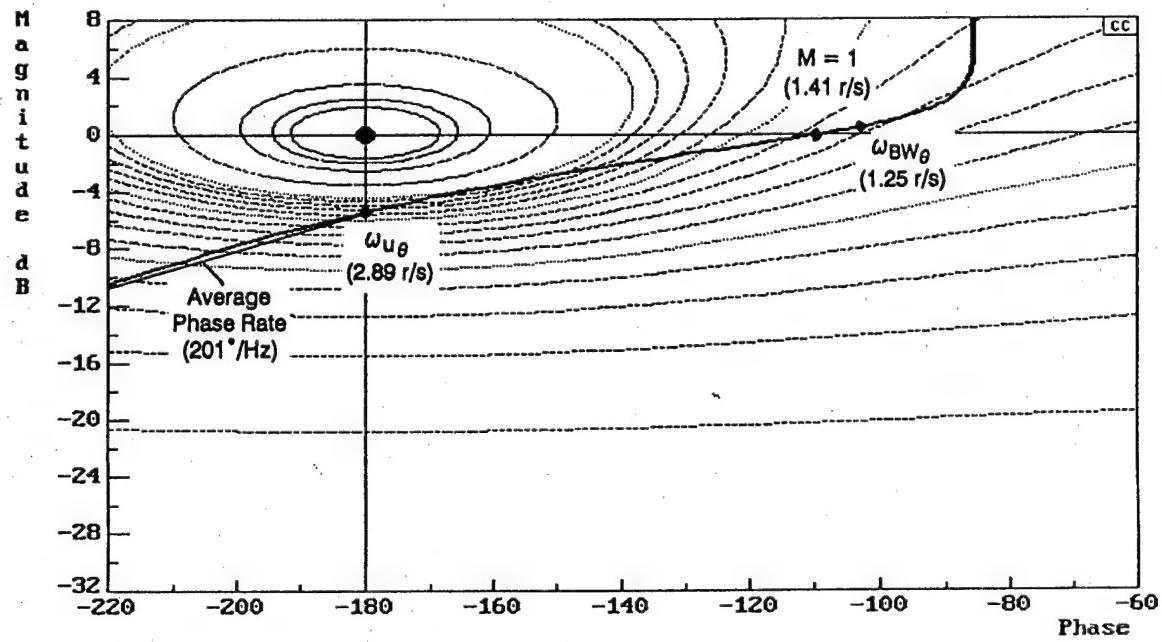
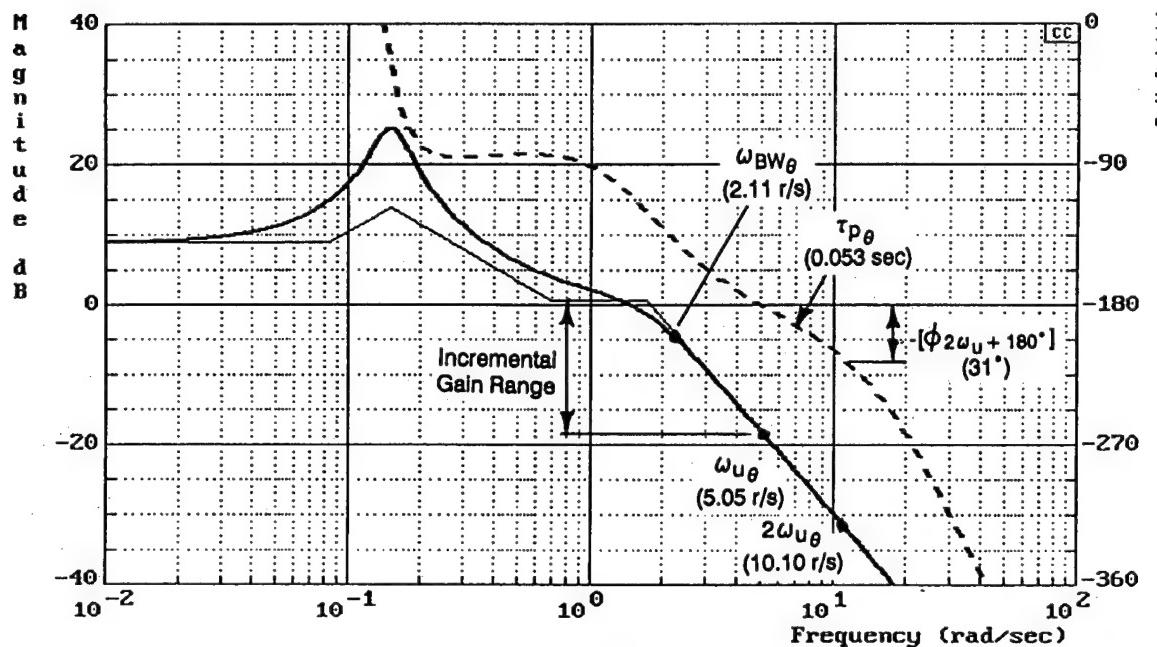


Figure B-6. Have PIO Configuration 3-13



$$\frac{\theta}{\delta} = \frac{1.18E+07 (.0845)(.699)}{[.16, .15][.68, 1.7][.6, 26][.7, 75]}$$

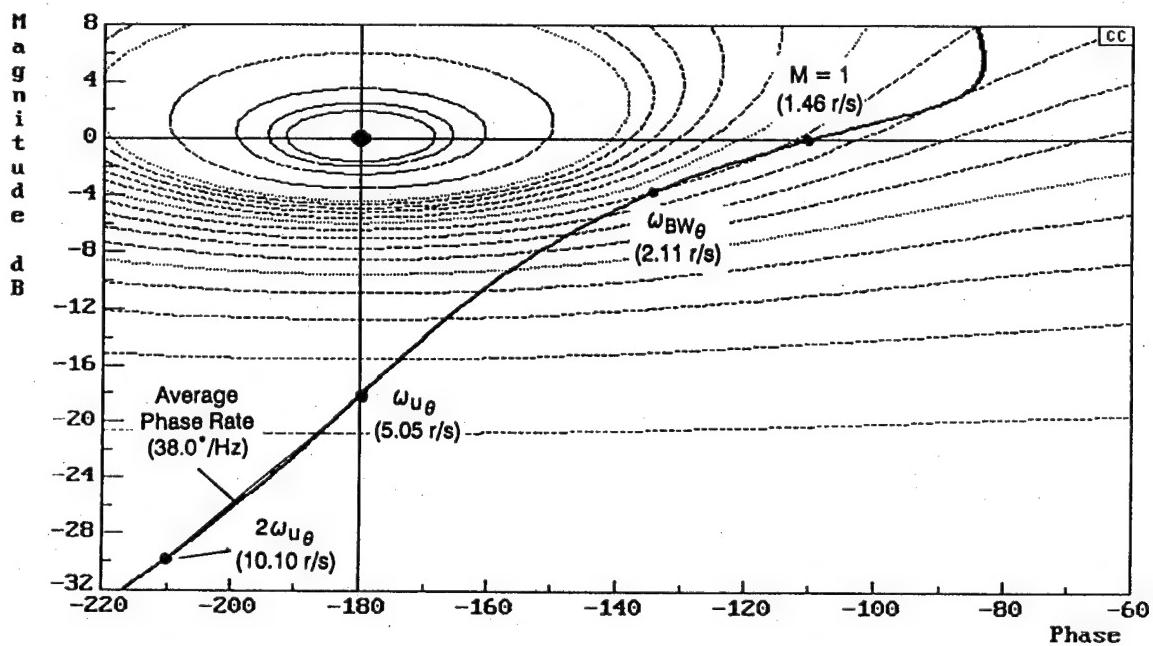
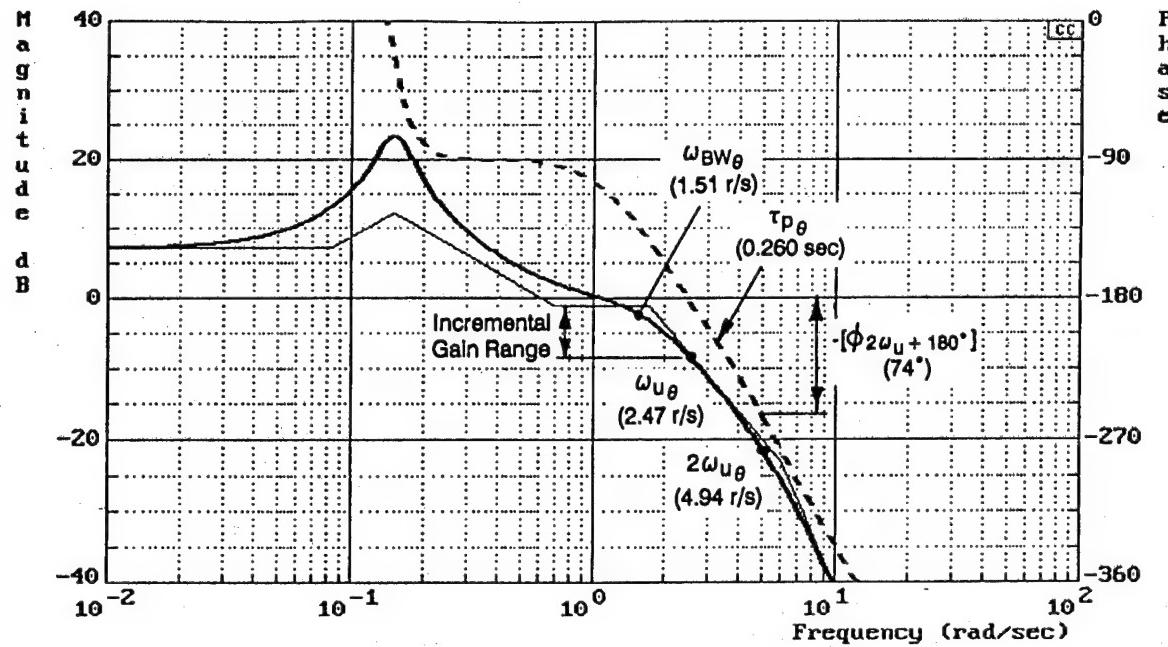


Figure B-7. Have PIO Configuration 5-1 (Baseline)



$$\frac{\theta}{\delta} = \frac{3.45E+08 (.0845)(.699)}{[.16, .15][.68, 1.7][.7, 6][.6, 26][.7, 75]}$$

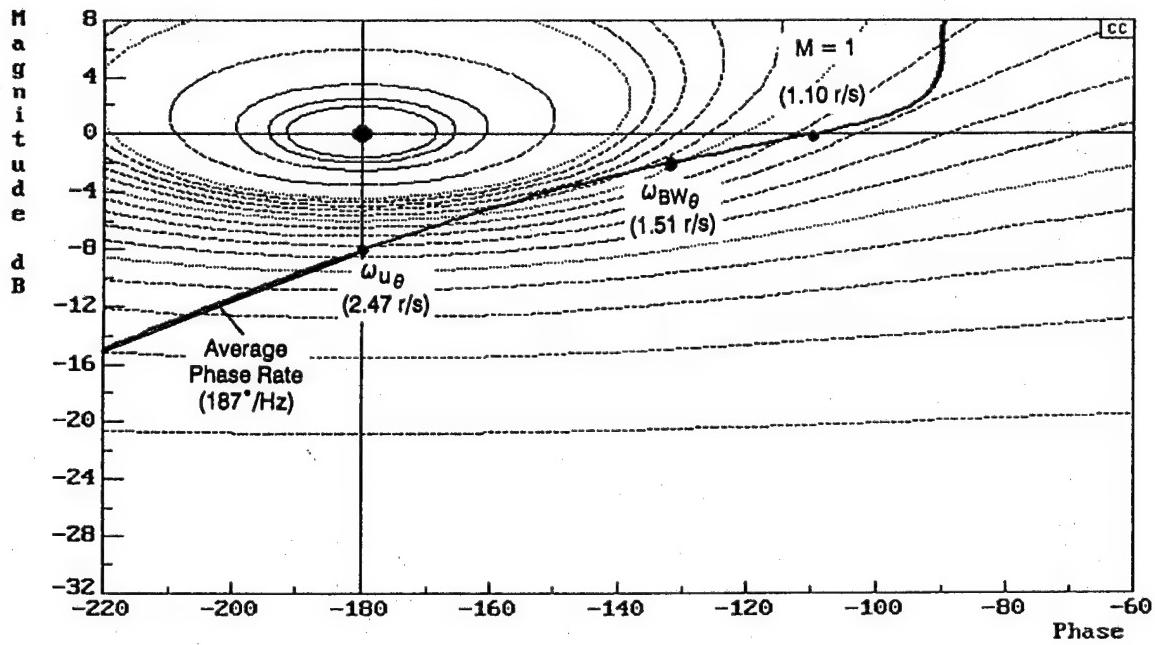
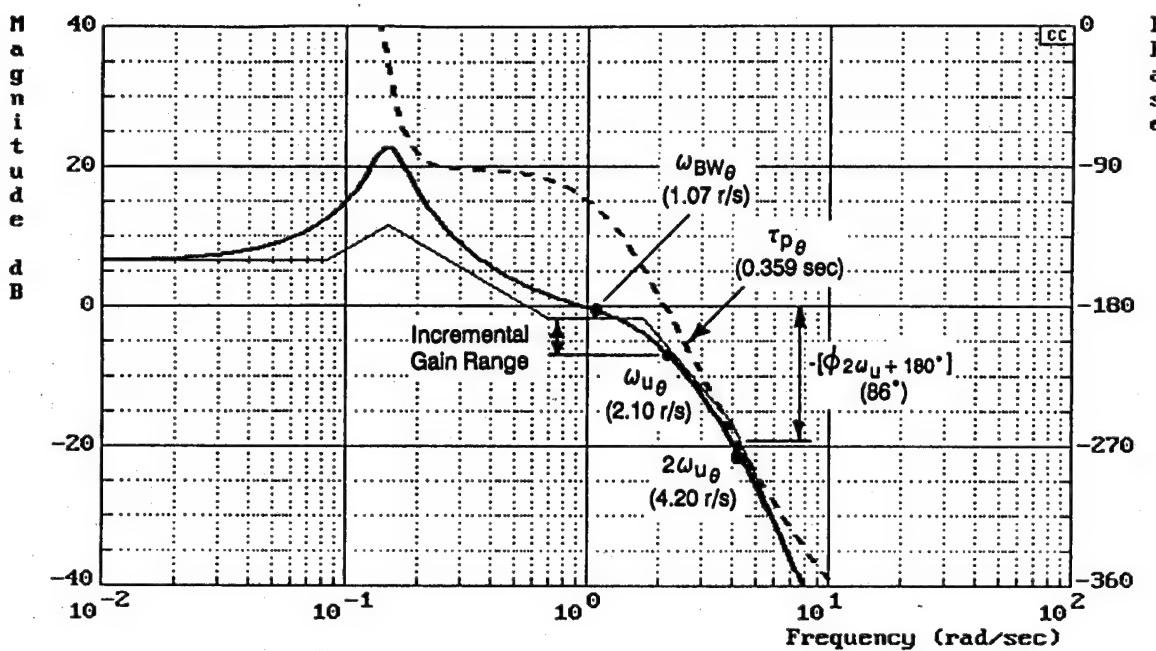


Figure B-8. Have PIO Configuration 5-9



$$\frac{\theta}{\delta} = \frac{1.43E+08 (.0845)(.699)}{[.16, .15][.68, 1.7][.7, 4][.6, 26][.7, 75]}$$

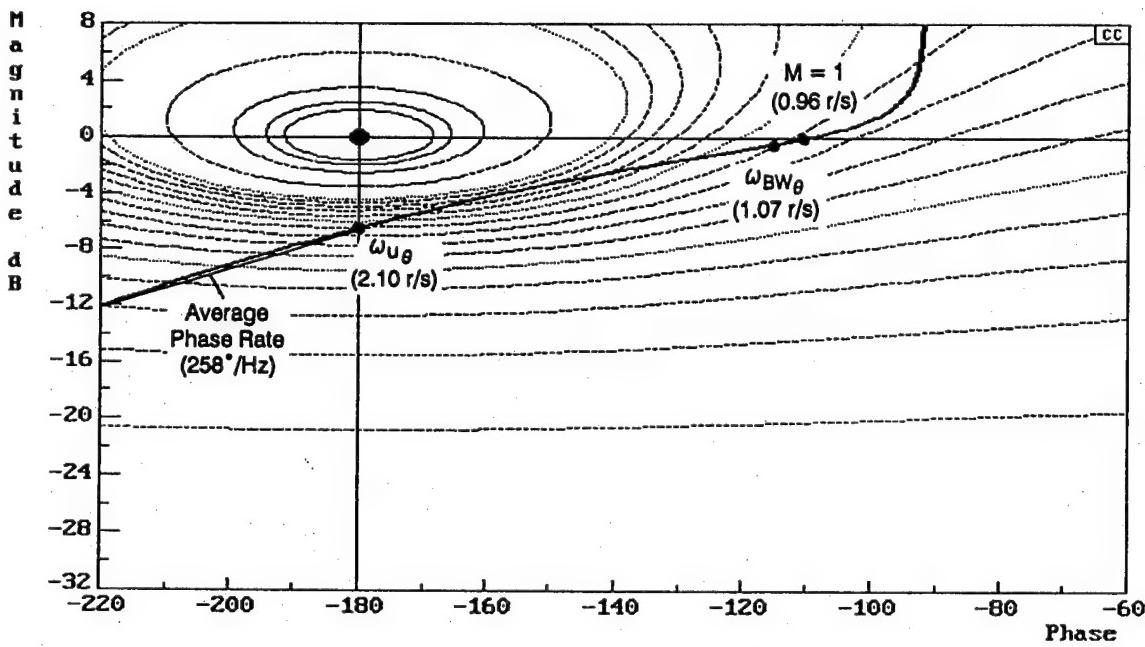
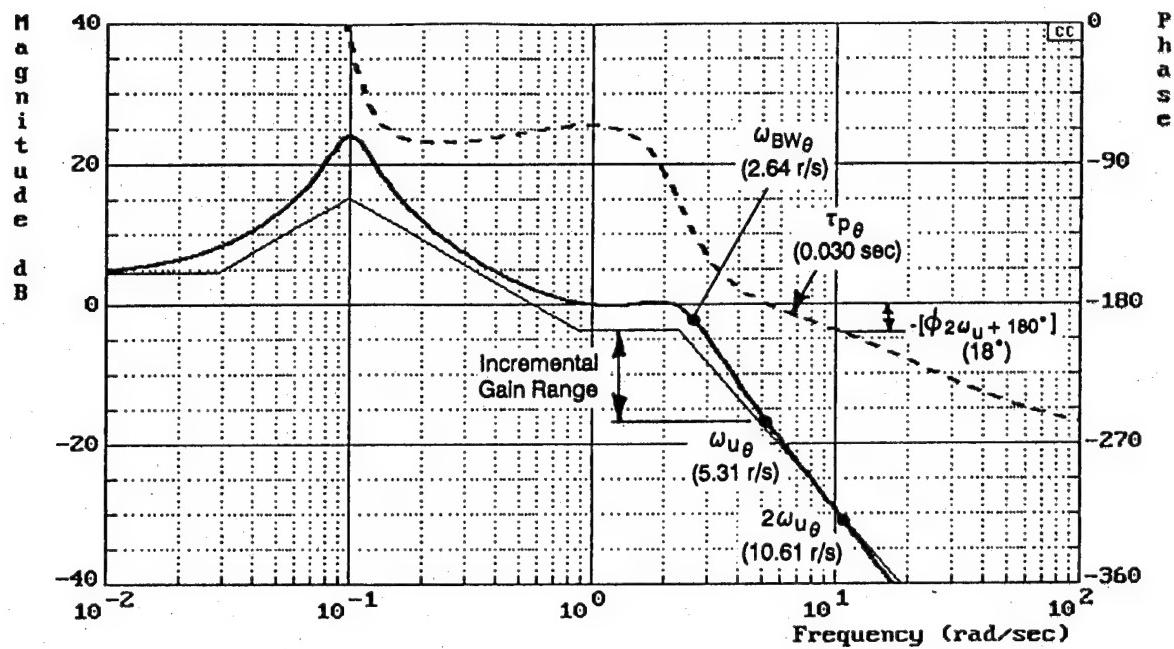


Figure B-9. Have PIO Configuration 5-10



$$\frac{\theta}{\delta} = \frac{86.9 (.0292)(.883)}{[.19, .1][.366, 2.3](25)}$$

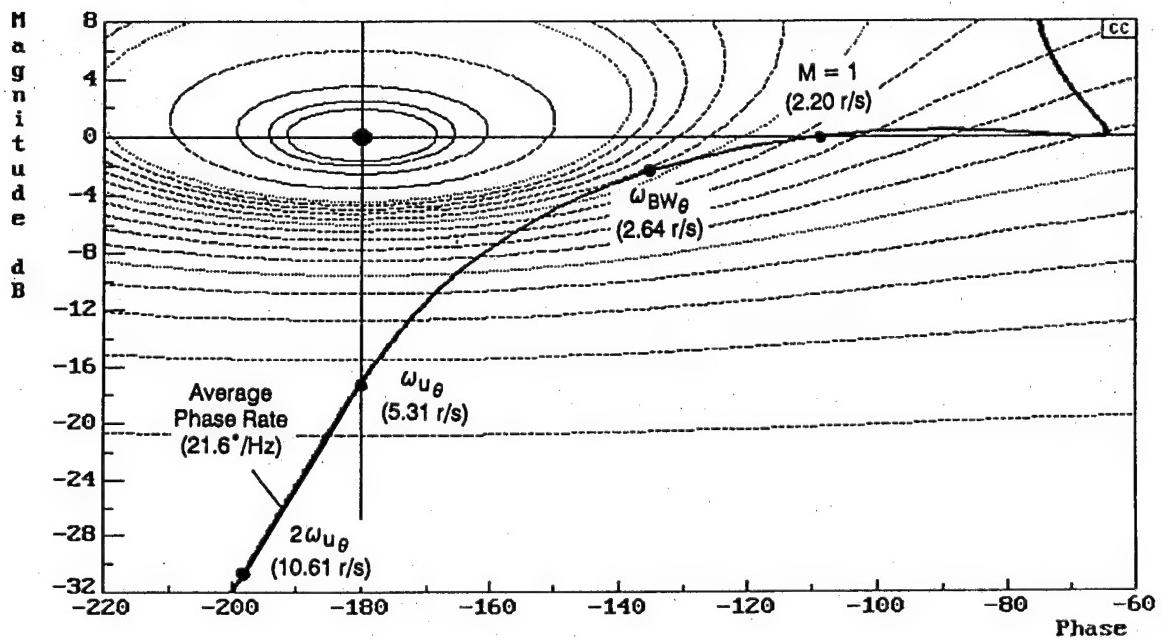
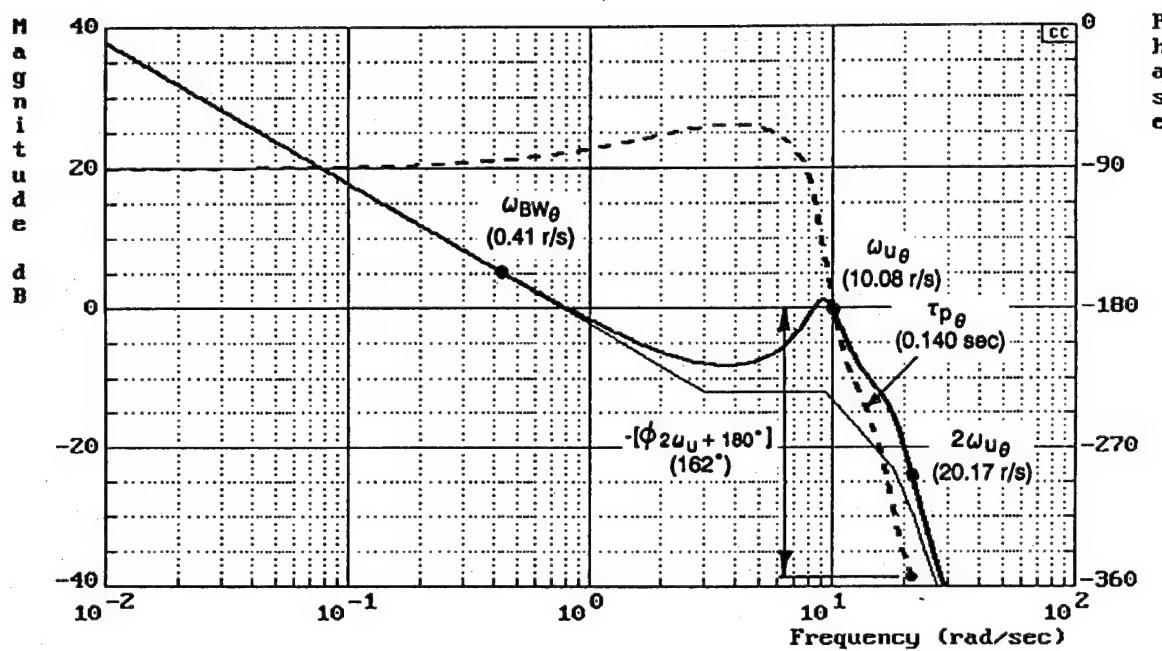


Figure B-10. X-15 Flight 1-1-5



$$\frac{\theta}{\delta} = \frac{153000 (3.08)}{(0)[.141, 9.34][.212, 17.8](21.7)}$$

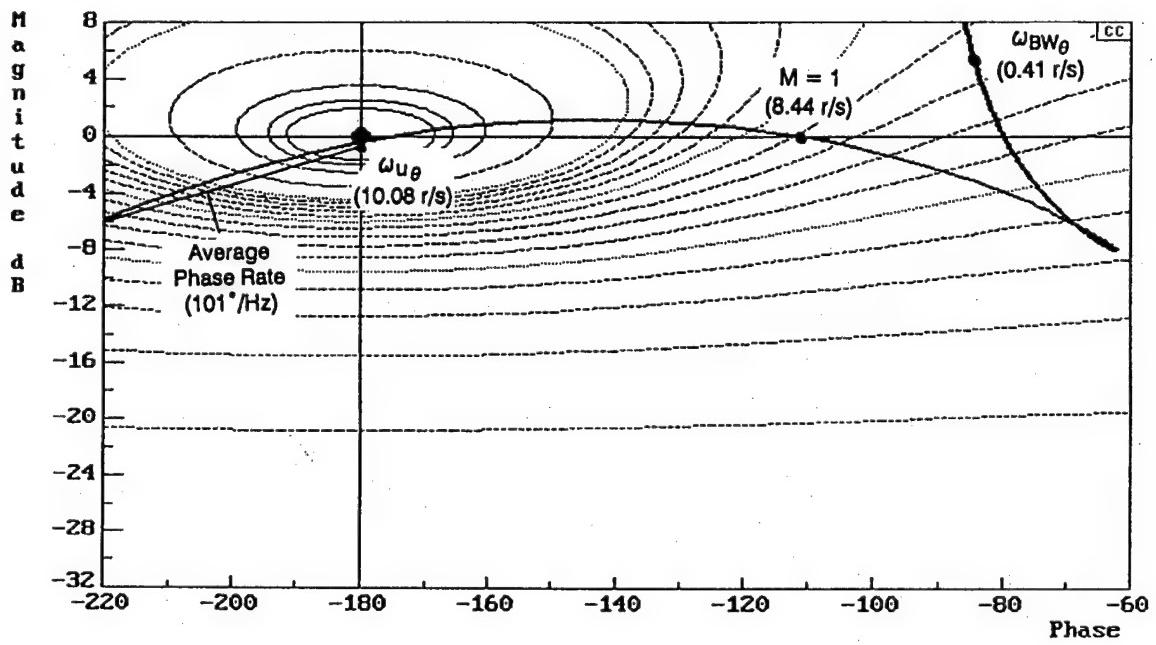
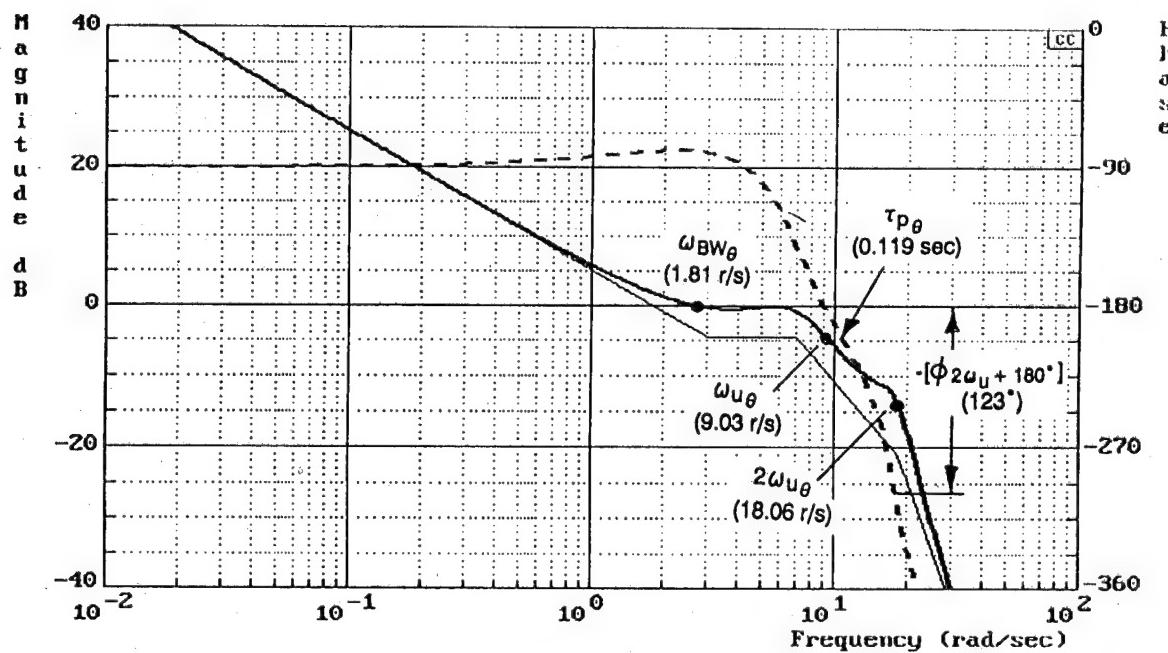


Figure B-11. T-38 with Bobweight Loop Closed



$$\frac{\theta}{\delta} = \frac{190000 (3.08)}{(0)[.39, 7.01][.18, 18](20)}$$

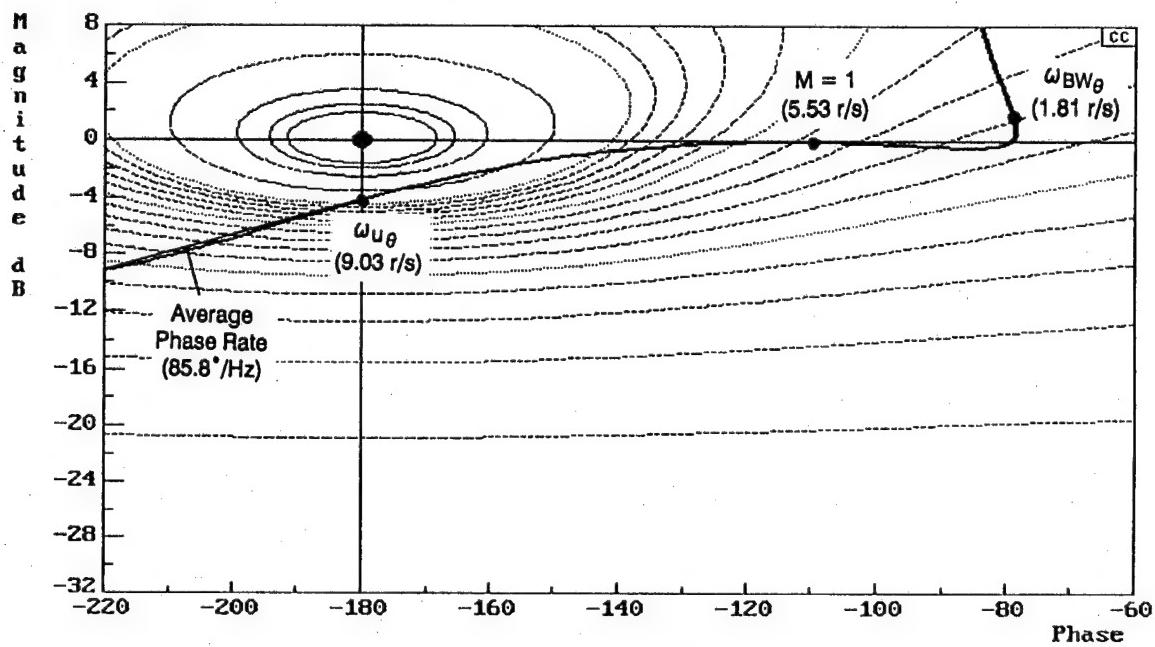
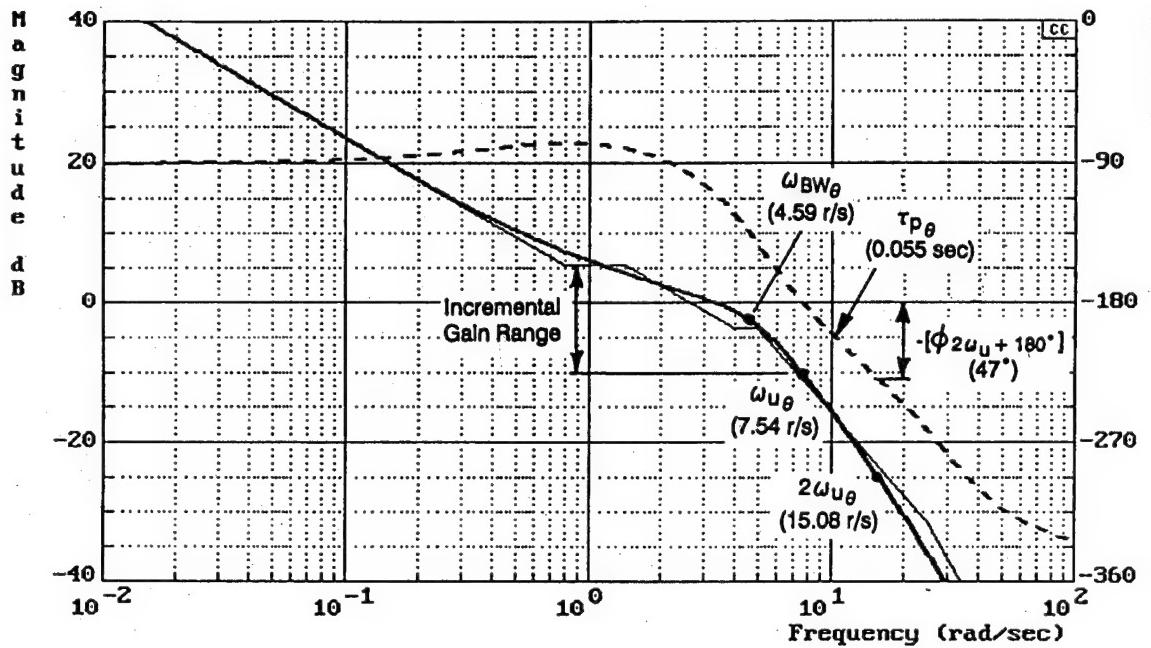


Figure B-12. T-38 with Bobweight Loop Open



$$\frac{\theta}{\delta} = \frac{10000 (.8)(4)[.671, 50.5]}{(0)(1.42)[.587, 4.95](24.7)[.647, 39.7](40.5)}$$

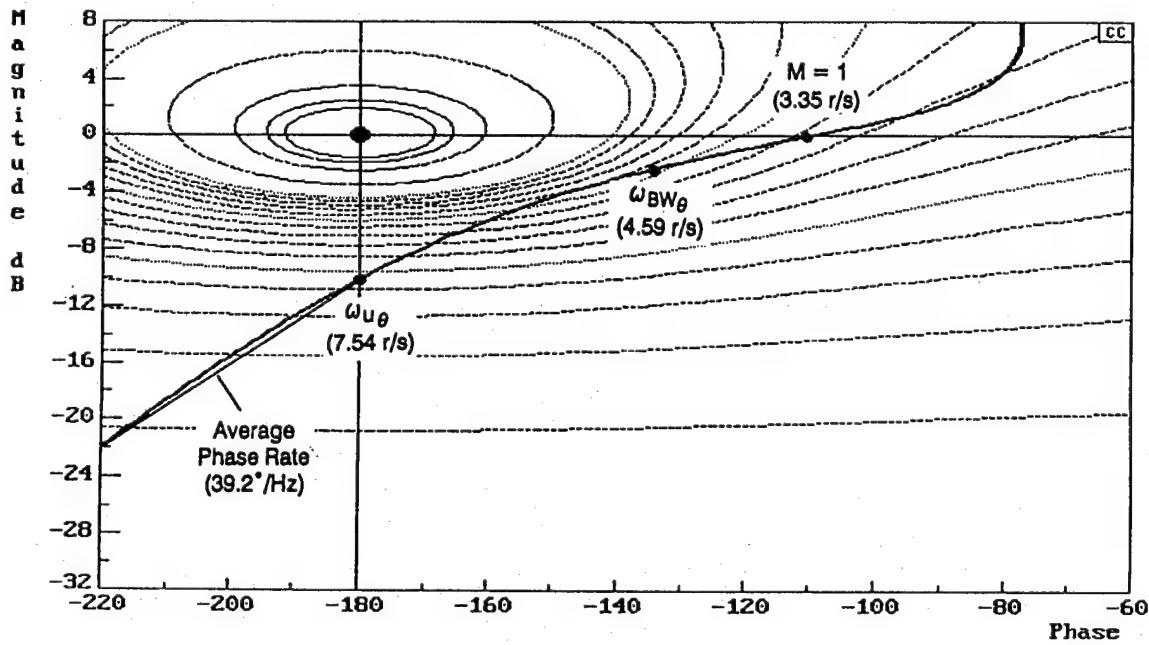
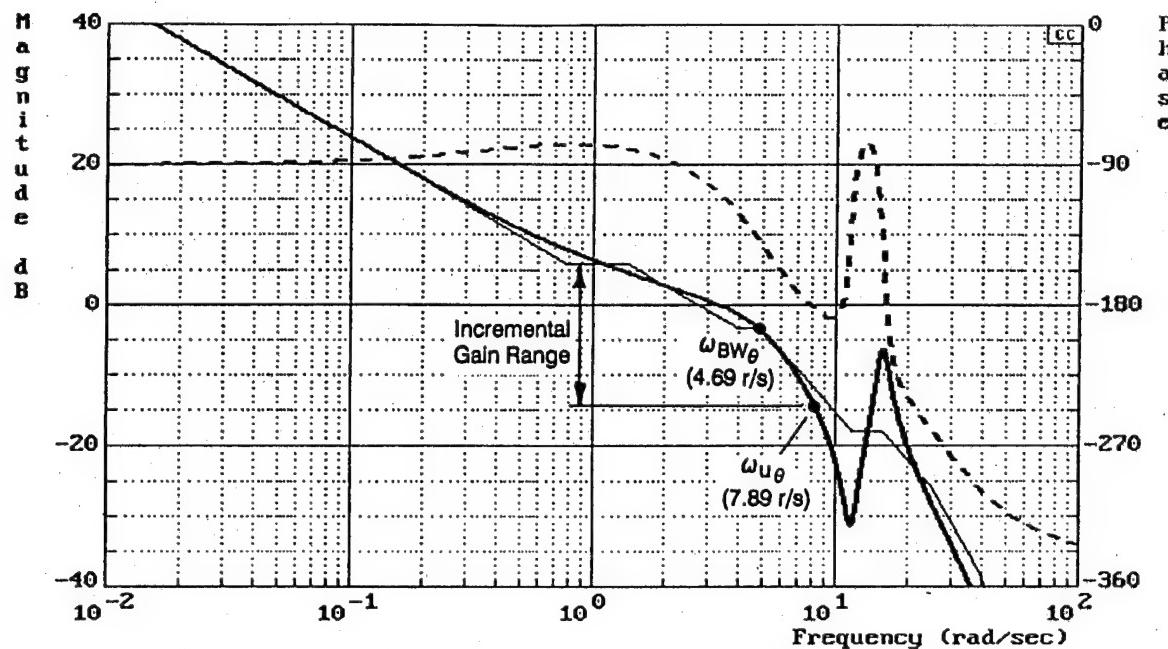


Figure B-13. YF-12 Rigid Body Only



$$\frac{\theta}{\delta} = \frac{19300 (.79)(4)[.0509, 11.6][.671, 50.5]}{(0)(1.42)[.587, 4.95][.05, 15.7](24.7)[.647, 39.7](40.5)}$$

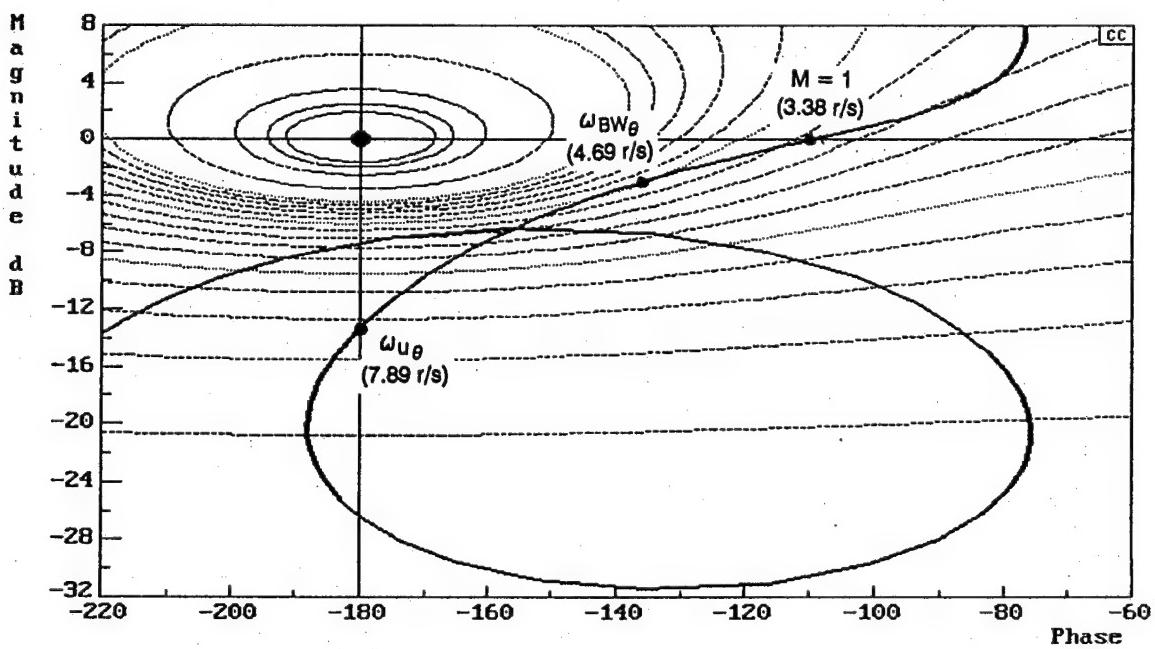
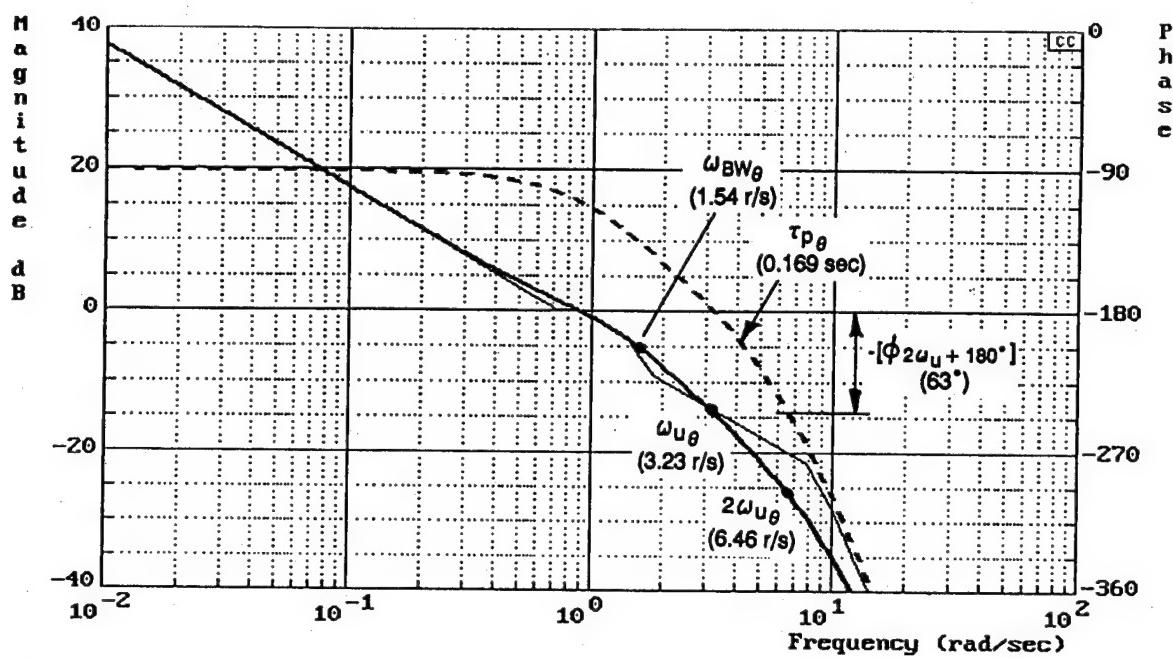


Figure B-14. YF-12 Rigid Body with Flexible Mode



$$\frac{\theta}{\delta} = \frac{214000 (.042)(.72)(1.5)(1.8)[.02, 32.8](50)}{(0)(.041)(.87)[.8, 1.4][.99, 7.67](10)[.49, 21][.71, 36.4](51.2)}$$

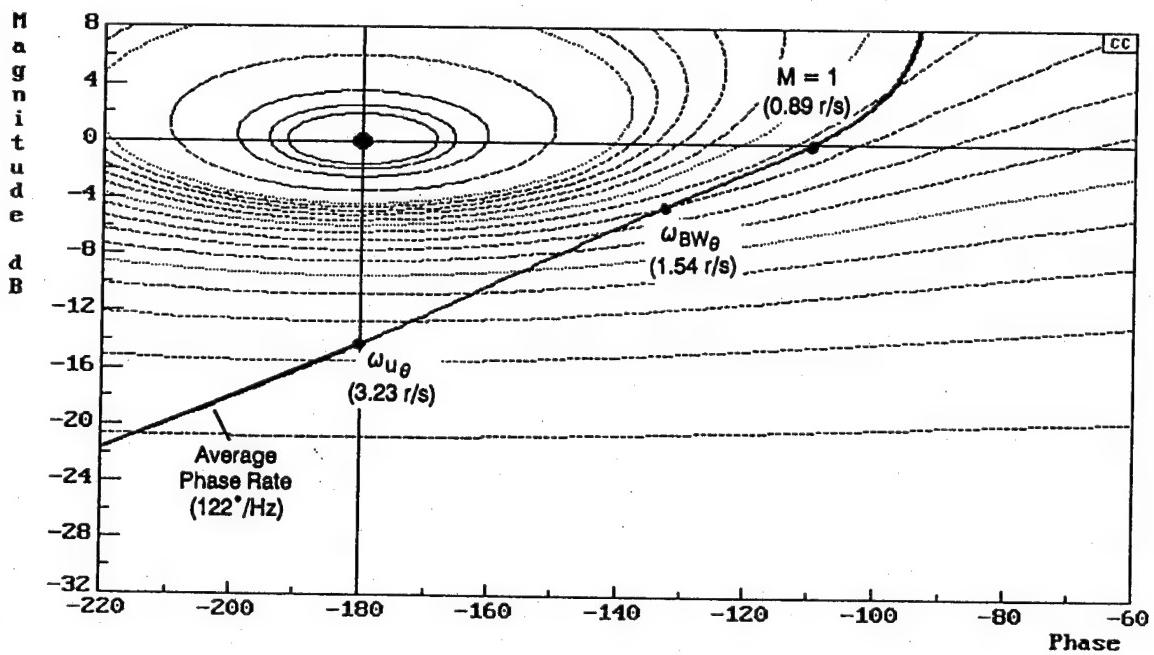
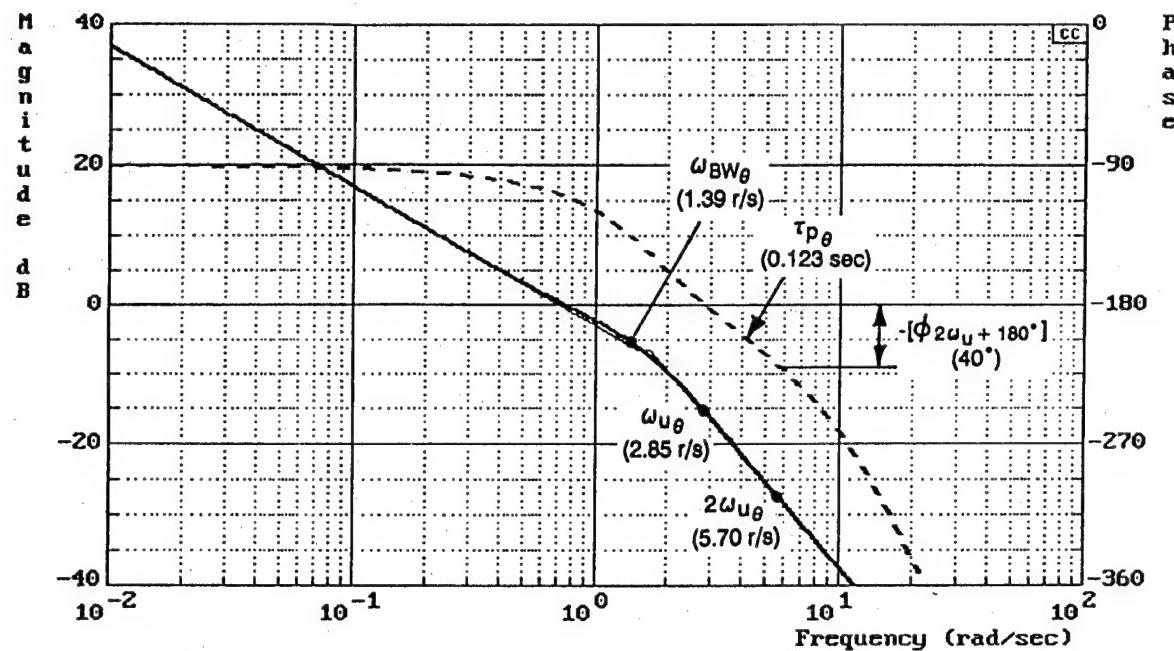


Figure B-15. Shuttle ALT-5



$$\frac{\theta}{\delta} = \frac{1.33(1.5)[- .866, 22.2]}{(0)[.74, 1.68][.866, 22.2]}$$

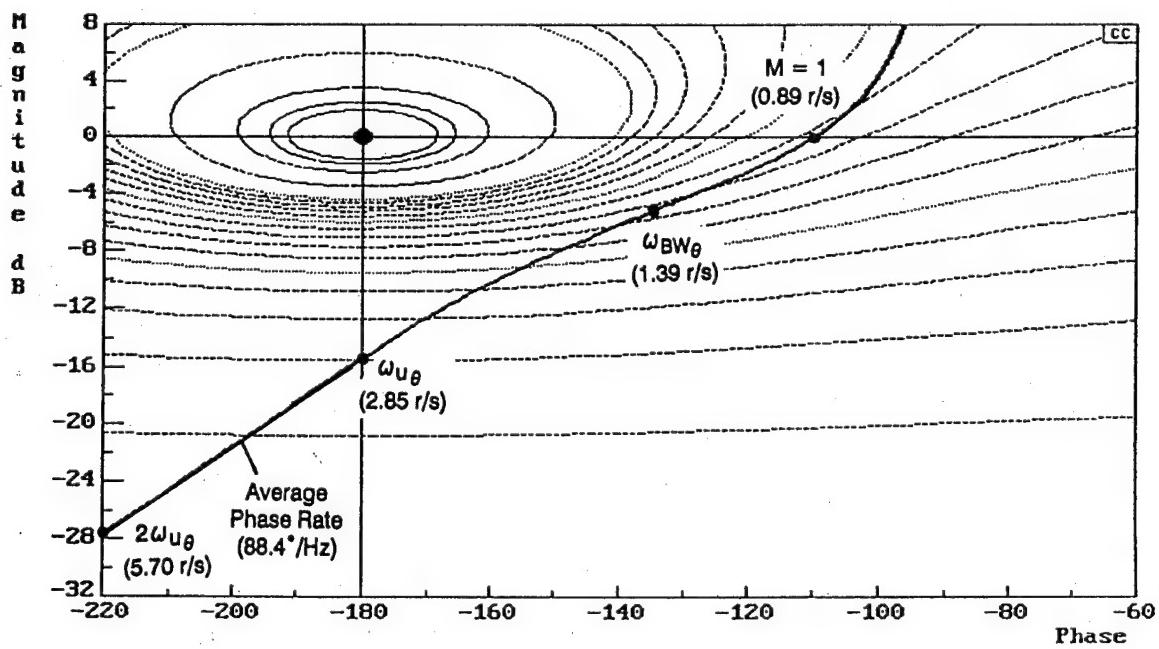
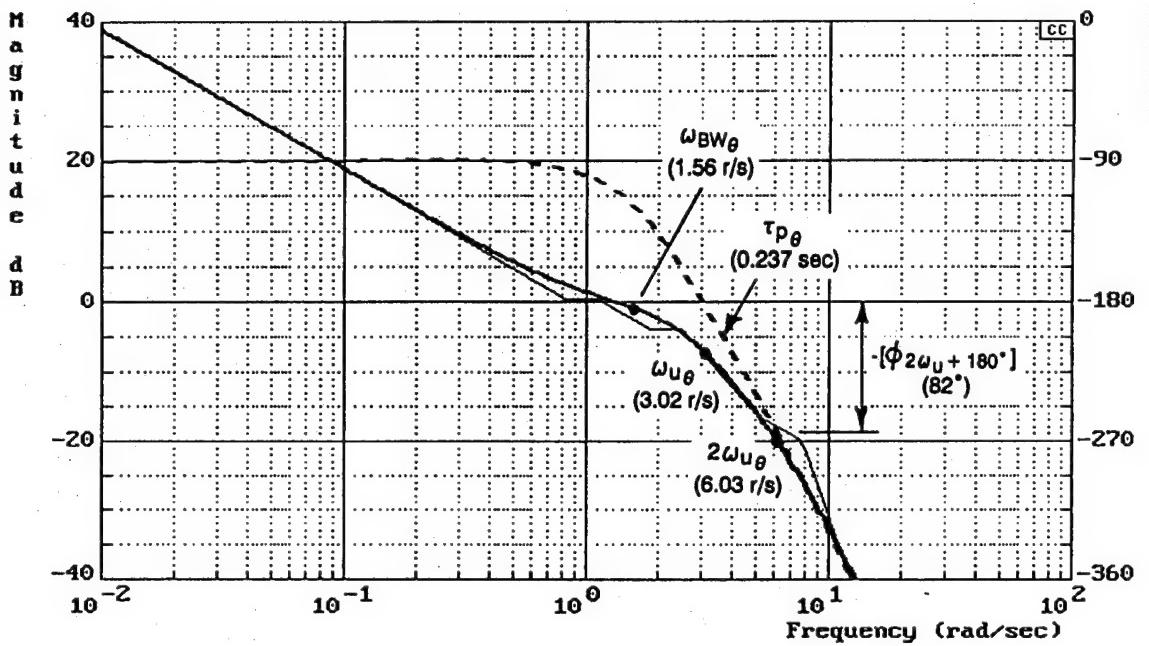


Figure B-16. Shuttle STS-4 (fit)



$$\frac{\theta}{\delta} = \frac{281000 (.826)(1.85)(5)[.864, 13.3][- .866, 34.6][- .866, 115]}{(0)(1.11)[.65, 2.49][.91, 7.42][0.782, 7.95][.866, 34.6][.653, 112][.845, 139]}$$

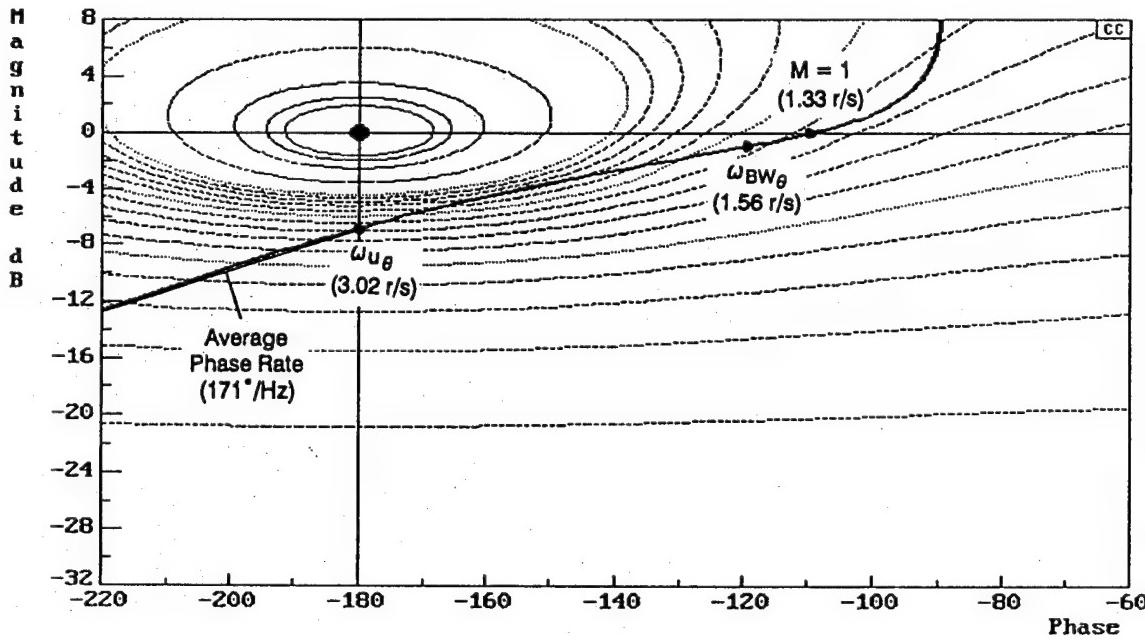
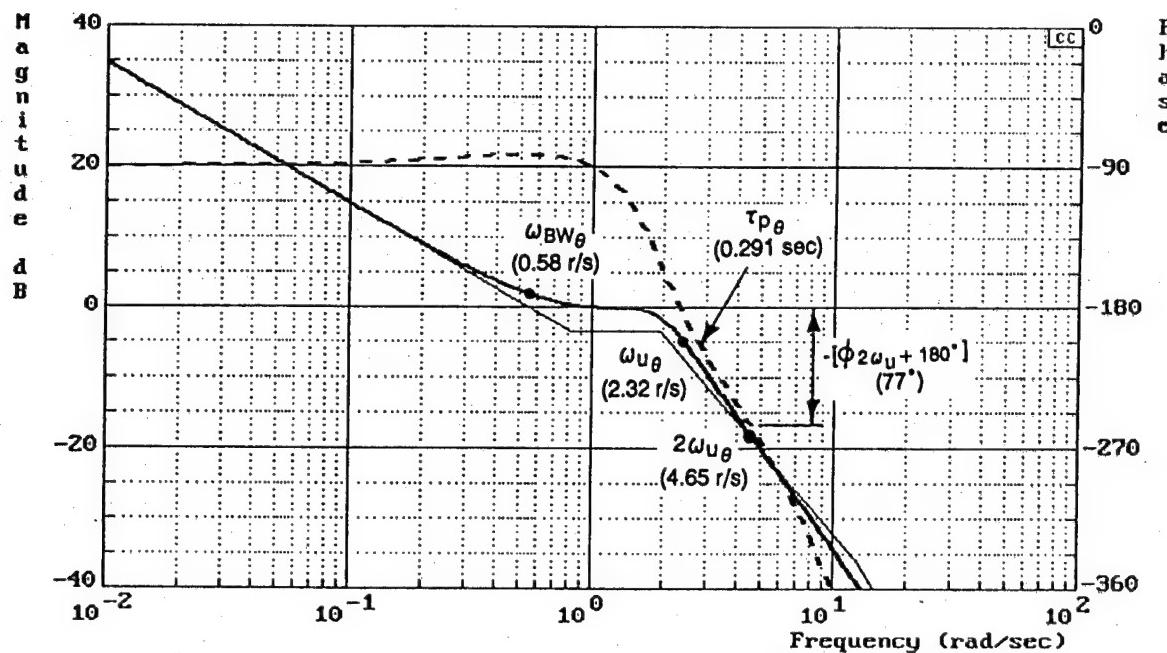


Figure B-17. F-8 DFBW CAS Mode + 100 msec Added Delay



$$\frac{\theta}{\delta} = \frac{2.42E+07 (.826)[- .866, 26.6][- .866, 34.6]}{(0)[.42, 1.91](12.5)[.866, 26.6][.866, 34.6](50)[.698, 126]}$$

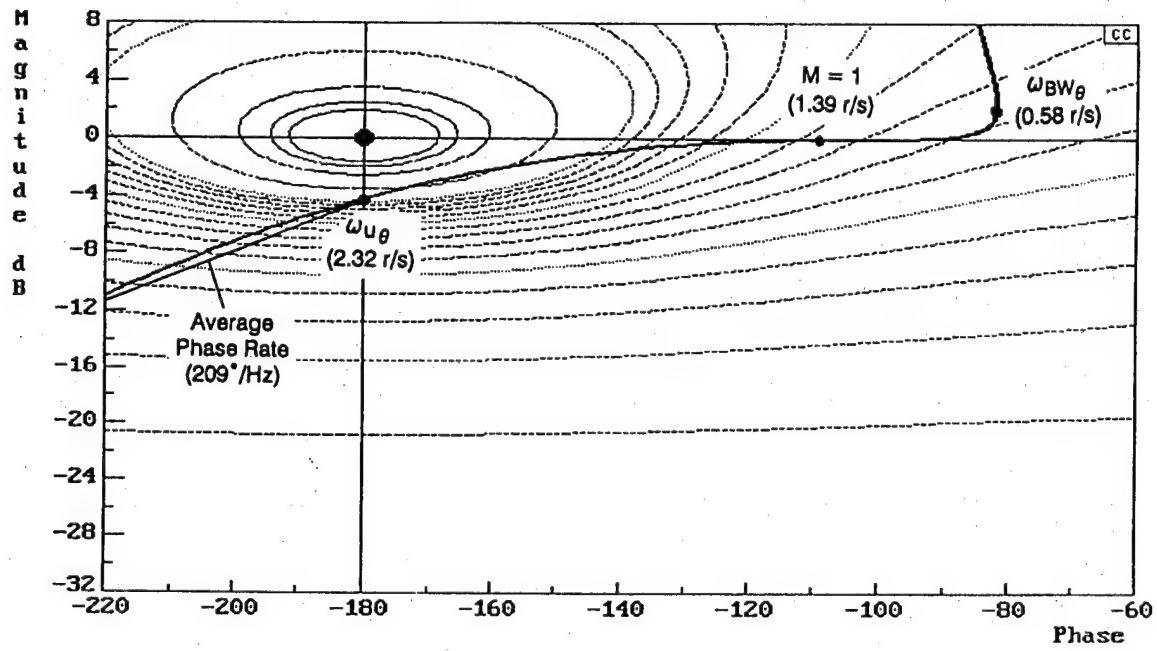
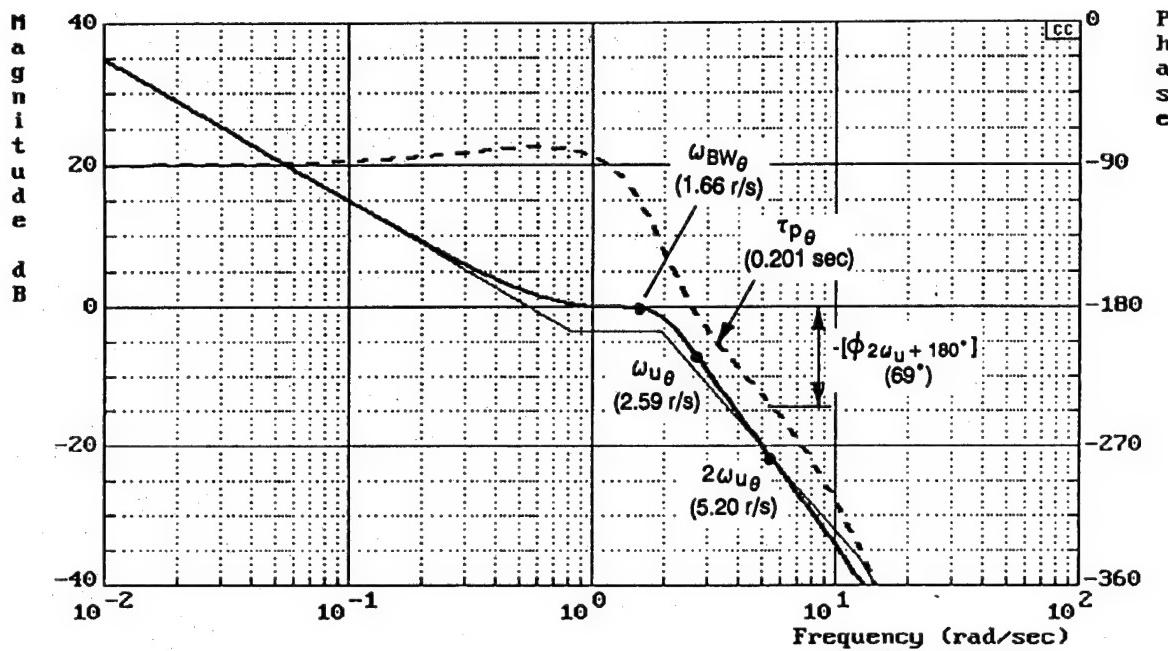


Figure B-18. F-8 DFBW Direct Mode + 100 msec Added Delay



$$\frac{\theta}{\delta} = \frac{2.44E+07 (.826)[-866, 26.6]}{(0)[.42, 1.91](12.5)[.866, 26.6](50)[.698, 126]}$$

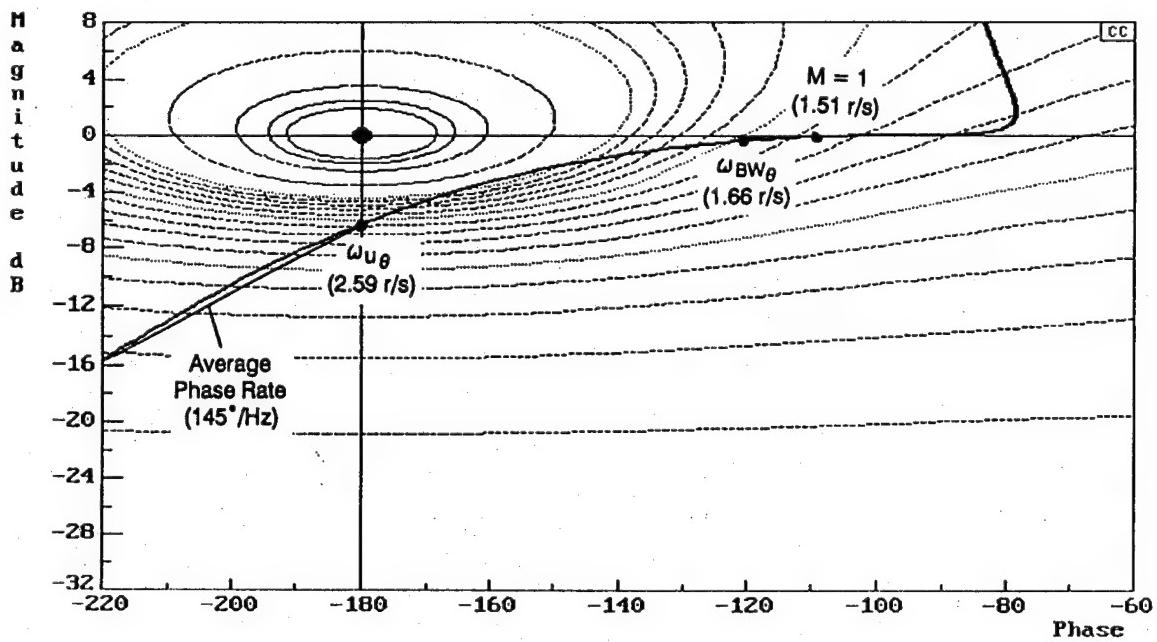
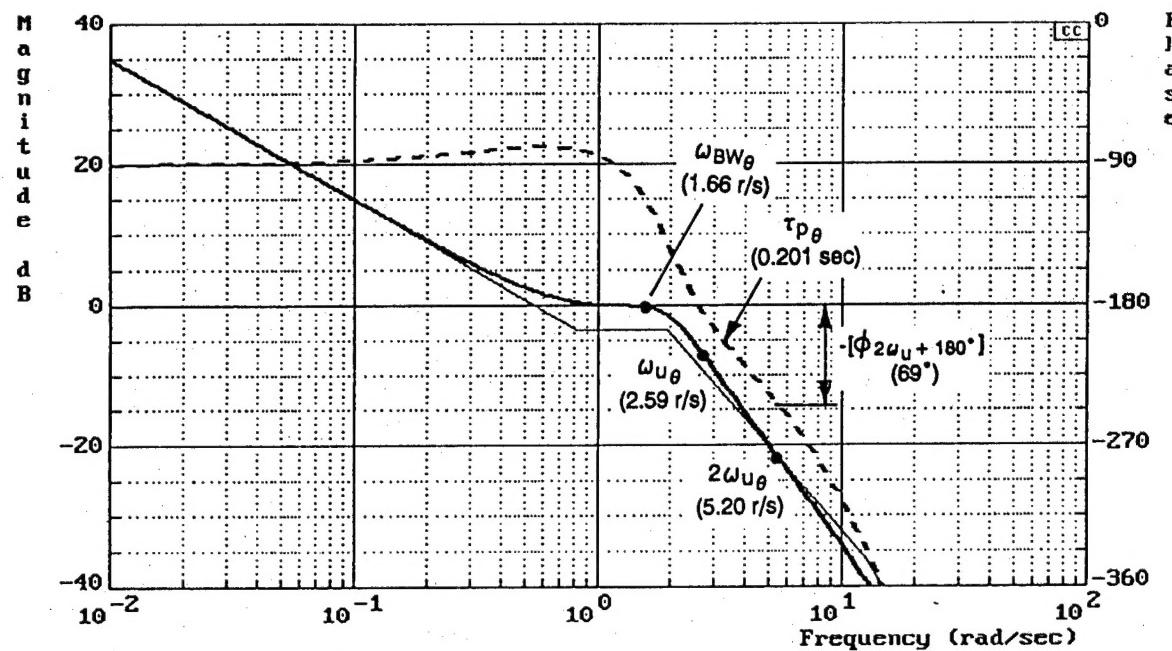


Figure B-19. F-8 DFBW Direct Mode



$$\frac{\theta}{\delta} = \frac{2.44E+07 (.826)[- .866, 26.6]}{(0)[.42, 1.91](12.5)[.866, 26.6](50)[.698, 126]}$$

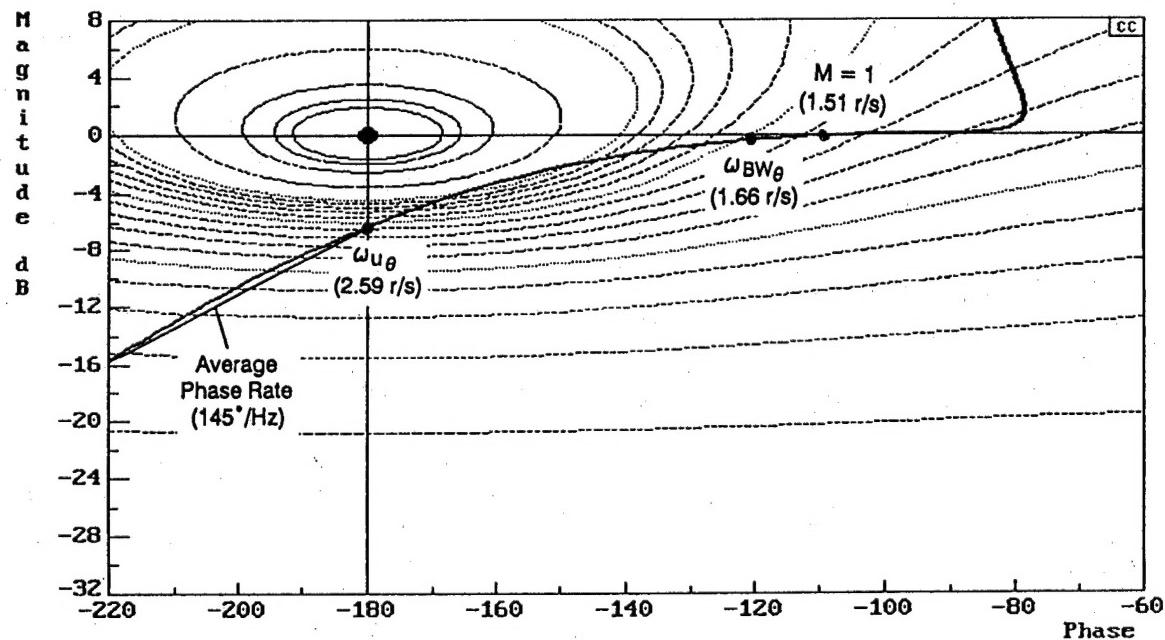


Figure B-20. F-8 DFBW SAS Mode

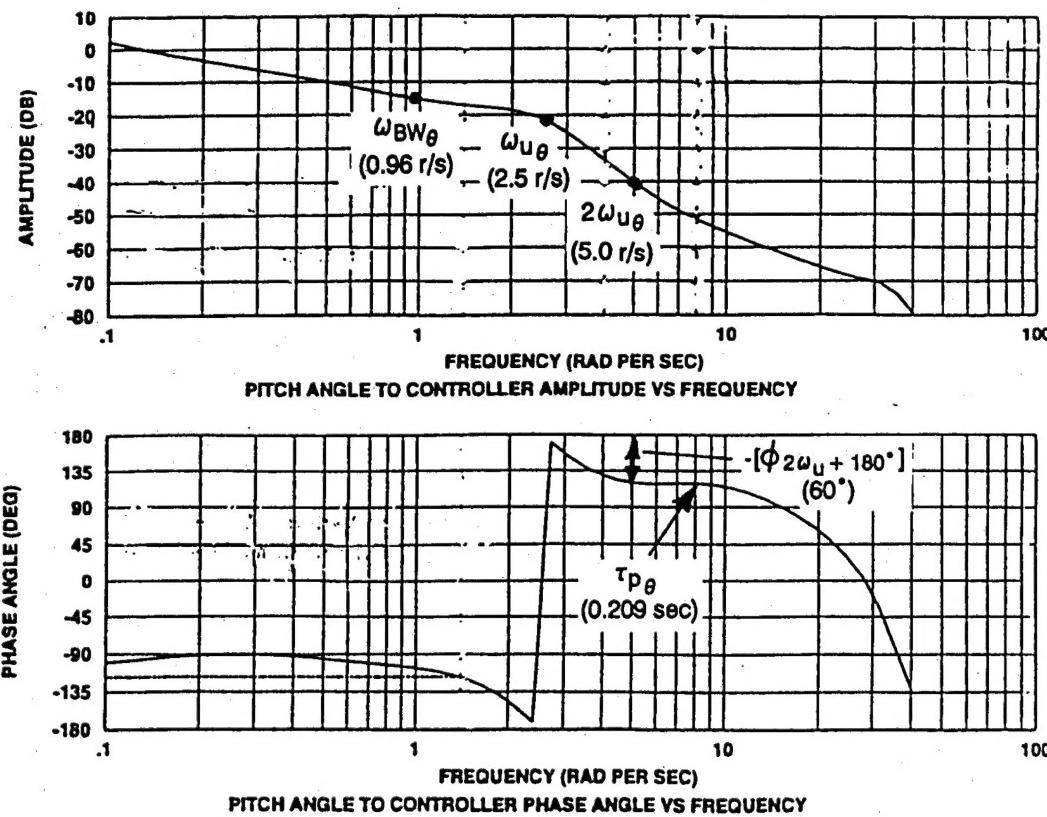


Figure B-21. B-2 Off-Nominal Approach (from Ref. B-10)

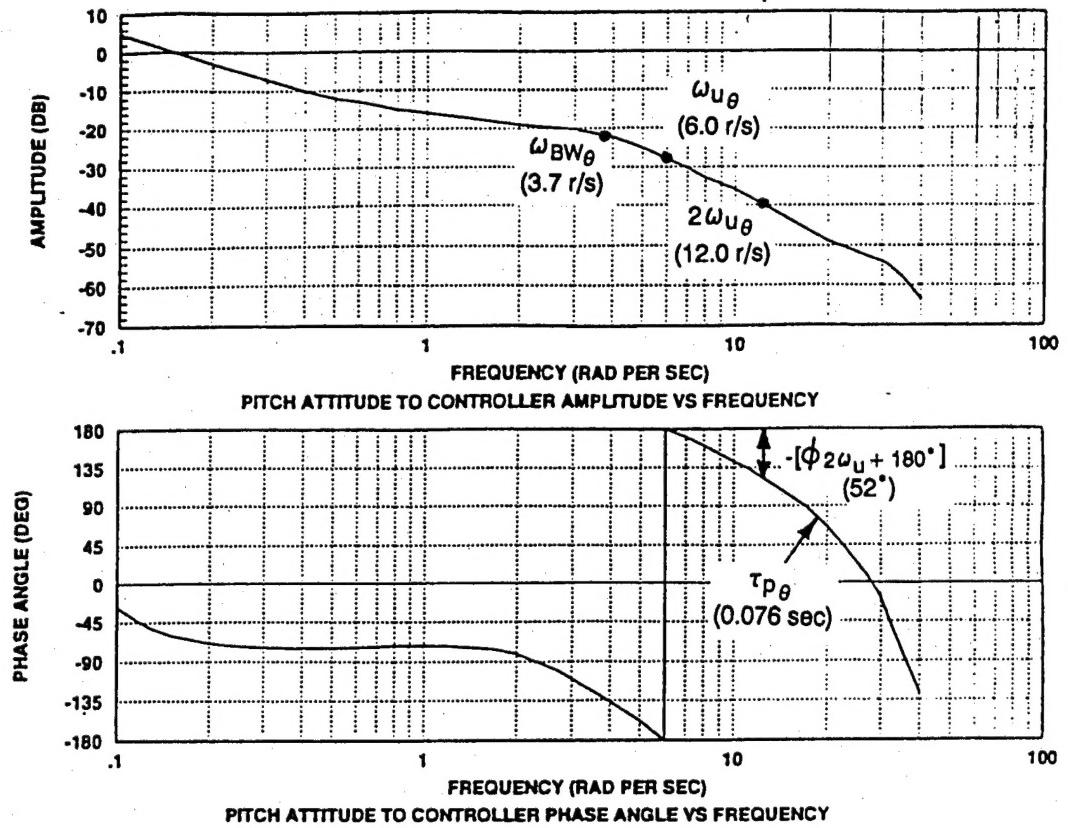


Figure B-22. B-2 Refueling (from Ref. B-10)

REFERENCES

- B-1. Bjorkman, Eileen A., *Flight Test Evaluation of Techniques to Predict Longitudinal Pilot Induced Oscillations*, AFIT/GAE/AA/86J-1, Dec. 1986.
- B-2. Matranga, Gene J., *Analysis of X-15 Landing Approach and Flare Characteristics Determined from the First 30 Flights*, NASA TN D-1057, July 1961.
- B-3. Heffley, Robert K., and Wayne F. Jewell, *Aircraft Handling Qualities Data*, NASA CR-2144, Dec. 1972.
- B-4. Taylor, Lawrence W., Jr., and John W. Smith, *An Analysis of the Limit-Cycle and Structural-Resonance Characteristics of the X-15 Stability Augmentation System*, NASA TN D-4287, Dec. 1967.
- B-5. Jex, Henry R., *Summary of T-38 PIO Analyses*, Systems Technology, Inc., STI-TR-239-1, July 1962.
- B-6. Smith, John W., and Donald T. Berry, *Analysis of Longitudinal Pilot-Induced Oscillation Tendencies of YF-12 Aircraft*, NASA TN D-7900, Feb. 1975.
- B-7. Teper, Gary L., Richard J. DiMarco, Irving L. Ashkenas, and Roger H. Hoh, *Analysis of Shuttle Orbiter Approach*, NASA CR 163108, July 1981.
- B-8. Myers, Thomas T., Donald E. Johnston, and Duane T. McRuer, *Space Shuttle Flying Qualities and Criteria Assessment*, NASA CR-4049, March, 1987.
- B-9. Berry, Donald T., Bruce G. Powers, Kenneth J. Szalai, and R. J. Wilson, "A Summary of an In-Flight Evaluation of Control System Pure Time Delays During Landing Using the F-8 DFBW Airplane," AIAA Paper No. 80-1626, Danvers, MA, 11 to 13 Aug. 1980.
- B-10. Givens, Margo L., *Evaluation of B-2 Susceptibility to Pilot-Induced Oscillations*, Northrop Grumman, B-2 Division, White Paper 120-4, 1 March 1994.
- B-11. Mitchell, David G., and Roger H. Hoh, *Development of a Unified Method to Predict Tendencies for Pilot-Induced Oscillations*, WL-TR-95-3049, June 1995.
- B-12. Smith, R. H., "The Smith-Geddes Criteria," presented at the SAE Aerospace Control and Guidance Systems Committee meeting, Reno NV, 11 Mar. 1993.
- B-13. Gibson, J. C., "The Prevention of PIO by Design," in *Active Control Technology: Applications and Lessons Learned*, AGARD, CP-560, Jan. 1995.